



УНИВЕРЗИТЕТ У БАЊОЈ ЛУЦИ
UNIVERSITY OF BANJA LUKA
ТЕХНОЛОШКИ ФАКУЛТЕТ
FACULTY OF TECHNOLOGY



PROCEEDINGS

OCTOBER 21-22, 2022

ACADEMY OF SCIENCES AND ARTS
OF THE REPUBLIC OF SRPSKA,
BANJA LUKA, REPUBLIC OF SRPSKA, B&H

INTERNATIONAL SCIENTIFIC CONFERENCE

XIV OF CHEMISTS,
CONFERENCE TECHNOLOGISTS AND
ENVIRONMENTALISTS
OF REPUBLIC OF SRPSKA

XIV CONFERENCE OF CHEMISTS, TECHNOLOGISTS AND
ENVIRONMENTALISTS OF REPUBLIC OF SRPSKA

BOOK OF PROCEEDINGS

Publisher:

University in Banjaluka, Faculty of Technology

Editorial board:

Borislav Malinović, PhD, dean

Design and computer processing

Pero Sailović, PhD

MSc Marina Rakanović

MSc Đorđe Vujčić

CIP - Каталогизација у публикацији
Народна и универзитетска библиотека
Републике Српске, Бања Лука

66(082)
661:663/664(082)
502(082)

CONFERENCE of Chemists, Technologists and Environmentalists
of Republic of Srpska (14 ; 2023)

[Book of proceedings] : international scientific conference /
XIV Conference of Chemists, Technologists and Environmentalists
of Republic of Srpska ; [editorial board Borislav Malinović]. - Banja
Luka : University in Banjaluka, Faculty of Technology, 2023 ([S.l. :
s.n.]). - 313 стр. ; 24 cm

Библиографија уз сваки рад.

ISBN 978-99938-54-98-2

COBISS.RS-ID 137637377

Organizing Committee:

PhD Pero Sailović, president, PhD Darko Bodroža, general secretary, M.Sc Maja Milijaš secretary, M.Sc Dajana Dragić, M.Sc Branka Ružičić, M.Sc Marina Rakanović, M.Sc Maja Katić, Sanda Pilipović, M.Sc Nebojša Gorgi, Biljana Vasić, Sanja Novaković, M.Sc Jovanka Kotur

Students: Vladimir Ivković, Jovan Savić, Nevena Janjić, Bojana Milinković, Danijela Lazić

Scientific Committee:

Dr Božana Odžaković, president, University of Banja Luka, **B&H**, Dr Nada Štrbac, co-president, University of Belgrade, **Serbia**, Dr Borislav Malinović, University of Banja Luka, **B&H**, Dr Vlada Veljković, University of Niš, **Serbia**, Dr Todor Vasiljević, Victoria University Melbourne, **Australia**, Dr Sanja Mahović-Poljačak, University of Zagreb, **Croatia**, Dr Csaba Horvath, University Obuda, Budapest, **Hungary**, Dr Mihail Kochubovski, University of Skopje, **Macedonia**, Dr Massimiliano Fenice, Universityt Della Tuscia, **Italy**, Dr Georgij Petriaszwili, Warshav University of Technology, **Poland**, Dr Mira Vukcević, University of Monte Negro, **Monte Negro**, Dr Ondrej Panák, University of Pardubice, **Czech Republic**, , Dr Pospiech Matej, University of Veterinary and Pharmaceutical Sciences, Brno, **Czech Republic**, , Dr Dani Dordevic, University of Veterinary and Pharmaceutical Sciences, Brno, **Czech Republic**, Dr Iskren Spiridonov, University of Chemical Technology and Metallurgy, **Bulgaria**, Dr Laura Benea, West University of Timisoara, **Romania**, Dr Savvas G. Vassiliadis, University of Piraeus, **Greece**, Dr Helena Prosen, University of Ljubljana, **Slovenia**, Dr Srecko Stopic, RWTH University Aachen, **Germany**, Dr Maria Iosune Cantalejo, UPNA, **Spain**, Dr Jurislav Babić, University of Osijek, **Croatia**, Dr Svetozar Milosavić, University of Kosovska Mitrovica, **Serbia**, Dr Petar Uskoković, University of Belgrade, **Serbia**, Dr Mitja Kolar, University of Ljubljana, **Slovenia**, Dr Dragiša Savić, , University of Niš, **Serbia**, Dr Dragan Vujadinović, University of East Sarajevo, **B&H**, Dr Biljana Pajin, University of Novi Sad, **Serbia**, Dr Sead Čatić, University of Tuzla, **B&H**, Dr Husein Vilić, University of Bihać, **B&H**, Dr Sanjin Gutić, University of Sarajevo, **B&H**, Dr Goran Trbić, University of Banja Luka, **B&H**, Dr Milica Balaban, University of Banja Luka, **B&H**, Dr Ljiljana Vukić, University of Banja Luka, **B&H**, Dr Ljiljana Topalić-Trivunović, University of Banja Luka, **B&H**, Dr Slavica Sladojević, University of Banja Luka, **B&H**, Dr Pero Dugić, University of Banja Luka, **B&H**, Dr Zoran Kukrić, University of Banja Luka, **B&H**, Dr Slavica Grujić, University of Banja Luka, **B&H**, Dr Milorad Maksimović, University of Banja Luka, **B&H**, Dr Branka Rodić-Grabovac, University of Banja Luka, **B&H**, Dr Rada Petrović, University of Banja Luka, **B&H**, Dr Dragana Grujić, University of Banja Luka, **B&H**, Dr Svjetlana Janjić, University of Banja Luka, **B&H**, Dr Zora Levi, University of Banja Luka, **B&H**, Dr Ladislav Vasilišin, University of Banja Luka, **B&H**

NOTE:

The authors have full responsibility for the originality and content of thier own papers



УНИВЕРЗИТЕТ У БАЊОЈ ЛУЦИ
UNIVERSITY OF BANJA LUKA
ТЕХНОЛОШКИ ФАКУЛТЕТ
FACULTY OF TECHNOLOGY



International scientific conference

"XIV CONFERENCE OF CHEMISTS, TECHNOLOGISTS AND ENVIRONMENTALISTS OF REPUBLIC OF SRPSKA"

under the auspices of



MINISTRY OF SCIENTIFIC AND TECHNOLOGICAL DEVELOPMENT, HIGHER
EDUCATION AND INFORMATION SOCIETY

MINISTRY OF AGRICULTURE, FORESTRY AND WATER MANAGEMENT



ACADEMY OF SCIENCES AND ARTS OF THE REPUBLICA OF SRPSKA

SPONSORS

OPTIMA GROUP and OIL RAFINERY MODRIČA

HOFSTETTER ENVIRONMENTAL SRL

SINEX LABORATORY

PREHTEH d.o.o.

DESTILACIJA ad

EAST CODE d.o.o.

MUNICIPALITY OF ČELINAC

J.P. DEP-OT

ASSOCIATION OF TECHNOLOGY ENGINEERS OF REPUBLIC OF
SRPSKA

EM PLUS d.o.o.

KESO GRADNJA d.o.o.

MARKWAY d.o.o.

EURO-LAB V d.o.o.

EKO-EURO TIM d.o.o.

MB-IMPEX d.o.o.

TRGO FORTUNA PLUS d.o.o.

EURO-INSPEKT d.o.o.

ABC PROJEKT d.o.o.

ŠTAMPARIJA PETROGRAF

CSK PRINT

CONTENTS

GENERAL AND APPLIED CHEMISTRY	5
SYNTHESIS AND ANTIPROLIFERATIVE ACTIVITY OF NITRO AND AMINO SUBSTITUTED BENZIMIDAZOLES AND BENZOTHIAZOLES.....	6
Marijana Hranjec, Livio Racané, Ida Boček, Leentje Persoons, Dirk Daelmans	
PHOTOLYSIS OF NADOLOL IN THE AQUATIC ENVIRONMENT: INSIGHTS INTO THE EFFECT OF BICARBONATES.....	15
Andrijana Vukojević, Maria M. Savanović, Stevan Armaković, Svetlana Peleliš, Sanja J. Armaković	
CAN E-CIGARETTES BE A THREAT TO ENVIRONMENT: HEAVY METALS ANALYSIS IN E-CIGARETTES FILTERS	21
Dijana Mihajlović, Nemanja Lončar, Ana Đurić, Bojana Đekanović, Dijana Jelić	
COMPARISON OF THREE EXTRACTION PROCEDURES FOR QUANTIFICATION OF Cu, Mn, Ni, Pb AND Zn IN THE PLANTS	27
Dijana Mihajlović, Vesna Antunović	
ANTIPROLIFERATIVE AND ANTIBACTERIAL ACTIVITY <i>IN VITRO</i> OF AMIDINO SUBSTITUTED 2-NAPHTHYLBENZAZOLES	33
Livio Racané, Lucija Ptiček, Marijana Hranjec, Leentje Persoons, Dirk Daelmans, Mihailo Banjananc, Vedrana Radovanović	
SOLVATOCHROMIC PROPERTIES OF NEWLY SYNTHESIZED ARYL AZO PYRIDONE DYES	42
Borko Matijević, Gorana Mrđan, Dušan Mijin, Jelena Lađarević, Suzana Apostolov, Đendi Vaštag	
CHEMICAL ENGINEERING	50
BIOBASED UNSATURATED POLYESTER RESINS REINFORCED WITH NATURAL FILLERS	51
Olga Pantić, Vesna Panić, Sanja Savić, Maja Marković, Melina Kalagasidis Krušić, Pavle Spasojević	
POSSIBILITIES OF CROSSLINKING SILICONE MATERIALS IN EXCESS OF CROSSLINKER WITH TWO TYPES OF FILLERS	56
Darko Manjenčić, Marko Paić, Vesna Cvijetinović, Vladan Mičić, Anja Manjenčić, Duško Kostić, Pero Dugić	
PHOSPHATE GLASSY FERTILIZERS	62
Vladimir S. Topalović, Jelena D. Nikolić, Srdjan D. Matijašević, Veljko V. Savić, Marija S. Djošić, Ana M. Vujošević, Snežana R. Grujić	
CHEMICAL TECHNOLOGY	67
MINEROLOGICAL AND CHEMICAL CHARACTERIZATION OF CLAY FROM THE ZAGONI SITE MUNICIPALITY OF BRATUNAC	68
Dragana Kešelj, Dragica Lazić, Zoran Petrović, Nebojša Vasiljević	
THE PHOTOSTABILITY AND DYEING ABILITY OF SOME ANTHRAQUINONE REACTIVE DYES FOR COTTON AND PAPER.....	75
Polya Miladinova, Dimitrina Todorova	
COMPARATIVE ANALYSIS OF BLEACHING OF SUNFLOWER OIL WITH COMMERCIAL BLEACHING EARTH AND BENTONITE POWDER ACTIVATED WITH SULFURIC ACID	83
Zoran Petrović, Jelena Mihajlović, Sabina Begić, Dragana Kešelj, Zorica Stojanović, Amir Fazlić	
BIOTECHNOLOGY	95
THE IMPACT OF pH VALUE AND TEMPERATURE ON POLYPHENOL RECOVERY, ANTIOXIDANT CAPACITY AND PHYSICAL PROPERTIES OF SERPYLLI HERBA'S WASTE EXTRACTS.....	96
Aleksandra A. Jovanović, Predrag M. Petrović, Mina Volić, Nataša Obradović, Bojana Balanč, Radoslava Pravilović, Branko M. Bugarski	
THE POSSIBILITY OF ANTIBIOTIC AZALOMYCIN B PRODUCTION BY COMBINING BENZOYL HYDRAZONE DERIVATIVES AND WASTE RAPESEED OIL GLYCEROL	105

Jovan Ćirić, Slavica Ilić, Sandra Konstantinović, Đorđe Lazarević, Marko Živković, Nikola Stanković

FOOD TECHNOLOGY 109

RED WINE COLOR AND STABILITY AS FUNCTION OF SIZE AND CONTENT OF SILICA GEL PARTICLES 110
Tanja Šaran, Dragan Vujadinović, Zoran Petković, Milan Vukić, Vesna Gojković, Vladimir Tomović

THE SEASONAL VARIATIONS OF BIOCHEMICAL COMPOSITION OF COW'S MILK ON THE SOUTHERN SERBIA TERRITORY 118
Jovan Ćirić, Slavica Ilić, Aleksandar Veličković, Ivan Stojković, Dragana Stanisavljević, Nebojša Milosavljević

THE EFFECTS OF ADDITION OF FLAXSEED TO THE CHARACTERISTICS OF BREAD 122
Gordana Jovanović, Ana Vasić, Ljubica Mijić, Ana Matić, Bojan Damnjanović

HABITS OF FLUID INTAKE WITH STUDENTS 128
Dragana Ilić Udovičić, Ana Matić, Danijela Damnjanović, Aleksandra Vasić

QUALITY CONTROL AND FOOD SAFETY 134

THE CONTENT OF TOTAL IRON IN *Urtica dioica* L. FROM DIFFERENT LOCALITIES IN SERBIA 135
Jelena Đuričić Milanković, Kosana Popović, Mirjana Antonijević Nikolić, Bojana Milutinović, Danijela Damnjanović, Dragana Ilić Udovičić

THE PRESENCE OF PHOSPHATE IN MEAT PRODUCTS FROM THE MARKET OF REPUBLIC OF SRPSKA 143
Biljana Pećanac, Dragan Brenjo

TEXTILE ENGINEERING 151

OPTIMIZATION OF THE CLASSICAL DYEING PROCESS OF PES KNITWEAR 152
Marija Kodrić, Suzana Đorđević, Nevena Tomić, Dragan Đorđević

INFLUENCE OF KNIT PATTERN ON DIMENSIONAL STABILITY OF KNITTED FABRICS 159
Sandra Stojanović, Dušan Trajković, Jelka Geršak, Miodrag Đorđević

GRAPHIC ENGINEERING AND DESIGN 166

A METHOD OF RANKING RESPONDENTS ACCORDING TO SENSE OF COLOR DIFFERENCES 167
Zoran Gazibarić, Predrag Živković, Vladimir Cviljušac, Miloš Ljubojević

AN OVERVIEW OF VARIOUS POSSIBILITIES OF 3D PRINTING TECHNIQUES IN THE PRODUCTION OF FLEXOGRAPHIC PRINTING PLATES 176
Sandra Dedijer, Nemanja Kašiković, Magdolna Pal, Živko Pavlović, Gojko Vladić, Ivana Tomić, Bojan Banjanin

CONTEMPORARY APPLICATIONS OF PULP MOULDED PACKAGING 184
Gojko Vladić, Nemanja Kašiković, Živko Pavlović, Stefan Đurđević, Gordana Bošnjaković, Teodora Gvoka

INFLUENCE OF THE SUBSTRATE ON THE PERMANENCE OF PRINTING INK 190
Branka Ružičić, Mladen Stančić, Đorđe Vujčić, Milijana Milić

REMARKS ABOUT PRINTING AUTOMATION 194
Thomas Hoffmann Walbeck, Živko Pavlović

ENVIRONMENTAL ENGINEERING AND ECOLOGY 199

DEPOSITION OF GOETHITE AND FERRIHYDRITE ONTO EXPANDED VERMICULITE SURFACE: CHEMICAL PROPERTIES AND POTENTIAL APPLICATION 200
Mladen Bugarčić, Aleksandar Jovanović, Aleksandar Marinković, Jovana Bošnjaković, Miroslav Sokić, Ana Radosavljević Mihajlović, Milan Milivojević

REMOVAL OF XENOBIOTICS FROM WASTEWATERS USING PHOTOLYSIS UNDER SUN-LIGHT IRRADIATION: EXPERIMENTAL APPROACH AND PROCESS DESIGN 206

Aleksandar Jovanović, Mladen Bugarčić, Nataša Knežević, Jovana Bošnjaković, Jelena Lukić, Antonije Onjia, Aleksandar Marinković

SOLAR STABILITY OF COMMERCIAL PESTICIDES THAT CONTRIBUTE TO THE QUALITY OF GRAPES AND FRUITS..... 211

Maria M. Savanović, Aleksandra Jovanoski Kostić, Andrijana Vukojević, Stevan Armaković, Jelena Kalajdžić, Biserka Milić, Mladen Kalajdžić, Svetlana Pelemiš, Sanja J. Armaković

COMPARATIVE ASSESSMENT OF ZINC IONS SORPTION AND RETENTION BY PROSPECTIVE UNCONVENTIONAL SOIL ADDITIVES 217

Ivana Smičiklas, Marija Egerić, Mihajlo Jović

A GREEN ADSORBENT BASED ON WHEAT STARCH FOR REMOVAL OF SELECTIVE ORGANIC POLLUTANTS FROM AQUEOUS SOLUTIONS 225

Nataša Karić, Marija Vukčević, Marina Maletić, Mirjana Ristić, Aleksandra Perić-Grujić, Katarina Trivunac

EFFECT OF ALKALI MODIFICATION ON ADSORPTION EFFICIENCY OF FLY ASH 231

Nataša Karić, Sara Živojinović, Marija Vukčević, Marina Maletić, Aleksandra Perić-Grujić, Katarina Trivunac

USE OF AGRICULTURAL WASTE AS RAW MATERIALS FOR OBTAINING GLASS AND GLASS-CERAMICS: A REVIEW 237

Vladimir S. Topalović, Jelena D. Nikolić, Veljko V. Savić, Srdjan D. Matijašević, Marija S. Djošić, Snežana N. Zildžović, Snežana R. Grujić

PHOTOCATALYTIC DECOMPOSITION OF DIFENOCONAZOLE FROM WASTEWATERS 242

Jovana Bošnjaković, Nataša Knežević, Srećko Manasijević, Aleksandar Jovanović, Mladen Bugarčić, Aleksandar Marinković

UTILIZATION OF CONSTRUCTION MATERIAL AND UNSATURATED RESIN FROM WASTE PET AS A STABILIZER FOR DESORBED METAL ION Pb^{2+} 247

Nataša Knežević, Jovana Bošnjaković, Aleksandar Jovanović, Mladen Bugarčić, Srećko Manasijević² Aleksandar Marinković

BIOCHAR AS EFFICIENT TOOL FOR SOIL AMMENDMENT 252

Zorica Lopičić, Anja Antanasković, Tatjana Šošarić, Vladimir Adamović, Marina Orlić, Jelena Petrović, Jelena Avdalović

A STUDY OF PV SYSTEM APPLICATION ON THE SUSTAINABLE DEVELOPMENT IN SERBIA 258

Dragana Todorović, Slavica Jovanović, Tijana Kevkić, Marija Stojanović Krasić, Nenad Milojević, Branko Drljača

TIME AND SEASONAL VARIATIONS OF PARTICULATE MATTER (PM) AND GASEOUS POLLUTANTS CONCENTRATIONS IN AMBIENT AIR OF VALJEVO, SERBIA 265

Jelena Đuričić Milanković, Dragana Đorđević, Slavica Ilić

ORGANIC BIO-DEGRADABLE WASTE IN FRUIT PRODUCTION 275

Milica Đeković Šević, Zoranka Malešević, Milan Šević, Tamara Bartošek

MATERIAL SCIENCE AND METALLURGY 283

SIMULATION OF THE IMPACT OF PREHEATING TEMPERATURE ON RAILWAY ALUMINOTHERMIC WELDING 284

Gvozden Jovanović, Vaso Manojlović, Miroslav Sokić, Alen Delić, Milorad Gavrilovski

OTHERS 291

STUDY OF ISOTHERMAL, KINETIC, AND THERMODYNAMIC PARAMETERS FOR SORPTION OF VANADIUM 292

Tamara T. Tadić, Bojana M. Marković, Aleksandra B. Nastasović, Ljiljana T. Suručić, Zvezdana P. Sandić, Antonije E. Onjia

REMOVAL OF LINDANE FROM AQUEOUS SOLUTION BY GLYCIDYL METHACRYLATE BASED CHELATING MACROPOROUS COPOLYMER: KINETICS AND MECHANISM..... 300

Tamara T. Tadić, Bojana M. Marković, Mila V. Ilić, Aleksandra B. Nastasović, Antonije E. Onjia

THE USE OF SOFT FOOD AS A VEHICLE FOR DRUG DELIVERY TO PEDIATRIC POPULATION – EFFECTS ON DISSOLUTION OF PROPRANOLOL 307

Maja Mirjanić, Aneta Stojmenovski, Biljana Gatarić, Nataša Bubić Pajić, Anđelka Račić

GENERAL AND APPLIED CHEMISTRY

Original scientific article

SYNTHESIS AND ANTIPROLIFERATIVE ACTIVITY OF NITRO AND AMINO SUBSTITUTED BENZIMIDAZOLES AND BENZOTHAZOLES

Marijana Hranjec¹, Livio Racané², Ida Boček¹, Leentje Persoons³, Dirk Daelmans³¹Department of Organic Chemistry, Faculty of Chemical Engineering and Technology, University of Zagreb, HR-10000 Zagreb, Croatia²Department of Applied Chemistry, Faculty of Textile Technology, University of Zagreb, HR-10000 Zagreb, Croatia³KU Leuven Department of Microbiology and Immunology, Laboratory of Virology and Chemotherapy, Rega Institute, Leuven, Belgium

Abstract

Nowadays heterocyclic compounds become unavoidable structural motifs and building blocks in organic and medicinal chemistry. Since benzimidazoles and benzothiazoles as one of the most important nitrogen heterocycles have great and versatile biological activities, these benzazoles become important structural scaffolds in the rational design of novel drugs in medicinal and pharmaceutical chemistry. These nitrogen scaffolds could be found in a variety of bioactive natural and synthetic medical and biochemical agents, which possess different chemical and pharmacological features. Within this work we present the synthesis, structural characterization and biological evaluation of methoxy and hydroxy substituted 2-benzimidazole and 2-benzothiazole derivatives bearing either nitro or protonated amino group at the benzazole scaffold (Figure 1). The targeted compounds were prepared by using conventional and well-optimized reactions of organic chemistry for the synthesis and cyclocondensation of benzimidazole and benzothiazole nuclei. All synthesized compounds were structurally characterized by means of ¹H and ¹³C NMR spectroscopy. The antiproliferative activity was evaluated on the panel of human cancer cells *in vitro*. Some of tested compounds showed prominent antiproliferative activity. Obtained results revealed the strong influence of the substituents placed at the phenyl as well as on the benzazole nuclei on biological activity.

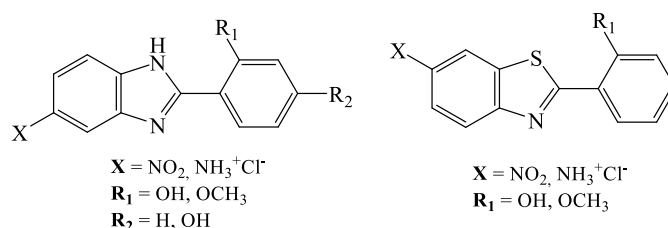


Figure 1. Benzimidazole and benzothiazole derivatives

Keywords: antiproliferative activity, benzimidazoles, benzothiazoles, synthesis.

Introduction

In the last two decades, heterocyclic molecules are playing an important role in the rational design of novel biologically active molecules being one of the greatest focuses of organic, medicinal and pharmaceutical chemists all over the world (Silverman, 2004). The most significant feature of the heterocycles is their great possibility to incorporate different functional groups either as substituents or as part of the ring itself, which enabled the optimization of suchlike skeletons towards more

efficient molecules (Časar, 2016). This ability has a particular interest in organic and medicinal chemistry, so the heterocycles became widely incorporated in the structure of many newly synthesized compounds in order to improve their biological features. Nitrogen-containing heterocycles have been one of the most studied types of heterocycles having great and extensive therapeutic potential and significance in medicinal chemistry (Akhtar, 2017). Among all nitrogen heterocycles, one of the most important subclasses are benzazoles, namely benzimidazoles and benzothiazoles which have proven to be fundamental, privileged and indispensable building motifs for the synthesis of novel biologically active molecules (Bansal, 2012; Sharma, 2013). Furthermore, because benzazole nuclei are actually a bioisoster of naturally occurring purine, suchlike derivatives have often a crucial role in the function of biologically important molecules like DNA, RNA or different proteins (Tariq, 2019; Keri, 2015). Based on all above-mentioned importance, there are a great number of natural and synthetic molecules, which consist of bezazole structural fragments showing versatile biological activities including antitumor, antimicrobial, antifungal, antiprotozoal, antihypertensive, antioxdant, anti-inflammatory *etc.* Activities (Yadav, 2015; Gill, 2015).

Recently, in our research group, we have evaluated several series of substituted 2-benzimidazole and 2-benzothiazole derivatives including amidino, cyano, carboxamido, nitro, amino, hydroxy and methoxy substituted derivatives, which have showed a great biological potential possessing promising antiproliferative, antitumor, antibacterial or antioxidant activity (Hranjec, 2007; Racané, 2010a; Racané, 2021b; Sović, 2019). Furthermore, we have also synthesized and studied tricyclic, tetracyclic and pentacyclic benzimidazole derivatives substituted with amidino, cyano and carboxamido side chains and showing great antiproliferative activity in submicromolar range of inhibitory concentrations (Perin, 2016a; Perin, 2017b). Among all benzimidazole/benzothiazole derivates, the most promising antiproliferative activity has been observe by amidino-substituted derivatives with compounds bearing cyclic 2-imidazolinylyl amidine group. In addition, many of our previously published and studied benzimidazole/benzothiazole derivatives with enhance biological activity have shown strong interaction with either DNA or RNA being classified as minor groove binders or intercalators which showed selective binding to these biomolecules (Hranjec, 2008b; Racané, 2021c).

In the last few years, our research has been focus on the study of antioxidative potential of benzazole derivatives, which possess good antiproliferative activity (Tireli, 2017; Cindrić, 2019). We have explored different benzazole derivatives, which have been substituted with versatile substituents to study the structure-activity relationship. Based on all obtained results, we have seen that the most important influence on the antioxidative and thus on antiproliferative activity have nitro, amino, amino protonated and variable number of methoxy and hydroxy groups (Beč, 2022). The focus within this research was to study the influence of nitro and amino protonated as well as hydroxy and methoxy groups on antiproliferative activity as well as the influence of the type of heteroatom (NH group in benzimidazole and S atom in benzothiazole) on biological activity. With this purpose, all synthesized compound were tested for their antiproliferative activity on a panel of human cancer cells *in vitro*.

Materials and Methods

Chemistry

General methods

All chemicals and solvents were purchased from commercial available suppliers. Melting points were recorded on SMP11 Bibby apparatus and were not corrected.

All NMR spectra were measured in DMSO-*d*₆ solutions using TMS as an internal standard. The ¹H and ¹³C NMR spectra were recorded on a Varian Bruker Avance III HD 400 MHz/54 mm Ascend.

Chemical shifts are reported in ppm (δ) relative to TMS. All compounds were routinely checked by TLC with Merck silica gel 60F-254 glass plates. Elemental analysis for C, H and N were performed on a Perkin-Elmer 2400 elemental analyzer. Where analyses are indicated only as symbols of elements, analytical results obtained are within 0.4% of the theoretical value.

Synthesis of benzothiazole derivatives

Compounds **2**, **4a** and **4b** were synthesized according to the previously published paper (Racan , 2022d).

2-(2-Hydroxyphenyl)benzothiazole-6-ammonium chloride (5a)

To a stirred solution of tin(II) chloride dihydrate (1.28 g, 5.0 mmol) in concd. hydrochloric acid (2.5 ml) and methanol (2.5 ml), 2-(2-hydroxyphenyl)-6-nitrobenzothiazole (**4a**) (0.272 g, 1.0 mmol) was added and heated to reflux for 30 min. The reaction mixture was poured onto ice, made slightly basic (pH 8-9) with 20 % NaOH and the product was extracted with diethyl-ether. The solvent was removed under reduced pressure and resulting crude amine was dissolved in 2-propanol (10 ml), concd. hydrochloric acid (0.165 ml, 2 mmol) was added and stirred at room temperature for 2 h. The resulting precipitate was filtered, washed with diethyl-ether and dried at 75 °C giving 0.256 g (92 %) of colorless solid; mp = 263 - 272 °C (dec.). ¹H NMR (600 MHz, DMSO-*d*₆) (δ ppm): 11.57 (bs, 1H, -OH), 8.16 (d, *J* = 7.2 Hz, Ar-*H*), 8.05 (d, 1H, *J* = 8.6 Hz, Ar-*H*), 7.96 (s, 1H, Ar-*H*), 7.42 – 7.38 (m, 2H, Ar-*H*), 7.12 (d, 1H, *J* = 8.1 Hz, Ar-*H*), 7.02 (m, 1H, Ar-*H*). ¹³C NMR (75 MHz, DMSO-*d*₆) (δ ppm): 165.3, 156.0, 150.0, 135.2, 132.1, 130.6, 128.1, 122.8, 120.5, 119.4, 118.0, 116.3, 114.7. Analysis calcd for C₁₃H₁₁ClN₂OS: C, 56.01; H, 3.98; N, 10.05. Found: C, 55.87; H, 4.08; N, 10.10.

2-(2-Methoxyphenyl)benzothiazole-6-ammonium chloride (5b)

To a stirred solution of tin(II) chloride dihydrate (1.28 g, 5.0 mmol) in concd. hydrochloric acid (2.5 ml) and methanol (2.5 ml), 2-(2-methoxyphenyl)-6-nitrobenzothiazole (**4b**) (0.286 g 1.0 mmol) was used and heated to reflux for 30 min. The reaction mixture was poured onto ice, made slightly basic (pH 8-9) with 20 % NaOH and the product was extracted with diethyl-ether. The solvent was removed under reduced pressure and resulting crude amine was dissolved in 2-propanol (15 ml), concd. hydrochloric acid (0.165 ml, 2 mmol) was added and stirred at room temperature for 2h. The resulting precipitate was filtered, washed with diethyl-ether and dried at 75 °C giving 0.220 g (75 %) of colorless solid; mp = 214 - 218 °C (dec.). ¹H NMR (600 MHz, DMSO-*d*₆) (δ ppm): 8.43 (dd, 1H, *J* = 7.8 Hz, *J* = 1.7 Hz, Ar-*H*), 8.18 (d, 1H, *J* = 2.0 Hz, Ar-*H*), 8.14 (d, 1H, *J* = 8.6 Hz, Ar-*H*), 7.60 -7.57 (m, 1H, Ar-*H*), 7.54 (dd, 1H, *J* = 8.6 Hz, *J* = 2.1 Hz, Ar-*H*), 7.33 (d, 1H, *J* = 8.1 Hz, Ar-*H*), 7.18 (m, 1H, Ar-*H*), 4.07 (s, 3H, -OCH₃). ¹³C NMR (75 MHz, DMSO-*d*₆) (δ ppm): 163.6, 157.0, 150.8, 136.1, 132.8, 128.6, 128.5, 123.2, 121.9, 121.1, 120.7, 116.6, 112.7, 56.1. Analysis calcd for C₁₄H₁₃ClN₂OS: C, 57.43; H, 4.48; N, 9.57. Found: C, 57.62; H, 4.38; N, 9.55.

Synthesis of benzimidazole derivatives

5(6)-nitro-2-(2-hydroxyphenyl)benzimidazole (7)

A mixture of 2-hydroxybenzaldehyde **3a** (1.00 g, 8.2 mmol), 4-nitro-1,2-phenylenediamine **6** (1.25 g, 8.2 mmol) and *p*-benzoquinone (0.88 g, 8.2 mmol) in absolute ethanol (10 mL) was obtained 1.140 g (55 %) of grey solid; mp > 270 °C; ¹H NMR (600 MHz, DMSO-*d*₆) (δ ppm): 13.52 (bs, 1H, OH), 12.32 (bs, 1H, NH_{benzimidazol}), 8.55 (s, 1H, Ar-*H*), 8.15 (t, *J* = 8.5 Hz, 2H, Ar-*H*), 7.83 (d, *J* = 8,8 Hz, 1H, Ar-*H*), 7.45 (t, *J* = 7.8 Hz, 1H, Ar-*H*), 7.15 – 7.00 (m, 2H, Ar-*H*).

¹³C NMR (75 MHz, DMSO-*d*₆) (δ ppm): not enough soluble. Analysis calcd for C₁₃H₉N₃O₃: C, 57.43; H, 4.48; N, 9.57. Found: C, 57.60; H, 4.70; N, 9.80.

General method for the synthesis of benzimidazole derivatives 10a-10b

Equimolar amounts of the corresponding aldehyde **9a-9b** and 4-nitro-1,2-phenylenediamine **7** in PPA (10 g) was stirred at temperature 180 °C for 2 hours. The cooled mixture was poured into ice-water (200 ml) and the resulting solution was made slightly basic (pH 8-9) with 20 % NaOH. After

extraction with ethyl-acetate, the organic layer was dried over MgSO₄ and evaporated to obtained powdered product.

5(6)-nitro-2-(2,4-dihydroxyphenyl)benzimidazole (10a)

Using above described method from 2,4-dihydroxybenzoic acid **9a** (0.38 g, 2.4 mmol) and 4-nitro-1,2-phenylenediamine **7** (0.37 g, 2.4 mmol) was obtained 0.455 g (70 %) of green solid; mp > 3000 °C; ¹H NMR (600 MHz, DMSO-*d*₆) (δ ppm): 13.33 (bs, 1H, NH_{benzimidazol}), 13.21(bs, 1H, NH_{benzimidazol}), 12.37 (bs, 1H, OH), 12.28 (bs, 1H, OH), 10.18 (s, 2H, OH), 8.53 (s, 1H, Ar-*H*), 8.39 (s, 1H, Ar-*H*), 8.13 (d, 2H, *J* = 8.91 Hz, Ar-*H*), 7.98 (bs, 2H, Ar-*H*), 7.81-7.70 (m, 2H, Ar-*H*), 6.49 (dd, 2H, *J*₁ = 8.58 Hz, *J*₂ = 2.19 Hz, Ar-*H*), 6.44 (d, *J* = 2.04 Hz, Ar-*H*). ¹³C NMR (75 MHz, DMSO-*d*₆) (δ ppm): not enough soluble. Analysis calcd for C₁₃H₉N₃O₄: C, 57.57; H, 3.34; N, 15.94. Found: C, 57.33; H, 3.14; N, 15.80.

5(6)-nitro-2-(2-methoxyphenyl)benzimidazole (10b)

Using above described method from 2-methoxybenzoic acid **9b** (1.00 g, 7.4 mmol) and 4-nitro-1,2-phenylenediamine **7** (1.13 g, 7.4 mmol) was obtained 0.550 g (38 %) of grey solid; mp > 300 °C; ¹H NMR (600 MHz, DMSO-*d*₆) (δ ppm): 12.64 (bs, 1H, NH_{benzimidazol}), 8.53 (d, 1H, *J* = 2.22 Hz, Ar-*H*), 8.37 (dd, 1H, *J*₁ = 7.76 Hz, *J*₂ = 1.56 Hz, Ar-*H*), 8.13 (dd, 1H, *J*₁ = 8.90 Hz, *J*₂ = 2.30 Hz, Ar-*H*), 7.80 (d, 1H, *J* = 8.90 Hz, Ar-*H*), 7.59-7.56 (m, 1H, Ar-*H*), 7.30 (d, 1H, *J* = 8.20 Hz, Ar-*H*), 7.17 (t, 1H, *J* = 7.90 Hz, Ar-*H*), 4.03 (s, 3H, OCH₃). ¹³C NMR (150 MHz, DMSO-*d*₆) (δ ppm): 159.1, 157.7, 143.0, 133.1, 130.6, 121.6, 120.1, 118.2, 117.7, 117.1, 112.8, 56.4. Analysis calcd for C₁₄H₁₁N₃O₃: C, 62.45; H, 4.12; N, 15.61. Found: C, 62.67; H, 4.25; N, 15.78.

General method for the synthesis of benzimidazole derivatives 8 and 11

To a stirred solution of tin(II) chloride dihydrate in concd. hydrochloric acid) and methanol, nitro substituted benzimidazoles **7** and **10b** were added and heated to reflux for 30 min. The reaction mixture was poured onto ice, made basic (pH 12-13) with 20 % NaOH and the product was extracted with ethyl-acetate. The solvent was removed under reduced pressure and resulting crude amine was dissolved in absolute ethanole (3 ml), concd. hydrochloric acid was added and stirred at room temperature for 2 h. The resulting precipitate was filtered, washed with diethyl-ether to give powdered products.

2-(2-hydroxyphenyl)benzimidazole ammonium chloride (8)

Using above described method from **7** (0.50 g, 3.62 mmol), tin(II) chloride dihydrate (3.09 g, 13.7 mmol) in MeOH (10 ml) and HCl_{conc.} (5 ml) to obtain 0.35 g (79%) amine which gave with HCl_{conc.} (133 mL) in EtOH_{abs.} desired hydrochloride salt as 0.30 g beige powder (73%); mp > 300 °C; ¹H NMR (600 MHz, DMSO-*d*₆) (δ ppm): 13.79 (bs, 2H, OH, NH_{benzimidazole}), 7.90 (d, *J* = 7.4 Hz, 1H, Ar-*H*), 7.36 (d, 2H, *J* = 8.36 Hz, Ar-*H*), 7.00 – 6.90 (m, 2H, Ar-*H*), 6.69 (d, 1H, *J* = 8.60 Hz, Ar-*H*), 6.58 (bs, 1H, Ar-*H*), 5.09-4.80 (bs, 3H, NH₃⁺).

¹³C NMR (75 MHz, DMSO-*d*₆) (δ ppm): not enough soluble. Analysis calcd for C₁₃H₁₂ClN₃O: C, 59.66; H, 4.62; N, 16.06. Found: C, 59.50; H, 4.38; N, 16.28.

2-(2-methoxyphenyl)benzimidazole ammonium chloride (11)

Using above described method from **10b** (0.15 g, 0.64 mmol), tin(II) chloride dihydrate (1.44 g, 6.4 mmol) in MeOH (4 ml) and HCl_{conc.} (4ml) to obtain 0.065 g (42%) amine which gave with HCl_{conc.} (30 μL) in EtOH_{abs.} desired hydrochloride salt as 0.44 g beige powder (85%); mp > 300 °C; ¹H NMR (600 MHz, DMSO-*d*₆) (δ ppm): 11.90 (bs, 1H, NH_{benzimidazol}), 8.37 (d, 1H, *J* = 7.32 Hz, Ar-*H*), 7.89 (d, 1H, *J* = 8.70 Hz, Ar-*H*), 7.81 (s, 1H, Ar-*H*), 7.74 (t, 1H, *J* = 8.40 Hz, Ar-*H*), 7.41 (d, 2H, *J* = 8.40 Hz, Ar-*H*), 7.28 (t, 1H, *J* = 7.60 Hz, Ar-*H*), 5.30-4.97 (bs, 3H, NH₃⁺), 4.10 (s, 3H, OCH₃). ¹³C NMR (150 MHz, DMSO-*d*₆) (δ ppm): 157.1, 156.8, 145.8, 134.6, 131.5, 129.5, 119.3, 116.7, 114.5, 112.4, 110.7, 110.4. Analysis calcd for C₁₄H₁₄ClN₃O: C, 60.98; H, 5.12; N, 15.24. Found: C, 60.75; H, 5.30; N, 15.40.

Biology

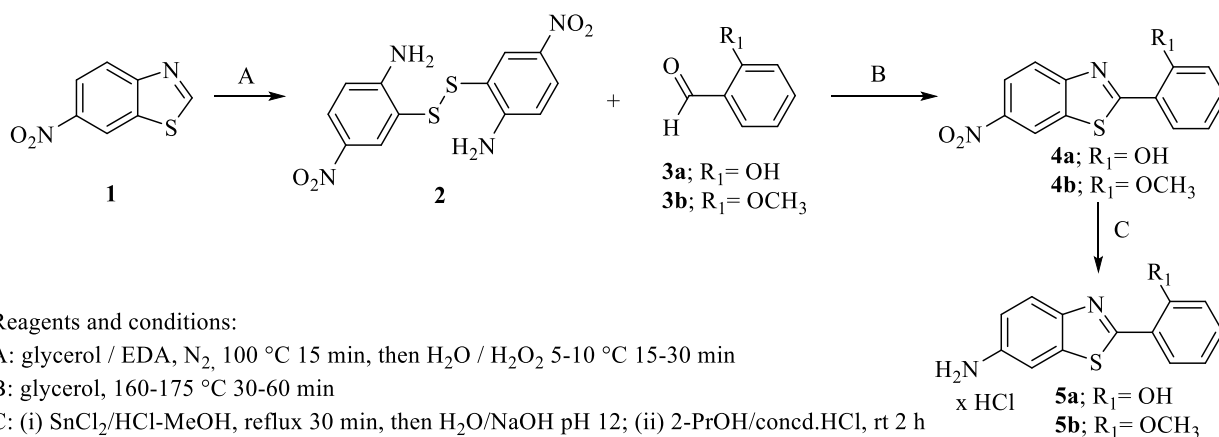
Cell culture and reference compounds

Human cancer cell lines were acquired from the American Type Culture Collection (ATCC, Manassas, VA, USA), DND-41 cell line was purchased from the Deutsche Sammlung von Mikroorganismen und Zellkulturen. All assays were done according to the previously published procedures. Culture media were purchased from Gibco Life Technologies, USA, and supplemented with 10% fetal bovine serum (HyClone, GE Healthcare Life Sciences, USA). Stock solutions were prepared in DMSO and *Vincristine* and *docetaxel* were used as references.

Results and discussion

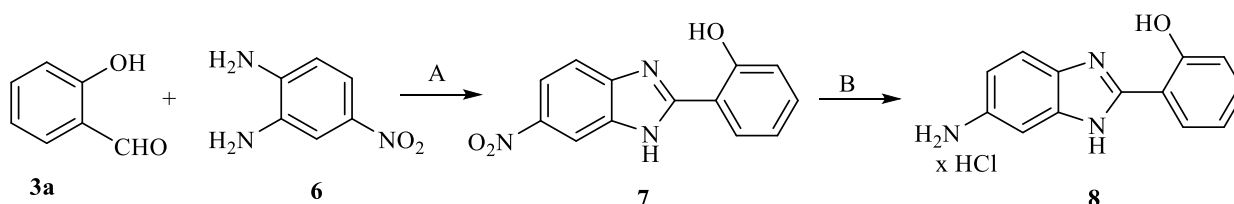
Chemistry

All targeted benzothiazole and benzimidazole derivatives were synthesized according to the experimental procedures shown in Scheme 1, 2 and 3.



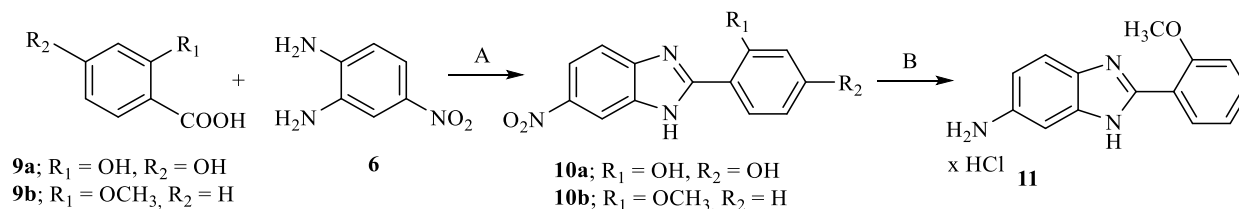
Scheme 1. Synthesis of benzothiazole derivatives **4a-4b** and **5a-5b**

Hydroxy and methoxy substituted benzothiazoles **4a** and **4b** were prepared according to the Scheme 1, in the green synthesis starting from disulphide **2**, prepared from 6-nitrobenzothiazole **1** in glycerol. Precursor **2** gave in cyclocondensation with chosen benzaldehydes **3a-3b** also in glycerol targeted compounds. Amino protonated derivatives obtained after the reduction with SnCl₂×2H₂O and HCl in MeOH followed with protonation in 2-PrOH with HCl. All benzothiazole derivatives obtained in moderate reaction yields. 2-(hydroxyphenyl)substituted benzimidazole derivative **7**, according to the Scheme 2, obtained in the condensation from 2-hydroxybenzaldehyd and 4-nitro-1,2-phenylenediamine **6** using *p*-benzoquinone as an oxidants. After the reduction and protonation, targeted amino protonated derivative **8** was prepared.



Scheme 2. Synthesis of benzimidazole derivatives **7** and **8**

2,4-dihydroxy and 2-methoxy substituted benzimidazoles **10a-10b** obtained according to the reaction Scheme 3, starting from corresponding benzoic acid and 4-nitro-1,2-phenylenediamine **6** using polyphosphoric acid. The synthesis of 2,4-dihydroxy substituted amino-benzimidazole was not successful and thus, only 2-methoxy substituted derivative bearing amino protonated group **11** was prepared using reduction and protonation. All hydrochloride salts were prepared in order to ensure better solubility important for biological testing.



Reagents and conditions:

A: PPA, heat, 180 °C

B: (i) SnCl₂/HCl-MeOH, reflux 30 min, then H₂O/NaOH pH 12; (ii) HCl_{conc.}, EtOH_{abs.}

Scheme 3. Synthesis of benzimidazole derivatives **10a-10b** and **11**

Antiproliferative activity *in vitro*

All prepared compounds were tested for their antiproliferative activity *in vitro* on a following human cancer cells: LN-229 - glioblastoma, Capan-1 - pancreatic adenocarcinoma, HCT-116 - colorectal carcinoma, NCI-H460 - lung carcinoma, DND-41 - acute lymphoblastic leukemia, HL-60 - acute myeloid leukemia, K-562 - chronic myeloid leukemia, and Z-138 - non-Hodgkin lymphoma (Table 1). As standard drugs, docetaxel and vincristine have been used and obtained results revealed that all tested compounds showed significantly lower activity in comparison to these antitumor drugs.

Table 1. Antiproliferative activity of tested compounds *in vitro*

Cpd	IC ₅₀ /μM							
	Cell lines							
	LN-229	Capan-1	HCT-116	NCI-H460	DND-	HL-60	K-562	Z-138
4a	>100	>100	>100	>100	>100	>100	>100	>100
4b	>100	>100	>100	>100	>100	>100	>100	>100
5a	>100	13.5	>100	>100	>100	62.4	>100	50.0
5b	>100	2.6	43.3	>100	43.4	17.7	>100	46.9
7	2.1	1.7	2.2	2.1	1.6	2.3	3.0	1.2
8	>100	>100	>100	>100	>100	>100	>100	>100
10a	83.7	4.3	48.7	43.5	12.1	10.6	68.5	8.8
10b	>100	29.1	>100	>100	69.5	50.4	87.0	53.8
11	>100	27.6	>100	83.5	56.4	61.8	>100	>100
Docetaxel	0.0041	0.0038	0.0025	0.0044	0.0025	0.0022	0.0085	0.0023
Vincristine	0.0027	0.0088	0.0079	0.0097	0.010	0.0033	0.017	0.031

The majority of the compounds exerted weak to moderate antiproliferative activity on the tested cell lines. Exceptionally compound **7**, 5(6)-nitro and 2-hydroxyphenyl substituted benzimidazole derivative, showed strong antiproliferative activity against all of the cancer cells without significant selectivity (IC₅₀ 1.2 – 2.3 μM). This compound has been chosen as a lead compound for further structure optimization to achieve even better antiproliferative activity and selectivity. Very strong antiproliferative activity was also shown by 5(6)-nitro and 2,4-dihydroxyphenyl substituted

benzimidazole **10a** with strong and selective activity against Capan-1 cells (IC₅₀ 4.3 μM) and good activity against DND-41 and HL-60 cells (IC₅₀ 12.1 and 10.6 μM, respectively).

Compounds **4a**, **4b** and **8** were not active at all. 2-methoxyphenyl benzothiazole ammonium chloride **5b** showed selective activity against Capan-1 cells in comparison to other cancer cells. Furthermore, 5(6)-nitro and 2-methoxyphenyl substituted derivative **10b** and 2-methoxyphenyl benzimidazole ammonium chloride **11** also showed moderate selective activity against Capan-1 cells. In general, we might conclude that benzimidazole derivatives were more active in comparison to benzothiazole derivatives with strong influence of the chosen substituents on the antiproliferative activity.

Conclusion

Within this work, we have synthesized and structurally characterized hydroxyl and methoxy substituted benzimidazole and benzothiazole derivatives bearing either nitro or amino protonated group on the benzazole nuclei. All compounds were prepared in order to evaluate their antiproliferative activity *in vitro* against several human cancer cells as well as to study the influence of the chosen substituents on the biological activity. Targeted compounds were prepared according to the well-optimized and previously published conventional methods for organic synthesis of benzimidazole and benzothiazole derivative.

Based on results obtained from antiproliferative testing, we might observe that the benzimidazole derivatives are in general more active in comparison to their benzothiazole analogues. Majority of active compounds showed selective activity against Capan-1 cancer cells.

The type of substituent placed at either the phenyl or benzazole nuclei as well as the type of benzazole nuclei has a strong impact on the antiproliferative activity. The most active compound has proven to be 5(6)-nitro and 2-hydroxyphenyl substituted benzimidazole derivative, with strong antiproliferative activity against all of the cancer cells (IC₅₀ 1.2 – 2.3 μM). This compound has been chosen for further optimization of the structure in order to design a promising antiproliferative agent.

Acknowledgments: We greatly appreciate the financial support of the Croatian Science Foundation under the projects 4379 entitled *Exploring the antioxidative potential of benzazole scaffold in the design of novel antitumor agents*.

References

- Akhtar, J., Khan, A. A., Ali, Z., Haider, R. & Shahar Yar, M. (2017). Structure-activity relationship (SAR) study and design strategies of nitrogen-containing heterocyclic moieties for their anticancer activities. *European Journal of Medicinal Chemistry*, 125, 143–189. <https://doi.org/10.1016/j.ejmech.2016.09.023>
- Bansal, Y. & Silakari, O. (2012). The therapeutic journey of benzimidazoles: A review. *Bioorganic and Medicinal Chemistry*, 20(21), 6208–6236. <https://doi.org/10.1016/j.bmc.2012.09.013>
- Beč, A., Mioč, M., Bertoša, B., Kos, M., Debogović, P., Kralj, M., Starčević, K. & Hranjec, M. (2022). Design, synthesis, biological evaluation and QSAR analysis of novel N-substituted benzimidazole derived carboxamides. *Journal of enzyme inhibition and medicinal chemistry*, 37, 1327–1339. <https://doi.org/10.1080/14756366.2022.2070910>
- Cindrić, M., Sović, I., Mioč, M., Hok, L., Boček, I., Roškarić, P., Butković, K., Martin-Kleiner, I., Starčević, K., Vianello, R., Kralj, M. & Hranjec, M. (2019). Experimental and Computational Study of the Antioxidative Potential of Novel Nitro and Amino Substituted Benzimidazole/Benzothiazole-2-Carboxamides with Antiproliferative Activity. *Antioxidants*, 8(10), 477. <https://doi.org/10.3390/antiox8100477>

- Časar, Z. (2016). Synthesis of Heterocycles in Contemporary Medicinal Chemistry, In Topics in Heterocyclic Chemistry, 1st Ed., Springer.
- Gill, R. K., Rawal, R. K. & Bariwal, J. (2015). Recent Advances in the Chemistry and Biology of Benzothiazoles. *Arch Pharm Chemistry In Life Sciences*, 348, 1–24. <https://doi.org/10.1002/ardp.201400340>
- Hranjec, M., Kralj, M., Piantanida, I., Sedić, M., Šuman, L., Pavelić, K. & Karminski-Zamola, G. (2007). Novel cyano- and amidino-substituted derivatives of styryl-2-benzimidazoles and benzimidazo[1,2-*a*]quinolines: Synthesis, photochemical synthesis, DNA binding and antitumor evaluation. Part 3. *Journal of Medicinal Chemistry*, 50, 5696–5711. <https://doi.org/10.1021/jm070876h>
- Hranjec, M., Piantanida, I., Kralj, M., Šuman, L., Pavelić, K. & Karminski-Zamola, G. (2008). Novel amidino-substituted thienyl- and furyl-vinyl-benzimidazole derivatives and their photochemical conversion into corresponding diaza-cyclopenta[*c*]fluorenes. Synthesis, interactions with DNA and RNA and antitumor evaluation. Part 4. *Journal of Medicinal Chemistry*, 51, 4899–4910. <https://doi.org/10.1021/jm8000423>
- Keri, R. S., Hiremathad, A., Budagumpi, S. & Nagaraja, B. M. (2015). Comprehensive Review in Current Developments of Benzimidazole-Based Medicinal Chemistry. *Chemical Biology and Drug Design*, 86, 19–65. <https://doi.org/10.1111/cbdd.12462>
- a) Perin, N., Nhili, R., Cindrić, M., Bertoša, B., Vušak, D., Martin-Kleiner, I., Laine, W., Karminski-Zamola, G., Kralj, M., David-Cordonnier, M. H. & Hranjec, M. (2016). Amino substituted benzimidazo[1,2-*a*]quinolines: Antiproliferative potency, 3D QSAR study and DNA binding properties. *European Journal of Medicinal Chemistry*, 122, 530–545. <https://doi.org/10.1016/j.ejmech.2016.07.007>
- b) Perin, N., Bobanović, K., Zlatar, I., Jelić, D., Kelava, V., Koštrun, S., Gabelica Marković, V., Brajša, K. & Hranjec, M. (2017). Antiproliferative activity of amino substituted benzo[*b*]thieno[2,3-*b*]pyrido[1,2-*a*]benzimidazoles explored by 2D and 3D cell culture system. *European Journal of Medicinal Chemistry*, 125, 722–735. <https://doi.org/10.1016/j.ejmech.2016.09.084>
- a) Racané, L., Tralić-Kulenović, V., Kraljević Pavelić, S., Ratkaj, I., Peixoto, P., Nhili, R., Depauw, S., Hildebrand, M. P., David-Cordonnier, M. H., Pavelić, K. & Karminski-Zamola, G. (2010). Novel Diamidino-Substituted Derivatives of Phenyl Benzothiazolyl and Dibenzothiazolyl Furans and Thiophenes: Synthesis, Antiproliferative and DNA Binding Properties. *Journal of Medicinal Chemistry*, 53, 2418–2432. <https://doi.org/10.1021/jm901441b>
- b) Racané, L., Cindrić, M., Zlatar, I., Kezele, T., Milić, A., Brajša, K. & Hranjec, M. (2021). Preclinical in vitro screening of newly synthesised amidino substituted benzimidazoles and benzothiazoles. *Journal of Enzyme Inhibition and Medicinal Chemistry*, 36, 163–74. <https://doi.org/10.1080/14756366.2020.1850711>
- c) Racané, L., Rep, V., Kraljević Pavelić, S., Grbčić, P., Zonjić, I., Radić Stojković, M., Taylor, M. C., Kelly, J. M. & Raić-Malić, S. (2021). Synthesis, antiproliferative and antitrypanosomal activities, and DNA binding of novel 6-amidino-2-arylbenzothiazoles. *Journal of Enzyme Inhibition and Medicinal Chemistry*, 1, 1952–1967. <https://doi.org/10.1080/14756366.2021.1959572>
- d) Racane, L., Ptiček, L., Fajdetić, G., Tralić-Kulenović, V., Klobučar, M., Kraljević Pavelić, S., Perić, M., Čipčić Paljetak, H., Verbanac, D. & Starčević, K. (2020). Green synthesis and biological evaluation of 6-substituted-2-(2-hydroxy/methoxy phenyl)benzothiazole derivatives as potential antioxidant, antibacterial and antitumor agents. *Bioorganic Chemistry*, 95, 103537. <https://doi.org/10.1016/j.bioorg.2019.103537>

- Sharma, P. C., Sinhmar, A., Sharma, A., Rajak, H. & Pathak, D. P. (2013). Medicinal significance of benzothiazole scaffold: an insight view. *Journal of Enzyme Inhibition and Medicinal Chemistry*, 28, 240–266. <https://doi.org/10.3109/14756366.2012.720572>
- Silverman, R. B. (2004). *The Organic Chemistry of Drug Design and Drug Action*, 2nd Ed. San Diego: Elsevier/Academic Press.
- Sović, I., Cindrić, M., Perin, N., Boček, I., Novaković, I., Damjanović, A., Stanojković, T., Zlatović, M., Hranjec, M. & Bertoša, B. (2019). Biological potential of novel methoxy and hydroxy substituted heteroaromatic amides designed as promising antioxidative agents: Synthesis, 3D-QSAR analysis and biological activity. *Chemical Research in Toxicology*, 32, 1880–1892. <https://doi.org/10.1021/acs.chemrestox.9b00256>
- Tariq, S., Kamboj, P. & Amir, M. (2019). Therapeutic advancement of benzothiazole derivatives in the last decennial period. *Arch Pharm Chemistry In Life Sciences*, 352, e1800170. <https://doi.org/10.1002/ardp.201800170>
- Tireli, M., Starčević, K., Martinović, T., Kraljević Pavelić, S., Karminski-Zamola, G. & Hranjec, M. (2016). Antioxidative and antiproliferative activities of novel pyrido[1,2-a]benzimidazoles. *Molecular Diversity*, 21, 201–210. <https://doi.org/10.1007/s11030-016-9702-y>
- Yadav, G. & Ganguly, S. (2015). Structure activity relationship (SAR) study of benzimidazole scaffold for different biological activities: A mini-review. *European Journal of Medicinal Chemistry*, 97, 419–443. <https://doi.org/10.1016/j.ejmech.2014.11.053>

Original scientific article

PHOTOLYSIS OF NADOLOL IN THE AQUATIC ENVIRONMENT: INSIGHTS INTO THE EFFECT OF BICARBONATES

Andrijana Vukojević^{1,2}, Maria M. Savanović^{1,2}, Stevan Armaković^{2,3}, Svetlana Pelemiš⁴, Sanja J. Armaković^{1,2}

¹Faculty of Sciences, Department of Chemistry, Biochemistry and Environmental Protection, University of Novi Sad, Trg D. Obradovića 3, Novi Sad 21000, Serbia

²Association for the International Development of Academic and Scientific Collaboration (AIDASCO), 21000 Novi Sad, Serbia

³Faculty of Sciences, Department of Physics, University of Novi Sad, Trg D. Obradovića 4, Novi Sad 21000, Serbia

⁴University of East Sarajevo, Faculty of Technology Zvornik, Karakaj bb, 75400 Zvornik, Republic of Srpska, Bosnia and Herzegovina

Abstract

Pharmaceuticals such as β -blockers have been widely recognized as a continuous threat to the environment. These compounds are discharged into the aquatic environment, while the traditional wastewater treatment plants cannot perform their efficient removal. Nadolol, a representative of the β -blockers family, has been detected in the treated wastewater at a concentration of 20 ± 0.5 ng/dm³. Although nadolol is helpful for humans, it shows a certain level of toxicity to aquatic organisms. Since bicarbonates are present in natural waters, observing their influence on the stability of pharmaceuticals detected in natural waters is essential. Therefore, nadolol has been subjected to photolytic degradation in the presence/absence of bicarbonates under different types of irradiation (simulated solar (SS), UV-LED, and UV irradiation). Due to bicarbonates in water, it is essential to discover their effect on the photolytic stability of nadolol in water. In the presence of 3 mmol/dm³ bicarbonate, the efficiency of direct photolysis is decreased under UV and UV-LED irradiation. In contrast, under SS irradiation presence of bicarbonates showed a slightly positive effect on nadolol degradation. Bicarbonates are a known radical scavenger, which explains their tendency to lower the degradation efficiency of nadolol under irradiation, where most radicals are formed.

Keywords: β -blockers, Stability, Water purification, UV, UV-LED, Simulated solar irradiation.

Introduction

Expeditious industrialization and urbanization have raised water demands and increased water pollution. A serious problem of this century is the continuous discharge of wastewater that has not been effectively purified into the environment. Therefore, steps for the remediation of contaminated water should be prioritized (Gupta et al., 2020). Pharmaceuticals have a substantial share of various pollutants discharged into the aquatic environment. Pharmaceuticals are already known to negatively affect aquatic organisms in terms of mutagenicity, while the impact on humans is still uncertain (Ratpukdi, 2014). Reusing treated wastewater, an often suggested method to achieve sustainable water cycle management, is also endangered by the presence of micropollutants. Urban and domestic wastewaters that reach sewage treatment facilities contain increasing amounts of pharmaceuticals, whether or not they have been metabolized. Many of these chemicals get beyond typical activated sludge wastewater treatment processes, reaching surface water streams and distributing them throughout the environment (Rosal et al., 2010).

For each pollutant in general, abiotic and biotic processes in surface waters define their fate. Abiotic transformations of any contaminant, including pharmaceuticals in surface waters, include hydrolysis and photolysis. Since pharmaceuticals are often designed for oral consumption and are typically resistant to hydrolysis, direct and indirect photolysis is thought to be the main pathway for their abiotic transformation in surface waters. Indirect photolysis involves natural photosensitizers, whereas direct photolysis of chemical compounds is generated by direct radiation absorption. When exposed to radiation, naturally occurring water components can either increase the photodegradation rate by generating strong oxidant species, including hydroxyl radicals and singlet oxygen, or decrease by radical scavenging (Andreozzi et al., 2003). Radiation wavelength and light intensity are other factors that significantly impact the rate of photodegradation for any specific pharmaceutical found in surface waters (Carlson et al., 2015).

Bicarbonates HCO_3^- , as inorganic salts, are present in various environmental waters, ranging from 0.4 to 4.0 mmol/dm^3 . Depending on the photolysis conditions, HCO_3^- can either promote photodegradation by producing reactive species ($\text{HCO}_3^{\bullet}/\text{CO}_3^{\bullet-}$) or inhibit photodegradation by reacting with radicals in water (Kang et al., 2018). The carbonate radical has a relatively high oxidation potential ($E_0 = 1.78 \text{ V}$, pH 7), but this radical is selective transient species that react with some organic compounds. Because of the high selectivity, photodegradation efficiency depends mainly on the type of organic compound (Orellana-García et al., 2015).

β -blockers are often prescribed pharmaceuticals extensively used to treat heart dysfunction and hypertension. These medications and their metabolites are considerably discharged into municipal, hospital, and industrial wastewaters. β -blockers are regarded as "pseudo persistent" substances because of their reported aqueous phase half-lives of 3.0 – 8.7 days. Even at low doses, β -blockers are toxic to aquatic organisms like fish, algae, and invertebrates (Xu et al., 2019). Nadolol, a representative of the β -blockers family, has been detected in the treated wastewater at a concentration of approximately 20 ng/dm^3 (Gabet-Giraud et al., 2010).

Due to bicarbonates in water, it is essential to discover their effect on the photolytic stability of nadolol in water. Therefore, the efficiency of direct photolysis in 3 mmol/dm^3 bicarbonate under UV, UV-LED, and SS irradiation were investigated. The degradation kinetics of nadolol was monitored by HPLC–PDA technique. Also, the change in pH during the photolysis under different irradiation was observed using a pH meter.

Materials and Methods

Nadolol ($\text{C}_{17}\text{H}_{27}\text{NO}_4$, $M_r = 309.4$, $\geq 99\%$ purity, Sigma–Aldrich) and sodium bicarbonate (NaHCO_3 , $M_r = 84.01$, $\geq 99\%$ purity, Kemika, Zagreb) were used without additional purification. The standard solutions of nadolol (0.05 mmol/dm^3) were made using ultrapure water (UPW, pH = 6.56, $\kappa = 0.055 \text{ }\mu\text{S/cm}$). The solutions were stored in the dark at a temperature of 4 °C. Acetonitrile (ACN, $\text{C}_3\text{H}_3\text{NO}$, 99.9% purity, Sigma-Aldrich, pro analysis) and orthophosphoric acid (H_3PO_4 , 85% purity, Lachema, Neratovice, Czech Republic, pro analysis), were used as mobile phase components for liquid chromatography.

A Pyrex glass cell with a plain window on which the light beam was focused (total volume of *ca.* 40 cm^3) was used for photolytic degradation of nadolol. Experiments were performed using 20 cm^3 of 0.05 mmol/dm^3 nadolol containing 3 mmol/dm^3 NaHCO_3 . Before irradiation, the reaction mixture was sonicated for 15 min in the dark to establish adsorption/desorption equilibrium. Also, before irradiation, the reaction mixture was thermostated at 25 °C using a water circulating jacket in a stream of O_2 (3.0 cm^3/min). The solution was stirred using a magnetic stirring bar during all experiments under continuous gas flow. A high-pressure mercury lamp (125 W, Philips, HPL-N, emission bands at 290, 293, 296, 304, 314, 335, and 366 nm, with maximum emission at 366 nm) was used as the

UV radiation source, UV LED Lamp (5W Enjoydeal, China, type: MR16 AC 85-265V/12) was used as an LED radiation source, and halogen lamp (50 W, Philips) was used as SS radiation source.

Aliquots of 0.50 cm³ were taken from the reaction mixture at the beginning of the experiment and at regular time intervals to monitor the kinetics of nadolol removal with High-Performance Liquid Chromatography with Diode Array Detection (HPLC–PDA, Shimadzu) equipped with an Eclipse XDB–C18 column (150 mm × 4.6 mm i.d., particle size 5 μm, 30 °C). The reaction mixture's highest volume variation due to aliquot sampling was *ca.* 10%. A 20 μL sample was injected and analyzed using the HPLC–PDA. The UV/vis PDA detector was set at 210 nm (suitable nadolol absorption wavelength). The gradient method of analysis was utilized in HPLC–PDA. The mobile phase (flow rate 0.7 cm³/min) was a mixture of ACN and water (0 min 15% ACN, which increased to 25% ACN for 6 min, after which 30% ACN was constant for the next 2 min; post time 1 min), the water is acidified with 0.1% H₃PO₄. The retention time for NAD was 5.8 ± 0.1 min. The reproducibility of repeated runs was around 3–10%.

For measuring the pH during the degradation, a combined glass electrode (pH-Electrode SenTix 20, WTW) connected to the pH meter was used (pH/Cond 340i, WTW).

Results and discussion

The impact of the radiation type (SS, UV, and UV-LED radiation) was investigated to assess the effect of various conditions on the efficiency of nadolol degradation. All experiments were under natural pH, *c.a.* 7.0. UV radiation was more effective than SS and UV-LED radiation. After 180 minutes of exposure to SS and UV-LED radiation, 3.0% and 11.0% of nadolol were degraded (Figures 1a and 1c). The degradation efficiency was higher when UV irradiation was used, 14.7% of the nadolol was degraded after 180 minutes (Figure 1b). The absorption spectrum of the substance of interest is the main factor determining this process's efficiency. Since nadolol's absorption maximum occurs at 210 nm, the results described were anticipated.

Further, the influence of HCO₃⁻ on degradation efficiency was examined. As seen in Figure 1, in the presence of 3 mmol/dm³ bicarbonate, the efficiency of direct photolysis is decreased under UV and UV-LED irradiation. After 180 min of UV and UV-LED irradiation, 9.2% and 6.5% of nadolol were less degraded (Figures 1b and 1c). In contrast, the presence of investigated anion showed a slightly positive effect on nadolol degradation under SS irradiation. After 180 min, the degradation efficiency of nadolol is higher by 1.5% (Figure 1a). These ions "steal" UV radiation from organic pollutants and act as scavengers of [•]OH presented in water, which explains its tendency to lower the degradation efficiency of nadolol under UV and UV-LED irradiation (Petala et al., 2015). While potentially formed carbonate radicals (reactions 1-3), which are highly selective, do not show affinity towards nadolol and do not increase degradation efficiency.

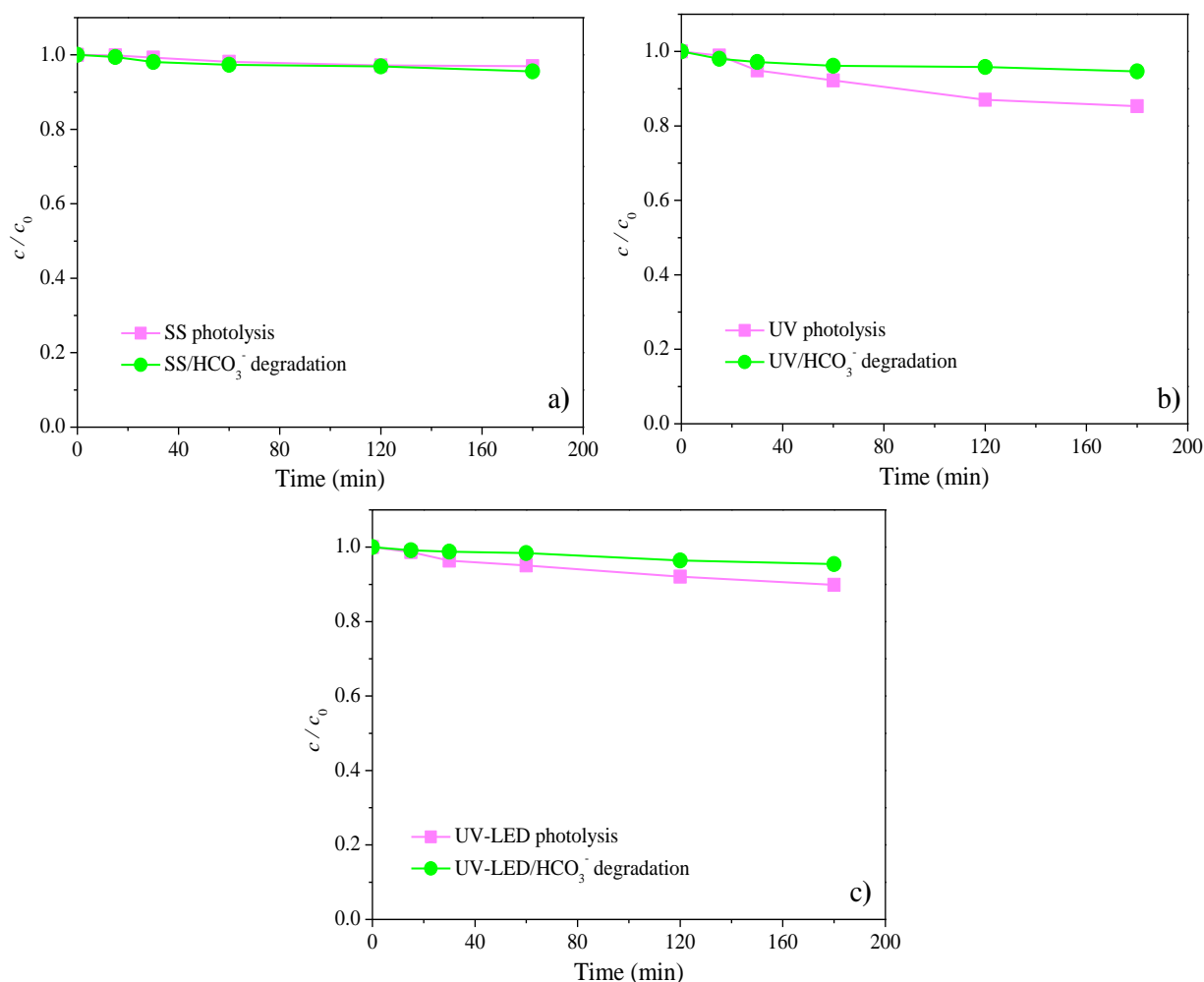


Figure 1. The degradation efficiency of nadolol (0.05 mmol/dm^3) in the presence of bicarbonates under a) SS, b) UV, and c) UV-LED irradiation



The pH change was monitored throughout each experiment (Figure 2). As shown in Figure 2b, during direct photolysis, the pH value increases slightly from 8.2 to 9.1 under SS irradiation, from 8.1 to 8.8 under UV irradiation, and from 8.2 to 9.2 under UV-LED irradiation during 180 min. The similar pH change with the application of SS, UV, and UV-LED irradiation implies the formation of similar intermediates. In the case of photolytic degradation of nadolol with bicarbonates, the pH value increases slightly from 8.9 to 9.9 under SS irradiation, from 8.9 to 9.7 under UV irradiation, and from 9.1 to 9.7 under UV-LED irradiation after 180 min (Figure 2a). In the absence and the presence of bicarbonate, an increase in pH value was observed, indicating the formation of more alkaline intermediates.

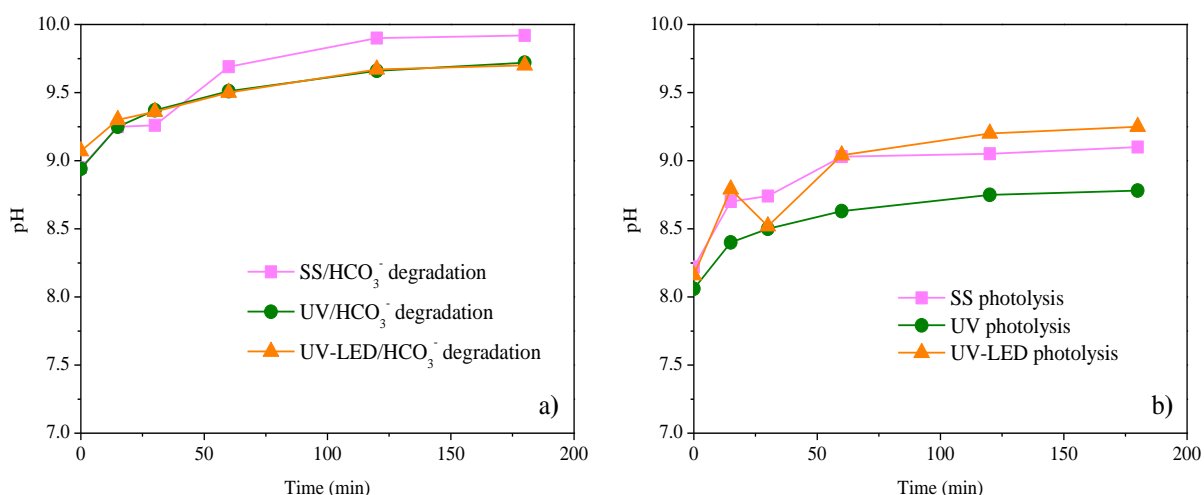


Figure 2. Change of pH during the photolytic degradation of nadolol under SS, UV, and UV-LED irradiation in the a) presence and b) absence of bicarbonates

Conclusion

Human society strives for constant development in which a clean natural environment plays an important role. The population's physical health and socioeconomic development depend on clean and safe water availability. Quality natural water is a global problem that has grown significantly due to increasing urbanization, industrialization, and intense agricultural activity. For this reason, research in removing pollutants from water and understanding the factors influencing their fate in water is of great importance. Pharmaceuticals are one of those polluting materials to which special attention must be paid because they are very stable and harmful to the living world.

This work studied the influence of bicarbonates on the photolytic degradation of nadolol water solution under different types of radiation (SS, UV, and UV-LED radiation). The degradation kinetics were monitored using high-performance liquid chromatography, and the pH change was observed using a pH meter. First, the photolytic degradation of nadolol using different types of radiation was investigated, where UV radiation showed to be the most efficient, wherein 14.7% of nadolol was degraded after 180 min of irradiation. Further, the kinetics of photolytic degradation in the presence of bicarbonates under different types of irradiation was monitored. The results showed that bicarbonates decrease removal efficiency under UV and UV-LED irradiation. Only 5.5% and 4.5% of nadolol were degraded after 180 min, respectively. Only in the presence of SS radiation is a slight increase in the degradation efficiency of nadolol by 1.5% after 180 min. In the photolytic degradation of nadolol, the potential bicarbonate radicals are not selective for nadolol. Moreover, bicarbonate anions absorb part of UV radiation, which explains the decrease in degradation efficiency of nadolol.

References

- Andreozzi, R., Marotta, R. & Paxéus, N. (2003). Pharmaceuticals in STP effluents and their solar photodegradation in aquatic environment. *Chemosphere*, 50(10), 1319–1330. [https://doi.org/10.1016/S0045-6535\(02\)00769-5](https://doi.org/10.1016/S0045-6535(02)00769-5)
- Carlson, J. C., Stefan, M. I., Parnis, J. M. & Metcalfe, C. D. (2015). Direct UV photolysis of selected pharmaceuticals, personal care products and endocrine disruptors in aqueous solution. *Water Research*, 84, 350–361. <https://doi.org/10.1016/j.watres.2015.04.013>
- Gabet-Giraud, V., Miège, C., Choubert, J. M., Ruel, S. M. & Coquery, M. (2010). Occurrence and removal of estrogens and beta blockers by various processes in wastewater treatment plants.

- Science of the Total Environment*, 408(19), 4257–4269. <https://doi.org/10.1016/j.scitotenv.2010.05.023>
- Gupta, N. K., Ghaffari, Y., Bae, J. & Kim, K. S. (2020). Synthesis of coral-like α -Fe₂O₃ nanoparticles for dye degradation at neutral pH. *Journal of Molecular Liquids*, 301, 1–9. <https://doi.org/10.1016/j.molliq.2020.112473>
- Kang, Y. M., Kim, M. K. & Zoh, K. D. (2018). Effect of nitrate, carbonate/bicarbonate, humic acid, and H₂O₂ on the kinetics and degradation mechanism of Bisphenol-A during UV photolysis. *Chemosphere*, 204, 148–155. <https://doi.org/10.1016/j.chemosphere.2018.04.015>
- Orellana-García, F., Álvarez, M. A., López-Ramón, M. V., Rivera-Utrilla, J. & Sánchez-Polo, M. (2015). Effect of HO[•], SO₄^{•-} and CO₃^{•-}/HCO₃^{•-} radicals on the photodegradation of the herbicide amitrole by UV radiation in aqueous solution. *Chemical Engineering Journal*, 267, 182–190. <https://doi.org/10.1016/j.cej.2015.01.019>
- Petala, A., Frontistis, Z., Antonopoulou, M., Konstantinou, I., Kondarides, D. I. & Mantzavinos, D. (2015). Kinetics of ethyl paraben degradation by simulated solar radiation in the presence of N-doped TiO₂ catalysts. *Water Research*, 81, 157–166. <https://doi.org/10.1016/j.watres.2015.05.056>
- Ratpukdi, T. (2014). Degradation of Paracetamol and Norfloxacin in Aqueous Solution Using Vacuum Ultraviolet (VUV) Process. *Journal of Clean Energy Technologies*, March, 168–170. <https://doi.org/10.7763/jocet.2014.v2.115>
- Rosal, R., Rodríguez, A., Perdigón-Melón, J. A., Petre, A., García-Calvo, E., Gómez, M. J., Agüera, A. & Fernández-Alba, A. R. (2010). Occurrence of emerging pollutants in urban wastewater and their removal through biological treatment followed by ozonation. *Water Research*, 44(2), 578–588. <https://doi.org/10.1016/j.watres.2009.07.004>
- Xu, J., Sun, H., Zhang, Y. & Alder, A. C. (2019). Occurrence and enantiomer profiles of β -blockers in wastewater and a receiving water body and adjacent soil in Tianjin, China. *Science of the Total Environment*, 650, 1122–1130. <https://doi.org/10.1016/j.scitotenv.2018.09.086>

Original scientific article

CAN E-CIGARETTES BE A THREAT TO ENVIRONMENT: HEAVY METALS ANALYSIS IN E-CIGARETTES FILTERS

Dijana Mihajlović¹, Nemanja Lončar², Ana Đurić², Bojana Đekanović², Dijana Jelić²

¹University of Banja Luka, Faculty of Agriculture, Banja Luka, Bosnia and Herzegovina

²student of 1st cycle study of the University of Banja Luka, Faculty of Natural Science and Mathematics, Banja Luka, Bosnia and Herzegovina

²University of Banja Luka, Faculty of Natural Science and Mathematics, Chemistry Department, Banja Luka, Bosnia and Herzegovina

Abstract

Electronic cigarettes (EC) proved to be very popular way of consuming nicotine, especially due to opinion that EC present a safer alternative to conventional tobacco products. There are many forms of EC in the market with different refills. In presented research, e-cigarettes filters were in the focus. The idea was to evaluate heavy metals content in used and unused e-cigarettes filters. Special attention was on environmental issue, since e-cigarettes filters (with potential heavy metals presence) could contribute to the environmental damage and threat, due to accumulation. Four heavy metals, namely Cr, Cd, Pb and Mn were quantified in the filters of the most popular e-cigarettes found in the market of Bosnia and Herzegovina. Determination of metal concentrations was done by method of atomic absorption spectrophotometry in the extracts obtained after the acid digestion of filters with concentrated nitric acid and hydrogen peroxide. The results of used e-cigarettes mean \pm standard deviation concentrations in the filters were as follows: 0.16 ± 0.05 mg Cd/kg, 4.61 ± 1.81 mg Pb/kg, 32.02 ± 5.31 mg Mn/kg and 2.59 ± 1.23 mg Cr/kg. On the other hand, heavy metal concentrations in the unused filters were significantly lower and amounted to 0.07 ± 0.00 mg Cd/kg, 0.035 ± 0.04 mg Pb/kg, 10.43 ± 0.14 mg Mn/kg and 0.98 ± 0.30 mg Cr/kg. Determined metal contents in the filters of smoked and unsmoked cigarettes were at similar levels to those found in the studies done worldwide. In order to obtain more detailed overview of the impact of these products on human health and the environment, it is necessary to continue with similar researches.

Keywords: tobacco products, heavy metals, electronic cigarettes.

Introduction

Among the diverse range of tobacco products available in the market worldwide, electronic cigarettes (EC) have become increasingly popular in many countries, including ours, especially in the last decade of the 21st century. Due to the serious health concerns of conventional tobacco products (Talhout, 2011; Drope & Schluger, 2018), there is an evident tendency for safer alternatives such as e-cigarettes (Gentzke, 2022). According to the U.S. Department of Health and Human Services (2016), e-cigarettes are especially popular among young and youth adults, and non-smokers in the United States. The main reasons for the popularity of e-cigarettes are probably successful marketing campaigns and their promotion as a healthier way of consuming nicotine.

On the other hand, some studies have shown that e-cigarettes are a source of exposure to toxic metals, including elements with known carcinogenic properties such as Pb, As, Cd, Ni, etc. (Goniewicz et al., 2014; Williams et al., 2013; Farsalinos et al., 2015). Williams and authors (2013) found the concentrations of nine heavy metals (Ni, Cr, Zn, etc.) in e-cigarette aerosol to be higher than or equal

to the concentrations smoke of conventional cigarettes. Similar results were found in another study done by the quantification of heavy metals in the liquids of the five most popular e-cigarette brands in the United States (Hess et al., 2017). In addition to increased amounts of Ni, Cr, Mn, and Pb found in the liquids of analyzed e-cigarettes, Hess et al. (2017) found significant differences between metal concentrations in the cigarettes of different brands.

Furthermore, there is a need to determine heavy metals in the filters of smoked cigarettes (butts). Cigarette butts are among the most common forms of litter in urban areas, accounting for between 22 and 46% of visible litter (Roder Green et al., 2014). They are also the second most found item of litter on beaches in the European Union (Kideys & Aydin, 2020) and the single most collected litter in the coastal environment in the last decade (Ocean Conservancy, 2021). Therefore, this type of litter represents a serious ecological problem not only due to possible accumulation in the environment but especially due to the presence of various pollutants: heavy metals (Moerman & Potts, 2011; Koutela et al., 2020), polycyclic aromatic hydrocarbons (Dobaradaran et al., 2019), nicotine (Roder Green et al., 2014), radionucleotides (Desideri et al., 2019), etc.

Considering that the consumption of e-cigarettes has become popular and that, according to our knowledge, no similar research has been done in Bosnia and Herzegovina (B&H) recently, we conducted our research as a preliminary step in assessing the quality control of e-cigarettes and heated tobacco products, consumed in our country, on potential health and environmental protection. During research, using the method of atomic absorption spectrophotometry after the acid digestion of analyzed samples, we determined the contents of four heavy metals: Cr, Cd, Pb, and Mn in the filters of cigarettes that are the most often smoked in e-cigarettes.

Materials and Methods

In April 2022, 15 e-cigarette filter samples were collected. These cigarettes belong to the Heets brand, produced by Philip Morris International, which was one of the most popular brands of cigars (also known as "heated tobacco sticks"), used for smoking in e-cigarettes and heated tobacco devices in our country. The sampled varieties of the Heets brand were: Blue Selection (8 samples), Siena Label (4), Purple Label (1), and Creation (1). All collected cigarettes were not more than 6 months old from the day of production, and in the case of smoked cigarettes, no more than 2 days old from the day of consumption. Two of the filters were sampled from the unused (unsmoked) cigarettes and 13 others from smoked cigarettes (Table 1).

The sampled filters were first manually separated from the cigarettes, gently chopped, and then dried in an air dryer at 60 °C. After drying, the filters were weighed on an analytical balance (cca. 1.0000 g) and transferred into glass beakers of 100 mL, where 10 mL of concentrated HNO₃ was added. The contents of beakers were heated and slowly boiled on a hot plate for 1,5 hours at 150 °C. After cooling, 3 mL of 30% hydrogen peroxide (H₂O₂) was added twice to the contents of beakers. The digested cooled samples were transferred to a 50 mL volumetric flask and diluted with distilled water. Afterwards, the solutions were filtered through acid-washed Whatman No.1 filter paper. The obtained extracts were stored in the laboratory refrigerator at 4 °C until the analysis.

The quantification of the examined heavy metals (Cr, Cd, Pb, and Mn) was done by the method of atomic absorption spectrophotometry (AAAnalyst 400 Perkin Elmer®, USA). Selected wavelengths of determined elements were as follows: Cd 228.80, Cr 357.87, Mn 279.48, and Pb 283.00 nm. Metals were quantified in the air/acetylen flame with an additional deuterium background correction of signal for Cd. Calibration standards included: 0.2, 0.5, 0.7, 0.9 mgCd/L, 1.0, 2.0, 3.0, 4.0 mgCr/L, 0.2, 0.4, 0.8, 1.0 mgMn/L, and 0.5, 1.0, 2.0, 4.0, 8.0 mgPb/L. Standard solutions were prepared by diluting a single element stock solution for AAS (1000 mg/l, Perkin Elmer, USA) with 2% HNO₃. The calibration equations for all elements were linear through zero, with a correlation coefficient higher than 0.995 prior to analysis. The measurement procedure also included the analysis of one calibration

blank and one calibration standard after each group of 10 extracts as a calibration check. All glassware and plastic material used during the analyses were immersed in 10% HNO₃ for 12 hours and later rinsed with deionized water to prevent any external contamination.

Results and discussion

The results of analysis (Table 1) showed that the content of all determined metals in the filters of unused (unsmoked) cigarettes was lower than in used (smoked) cigarettes, except for Cd, whose content was the same in the filters of used cigarettes (0.07 mg/kg) and in the two samples of unsmoked cigarettes (samples F1 and F2, Table 1).

Table 1. Determined concentrations of heavy metals (mg/kg) in analyzed filters of e-cigarettes

Sample mark	Brand	Character	Cd (mg/kg)	Cr (mg/kg)	Mn (mg/kg)	Pb (mg/kg)
F1	Heets Sienna Label	unused	0.07	0.68	10.29	0.00
F2	Heets Sienna Label	unused	0.07	1.27	10.57	0.07
F3	Heets Sienna Label	used	0.17	2.02	31.67	2.67
F4	Heets Sienna Label	used	0.13	1.32	24.47	0.57
F5	Heets Silver Select.	used	0.22	5.54	33.49	6.56
F6	Heets Creations	used	0.15	1.48	28.62	4.14
F7	Heets Blue Selection	used	0.14	2.11	30.74	5.26
F8	Heets Blue Selection	used	0.22	2.33	31.30	4.64
F9	Heets Blue Selection	used	0.15	3.83	45.62	2.82
F10	Heets Blue Selection	used	0.15	2.04	38.22	6.59
F11	Heets Blue Selection	used	0.15	2.56	33.06	5.66
F12	Heets Blue Selection	used	0.21	2.31	30.67	5.02
F13	Heets Blue Selection	used	0.22	2.24	32.88	5.58
F14	Heets Blue Selection	used	0.07	1.58	26.62	3.70
F15	Heets Purple Label	used	0.07	4.34	28.94	6.77

Furthermore, the content of metals in the analyzed used cigarette filters decreased in the following order: Mn>Pb>Cr>Cd (Figure 1, Table 1). A similar sequence of metal concentrations was found in the unused cigarettes (Mn>Cr>Pb>Cd), with the exception of Pb and Cr. A higher amount of Pb compared to Cr was detected in the filters of the used cigarettes, while in unused filters the order of their content was the opposite.

In the study conducted in Greece (Koutela et al., 2020), the contents of eleven heavy metals, among them Pb, Cr, and Cd, were analyzed in the two brands of e-cigarette filters. For these three elements, the researchers found the same decreasing order of concentrations in the filters of used and unused cigarettes: Cr>Pb>Cd, which is the same order of determined concentrations found in the unused cigarettes in our work. Also, Koutela et al. (2020) found slightly lower concentrations of Cr and Pb in used than in unused filters, while the concentrations of Cd were under the limit of detection in both groups of samples. In addition, they quantified the content of metals in the filters of conventional cigarettes and found the same order of their presence as in the filters of e-cigarettes. Also, a slightly lower content of Pb, Cr, and Cr was determined in conventional cigarette filters compared to those belonging to e-cigarettes.

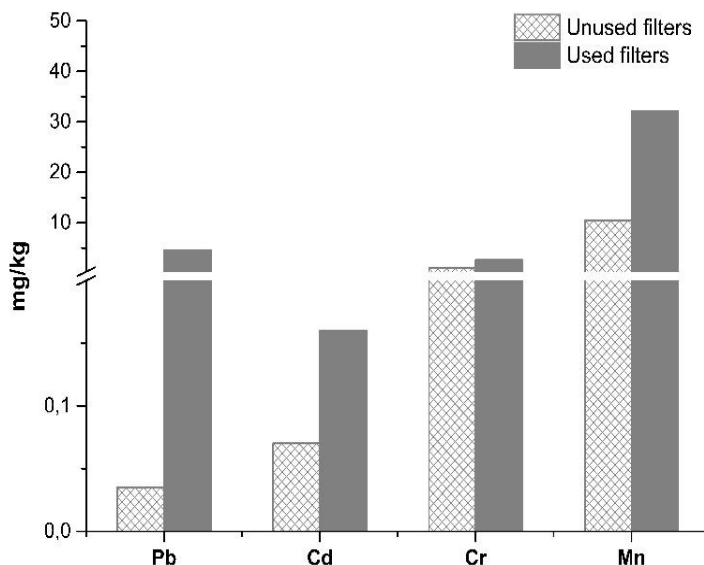


Figure 1. Determined average concentrations of heavy metals in the filters of e-cigarettes

Moreover, in the analysed filter samples, we found significantly higher concentrations of Pb in the used filters (4.61 ± 1.81 mg Pb/kg) compared to the unused filters (0.035 ± 0.04 mg Pb/kg). During the study of conventional cigarettes, Michael et al. (2022) determined significantly higher content of Cd and Pb in the butts of smoked cigars than in the butts of unsmoked cigars, as well as in the parts of cigarettes filled with tobacco. Furthermore, in a study conducted in Canada, Shaller et al. (2016) analyzed the composition of aerosols produced after smoking heated tobacco sticks and determined that the content of examined toxic metals (Hg, As, Pb, Cd) were within the levels allowed by Canadian regulations. Besides, they found that among the examined metals, Pb was the most abundant in the aerosols.

Conclusion

Electronic cigarettes (EC) and other alternative ways of consuming nicotine have become increasingly popular in the 21st century worldwide, but the facts about their health and environmental influence have not been thoroughly and sufficiently investigated. Also, the permitted levels of pollutants in these products are not defined by legislation in a large number of countries, as well as in B&H. This paper presents the results of preliminary research conducted with the aim of assessing the content of e-cigarettes, present in the markets in our country, and also potential risk on the environment and human health by quantifying four heavy metals: Pb, Cd, Cr, and Mn in the filters of cigarettes used for smoking in e-cigarettes and heated tobacco devices. The determined contents of metals in the filters of used e-cigarettes were as follows: 0.16 ± 0.05 mg Cd/kg, 4.61 ± 1.81 mg Pb/kg, 32.02 ± 5.31 mg Mn/kg and 2.59 ± 1.23 mg Cr/kg. On the other hand, heavy metal concentrations in the unused filters were significantly lower and amounted to 0.07 ± 0.00 mg Cd/kg, 0.035 ± 0.04 mg Pb/kg, 10.43 ± 0.14 mg Mn/kg and 0.98 ± 0.30 mg Cr/kg. By comparing our results with some studies done on similar products around the world, we could conclude that the determined metal contents in the order of their presence in the filters of smoked and unsmoked cigarettes were at similar levels to those found by other authors, even if they used different methodologies of sampling and quantification of heavy metals. In order to obtain a clearer and more detailed overview of the impact of these products on human health and the environment, it is necessary to continue with provision of similar research projects.

References

- Desideri, D., Meli, M. A. & Roselli, C. (2019). Leaching tests to assess the release of ²¹⁰Po from discarded cigarette butts. *Microchemical Journal*, *145*, 42–46. <https://doi.org/10.1016/j.microc.2018.10.008>
- Dobaradaran, S., Schmidt, T. C., Lorenzo-Parodi, N., Jochmann, M. A., Nabipour, I., Raeisi, A., Stojanović, N. & Mahmoodi, M. (2019). Cigarette butts: an overlooked source of PAHs in the environment? *Environmental Pollution*, *249*, 932–939. <https://doi.org/10.1016/j.envpol.2019.03.097>
- Drope, J. & Schluger, N. W. (2018). *The tobacco atlas*. American Cancer Society.
- European Commission (2019). Directive (EU) 2019/904 of the European Parliament and the Council on the reduction of the impact of certain plastic products on the environment. OJ L 155, 1–19.
- Farsalinos, K. E., Voudris, V. & Poulas, K. (2015). Are metals emitted from electronic cigarettes a reason for health concern? A risk-assessment analysis of currently available literature. *International Journal of Environmental Research and Public Health*, *12*(5), 5215–5232. doi:10.3390/ijerph120505215
- Gentzke, A. S., Wang T. W., Cornelius, M., Park-Lee, E., Ren, C., Sawdey, M. D., Cullen, K. A., Loretan, C., Jamal, A. & Homa, D. M. (2022). *Morbidity and Mortality Weekly Report*, *71*(No. SS-5), 1–29. <https://www.cdc.gov/mmwr/71/ss/ss7105a1.htm>
- Goniewicz, M. L., Knysak, J., Gawron, M., Kosmider, L., Sobczak, A., Kurek, J., Prokopowicz, A., Jablonska-Czapla, M., Rosik-Dulewska, C., Havel, C., Jacob, P. & Benowitz, N. (2014). Levels of selected carcinogens and toxicants in vapour from electronic cigarettes. *Tobacco Control*, *23*(2), 133–139. doi:10.1136/tobaccocontrol-2012-050850859
- Hess, C. A., Olmedo, P., Navas-Acien, A., Goessler, W., Cohen, J. E. & Rule, A. M. (2017). E-cigarettes as a source of toxic and potentially cancerogenic metals. *Environmental Research*, *152*, 221–225. <http://dx.doi.org/10.1016/j.envres.2016.09.026>
- Kideys, A. E. & Aydin, M. (2020). Marine Litter Watch (MLW) European Beach Litter Assessment 2013-2019. ETC/ICM Technical Report 2/2020, 26 pp.
- Koutela, N., Fernandez, E., Saru, M. & Psillakis, E. (2020). A comprehensive study on the leaching of metals from heated tobacco stick and cigarettes in water and natural waters. *Science of the Total Environment*, *714*, 136700. <https://doi.org/10.1016/j.scitotenv.2020.136700>
- Michael, M., Meyyazhagan, A., Velayudhannair, K., Pappuswamy, M., Maria, A., Xavier, V., Balasubramaniam, B., Baskaran, R., Kamyab, H., Vasseghian, Y., Chelliapan, S., Safa, M., Moradi, Z. & Khadimallah, M. A. (2022). The content of heavy metals in cigarettes and the impact of their leachates on the aquatic ecosystem. *Sustainability*, *14*, 4752. <https://doi.org/10.3390/su14084752>
- Moerman, J. W. & Potts, G. E. (2011). Analysis of metals leached from smoked cigarette litter. *Tobacco Control*, *20*, i30–i35. <https://doi.org/10.1136/tc.2010.040196>
- Ocean Conservancy (International Coastal Cleanup) /<https://oceanconservancy.org/trash-free-seas/international-coastal-cleanup/annual-data-release/accesed> on 01.07.2022.
- Roder Green, A. L., Putschew, A. & Nehls, T., (2014). Littered cigarette butts as a source of nicotine in urban waters. *Journal of Hydrology*, *519*, 3466–3474. <https://doi.org/10.1016/j.jhydrol.2014.05.046>.
- Shaller, J., Keller, D., Poget, L., Pratte, P., Kaelin, E., McHugh, D., Cudazzo, G., Smart, D., Tricker, A. R., Gautier, L., Yerly, M., Piers, R. R., Le Bouhellec, S., Ghosh, D., Hofer, I., Gracia, E., Vanscheeuwijck, P. & Maeder, S. (2016). Evaluation of the tobacco heating system 2.2. Part 2: Chemical composition, genotoxicity, cytotoxicity, and physical properties of the aerosol,

Regulatory toxicology and Pharmacology, 81, S27–S47.
<http://dx.doi.org/10.1016/j.yrtph.2016.10.001>

Talhout, R., Schulz, T., Florek, E., Van Benthem, J., Wester, P. & Opperhuizen, A. (2011). Hazardous compounds in tobacco smoke. *International Journal of Environmental Research and Public Health*, 8, 613–628. <https://doi.org/10.3390/ijerph8020613>

U.S. Department of Health and Human Services (2016). E-cigarette use among youth and young adults: A report of the surgeon general. Atlanta: U.S. Department of Health and Human Services, Centers for Disease Control and Prevention, National Center for Chronic Disease Prevention and Health Promotion, Office on Smoking and Health.

Williams. M., Villarreal, A., Bozhilov, K., Lin, S. & Talbot, P. (2013). Metal and silicate particles including nanoparticles are present in electronic cigarette cartomizer fluid and aerosol. *PloS One*, 8(3), e57987. <https://doi.org/10.1371/journal.pone.0057987>

Original scientific article

COMPARISON OF THREE EXTRACTION PROCEDURES FOR QUANTIFICATION OF Cu, Mn, Ni, Pb AND Zn IN THE PLANTS

Dijana Mihajlović¹, Vesna Antunović²

¹University of Banja Luka, Faculty of Agriculture, Banja Luka, B&H

²University of Banja Luka, Faculty of Medicine, Banja Luka, B&H

Abstract

During this research, the content of five potentially toxic elements (Cu, Mn, Ni, Pb and Zn) was determined in different plant material by atomic absorption spectrophotometry after three methods of acid digestion: 1. HNO₃+H₂O₂+HClO₄ (10:3:1), 2. aqua regia+H₂O₂ (5:1), 3. HNO₃+H₂SO₄+HClO₄ (5:1:1). Analyzed plant samples were hay and quinoa shoots, vine tree and pear and apple leaves. Additional quality control was done with certified reference sample of the rye grass ERM[®]-CD281. Obtained results showed that the most effective extraction procedure for quantification of Cu, Mn, Ni and Pb in the examined plant samples was acid digestion with mixture of aqua regia and 30% H₂O₂. On the other hand, digestion with concentrated nitric acid followed by addition of hydrogen peroxide and perchloric acid was the most efficient procedure in the case of the Zn contents determination.

Keywords: potentially toxic elements, acid digestion, plant material.

Introduction

Potentially toxic elements (PTEs) are found naturally in the environment but also due to the various anthropological sources: industry, urbanization, traffic etc. (Bradl, 2005; Hooda, 2010). Quantification of PTEs in plants is important as an indicator of environmental pollution, and in the case of edible and medical plants for assessing their impact on human health due to the possible serious damages caused by their elevated content, especially pronounced for some toxic elements (Hg, As, Pb, Cd), and/or by lack of essential microelements necessary for the normal functioning of living cells (Cu, Zn, Ni etc.). Therefore, plant analyses are important for diagnosing of mineral nutrition defects and solving practical field problems (Kabata-Pendias, 2011).

According to the literature (Campbell & Plank, 1998; Beneton 2001; Uddin et al., 2016), a large number of wet acid digestions have been used to extract PTEs from plant tissues. During these procedures, the samples were destroyed and solubilized due to aggressive reagents and heating. Wet digestion is also accompanied by the mineralization of organic matter in the aqueous phase due to the addition of oxidizing reagents (hydrogen peroxide or concentrated acids). However, sometimes it was impossible to completely end the decomposition of organic matter. In these cases, undegraded organic compounds partially remained in the extraction solution and interfered with further assay (Sleimi et al., 2022). Hence, the selection of a suitable digestion procedure is important for the quantification of PTEs.

Sampling is the first step done before the chemical analysis, which has to be planned and provided properly. Variables which significantly affect the final results and their interpretation are plant species, age, plant part, minimum number of the plants to sample and time of sampling (Bell, 2000). Sample preparation is the next important step in the further analytical procedure, which includes

transporting, decontamination (washing or cleaning the plant tissues), drying, particle size reduction, and storage (Campbell & Plank, 1998). According to the same authors, other critical factors in wet digestion procedures besides selection of reagents are: temperature, time, mass of the analysed samples, and final volume of getted extract. Hence, wet digestion procedures generally require analyst supervision and intervention. On the other hand, every analytical technique used for the quantification of PTEs has its own characteristics: accuracy, limit of detection, elemental coverage, single or multielement determination, etc. (Beneton, 2001). Finally, the major influence on the variation of the results in elemental analysis of plants has been the steps in the extraction solutions preparation (Uddin et al., 2016; Sleimi et al., 2022).

Furthermore, the variety of extraction procedures used in environmental research causes difficulties in comparing the obtained results. Considering all that has stated, the aim of this study was to estimate the efficiency of three different extraction procedures by their application to a certified reference standard and six different samples of the plant material. The quantification of the examined elements (Cu, Mn, Ni, Pb, and Zn) was done by the method of atomic absorption spectrofotometry.

Materials and Methods

Our work was focused on the different extraction procedures of potentially toxic elements through wet digestion with different acid mixtures: 1. $\text{HNO}_3+\text{H}_2\text{O}_2+\text{HClO}_4$ (10:3:1), 2. aqua regia+ H_2O_2 (5:1), 3. $\text{HNO}_3+\text{H}_2\text{SO}_4+\text{HClO}_4$ (5:1:1), carried out on sellected plant samples: shoots of hay and quinoa, stem of vine and leaves of pear and apple. Additional quality control was done with certified standard reference material ERM[®] CD281, that is rye grass, provided by the Institute for reference materials and measurements of the European Commision's Joint Research Centre (Geel, Belgium).

One gram of the plant powder, previously dried in an air dryer at 60 °C and milled, was weighted on an analytical balance and transferred into tubes of the heating block (InKjel M, Behr Labor-technik GmbH). Extraction was performed via three acid digestions, which included: 1. addition of 20 mL of concentrated HNO_3 and boiling the content in the tube for 2 hours at 150 °C, and after cooling to room temperature addition of 3 mL 30% H_2O_2 in two consecutive steps, followed by gentle boiling for 15 minutes. Following that, 2 mL of the 70% HClO_4 was added to the cooled solutions, evaporated, transferred to a 100 mL volumetric flask, diluted with deionized water, and filtrated (Perquel et al. 1993); 2. addition of the 25 mL of aqua regia (HNO_3 : HCl =1:3) and 5 mL of 30% H_2O_2 , boiling at 80 °C until a clear solution was obtained. After cooling, the digested samples were diluted to 50 mL with deionized water and filtered (Rodrigues-Flores & Rodrigues-Castellon, 1982); 3. addition of the 15 mL of the $\text{HNO}_3+\text{H}_2\text{SO}_4+\text{HClO}_4$ mixture (5:1:1), digestion at 80 °C until the solution became transparent. The resultant solution was diluted to 50 mL with deionized water and then filtrated (Allen et al., 1986). In all three extraction procedures, filtration was done by using Whatman number 42 filter paper. The obtained solutions were kept at 4 °C until the analysis.

All AAS measurements were carried out using AAnalyst 400 Perkin Elmer[®] (USA). Standard solutions for measurements were prepared using commercial standards for AAS (Perkin Elmer, USA) and an appropriate diluent extractant. The selected wavelenghts of determined elements were as follows: Cu 324.75, Mn 279.48, Ni 232.00, Pb 283.00, and Zn 213.70 nm. The elements were quantified in the air/acetylen flame with additional deuterium background correction of signal for Ni and Zn. All analytical procedures were triplicated and made with glassware and plastic material prewashed with 10% HNO_3 .

Results and discussion

Three extraction methods were first applied to the certified plant material (rye grass, ERM[®] CD281). The certified and experimental results for five potentially toxic elements are given in Table 1. In order

to evaluate the analytical accuracy of applied methods, certified and experimental (measured) values obtained after analyses of the standard reference material were compared, and the percentage of recovery for each metal was calculated as:

$$\% \text{ Recovery} = [\text{experimental values (mg/kg)} / \text{certified values (mg/kg)}] * 100 \% \quad (1)$$

The obtained results (Table 1) for the reference sample, rye grass, ERM[®] CD281, showed that wet digestion with aqua regia and hydrogen peroxide, as well as a mixture of nitric acid, hydrogen peroxide and perchloric acid, provides very good recovery values in the range of 86.93-102.69% for all five elements.

Table 1. Certified and measured concentrations of potentially toxic elements (mean±SD) in the standard reference material ERM[®] CD281

Element (mg/kg)	Certified value (mean±SD)	Extraction reagents	Measured v. (mean±SD)	Recovery (%)
Cu	10.20±0.50	HNO ₃ +H ₂ O ₂ +HClO ₄	8.87±0.35	86.93
		HNO ₃ +HCl	9.33±0.18	91.50
		HNO ₃ +H ₂ SO ₄	8.47±0.14	83.04
Zn	30.50±1.1	HNO ₃ +H ₂ O ₂ +HClO ₄	30.66±0.70	100.52
		HNO ₃ +HCl	31.32±0.52	102.69
		HNO ₃ +H ₂ SO ₄	27.26±0.72	89.38
Ni	15.20±0.6	HNO ₃ +H ₂ O ₂ +HClO ₄	13.70±0.70	90.13
		HNO ₃ +HCl	13.76±0.79	90.53
		HNO ₃ +H ₂ SO ₄	10.70±0.72	70.39
Mn	82±4.00	HNO ₃ +H ₂ O ₂ +HClO ₄	74.97±2.94	91.42
		HNO ₃ +HCl	76.49±3.46	93.28
		HNO ₃ +H ₂ SO ₄	59.28±2.17	72.30
Pb	1.67±0.11	HNO ₃ +H ₂ O ₂ +HClO ₄	1.70±0.02	101.88
		HNO ₃ +HCl	1.66±0.03	99.40
		HNO ₃ +H ₂ SO ₄	1.28±0.02	76.65

Comparable recovery rates were obtained for Zn (100.52%) and Pb (101.88%) using an extraction method with a mixture of nitric acid, hydrogen peroxide and perchloric acid, while the recoveries after the provided wet digestion with aqua regia were 102.69% for Zn and 99.40% for Pb. Tested elements were extracted satisfactorily with mixture of concentrated nitric and sulfuric acid, while the recovery rates (70.39% - 89.38%) were somewhat lower values compared to the other two methods. Determined concentrations of the PTEs in the examined plant samples implied on similar extraction potential of aqua regia and a mixture of nitric acid, hydrogen peroxide and perchloric acid (Figure 1, Table 2). Generally, greater concentrations of all determined elements were obtained after these two extraction procedures compared to digestion with a mixture of nitric and sulfuric acid.

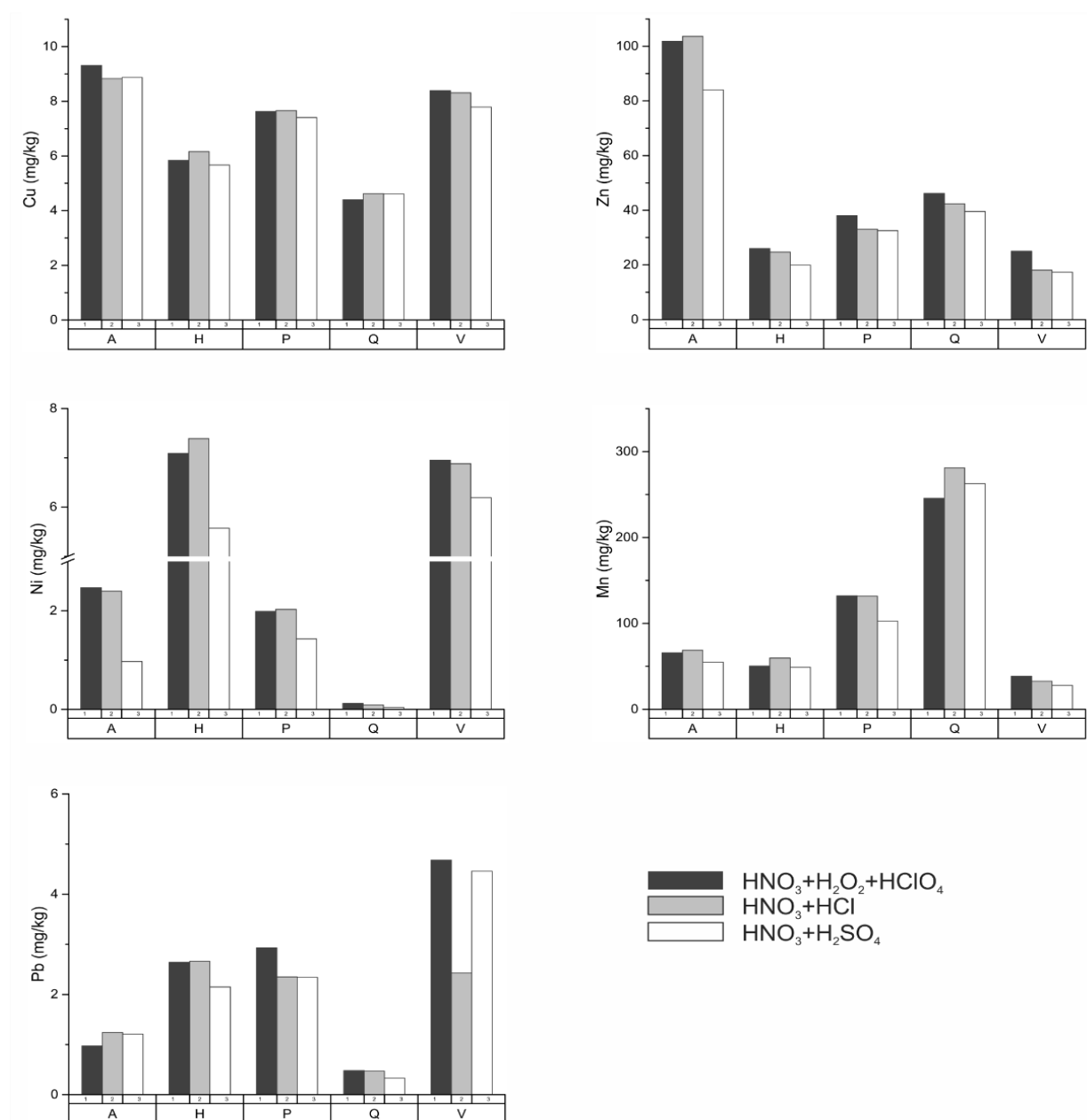


Figure 1. Determined average concentrations of potentially toxic elements in analyzed samples (A, P- leaves of pear and apple, H,Q- shoots of hay and quinoa, and V-steam of vine tree) by three extraction procedures

Aqua regia has been proposed as one of the best acid mixtures used for digestion of samples with low organic matter and/or carbonate contents, such as sediments and soils (Rao et al., 2008). The addition of H₂O₂ in this mixture provides further oxidation of organic matter from the analysed samples, resulting in higher extraction efficiency (Idera et al., 2015). Concentrated HNO₃, as well as mixtures of HNO₃ and HClO₄ or HNO₃ and H₂O₂, were found to be good digestion reagents for extraction of PTEs from plants and other organic samples, with only minor differences in extraction potential (Mokoena et al., 2020; Shaibur et al., 2010). According to Perquel and al. (1993), digestion with all three reagents could provide a higher efficiency and less time of digestion. On the other hand, use of sulfuric acid provides fast and complete oxidation of organic compounds, but it is followed by higher

energy consumption for heating because of the higher boiling point of H₂SO₄ and the presence of insoluble compounds that can interfere during quantification of metals (Hoenig, 2001).

Table 2. Determined concentrations of potentially toxic elements (mean±SD) in analyzed plant samples (A, P- leaves of pear and apple, H,Q- shoots of hay and quinoa and V-steam of vine tree)

Plant sample	Extraction reagents	Cu (mg/kg)	Zn (mg/kg)	Ni (mg/kg)	Mn (mg/kg)	Pb (mg/kg)
A	HNO ₃ +H ₂ O ₂ +HClO ₄	9.31±0.17	101.85±0.56	2.47±0.03	65.86±0.02	0.97±0.17
	HNO ₃ +HCl	8.83±0.50	103.60±3.30	2.40±0.03	68.78±0.44	1.24±0.03
	HNO ₃ +H ₂ SO ₄	8.87±0.18	84.02±1.86	0.97±0.14	54.95±0.74	1.21±0.04
P	HNO ₃ +H ₂ O ₂ +HClO ₄	7.63±0.22	38.09±0.58	1.99±0.25	132.07±1.34	2.93±0.21
	HNO ₃ +HCl	7.66±0.22	33.06±0.27	2.03±0.13	131.70±3.32	2.35±0.21
	HNO ₃ +H ₂ SO ₄	7.41±0.12	32.56±0.56	1.43±0.19	102.61±1.56	2.34±0.11
H	HNO ₃ +H ₂ O ₂ +HClO ₄	5.84±0.29	25.99±0.80	7.09±0.49	50.38±1.46	2.64±0.54
	HNO ₃ +HCl	6.16±0.04	24.71±0.56	7.39±0.37	59.67±1.85	2.66±0.06
	HNO ₃ +H ₂ SO ₄	5.67±0.15	19.90±0.62	5.57±0.11	48.86±1.43	2.15±0.05
Q	HNO ₃ +H ₂ O ₂ +HClO ₄	4.40±0.60	46.14±0.32	0.12±0.02	245.61±1.36	0.48±0.04
	HNO ₃ +HCl	4.62±0.37	42.35±0.59	0.09±0.01	281.06±6.02	0.47±0.04
	HNO ₃ +H ₂ SO ₄	4.61±0.02	39.54±0.59	0.04±0.01	262.74±2.01	0.33±0.02
V	HNO ₃ +H ₂ O ₂ +HClO ₄	8.39±0.11	25.01±1.10	6.95±0.37	38.45±0.48	4.68±0.05
	HNO ₃ +HCl	8.31±0.31	18.09±0.23	6.88±0.34	32.84±0.29	2.43±0.35
	HNO ₃ +H ₂ SO ₄	7.79±0.18	17.34±0.42	6.19±0.05	27.86±0.08	4.64±0.43

Our result indicate that the most effective extraction procedure for quantification of Cu, Mn, Ni and Pb in the examined plant samples was acid digestion with mixture of aqua regia with addition of hydrogen peroxide, while the digestion with concentrated nitric acid followed by addition of H₂O₂ and HClO₄ was the most efficient procedure in the case of the Zn contents determination.

Conclusion

This research indicates that among the examined extractants, aqua regia with the addition of H₂O₂ showed maximum extraction capacity in the quantification of Cu, Mn, Ni, and Pb. On the other hand, wet digestion provided with a combination of HNO₃, H₂O₂ and HClO₄ resulted in a slightly smaller efficiency in the case of quantification of those four elements and the highest efficiency in the determination of Zn content. Besides, during the research, it was found that the accuracy of the both these methods of wet digestion for the analysis of the standard reference material was satisfactory. Considering all the obtained results, we could conclude that an acid mixture composed of aqua regia+H₂O₂ and HNO₃+H₂O₂+HClO₄ could be successfully used for the wet digestion of various plant samples as an extraction method for the determination of Cu, Mn, Ni, Pb, and Zn contents by the method of atomic absorption spectrophotometry. The efficiency and benefits of both methods for quantification of the PETs in specific plant parts (leaves, shoots, roots) and samples could be further explored.

References

- Allen, S. E., Grimshaw, H. M. & Rowland, A. P. (1986). Chemical analysis. In: Moore, P. D., Chapman, S. B. (Eds.), *Methods in Plant Ecology*, Oxford: Blackwell Scientific Publication, London, 285–344.
- Bell, R. W. (2000). Temporary nutrient deficiency-a difficult case for diagnostic and prognosis by plant analysis. *Communications in Soil Science and Plant Analysis*, 31, 1847–1861. <https://doi.org/10.1080/00103620009370542>

- Beneton, J. Jr. (2001). *Laboratory guide for conducting soil tests and plant analysis*. CRC Press LLC, Boca Raton.
- Bradl, H. B. (2005). Sources and origins of heavy metals. in Bradl, H. B., Ed. *Heavy metals in the environment*. Elsevier, Ltd. London.UK.
- Campbell, R. C. & Plank, O. C. (1998). Handbook of reference methods for plant analysis, In Y. P. Kalra (Ed.) *Preparation of Plant Tissue for laboratory analysis* (pp.37-50) Taylor & Francis Group, Boca Raton.
- Hooda, P. A. (2010). *Trace Elements in Soils*. Blackwell Publishing Ltd.
- Hoening, M. (2001). Preparation steps in environmental trace element analysis-Facts and traps. *Talanta*, 54, 1021–1038. [https://doi.org/10.1016/s0039-9140\(01\)00329-0](https://doi.org/10.1016/s0039-9140(01)00329-0)
- Idera, F., Omotola, O., Adedayo, A. & Paul, U. J. (2015). Comparison of Acid Mixtures Using Conventional Wet Digestion Methods for Determination of Heavy Metals in Fish Tissues. *Journal of Scientific Research & Reports*, 8(7), 1–9. <https://doi.org/10.9734/JSRR/2015/19717>
- Kabata-Pendias, A. (2011). *Trace elements in soils and plants*. 4th Edition, CRC Press.
- Mokoena, D. P., Mngadi, S. V. & Nomngongo, P. N. (2020). Microwave-assisted extraction of trace metals from sediments using dilute hydrogen peroxide and dilute nitric acid prior to their determination by inductively coupled plasma-optical emission spectrometry. *Current Analytical Chemistry*, 16(8), 970–978. <https://doi.org/10.2174/1573411016666200318144655>
- Pequerul, A., Perez, C., Madero, P., Val, J. & Mange, E. (1993). A rapid wet digestion method for plant analysis, in Optimization of Plant Nutrition (eds. Fragoso, M.A.C. and van Beusichem). *Development in Plant and Soil Sciences*, 53, 3–6.
- Rao, C. R. M., Sahuquillo, A. & Lopez-Sanchez, J. F. (2008). A review of the different methods applied in environmental geochemistry for single and sequential extraction of trace elements in soils and related materials. *Water, Air and Soil Pollution*, 189(1), 291–333. <https://doi.org/10.1007/s11270-007-9564-0>
- Rodrigues-Flores, M. & Rodrigues-Castellon, E. (1982). Lead and cadmium levels in soil and plants near highways and their correlation with traffic density. *Environmental Pollution Ser. B*, 4, 281–290. [https://doi.org/10.1016/0143-148X\(82\)90014-3](https://doi.org/10.1016/0143-148X(82)90014-3)
- Shaibur, M. R., Shamim, A. H., Huq, S. M. I. & Kawai, S. (2010). Comparison of digesting capacity of nitric acid and nitric acid-perchloric acid mixture and the effect of lanthanum chloride on potassium measurement. *Nature and Science*, 8(5), 157–162. <https://doi.org/10.7537/marsnsj080510.18>
- Sleimi, N., Bankaji, I., Kouki, R., Dridi, N., Duarte, B. & Cacador, I. (2022). Assessment of extraction methods of trace metallic elements in plants: Approval of common method. *Sustainability*, 14, 1428. <https://doi.org/10.3390/su14031428>
- Uddin, A. H., Khalid, R. S., Alaama, M., Abdulkader, A. M., Kasmuri, A. & Abbas, S. A. (2016). Comparative study of three digestion methods for elemental analysis in traditional medicine products using atomic absorption spectrometry. *Journal of Analytical Science and Technology*, 7, 6. <https://doi.org/10.1186/s40543-016-0085-6>

Original scientific article

ANTIPROLIFERATIVE AND ANTIBACTERIAL ACTIVITY *IN VITRO* OF AMIDINO SUBSTITUTED 2-NAPHTHYLBENZAZOLES

Livio Racané¹, Lucija Ptiček¹, Marijana Hranjec², Leentje Persoons³, Dirk Daelmans³, Mihailo Banjananc⁴, Vedrana Radovanović⁴

¹Department of Applied Chemistry, Faculty of Textile Technology, University of Zagreb, HR-10000 Zagreb, Croatia

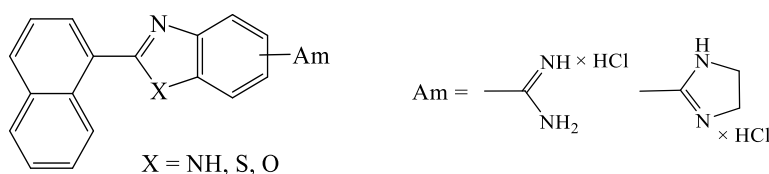
²Department of Organic Chemistry, Faculty of Chemical Engineering and Technology, University of Zagreb, HR-10000 Zagreb, Croatia

³KU Leuven Department of Microbiology and Immunology, Laboratory of Virology and Chemotherapy, Rega Institute, Leuven, Belgium

⁴Pharmacology in vitro, Fidelta Ltd., Prilaz baruna Filipovića 29, 10000 Zagreb, Croatia

Abstract

Taking into account that benzimidazole, benzothiazole and benzoxazole nuclei, as a part of nitrogen heterocycles, are highly-privileged building structural motifs in organic and medicinal chemistry, they played unavoidable role in the rational drug design. Among their versatile pharmacological features, the most important ones are antimicrobial, antitumor, antiviral, anti-inflammanory, antihistaminic, antioxidant, *etc.* On the other hand, amidines are known as important pharmacophore functional groups usually placed at the termini of the biologically active molecules. They are a structural parts of the numerous biologically active compounds and many important medical and biochemical agents. Amidine groups, usually in cationic form, could significantly contribute to the molecule/possible biological target complex stability. Herein we present the synthesis, structural characterization and biological evaluation of amidino substituted benzimidazole and benzothiazole derivatives substituted with 2-naphthyl ring. All targeted compounds have been synthesized according to the conventional methods of organic synthesis. They have been evaluated on the several human cancer cell lines for their antiproliferative activity *in vitro*. Additionally, all synthesized compounds have been tested against several Gram negative and Gram positive bacterial strains *in vitro*.



Keywords: amidines, antibacterial activity, antiproliferative activity, benzimidazoles, benzothiazoles.

Introduction

Among all known heterocyclic compounds and specially nitrogen heterocycles, benzazoles, including benzoxazoles, benzimidazole and benzothiazole moieties have been recognized as important and unavoidable constituents and structural motifs of versatile biologically important molecules in medicinal and pharmaceutical chemistry (Tariq, 2019; Yaday, 2015; Kale, 2019; Silakari, 2018). Owing to their wide range of different biological activities, these heterocycles are still privileged

structural motifs in the rational design of novel drugs (Akthar, 2017; Mahdi Alzhrani, 2022). Suchlike derivatives display versatile biological features including antiproliferative, antitumor, antibacterial, antifungal, antiprotozoal, antihypertensive, antioxidant, antihistaminic *etc.* activities (Ali, 2020; Bansal, 2012; Keri, 2015).

On the other hand, amidines are pharmacophore groups which could be found in the structure of many known biologically active molecules, mostly being placed at the termini of the molecules (Rescifina, 2014). On that way this functional groups usually in the cationic form, could improve and enhance the interaction with the possible biological targets, like DNA, RNA or proteins (Tidwell & Boykin, 2003). If the biological target is DNA or RNA, it has been proven that amidines contribute significantly to the molecule/possible biological target complex stability through H-bonding and electrostatic interactions and thus, enhance the biological activity (Depauw, 2019). In our research group, we have published several papers describing the biological activity of amidino substituted benzazole derivatives (Lončar, 2021; Hranjec, 2008a). All results obtained from the antiproliferative testing *in vitro* as well as from the additional biological experiments, we have concluded that the introduction of one or two positively charged amidine moieties at the end of the heteroaromatic benzazole derivatives, has significantly improve the biological activity of studied derivatives (Racané, 2010a). Among all types of amidino groups, the most significant influence on the improvement of biological activity was displayed within the derivatives bearing cyclic 2-imidazoliny amidine group, which showed stronger activity when compared to the aliphatic types of amidines (Racané, 2021b). Additionally, we have confirmed that the amidino-substituted benzazole derivatives bind strongly to an electronegatively charged molecule such as DNA/RNA, mostly as groove binders or intercalators. Furthermore, we have shown that some amidino substituted benzimidazole and benzothiazole derivatives displayed strong antitumor activity by intercalating into ds-RNA and ct-DNA, or by binding into the minor groove of AT-DNA, ss-RNA or showed sequence-selective binding in the A-T rich side of ct-DNA (Racané, 2014c; Cindrić, 2017).

Herein we present the synthesis and biological activity on 2-naphthyl substituted 2-benzazoles bearing either cyclic amidino or unsubstituted amidino group at the benzazole nuclei. All compounds were tested for their antiproliferative and antibacterial activity *in vitro* on several human cancer cells as well as several bacterial strains. Based on the SAR study, we might conclude that the type of the heteroatom placed at the azole nuclei as well as the type of the amidine substituent has a great impact on the biological activity.

Materials and Methods

Chemistry

General methods

Melting points were determined by means of Original Kofler Mikroheitztisch apparatus (Reichert, Wien). ^1H NMR and ^{13}C NMR spectra were recorded with the Bruker Avance DPX-300 or Bruker AV-600 using TMS as internal standard. Chemical shifts are reported in parts per million (ppm) relative to TMS. Elemental analyses for carbon, hydrogen and nitrogen were performed on Perkin-Elmer 2400 elemental analyser. Analyses are indicated as symbols of elements, and analytical results obtained are within 0.4% of the theoretical value.

Synthesis of benzoxazole and benzothiazole derivatives 3a-3d

General procedure for synthesis of 3a-3d

A mixture of 1-naphthoic acid (**1**) (0.5 mmol) and 5-amidino-substituted 2-aminophenols hydrochloride **2a-2b** or 5-amidino-substituted 2-aminothiophenoles **2c-2d** (0.5 mmol) in polyphosphoric acid (10-12 g) was gradually heated to 160 °C until the mixture became homogenous and then at 180 °C for 2 h. The reaction mixture was poured in water (150 mL), cooled and made alkaline with 20% NaOH. The obtained free base was filtered, washed with water and dried under

vacuum over KOH. To a mixture of crude base in ethanol (5 ml) 36% hydrochloride acid (0.087 ml, 1 mmol) was added and stirred at room temperature for 1-2 h, diethyl ether (10 ml) was added, and then cooled overnight. The resulting precipitate was filtered and purified by crystallization.

6-Amidino-2-(naphthalene-1-yl)benzoxazole hydrochloride (3a)

Using 1-naphthoic acid (**1**) (86 mg), 2-amino-5-amidinophenol dihydrochloride (**2a**) (112 mg) and crystallization from ethanol gave 66 mg (41 %) of white solid; mp = 281 – 285 °C. ¹H NMR (300 MHz, DMSO-*d*₆) (δ ppm): 9.55 (s, 2H, –C(NH₂)⁺), 9.42 (d, 1H, *J* = 8.4 Hz Ar-*H*), 9.29 (bs, 2H, –C(NH₂)⁺), 8.53 (d, 1H, *J* = 7.1 Hz, Ar-*H*), 8.42 (s, 1H, Ar-*H*), 8.31 (d, 1H, *J* = 7.9 Hz, Ar-*H*), 8.20 – 8.11 (m, 2H, Ar-*H*), 7.94 (d, 1H, *J* = 8.6 Hz, Ar-*H*), 7.87 – 7.66 (m, 3H, Ar-*H*). ¹³C NMR (75 MHz, DMSO-*d*₆) (δ ppm): 165.2, 164.8, 148.9, 145.6, 133.4, 133.3, 129.9, 129.7, 128.8, 128.1, 126.6, 125.3, 125.2, 124.9, 124.7, 121.6, 120.1, 111.2. Analysis calcd for C₁₈H₁₄ClN₃O (323.78): C, 66.77; H, 4.36; N, 10.95. Found: C, 66.89; H, 4.25; N, 10.99.

6-(4,5-Dihydro-1H-imidazol-2-yl)-2-(naphthalene-1-yl)benzoxazole hydrochloride (3b)

Using 1-naphthoic acid (**1**) (86 mg), 2-Amino-5-(4,5-dihydro-1H-imidazol-2-yl)phenol hydrochloride dihydrate (**2b**) (125 mg) and crystallization from ethanol gave 79 mg (45 %) of white solid; mp > 300 °C. ¹H NMR (300 MHz, DMSO-*d*₆) (δ ppm): 10.89 (s, 2H, –C(NH–)₂⁺), 9.42 (d, 1H, *J* = 8.5 Hz, Ar-*H*), 8.61 (s, 1H, Ar-*H*), 8.54 (d, 1H, *J* = 7.3 Hz, Ar-*H*), 8.30 (d, 1H, *J* = 8.3 Hz, Ar-*H*), 8.20 (d, 1H, *J* = 8.4 Hz, Ar-*H*), 8.16 – 8.08 (m, 2H, *J* = 6.7 Hz, Ar-*H*), 7.85 – 7.65 (m, 3H, Ar-*H*), 4.06 (s, 4H, –CH₂CH₂–). ¹³C NMR (151 MHz, DMSO-*d*₆) (δ ppm): 165.1, 164.4, 149.0, 146.1, 133.3, 133.2, 129.9, 129.6, 128.6, 127.9, 126.4, 125.3, 125.1, 125.0, 121.5, 120.3, 118.8, 111.5, 44.2. Analysis calcd for C₂₀H₁₆ClN₃O (349.81): C, 68.67; H, 4.61; N, 12.01. Found: C, 68.58; H, 4.63; N, 10.04.

6-Amidino-2-(naphthalene-1-yl)benzothiazole hydrochloride (3c)

Using 1-naphthoic acid (**1**) (86 mg), 2-amino-5-amidiniumbenzenethiolate (**2c**) (84 mg) and crystallization from ethanol-diethylether gave 55 mg (32 %) of white solid; mp = 267 – 271 °C. ¹H NMR (300 MHz, DMSO-*d*₆) (δ ppm): 9.60 (bs, 2H, –C(NH₂)⁺), 9.37 (bs, 2H, –C(NH₂)⁺), 9.05 (d, 1H, *J* = 8.0 Hz Ar-*H*), 8.78 (s, 1H, Ar-*H*), 8.41 (d, 1H, *J* = 8.5 Hz, Ar-*H*), 8.24 (d, 1H, *J* = 8.2 Hz, Ar-*H*), 8.19 – 8.08 (m, 2H, Ar-*H*), 8.02 (d, 1H, *J* = 8.4 Hz, Ar-*H*), 7.78 – 7.64 (m, 3H, Ar-*H*). ¹³C NMR (75 MHz, DMSO-*d*₆) (δ ppm): 171.4, 165.5, 156.6, 134.8, 133.7, 132.2, 130.4, 129.5, 129.1, 128.7, 128.1, 126.9, 126.3, 125.6, 125.3, 125.1, 123.3, 123.2. Analysis calcd for C₂₈H₁₄ClN₃S (339.84): C, 63.62; H, 4.15; N, 12.36. Found: C, 63.74; H, 4.14; N, 12.28.

6-(4,5-Dihydro-1H-imidazol-2-yl)-2-(naphthalene-1-yl)benzothiazole hydrochloride (3d)

Using 1-naphthoic acid (**1**) (86 mg), 2-amino-5-(4,5-dihydro-1H-imidazol-3-ium-2-yl)-benzenethiolate hydrate (**2d**) and crystallization from ethanol gave 70 mg (38 %) of white solid; mp = 297 – 302 °C. ¹H NMR (300 MHz, DMSO-*d*₆) (δ ppm): 10.94 (s, 2H, –C(NH–)₂⁺), 9.04 (d, 1H, *J* = 8.2 Hz, Ar-*H*), 8.97 (d, 1H, *J* = 1.4 Hz, Ar-*H*), 8.45 (d, 1H, *J* = 8.6 Hz, Ar-*H*), 8.27 – 8.09 (m, 4H, Ar-*H*), 7.77 – 7.65 (m, 3H, Ar-*H*), 4.08 (s, 4H, –CH₂CH₂–). ¹³C NMR (75 MHz, DMSO-*d*₆) (δ ppm): 164.6, 156.8, 153.32, 146.6, 135.0, 133.6, 132.3, 130.5, 129.5, 128.7, 128.1, 126.9, 126.6, 125.5, 125.3, 123.7, 123.6, 119.1, 44.5. Analysis calcd for C₂₀H₁₆ClN₃S (365.88): C, 65.65; H, 4.41; N, 11.48. Found: C, 65.60; H, 4.48; N, 11.48.

Synthesis of benzimidazole derivatives 6a-6b

The synthesis and structural characterization of amidino substituted benzimidazole derivatives **6a-6b** were previously published (Perin, 2017).

Antiproliferative activity *in vitro*

Cell culture, proliferation assay and reference compounds

Human cancer cell lines were purchased from the American Type Culture Collection (ATCC, Manassas, VA, USA), DND-41 cell line was purchased from the Deutsche Sammlung von Mikroorganismen und Zellkulturen. All assays were done according to the previously published procedures. Culture media were purchased from Gibco Life Technologies, USA, and supplemented with 10% fetal bovine serum (HyClone, GE Healthcare Life Sciences, USA). Stock solutions were prepared in DMSO and *Vincristine* and *docetaxel* were used as references. Adherent cell lines LN-229, HCT-116, NCI-H460, LS513 and Capan-1 cells were seeded at a density between 500 and 1500 cells per well, in 384-well tissue culture plates (Greiner). After overnight incubation, cells were treated with seven different concentrations of the test compounds, ranging from 100 to 0.006 μ M. Cells were incubated for 72 hours with compounds and were then analyzed using the CellTiter 96® AQueous One Solution Cell Proliferation Assay (MTS) reagent (Promega) according to the manufacturer's instructions. Absorbance of the samples was measured at 490 nm using a SpectraMax Plus 384 (Molecular Devices), and OD values were used to calculate the 50% inhibitory concentration (IC₅₀). Compounds were tested in at least two independent experiments.

Antibacterial activity in vitro

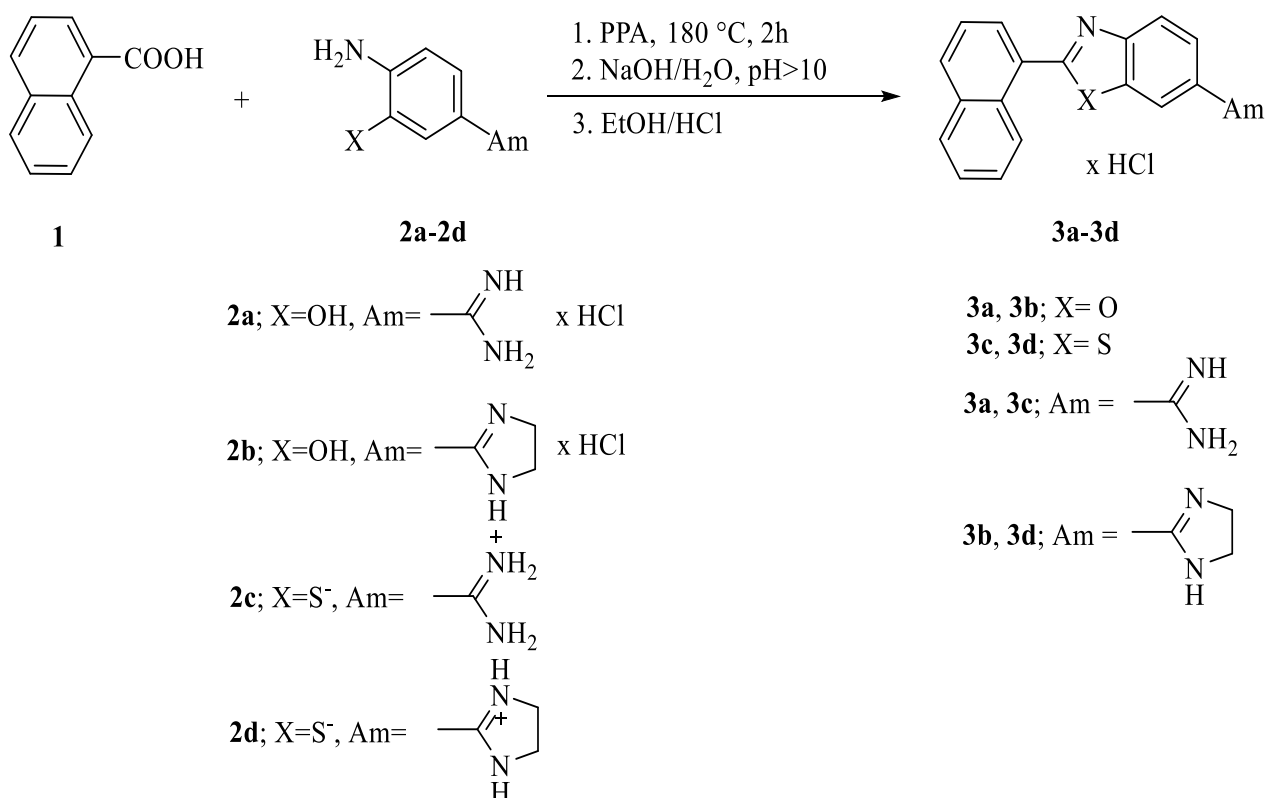
In this experiment standard antibiotics *Ampicillin*, *Ceftazidime*, *Ciprofloxacin* and *Meropenem* were tested. Broth microdilution testing was performed according to CLSI (Clinical Laboratory Standards Institute) guidelines. MIC (minimal inhibitory concentration) value was defined as the last tested concentration of compound at which there is no visible growth of bacteria. Inoculums for each microorganism were prepared using the direct colony suspension method where broth solutions that achieved turbidity equivalent to 0.5 McFarland standard were additionally diluted 100x with Ca adjusted MH media (Becton Dickinson). All test plates were incubated for 16 – 24h at 37 °C. MIC values for reference antibiotics against quality control strains were used for confirming the validity of the screen.

Results and discussion

Chemistry

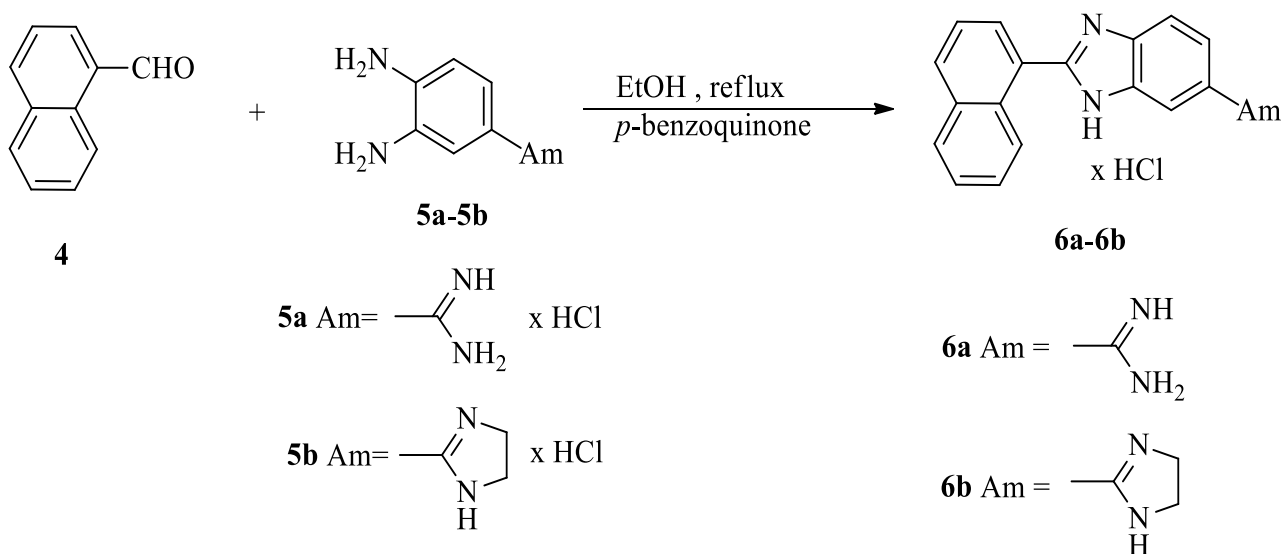
Amidino substituted benzoxazole, benzothiazole and benzimidazole derivatives were synthesized following the experimental protocols presented in Scheme 1 and 2. All compounds were prepared as hydrochloride salts were prepared in order to ensure better solubility important for biological testing. For the synthesis of targeted amidino substituted benzoxazoles and benzothiazoles, the corresponding amidino substituted precursors **2a-2d** as hydrochloride salts were prepared by previously published procedures. Synthesis of 2-amino-5-amidinophenol dihydrochloride **2a** and 2-Amino-5-(4,5-dihydro-1*H*-imidazol-2-yl)phenol hydrochloride dihydrate **2b** were carried out according to the literature (Ptiček, 2021), while 2-amino-5-amidiniumbenzenethiolate (**2c**) and 2-amino-5-(4,5-dihydro-1*H*-imidazol-3-ium-2-yl)-benzenethiolate hydrate **2d** were synthesized according to the literature (Racané, 2008d).

2-Naphthyl substituted benzoxazole and benzothiazole derivatives obtained in the reaction of cyclocondensation of precursors **2a-2d** with 2-naphthoic acid **1** using polyphosphoric acid at high temperature. After the treatment with aq. NaOH the free bases were isolated which were then converted, with concentrated hydrochloric acid in absolute ethanol, into the corresponding hydrochloride salts in moderate reaction yields.



Scheme 1. Synthesis of benzoxazole **3a-3b** and benzothiazole derivatives **3c-3d**

The targeted amidino substituted 2-naphthyl benzimidazole derivatives **6a-6b** obtained by the condensation from 2-naphthylcarbaldehyd **4** and previously synthesized 4-amidino substituted 1,2-phenylenediamines **5a-5b** in absolute ethanol using *p*-benzoquinone as an oxidants (Hranjec, 2007b; Racane, 2021e).



Scheme 2. Synthesis of benzimidazole derivatives **6a** and **6b**

Antiproliferative activity *in vitro*

All prepared amidino-substituted benzazole derivatives were tested for their antiproliferative activity *in vitro* on a following human cancer cells: LN-229 - glioblastoma, Capan-1 - pancreatic adenocarcinoma, HCT-116 - colorectal carcinoma, NCI-H460 - lung carcinoma, DND-41 - acute lymphoblastic leukemia, HL-60 - acute myeloid leukemia, K-562 - chronic myeloid leukemia, and Z-138 - non-Hodgkin lymphoma (Table 1). Docetaxel and Vincristine have been used as standard drugs. All tested compounds showed lower antiproliferative activity in comparison to these antitumor drugs.

Table 1. Antiproliferative activity of tested compounds *in vitro*

Cpd	IC ₅₀ /μM							
	<i>Cell lines</i>							
	LN-229	Capan-1	HCT-116	NCI-H460	DND-	HL-60	K-562	Z-138
3a	37.8	8.9	32.2	40.5	6.1	6.5	26.9	3.8
3b	6.1	5.2	40.0	10.8	2.1	2.5	3.5	2.0
3c	46.8	38.4	45.7	44.4	19.1	42.9	38.8	31.5
3d	1.9	3.1	7.1	4.0	1.3	1.2	2.0	1.9
6a	>100	50.7	>100	>100	13.6	77.3	84.0	32.5
6b	43.3	29.6	45.2	34.4	7.6	12.5	50.4	9.5
Docetaxel	0.0041	0.0038	0.0025	0.0044	0.0025	0.0022	0.0085	0.0023
Vincristine	0.0027	0.0088	0.0079	0.0097	0.010	0.0033	0.017	0.031

All tested compounds exerted moderate to strong antiproliferative activity on the tested cell lines. 2-Imidazolynyl substituted benzothiazole derivative **3d**, showed strong antiproliferative activity against all of the cancer cells without significant selectivity between tested cells (IC₅₀ 1.2 – 7.1 μM). This compound has been chosen as a lead compound for further structure optimization to achieve better antiproliferative activity and selectivity. Very strong antiproliferative activity was also shown by 2-Imidazolynyl substituted benzoxazole derivative **3b** with strong and selective activity against DND-41, HL-60 and Z-138 cells (IC₅₀ 2.1, 2.5 and 2.0 μM, respectively) and good activity against K-562 cells (IC₅₀ 3.5 μM). 2-Imidazolynyl substituted benzimidazole derivative **6b** showed selective activity against DND-41 cells (IC₅₀ 7.6 μM).

In general, we might conclude that benzimidazole derivatives were less active in comparison to benzoxazole and benzothiazole analogues with strong influence of the amidino group placed at the benzazole nuclei on the antiproliferative activity. Obtained results revealed that the cyclic amidino group enhanced antiproliferative activity in comparison to unsubstituted amidino group.

Additionally, all prepared amidino-substituted benzazole derivatives were tested also for their antibacterial activity against some Gram-positive and Gram-negative bacterial strains including *E.coli*, *S. Aureus* and *S. Pneumoniae*. Four antibiotics were used as a standard drugs for comparison: *Ampicillin*, *Ceftazidime*, *Ciprofloxacin* and *Meropenem*. Obtained results are presented in the Table 2. Tested compounds were less active when compared to standard drugs.

According to the obtained results, we might observe that benzoxazole and benzothiazole derivatives showed the same moderate antibacterial activity against chosen bacterial strains (MIC 16-64 μM). There was no influence of the type of benzazole nuclei as well as the type of the amidine substituent placed at the benzazole nuclei on the antibacterial activity. Benzimidazole derivatives were less active when compared to the benzoxazole and benzothiazole analogues.

Table 2. Antibacterial activity of tested compounds *in vitro*

Cpd	MIC/ μ M			
	<i>Bacterial strains</i>			
	<i>S. aureus</i> ATCC 29212	<i>E. coli</i> ATCC 29213	<i>E. coli</i> efflux del	<i>S. pneumoniae</i> ATCC 49619
3a	16	32	16	32
3b	16	>64	16	64
3c	16	32	16	32
3d	16	>64	16	64
6a	32	>64	32	>64
6b	32	>64	32	32
Ampicillin	1	1	2	<0.125
Ceftazidime	16	0.25	0.25	0.25
Ciprofloxacin	0.25	<0.125	<0.125	0.25
Meropenem	<0.125	<0.125	<0.125	<0.125

Conclusion

Within this research, we have synthesized amidino-substituted benzoxazole, benzothiazole and benzimidazole derivatives bearing either cyclic 2-imidazolynyl or unsubstituted amidino group on the benzazole nuclei. Targeted compounds were prepared in order to evaluate their antiproliferative activity *in vitro* against several human cancer cells as well as antibacterial activity *in vitro*. Additionally, the main purpose was to study the influence of the type of benzazole nuclei and amidino substituents on the biological activity. Benzazole derivatives were prepared according to the well-optimized and previously published conventional methods for organic synthesis of benzazole derivatives, mostly published by our research group.

Obtained results for antiproliferative and antibacterial activity *in vitro*, revealed that the benzimidazole derivatives are in general less active in comparison to their benzoxazole and benzothiazole analogues. Regarding the antiproliferative activity, the most active compound has proven to be benzothiazole derivative substituted with cyclic amidino group **3d** with strong activity against several cancer cells. This derivative has been chosen for further structure optimization in order to design a more active and selective antiproliferative agent. Additionally, from the results we might conclude that cyclic amidino group enhanced the antiproliferative activity in comparison to unsubstituted amidino group. Benzoxazoles and benzothiazoles showed better antibacterial activity in comparison to benzimidazole derivatives with 2-imidazolynyl substituted derivatives being slightly more active.

Acknowledgments: We greatly appreciate the financial support of the Croatian Science Foundation under the projects 4379 entitled *Exploring the antioxidative potential of benzazole scaffold in the design of novel antitumor agents*.

References

Akhtar, J., Khan, A. A., Ali, Z., Haider, R. & Shahar Yar, M. (2017). Structure-activity relationship (SAR) study and design strategies of nitrogen-containing heterocyclic moieties for their anticancer activities. *European Journal of Medicinal Chemistry*, 125, 143–189. <https://doi.org/10.1016/j.ejmech.2016.09.023>

- Ali, I., Batool, F., Syeda Andled, Z. N., Amjad, I., Sameh, O. M., Nocentini, A., Siham, A. A. & Supuran, C. T. (2020). Benzothiazole derivatives as anticancer agents. *Journal of Enzyme Inhibition and Medicinal Chemistry*, 35, 265–279. <https://doi.org/10.1080/14756366.2019.1698036>
- Bansal, Y. & Silakari, O. (2012). The therapeutic journey of benzimidazoles: A review. *Bioorganic and Medicinal Chemistry*, 20, 6208–6236. <https://doi.org/10.1016/j.bmc.2012.09.013>
- Cindrić, M., Jambon, S., Harej, A., Depauw, S., David-Cordonnier, M. H., Kraljević Pavelić, S., Karminski-Zamola, G. & Hranjec, M. (2017). Novel amidino substituted benzimidazole and benzothiazole benzo[b]thieno-2-carboxamides exert strong antiproliferative and DNA binding properties. *European Journal of Medicinal Chemistry*, 136, 468–479. <https://doi.org/10.1016/j.ejmech.2017.05.014>
- Tidwell, R. R. & Boykin, D. W. (2003). Dicationic DNA Minor Groove Binders as Antimicrobial Agents, In M. Demeunynck, C. Bailly, W. D. Wilson (Ed.). *Small Molecule DNA and RNA Binders*, Vol. 2 (pp. 414–501.). Wiley-VCH
- Depauw, S., Lambert, M., Jambon, S., Paul, A., Peixoto, P., Nhili, R., Marongiu, L., Figeac, M., Dassi, C., Paul-Constant, C., Billoré, B., Kumar, A., Farahat, A. A., Ismail, M. A., Mineva, E., Sweat, D. P., Stephens, C. E., Boykin, D. W., Wilson, W. D. & David-Cordonnier, M. H. (2019). Heterocyclic Diamidine DNA Ligands as HOXA9 Transcription Factor Inhibitors: Design, Molecular Evaluation, and Cellular Consequences in a HOXA9-Dependant Leukemia Cell Model. *Journal of Medicinal Chemistry*, 62, 1306–1329. <https://doi.org/10.1021/acs.jmedchem.8b01448>
- a) Hranjec, M., Piantanida, I., Kralj, M., Šuman, L., Pavelić, K. & Karminski-Zamola, G. (2008). Novel amidino-substituted thienyl- and furyl-vinyl-benzimidazole derivatives and their photochemical conversion into corresponding diaza-cyclopenta[c]fluorenes. Synthesis, interactions with DNA and RNA and antitumor evaluation. Part 4. *Journal of Medicinal Chemistry*, 51, 4899–4910. <https://doi.org/10.1021/jm8000423>
- b) Hranjec, M., Kralj, M., Piantanida, I., Sedić, M., Šuman, L., Pavelić, K., Karminski-Zamola, G. (2007). Novel cyano- and amidino-substituted derivatives of styryl-2-benzimidazoles and benzimidazo[1,2-*a*]quinolines: Synthesis, photochemical synthesis, DNA binding and antitumor evaluation. Part 3. *Journal of Medicinal Chemistry*, 50, 5696–5711. <https://doi.org/10.1021/jm070876h>
- Kale, M. & Chavan, V. (2019). Exploration of the Biological Potential of Benzoxazoles: An Overview. *Mini-Reviews in Organic Chemistry*, 16, 112–126. <https://doi.org/10.2174/1570193X15666180627125007>
- Keri, R. S., Hiremathad, A., Budagumpi, S. & Nagaraja, B. M. (2015). Comprehensive Review in Current Developments of Benzimidazole-Based Medicinal Chemistry. *Chemical Biology and Drug Design*, 86, 19–65. <https://doi.org/10.1111/cbdd.12462>
- Lončar, B., Perin, N., Mioč, M., Boček, I., Grgić, L., Kralj, M., Tomić, S., Radić Stojković, M. & Hranjec, M. (2021). Novel amino substituted tetracyclic imidazo[4,5-*b*]pyridine derivatives: Design, synthesis, antiproliferative activity and DNA/RNA binding study. *European Journal of Medicinal Chemistry*, 217, 113342. <https://doi.org/10.1016/j.ejmech.2021.113342>
- Alzhrani, Z. M. M., Alam, M. M. & Nazreen, S. (2022). Recent Advancements on Benzimidazole: A Versatile Scaffold in Medicinal Chemistry. *Mini-Reviews in Medicinal Chemistry*, 22, 365–386. <https://doi.org/10.2174/1389557521666210331163810>
- Perin, N., Starčević, K., Perić, M., Čipčić Paljetak, H., Matijašić, M., Stepanić, V., Verbanac, D., Karminski-Zamola, G. & Hranjec, M. (2017). Synthesis and SAR study of novel amidino 2-substituted benzimidazoles as potential antibacterial agents. *Croatica chemica acta*, 90, 145–154. <https://doi.org/10.5562/cca3147>

- Ptiček, L., Hok, L., Grbčić, P., Topić, F., Cetina, M., Rissanen, K., Kraljević Pavelić, S., Vianello, R. & Racané, L. (2021). Amidino Substituted 2-Aminophenols: Biologically Important Building Blocks for the Amidino-Functionalization of 2-Substituted Benzoxazoles. *Organic & Biomolecular Chemistry*, 19, 2784–2793. <https://doi.org/10.1039/D1OB00235J>
- a) Racané, L., Tralić-Kulenović, V., Kraljević Pavelić, S., Ratkaj, I., Peixoto, P., Nhili, R., Depauw, S., Hildebrand, M. P., David-Cordonnier, M. H., Pavelić, K. & Karminski-Zamola, G. (2010). Novel Diamidino-Substituted Derivatives of Phenyl Benzothiazolyl and Dibenzothiazolyl Furans and Thiophenes: Synthesis, Antiproliferative and DNA Binding Properties. *Journal of Medicinal Chemistry*, 53, 2418–2432. <https://doi.org/10.1021/jm901441b>
- b) Racané, L., Cindrić, M., Zlatar, I., Kezele, T., Milić, A., Brajša, K. & Hranjec, M. (2021). Preclinical in vitro screening of newly synthesised amidino substituted benzimidazoles and benzothiazoles. *Journal of Enzyme Inhibition and Medicinal Chemistry*, 36, 163–74. <https://doi.org/10.1080/14756366.2020.1850711>
- c) Racané, L., Stojković, R., Tralić-Kulenović, V., Cerić, H., Đaković, M., Ester, K., Mišir Krpan, A. & Radić Stojković, M. (2014). Interactions with polynucleotides and antitumor activity of amidino and imidazolyl substituted 2-phenylbenzothiazole mesylates. *European Journal of Medicinal Chemistry*, 86, 406–419. <https://doi.org/10.1016/j.ejmech.2014.08.072>
- d) Racané, L., Tralić-Kulenović, V., Mihalić, Z., Pavlović, G. & Karminski-Zamola, G. (2008). Synthesis of new amidino-substituted 2-aminothiophenoles: mild basic ring opening of benzothiazole. *Tetrahedron*, 64, 11594–11602. <https://doi.org/10.1016/j.tet.2008.10.026>
- e) Racané, L., Zlatar, I., Perin, N., Cindrić, M., Radovanović, V., Banjanac, M., Shanmugam, S., Radić Stojković, M., Brajša, K. & Hranjec, M. (2021). Biological Activity of Newly Synthesized Benzimidazole and Benzothiazole 2,5-Disubstituted Furane Derivatives. *Molecules*, 26, 4935–4956. <https://doi.org/10.3390/molecules26164935>
- Rescifina, A., Zagni, C., Varrica, M. G., Pistarà, V. & Corsaro, A. (2014). Recent advances in small organic molecules as DNA intercalating agents: Synthesis, activity, and modeling. *European Journal of Medicinal Chemistry*, 74, 95–115. <https://doi.org/10.1016/j.ejmech.2013.11.029>
- Silakari, O. (2018). *Key Heterocycle Cores for Designing Multitargeting Molecules*, Elsevier.
- Tariq, S., Kamboj, P., Amir, M. (2019). Therapeutic advancement of benzothiazole derivatives in the last decennial period. *Arch Pharm Chemistry In Life Sciences*, 352, e1800170. <https://doi.org/10.1002/ardp.201800170>
- Yadav, G., Ganguly, S. (2015). Structure activity relationship (SAR) study of benzimidazole scaffold for different biological activities: A mini-review. *European Journal of Medicinal Chemistry*, 97, 419–443. <https://doi.org/10.1016/j.ejmech.2014.11.053>

Original scientific article

SOLVATOCHROMIC PROPERTIES OF NEWLY SYNTHESIZED ARYL AZO PYRIDONE DYES

Borko Matijević¹, Gorana Mrđan¹, Dušan Mijin², Jelena Lađarević², Suzana Apostolov¹, Đenđi Vaštag¹

¹University of Novi Sad, Faculty of Sciences, Department of Chemistry, Biochemistry and Environmental Protection, Novi Sad, Serbia

²University of Belgrade, Faculty of Technology and Metallurgy, Belgrade, Serbia

Abstract

Pyridone aryl azo dyes belong to a class of compounds that have wide application, not only as agents for coloring various materials in many branches of the industry but also in medicine as biologically active compounds. It has been proven that they have anti-tumor, anti-inflammatory, and anti-tuberculosis activity and are widely used for therapeutic purposes. Their application can highly depend on the inter- or intra- molecular interactions that occur between the dissolved compound and the surrounding medium. Therefore, the study of these interactions is of great importance for newly synthesized compounds. The spectrophotometric method can be used to examine intermolecular interactions thoroughly by studying the solvatochromic properties of newly synthesized compounds in different molecular environments. To this end, absorption spectra of seven newly synthesized aryl azo pyridone dyes based on 5-((disubstituted phenyl)diazenyl)-6-hydroxy-4-methyl-2-oxo-1,2-dihydropyridine-3-carbonitrile were recorded in ten solvents of different properties. The spectra were recorded in the range from 300 to 600 nm and showed one absorption maximum. By applying different models based on the principle of multiple linear correlations of solvatochromic energies (LSER method), information about the effects of certain interactions that take place between the tested compounds and the surrounding medium were obtained.

Keywords: Aryl azo dyes, solvatochromism, intermolecular interactions, spectrophotometry.

Introduction

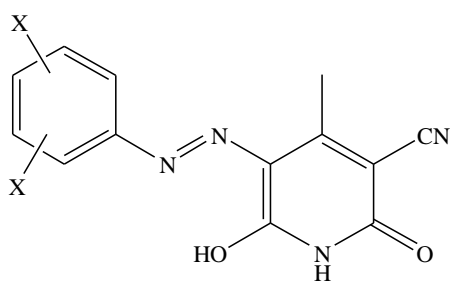
Azo dyes are compounds containing at least one diazenyl group ($R-N=N-R'$) in their structure and account for more than 60% of the known commercial dyes. During synthesis, when the coupling component is a pyridone derivative, and the diazo component is a carbocyclic or heterocyclic compound, aryl azo pyridone dyes are obtained (Chudgar & Oakes, 2003; Radojković-Veličković & Mijin, 2001). These dyes are widely used due to their high molar extinction coefficient and great resistance to light and wet processing (Lubai et al., 1986; Christie, 2001). Mostly they are applied in the textile industry for dyeing synthetic fabrics, but also as components of LCD screens and ink-jet graphic colors (Oberholzer, 2005; Seto et al., 2006; Tanaka et al., 2012). Recent medical and biological research in the field of azo derivatives has opened up the possibility of their use as antimicrobial, antioxidant, and antitumor agents (Ashkar et al., 2012; El-Sonbati et al., 2017; Mishra et al., 2019). Considering previous studies, it is clear that newly synthesized compounds based on azo dyes would be interesting candidates for the investigation of potential biological activity. Every biological study is preceded by a detailed physicochemical characterization. UV-Vis spectrophotometry is a simple, economic method used to obtain information about inter- and intramolecular interactions that occur between dissolved substances and the surrounding medium. The strength and type of these interactions can have a great influence on the activity of a molecule,

and their quantification is important for the further potential application of the investigated compound. In this paper absorption spectra of seven newly synthesized aryl azo pyridone dyes have been recorded in nine solvents of different properties in the range from 300 to 600 nm. The influence of the solvent on the shifts of absorption maxima was interpreted with two solvatochromic models, first proposed by Kamlet and Taft and second by Catalan, using the LSER method (Linear Solvation Energy Relationship). This way, information about the intermolecular interactions that take place between the newly synthesized azo dyes and the selected solvents was obtained.

Materials and Methods

Seven derivatives of 5-(disubstituted phenylazo)-3-cyano-6-hydroxy-4-methyl-2-pyridone were synthesized and characterized at the Department of Organic Chemistry, Faculty of Technology and Metallurgy in Belgrade. Absorption spectra of newly synthesized compounds were recorded in the range from 300 to 600 nm in nine solvents of different properties, four of which are protic (methanol, *i*-butanol, *t*-butanol, and acetic acid) and five aprotic solvents (acetonitrile (ACN), dimethylsulfoxide (DMSO), *N,N*-dimethylformamide (DMF), chloroform and diethyl-ether). All solvents used were with a high degree of purity and quality for spectrophotometric measurements, manufactured by Sigma Aldrich. Solutions recorded were prepared in concentrations of 4×10^{-5} mol dm⁻³, and the obtained data were processed in Origin 8.0 and Microsoft Office Excel 2007. The structure and numbering of the investigated compounds are given in Table 1.

Table 1. Structure and numeration of investigated azo dyes

	X		
	Compound	Position	Substituent
	1	3, 5	CH ₃
	2	2, 4	CH ₃
	3	2, 6	Cl
	4	2, 6	CH ₃
	5	3, 5	Cl
	6	2, 4	NO ₂
	7	2, 4	OCH ₃

Quantitative analysis of the interactions that occur between the investigated dyes and the surrounding medium was done by the LSER method, using two solvatochromic models, Kamlet-Taft's (1) (Kamlet & Taft 1976; Taft & Kamlet, 1976; Kamlet et. al., 1977) and Catalan's (2) (Catalan & Hopf, 2004; Catalan, 2009) according to the following equations:

$$v_{max} = v_0 + a \cdot \alpha + b \cdot \beta + s \cdot \pi \quad (1)$$

v_{max} - frequency in the used solvent, v_0 - frequency in the standard solvent, α - acidity, β - basicity, π^* - polarizability/dipolarity of the solvent, while **a**, **b** and **s** are the regression coefficients of this equation.

$$v_{max} = v_0 + a \cdot SA + b \cdot SB + c \cdot SP + d \cdot SdP \quad (2)$$

v_{max} - frequency in the used solvent, v_0 - frequency in the standard solvent, *SA* - acidity, *SB* - basicity, *SP* - polarizability и *SdP* - dipolarity of the solvent, and **a**, **b**, **c** and **d** are the regression coefficients of this equation.

Results and discussion

Depending on the properties of the used solvent and its ability to enter into various interactions with the dissolved substance, changes in the absorption spectrum of the given compound can occur related

to the spectrum of the same compound in the gaseous state. This phenomenon is defined as solvatochromism and is used to study the structure and reactivity of organic compounds using the linear solvation energy relationship (LSER) method. The solvatochromic effect have only those organic molecules whose chromophores contain π -electrons and free electron pairs, i.e. where $\pi \rightarrow \pi^*$ or $n \rightarrow \pi^*$ electron transitions can occur (Kamlet et. al., 1977). Figure 1 represents spectra of compound **2** recorded in all solvents, four protic (a) and five aprotic (b).

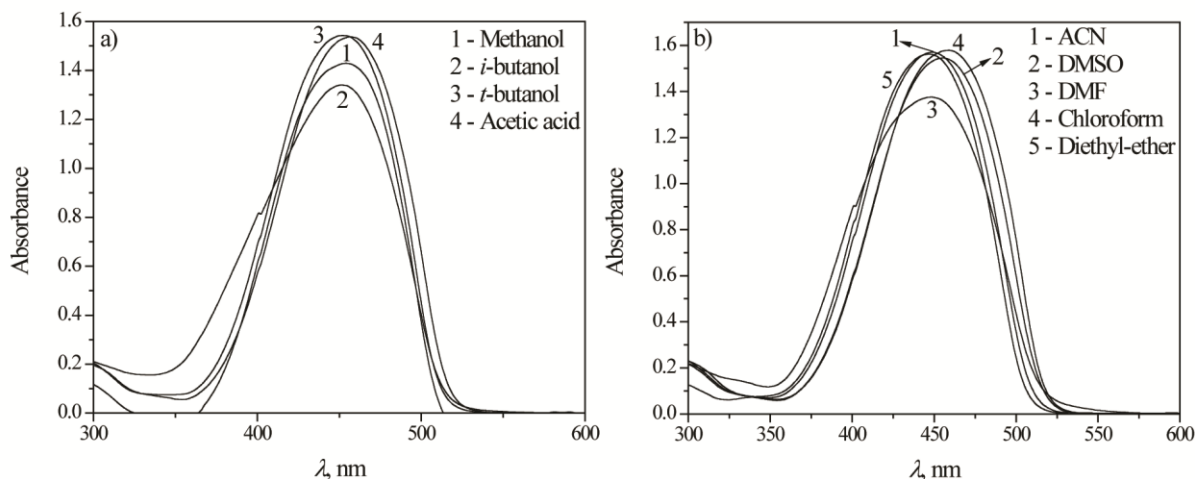


Figure 1. Spectra of compound **2** recorded in protic (a) and aprotic (b) solvents

Table 2. Absorption frequencies of azo dyes recorded in all solvents used

Compound/ Solvent	Methanol	<i>i</i> -butanol	<i>t</i> -butanol	Acetic acid	ACN	DMSO	DMF	Chloroform	Diethyl ether
1	22.70	22.84	22.81	22.68	22.82	22.76	22.85	22.89	22.99
2	22.05	22.14	22.21	22.12	22.25	22.20	22.23	22.36	22.41
3	24.98	25.06	25.18	24.94	25.24	25.17	25.20	25.31	25.43
4	23.10	23.17	23.22	23.10	23.25	23.22	23.30	23.44	23.48
5	23.72	23.75	23.81	23.70	23.86	23.85	23.82	23.88	23.94
6	22.65	22.71	22.74	22.65	22.73	22.74	22.73	22.86	22.96
7	20.62	20.65	20.73	20.60	20.81	20.75	20.76	20.84	20.96

Observing the spectra presented in Figure 1, it can be seen that there is one absorption maximum in all solvents. Similar spectra are obtained for the remaining compounds. Also, it can be noted that more significant shifts are represented within aprotic solvents, due to a much greater variety of their properties compared to the protic solvents. Absorption frequencies at the maximum absorbance for all tested compounds (wave numbers) are shown in Table 2.

The absorption maxima of seven tested dyes are in the range of wavelengths from 390 to 485 nm. The reason for such a wide range is already mentioned variety of the solvents used and also the great variety of substituents attached to the benzene ring of azo derivatives (methyl, methoxy, chloride, and nitro). Calculated wave numbers (Table 2) were correlated with empiric polarity parameter (E_T^N , Table 3) and significant dependencies were obtained. One of them, obtained for compound **2**, is shown in Figure 2, while similar dependencies were obtained for all other investigated compounds.

Table 3. Parameters used for correlations

Solvent	E_T^N	Kamlet-Taft's parameters			Catálan's parameters			
		α	β	π	SA	SB	SP	SdP
Methanol	0.762	0.98	0.66	0.60	0.605	0.545	0.608	0.904
<i>i</i> -butanol	0.552	0.79	0.84	0.40	0.311	0.828	0.657	0.684
<i>t</i> -butanol	0.389	0.42	0.93	0.41	0.145	0.928	0.632	0.732
Acetic acid	0.648	1.12	0.45	0.64	0.689	0.390	0.651	0.676
ACN	0.460	0.19	0.40	0.75	0.044	0.286	0.645	0.974
DMSO	0.444	0.00	0.76	1.00	0.072	0.647	0.830	1.000
DMF	0.386	0.00	0.69	0.88	0.031	0.613	0.759	0.977
Chloroform	0.259	0.44	0.00	0.58	0.047	0.071	0.783	0.614
Diethyl ether	0.117	0.00	0.47	0.27	0.000	0.562	0.617	0.385

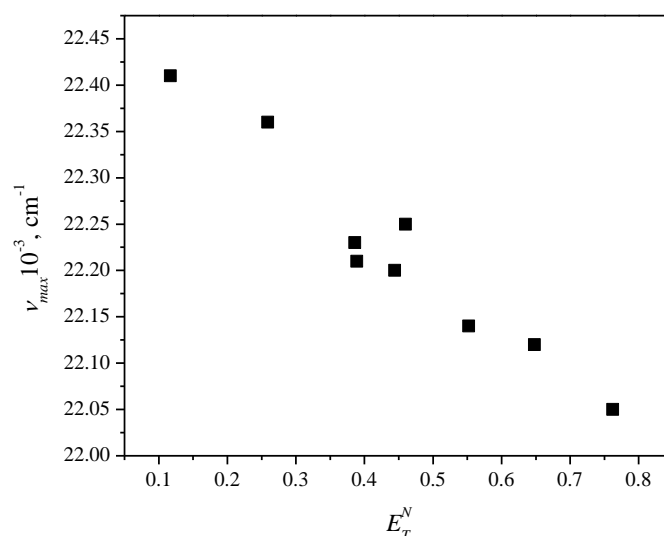


Figure 2. Correlation obtained between values of wave numbers of compound **2** and E_T^N

From Figure 2 it can be seen that with increasing the polarity of the solvent, the values of the wave numbers decrease, that is, there is a shift of the absorption maxima towards higher wavelengths (bathochromic shift). This is a characteristic of $\pi \rightarrow \pi^*$ electronic transitions in molecules (Antić-Jovanović, 2006), so it can be concluded that precisely these transitions are present in the investigated compounds, which is in agreement with the results published so far (Mirković et al., 2018).

Further correlations were made with the parameters of solvatochromic models (Table 3) in order of quantitative analysis of the interactions that occur between the synthesized azo dyes and the solvents used.

Kamlet-Taft's solvatochromic model

Results obtained using Kamlet-Taft's solvatochromic model, as well as statistical parameters are presented in Table 4. Table 5 gives these results in percentages for easier interpretation of the solvent's effects. Observing the values of regression coefficients (a, b and s) it can be concluded that the highest impact on absorption shifts within compounds **1**, **2**, **4**, and **6** have polarizability and dipolarity of the solvents used, while for compounds **3**, **5**, and **7** acidity is the solvent's property that affects the most. For all compounds basicity of the solvents has the lowest impact on spectral changes. A negative sign in front of every value of regression coefficients indicates that with the increase of solvent's acidity, basicity, and polarizability/dipolarity bathochromic shifting of the absorption maxima of the investigated dyes is expected. Observing the values of correlation coefficients obtained

for all compounds ($r^2 = 0.909-0.994$), it is assumed that the selected solvatochromic model is suitable for interpreting the solvatochromism of azo dyes.

Table 4. Results obtained using Kamlet-Taft's solvatochromic model

	$\nu_0 \cdot 10^{-3}, \text{cm}^{-1}$	$a \cdot 10^{-3}, \text{cm}^{-1}$	$b \cdot 10^{-3}, \text{cm}^{-1}$	$s \cdot 10^{-3}, \text{cm}^{-1}$	r^2	F
1	23.114 (± 0.050)	-0.182 (± 0.031)	-0.087 (± 0.045)	-0.274 (± 0.057)	0.909	17
2	22.574 (± 0.037)	-0.214 (± 0.023)	-0.210 (± 0.033)	-0.227 (± 0.042)	0.965	46
3	25.618 (± 0.021)	-0.337 (± 0.013)	-0.200 (± 0.019)	-0.305 (± 0.024)	0.994	273
4	23.671 (± 0.055)	-0.251 (± 0.034)	-0.247 (± 0.050)	-0.269 (± 0.063)	0.944	28
5	24.017 (± 0.023)	-0.172 (± 0.014)	-0.099 (± 0.022)	-0.113 (± 0.026)	0.971	57
6	23.081 (± 0.047)	-0.178 (± 0.029)	-0.149 (± 0.043)	-0.268 (± 0.054)	0.924	20
7	21.083 (± 0.021)	-0.242 (± 0.013)	-0.169 (± 0.019)	-0.217 (± 0.024)	0.989	145

Table 5. Percentage shares of the regression coefficients of the Kamlet-Taft's model

Compound	a, %	b, %	s, %
1	33.52	16.02	50.46
2	32.87	32.26	34.87
3	40.02	23.75	36.23
4	32.72	32.20	35.07
5	44.79	25.78	29.43
6	29.92	25.04	45.04
7	38.54	26.91	34.55

In order to confirm the correctness of the used solvatochromic model, experimentally obtained values of absorption frequencies ($\nu_{exp} \cdot 10^{-3}, \text{cm}^{-1}$) were correlated with values obtained by theoretical calculations ($\nu_{calc} \cdot 10^{-3}, \text{cm}^{-1}$). Results are presented in Figure 3. Figure 3 shows great linear dependency with the value of correlation coefficient $r^2 = 0.999$ which indicates that the chosen solvatochromic model is adequate for the interpretation of the solvatochromism of the synthesized aryl azo dyes.

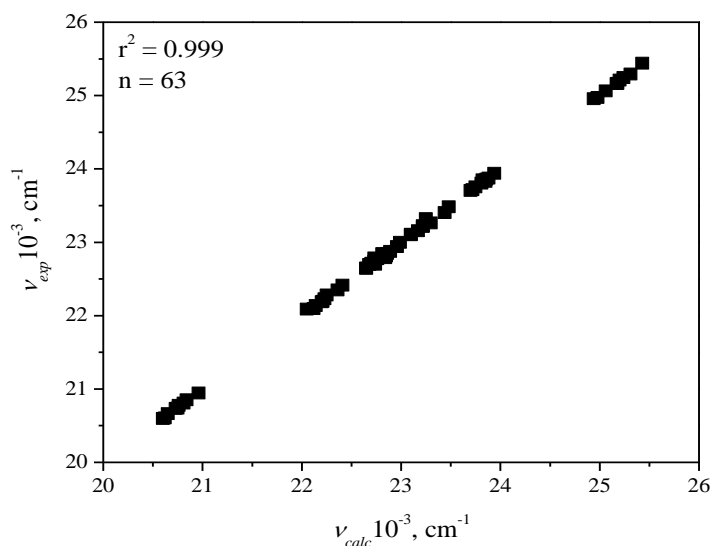


Figure 3. Correlation of calculated values with experimentally obtained results (Kamlet-Taft)

Catalan's solvatochromic model

Another solvatochromic model was used for quantification of the solvent's effect on spectral changes of synthesized aryl azo pyridone dyes. Results obtained using Catalan's model are presented in Tables 6 and 7.

Table 6. Results obtained using Catalan's solvatochromic model

	$\nu_0 \cdot 10^{-3}, \text{cm}^{-1}$	$a \cdot 10^{-3}, \text{cm}^{-1}$	$b \cdot 10^{-3}, \text{cm}^{-1}$	$c \cdot 10^{-3}, \text{cm}^{-1}$	$d \cdot 10^{-3}, \text{cm}^{-1}$	r^2	F
1	23.182 (± 0.145)	-0.305 (± 0.058)	/	-0.176 (± 0.028)	-0.224 (± 0.071)	0.922	12
2	22.573 (± 0.092)	-0.339 (± 0.037)	-0.125 (± 0.034)	/	-0.265 (± 0.045)	0.978	44
3	25.721 (± 0.158)	-0.564 (± 0.063)	-0.115 (± 0.058)	-0.292 (± 0.227)	-0.219 (± 0.078)	0.965	28
4	23.605 (± 0.174)	-0.385 (± 0.070)	-0.138 (± 0.063)	/	-0.320 (± 0.085)	0.944	17
5	24.030 (± 0.120)	-0.279 (± 0.048)	-0.062 (± 0.044)	/	0.084 (± 0.059)	0.923	12
6	23.066 (± 0.143)	-0.257 (± 0.057)	-0.056 (± 0.052)	/	-0.308 (± 0.070)	0.931	13
7	21.214 (± 0.173)	-0.401 (± 0.069)	-0.118 (± 0.063)	-0.281 (± 0.247)	-0.160 (± 0.085)	0.924	12

Table 7. Percentage shares of the regression coefficients of the Catalan's model

Compound	a, %	b, %	c, %	d, %
1	43.26	/	24.96	31.78
2	46.50	17.15	/	36.35
3	47.39	9.66	24.54	18.40
4	45.67	16.37	/	37.96
5	65.65	14.59	/	19.76
6	41.38	9.02	/	49.60
7	41.77	12.29	29.27	16.67

Within this, model the highest impact on spectral changes of azo dyes has the acidity of the solvents used (except for compound **6**). Some smaller effects have polarizability and dipolarity and again, the smallest impact on solvatochromism has solvent's basicity. Negative values of all regression coefficients indicate the same trend – with the increase of solvent's acidity, basicity, polarizability, and dipolarity bathochromic shifting of the absorption maxima of the investigated dyes is expected. Values of obtained correlation coefficients are in the range from 0.922 to 0.978 and it is assumed that this model is also suitable for interpretation of solvatochromism of investigated azo dyes. In order to confirm the previously stated assumption experimentally obtained values of absorption frequencies ($\nu_{exp} \cdot 10^{-3}, \text{cm}^{-1}$) were correlated with values obtained by theoretical calculations ($\nu_{calc} \cdot 10^{-3}, \text{cm}^{-1}$) for Catalan's model (Figure 4).

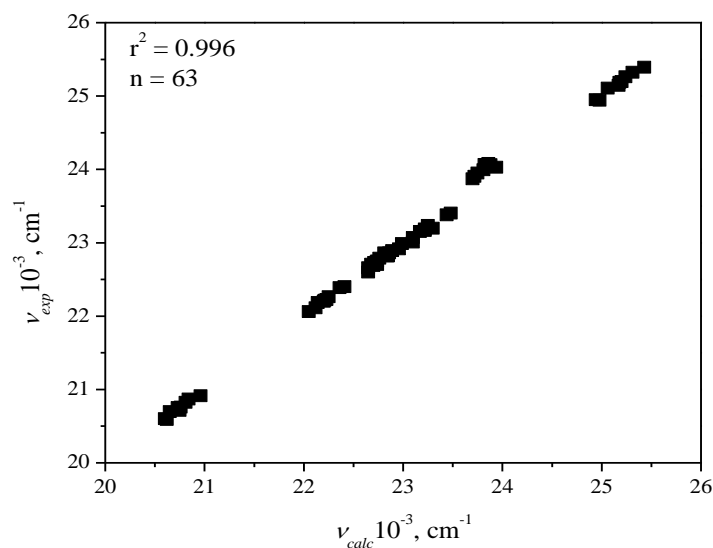


Figure 4. Correlation of calculated values with experimentally obtained results (Catalan)

A high correlation coefficient value obtained again ($r^2 = 0.996$) shows that Catalan's model is also suitable for the determination of solvatochromic properties of synthesized azo dyes.

Conclusion

In this paper, the effect of solvent on spectral changes of seven newly synthesized aryl azo pyridone dyes was determined by the linear solvation energy relationship method (LSER), with the use of two different solvatochromic models – Kamlet-Taft's and Catalan's. Results obtained showed that the highest impact on solvatochromism of investigated dyes, in general, has solvent acidity, followed by dipolarity and polarizability of the solvents. The smallest impact on absorption shift has the basicity of the solvent used. The negative value of every regression coefficient in both models indicates that with the increase of solvent's acidity, basicity, polarizability, and dipolarity bathochromic shifting of the absorption maxima of the investigated will occur. Obtained results as a part of physico chemical characterization of newly synthesized dyes can be further used for studies of potential biological activity.

Acknowledgement: The authors acknowledge financial support of the Ministry of Education, Science and Technological Development of the Republic of Serbia (Grant No. 451-03-68/2022-14/200125)".

References

- Antić–Jovanović, A. (2006). *Molekulska spektroskopija-spektrohemijski aspekti*. Fakultet za fizičku hemiju, Beograd.
- Ashkar, S. M., El-Asasery, M. A., Touma, M. M. & Elnagdi, M. H. (2012). Synthesis of some novel biologically active disperse dyes derived from 4-methyl-2,6-dioxo-1-propyl-1,2,5,6-tetrahydropyridine-3-carbonitrile as coupling component and their colour assessment on polyester fabrics. *Molecules* 17(8), 8822–8831. <https://doi.org/10.3390/molecules17088822>
- Catalan, J. & Hopf, H. (2004). Empirical treatment of the inductive and dispersive components of solute-solvent interactions: The solvent polarizability (SP) scale. *European Journal of Organic Chemistry*, 2004(22), 4694–4702. <https://doi.org/10.1002/ejoc.200400311>
- Catalan, J. (2009). Toward a generalized treatment of the solvent effect based on four empirical scales: Dipolarity (SdP, a new scale), polarizability (SP), acidity (SA) and basicity (SB) of the medium. *Journal of Physical Chemistry B*, 113(17), 5951–5960. <https://doi.org/10.1021/jp8095727>
- Christie, R. M. (2001). *Colour Chemistry*. Royal Society of Chemistry: Cambridge.
- Chudgar, R. J. & Oakes, J. (2003). Dyes, Azo, Kirk-Othmer Encyclopedia of Chemical Technology, 9, 349–430. <https://doi.org/10.1002/0471238961.01261503082104.a01.pub2>
- El-Sonbati, A. Z., Diab, M. A. & Morgan, Sh. M. (2017). Thermal properties, antimicrobial activity and DNA binding of Ni(II) complexes of azo dye compounds. *Journal of Molecular Liquids*, 225, 195–206. <https://doi.org/10.1016/j.molliq.2016.11.047>
- Kamlet, M. J. & Taft, R. W. (1976). The solvatochromic comparison method. I. The β -scale of solvent hydrogen-bond acceptor (HBA) Basicities. *Journal of the American Chemical Society*, 98(2), 377–383. <https://doi.org/10.1021/ja00418a009>
- Kamlet, M. J., Abboud, J. L. & Taft, R. W. (1977). The solvatochromic comparison method. 6. The π^* scale of solvent polarities. *Journal of the American Chemical Society*, 99(18), 6027–6038. <https://doi.org/10.1021/ja00460a031>
- Lubai, C., Xing, C., Kunyu, G. & Jiazhen, H. (1986). Colour and constitution of azo dyes derived from 2-thioalkyl-4,6-diaminopyrimidines and 3-cyano-1,4-dimethyl-6-hydroxy-2-pyridone

- as coupling component. *Dyes and Pigments*, 7, 373–388. [https://doi.org/10.1016/0143-7208\(86\)80005-5](https://doi.org/10.1016/0143-7208(86)80005-5)
- Mirković, J., Božić, B., Vitnik, V., Vitnik, Ž., Rogan, J., Poleti, D., Ušćumlić, G. & Mijin, D. (2018). Structural, spectroscopic and computational study of 5-(substituted phenylazo)-3-cyano 1-ethyl-6-hydroxy-4-methyl-2-pyridones. *Coloration Technology*, 134(1), 33–43. <https://doi.org/10.1111/cote.12321>
- Mishra, V. R., Ghanavatkar, C. W. & Sekar, N. (2019). UV protective heterocyclic disperse azo dyes: Spectral properties, dyeing, potent antibacterial activity on dyed fabric and comparative computational study. *Spectrochimica Acta – Part A: Molecular and Biomolecular Spectroscopy*, 223, Article No. 117353. <https://doi.org/10.1016/j.saa.2019.117353>
- Oberholzer, M. (2005). Concentrated storage-stable aqueous dye solution without any solubilizer content. WO 2005116143
- Radojković-Veličković, M. & Mijin, D. (2001). *Organske boje i pigmenti*, Tehnološko-metalurški fakultet, Beograd.
- Seto, N., Kato, Y. & Fujimori, T. (2006). Colored curable compositions containing phthalocyanine and pyridone azo dyes and manufacture of color filters using them with excellent light and heat resistance. JP 2006071
- Taft, R. W. & Kamlet, M. J. (1976). The solvatochromic comparison method. 2. The α -scale of solvent hydrogen-bond donor (HBD) Acidities. *Journal of the American Chemical Society*, 98(10), 2886–2894. <https://doi.org/10.1021/ja00426a036>
- Tanaka, M., Kawamura, M., Murai, Y., Hirose, M. & Miyazak, T. (2012). Colorant compound and ink including the colorant compound. US 8211221.

CHEMICAL ENGINEERING

Preliminary Report

BIOBASED UNSATURATED POLYESTER RESINS REINFORCED WITH NATURAL FILLERS

Olga Pantić¹, Vesna Panić², Sanja Savić¹, Maja Marković², Melina Kalagasidis Krušić³, Pavle Spasojević²

¹Institute of Chemistry, Technology and Metallurgy, University of Belgrade, Belgrade, Serbia

²Innovation Center of Faculty of Technology and Metallurgy, University of Belgrade, Belgrade, Serbia

³Faculty of Technology and Metallurgy, University of Belgrade, Belgrade, Serbia

Abstract

Using natural fillers can provide several benefits as they are abundant, low cost, and non-toxic. In this paper two different natural fillers were examined, rosehip seed flour and hemp fibres, both of which were varied in weight ratios. A highly biobased unsaturated polyester resin was synthesized as a matrix. Characterization of thus obtained composite materials consisted of examining mechanical properties by uniaxial tensile test, FTIR spectroscopy and gel content analysis.

Keywords: biobased materials, natural fillers, itaconic acid, sustainable development.

Introduction

Polymer composite materials consist of two phases, polymer matrix phase and reinforcement (fillers). Polymer matrices keep intact the fillers that contribute to the strength of composite materials. Composite materials are considered as vital materials in the modern world due to their combined properties, namely their light weight, good stiffness, high strength, high temperature stability, resistance to moisture, weather and corrosion stability, which are not possible with the individual components (Devaraju & Alagar, 2019).

In recent years biobased polymer composites have been the subject of many research projects in both industry and academia (Li et al., 2019). Growing global environmental and social concern, the high rate of depletion of petroleum and new environmental regulations has forced the search for new composite materials and green materials, compatible with the environment.

Unsaturated polyester resins (UPRs) are the most adaptable and industrially important group of thermosetting polymers. UPRs are the most widely used thermosetting polymer resins in the form of coating and matrices, making up around three fourths of all the thermoset resins used in the production of polymer composite materials (Devaraju & Alagar, 2019).

Commercially available UPRs are mainly synthesized from petroleum (Ahamad et al., 2001; Malik et al., 2000), containing two main components, namely unsaturated polyesters and reactive diluents. Unsaturated polyester is synthesized by the polycondensation of diacids with diols. These diacids and diols are mostly extracted and produced from petroleum. Furthermore, it has been found that the industrially used reactive diluent styrene poses a potential health risk and has a negative effect on the environment (Li et al., 2019). Transitioning to biobased UPRs is a complex, costly and time-consuming process. Using different combinations of petroleum based and biobased monomers can be the first step to achieving a fully biobased UPR, since acting in this way lowers the dependence of petroleum (Zhu et al., 2016).

In contrast to the polymer matrix phase, the use of biobased fillers is far more present. Natural fillers are renewable and are cheaper alternatives to synthetic or inorganic ones and have several advantages

such as low density and biodegradability (Satyanarayana et al., 2009; Taj et al., 2007). In this paper one set of experiments was conducted where hemp fibres were used as filler, while the second set of experiments was conducted where rosehip seed flour was used as filler. The criteria for these fillers was their difference in shape, i.e. round particles and fibres.

We examined how two different shapes of natural fillers affected the properties of a highly biobased UPR. UPR was prepared from itaconic acid, succinic acid, propylene glycol, neopentyl glycol with dimethyl itaconate as a reactive diluent. The obtained composite materials were characterized by uniaxial tensile testing, FTIR spectroscopy and gel content analysis.

Materials and Methods

Itaconic acid, succinic acid, propylene glycol, neopentyl glycol, hydroquinone and toluene were supplied from Acros Organics. The catalyst, FASCAT 4100 was procured from PMC Organometallics. The initiator, methyl ethyl ketone peroxide, activator, cobalt octoate, and reactive diluent dimethyl itaconate (DMI) were all supplied by Sigma Aldrich. All chemicals were used as received.

UPRs are obtained by the polycondensation reaction between itaconic acid, succinic acid, propylene glycol and neopentyl glycol, with the mole ratio of 1:1:1.05:1.05, respectively. Toluene (0.5 wt.% based on monomers) was used to increase the rate of water removal. Hydroquinone (150 ppm) was added as a free radical scavenger and the components were mixed. The reaction was carried out in a three-neck round-bottom flask equipped with a stirrer, Dean-Stark and thermometer, and under nitrogen atmosphere. The temperature range was 110 to 190 °C and was raised by 10 °C every hour. The reaction was carried out until the acid value reached 35. Obtained prepolymer was cooled to 90 °C and diluted in dimethyl itaconate (60% w/w with respect to the prepolymer).

The prepared UPRs were mixed with methyl ethyl ketone peroxide (2.5% w/w) and cobalt octoate (1% w/w), after natural fillers were added in different weight ratios (10, 20 wt.%). Preparation of reinforcements included sifting rosehip seed flour through 300 µm sieves and drying in an air oven at 70 °C for 5 hours, while hemp fibres were cut to length of 3000 µm. After homogenization, the mixtures were poured into Teflon moulds, which were placed in an air oven for 24 hours at 60 °C to cure. Additionally, all the samples were kept at 120 °C for 2 hours to harden. The acid value was defined as the number of milligrams of KOH needed to neutralize 1 g of resin and was measured according to ASTM D465-01. Around 0.5 g of resin was titrated with a KOH equimolar solution of toluene and isopropyl alcohol (0.3 mol/L).

Chemical composition of obtained composite materials were determined by Fourier Transform Infrared spectroscopy. The Fourier Transform Infrared (FTIR) spectra of powdered samples were recorded in transmittance mode for the wavelength range of 600 – 4000 cm⁻¹ with a resolution of 4 cm⁻¹, using Nicolet™iS10 FTIR Spectrometer.

The gel content was calculated by extraction in tetrahydrofuran (THF). The cured samples were cut into rectangular shapes, with dimensions of 40 × 10 × 4 mm, and their weight was determined (W_i). Such prepared samples were immersed into THF for 28 days at room temperature. The insoluble fractions, which correspond to the inflated polymer network, were filtered, carefully dried under vacuum, and then measured (W_{sol}). The gel content was calculated as follows:

$$GC (\%) = W_{sol} / W_i \times 100 \quad (1)$$

The uniaxial tensile mechanical properties of the investigated composite materials were evaluated using the Shimadzu Autograph AGS-X servo-hydraulic testing machine, equipped with a 1 kN load cell at room temperature according to ASTM D638. Four measurements were performed for each sample, at a testing rate of 2 mm/min. The average values of the break stress and break stroke strain,

the standard deviations and Young's modulus were determined. Young's modulus was calculated by the software TRAPEZIUM X from the linear part of the stress-strain curve.

Results and discussion

The chemical structure of cured UPR (c-UPR), rosehip seed flour (RSF) and hemp fibres (HF) were analyzed by FTIR spectroscopy and corresponding spectra are shown in Figure 1. The spectra of c-UPR show a band at 1720 cm^{-1} that corresponds to C=O stretching vibrations, that derives from itaconic acid and succinic acid, and indicate an ester bond forming between carboxyl and hydroxyl groups (Baharu et al., 2015; Brännström et al., 2017). Band at 2950 cm^{-1} found in this spectra correspond to C-H stretching vibrations. Bands from 1300 to 1000 cm^{-1} are related to C-O-C and C-O vibrations of ester bonds.

The FTIR spectra of both RSF and HF show a broad characteristic band at 3310 cm^{-1} which corresponds to -OH stretching vibrations. The double peaks at 2925 and 2850 cm^{-1} are related to C-H stretching. FTIR spectra of RSF shows a specific band maximum in the 1200 to 1000 cm^{-1} region. This region is dominated by ring vibrations overlapped with stretching vibrations of C-OH side groups and the C-O-C glycosides bond vibration (Neagu et al., 2013). FTIR spectra of HF shows a characteristic band at 1020 cm^{-1} which corresponds to C-OH vibrations (Dai & Fan, 2010).

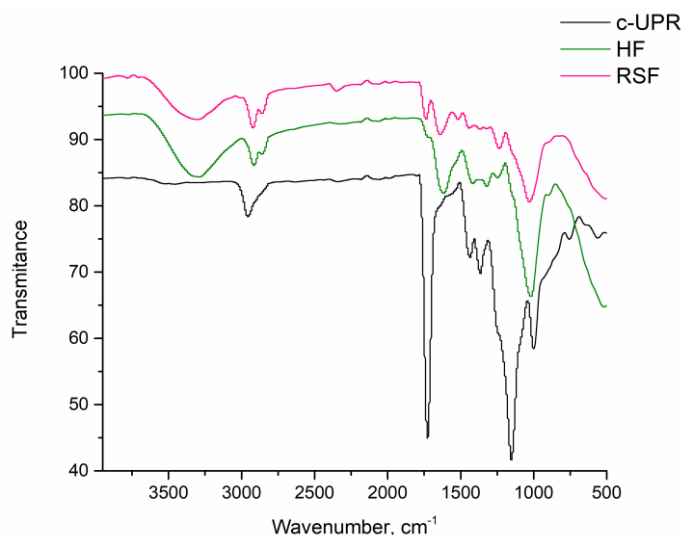


Figure 1. FTIR spectra of c-UPR, HF and RSF

The FTIR spectra of obtained composite materials with different weight ratios of natural fillers are shown in Figure 2. Wide band at 3310 cm^{-1} corresponds to -OH stretching vibrations and it increases with increasing filler ratio. It is noticeable that samples where hemp fibers were used as filler have more -OH groups present in its structure than samples where rosehip seed flour was used as filler, since the increasing of this band is more prominent. It is also noticeable that all composite materials formed peaks at 2850 and 2350 cm^{-1} when compared to c-UPR. The peak at 2850 cm^{-1} corresponds to C-H symmetrical stretching vibrations.

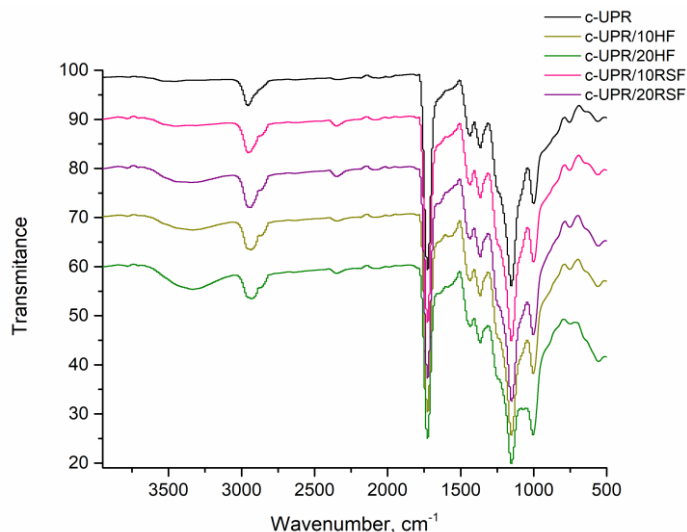


Figure 2. FTIR spectra of obtained composite materials

Gel content analysis was used to assess the degree of crosslinking. Namely, unreacted monomers, oligomers and non-crosslinked polymer chains would dissolve in THF and leach out from the sample. In other words, a lower value of gel content indicated a lower degree of crosslinking. The results of this analysis are very indicative of mechanical properties. The obtained values of gel content are given in Table 1. It is noticeable that weight ratio of fillers doesn't affect the degree of crosslinking since in both sets of composite materials similar value of gel content are obtained. Furthermore, the presence of rosehip seed flour has a greater effect on the polymerization reaction than hemp fibers since samples that used this type of filler have lower degree of crosslinking when compared to samples that used hemp fibers as filler.

Table 1. Results of gel content analysis (GC) and uniaxial tensile testing

Samples	GC, %	Young's modulus, MPa	Break stress, MPa	Break strain, %
c-UPR	99.44	974.3	29.2	666
c-UPR/10RSF	87.92	553.1	10.7	2.9
c-UPR/20RSF	87.25	332.8	5.2	2.3
c-UPR/10HF	91.72	746.5	23.6	4.5
c-UPR/20HF	92.25	873.7	23.6	3.4

The mechanical properties of obtained composite materials as well as neat UPR were examined by uniaxial tensile test. The obtained results are summarized in Table 1. Highest break stress was obtained for c-UPR, presence of fillers lowered this value. The drop in break stress is more prominent for samples that used rosehip seed flour as filler, and it is clear that with growing weight ratio break stress is decreasing. It is interesting that samples with hemp fiber fillers also showed a drop in break stress value, but the weight ratio doesn't seem to affect this parameter.

The presence of natural fillers has led to weakening of mechanical properties, this is mainly due to the lower crosslink density witnessed by lower values of gel content. Furthermore, lower mechanical properties could be a consequence of poor interactions between fillers and resin. Potentially, when the compatibility problem is resolved, characterization of samples with higher filler content could be the next step. Using higher contents of filler could result in composite materials with desired mechanical properties while also being lightweight, which are commercially favorable properties.

Conclusion

In this paper hemp fibres and rosehip seed flour particles were used as fillers for a highly biobased UPR. Their potential as composite material fillers were examined using several different methods. FTIR spectroscopy showed little interactions between resin and natural fillers. This was confirmed by poor mechanical properties of both composite materials when compared to neat UPR. To achieve better mechanical properties, it is necessary to increase these interactions. To achieve this objective several approaches can be used, such as chemical modifications of natural fillers, physical modifications of natural fillers and modifying the UPR matrix by additives and using compatibilizers to provide increased interactions among composite components.

Acknowledgement: This work was supported by the Ministry of Education, Science and Technological Development of the Republic of Serbia (Contract No. 451-03-68/2022-14/200026).

References

- Ahamad, A., Mohan, A., Safeer, M. & Thachil, E. T. (2001). Synthesis of unsaturated polyester resin—Effect of anhydride composition. *Designed Monomers and Polymers*, 4(3), 260–267. <https://doi.org/10.1163/156855501750536242>
- Baharu, M. N., Kadhum, A. A. H., Al-Amiery, A. A. & Mohamad, A. B. (2015). Synthesis and characterization of polyesters derived from glycerol, azelaic acid, and succinic acid. *Green Chemistry Letters and Reviews*, 8(1), 31–38. <https://doi.org/10.1080/17518253.2014.991810>
- Brännström, S., Malmström, E. & Johansson, M. (2017). Biobased UV-curable coatings based on itaconic acid. *Journal of Coatings Technology and Research*, 14(4), 851–861. <https://doi.org/10.1007/s11998-017-9949-y>
- Dai, D. & Fan, M. (2010). Characteristic and performance of elementary hemp fibre. *Materials Sciences and Applications*, 1(06), 336. <http://dx.doi.org/10.4236/msa.2010.16049>
- Devaraju, S. & Alagar, M. (2019). Unsaturated Polyester–Macrocomposites. In *Unsaturated Polyester Resins* (pp. 43–66). Elsevier.
- Li, Q., Ma, S., Xu, X. & Zhu, J. (2019). Bio-based unsaturated polyesters. In *Unsaturated Polyester Resins* (pp. 515–555). Elsevier.
- Malik, M., Choudhary, V. & Varma, I. K. (2000). Current status of unsaturated polyester resins. *Journal of Macromolecular Science, Part C: Polymer Reviews*, 40(2–3), 139–165. <https://doi.org/10.1081/MC-100100582>
- Neagu, M., Pascu, D. E., Traistaru, G. A., Cretu, G., Nechifor, A. C., Bunaciu, A. A. & Aboul-Enein, H. Y. (2013). Membrane separation and concentration study of biological active compounds. *Analytical Chemistry Letters*, 3(5–6), 314–321. <https://doi.org/10.1080/22297928.2013.861165>
- Satyanarayana, K. G., Arizaga, G. G. & Wypych, F. (2009). Biodegradable composites based on lignocellulosic fibers—An overview. *Progress in polymer science*, 34(9), 982–1021. <https://doi.org/10.1016/j.progpolymsci.2008.12.002>
- Taj, S., Munawar, M. A. & Khan, S. (2007). Natural fiber-reinforced polymer composites. *Proceedings-Pakistan Academy of Sciences*, 44(2), 129.
- Zhu, Y., Romain, C. & Williams, C. K. (2016). Sustainable polymers from renewable resources. *Nature*, 540(7633), 354–362. <https://doi.org/10.1038/nature21001>

Original scientific article

POSSIBILITIES OF CROSSLINKING SILICONE MATERIALS IN EXCESS OF CROSSLINKER WITH TWO TYPES OF FILLERS

Darko Manjenčić¹, Marko Paić¹, Vesna Cvijetinić², Vladan Mičić², Anja Manjenčić³, Duško Kostić², Pero Dugić⁴

¹Faculty of Maritime Academic Studies Belgrade, Bulevar vojvode Putnika 7, 11000 Belgrade, Serbia

²University of East Sarajevo, Faculty of Technology, Karakaj 34a, 75400 Zvornik, Republic of Srpska, Bosnia and Herzegovina

³University of Belgrade, Faculty of Medicine, Dr Subotića 8, Belgrade, Serbia

⁴University of Banja Luka, Faculty of Technology, Bulevar vojvode Stepe Stepanovića 73, 78 000 Banja Luka, Bosnia and Herzegovina

Abstract

Due to their polymer networks, nanocomposites are mainly used in those applications where traditional networks are not able to meet the needs satisfactorily. One of the goals of this study is, therefore, to develop a process that would enable the manufacture of silicone polymer networks with improved mechanical, elastic and thermal properties. The motivation behind this goal was the desire to develop new composite materials with unique mechanical, or thermo-mechanical properties that would allow silicone materials to be used in a wider range of applications. The paper analyzes the influence of the siloxane matrix structure and addition of nanofillers on the mechanical properties of siloxane elastomers. The focus of the study is the influence of possible interactions between the fillers and polymer matrices at the supramolecular level on the mechanical properties of siloxanes. It can be concluded that the addition of nanosilicon(IV)oxide leads to the increase in tensile strengths of the samples, where the increase is more significant at higher filler loadings, that is, the samples with 5 wt% of the filler. The elongation at break also increases with the addition of the filler, so that the fillers, along with increasing the strength, increased the elasticity of the siloxane materials. The focus of the study was to investigate the influence of nanoparticles on the properties of elastomeric materials based on different siloxane precursors. FTIR spectroscopy confirmed the presumed structure of the polysiloxane and the obtained siloxane elastomeric nanocomposites. It was found that the addition of silicon(IV)oxide nanoparticles leads to an increase in hardness and tensile strength of the siloxane elastomers.

Keywords: elastomers, nanocomposites, silica, silicones.

Introduction

Designing the properties of materials, or material structuring, is particularly important for their application. One of the methods that may be used in materials design is crosslinking the ensembles of siloxane macromolecules in composite materials.

Research in the field of nanocomposite materials is mainly focused on the structure-properties relationship. Considering the fact that polymer nanocomposites are becoming the pillar of modern polymer industry, the durability of these materials in different exploitation settings and degradation upon usage lifespan are increasingly seen as the key areas of research (Witt et al., 2013; Xie et al., 2017).

Polyorganosiloxanes (whose general formula is $-(\text{SiR}_2\text{-O})_n-$, where R represent a monovalent organic substituent) are the first commercial category of polymers with an inorganic structure of the main

chain, which has even become the most important such category today. The most common substituents on the atom of silicon are methyl, phenyl, 1,1,1-trifluoropropyl, hydrogen and vinyl group, the most important being polydimethylsiloxane, PDMS. The unique combination of PDMS properties is a result of the characteristic siloxane bond. PDMS is an extremely flexible molecule with an almost free rotation along the main chain. The freedom of movement in the PDMS molecule, both in rotation and in the mobility of the segmental chain, allows for the increase in the interchain spacing, whereas weak intermolecular interactions make it significantly more elastic compared to corresponding carbon polymers, which gives them numerous unusual properties. Flexibility and weak intermolecular forces also result in low surface energy, low solubility and low dielectric constant. Polydimethylsiloxanes are transparent and resistant to UV light and ozone, and they are very stable to atomic oxygen. Other interesting features of polydimethylsiloxane materials are permeability for numerous gases, hydrophobicity, ability to form films, surface activity, and extreme chemical and physical inertness. Siloxanes are widely used in medicine owing to their high biocompatibility, biological inertness, non-toxicity (they do not cause irritation), efficiency (characterized by their ability to be applied to the skin and to be permeable to therapeutic substances) and stability (high chemical inertness and ability to retain physical and chemical properties at the skin's temperature), (Owen, 1981; Sanchez & Ribol, 1994). The crosslinking process most commonly used nowadays in polysiloxane chains is known as "addition reaction" (Figure 1). Numerous parameters are investigated in addition reactions in silicon coatings – namely, the structure of the reactive silicon polymer (the type and number of functional alkenyl groups per molecule and molecular mass), the type and structure of the crosslinker, the type, functionality and structure of the siloxane resin, etc. Since functional silicone polymers are becoming more and more available, addition reactions in silicone coatings have now started to develop (Kanar, 2006; Okumara & Ito, 2001).

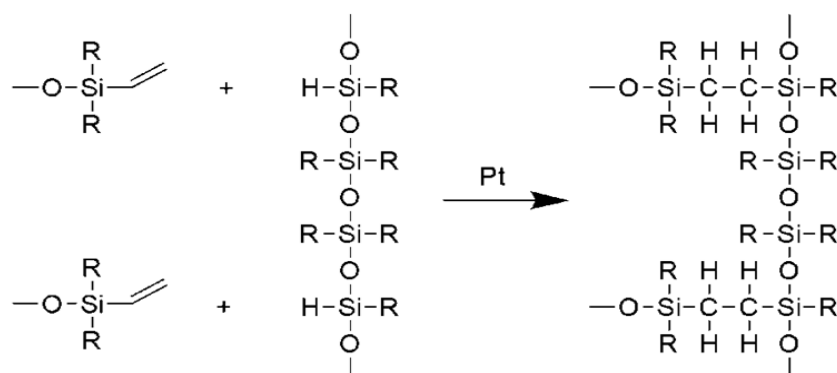


Figure 1. Addition crosslinking of siloxane by hydrogen siliconization using a Pt - catalyzed

Materials and Methods

Materials

Vinylpolydimethyldisiloxane (HANSA SFA 42500, manufactured by CHT GMBH BEZEMA) with a content of vinyl of 0.19 mmol/g, Mw 34 500 g/mol, Brookfield viscosity at 20 °C -500 mPas. Methyl Hydrogen Polysiloxane fluid (HANSA SFA 11230, manufactured by CHT GMBH BEZEMA) with a content of hydrogen of 2.3 mmol/g, Mw 19 800 g/mol, Brookfield viscosity at 25 °C of 210 mPas. Methyl silicone resin (ALPA-RETARD manufactured by CHT GMBH BEZEMA) with a 20% content of the active component, Mw 5640 g/mol $\text{Me}_n\text{SiH}_m\text{O}_y$ type, viscosity at 25 °C was 75 mPas. A complex of platinum polydimethylsiloxane containing vinyl groups (ALPA-KAT manufactured by CHT GMBH BEZEMA) with a content of vinyl of 0.5 mmol/g, Brookfield viscosity at 20 °C of 800 mPas. Silicon(IV)oxide with a specific surface area of 130 m²/g and an average size of primary

particles of 16 nm (Aerosil R 972 (hydrophobic filler), manufactured by Degussa). Silicon(IV)oxide with a specific surface area of 200 m²/g and an average size of primary particles of 12 nm (Aerosil A 200 (hydrophilic filler), manufactured by Degussa).

With the Methyl Hydrogen Polysiloxane crosslinker, a number of methyl groups was substituted by hydrogen —polymethylhydrosiloxane, HPDMS, (CH₃)₃Si-O-((CH₃)Si(H)-O)_n-Si(CH₃)₃. The structure of this network precursor was given in Figure 2.

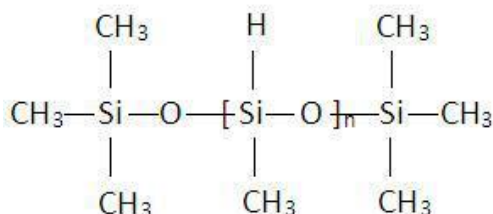


Figure 2. The structure of polymethylhydrosiloxane

Preparation of siloxane elastomers and siloxane nanocomposites

Siloxane elastomers were prepared by a conventional method, with the hydrogen- and vinyl-siloxane ratios of 65:35. All syntheses were performed by the addition of the catalyst (0.2 wt%) and the inhibitor (0.1 wt%), calculated on the total weight of monomers. First, all components were mixed in a round bottom flask at room temperature on a magnetic stirrer for 1 h at 100 rpm. Nanocomposites were synthesized by adding of 1, 5, 20 % hydrophobic and hydrophilic fillers immediately to the reaction mixture and mixing thoroughly all the components for 1 h. The reaction mixture was then treated in an ultrasonic bath for 15 min and poured into the mold. Then the samples were poured into molds and cured at 80 °C for 1 h in a vacuum oven. The major difference between hydrophilic and hydrophobic silicon dioxides is, in fact, in the difference between silanol and siloxane functional groups within a particular silicon dioxide, as shown in Figure 3. Hydrophobic behavior is a consequence of the reaction between the hydrophilic silanol group with organic groups.

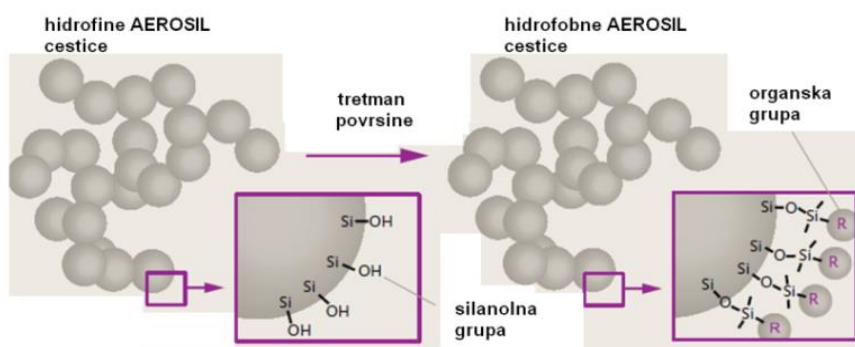


Figure 3. Surface treatment which converts hydrophilic AEROSIL® into hydrophobic AEROSIL

Characterization of obtained materials

Infrared spectroscopy (FTIR) - FTIR spectrophotometer

Silicon samples were tested on a Thermo-Nicolet Nexus 670FTIR spectrometer. The measurements were made using an ATR (attenuated total reflection) accessory with a single reflection on a germanium crystal. The same pressure was used for each sample in order to obtain the same air penetration depth. Each sample was scanned 100 times at a resolution of 4 cm⁻¹. A deuterated triglycine sulfate, DTGS, was used as a detector. The spectra were analyzed using a Thermo-Nicolet Omnic 6.0 software.

Mechanical properties

Mechanical properties such as tensile strength and elongation at break were calculated based on the ASTM 412-98a standard, on a universal INSTRON device, model 1195 (England), at 50 cm/min. Hardness was determined using the ASTM D2240 standard with a 306L type a durometer model. Hardness values are expressed in hardness units (Shore A).

Results and discussion

Physical properties of elastomeric materials are directly dependent on the concentration of elastically active network chains, on the number and type of junctions, which, in turn, depend in a certain way on the composition of the crosslinking system applied. The structure of an elastomeric material can be reduced and improved using novel silicon dioxide fillers. The results of the FTIR analysis for the molecular structure of the samples of silicone elastomers without the addition of nano fillers are given in Figure 4 and Table 1. Two sharp bands at 2961 cm^{-1} and 2905 cm^{-1} originated from the asymmetric and symmetric C-H stretching vibrations of Si-CH₃. Characteristic peaks of the siloxane matrix that originated from the functional groups Si-CH₃, Si-O-Si, and Si-C are clearly observed. The absence of peaks at wave lengths greater than 3000 cm^{-1} shows the quantitative reaction of the C=C double bond in vinyl siloxanes. H/Vi 65/35 siloxanes with a lower proportion of vinyl siloxane do not give a peak of lower intensity at 3080 cm^{-1} , which shows that all double bonds have reacted (Figure 4).

Table 1. Characteristic bands in the FTIR spectrum for the samples of silicone elastomers without the addition of nano fillers

Wavelength, cm^{-1}	Functional group
3000 - 2800 cm^{-1}	CH ₃ and CH ₂ group
1450 cm^{-1}	Asymmetric elongation of CH ₃
~1420 cm^{-1}	CH ₂ bending
~1260 cm^{-1}	Si-CH ₃
~1250 cm^{-1}	(CH ₃) ₃ - Si
1130 - 1000 cm^{-1}	Si-O-Si
1000 cm^{-1}	Si-O
790 cm^{-1}	Si-C and CH ₃ twisting

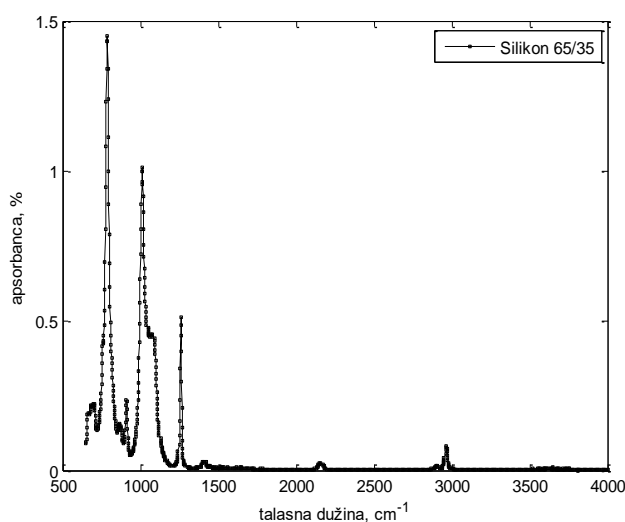


Figure 4. FTIR spectrum of crosslinked siloxane elastomer obtained from HPMS and ViPDM: SiH/Vi 65/35 without the addition of nano fillers

Figure 5 shows that the filler did not react chemically with the polymer matrix, though there were physical interactions resulting from the structural similarities between the filler and the matrix. These

similarities were also the reason for intensive interaction between the SiO₂ hydrophobic fillers and the siloxane matrix. The highest Si-O range moved at 1100 cm⁻¹ in the composites containing hydrophilic silicon(IV) oxide, which is indicative of a lower intensity of physical interaction between the filler and the matrix. Based on the surface activity and the geometry of the filler, filler-filler and polymer-polymer systems exhibited only physical interactions as the primary reinforcement mechanism. The absence of hydroxyl bond vibrations between 3200 cm⁻¹ and 4000 cm⁻¹ signifies that the surface OH groups of the fumed silica were successfully consumed by bonding with the silicon atom in the siloxane moiety in the PDMS. The addition of nanoparticles into the samples of Sil H/Vi 65/35 did not affect the positions of bands in the FTIR spectra of the obtained siloxanes, because the system already had an excess of H from poly(methylhydrosiloxane), so that the added nanoparticles can only react with poly(methylhydrosiloxane), which does not result in the formation of new bands in the FTIR spectrum.

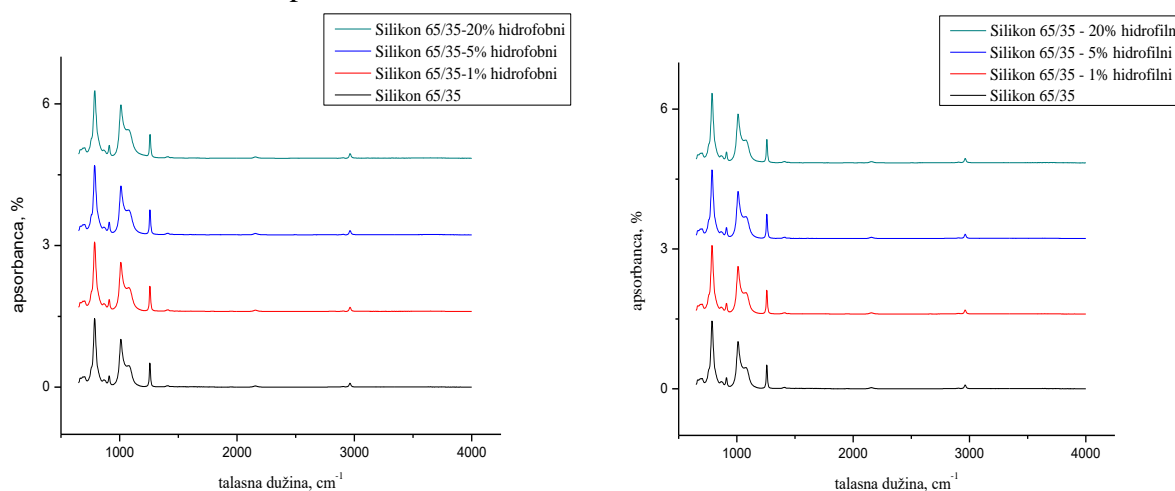


Figure 5. FTIR spectra of crosslinked siloxane elastomers obtained from HPMS and ViPDM: Sil H/Vi 65/35 with the addition of 1, 5, 20 % hydrophobic and hydrophilic fillers

The research conducted on HPDMS (Methyl Hydrogen Polysiloxane) and ViPDM (Vinyl polydimethylsiloxane) – Sil H/Vi (Methyl Hydrogen Polysiloxane and Vinyl polydimethylsiloxane) 65/35 siloxanes used as precursors for crosslinking shows that the mobility of the ensembles of macromolecules around the nanofiller particles changes depending on the content of the nanofiller, which is the explanation for the effect they have on material reinforcement. Table 2 gives the data on the mechanical properties of the synthesized samples of siloxane composites with the addition of hydrophobic and hydrophilic fillers. The values given are tensile strength (maximum load), elongation at break, energy necessary to deform the sample, and hardness (according to Shore A). With a Sil H/Vi 65/35 ratio, tensile strength is unexpectedly low – 0.546 MPa, and elongation is 37.48%, probably due to a better configuration of the network formed; this is because in this case there are no vinyls that were not used up in the reaction, but only an excess of HPDMS, which, again, have a lower molar mass, and thus more easily incorporated into the network topology. Table 2 clearly shows that the addition of nanosilicon (IV) oxide increases the tensile strength in the samples, with more significant increases occurring only with 5wt% filler loadings and higher. Elongation at break also rises with the addition of the filler which means that the filler, apart from increasing the strength, also increases the elasticity of silicone materials. This is to be expected considering the chemical composition of the filler and the matrix, thus proving that silicon dioxide fillers are beneficial for optimizing the desired properties of silicone elastomers. Moreover, the comparison of the energy required to deform or break the sample, shows that the increase in the content of the filler also increases the energy of deformation of crosslinked siloxane elastomers.

Table 2. Mechanical properties of siloxane elastomers HPDMS and ViPDMS- Sil H/Vi 65/35 with the addition of hydrophobic and hydrophilic fillers

Samples	Tensile strength, MPa	Elongation at break, %	Strain energy, J	Hardness, Shore A
Sil H/Vi 65/35	0.546	37.48	0.00638	62
Sil H/Vi 65/35-1-h-phob	0.787	37.29	0.00680	65
Sil H/Vi 65/35-2-h-phob	1.132	36.78	0.011	65
Sil H/Vi 65/35-5-h-phob	2.97	44.82	0.031	70
Sil H/Vi 65/35-10-h-phob	6.82	80.21	0.065	71
Sil H/Vi 65/35-20-h-phob	5.307	86.38	0.053	73
Sil H/Vi 65/35-1-h-phil	0.699	39.39	0.0061	64
Sil H/Vi 65/35-2-h-phil	1.584	45.08	0.0086	65
Sil H/Vi 65/35-5-h-phil	2.46	97.19	0.014	67
Sil H/Vi 65/35-10-h-phil	3.84	138.19	0.046	70
Sil H/Vi 65/35-20-h-phil	6.65	186.34	0.326	75

Conclusion

Siloxanes or polysiloxanes, are most certainly one of the most interesting classes of polymers. They have unique properties that distinguish them from all other polymers, they exhibit extremely high mobility of polymer segments and equilibrium flexibility, which gives them extra ordinary surface properties and lowest glass transition temperatures among all polymers. The synthesis of siloxane elastomers involves the process of vulcanization as a result of crosslinking linear siloxane polymers, the so-called reactive polymers. FTIR spectroscopy confirmed the structure of polysiloxane and the obtained elastomer nanocomposites as expected. It was established that the addition of highly active silicon(IV) oxide increases hardness and tensile strength. The results clearly lead to the conclusion that the addition of nanosilicon(IV) oxide causes the increase in the tensile strength of the samples, where the increase is more significant at higher filler loadings, that is, the samples with 5 wt% of the filler. The increase in elongation at break in the materials with hydrophilic silicon dioxide is noticeable, though lower when compared to nanocomposites with hydrophobic fillers, due to the lower interaction between the hydrophobic matrix and hydrophilic fillers, or the lower compatibility of the two phases. The improvement in the mechanical properties is a result of the increase in network density, thus proving that silicon(IV) oxide fillers are a very good option for optimizing the properties of siloxane elastomers.

References

- Kanar, N. (2006). Silicone PSAs: Trends in the east and west. *29th Pressure Sensitive Tape Council Technical Seminar*. Las Vegas.
- Okumura, Y. & Ito, K. (2001). The polyrotaxane gel: a topological gel by figure-of-eight cross-links. *Adv. Mater*, 13, 485–487.
[https://doi.org/10.1002/15214095\(200104\)13:7%3C485::AID-ADMA485%3E3.0.CO;2-T](https://doi.org/10.1002/15214095(200104)13:7%3C485::AID-ADMA485%3E3.0.CO;2-T)
- Owen, M. J. (1981). Why silicones behave funny. *Chemtech*, 11(5), 288–292.
- Sanchez, C. & Ribol, F. (1994). Design of hybrid organic-inorganic materials synthesized via sol-gel chemistry. *New Journal of Chemistry*, 18(10), 1007–1047.
- Xie, Y., Geng, C., Liu, X., Xu, S., Xing, W., Zhang, Z., Zhang, Z. H., Zhang, Y. & Bi, W. (2017). Synthesis of highly stable quantum-dot silicone nanocomposites via in situ zinc-terminated polysiloxane passivation. *Nanoscale*, 43 (9), 16836–16842.
- Witt, N., Tang, Y., Lin, Y. & Fang, L. (2013). Silicone rubber nanocomposites containing a small amount of hybrid fillers with enhanced electrical sensitivity. *Mater Des.* 45, 548–554.
<http://dx.doi.org/10.1016%2Fj.matdes.2012.09.029>

Original scientific article

PHOSPHATE GLASSY FERTILIZERS

Vladimir S. Topalović¹, Jelena D. Nikolić¹, Srdjan D. Matijašević¹, Veljko V. Savić¹, Marija S. Djošić¹, Ana M. Vujošević², Snežana R. Grujić³

¹Institute for the Technology of Nuclear and other Mineral Raw Materials-Belgrade, Serbia

²University of Belgrade, Faculty of Agriculture-Belgrade, Serbia

³University of Belgrade, Faculty of Technology and Metallurgy-Belgrade, Serbia

Abstract

The main goal of agricultural production should be the production of a sufficient amount of agricultural products with the least possible impact on the environment. In traditional agricultural production, to obtain a satisfactory yield, artificial fertilizers are used, which have multiple negative impacts on the environment. Glassy fertilizers are a type of fertilizer that, at least according to previous research, do not have a negative impact on the environment, and at the same time the use of these fertilizers yields no less than when using traditional fertilizers. Glassy fertilizers are fertilizers with controlled dissolution, they do not pollute groundwater or surface water, and the pH of the soil does not change with their use, by changing the composition they can adapt to the requirements of each crop individually, etc. The paper presents three phosphate glassy fertilizers of different chemical compositions, obtained at the Centre for Inorganic Technologies, ITNMS. The method of obtaining glassy fertilizers, their dissolution rates in a medium that simulates soil conditions, the changes in pH values of solutions for different dissolution times, and the effect of temperature on dissolution rates are shown. Also, the results of the influence of glass fertilizers on plant cultures in real conditions are presented.

Keywords: glassy fertilizers, phosphate, dissolution rate.

Introduction

Controlled release fertilizers (CR fertilizers) are those materials that have nutrients for the plant and can dissolve after some time from the moment of introduction into the soil ("to delay their availability"), they are available to the plant much longer than conventional fertilizers (Calabi-Floody et al, 2018). One of the groups of ecological CR fertilizers is glassy fertilizers (GF). These glasses have a polymer structure, and the glass network can be made up of one, two, or more network builders, while cations of different metals are placed in the cavities (Ersundu et al., 2022). Various macro (K, P, Mg, Ca) and micro (B, Fe, Mo, Cu, Zn, Mn) nutrients, necessary for the growth and development of plants, can be included in the composition of glass in a relatively simple way (Cacini et al, 2020). The dissolution of glass is a complex process that takes place in several stages and which, apart from the chemical composition and granulation of the glass, also depends on the temperature, pH of the solvent, time of action, etc. (external conditions). The total dissolution time can be designed to favor or inhibit one of these phases. During the growing season, plants intensively consume the components that are separated from the glass, and thus the driving force for the dissolution process increases. The solubility of glassy fertilizers can be adjusted to a certain plant culture or natural conditions (climate

and soil characteristics), by changing the chemical composition and granulation of the glass (Sirotkin et al, 2012).

The use of GF in agricultural production has a positive impact on the natural environment and does not lead to a decrease in yield, they do not wash into the lower layers of the soil because the unused part of the glass remains in the upper layers of the soil, the nutrients are easily accessible, etc. (Szumera et al, 2005). Research shows that by using GF, plants get a sufficient amount of nitrogen because these glasses encourage the activity of microorganisms from the soil to bind nitrogen from the air into forms suitable for plant nutrition (Karapetyan et al, 2004).

This paper presents three phosphate GF of different chemical compositions, obtained at the Center for Inorganic Technologies, ITNMS. The method of obtaining glassy fertilizers, their dissolution rates in a medium that simulates soil conditions and the effect of temperature on dissolution rates are shown. Also, the results of the influence of glass fertilizers on plant cultures in real conditions are presented.

Materials and Methods

The appropriate glass batches compositions were prepared from reagent-grade raw materials $(\text{NH}_4)_2\text{HPO}_4$, K_2CO_3 , CaCO_3 , SiO_2 , MgO , ZnO , Fe_2O_3 , CuO , B_2O_3 , and MnO_2 in an open porcelain crucible (the preparation of the glass batches described in the patent, number 61428 (2021)-The Intellectual Property Office of the Republic of Serbia). The glasses mixture was melted at $T = 1100$ °C (GF2) and 1300 °C (GF1, GF3) for $t=1\text{h}$ in an electric furnace, and the melt was quenched on a steel plate. Powder X-ray diffraction (XRD) analysis confirmed the quenched melt to be vitreous (data not shown). The chemical composition of glass was determined by gravimetric (Si) and spectroscopic methods, *i.e.*, by AAS using a PERKIN ELMER 703 instrument (Ca, K, Mg, Cu, Zn, Fe, B-standard solutions 1000 $\mu\text{g}/\text{ml}$) and UV/VIS spectroscopy using a PHILIPS 8610 spectrophotometer (P- standard solutions 1000 $\mu\text{g}/\text{ml}$) The chemical composition of the glasses is presented in Table 1.

The chemical stability of the glasses (granulation 0.3-0.65 mm) was determined in a 2% citric acid solution (a solution that simulates the environment around plant roots) at several temperatures.

Results and discussion

Table 1. presents the analyzed composition of the glasses.

Table 1. Chemical composition of glasses

	Macronutrients			SiO ₂	Micronutrients				
	P ₂ O ₅	K ₂ O	CaO +MgO		ZnO	CuO	Fe ₂ O ₃	MnO	B ₂ O ₃
CRG1	65	17	10	3	-	-	-	-	5
CRG2	60	22	10	2	0.5	2	3	0.5	-
CRG3	45	25	25	3	1	-	-	1	-

For the analysis of structure, this glasses were considered as a binary one: $z\text{Me}_{2/x}\text{O} \cdot (1-z)\text{NFO}$ where Me are ion modifiers (K, Ca, Mg, Zn, Cu, Fe, Mn), z is a molar fraction of oxides and x is the valence of the Me atoms; NF is network former ions (P, Si, B). For $0 \leq z \leq 0.5$ the glass is ultraphosphate and for $z > 0.5$ the glass is polyphosphate (Brow, 2000). Based on the chemical analysis of the glasses (Table 1), it is concluded that the CRG1 and CRG2 belong to ultraphosphate glasses, while CRG3 belongs to the group of polyphosphate glasses. Figure 1 shows the chemical stability of all three glasses in an acidic environment at a temperature of 37 °C. From Figure 1, it can be seen that the concentration profiles are similar. The dissolution process is initially very intense (initial phase),

while after 15 h it slows down significantly (transitional phase) and enters the stationary phase (final phase). CRG1 and CRG3 dissolve faster than CRG2 (Figure 2) because the composition of this glass contains divalent and trivalent cations that connect the phosphate network and make it more resistant. Divalent cations form chelate structures, which are more resistant to the action of acids. CRG1 dissolves and has a slightly higher dissolution rate than CRG3. Including B_2O_3 into phosphate glasses often improve their chemical durability because of the formation of P-O-B bonds, which exhibit higher resistance to hydrolysis than P-O-P bonds. This small difference in dissolution rate is probably because the ionicity of the P-O-Ca bond is lower than that of the B-O-Ca and B-O-K bonds and it is more flexible and less resistant to the action of H^+ ions (Lee et al, 2022).

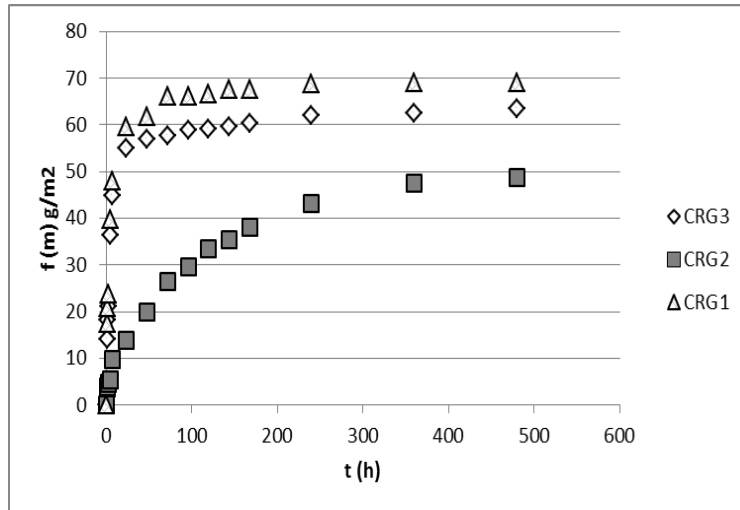


Figure 1. Dependence of normalized mass release $f(m)$ on dissolution time at 37 °C

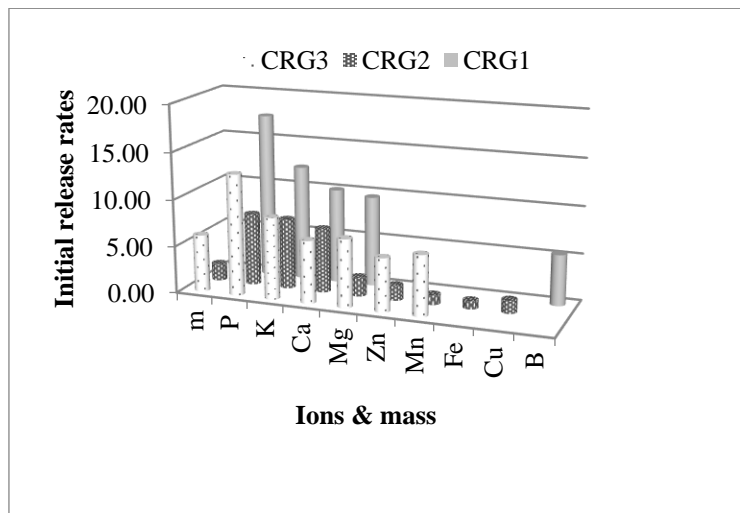


Figure 2. Initial release rates of the ions and mass

Figure 3 shows the influence of temperature on the dissolution process of CRG3. The concentration profiles for the other two glasses are similar (data not shown). It can be seen that with increasing temperature, the initial phase is shortened and the changes become abrupt (sharper). The final phase expands and the slopes of changes in this phase increase with temperature.

All three vitreous fertilizers were tested in real conditions for feeding different plants, in the greenhouse of the Faculty of Agriculture, University of Belgrade.

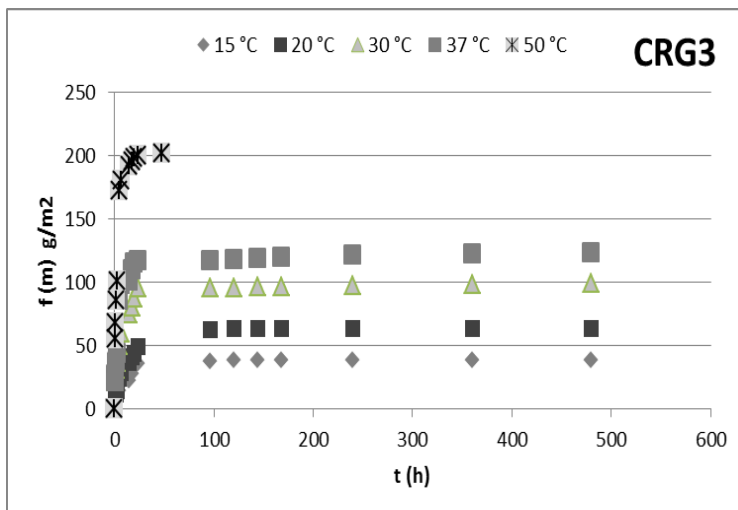


Figure 3. Dependence of normalized mass release f(m) on dissolution time for CRG3

The obtained results show that these fertilizers have a positive effect on the growth and development of plant crops. Table 2 shows some of the basic statistics indicators for examined quality parameters of Capsicum annum L seedlings fed with CRG2.

Table 2. The basic statistics indicators for examined quality parameters of Capsicum annum L seedlings

Parameters	Dosage of phosphate glass	I _v Interval of variation	$\bar{x} \pm S \bar{x}$ Arithmetical mean \pm Standard error	M _e Median	C _v (%) Coefficient of variation
Plant height (cm)	0 (test)	25.1– 40.3	31.370 \pm 1.638	30.450	16.508
	1 g/l	33.4 – 41.4	37.350 \pm 0.890	37.000	7.535
	2 g/l	25.6 – 37.9	32.690 \pm 1.297	33.700	12.545
	3 g/l	28.4 – 40.7	34.370 \pm 1.279	34.150	11.764
	4 g/l	23.8 – 35.4	30.700 \pm 1.271	31.650	13.090
Number of leaves	0 (test)	17.0 – 55.0	28.4 \pm 3.407	26.000	37.931
	1 g/l	24.0 – 33.0	27.3 \pm 0.803	26.500	9.307
	2 g/l	21.0 – 31.0	25.4 \pm 1.861	24.500	13.789
	3 g/l	15.0 – 33.0	22.8 \pm 0.876	21.500	25.807
	4 g/l	13.0 – 36.0	26.2 \pm 2.973	30.500	35.886

Based on the parameters of development examined it was determined that the glass dosage of 1 g/l is optimal. This dosage was affected significantly by an increase in average height and the overground mass of the plants. Concerning other additives for improvement of the substrates (mineral fertilizers, vermicompost, etc.), by addition of polyphosphate glass, better development of pepper seedlings was attained.

Conclusion

This paper presents three phosphate glassy fertilizers (CRG1, CRG2, and CRG3) of different chemical compositions, the method of obtaining them, their dissolution rates in a medium that simulates soil conditions, and the effect of temperature on dissolution rates. The dissolution process is initially very intense (initial phase), while after 15 h it slows down significantly (transitional phase)

and enters the stationary phase (final phase). CRG1 and CRG3 dissolve faster than CRG2 because the composition of this glass contains divalent and trivalent cations that connect the phosphate network and make it more resistant. With increasing temperature, the initial phase is shortened and the changes become abrupt. The obtained results show that these fertilizers have a positive effect on the growth and development of plant crops. Based on the parameters of development examined it was determined that the CRG2 dosage of 1 g/l is optimal for pepper seedlings (*Capsicum annuum* L).

Acknowledgment: This work was supported by the Ministry of Education, Science and Technological Development of the Republic of Serbia (Contract No. 451-03-68/2022-14/200023 and Contract No. 451-03-68/2022-14/200135).

References

- Brow, R. K. (2000). Review: the structure of simple phosphate glasses. *Journal of Non-Crystalline Solids*, 263&264, 1–28. [https://doi.org/10.1016/S0022-3093\(99\)00620-1](https://doi.org/10.1016/S0022-3093(99)00620-1)
- Cacini, S., Rinaldi, S., Massa, D., Nesi, B., Epifani, R. & Trinchera, A. (2020). The effect of a glass matrix fertilizer and compost amendment on plant growth and mineral nutrition of two container-grown *Rose* spp. Cultivars. *Scientia Horticulturae*, 274, 109660. <https://doi.org/10.1016/j.scienta.2020.109660>
- Calabi-Floody, M., Medina, J., Rumpel, C., Condrón, L. M., Hernández, M., Dumont, M. & Mora, M. (2018). Chapter Three-Smart fertilizers as a strategy for sustainable agriculture, *Advances in Agronomy*, 147, 119–157. <https://doi.org/10.1016/bs.agron.2017.10.003>
- Ersundu, M. C., Kuzu, B. & Ersundu, A. E. (2022). Structural properties and dissolution behavior of new generation controlled release phosphate glass fertilizers. *Journal of Non-Crystalline Solids*, 576, 121239. <https://doi.org/10.1016/j.jnoncrysol.2021.121239>
- Lee, S., Shiraki, S., Nagata, F., Kato, K., Sakurai, M. & Kasuga, T. (2022). Structure and dissolution behavior of boron-containing calcium phosphate invert glasses. *Journal of Non-Crystalline Solids*, 590, 121690. <https://doi.org/10.1016/j.jnoncrysol.2022.121690>
- Karapetyan, G., Karapetyan, K., Maksimov, L. (2004). Glassy environmentally friendly fertilizers of prolonged action. *Phosphorus Bulletin*, 15, 60–67. https://www.jstage.jst.go.jp/article/prb1992/15/0/15_60/_pdf
- Sirotkin, S., Meszaros, R. & Wondraczek, L. (2012). Chemical Stability of Zn-Na₂O-SO₃-P₂O₅. *International Journal of Applied Glass Science*, 3(1), 44–52. <https://doi.org/10.1111/j.2041-1294.2011.00076.x>
- Szamera, M., Waclawska, I., Mozgawa, W. & Sitarz, M. (2005). Spectroscopic study of biologically active glasses, *Journal of Molecular Structure*, 744–747, 609–614. <https://doi.org/10.1016/j.molstruc.2005.01.023>

CHEMICAL TECHNOLOGY

Original scientific article

MINEROLOGICAL AND CHEMICAL CHARACTERIZATION OF CLAY FROM THE ZAGONI SITE MUNICIPALITY OF BRATUNAC

Dragana Kešelj¹, Dragica Lazić¹, Zoran Petrović¹, Nebojša Vasiljević¹

¹University of East Sarajevo, Faculty of Technology Zvornik, Republic of Srpska, Bosnia and Herzegovina

Abstract

Clay is the basic raw material for obtaining various ceramic materials. In nature, it is formed by the decomposition of complex silicate rocks, which form clays of different physical characteristics, mineral and chemical composition. The aim of this work was to perform mineralogical and chemical characterization of clay from the locality Zagoni, municipality of Bratunac. Chemical analysis revealed a high content of SiO₂ (59.39%) and a relatively low content of other components, which are chemical contaminants of clay (Fe₂O₃ + TiO₂ + CaO + MgO). Based on the obtained experimental results, the clay can be classified into semi-acidic clays with a low content of coloring oxides. The presence of quartz and kaolinite minerals was registered in the clay by XRD and thermal methods of analysis. The granulometric composition of this clay is uneven, and fifty percent of the particles have an average diameter of 8.54 μm. The examination determined that the clay "Zagoni" swells poorly under the action of water.

Keywords: clay, kaolin, quartz, mineralogical composition, chemical analysis.

Introduction

Clay is a polymineral raw material, which is formed due to mechanical and chemical decomposition of rock masses. The composition of clay includes clay minerals (kaolinite, montmorillonite, illite, dickite, nacrite, etc.), then various carbonates, iron oxides, quartz, etc. (Brzaković, 2000; Kostić-Gvozdrenović & Ninković, 1997; Tecilović-Stevanović, 1990; Hamzabegović, 2015).

For decades, clay has been successfully used in many industries, such as the building materials industry, refractory ceramics, electrical ceramics, but also in the field of ceramic art (Filipović-Petrović et al., 2018). It was initially used to build simple ceramic pottery. Over time, the range of clay products increased, from low-quality products (pots and vases made of clay, pots obtained by drying, etc.), through baked clay products (these products were of low quality and could not tolerate high temperatures) to baked products of high quality and resistance to high temperatures (fire resistance).

The suitability of clays for different uses in certain industries and their capability to fulfill certain technological requirements are influenced by their physical-chemical, mineral and technological characteristics. Therefore, it is extremely important to characterize the clay before its application, which means determining the chemical and mineral composition, granulometric composition, as well as different technological characteristics (sensitivity to drying, plasticity, swelling, etc.).

Clays can be classified according to different parameters: origin, mineralogical composition, Al₂O₃+TiO₂ content, content of colored oxides, refractoriness, sintering ability, content of finely dispersed fractions, etc. (Brzaković, 2000; Kostić-Gvozdrenović & Ninković, 1997; Tecilović-Stevanović, 1990; Hamzabegović, 2015; Filipović-Petrović et al., 2018).

According to the content of $\text{Al}_2\text{O}_3 + \text{TiO}_2$ in the annealed state, clays are classified as high-base, base, semi-acidic and acidic clays (Table 1).

Table 1. Classification of clays according to the content of $\text{Al}_2\text{O}_3 + \text{TiO}_2$ in the annealed state

A group of clay raw materials	Content of $\text{Al}_2\text{O}_3 + \text{TiO}_2$ (%)
High-base	>40
Base	30-40
Semi-acidic	15-30
Acidic	< 15

The color of the clay can vary from white, yellow, gray, to even black. The presence of components which do not belong to clay minerals determines the color of the clay and the ceramic material obtained from it. These components include organic matter, iron oxides, titanium oxide, etc. (Vulićević-Krstić, 1981). Clays can also be classified according to the content of colored oxides (Fe_2O_3 and TiO_2) (Table 2) into those with very low, low, medium and high content of colored oxides.

Table 2. Classification of clays according to the content of colored oxides

A group of clay raw materials	Content of Fe_2O_3 (%)	Content of TiO_2 (%)
with a very low content of colored oxides	-	<1
with a low content of colored oxides	< 1.6	<1
with a medium content of colored oxides	1.5-3	1-2
with a high content of colored oxides	> 3	>2

The ability of clay to absorb and retain water is a property that is closely related to the plasticity of clay. Hygroscopicity depends on the specific surface area of the clay particles, and is larger if the particles are smaller or finer. Closely related to water absorption is the notion of normal clay consistency, which gives clay dough with the highest plasticity and tear strength. In practical application, the term normal consistency of clay dough means a consistency in which the clay contains the maximum amount of water, and the clay mass does not stick to the fingers. According to their absorption or hydrophilicity, clays can be divided into high-plasticity, medium-plasticity and low-plasticity clays.

Aluminum hydrosilicates (clay minerals) are minerals that are the main constituents of clay (Bravin, 1999). In addition to clay minerals, clay may also contain quartz (SiO_2), limestone (CaCO_3), dolomite ($\text{CaCO}_3 \cdot \text{MgCO}_3$), hematite (Fe_2O_3), gypsum ($\text{CaSO}_4 \cdot \text{H}_2\text{O}$), organic substances, etc. Clay minerals are divided into two major groups: kaolinite and montmorillonite. The kaolinite group of minerals includes: kaolinite, dickite, nacrite $[(\text{Al}_2(\text{Si}_2\text{O}_5)(\text{OH})_4)]$, halloysite $(\text{Al}_2(\text{Si}_2\text{O}_5)(\text{OH})_4 \cdot 2\text{H}_2\text{O})$ and allophane $[(\text{Al}_2\text{O}_3 \cdot \text{SiO}_2 \cdot n\text{H}_2\text{O})]$ (Tecilović-Stevanović, 1990).

The montmorillonite group includes pyrophyllite $[(\text{Al}_2(\text{Si}_2\text{O}_5)_2(\text{OH})_2)]$, montmorillonite $[(\text{Al}_2(\text{OH})_2\text{Si}_4\text{O}_{10}) \cdot n\text{H}_2\text{O}]$, illite $[(\text{K}, \text{H}_3\text{O})\text{Al}_2[(\text{H}_2\text{O}, \text{OH})_2](\text{Si}, \text{Al})_4\text{O}_{10})]$ and chlorite $[(3\text{Mg}(\text{OH})_2\text{Mg}_3(\text{Si}_2\text{O}_5)_2(\text{OH})_2)]$.

The starting parameters in the characterization and evaluation of clay quality are chemical composition, mineral composition, granulometric composition, plasticity, sensitivity to drying, shrinkage during drying and baking, etc. The whole range of physical, mechanical and technological properties of clay as a raw material for ceramic products is directly dependent on the chemical composition.

Also, all calculations of raw material mixtures in the ceramic industry are based on data on the chemical composition of clay as a raw material. Clay is a complex polymineral system composed of a large number of chemical elements. It usually contains the following elements: Si, Al, Ti, Fe, Ca, Mg, Na, K, Cr, Mn, P, S, H, and in rare cases: Zr, Ni, Co, Ba, Be, Pb, B, C, Cl, F, etc. (Kovačević et al., 2007; Tzozue et al., 2017).

The most important deposits of kaolin raw materials in Bosnia and Herzegovina are located in several ore districts, of which the Srebrenica-Bratunac ore region is very important with the following deposits: "Smoljave-Zagoni", "Tegare", "Borići", as well as several sites with kaolinite phenomena such as: "Bjelavac", "Sikirići", "Vukosavljevići", "Crni Guber" and "Jadar" near Srebrenica and Bratunac. The aim of this paper is to mineralogically and chemically characterize the clay from the Zagoni site, Bratunac municipality.

Materials and Methods

The test methods used in this paper for chemical and mineralogical characterization of clay from the site "Zagoni", Bratunac municipality, are as follows: chemical analysis, thermal analysis, XRD analysis, laser method for determining granulometric composition, swelling ability, and determination of specific mass of clay.

Loss by annealing, moisture content, granulometric composition and thermal analysis were determined on a clay sample which was previously crushed in a mortar and then sifted through a DIN 20 sieve.

Sample preparation for chemical analysis, swelling ability and determination of specific clay mass was performed by drying the sample to a constant mass at 105-110 °C after being crushed and sieved through a DIN 20 sieve (Lee & Yeh, 2008; Randelović et al., 2011; Mitrović et al., 2009; Filipović-Petrović et al., 2008).

The Swell Index or Free Swell (Swelling) test procedure is used to determine the general swelling characteristics of clay. Test method ASTM - D5890 is used to determine the swell index. A 2g sample of dried and finely ground clay is dispersed into a 100 ml graduated cylinder in 0.1g increments. A minimum of 10 minutes must pass between additions to allow for full hydration and settlement of the clay to the bottom of the cylinder. These steps are followed until the entire 2g sample has been added to the cylinder. The sample is then covered and protected from disturbances for a period of 16 - 24 hours, at which time the level of the settled and swollen clay is recorded to the nearest 0.5 ml. The ability to swell depends on the mineral composition, type, shape and specific surface area of clay particles (Table 3) (Vulićević-Krstić, 1981; Filipović-Petrović et al., 2008).

The density of clay refers to the ratio of the mass of an absolutely dry clay sample to the volume that includes pores. Of the many procedures for determining the specific mass, the pycnometer method is the most widely used. There are two techniques for determining the density of clay using the pycnometer method, and they differ in the way air is removed from open pores, cracks and cavities. In the first one, the air is removed by vacuuming, whereas the second one uses boiling the sample with liquid immersion.

Table 3. Influence of mineral composition on swelling ability

Mineral	Particle size (10 ⁻¹⁰ m)	Specific surface area (m ² /g)	Propensity to swell
Montmorillonite	20	800	High
Illite	200	80	Medium
Kaolinite	1000	15	Low

The size and distribution of clay particles was determined on a laser particle size analyzer "Mastersizer 3000" in the laboratory of the Faculty of Technology Zvornik. X-ray diffraction measurements were performed on a Bruck D8 Endeavor powder diffractometer operating on the principle of Bragg-Brentan geometry, with a Ni-filter, using an X-ray tube with cobalt anticathode (CoK_α) with a $\lambda=1.78897 \text{ \AA}$ wavelength radiation. Thermal analysis of a clay sample from Zagoni, Bratunac municipality, was performed on a Netzsch-Gerätebau GmbH - STA 409 CD Simultaneous thermal analyzer, under the following conditions: inert material - Al₂O₃, atmosphere - air, heating rate - 15.0 °C/min and maximum temperature of 1200 °C.

Results and discussion

The whole range of physical, mechanical and technological properties of ceramic raw materials is directly dependent on the chemical composition of the clay. The starting point in the assessment of the quality of clay from the site "Zagoni", municipality of Bratunac, was the chemical analysis. Chemical composition analysis for the purpose of this study included the determination of moisture (W), loss on ignition at 1000 °C (LOI) and determination of the content of SiO₂, Al₂O₃, Fe₂O₃, TiO₂, CaO and MgO.

Chemical analysis of clay (Table 4) revealed a high content of SiO₂ (59.39%) and a relatively low (less than 5%) content of other components (Fe₂O₃+TiO₂+CaO+MgO), which are chemical contaminants of clay.

Table 4. Chemical analysis of the clay sample "Zagoni"

Component	SiO ₂ (%)	Al ₂ O ₃ (%)	Fe ₂ O ₃ (%)	TiO ₂ (%)	CaO (%)	MgO (%)	Loss on Ignition(LOI) at 1000 °C (%)	W (%)
Clay „Zagoni“	59.39	19.16	1.14	1.22	0.7	1.8	7.02	0.49

According to the content of Al₂O₃+TiO₂ in the annealed state (21.92%), the clay from the locality Zagoni, municipality Bratunac, is classified as semi-acidic clay, while according to the content of colored oxides (Fe₂O₃ and TiO₂) it is classified as the clay with a low content of colored oxides. Thermal analysis was used to examine the physico-chemical changes of clay that occur during annealing.

The obtained thermogram (Figure 1) shows the occurrence of phase transformations in the form of temperature maxima at endothermic and exothermic peaks. Two intense peaks are observed: the first at 596.9 °C is characteristic of the endothermic process of dehydration of kaolinite, while the second peak at 1020.6 °C is responsible for the phase transformation of kaolinite into mullite.

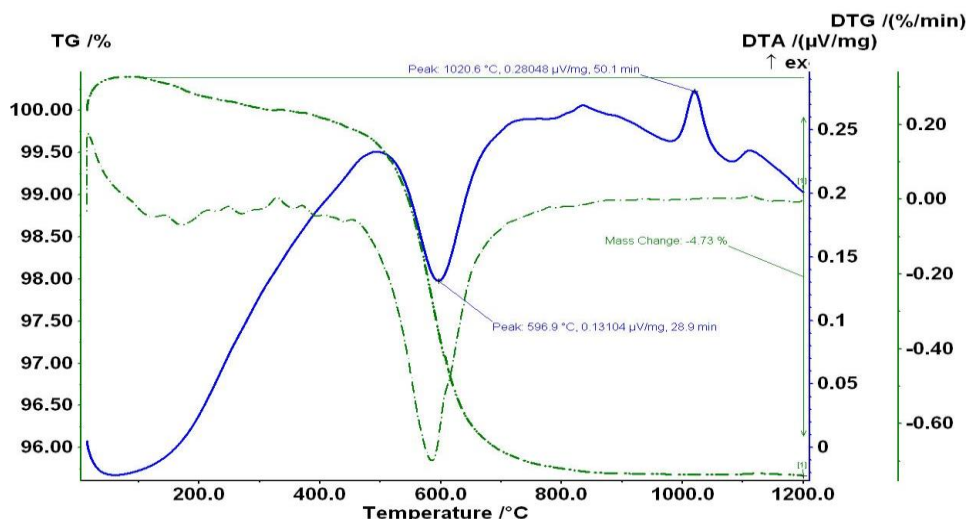


Figure 1. Thermogram of the clay sample "Zagoni"

Comparison of the obtained thermogram of the clay sample "Zagoni" with the thermogram of the standard sample of kaolinite (Figure 2) also confirms the presence of kaolinite in the tested sample. Based on the surface of the peaks, it can be concluded that the sample of clay "Zagoni" is not pure kaolinite, because the surface of the peak corresponding to the dehydration of kaolinite is lower.

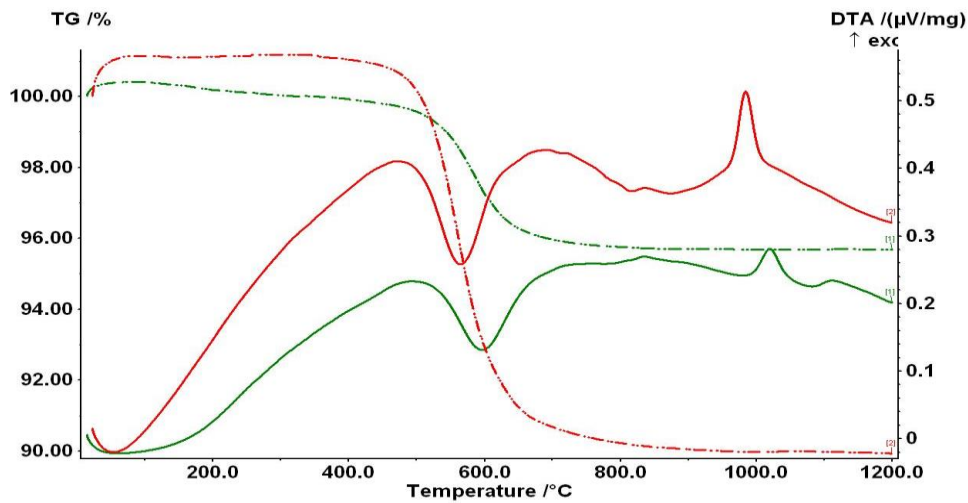


Figure 2. Comparative thermogram of the clay sample "Zagoni" (-) and the kaolinite sample (-)

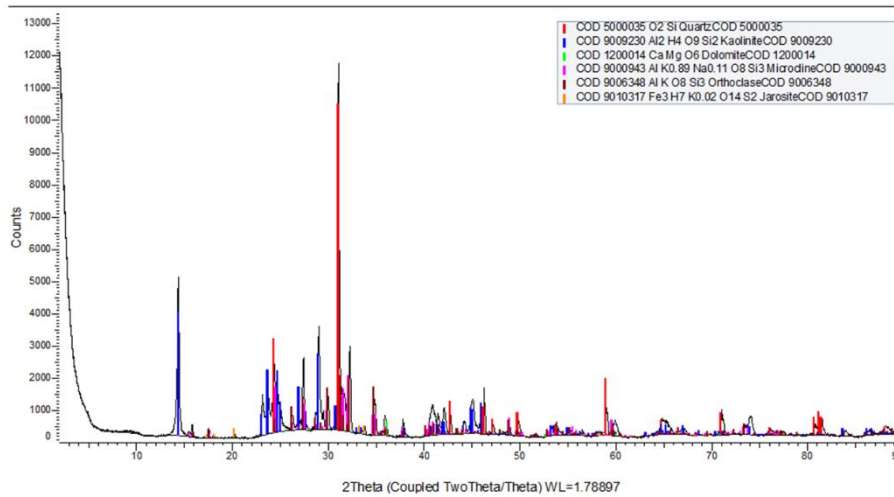


Figure 3. Diffractogram of the clay sample "Zagoni"

Based on the results of XRD analysis (Figure 3), the presence of quartz, kaolinite and dolomite minerals is noticed, and the presence of orthoclase and jarosite is very low.

Based on the chemical analysis (Table 4) and the stoichiometric ratio of SiO_2 and Al_2O_3 masses in kaolinite, the quartz content in the clay sample "Zagoni" can be approximately determined using relation (1).

$$Q = \% \text{SiO}_2 - 1.175\% \text{Al}_2\text{O}_3 = 59.39 - 1.175 \times 19.16 = 32.18\% \quad (1)$$

Clays are polydisperse systems, which means that one of the important characteristic is granulometric composition (grain size and particle distribution).

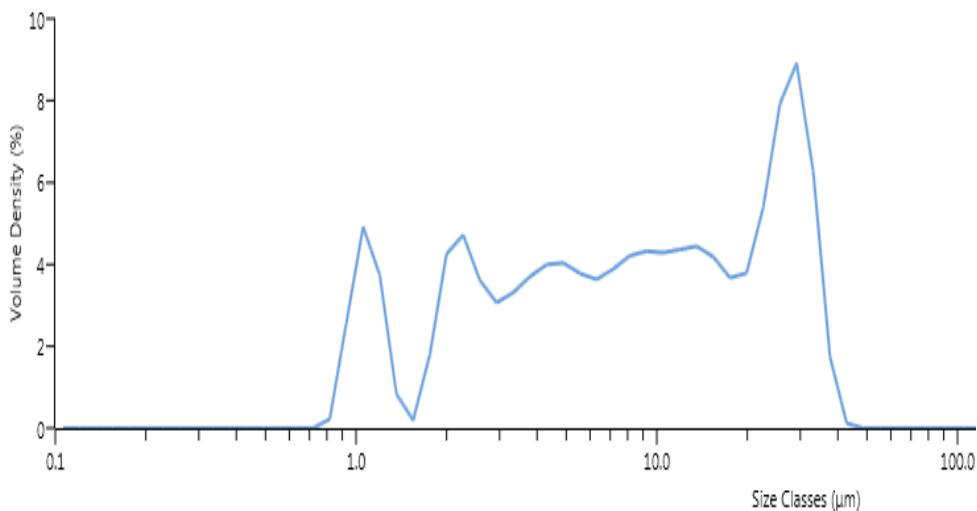


Figure 4. Particle size distribution in the clay sample "Zagoni"

Analysis of the size and distribution of clay particles in the sample "Zagoni" (Figure 4, Table 5) by the laser method showed varying particles size and the mean diameter of 8.54 µm in fifty percent of the particles. Figure 4 clearly shows the distribution of particles into two different groups. The first group, with a granulation of about 1 µm, are characteristic of kaolinite in the sample, while the group of larger particles represent impurities in the examined sample.

Table 5. Granulometric composition in the clay sample "Zagoni"

P,%	10	50	90
Clay sample „Zagoni“ (µm)	1.35	8.54	29.4

The density (ρ) of the clay sample "Zagoni" was determined by the pycnometer method. Air was removed from open pores, cracks and cavities in the clay sample using two techniques: "vacuuming" and "boiling" water with a clay sample.

The density values obtained by the two techniques were similar: $\rho_v = 2.61 \text{ g/cm}^3$ for the "vacuum" method and $\rho_k = 2.54 \text{ g/cm}^3$ for the "boiling" method .

The Swell Index is expressed in $\text{cm}^3/2\text{g}$ of the sample. If the volume of clay inside the graduated cylinder is less than 20, then the swelling is less than $20 \text{ cm}^3/2\text{g}$ of the sample.

Clays with a volume of over 20 are said to swell to a large degree, while the opposite is the case with the clay sample "Zagoni".

Conclusion

Chemical analysis of the clay from the Zagoni site, Bratunac municipality, revealed a high content of SiO_2 (59.39%) and a relatively low (less than 5%) content of other components that represent chemical contaminants of clay ($\text{Fe}_2\text{O}_3 + \text{TiO}_2 + \text{CaO} + \text{MgO}$). Based on the chemical analysis (the content of $\text{Al}_2\text{O}_3 + \text{TiO}_2$ and the content of colored oxides Fe_2O_3 and TiO_2), this clay is classified as semi-acidic and low in the content of colored oxides.

Thermal analysis and XRD analysis revealed the presence of quartz, kaolinite and dolomite minerals. Chemical analysis and stoichiometric ratio of SiO_2 and Al_2O_3 masses in kaolinite showed that the clay from the Zagoni site is contaminated with quartz, whose approximate content is 32.18%.

Previous results show that the clay sample from Zagoni site, Bratunac municipality can be used as a ceramic material.

References

- Bravin, K. (1999). *Inženjerska geologija*. Varaždin: Geotehnički fakultet, Sveučilište u Zagrebu.
- Brzaković, P. (2000). *Priručnik za proizvodnju i primenu građevinskih materijala nemetalnog porekla, Knjiga 2: Betoni i betonski prefabrikati, građevinska keramika, mineralna vuna*. Beograd: Orion Art.
- Filipović-Petrović, L., Miladinović, M., Vujić, V. & Despotović, S. (2008). Chemical-mineralogical and ceramic characteristics dark clay „Jovanovića Brdo”. *21st International Symposium on Mineral Processing*, (pp. 96–100). Bor, Srbija.
- Filipović-Petrović, L., Stanojević, D., Antonijević-Nikolić, M. & Mijić, L. (2018). Mineraloška, fizičko-hemijska i keramička svojstva gline Brezaci. *Zaštita materijala*, 59, 39–44. <https://doi.org/10.5937/ZasMat1801039F>
- Hamzabegović, A. (2015). *Glina kao mineralana sirovina, Zemaljski muzej Bosne I Hercegovine*. Sarajevo: Zemaljski muzej Bosne I Hercegovine.
- Kostić-Gvozdrenović, L. & Ninković, R. (1997). *Neorganska hemijska tehnologija*. Beograd: Tehnološko-metalurški fakultet, Univerzitet u Beogradu.
- Kovačević-Zelić, B., Domitrović, D. & Veinovič, Ž. (2007). Laboratorijska ispitivanja bentonitnih glina za potrebe projektiranja i izgradnje odlagališta. *Rudarsko-geološko-naftni zbornik*, 19, 99–110. Retrieved from <https://hrcak.srce.hr/19297>
- Lee, V. & Yeh, T. (2008). Sintering effects on the development of mechanical properties of fired clay ceramics. *Materials Science and Engineering: A*, 485, 5–13. <https://doi.org/10.1016/j.msea.2007.07.068>
- Mitrović, A., Komljenović, M. & Ilić, B. (2009). Ispitivanje mogućnosti korišćenja domaćih kaolinskih glina za proizvodnju metakaolina. *Hemijska industrija*, 63, 107–113. <https://doi.org/10.2298/HEMIND0902107M>
- Randelović, M., Purenović, M., Zarubica, A., Mladenović, I. & Purenović, J. (2011). Fizičko-hemijska karakterizacija bentonita i njegova primena u uklanjanju Mn²⁺ iz vode. *Hemijska industrija*, 65, 381–387. <https://doi.org/10.2298/HEMIND110322029R>
- Tecilović-Stevanović, M. (1990). *Osnovi tehnologije keramike*. Beograd: Tehnološko-metalurški fakultet, Univerzitet u Beogradu.
- Tzozue, D., Nzeugang, A., Mache, J., Loweh, S. & Fagel, N. (2017). Mineralogical, physico-chemical and technological characterization of clays from Maroua (Far-North, Cameroon) for use in ceramic bricks production. *Journal of Building Engineering*, 11, 17–24. <https://doi.org/10.1016/j.jobbe.2017.03.008>
- Vulićević-Krstić, L. (1981). *Kontrola sirovina, procesa i proizvoda, sa praktikumom za vežbe sa pitanjima i zadacima*. Beograd: Naučna knjiga.

Original scientific article

THE PHOTOSTABILITY AND DYEING ABILITY OF SOME ANTHRAQUINONE REACTIVE DYES FOR COTTON AND PAPER

Polya Miladinova¹, Dimitrina Todorova²

¹Organic Synthesis Department, University of Chemical Technology and Metallurgy, Sofia, Bulgaria

²Department of Pulp, Paper and Printing Arts, University of Chemical Technology and Metallurgy, Sofia, Bulgaria

Abstract

Anthraquinone dyes and their derivatives are a type of colorants with excellent color properties, light and wet fastness and are widely used as dyes, pigments, and colorants in cosmetics, drugs and foods. Furthermore, they have a variety of interesting biological activities and pharmacological effects, such as antiviral, antioxidant, antibacterial, anti-cancer and anti-inflammatory, and to prevent osteoporosis and hypoglycemic activity. The photostability of two blue anthraquinone reactive dyes, synthesized by as in water solution and dyed samples of cotton and paper have been investigated. A comparative analysis has been made with two commercial direct dyes from the Solenis Pergasol™ range. The dyeing of cotton fabrics was carried out with dyes at 2% depth o.w.f. Aiming to prepare woodfree paper for printing and packaging, wet-end chemical additives have been added, in the following sequence: dye fixative - 1% of o.d.f., dye - 0.6% of o.d.f., sizing agent - 1% of o.d.f. and retention additive – 0.05% of o.d.f. The optical properties - L*, a*, b*, C*, and h* from the CIE Lab color space of the resulting textile and paper samples have been examined. As a result of the studies carried out it was found out that the photostability of the examined reactive dyes is about 20-25% higher than that of direct dyes. Bearing in mind that the color characteristics of the dyed samples of cotton and paper do not change significantly during irradiation, it could be concluded that the synthesized anthraquinone dyes are suitable for dyeing of cellulosic materials.

Keywords: triazine reactive dyes, anthraquinone dyes for cotton and paper, photostability.

Introduction

Cotton and paper are the major cellulose fibers and they have a unique combination of properties, including high strength, durability, softness, good dyeability and biodegradability.

Direct dyes are widely used to dye cotton and paper for over 100 years (Benkhaya, 2020; Drzewińska, 2008; Hande, 2022; Holmes, 1922; Ishegbe et al., 2014; Society of Dyers and Colourists, 1995). Pergasol direct dyes are water-soluble synthetic dyes. Chemically they are azo dyes or solubilized pigments. They are used in alkaline or neutral solution especially for dyeing cellulosic material (such as cotton or paper) directly in the presence of electrolytes. Anionic Pergasol™ direct dyes contain several sulfonic or carboxyl groups to activate the dye soluble in water. In solution, the dyes are dissociated into a dye anion and a colorless cation for instance sodium. The dye molecules also exhibit a linear and planar structure, which allows the dye to attach to the cellulose chains in the fiber via intermolecular bonding. Anionic Pergasol dyes are especially suitable for dyeing wood-free papers or papers containing small amounts of lignin and should be added as early as possible, allowing sufficient time for uptake by the stock. In most cases the use of a fixing aid is suggested. Sizing and other process chemicals should preferably be added after the dyes. Cationic Pergasol™ direct dyes have amine groups, providing a net positive charge. The combination of positive charge and relatively

large, planar shape means that cationic direct dyes bond readily to fiber surfaces. Because of their more rapid uptake, cationic dyes are highly suitable for continuous application. Before adding these dyes, it is advisable to be neutralized troublesome anionic trash with cationic fixative for aluminium sulphate (Solenis, 2019). Direct dyes have good light fastness, poor wash fastness, shorter dyeing cycle. However, they bind with cellulose fibres through weak physical forces due to which cotton dyed with direct dyes bleeds when washed (Porter, 1973).

Anthraquinone dyes are very well known in literature, being the second largest class of textile dyes after azo dyes and are used for dyeing of different type of fibres (Baqi, 2022). They are distinguished by their brilliance, good light-fastness and stability of the chromophore under both acid and alkaline conditions. The color of anthraquinone dyes is partially associated with the anthraquinone nucleus and modified by the type, number, and position of substituents. Anthraquinone dyes give a wide range of colors in almost the whole visible spectrum, but they are most commonly used for green, blue and violet hues. Some of the very important blue dyes are derivatives of sodium salt of 1-amine-4-bromo-anthraquinone-2-sulphonic acid (bromamine acid). They are widely used as dyes, pigments and colorants in cosmetics, drugs and foods (Lv et al., 2017; Oprisan et al., 2007; Oyewale et al., 2020; Patel & Patel, 2009).

Among the anthraquinone dyes the reactive ones are the most important class of dyes since they can be linked with the textile fibres through covalent bonds, thus the colored fibres have high fastness to wet treatment. These dyes are widely used in the textile industries for dyeing of cotton, wool, silk, polyamides and other synthetic fibres and have only limited use on practical application in the papermaking process and single reports on laboratory experiments (Shan et al., 2015; Zhang et al., 2019).

Bearing in mind above mentioned, it was of interest to study the photostability and dyeing ability of some anthraquinone reactive dyes and to compare them with some commercial direct dyes used for dyeing of cotton and paper.

Materials, analysis and equipment

We synthesized the anthraquinone dyes as it was reported before (Konstantinova & Miladinova, 2008). Bromamine acid, cyanuric chloride (98%), allylamine and ammonia (25% water solution) were Sigma-Aldrich (Merck) products. The direct dyes Pergasol Türk F-2GN and Pergasol Türk R were Solenis products.

Electronic absorption spectra were recorded on a Hewlett Packard 8452A UV/Vis spectrophotometer in water (concentration 2×10^{-4} g.ml⁻¹).

Dyeing with synthesized reactive dyes (Exhaust at 80 °C) and with direct dyes was performed on 100% cotton (15 x 25 cm) according to standard procedures (Miladinova & Todorova, 2022; Parvinzadeh & Najafi, 2008).

The used fibre raw material for obtaining paper samples is a mixture of bleached kraft cellulose from sprues wood (delivered by SCA, Sweden) and bleached kraft cellulose from beech wood (delivered by Svilosa AD, Bulgaria) in ratio 1:1. The used kraft cellulose were refined by laboratory Jokro mill method with six refining units, acc. ISO 5264-3:1979. The refining concentration in each unit was 6% (16g o.d.f in 267ml water). The celluloses were refined separately and the Schopper Riegler Value as degree SR (ISO 5267-1/AC:2004) of the obtained pulp mixture was 30 °SR.

Aiming to prepare wood-free paper for printing and packaging, wet-end chemical additives have been added to the obtained cellulose fiber raw material, in the following sequence:

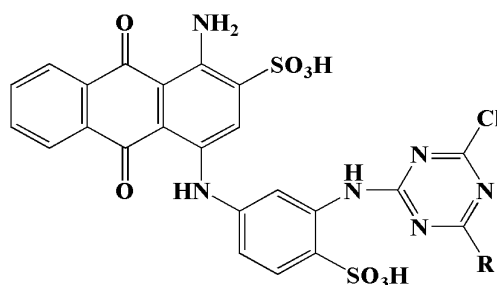
- dye fixative - 1% of o.d.f. (Kemira® Levogen E 1063 LQ);
- investigated two direct and two reactive dyes - 0.6% of o.d.f.;
- alkylketendimer (AKD) sizing agent - 1% of o.d.f (Kemira® Fennosize KD 157YC);

- cationic retention additive – 0.05% of o.d.f. (modified polyacrylamide with molecular weight 11.10^6 g/mol and charge density +1.05 from Ciba Specialty Chemicals-Ciba® Percol®Co (Basel, Switzerland)).

After preparation of each cellulose mixture, the papermaking process was simulated by using laboratory paper-sheet machine. Paper suspensions with concentration of 2% were prepared and paper samples were obtained on paper laboratory machine (Rapid-Kothen, Germany) acc. ISO 5269-2:2005, with a basic weight of 70 g/m^2 , with drying conditions of $-96 \text{ }^\circ\text{C}$ and duration of 7 minutes. The color coordinates L^* , a^* , b^* , C^* , h^* from the CIE Lab color space by Konica Minolta Spectrophotometer CM-3630 from Frank – PTI, according to ISO 5631-2:2008. Irradiation of the dyes (in solution) and the dyed cotton and paper was performed in a Suntest CPS equipment (Heraeus) supplied with a Xenon lamp (Hanau, 1.1 kW, 765 W.m^{-2} , wavelength $\lambda_{\text{max}} = 290 \text{ nm}$).

Results and discussion

The anthraquinone dyes object of the present study can be presented by the following general formula 1:



Formula 1

where the meanings of **R** are $-\text{NH}_2$ (dye RD1) and $-\text{NHCH}_2\text{CH}=\text{CH}_2$ (dye RD2). We synthesized them as it was described before (Konstantinova & Miladinova, 2008). Direct dyes Pergasol Türk F-2GN (dye Dir1) and Pergasol Türk R (dye Dir2) are Solenis products and they were used for comparison with synthesized dyes. The absorption spectra of the investigated dyes were recorded in water with concentration $2 \times 10^{-4} \text{ g.ml}^{-1}$) and are presented in Figure 1.

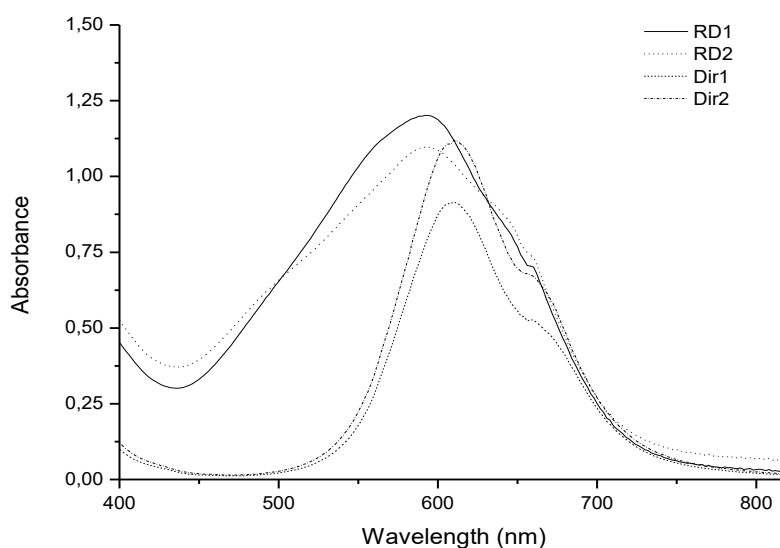


Figure 1. Absorption spectra of the investigated dyes in water

As can be seen from the presented spectra, the reactive dyes DR1 and RD2 absorb in range of 450-700 nm with $\lambda_{\max} = 592$ nm and direct dyes Dir1 and Dir2 - in range of 500-700 nm with λ_{\max} at 610 nm.

Dyeing of cotton fabrics

Cotton fabrics were dyed with the investigated dyes at 2% depth o.w.f. according to procedures mentioned above. Materials with an intense blue color were obtained.

The dye exhaustion (%) and dye fixation ratio (%F) was determined spectrophotometrically. The extraction rate of the dyes was found to be between 85-90% and the fixation rate was found to be 91-93%.

Photostability of the dyes

In order to determine what is the photostability of the dyes, the solutions of the dyes in water with concentration $1 \cdot 10^{-4}$ g/ml were subjected to irradiation for 2 hours by UV light in a Suntest equipment. As during the irradiation no change was observed in the absorption spectra (λ_{\max}) of the dyes, the course of the photodegradation was monitored colorimetrically, i.e. the dependence of the concentration of the dye on the time of irradiation was determined using the method of the standard calibration curve. The data obtained is presented in Figure 2.

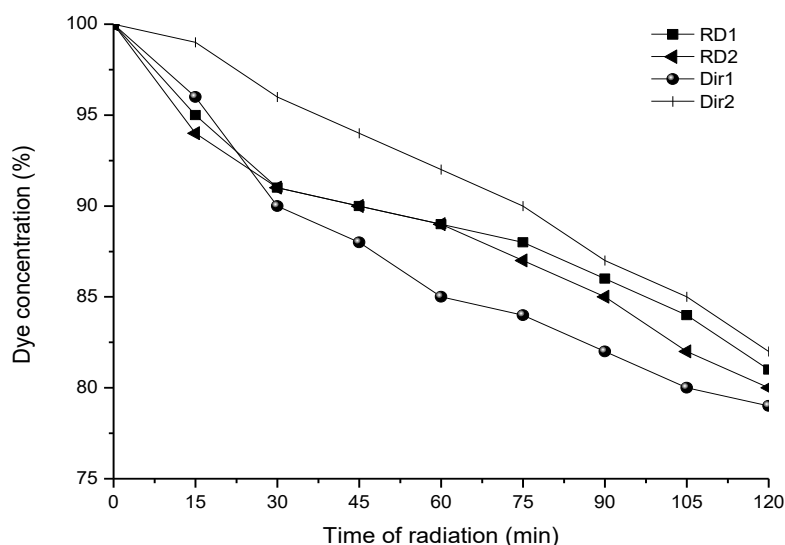


Figure 2. Dependence of the concentration of the dye (%) in water on the time of irradiation (min)

One can see from the figure that the photostability of the investigated dyes is similar. The high photostability (79-82%) of the dyes is due to the presence of hydroxy or amine groups located near the azo groups (at direct dyes) or carboxylic groups (at reactive dyes) and the possibility to forming hydrogen bonds.

Photostability of colored cotton

In order to study the photostability of the colored cotton, the last ones were subjected to irradiation by UV light in a Suntest equipment and examined for its optical properties – color coordinates L^* , a^* , b^* , C^* , h^* from the CIE Lab color space before and after irradiation for 8 hours. The data obtained are given in Table 1 and Table 2.

Table 1. Optical properties of the dyed with reactive dyes cotton textiles

Simple/Dyed with	Illuminant	L*	a*	b*	C*	h*	
non-radiated	RD1	D65_10	63.95	-2.86	-16.78	17.03	260.3
		A_10	62.26	-5.95	-19.37	20.26	252.9
		C_2	63.19	0.74	-18.11	18.12	272.3
	RD2	D65_10	61.57	-2.02	-16.75	16.87	263.1
		A_10	59.99	-5.26	-19.06	19.78	254.6
		C_2	60.86	1.47	-17.99	18.03	274.7
radiated	RD1	D65_10	64.31	-2.86	-15.42	15.68	259.5
		A_10	62.75	-5.64	-17.82	18.69	252.4
		C_2	63.62	0.41	-16.63	16.64	271.4
	RD2	D65_10	61.93	-2.03	-15.99	16.12	262.8
		A_10	60.42	-5.13	-18.21	18.92	254.3
		C_2	61.25	1.27	-17.17	17.21	274.2

Table 2. Optical properties of the dyed with direct dyes cotton textiles

Simple/Dyed with	Illuminant	L*	a*	b*	C*	h*	
non-radiated	Dir1	D65_10	60.3	-29.26	-29.6	41.62	225.3
		A_10	54.12	-39.02	-41.12	56.69	226.5
		C_2	58.11	-20.82	-33.91	39.79	238.4
	Dir2	D65_10	74.10	-23.72	-17.35	29.39	216.2
		A_10	69.98	-28.79	-24.98	38.12	221.0
		C_2	72.90	-20.27	-19.74	28.30	224.2
radiated	Dir1	D65_10	60.70	-28.26	-26.94	39.04	223.6
		A_10	54.98	-36.52	-37.66	52.46	225.9
		C_2	58.72	-20.79	-30.87	37.22	236.1
	Dir2	D65_10	74.33	-23.08	-17.63	29.04	217.4
		A_10	70.27	-28.08	-25.13	37.68	221.8
		C_2	73.14	-19.55	-19.99	27.97	225.6

From the data presented in Table 1 and Table 2, it can be seen that all dyed samples have a blue greenish color that does not change as a result of irradiation. No significant change in shade is noticeable either. However, a decrease in the intensity of the blue color was observed in the samples dyed with dye Dir1. A change was observed in the lightness of the studied samples and as seen from the data, it increased as a result of the irradiation. The color saturation decreases after irradiation. As the result from the investigations, we concluded that the changes observed in the studied samples are commensurable.

Photostability of colored paper

Based on previous research (Miladinova & Todorova, 2022) the chosen consumption of the investigated dyes in the paper was 0,6% of o.d.f. In order to study the photostability of the paper, the samples were subjected to irradiation by UV light in a Suntest equipment for 12 hours. The obtained paper samples were being examined for its optical properties – color coordinates L*, a*, b*, C*, h*

from the CIE Lab color space by Konica Minolta Spectrophotometer CM-3630 from Frank – PTI, according to ISO 5631-2:2008. For each sample, ten measurements were made at different locations on the surface. Before the measurements, the samples were conditioned at 50% RH and 23 ± 2 °C for 72 h. The data obtained is given in Table 3 and Table 4.

Table 3. Optical properties of the dyed with reactive dyes paper

Simple	Illuminant	L*	a*	b*	C*	h*	
Dyed, non-radiated	RD1	D65_10	65.27	-0.84	-13.55	13.58	266.5
		A_10	64.12	-2.88	-15.21	15.48	259.3
		C_2	64.70	2.13	-14.55	14.7	278.3
	RD2	D65_10	65.82	-1.96	-13.45	13.59	261.7
		A_10	64.55	-4.06	-15.39	15.92	255.2
		C_2	65.23	0.96	-14.50	14.54	273.8
Dyed, radiated	RD1	D65_10	65.25	-0.51	-13.26	13.02	264.6
		A_10	64.33	-2.15	-15.19	14.99	257.1
		C_2	64.51	1.98	-14.05	13.89	277.1
	RD2	D65_10	65.90	-1.75	-12.73	13.01	259.3
		A_10	64.65	-3.82	-14.63	15.03	253.6
		C_2	64.98	0.74	-13.80	13.97	272.6

Table 4. Optical properties of the dyed with direct dyes paper

Simple	Illuminant	L*	a*	b*	C*	h*	
Dyed, non-radiated	Dir1	D65_10	73.55	-27.43	-18.95	33.34	214.6
		A_10	68.87	-32.46	-27.85	42.77	220.6
		C_2	72.14	-23.06	-21.84	31.76	223.4
	Dir2	D65_10	75.02	-23.53	-14.54	27.66	211.7
		A_10	71.21	-25.36	-22.01	33.58	220.9
		C_2	73.86	-19.74	-17.00	26.06	220.7
Dyed, radiated	Dir1	D65_10	73.78	-26.68	-17.52	31.24	211.5
		A_10	69.82	-31.56	-26.75	40.57	219.4
		C_2	74.19	-22.16	-20.64	29.88	220.6
	Dir2	D65_10	74.89	-22.78	-13.77	25.55	210.2
		A_10	70.24	-23.58	-21.01	31.39	219.2
		C_2	72.56	-17.94	-15.92	24.12	219.2

From the data presented in Table 3 and Table 4, it can be seen that all dyed samples have a blue greenish color that does not change as a result of irradiation. No significant change in shade is noticeable either. However, a decrease in the intensity of the blue color was observed in the samples dyed with dye Dir1 and Dir2. A change was observed in the lightness of the studied samples and as seen from the data, it increased as a result of the irradiation. The color saturation decreases after irradiation. As the result from the investigations, we concluded that the changes observed in the studied samples are commensurable.

Conclusions

As a result of our research, it can be concluded that the synthesized of us reactive dyes RD1 and RD2 have high exhaustion and dye fixation ratio. The dyes, as well as the cotton and paper samples dyed with them, show good photostability, comparable to that of the direct dyes Dir1 and Dir2 used in practice for paper dyeing. This makes the investigated reactive dyes suitable for dyeing of cotton and paper.

References

- Baqi, Y. (2022). Anthraquinone Dyes: A synthetic and chemical characterization protocol for an industrial chemistry laboratory course. *Journal of Chemical Education*, 99(3), 1441–1447. <https://doi.org/10.1021/acs.jchemed.1c00865>
- Benkhaya, S., M`rabet, S. & El Harfi, A. (2020). A review on classifications, recent synthesis and applications of textile dyes. *Inorganic Chemistry Communications*, 115, 107891. <https://doi.org/10.1016/j.inoche.2020.107891>
- Drzewińska, E. (2008). Influence of Chemithermomechanical Pulp on the Colour of Pulps Dyed with Direct Dyes. *Fibres and textiles in eastern Europe*, 16(2), 105–107. <http://www.fibtex.lodz.pl/article137.html>
- Hande, P., Kulkarni, K. S., Adivarekar, R. V., Bhagwat, S. S. & Bhate, P. M. (2022). A process for dyeing cotton with direct dyes possessing primary aromatic amino groups furnishing wash fastness exhibited by reactive dyes. *Coloration Technology*, 138(3), 248–254. <https://doi.org/10.1111/cote.12586>
- Holmes, W. C. (1922). Application of the direct dyes in coloring paper. *Journal of Industrial & Engineering Chemistry*, 14(10), 958–960. <https://doi.org/10.1021/ie50154a038>
- Ishegbe, J. E., Bello, K. A. & Kogo, A. A. (2014). Synthesis and application of direct dyes derived from terephthalic and isophthalic acids on cotton fabrics, *IOSR Journal of Polymer and Textile Engineering (IOSR-JPTE)*, 1(3), 50–58. <https://doi.org/10.9790/019X-0135058>
- Konstantinova, T. & Miladinova, P. (2008). On the synthesis and application of ecologically tolerant dyes and pigments. In A. R. Lang (Ed.), *Dyes and Pigments - New Research*, (pp. 383–403.). Nova Science Publishers.
- Lv, D., Cui, J., Wang, Y., Zhu, G., Zhang, M. & Li, X. (2017). Synthesis and color properties of novel polymeric dyes based on grafting of anthraquinone derivatives onto o-carboxymethyl chitosan. *RSC Advances*, 7, 33494–33501. <https://doi.org/10.1039/C7RA04024E>
- Miladinova, P. M. & Todorova, D. A. (2022). Synthesis, characterization, and application of new reactive triazine dye on cotton and paper. *Fibers and Polymers*, 23, 1614–1620. <https://doi.org/10.1007/s12221-022-4020-8>
- Oprisan, L., Slavila, N. & Sebe, I. (2007). Bromamine acid derivated dyes. *U.P.B. Sci. Bull., Series B*, 69(2), 43–48. <https://www.yumpu.com/en/document/view/26128537/>
- Oyewale, A. O., Bello, K. A., Omotola, M. B. & Tukur, A. R. (2020). Synthesis, characterization, antimicrobial activity and dyeing potential on leather using bromamine-derived anthraquinone acid dyes. *ChemSearch Journal*, 11(2), 52–63. <http://www.ajol.info/index.php/csj>
- Parvinzadeh, M. & Najafi, H. (2008). Textile softeners on cotton dyed with direct dyes: Reflectance and fastness assessments. *Tenside Surfactants Detergents*, 45, 13–16. <https://doi.org/10.3139/113.100357>

- Patel, N. B. & Patel, A. L. (2009). Novel acid anthraquinone dyes and their application on various fibres and microbial studies. *Asian Journal of Chemistry*, 21(6), 4435–4443. <https://asianjournalofchemistry.co.in>
- Porter, J. J. (1973). The stability of acid, basic, and direct dyes to light and water. *Textile Research Journal*, 43 (12), 735–744. <https://doi.org/10.1177/004051757304301209>
- Shan, B., Tong, X., Xiong, W., Qiu, W., Tang, B., Lu, R., Ma, W., Luo, Y. & Zhang, S. (2015). A new kind of h-acid nonoazo-anthraquinone reactive dyes with surprising colour. *Dyes and Pigments*, 123, 44–54. <https://doi.org/10.1016/j.dyepig.2015.07.001>
- Society of Dyers and Colourists. (1995). *Cellulosics Dyeing*. Society of Dyers and Colourists.
- Solenis. (2019). *Paper colorants*. Solenis.
- Zhang, H., Hou, A., Xie, K. & Gao, A. (2019). Smart color-changing paper packaging sensors with pH sensitive chromophores based on azo-anthraquinone reactive dyes. *Sensors & Actuators: B. Chemical*, 286, 362–369. <https://doi.org/10.1016/J.SNB.2019.01.165>

Original scientific article

COMPARATIVE ANALYSIS OF BLEACHING OF SUNFLOWER OIL WITH COMMERCIAL BLEACHING EARTH AND BENTONITE POWDER ACTIVATED WITH SULFURIC ACID

Zoran Petrović¹, Jelena Mihajlović¹, Sabina Begić², Dragana Kešelj¹, Zorica Stojanović³, Amir Fazlić⁴

¹University of East Sarajevo, Faculty of Technology, Zvornik, RS/B&H

²University of Tuzla, Faculty of Technology, Tuzla, FB&H /B&H

³Victoriaoil Ltd., Šid, Serbia

⁴University of Sarajevo, Faculty of Science, Sarajevo, FB&H /B&H

Abstract

Commercial activated earths and activated clays based on aluminosilicate minerals, from different manufacturers, as well as activated carbon, are used for bleaching vegetable oils. Their structural and chemical composition, specific surface area and porosity are a good basis for application in the bleaching process of vegetable oils, which improves the color, reduces the peroxide number and soap content, and reduces and/or completely removes undesirable compounds.

In this paper, bentonite powder ("Bentoprodukt" a.d. Šipovo, Republic of Srpska) was activated with 8 wt% H₂SO₄ at the following parameters: mass of calcined bentonite powder 160 g, mass of 8 wt% H₂SO₄ solution 800 g, activation temperature 95 °C and contact time 30 minutes. The characterization of bentonite powder before and after activation, and commercial bleaching earth was performed using several test methods (XRPD, FTIR, BET, SEM/EDS).

Bleaching of raw sunflower oil ("Bimal" a.d. Brčko) with activated bentonite powder and commercial bleaching earth was carried out in laboratory conditions at the following parameters: temperature 95 °C, time 30 minutes and proportions of bleaching agents 0.2 wt%; 1.0 wt%; 2.0 wt% and 3.0 wt%. In sunflower oil samples before and after bleaching, soap content, peroxide number, color, then fatty acid composition by gas chromatography (GC-FID) and oil loss in the bleaching process were determined.

The test results showed that the activation of bentonite powder leads to an increase in its BET specific surface area, micropore surface area and volume, higher adsorption capacity, but also a decrease in particle size. The effects of bleaching of sunflower oil are: no residual soaps, reduction of peroxide value and small changes in the composition of fatty acids. The obtained values are in accordance with the Rulebook on the quality of sunflower edible oil, and the effects of bleaching with activated bentonite powder are similar to the effects of bleaching with commercial bleaching earth.

Keywords: bentonite powder, sulfuric acid activation, sunflower oil, commercial bleaching earth, bleaching effects.

Introduction

Commercial bleaching earths and active clays, due to their structural and chemical composition, are widely used in various branches of industry. One of these applications is based on the adsorption processes of refining, that is, the purification of various semi-products and products, such as edible oils, beer, motor oils, etc.

Edible vegetable oils are a necessary nutritional resource for human health (Zhou et al., 2020), however, raw edible oils contain undesirable substances having a nuisance or toxicity for the consumer (Zio et al., 2020). Because of the above, before their use for food purposes, they need to be subjected to a purification or refining process (Gharby, 2022) that aims at removing compounds such as phospholipids, free fatty acids, oxidation products, pigments, and other undesirable components (Almeida et al., 2019). Bleaching of oils is a process by which unwanted substances are removed by intimately mixing an adsorbent with oil, under certain conditions (Richardson, 1978). That is a common method in the industry (Sedghamiz et al., 2019), that may use commercial activated earths and activated clays based on aluminosilicate minerals, from different manufacturers, as well as activated carbon, as adsorbents. Their structural and chemical composition (Foletto et al., 2006; Foletto et al., 2011), specific surface area and porosity (Emmerich et al., 2010) are a good basis for application in the bleaching process of vegetable oils, which improves the color (Topkafa et al., 2013), reduces the peroxide number and soap content (Shah et al., 2018; Sedaghat Boroujeni et al., 2020), and reduces and/or completely removes undesirable compounds (Mukasa-Tebandeke et al., 2014). Although naturally active clays show a high adsorption capacity and possess some bleaching activity (Usman et al., 2012), the most common agents for bleaching of vegetable oils are acid activated clays (Okoronkwo & Jeje, 2012). Activated bentonite is considered as ideal clay material owing to its higher bleaching efficiency (Yassin et al., 2022) due to desired changes in its adsorptive properties occurring as a result of acid activation (Kashani Motlagh et al., 2011). In this paper, a comparative analysis of the bleaching of sunflower oil with commercial bleaching earth and bentonite powder activated with sulfuric acid was performed.

Materials and Methods

Materials

- natural bentonite powder from the company "Bentoprodukt" Šipovo (montmorillonite content 90 wt%, moisture content 9.8 wt% at 105 °C, 0.063 mm sieve residue 28.9%),
- 8 wt% sulfuric acid solution (H₂SO₄),
- commercial bleaching earth,
- unbleached sunflower oil (NSU) of the company "Bimal" Brčko,
- other chemicals and reagents required for the characterization of activated bentonite powder, commercial bleaching earth, and sunflower oil before and after bleaching.

Methods

Activation of bentonite powder with sulfuric acid

Before activation, bentonite powder (BPJM) was heated for 2 h at a temperature of 450 °C, and then the measured mass was activated with sulfuric acid (H₂SO₄) at the following parameters in laboratory conditions:

- 160 g of bentonite powder,
- 800 g of 8 wt% H₂SO₄ solution,
- temperature and activation time (95 °C and 30 minutes),

After activation, filtering, washing with water and neutralization with a 2 wt% Ca(OH)₂ solution to a pH value of 4-5 were performed. Then the activated bentonite powder was dried, ground and sieved on a 180 μm sieve.

Characterization of activated bentonite powder and commercial bleaching earth

In order to define the physicochemical characteristics of activated bentonite powder (ABPJM) and commercial bleaching earth (KZB), their structural and chemical composition, textural and

morphological characteristics and particle size distribution (D50), the characterization of the samples was performed using the test methods given below.

X-ray powder diffraction (XRPD)

Activated bentonite powder (ABPJM) and commercial bleaching earth (KZB) samples were scanned on a multipurpose *Rigaku SmartLab* X-ray diffractometer of parafocal Bragg-Brentano geometry, using a *D/teX Ultra 250* strip detector in 1D standard mode with a $\text{CuK}\alpha_{1,2}$ radiation source ($U = 40$ kV, $I = 30$ mA). XRPD data were collected at angular range between 2° and $80^\circ 2\theta$, with a step size of 0.01° and scan speed of $5^\circ/\text{min}$, and silicon (low background) sample holder was used (Petrović et.al, 2022). Crystalline phases were identified using *Rigaku PDXL 2.0* software (with ICDD PDF-2 database).

Fourier transform infrared (FTIR) spectroscopy

This method was used for a more complete definition of the structural or phase composition of activated bentonite powder (ABPJM) and commercial bleaching earth (KZB). The spectra of these samples were recorded on an *IRAffinity-1S Shimadzu* infrared spectrophotometer, using the ATR method (*MIRacle 10*).

Low-temperature nitrogen adsorption method (BET)

The low-temperature nitrogen adsorption method (BET method) was used to determine the textural characteristics of activated bentonite powder (ABPJM) and commercial bleaching earth (KZB), on a *Micromeritics Gemini VII 3.04* device.

Scanning electron microscopy/energy dispersive spectrometry (SEM/EDS)

Morphological characteristics of activated bentonite powder (ABPJM) and commercial bleaching earth (KZB) were recorded with a scanning electron microscope *JEOL-JSM-6460LV*. The samples were gold-sputtered using a *BAL-TEC SCD 005* device, with a current of 30 mA, from a distance of 50 mm for 180 s, and with an instrument resolution of 3-4 nm and a magnification of 500-3000 times. Micro-elemental analysis was performed by energy dispersive spectrometry (EDS) using Bruker QUANTAX 200 EDS spectrometer (detection of elements $Z \geq 5$, detection limit: ~ 0.1 wt%, resolution 126 eV), and EDS spectra were analyzed using Noran System Six.

Bleaching of sunflower oil with bleaching agents

Bleaching of crude sunflower oil (NSU) by bentonite powder activated by sulfuric acid (ABPJM) and by commercial bleaching earth (KZB) in laboratory conditions was carried out under the temperature 95°C , bleaching time 30 minutes and doses of bleaching agents (wt%) of 0.2; 1.0; 2.0 and 3.0. A previously calculated mass of bleaching agent was added to a certain amount of raw sunflower oil heated to a temperature of 95°C , and intensively mixed for 30 minutes. After that, bleached sunflower oil was filtered on vacuum filtration equipment.

Characterization of sunflower oil before and after bleaching

To determine the effects of sunflower oil bleaching, the methods prescribed by the regulation on edible vegetable oils (Službeni glasnik BiH, broj 2/11) were used to determine the soap content, peroxide number, color, fatty acid composition (GC), and oil losses.

Results and discussion

Test results of bleaching agents

X-ray powder diffractometry (XRPD) results

Recorded XRPD spectra of bentonite powder samples activated by sulfuric acid (ABPJM), and commercial bleaching earth (KZB) are shown in Figure 1.a and 1.b.

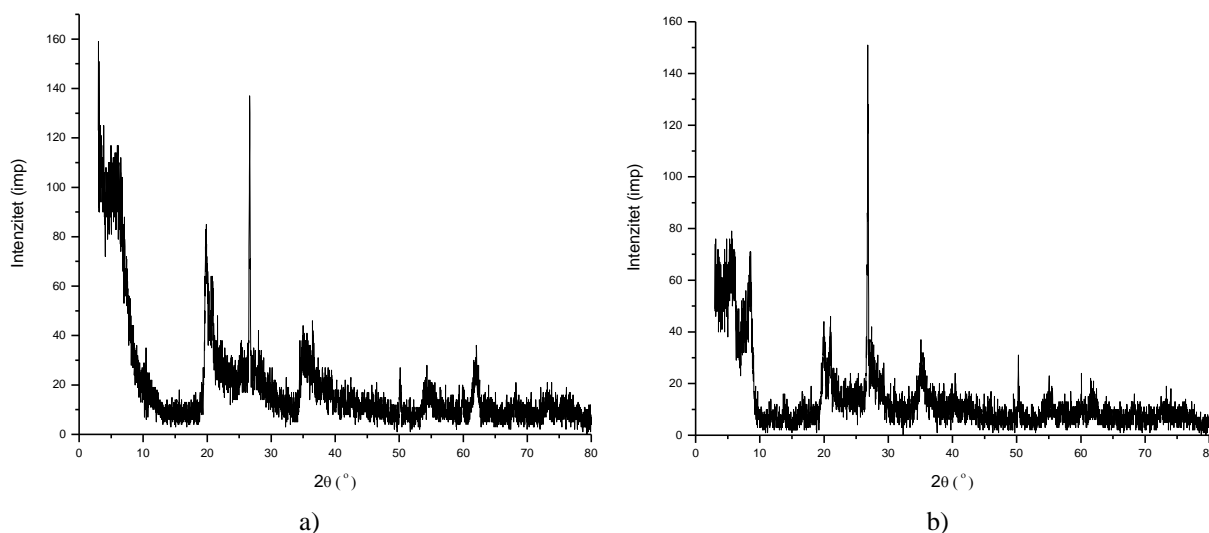


Figure 1. Diffractograms of samples: a) ABPJM; b) KZB

Montmorillonite (PDF#13-0135), nontronite (PDF#29-1497) and quartz (PDF#79-1906) phases were identified in a sample of bentonite powder activated with 8 wt% sulfuric acid (ABPJM), and in a sample of commercial bleaching earth (KZB) in addition to the phases of the smectite group and quartz, peaks for phyllosilicate minerals, e.g. palygorskite (PDF#31-0783), were identified (Petrović et. al, 2022).

Results of FTIR spectrophotometry

Figure 2 shows the FTIR spectra of bentonite powder activated with 8% sulfuric acid (ABPJM), and commercial bleaching earth (KZB), in the range of wave numbers from 4000 – 500 cm^{-1} . Bands characteristic for the presence of the smectite group of clay identified by the XRPD method can be identified on these spectra. For example, the band at $\sim 3620 \text{ cm}^{-1}$ originates from stretching vibrations of OH groups coordinated by the octahedral Al^{3+} cation, and the bands at ~ 3400 and 1630 cm^{-1} originate from stretching and bending OH vibrations from water. Si-O and Si-O-Si stretching vibrations are characteristic for the region $1020\text{-}990 \text{ cm}^{-1}$, and the band at $\sim 915 \text{ cm}^{-1}$ originates from Al-Al-OH bending vibrations. Bands at ~ 680 and 550 cm^{-1} originate from Si-O and Al-O-Si vibrations, and a broad band in the range $\sim 790\text{-}770 \text{ cm}^{-1}$ indicates the presence of quartz (Petrović et.al, 2022).

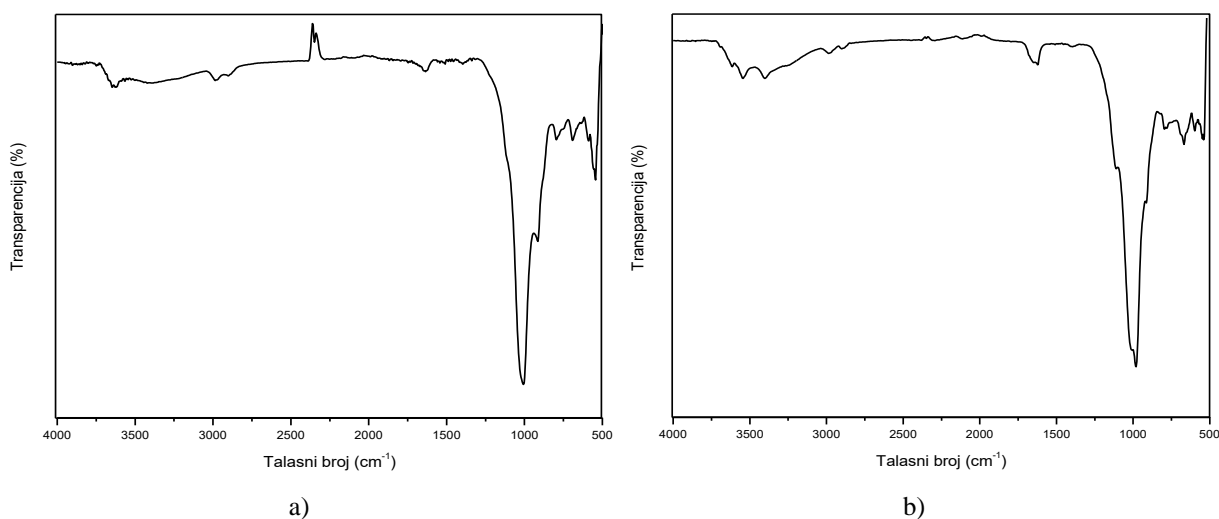


Figure 2. FTIR spectrum of samples: a) ABPJM; b) KZB

Results of the low-temperature nitrogen adsorption method (BET)

Using the method of low-temperature nitrogen adsorption (BET), it was determined that the adsorption isotherms of bentonite powder samples, before and after activation with 8% m/m sulfuric acid solution, are type II, which is characteristic of mesoporous materials with pores in the form of cracks. Unactivated bentonite powder has a relatively small specific surface area (83.1058 m²/g) and an underdeveloped porous structure. Table 1 shows some textural characteristics of samples of bentonite powder activated by sulfuric acid (ABPJM) and commercial bleaching earth (KZB).

Table 1. Textural characteristics of commercial bleaching earth (KZB) and activated bentonite (ABPJM)

Characteristics	Samples	
	KZB	ABPJM
Specific surface area, SP_{BET} , m ² /g	170.6072	195.8427
Constant, C_{BET}	357.5192	395.6569
Microporous volume, $V_{\mu p}$, cm ³ /g	0.020798	0.016072
External specific surface area, SP_{ext} , m ² /g	122.9679	163.6965
Microporous surface area, $S_{\mu p}$, m ² /g	47.6393	32.1462
Average pore diameter, d_p , nm	6.6506	3.03556

Analyzing the results given in Table 1 it can be concluded that activation with sulfuric acid led to an increase in the specific surface area of bentonite powder by about 2.36 times (195.84 m²/g), but also to a decrease in the average pore diameter from 6.60 nm to 3.04 nm. The decrease in mean pore diameter is a consequence of the development of a porous structure in the range of small mesopores (2-6 nm). The obtained results indicate that the applied bentonite activation process improves its textural characteristics, both in terms of specific surface area and porosity, primarily in the domain of small mesopores. Commercial bleaching earth (KZB) has a 14.85% lower specific surface value than activated bentonite powder (ABPJM), and at the same time a larger micropore volume by 22.72%, micropore area by 32.52%, as well as a larger mean pore diameter by 54.36% of the activated bentonite powder.

In previous research (Petrović et al., 2022), it was determined that the activation of bentonite powder from the same location (with 92 wt% montmorillonite content) with 8 wt% hydrochloric acid resulted in a significantly greater increase in specific surface area (316.25 m²/g). Activation of bentonite clay with a lower content of montmorillonite (locality Gerzovo, Mrkonjić Grad) with 20% sulfuric acid resulted in a significantly greater improvement in textural characteristics (Petrović et al., 2014; Petrović et al., 2016) compared to the textural characteristics of the examined bentonite powder ABPJM in this paper.

Results of the method of scanning electron microscopy/energy dispersive spectrometry (SEM/EDS)

Figure 3 shows SEM micrographs of tested samples of bentonite powder activated with 8 wt% sulfuric acid (ABPJM), and commercial bleaching earth (KZB). Activation of natural bentonite powder resulted in activated bentonite powder (ABPJM) with smaller particle sizes, which are at the same time smaller than the particle sizes of commercial bleaching earth (KZB).

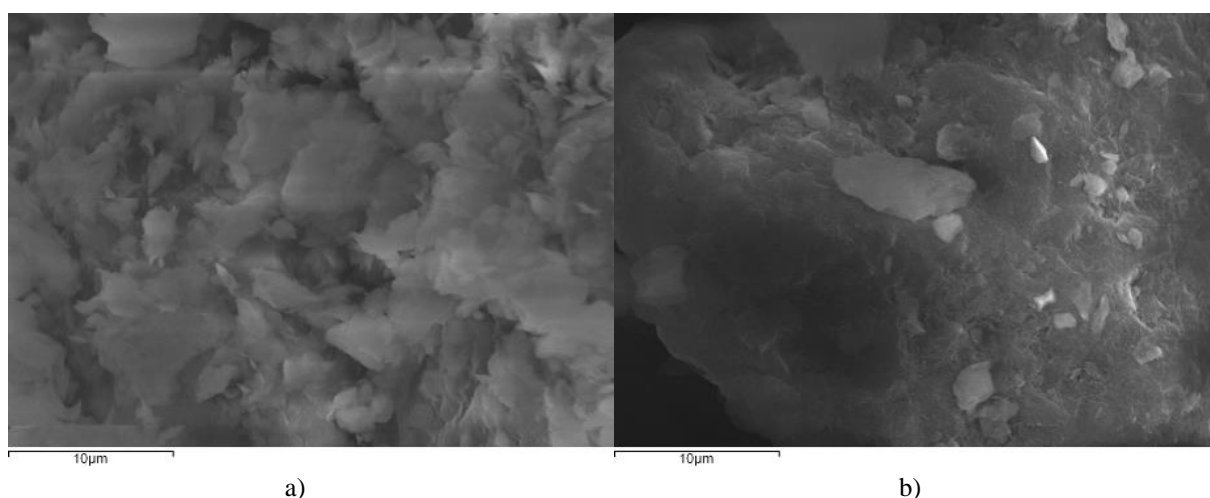


Figure 3. SEM micrograph of samples with a magnification of 3000 times: a) ABPJM; b) KZB

Micro-elemental analysis (EDS) of tested samples of bentonite powder, activated with 8 wt% sulfuric acid, and commercial bleaching earth, determined the proportion of elements in the selected regions, based on which the proportion of oxides in bleaching agents was calculated (Table 2). The results of the EDS analysis show that activated bentonite powder was obtained by activating bentonite powder with a slight change in the proportion of individual oxides. There was an increase in the proportion of SiO₂ (4.34 wt%), a decrease in various proportions of Al₂O₃ (1.42 wt%), Fe₂O₃ (0.84 wt%) and CaO (1.36 wt%), and a complete removal of TiO₂. Commercial bleaching earth contains a higher proportion of SiO₂ (8.03 wt%), Fe₂O₃ (0.10 %), CaO (6.49 wt%), and Al₂O₃ was not detected in the selected regions. It should be noted that commercial bleaching earth contains 1.40 wt% K₂O.

Table 2. Proportions of oxides in ABPJM and KZB samples

Component	SiO ₂ , wt%	Al ₂ O ₃ , wt%	Fe ₂ O ₃ , wt%	CaO, wt%	K ₂ O, wt%
ABPJM	80.29	16.03	2.75	0.94	-
KZB	88.32	-	2.85	7.43	1.40

Results of sunflower oil tests before and after bleaching

The soap content in raw sunflower oil (NSU) and in sunflower oil samples after bleaching with activated bentonite and commercial bleaching earth is 0.00 mg/kg. The peroxide value is a measure of oxidation and change in oil quality (mmol/kg), the value of which is prescribed by the relevant

national regulations. Table 3 shows the values of the peroxide number of sunflower oil before and after bleaching with activated bentonite and commercial bleaching earth.

Table 3. Results of determining the peroxide value of sunflower oil before and after bleaching

Oil samples	Peroxide number PoZ, mmol/kg
NSUJ	6.530
BSU KZB0,2	5.750
BSJKZB1,0	4.377
BSU KZB2,0	3.316
BSU KZB3,0	1.229
SUBPJM0,2	2.464
SUBJM1,0	1.923
SUZBBPJM2,0	1.576
SUBPJM3,0	1.357

As the bleaching agent concentration increases, the peroxide value of the bleached oil decreases. It should be pointed out that activated bentonite powder is significantly more effective in reducing the peroxide number than commercial bleaching earth.

The color of bleached oils with bleaching agents can be determined visually, with Lovibond or by the spectrophotometric method. In this paper, the color was determined with the Lovibond PFX 995 device according to the RYBN scale and the GARDNER scale. It can be concluded that there was a change in the color of the sunflower oil after bleaching with bleaching agents (ABPJM, KZB), but adequate clarity of the oil was not achieved. The assumption is that the reason for the greater turbidity of the bleached oil samples is a defective vacuum filtration apparatus, so smaller particles of bleaching agents were left behind. The effects of discoloration are slightly lower in oil samples bleached with activated bentonite powder (ABPJM) than the effects of using commercial earth (KZB). In earlier research on the bleaching of sunflower oil from the same manufacturer with homemade bentonite activated by 20% m/m sulfuric acid, significantly better results were achieved in changing the color of the starting oil (Petrović et al., 2016).

Results of determining the fatty acid composition of sunflower oil by gas chromatography

The composition of fatty acids, as the main components of vegetable oils, has the greatest influence on their quality, and depending on the presence of double bonds in the molecule, they are distinguished by saturated fatty acids (SFA), monounsaturated fatty acids (MUFA) and polyunsaturated fatty acids (PUFA). The most important representatives of SFA are stearic, palmitic, myristic and lauric acid, and of MUFA is oleic acid. Polyunsaturated fatty acids are characterized by the presence of two or more double bonds, and the most significant representatives are linoleic and α -linoleic acid, which cannot be synthesized in the body and are defined as essential acids very important for certain physiological processes in the body (Đurović et al., 2021). Sunflower oil is characterized by a high proportion of unsaturated fatty acids (mainly linoleic and linoleic acids), and it is considered one of the best vegetable oils in terms of nutritional properties.

The fatty acid composition of sunflower oil before and after bleaching with activated bentonite powder and commercial bleaching earth was determined by gas chromatography (GC) on an Agilent Technologies 7890 type gas chromatograph with a flame ionization detector (FID). After recording sunflower oil samples before and after bleaching, the retention time for individual components (fatty acids) is determined from the obtained chromatograms. Then, the concentrations of fatty acids are determined from the area and height of the peaks, i.e. individual proportions of fatty acids in sunflower oil samples. Figure 4 shows the chromatogram of unbleached sunflower oil (NSU), and Table 4 shows its fatty acid composition.

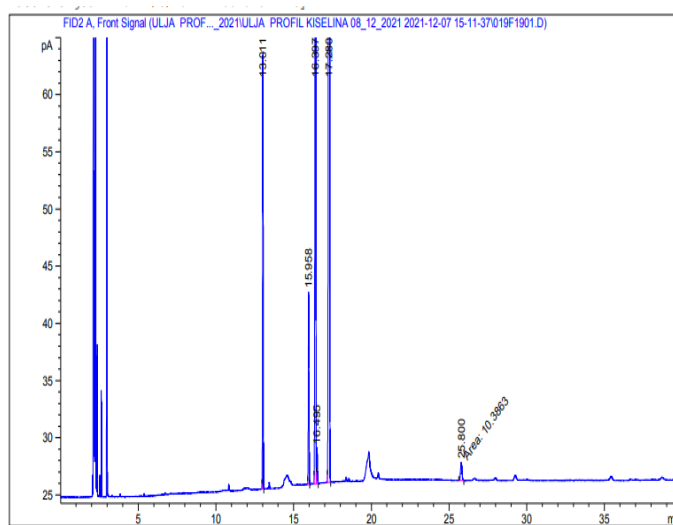


Figure 4. Chromatogram of unbleached sunflower oil (NSU)

Table 4. Fatty acid composition of unbleached sunflower oil (NSU)

Fatty acid	Designation	Fatty acid type	Content, wt%
Palmitic	C16:0	Saturated fatty acid (SFA)	6.43577
Stearic	C18:0	Saturated fatty acid (SFA)	3.48085
Oleic	C18:1	Monounsaturated fatty acid (MUFA)	29.62076
Linoleic	C18:2	Polyunsaturated fatty acid (PUFA)	59.12150
Behenic	C22:0	Saturated fatty acid (SFA)	0.69442

In a sample of unbleached sunflower oil (NSU), the proportion of saturated (palmitic, stearic and behenic), monounsaturated and polyunsaturated fatty acids was determined by gas chromatography. The largest mass fraction of this oil is linoleic acid, as a polyunsaturated fatty acid (59.12 wt%), followed by oleic acid, as a monounsaturated fatty acid (29.62 wt%) and palmitic, stearic and behenic acids, as saturated fatty acids (10.61 wt%). These, as well as other vegetable oils, are subject to thermal degradation due to their higher content of unsaturated fatty acids (Đuričić et.al., 2019).

Figure 5 shows the chromatograms of sunflower oil samples bleached with 0.2% activated bentonite powder and commercial bleaching earth (SUABPJM0.2; SUKZB0.2), and Table 5 and Table 6 show the fatty acid composition of sunflower oil after bleaching with different proportions of bleaching agents.

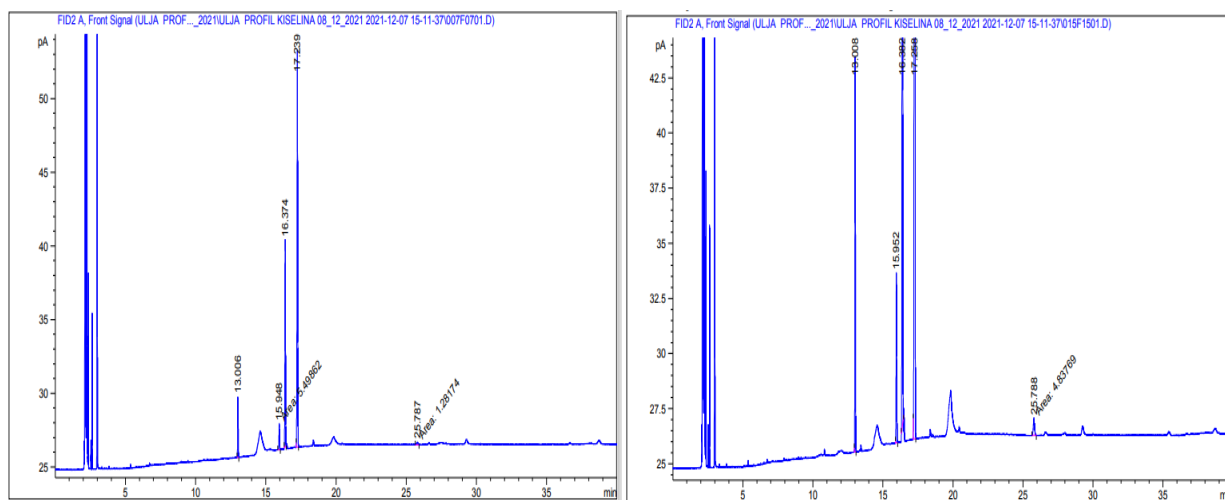


Figure 5. Chromatograms of sunflower oil bleached with activated bentonite (SUABPJM0,2) and commercial bleaching earth (SUKZB0,2)

Table 5. Fatty acid composition of sunflower oil bleached with activated bentonite powder

Fatty acid (designation)	Samples of sunflower oil bleached with activated bentonite/content of fatty acids, wt%			
	SUABPJM0,2	SUABPJM1,0	SUABPJM2,0	SUABPJM3,0
Palmitic (C16:0)	6.76387	6.55710	6.69708	6.62866
Stearic (C18:0)	3.56436	3.49942	3.57005	3.56686
Oleic (C18:1)	28.86138	29.26400	28.85581	28.95316
Linoleic (C18:2)	59.97954	59.67099	60.12983	60.11540
Behenic (C22:0)	0.83086	1.00848	0.74723	0.73591

Table 6. Fatty acid composition of sunflower oil bleached with commercial bleaching earth

Fatty acid (designation)	Samples of sunflower oil bleached with commercial bleaching earth/content of fatty acids, wt%			
	SUKZB0,2	SUKZB1,0	SUKZB2,0	SUKZB3,0
Palmitic (C16:0)	6.60466	6.70676	6.67418	6.61437
Stearic (C18:0)	3.55890	3.57828	3.57208	3.56525
Oleic (C18:1)	29.03599	29.04598	29.05314	29.07031
Linoleic (C18:2)	60.10005	59.97751	60.00552	60.06984
Behenic (C22:0)	0.70040	0.69147	0.69508	0.68023

In sunflower oil samples, after bleaching with activated bentonite powder and commercial bleaching earth in doses of 0.2 wt%; 1.0 wt%; 2.0 wt% and 3.0 wt%, there was a slight change in the fatty acid composition, i.e. the proportion of saturated, monounsaturated and polyunsaturated fatty acids, and these changes are shown in Table 7. Based on the GC results, it can be concluded that bleaching sunflower oil with a higher proportion of activated bentonite powder leads to a slight increase in the content of saturated fatty acids and polyunsaturated fatty acids, and a decrease in monounsaturated fatty acids. Similar changes in the fatty acid composition were achieved by bleaching sunflower oil with commercial bleaching earth.

Table 7. Changes in mass fractions of certain types of fatty acids in sunflower oil samples after bleaching

Fatty acid type	Sunflower oil samples bleached with activated bentonite powder and commercial soil/proportion of different types of fatty acids, wt%			
	SUABPJM0,2	SUABPJM 1,0	SUABPJM 2,0	SUABPJM 3,0
SFA	11.16	11.07	11.01	10.93
MUFA	28.86	29.26	28.86	28.95
PUFA	59.98	59.67	60.13	60.12
Fatty acid type	SUKZB0,2	SUKZB 1,0	SUKZB 2,0	SUKZB 3,0
SFA	10.86	10.98	10.94	10.86
MUFA	29.04	29.05	29.05	29.07
PUFA	60.10	59.98	60.01	60.07

Results of determination of oil losses in the bleaching process

In the process of bleaching sunflower oil, certain losses of oil occur, which remain in the oil cake after vacuum filtration. Oil losses depend on the type of bleached oil, the bleaching agent, as well as the filtration equipment. Test results show that oil losses decrease with increasing bleaching agents, and that they are slightly lower in sunflower oil samples bleached with activated bentonite powder compared to commercial bleaching earth. These losses are slightly higher than the losses achieved by bleaching sunflower oil of the same manufacturer with activated bentonite (Petrović et al., 2016).

Conclusion

Bentonite clays, due to their structural and chemical composition, and the possibility of modification by various procedures, are widely used in various branches of industry, and one of them is application

in adsorption processes. In the production of edible vegetable oils in the company "Bimal" Brčko, Bosnia and Herzegovina, imported commercial bleaching earths are used for bleaching raw oils, and at the same time, Republika Srpska has relatively large supplies of high-quality calcium bentonite. Chemical activation of bentonite with mineral acids (H_2SO_4 , HCl , etc.) is performed according to various parameters (acid concentration, ratio of bentonite and activation agents, activation temperature, activation time, etc.). Activation parameters mostly depend on the characteristics of natural bentonite, as well as uses of activated bentonite.

In this paper, the activation of bentonite powder with a montmorillonite content of 92 wt% was performed with an 8 wt% H_2SO_4 solution, under laboratory conditions. Bentonite powder was annealed for 2 h at a temperature of 450 °C before activation. The effects of activation were investigated using different test methods (XRPD, FTIR, BET and SEM/EDS). Using the XRPD method, the phases of montmorillonite, nontronite and quartz were identified in the sample of activated bentonite powder, and in the sample of commercial bleaching earth, in addition to the phases of the smectite group and quartz, peaks for phyllosilicate minerals, e.g. palygorskite, were identified. The results of FTIR spectroscopy of bentonite powder after activation and commercial bleaching earth confirmed the results of the phase composition of the samples, obtained by the XRPD method. The adsorption isotherm of the sample of activated bentonite powder is of type IIb, which is characteristic of mesoporous materials with pores in the form of cracks.

The activation of homemade bentonite powder with sulfuric acid led to an increase in the specific surface by about 2.36 times ($195.84 \text{ m}^2/\text{g}$), but also to a decrease in the average pore diameter from 6.60 nm to 3.04 nm. The decrease in mean pore diameter is a consequence of the development of a porous structure in the range of small mesopores (2-6 nm). Commercial bleaching earth has a 14.85% lower specific surface value than the activated bentonite powder, and at the same time a 22.72% higher micropore volume, a 32.52% higher micropore surface and a 54.36% higher mean pore diameter than the activated bentonite powder. In earlier studies of the activation of bentonite powder of a higher proportion of montmorillonite, by 8 wt% HCl , as well as the activation of bentonite clay from the same sites, by 20 wt% H_2SO_4 , it was determined that there was a significantly greater increase in their specific surface area. SEM images of the activated bentonite powder in this research showed that the activation resulted in a decrease in the particle sizes, which are at the same time smaller than the particle sizes of commercial soil.

The results of the EDS analysis show that the activation of the bentonite powder resulted in an activated bentonite powder with a slight change in the proportion of individual oxides, i.e. there was an increase in the proportion of SiO_2 , a decrease in liters of Al_2O_3 , Fe_2O_3 and CaO , and a complete removal of TiO_2 . Commercial bleaching earth contains a higher proportion of SiO_2 , Fe_2O_3 and CaO than activated bentonite powder. Also, this clay contains K_2O , but no Al_2O_3 was detected.

The bleaching effects of sunflower oil with activated bentonite and commercial earth were determined by standardized and/or internal methods of testing soap content, peroxide number, color, fatty acid composition and oil losses in the bleaching process. The test results of the bleached sunflower oil showed that there were no residual soaps, that the value of the peroxide value was significantly reduced, and better bleaching efficiency was obtained with activated bentonite. The results of determining the color of the sunflower oil samples, after bleaching by bentonite powder, showed that there was a change in color, but the appropriate clarity of the oil was not achieved, and some of the reasons may be inadequate filtration equipment and no addition of activated carbon, so it is necessary to examine the effects of combining bleaching agent with activated carbon. The effects of applying commercial bleaching earth were similar to the effects of activated bentonite powder.

The results of determining the fatty acid composition of unbleached sunflower oil by gas chromatography showed that the largest fractions of this oil are: linoleic acid (59.12 wt%), oleic acid (29.62 wt%), and palmitic, stearic and behenic acids (10.61 wt%). By bleaching sunflower oil with a higher dose of activated bentonite powder, there is a slight increase in the content of saturated fatty

acids and polyunsaturated fatty acids, and a decrease monounsaturated fatty acids. Similar changes in fatty acid composition were achieved by bleaching sunflower oil with commercial bleaching earth. In the process of bleaching sunflower oil, there are certain oil losses that remain in the oil cake after vacuum filtration. However, the oil losses decrease with the increase in the proportion of bleaching agents, and they are slightly lower in the sunflower oil samples bleached with activated bentonite powder, compared to the commercial bleaching earth.

Research into the activation of domestic bentonite powder and its application for bleaching sunflower and other types of oil should be continued in order to achieve appropriate efficiency and eventual application in industrial conditions instead of importing commercial bleaching earth.

References

- Almeida, E. S., Carvalho, A. C. B., de Souza Soares, I. D., Valadares, L. F., Mendonça, A. R. V., Silva, Jr. I. J. & Monteiro, S. (2019). Elucidating how two different types of bleaching earths widely used in vegetable oils industry remove carotenes from palm oil: Equilibrium, kinetics and thermodynamic parameters. *Food Research International*, 121, 785–797. <https://doi.org/10.1016/j.foodres.2018.12.061>
- Đuričić, I., Jović, M., Todorović, V., Šobajić, S., Đuričić, I., Jović, M., Todorović, V. & Šobajić, S. (2019). Analysis of fatty acid composition in edible oil by gas chromatography. *Hrana i ishrana*, 60(1), 24–29. <http://dx.doi.org/10.5937/HraIsh1901024D>
- Đurović, A., Kravić, S., Stojanović, Z., Lužaić, Romanić, R. & Grahovac, N. (2021). Karakterizacija masnokiselinskog sastava mešanih ulja suncokreta i lana sa aspekta faktora nutritivnog karaktera. *Uljarstvo*, 52(1), 35–41. <http://fiver.ifvcns.rs/handle/123456789/3126>
- Emmerich, K., Steudel, A., Schuhmann, R., Weidler, P. G., Ruf, F. & Sohling, U. (2010). Mineralogical and physicochemical characterization of a natural bleaching earth containing sepiolite suitable for fastfiltration and bioseparation. *Clay Minerals*, 45, 477–488. <https://doi.org/10.1180/claymin.2010.045.4.477>
- Foletto, E. L., Colazzo, G. C., Volzone, C. & Porto, L. M. (2011). Sunflower oil bleaching by adsorption onto acid-activated bentonite. *Brazilian Journal of Chemical Engineering*, 28(1), 169–174. <https://doi.org/10.1590/S0104-66322011000100018>
- Foletto, E. L., Volzone, C. & Porto, L. M. (2006). Clarification of cottonseed oil: how structural properties of treated bentonites by acid affect bleaching efficiency. *Latin American Applied Research*, 36, 37–40. http://www.scielo.org.ar/scielo.php?script=sci_arttext&pid=S0327-07932006000100006
- Gharby, S. (2022). Refining vegetable oils: Chemical and physical refining. *Scientific World Journal*, 2022, 1–10. <https://doi.org/10.1155/2022/6627013>
- Kashani Motlagh, M. M., Youzbashi, A. A. & Amiri Rigi, Z. (2011). Effect of acid activation on structural and bleaching properties of a bentonite. *Iranian Journal of Materials Science & Engineering*, 8(4), 50–56. <http://ijmse.iust.ac.ir/article-1-383-en.pdf>
- Mukasa-Tebandeke, I. Z., Ssebuwufu, P. J. M., Nyanzi, S. A., Schumann, A., Nyakairu, G. W. & Lugolobi, F. (2014). Using trace metals, peroxide, acid and iodine values to characterize oils bleached using clays from Central and Eastern Uganda. *Bulletin of Pure & Applied Sciences-Geology*, 33f(1and2), 9–23. <https://doi.org/10.5958/2320-3234.2014.00002.X>
- Okoronkwo, A. E. & Jeje, A. O. (2012). Studies on the efficiency of oyster shell and kaolin as adsorbents for bleaching of palm oil. *Knowledge Review*, 26(2), 15–18. <https://www.globalacademicgroup.com/journals/knowledge%20review/STUDIES%20ON%20THE%20EFFICIENCY%20OF%20OYSTER.pdf>

- Petrović, Z., Dugić, P., Aleksić, V., Begić, S., Sadadinović, J., Mičić, V. & Kljajić, N. (2014). Composition, structure and textural characteristic of domestic acid activated bentonite. *Contemporary materials*, 5(1), 133–139. <https://doi.org/10.7251/COMEN1401133P>
- Petrović, Z., Đokić, A., Botić, T., Begić, S., Kešelji, D. & Milovanović, M. (2022). Struktura bentonitnog praha aktiviranog hlorovodoničnom kiselinom. In I. Džombić (Ed.), *Proceedings – International Conference “XI Međunarodna konferencija o društvenom i tehnološkom razvoju”*. (pp. 521–589). Banjaluka: PIM University of Banja Luka. <http://conf.univerzitetpim.com/zbornik-radova/>
- Petrović, Z., Maksimović, R., Begić, S. & Knezić, N. (2016). Primjena hemijski aktiviranog domaćeg bentonita za bijeljenje jestivih biljnih ulja. In Lj. Vukic (Ed.), *Proceedings – “XI conference of chemists, technologists and environmentalists of republic of srpska”*. (pp. 225–234). Banjaluka: University of Banjaluka, Faculty of Technology. <http://ekonferencije.com/conference/downloadConferenceFile/232/11>
- Richardson, L. L. (1978). Use of bleaching, clays, in processing edible oils. *Journal of the American Oil Chemists' Society*, 55(11), 777–780. <https://doi.org/10.1007/BF02682647>
- Sedghamiz, M. A., Attar, F. & Raeissi, S. (2019). Experimental investigation of acid regeneration of spent bleaching clay de-oiled by the in-situ transesterification process at various operating conditions. *Process Safety and Environmental Protection*, 124, 121–127. <https://doi.org/10.1016/j.psep.2019.01.029>
- Sedaghat Boroujeni L., Ghavami, M., Piravi Vanak, Z. & Ghasemi Pirbalouti, A. (2020). Optimization of sunflower oil bleaching parameters: using response surface methodology (RSM). *Food Science and Technology, Campinas*, 40(Suppl. 1), 322–330. <https://doi.org/10.1590/fst.10919>
- Shah, S. N., Mahesar, S. A., Sherazi, S. T. H., Panhwar, M. A., Nizamani, S. M. & Kandhro, A. A. (2018). Influence of commercial refining on some quality attributes of sunflower oil. *Ukrainian Food Journal*, 7(2), 234–243. <https://doi.org/10.24263/2304-974X-2018-7-2-6>
- Službeni glasnik BiH, broj 2/11 „Pravilnik o jestivim biljnim uljima, jestivim biljnim mastima i majonezama“. https://www.fsa.gov.ba/old/images/pravni-propisi/bs-Pravilnik_o_jestivim_biljnim_uljima_jestivim_biljnim_mastima_i_majonezama_21-11.pdf
- Topkafa, M., Ayyildiz, H. F., Arslana, F. N., Kucukkolbasi, S., Durmaz, F., Sen, S. & Kara, H. (2013). Role of different bleaching earths for sunflower oil in a pilot plant bleaching system. *Polish Journal of Food and Nutrition Sciences*, 63(3), 147–154. <https://doi.org/10.2478/v10222-012-0077-1>
- Usman, M. A., Ekwueme, V. I., Alaje, T. O. & Mohammed, A. O. (2012). Characterization, acid activation, and bleaching performance of Ibeshe clay, Lagos, Nigeria. *International Scholarly Research Notices*, 2012, 1–5. <https://doi.org/10.5402/2012/658508>
- Yassin, J. M., Shiferaw, Y. & Tedla, A. (2022). Application of acid activated natural clays for improving quality of Niger (*Guizotia abyssinica* Cass) oil. *Heliyon*, 8(4), 1–7. <https://doi.org/10.1016/j.heliyon.2022.e09241>
- Zhou, Y., Zhao, W., Lai, Y., Zhang, B. & Zhang, D. (2020). Edible plant oil: Global status, health issues, and perspectives. *Frontiers in Plant Science*, 11, 1315. <https://doi.org/10.3389/fpls.2020.01315>
- Zio, S., Cisse, H., Zongo, O., Guira, F., Tapsoba, F., Somda, N. S., Hama-Ba, F., Songre-Ouattara, L. T., Zongo, C., Traore, Y. & Savadogo, A. (2020). The oils refining process and contaminants in edible oils: A review. *Journal of Food Technology Research*, 7(1), 9–47. <https://doi.org/10.18488/journal.58.2020.71.9.47>

BIOTECHNOLOGY

Original scientific article

THE IMPACT OF pH VALUE AND TEMPERATURE ON POLYPHENOL RECOVERY, ANTIOXIDANT CAPACITY AND PHYSICAL PROPERTIES OF SERPYLLI HERBA'S WASTE EXTRACTS

Aleksandra A. Jovanović¹, Predrag M. Petrović¹, Mina Volić¹, Nataša Obradović¹, Bojana Balanč¹, Radoslava Pravilović², Branko M. Bugarski²

¹University of Belgrade, Innovation centre of Faculty of Technology and Metallurgy, Belgrade, Serbia

²University of Belgrade, Faculty of Technology and Metallurgy, Belgrade, Serbia

Abstract

In the present study, Serpylli herba's waste extracts were prepared using 50% ethanol (pH 6) and 50% ethanol with hydrochloric acid (pH 1.2), using maceration (25 °C) and heat-assisted extraction (HAE, 80 °C). The best extraction conditions were determined *via* analyzing total polyphenol (TPC) and flavonoid contents (TFC), antioxidant capacity, extraction yield, zeta potential, density, and surface tension. In maceration and HAE, TPC were 1.18±0.06 and 1.43±0.05 mg GAE/mL (pH 6), and 0.69±0.05 and 0.86±0.02 mg GAE/mL (pH 1.2). The same trend is noticed in the case of TFC: 0.33±0.01 and 0.42±0.02 mg CE/mL (pH 6) and 0.24±0.01 and 0.27±0.01 mg CE/mL (pH 1.2). ABTS radical scavenging activity was 775.0±3.5 and 623.8±5.1 mmol Trolox/mL (pH 6), and 269.2±3.1 and 327.9±7.7 mmol Trolox/mL (pH 1.2). In DPPH assay, IC₅₀ was 1.64±0.04 and 1.48±0.03 mg/mL (pH 6), and 7.59±0.07 and 5.11±0.09 mg/mL (pH 1.2). Extraction yield was 0.541±0.049 and 0.583±0.019% (pH 6), and 0.938±0.057 and 0.889±0.060% (pH 1.2). Zeta potential was -2.58±0.02 and -2.08±0.10 mV (pH 6), and 1.49±0.37 and 1.08±0.09 mV (pH 1.2). Density was 0.945±0.001 and 0.949±0.001 g/mL (pH 6), and 1.008±0.001 and 1.010±0.001 g/mL (pH 1.2). Surface tension was 29.2±0.3 and 30.5±1.0 mN/m (pH 6), and 32.6±2.3 and 36.5±2.3 mN/m (pH 1.2). The best properties were determined in the extract obtained in HAE at pH 6. The aim of this study is to provide evidence of the physico-chemical properties of Serpylli herba's waste extracts that can add value and improve the quality of existing food, pharmaceutical, and cosmetic products.

Keywords: antioxidant capacity, density, polyphenols, Serpylli herba waste, surface tension.

Introduction

There is a growing interest in extracting polyphenol compounds from various plant materials intending to produce a safe, natural, and low-cost alternative to synthetic antioxidant compounds (Čadanović-Brunet et al., 2006). Different polyphenol extraction procedures, which vary in nature of plant material, solvent-to-solid ratio, extraction time, temperature, type and pH value of the extraction medium, were established (Both et al., 2014; Dent et al., 2013; Jovanović et al., 2021). Traditional procedures for obtaining plant extracts include maceration, percolation, Soxhlet extraction, leaching, etc. However, the mentioned methods possess various disadvantages, such as low extraction yield, prolonged extraction time, a large amount of the extraction medium and plant material, and consequently negative environmental impact (Jovanović et al., 2017). Thus, the application of novel extraction methods, such as heat-assisted extraction, which provide solvent saving, shorter extraction time, and higher extraction yield, have been evaluated (Dent et al., 2013; Jovanović et al., 2022; Tameshia et al., 2010; Oniszczuk & Podgórski, 2015). The pH of the extraction medium is an

important factor that impacts the solubility of the target components. Herbal sources contain various polyphenol compounds that have different solubility at different pH values (Wissam et al., 2012). Additionally, various research papers showed the presence of different bioactive components in plant waste, thus the extracts from the mentioned by-product can be incorporated in food, pharmaceutical, and cosmetic formulations (Panić et al., 2018; Sagar et al., 2018; Saha & Basak, 2020).

Thymus serpyllum L. (Lamiaceae), known as creeping thyme, wild thyme, or mother of thyme, is thyme species native to the Mediterranean region (Greece, Italy, and Spain) and extensively cultivated in France, Spain, Portugal, Greece, and the United States (California). *T. serpyllum* contains 0.4-2.3% volatile oil consisting of highly variable amounts of polyphenols, alcohols; and monoterpene hydrocarbons. Depending on sources, thymol or carvacrol are its major polyphenols (Khan & Abourashed, 2010). Serpylli herba has shown bronchodilatory activity on the smooth muscle of the trachea and spasmolytic activity on the ileum *in vitro* (Jovanović et al., 2022; Khan & Abourashed, 2010). The mentioned effects are probably related to unidentified non-phenolic compounds, not due to thymol and carvacrol (Khan & Abourashed, 2010). Additionally, fresh and dried Serpylli herba is reportedly used as an anthelmintic, antioxidant, antimicrobial, analgesic, carminative, sedative, diaphoretic, and expectorant, in rheumatism, skin problems, chronic gastritis, diarrhea, lack of appetite, acute bronchitis, laryngitis, whooping, cough, and cancer, usually in the form of an infusion, tincture, or essential oil (Jovanović et al., 2022; Khan & Abourashed, 2010).

The present study aimed to examine the influence of pH value and temperature on polyphenol and flavonoid contents, ABTS and DPPH radical scavenging activity, extraction yield, zeta potential, density, and surface tension of Serpylli herba's waste extracts.

Materials and Methods

Plant material, reagents, and standards

Air-dried and milled *T. serpyllum* waste (particle size of 0.3 mm that cannot be an integral part of the tea products for the market) was from the Institute for Medicinal Plants Research "Dr Josif Pančić", Pančevo, Serbia. The following reagents were used: ethanol and sodium carbonate (Fisher Scientific, UK), Folin-Ciocalteu reagent and gallic acid (Merck, Germany), potassium persulfate (Centrohem, Serbia), sodium nitrite (Alkaloid, Macedonia), 1M sodium hydroxide solution (Alfapanon, Serbia), 2,2'-azino-bis(3-ethylbenzothiazoline-6-sulphonic acid) or ABTS, 6-hydroxy-2,5,7,8-tetramethylchroman-2-carboxylic acid or Trolox, 2,2-diphenyl-1-picrylhydrazyl or DPPH, aluminum chloride, hydrochloric acid, and catechin (Sigma-Aldrich, USA).

Extract preparation

The extracts were prepared by using waste of dried *T. serpyllum*, 50% ethanol as an extraction solvent (pH 6) or 50% ethanol with hydrochloric acid (pH 1.2), and maceration (25 °C, 60 min) or heat-assisted extraction (HAE, 80 °C, 15 min), in the incubator shaker (KS 4000i control, IKA, Germany). A necessary amount of hydrochloric acid was added to the ethanol/water mixture to regulate the pH of the extraction medium. All extracts were prepared in triplicate.

Determination of total polyphenol and flavonoid contents

Total polyphenol content (TPC) was determined using the previously described Folin-Ciocalteu assay (Jovanović et al., 2022). The results are expressed as milligrams of gallic acid equivalents per milliliter of liquid extract (mg GAE/mL).

Total flavonoid content (TFC) was estimated using the previously described spectrophotometrically procedure (Jovanović et al., 2022). The results were presented as milligrams of catechin equivalents per milliliter of liquid extract (mg CE/mL).

Determination of antioxidant capacity

The antioxidant activity of the extracts was measured according to previously published ABTS and DPPH assays (Jovanović et al., 2022). The antioxidant potential was expressed as mmol of Trolox equivalents per mL of liquid extract (mmol Trolox/mL, ABTS assay) and as IC₅₀, the concentration required to scavenge 50% of free DPPH radicals (mg/mL, DPPH assay). All absorbance readings were performed on UV spectrophotometer, UV-1800 (Shimadzu, Japan).

Determination of extraction yield

The extraction yield was expressed as the dry matter content of the extract, dry matter content = $100 - ((a-b) \cdot 100) / m$, where a represents the weight of the vessel containing the extract before drying (g), b represents the weight of the vessel containing the extract after drying in Memmert 30-1060 (Mettler GmbH, Germany) at 105 °C to constant mass (approximately 2 h), and m represents the weight of the sample. Dry matter content is expressed as %.

Analysis of zeta potential, density, and surface tension

The zeta potential of the extracts was determined by photon correlation spectroscopy in Zetasizer Nano Series, Nano ZS (Malvern Instruments Ltd., UK). Each sample was measured three times at room temperature.

Density and surface tension were measured using silicon crystal as the immersion body and Wilhelmy plate, respectively, in Force Tensiometer K20 (Kruss, Germany). Each extract was examined three times at room temperature.

Statistical analysis

The statistical analysis was performed by using the analysis of variance (one-way ANOVA) followed by Duncan's *post hoc* test (STATISTICA 7.0). The statistical difference was considered significant at $p < 0.05$, $n = 3$.

Results and discussion

Total polyphenol and flavonoid contents

As can be seen from Table 1, the pH value of the extraction medium, as well as the used extraction technique, more precisely temperature, had a statically significant influence on polyphenol content in *T. serpyllum* ethanol extracts. Namely, polyphenol yield was significantly higher at pH 6 (1.18±0.06 mg GAE/mL for maceration and 1.43±0.05 mg GAE/mL for HAE) in comparison to the samples obtained at pH 1.2 (0.69±0.05 mg GAE/mL for maceration and 0.86±0.02 mg GAE/mL for HAE). In addition, the extracts obtained at 80 °C have shown higher TPC compared to the samples from maceration. The same trend is noticed in the case of TFC, where the extract obtained at pH 6 in HAE possessed the highest TFC (0.42±0.02 mg CE/mL), followed by the extract prepared at the same pH in maceration (0.33±0.01 mg CE/mL). Statistically significant lower flavonoid yield was in the extracts prepared at pH 1.2 (0.24±0.01 and 0.27±0.01 mg CE/mL, for maceration and HAE, respectively).

Table 1. Total polyphenol content (TPC), total flavonoid content (TFC), and antioxidant capacity (ABTS and DPPH assays) of Serpylli herba waste extracts obtained using 50% ethanol (pH 6) or 50% ethanol with hydrochloric acid (pH 1.2), and maceration (MAC, 25 °C) or heat-assisted extraction (HAE, 80 °C)

samples	TPC [mg GAE/mL]	TFC [mg CE/mL]	ABTS [mmol Trolox/mL]	DPPH IC ₅₀ [mg/mL]
MAC pH 1.2	0.69±0.06 ^{d*}	0.24±0.01 ^d	269.2±3.1 ^d	7.59±0.07 ^d
MAC pH 6	1.18±0.06 ^b	0.33±0.00 ^b	775.0±3.5 ^a	1.64±0.04 ^b
HAE pH 1.2	0.86±0.02 ^c	0.27±0.01 ^c	327.9±7.7 ^c	5.11±0.09 ^c
HAE pH 6	1.43±0.05 ^a	0.42±0.02 ^a	623.8±5.1 ^b	1.48±0.03 ^a

*Values with different letters (a-d) in the variable group showed statistically significant differences ($p < 0.05$; $n = 3$; analysis of variance, Duncan's *post-hoc* test); GAE, gallic acid equivalent; CE, catechin equivalent; IC₅₀ (mg/mL), the concentration of the extract required to neutralize 50% of DPPH radicals.

According to the literature, the content of extracted polyphenols increased with the decrease in pH values, but only up to a certain level. Namely, Librán et al. (2013) have reported that polyphenol concentration in grape extracts increased with the decrease in pH value up to 2, or even 4, in the case of polyphenols from pomegranate peel (Motikar et al., 2021). Although the acidic condition provides the breaking interactions between polyphenols and sugar or proteins polymers, and the protonation of polyphenol molecules, consequently leading to the stronger polyphenol-solvent interaction and faster penetration of the extraction medium through the herbal matrix (El-Abbassi et al. 2014; Motikar et al., 2020), it can be concluded that acidic pH value (1.2) used in the case of *T. serpyllum* extracts was too low.

The presented results of the influence of the temperature on TPC and TFC are in accordance with the literature data, where the higher temperature was a significant factor in maximizing the polyphenol yield in *Rosmarinus officinalis*, *Origanum vulgare*, *O. majorana*, and *Salvia officinalis* extracts (Dent et al., 2013; Hossain et al., 2011). Namely, high temperature causes the disruption of plant cells and their structures that lead to the increase of membrane permeability and breakdown of bonds between secondary metabolites structure compounds. Additionally, higher temperature decreases surface tension and viscosity of the extraction solvent, helps wetting of the plant material and solvent penetration through the plant matrix, consequently increasing mass transfer and polyphenol recovery. The all mentioned mechanisms cause the improvement and acceleration of the extraction process, i.e. better extraction efficiency (Jovanović et al., 2017).

Antioxidant capacity of the extracts

The antioxidant capacity of Serpylli herba waste extracts is determined using ABTS and DPPH assays, and the results are presented in Table 1. Considering that these methods are based on different reactions, the results obtained thereof may provide good insight into the overall antioxidant capacity of the extracts. It can be noticed that both, the pH value of the extraction solvent and extraction temperature have shown a statically significant impact on ABTS and DPPH radical scavenging activity of Serpylli herba ethanol extracts.

In specific, ABTS antioxidant activity was significantly higher in the extracts prepared at pH 6 (775.0±3.5 and 623.8±5.1 mmol Trolox/mL, for maceration and HAE, respectively) compared to their parallels prepared at pH 1.2 (269.2±3.1 and 327.9±7.7 mmol Trolox/mL). However, the extract from maceration prepared at pH 6 has shown statistically significantly higher ABTS radical scavenging potential compared to the HAE parallel. It can be explained by the fact that different polyphenol and flavonoid compounds are extracted in different extraction mediums, and probably the polyphenols and flavonoids extracted at pH 6 can be thermosensitive and at 80 °C their degradation occurs (Kalušević et al., 2022). Additionally, various unquantified polyphenols, non-phenolic compounds, as well as synergism can be also responsible for the antioxidant capacity of the extracts (Imeh and Khokhar, 2002). Previous studies reported that the correlation between antioxidant

potential and polyphenol concentration depends not only on the TPC determined using the Folin-Ciocalteu method but also on the composition of the extracts (Librán et al., 2013; Rajakaruna et al., 2021). The significant better antioxidant potential of the extracts prepared at pH 6 (compared to pH 1.2) is correlated to the previously discussed TPC and TFC. Since that pH represents one of the most important factors that can directly influence the polyphenols yield, antioxidant capacity, and stability of the extracts, several studies have shown that acidic conditions are associated with higher polyphenol and flavonoid yield, and consequently higher antioxidant potential (Putnik et al., 2016; Rajakaruna et al., 2021; Wang et al., 2013). Although according to the literature, the increased acidity provided a better release of polyphenols and flavonoids, and thus, enhanced the antioxidant potential of different plant extracts, in the present study, the pH value was significantly lower than optimal. Therefore, various pH values (>1.2 and >6) should be investigated in future experiments. The combination of herbal source, extraction solvent, and extraction procedure can significantly influence antioxidant capacity and it should be investigated and optimized for every plant matrix.

In the DPPH assay, lower IC_{50} (higher antioxidant potential) was measured for the extracts prepared at pH 6, 1.64 ± 0.04 mg/mL for maceration and 1.48 ± 0.03 for HAE, whereas the extracts prepared at acidic pH have shown significantly higher IC_{50} , 7.59 ± 0.07 and 5.11 ± 0.09 mg/mL, maceration and HAE, respectively. The obtained results are in correlation with polyphenol and flavonoid concentrations. Miraj et al. (2017) have reported that the antioxidant activity of aromatic plants from the Lamiaceae family has arisen from the higher content of some representatives of polyphenols, such as rutin, quercetin, chlorogenic acid, rosmarinic acid, and similar. According to the literature, the reduction of DPPH radicals may be due to the reducing property of flavonoids (Jovanović et al., 2022). The highest values of DPPH antioxidant activity of the extracts obtained by HAE revealed that the mentioned technique generates high extraction efficiency in the matter of antioxidant compounds in different extraction mediums, ethanol-water and ethanol-water-hydrochloric acid. Higher temperature assists polar solvents to penetrate the structure of plant cells causing the solubilisation and hydrogen bond breaking. Therefore, in that surrounding, there is a gradual increase of released polyphenols and flavonoids, which can scavenge and neutralize the free radical species, superoxide anions, etc. (Radomir et al., 2019).

Physical characterization of the extracts

Physical characteristics, including extraction yield (EY), zeta potential (ζ) density (ρ), and surface tension (γ) of *T. serpyllum* ethanol extracts, obtained in maceration and HAE at pH 1.2 and 6, are presented in Table 2.

The extraction yield was expressed as the dry matter content of Serpylli herba ethanol extracts (%). Although it was expected, the extraction technique did not have a significant influence on the extraction yield (Table 2). Teofilović et al. (2016) have reported that the extraction yield can be influenced by the gradient of concentrations between free solvent and internal liquid (bonded solvent with the plant particles), the particle size of plant material, porosity, microcapillary, and the contact between solvent and plant particles. Certainly, the amount and polarity of solvent from one side, and the solid-to-solvent ratio for another, can directly affect the value of the extraction yield. On the other hand, at acidic pH value, extraction yield was statistically significantly higher ($0.938 \pm 0.057\%$ for maceration and $0.889 \pm 0.060\%$ for HAE) compared to the extracts prepared at pH 6 ($0.541 \pm 0.049\%$ for maceration and $0.583 \pm 0.019\%$ for HAE). At lower pH values, there is a significant breaking of interactions between polyphenol and structure compounds which consequently enhances the release of different compounds in addition to polyphenols, such as sugars, lipids, and proteins into the extraction medium, and increases the extraction yield (El-Abbassi et al. 2014; Jovanović et al., 2022; Motikar et al., 2020). Thus, the highest extraction yield does not always correlate with a higher concentration of target compounds. Leal et al. (2008) have reported that organic acid (quinic, tartaric, and malic acids) and rhamnose can also affect value of extraction yield.

Table 2. The extraction yield (EY), zeta potential, density, and surface tension of *Serpylli* herba extracts obtained using 50% ethanol (pH 6) or 50% ethanol with hydrochloric acid (pH 1.2), and maceration (MAC, 25 °C) or heat-assisted extraction (HAE, 80 °C)

samples	EY [%]	zeta potential [mV]	denisty [g/mL]	surface tension [mN/m]
MAC pH 1.2	0.938±0.057 ^a	1.49±0.37 ^{c*}	1.008±0.01 ^b	32.6±2.3 ^a
MAC pH 6	0.541±0.049 ^b	-2.58±0.02 ^a	0.945±0.00 ^d	29.2±0.3 ^b
HAE pH 1.2	0.889±0.060 ^a	1.08±0.09 ^c	1.010±0.0a	36.5±2.3 ^a
HAE pH 6	0.583±0.019 ^b	-2.08±0.10 ^b	0.949±0.02 ^c	30.5±1.0 ^b

*Values with different letters (a-c) in the variable group showed statistically significant differences (p<0.05; n=3; analysis of variance, Duncan's *post-hoc* test).

Determination of zeta potential of the plant extracts represents one of the most important variables from the aspect of extract encapsulation into various carriers, as well as for their potential use in coagulation and flocculation in drinking water treatment. The higher value of zeta potential (absolute value) is related to better stability of the system. However, in the case of all investigated *Serpylli* herba waste extracts, the values were quite low (Table 2). For extracts obtained at pH 6, zeta potential amounted -2.58±0.02 and -2.08±0.10 mV, for maceration and HAE, respectively, while the zeta potential of their parallels prepared at pH 1.2 was 1.49±0.37 and 1.08±0.09 mV. It can be noticed that the extracts prepared at pH 6 exhibited negative, but higher zeta potential (absolute value). It suggested that *T. serpyllum* extracts prepared at a higher pH value possess anionic proteins that could be used in the treatment of drinking water and wastewater because anionic extracts could coagulate and flocculate negatively charged particles through adsorption and bridging actions. Statistically significantly lower zeta potential (and positive) was in the extracts prepared at pH 1.2. According to Skaf et al. (2021), the extraction rate of the various compounds soluble in the used extraction medium with different pH values can be the reason for the mentioned variations of zeta potential for the extracts. *Serpylli* herba waste extracts from maceration possessed higher values of zeta potential in comparison to their parallels from HAE. Namely, in *Moringa oleifera* extracts, zeta potential values depended on the extraction conditions and were 2-15 mV (Skaf et al., 2021). Jones (2018) has examined the zeta potential of Hibiscus crude extracts (-6.4 and -8.3 mV) intending to investigate the potential application in coagulation in water treatment as well.

Based on density measurements, a significantly higher density was obtained for the extract prepared at pH 1.2 (1.008±0.001 g/mL for maceration and 1.010±0.001 g/mL for HAE), whereas the density of their parallels prepared at pH 6 was 0.945±0.001 and 0.949±0.001 g/mL, which was correlated with their extraction yields (Table 2). However, the density of the extracts from HAE was slightly higher in comparison to their parallels from maceration. According to Mladenović et al. (2018), the extraction conditions and techniques significantly affect the density of the extracts, and in addition, density correlates to the extraction yield. Furthermore, the density of coffee extracts was in the range of 1.030 to 1.350 g/mL increasing with the increase of the dry substances' mass fraction (Khomiyakov et al., 2020).

The surface tension was significantly lower for the extracts prepared at pH 6 (29.2±0.3 and 30.5±1.0 mN/m, maceration and HAE, respectively) compared to the extracts obtained at pH 1.2 (32.6±2.3 and 36.5±2.3 mN/m, maceration and HAE, respectively). Nevertheless, the extraction technique did not have a significant impact on the surface tension of the extracts. As the values of surface tension of *T. serpyllum* extracts increase (at acidic pH value, Table 2), a decrease in the polyphenol concentration can be noticed (Table 1). Pellati et al. (2013) have reported that in the case of lower surface tension of the extraction medium, better adsorption of polyphenols by the solvent is provided. Furthermore, quick penetration of the extraction solvent to the herbal matrix causes an increase in surface contact, as well as a better release of polyphenols. Peng et al. (2016) have also shown that lower surface

tension is related to the relatively low interaction between molecules of water through hydrogen bonds that can provide higher mass transfer, as well as better polyphenol diffusion.

Conclusion

The present study aimed to examine the impact of pH value and temperature on polyphenol and flavonoid contents, ABTS and DPPH radical scavenging activity, extraction yield, zeta potential, density, and surface tension of Serpylli herba's waste extracts. Both, pH value and extraction temperature had a statically significant influence on polyphenol and flavonoid contents, as well as antioxidant activity. The highest TPC, TFC, and DPPH radical scavenging potential were determined in the extract prepared at pH 6 in heat-assisted extraction. On the other hand, the highest extraction yield, density, and surface tension were measured in the extracts prepared at pH 1.2, while the highest zeta potential was in the extract prepared at pH 6 in maceration. The presented study provides evidence of the physico-chemical properties of Serpylli herba's waste extracts that can add value and improve the quality of existing food, pharmaceutical, and cosmetic formulation, as well as in diagnostic tests and drinking water and wastewater treatment.

References

- Both, S., Chemat, F. & Strube, J. (2014). Extraction of polyphenols from black tea – Conventional and ultrasound assisted extraction. *Ultrasonic Sonochemistry*, 21, 1030–1034. <https://doi.org/10.1016/j.ultsonch.2013.11.005>
- Dent, M., Dragović-Uzelac, V., Penić, M., Brnčić, M., Bosiljkov, T. & Levaj, B. (2013). The effect of extraction solvents, temperature and time on the composition and mass Fraction of polyphenols in Dalmatian wild sage (*Salvia officinalis* L.) extracts. *Food Technology and Biotechnology*, 51, 84–91.
- Hossain, M. B., Barry-Ryan, C., Martin-Diana, A. B. & Brunton, N. P. (2011). Optimisation of accelerated solvent extraction of antioxidant compounds from rosemary (*Rosmarinus officinalis* L.), marjoram (*Origanum majorana* L.) and oregano (*Origanum vulgare* L.) using response surface methodology. *Food Chemistry*, 126, 339–346. <https://doi.org/10.1016/j.foodchem.2010.10.076>
- Čadanović-Brunet, J., Djilas, S., Četković, G., Tumbas, V., Mandić, A. & Čadanović, V. (2006). Antioxidant activities of different *Teucrium montanum* L. extracts. *International Journal of Food Science and Technology*, 41, 667–673. <https://doi.org/10.1111/j.1365-2621.2006.01133.x>
- Imeh, U. & Khokhar, S. (2002). Distribution of conjugated and free phenols in fruits: antioxidant activity and cultivar variations. *Journal of Agricultural and Food Chemistry*, 50, 6301–6306. <https://doi.org/10.1021/jf020342j>
- Jones, N. (2018). The zeta potential in crude extracts of some hibiscus plants for water treatment. *Arid Zone Journal of Engineering, Technology and Environment*, 14(1), 85–93.
- Jovanović, A., Petrović, P., Djordjević, V., Zdunić, G., Šavikin, K. & Bugarski, B. (2017). Polyphenols extraction from plant sources. *Lekovite Sirovine*, 37, 45–49. <https://doi.org/10.5937/leksir1737045J>
- Jovanović, A., Djordjević, V., Petrović, P., Pljevljakušić, D., Zdunić, G., Šavikin, K. & Bugarski, B. (2021). The influence of different extraction conditions on polyphenol content, antioxidant and antimicrobial activities of wild thyme. *Journal of Applied Research on Medicinal and Aromatic Plants*, 25, 100328. <https://doi.org/10.1016/j.jarmap.2021.100328>
- Jovanović, A., Vajić, J., Mijin, D., Zdunić, G., Šavikin, K., Branković, S., Kitić, D. & Bugarski, B. (2022). Polyphenol extraction in microwave reactor using by-product of *Thymus serpyllum* L.

- and biological potential of the extract. *Journal of Applied Research on Medicinal and Aromatic Plants*, 31(10), 100417. <https://doi.org/10.1016/j.jarmap.2022.100417>
- Kalušević, A., Salević, A., Jovanović, A., Trifković, K., Veljović, M., Pravilović, R. & Nedović, V. (2022). Encapsulation of Plant Extracts in Encapsulation, Lević, S., Nedović, V. & Bugarski B. (Ed.), In *Food Processing and Fermentation*. Taylor & Francis Group, <https://doi.org/10.1201/9780429324918-7>
- Khan, I. & Abourashed, E. (2010). *Leung's encyclopedia of common natural ingredients used in food, drugs, and cosmetics*. John Wiley & Sons, Inc.
- Khomyakov, A. P., Mordanov, S. V. & Khomyakova, T. V. (2020). The experimental data on the density, viscosity, and boiling temperature of the coffee extract. *IOP Conf. Series: Earth and Environmental Science*, 548, 022040. <https://doi.org/10.1088/1755-1315/548/2/022040>
- Librán, C., Mayor, L., Garcia-Castello, E. & Vidal-Brotons, D. (2013). Polyphenol extraction from grape wastes: Solvent and pH effect. *Agricultural Sciences*, 4(9B), 56–62. <https://doi.org/10.4236/as.2013.49B010>
- Leal, F. P., Maia, B. N., Carmello, A. C. K., Catharino, R. R., Eberlin, M. N. & Meireles, M. A. A. (2008). Sweet basil (*Ocimum basilicum*) extracts obtained by supercritical fluid extraction (SFE): global yields, chemical composition, antioxidant activity, and estimation of the cost of manufacturing. *Food and Bioprocess Technology*, 1, 326–338. <https://doi.org/10.1007/s11947-007-0030-1>
- Miraj, S., Kopae, M. R. & Kiano, S. (2017). *Melissa officinalis* L: A review study with an antioxidant prospective. *Journal of Evidence-Based Complementary & Alternative Medicine*, 22(3), 385–394. <https://doi.org/10.1177/2156587216663433>
- Mladenović, J., Đurić, M., Šekularac, G., Brković, D., Stepanović, J., Mašković, P. & Bošković Rakočević, Lj. (2018). Determination of the content of bioactive components in different extracts of *Portulaca oleracea* L. *Acta Agriculturae Serbica*, 23, 223–231. <https://doi.org/10.5937/AASer1846223M>
- Motikar, P. D., More, P. R. & Arya, S. S. (2021). A novel, green environment friendly cloud point extraction of polyphenols from pomegranate peels: a comparative assessment with ultrasound and microwave-assisted extraction. *Separation Science and Technology*, 56(6), 1014–1025. <https://doi.org/10.1080/01496395.2020.1746969>
- Oniszczyk, A. & Podgórski, R. (2015). Influence of different extraction methods on the quantification of selected flavonoids and phenolic acids from *Tilia cordata* inflorescence. *Industrial Crops and Products*, 76, 509–514. <https://doi.org/10.1016/j.indcrop.2015.07.003>
- Panić, M., Radić Stojković, M., Kraljić, K., Škevin, D., Radojčić Redovniković, I., Gaurina Srček, V. & Radošević, K. (2019). Ready-to-use green polyphenolic extracts from food by-products. *Food Chemistry*, 283, 628–636. <https://doi.org/10.1016/j.foodchem.2019.01.061>
- Pellati, F., Prencipe, F. P., Bertelli, D. & Benvenuti, S. (2013). An efficient chemical analysis of phenolic acids and flavonoids in raw propolis by microwave-assisted extraction combined with high-performance liquid chromatography using the fused-core technology. *Journal of Pharmaceutical and Biomedical Analysis*, 81–82, 126–132. <https://doi.org/10.1016/j.jpba.2013.04.003>
- Peng, X., Duan, M. H., Yao, X. H., Zhang, Y. H., Zhao, C. J., Zu, Y. G. & Fu, Y. J. (2016). Green extraction of five target phenolic acids from *Lonicerae japonicae* flos with deep eutectic solvent. *Separation and Purification Technology*, 157, 249–257. <https://doi.org/10.1016/j.seppur.2015.10.065>
- Putnik, P., Bursać Kovačević, D., Radojčin, M. & Dragović-Uzelac, V. (2016). Influence of acidity and extraction time on the recovery of flavonoids from grape skin pomace optimized by

- response surface methodology. *Chemical and Biochemical Engineering Quarterly*, 30(4), 455–464. <https://doi.org/10.15255/CABEQ.2016.914>
- Radomir, A.-M., Cătălina Guță, I., Cocuța Buciumeanu, E. & Letiția Pîrvu, M. (2019). Optimization of microwave extraction method of total polyphenols from *Melissa officinalis* L. vitroplants. *Biologie*, 28(1), 112–118.
- Rajakaruna, A., Manful, C., Abu-Reidah, I., Critch, A., Vidal, N., Pham, T., Cheema, M. & Thomas, R. (2021). Application of solvent pH under pressurized conditions using accelerated solvent extraction and green solvents to extract phytonutrients from wild berries. *Food Bioscience*, 47, 101471. <https://doi.org/10.1016/j.fbio.2021.101471>
- Sagar, N. A., Pareek, S., Sharma, S., Yahia, E. & Lobo, M. G. (2018). Fruit and vegetable waste: Bioactive compounds, their extraction, and possible utilization. *Comprehensive Reviews in Food Science and Food Safety*, 17(3), 512–531. <https://doi.org/10.1111/1541-4337.12330>
- Saha, A. & Basak, B. (2020). Scope of value addition and utilization of residual biomass from medicinal and aromatic plants. *Industrial Crops and Products*, 145, 111979. <https://doi.org/10.1016/j.indcrop.2019.111979>
- Skaf, D., Punzi, V., Rolle, J. & Cullen, E. (2021). Impact of *Moringa oleifera* extraction conditions on zeta potential and coagulation effectiveness. *Journal of Environmental Chemical Engineering*, 9(1), 104687. <https://doi.org/10.1016/j.jece.2020.104687>
- Tameshia, B. S., Parameswarakumar, M., Kequan, Z. & Sean, O. (2010). Microwave-assisted extraction of phenolic antioxidant compounds from peanut skins. *Food Chemistry*, 120, 1185–1192. <https://doi.org/10.1016/j.foodchem.2009.11.063>
- Teofilović, B. (2016). *Biochemical and chemical characterization of basil extracts and influence of pharmaceutical technological formulations on the glycemic, lipid and oxidative status in experimental animals* (Doctoral dissertation). University of Novi Sad, Medical Faculty, Novi Sad, Serbia. <https://www.cris.uns.ac.rs/DownloadFileServlet/Disertacija148180213455513.pdf>
- Wissam, Z., Ghada, B., Wassim, A. & Warid, K. (2012). Effective extraction of polyphenols and proanthocyanidins from pomegranate's peel. *International Journal of Pharmacy and Pharmaceutical Sciences*, 4, 675–682.
- Wang, C., Shi, L., Fan, L., Ding, Y., Zhao, S., Liu, Y. & Ma, C. (2013). Optimization of extraction and enrichment of phenolics from pomegranate (*Punica granatum* L.) leaves. *Industrial Crops and Products*, 42, 587–594. <https://doi.org/10.1016/j.indcrop.2012.06.031>

Original scientific article

THE POSSIBILITY OF ANTIBIOTIC AZALOMYCIN B PRODUCTION BY COMBINING BENZOYL HYDRAZONE DERIVATIVES AND WASTE RAPESEED OIL GLYCEROL

Jovan Ćirić^{1,2}, Slavica Ilić², Sandra Konstantinović², Đorđe Lazarević³, Marko Živković³, Nikola Stanković⁴

¹Toplica Academy of Vocational Studies – Department of Agricultural and Food Studies, Prokuplje, Serbia

²Faculty of Technology, University of Niš, Leskovac, Serbia

³Faculty of Electronic Engineering, University of Niš, Niš, Serbia

⁴Faculty of Sciences and Mathematics, Department of Biology, University of Niš, Niš, Serbia

Abstract

Previous research has shown that Schiff bases have a stimulating effect on the production of the antibiotic Azalomycine B by the bacterium *Streptomyces hygroscopicus*. Also, it was confirmed that waste glycerol obtained in biodiesel production from vegetable and inedible oils can be the common starting material for valuable industrial products such as antibiotics. In this paper, the results of studying the possibility of combining isatin derivatives of benzoyl hydrazone as a nitrogen source with waste glycerol, obtained in the rapeseed oil-based biodiesel production, as a carbon source for manufacturing antibiotic Azalomycine B by *S. hygroscopicus* CH-7 strain are presented. Depending on the nitrogen source (benzoyl hydrazone derivatives), the achieved maximal concentrations of azalomycine B range from 33 to 50 µg/ml, and the biomass content range from 5.5 to 5.9 g/l. The highest maximal concentration of Azalomycine B (50 µg/ml) and the specific rate of production (1.3 µg/g/d) were achieved in the medium with 5-chloroisatin-3 (4'-hydroxy) benzoylhydrazone. In general, the main difference in the structure of these compounds is the substituent at position 5, and chlorine in this case did not have a negative effect on antibiotic production.

Keywords: benzoyl hydrazone, waste glycerol, antibiotics.

Introduction

The Schiff bases possess many diverse biological activities (Konstantinović et al., 2008). It was confirmed that the usage of some of them as a nitrogen source for antibiotic production by *S. hygroscopicus* has a stimulative effect on Azalomycine B production (Ilić et al., 2010; Ćirić et al., 2016). Most of those studied isatin derivatives were synthesized in crude glycerol as a green solvent, and similar compounds have a positive effect on antibiotic production. Also, it was confirmed that waste glycerol obtained in biodiesel production can be a valuable starting material for some industrial processes (Konstantinović et al., 2016).

This paper aims to study the effect of the benzoyl hydrazone derivatives (isatin-3-(4'-hydroxy)benzoylhydrazone and 5-chloroisatin-3-(4'-hydroxy)benzoylhydrazone) in combination with waste glycerol obtained in rapeseed oil-based biodiesel production on the production of the antibiotic. The main difference between these two compounds is as a substituent at position 5.

Materials and Methods

The *S. hygroscopicus* CH-7 (NCAIM (P) B-001336) strain from the Microbial collection of the Faculty of Chemistry and Institute of Chemistry, Technology, and Metallurgy in Belgrade, Serbia

(Vučetić et al., 1994; Kradžić et al., 1991) was cultivated on the experimental fermentation media at 30 °C during 168 hours with shaking at 180 rpm. The content of the fermentative media was: (pure or waste glycerol 15 g/l; soybean 10 g/l; benzoyl hydrazone derivatives 5 g/l; CaCO₃ 3 g/l; NaCl 3 g/l; MgSO₄ x 7 H₂O 0.5 g/l; (NH₄)₂HPO₄ 0.5 g/l; K₂HPO₄ 1 g/l. The benzoyl hydrazone derivatives, which have added isatin and hydroxyl group or 5-chloroisatin and the hydroxyl group at the 3,5-position, were synthesized in the Laboratory for chemical technologies in the Faculty of Technology in Leskovac, Serbia. The results were obtained by spectrophotometrically measuring absorbance (Perkin-Elmer Lambda 15 UV/VIS) at $\lambda_{max} = 252$ nm for Azalomycine B (Vučetić et al., 1994; Kradžić et al., 1991). Microbial growth was determined by measuring the dry weights of cells (Kradžić et al., 1991). The concentrations of glycerol were determined using the HPLC method by Agilent 1100 Series chromatograph with Aminex HPX-87H column (Ćirić, 2017).

Results and discussion

To study the possibility of the yield increase of Azalomycin B, as well as the higher consumption of waste glycerol obtained in rapeseed oil-based biodiesel production, the influence of benzoyl hydrazone derivatives, as a source of nitrogen, on the bacterium *Streptomyces hygroscopicus* CH-7 gained in media with pure and waste glycerol, was studied. Table 1 shows the effect of benzoyl hydrazone derivatives on the maximum concentration of dry biomass, the total consumption of glycerol, and the production of antibiotics, while Figure 1 shows the change in the concentration of dry biomass, glycerol, and the antibiotic Azalomycin B. An almost identical increase in biomass was observed in the first 96 h of fermentation and after that, there was a decline, whereby growth with a maximum concentration of dry biomass of 5.9 g/l was achieved in the medium with isatin-3-(4'-hydroxy)benzoylhydrazone. The lower consumption of waste glycerol is also evident at 16% and 17% of the available amount compared to pure glycerol (41% and 29%). Regardless of the weaker growth and consumption of glycerol, than was observed in media with pure glycerol, the highest concentration of Azalomycin B (50 µg/ml) was achieved in the medium with 5-chloroisatin-3-(4'-hidroxy) benzoylhydrazone with a specific production rate of 1.3 µg/g/d, which is 19% that is 60% more than in the medium with pure glycerol. In contrast to that, in the medium with isatin-3-(4'-hydroxy)benzoylhydrazone, the higher values were obtained in combination with pure glycerol (52 µg/ml and 0.8 µg/g/d). There is no literature data for the research with the same or similar compounds and their effect on the microbial synthesis of antibiotics.

Table 1. Effect of benzoyl hydrazone derivatives as a nitrogen source on the maximum concentration of dry biomass (DBM), consumption of glycerol (Δ glyc), achieved maximum concentration (C_{max}), and specific production rate (q_p) of the antibiotic azalomycin B, during the cultivation of the *Streptomyces hygroscopicus* CH-7 in glycerol media

Characteristics of bioprocess										
Source of nitrogen	Pure glycerol			Waste glycerol						
	DBM	Δ glyc		Azalomycin B		DBM	Δ glyc		Azalomycin B	
	X_{max}			C_{max}	q_p	X_{max}			C_{max}	q_p
	g/l	mg/ml	%	µg/ml	mg/g/d	g/l	mg/ml	%	µg/ml	mg/g/d
isatin-3-(4'-hydroxy)benzoylhydrazone	8.2	6.3	41	52	0.8	5.9	2.3	17	33	0.7
5-chloroisatin-3-(4'-hydroxy)benzoylhydrazone	6.8	4.2	29	42	0.8	5.5	2.2	16	50	1.3

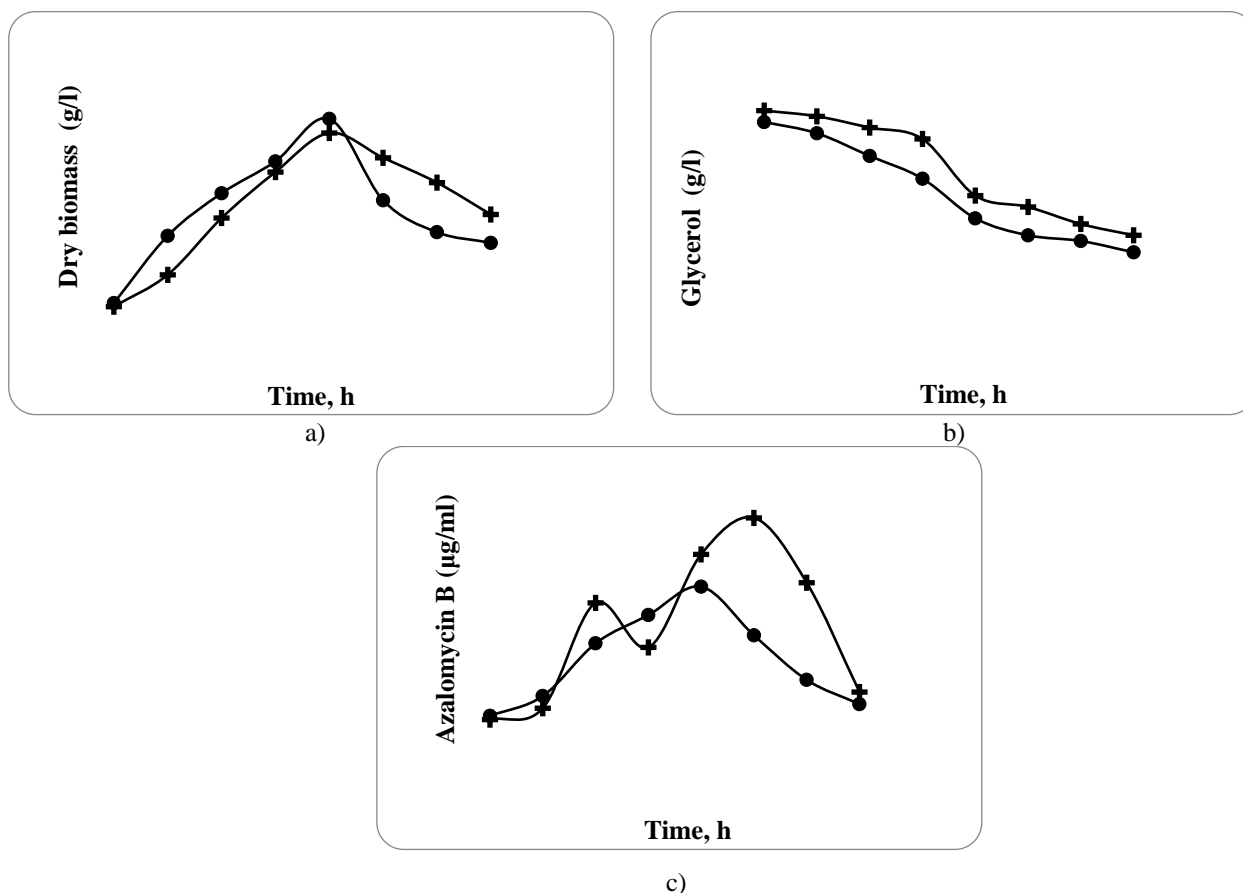


Figure 1. The change in concentration of dry biomass (a), the concentration of glycerol (b), and the concentration of antibiotic azalomycin B (c) during the cultivating *Streptomyces hygroscopicus* CH-7 in media with isatin-3-(4'-hydroxy)benzoylhydrazone (●) and 5-chloroisatin-3-(4'-hydroxy)benzoylhydrazone (+)

Conclusion

The achieved results are significant because they open up new possibilities for the common utilization of waste glycerol obtained in biodiesel production of biodiesel from rapeseed oil. Unlike the other processes and other microorganisms, chlorine, in this case as a substituent at position 5, did not have a negative effect on antibiotic production, even the opposite. The maximum achieved values of the antibiotic concentration were lower than in the previously published research with conventional media. To achieve better future results, additional purification of waste glycerol obtained in rapeseed oil-based biodiesel production is recommendable.

References

- Ćirić, J., Konstantinović, S., Ilić, S., Gojgić-Cvijović, G., Savić, D. & Veljković, V. (2016). The impact of isatin derivatives on antibiotic production by *Streptomyces hygroscopicus* CH-7. *Chemical Industry*, 70 (2), 123–128. <https://doi.org/10.2298/HEMIND141127019C>
- Ćirić, J. (2017). The microbial utilization of waste glycerol from biodiesel production, Doctoral dissertation, University of Niš
- Ilić, S. B., Konstantinović, S. S., Savić, D. S., Veljković, V. B. & Gojgić-Cvijović, G. (2010). The impact of Schiff bases on antibiotic production by *Streptomyces hygroscopicus*. *Medicinal Chemical Research*, 19, 690–697. <https://doi.org/10.1007/S00044-009-9223-7>

- Karadžić, I., Gojgić-Cvijović, G. & Vučetić, J. (1991). Hexaene H-85, A hexaene H-85 macrolide complex. *Journal of Antibiotics* 12, 1452–1453.
- Konstantinović, S. S., Radovanović, B. C., Sovilj, S. P. & Stanojević, S. S. (2008). Antimicrobial activity of some isatin-3-thiosemicarbazone complexes. *Journal of Serbian Chemical Society*, 72, 7–13. <https://doi.org/10.2298/JSC0801007K>
- Konstantinović, S., Danilović, B., Ćirić, J., Ilić, S., Savić, D. & Veljković, V. (2016). Valorization of crude glycerol from biodiesel production. *Chemical Industry and Chemical Engineering Quarterly*, 22(4), 461–489. <https://doi.org/10.2298/CICEQ160303019K>
- Vučetić, J., Karadžić, I., Gojgić-Cvijović, G. & Radovanović, E. (1994). Improving hexaene H-85 production by *Streptomyces hygroscopicus*. *Journal of Serbian Chemical Society*, 59, 973–980.

FOOD TECHNOLOGY

Original scientific article

RED WINE COLOR AND STABILITY AS FUNCTION OF SIZE AND CONTENT OF SILICA GEL PARTICLES

Tanja Šaran¹, Dragan Vujadinović¹, Zoran Petković², Milan Vukić¹, Vesna Gojković¹, Vladimir Tomović³

¹University of East Sarajevo, Faculty of Technology Zvornik, Bosnia and Herzegovina

²Zeochem Ltd Zvornik, Bosnia and Herzegovina

³University of Novi Sad, Faculty of Technology, Serbia

Abstract

Wine is a complex natural product influenced by many factors. Red wine is an alcoholic drink obtained by fermentation of grape juice. In addition to the qualities and degrees of ripeness of grapes, the production process, stabilization, and maturation are necessary for obtaining high quality wines. Clarification is a physical operation to remove deposited matter from wine. After fermentation, the process of clarification removes the precipitate and proteins, which preventively influence on the microbiological stability and quality of the red wine. Thanks to their negative charge, silica particles bind protein molecules to themselves. The main goal of this paper was to examine the influence of different concentration and sizes of silica gel particles on the stability of red wines. Red wine is prepared from varieties Kaberne, Vranac and Merlo. In total, 29 models were prepared to which four types of amorphous silica gel were added in different quantities (from 0.5 to 2 g/l). The following types of silica gel were used: I-SiO₂ (silica gel 60A, ACM 0-10µm); II-SiO₂ (silica gel 60A, SCR 0-40µm); III-SiO₂ (silica gel 60A, TSP 0-40µm); IV-SiO₂ (silica gel 90A, SCR 0-40µm). With the addition of silica gel to red wine, there was a decrease in the value of the content of total acids, as well as tartarate salts, which leads to an increase in the stability of the wine. An increase in the amount of added silica gel showed an improvement in the properties of red wine. The most optimal results were achieved with the addition of 1.5 to 2.0 g of silica gel. Among them, the best results were shown by the models M1.4, M6.4 and M7.4.

Keywords: wine clarification, red wine, silica gel, wine stabilisation.

Introduction

Red wine is an alcoholic drink obtained by fermentation more widely (grape juice). The process of obtaining red wine involves maceration, which represents the difference compared to the production of white wine. With the progress of human society, wine production has been perfected, however, the basic processes, which make wine what it is, have remained unchanged. The earliest records show that in Asia wine was ruled as much as 12 thousand years ago (Jackson, 2020). In addition to the qualities and degrees of grape ripeness, the final quality of wines is largely influenced by climatic and other agroecological environmental factors. Among the ingredients of red wine a very important place is occupied by phenolic compounds, micro and macroelements (Reynolds, 2021; Ribéreau-Gayon et al., 2021; Teng et al., 2020). Maceration is one of the processes aimed at moving individual ingredients from solid parts of grapes to a liquid phase (Aleixandre-Tudo & du Toit, 2018) During the maceration process, there is a build-up of aromatic, nitrogenous and mineral substances as well as phenolic compounds that make up the color and structure of the wine (anthocyanins and tannins) (Bakker & Clarke, 2011).

In wine production, alcoholic fermentation represents an anaerobic transformation of sugar into ethanol and carbon dioxide. Winemakers today use two types of yeasts that have wide application. These are *Saccharomyces cerevisiae* and *Saccharomyces bayanus* yeast (Bisson, 2004). The best yeast is considered selected wine yeast from grapes (Mills et al., 2008). During fermentation, other biochemical and chemical reactions take place simultaneously, which allow the translation of grape juice into wine. In addition to ethanol, higher alcohols, esters, glycerol, diacetyl and 2,3-butandiol are formed (Malfeito-Ferreira, 2021; Sumby et al., 2019).

Wine stabilization represents a group of operations that prevent the appearance of turbidity and precipitation after closing in bottles. Wines kept in basement courts should be checked regularly in terms of volatile acids and sulphur dioxide (Salaha et al., 2008; Snopek et al., 2018). The increase in volatile acids represents the first sign of some of the spoilage of wine. Maintaining a certain concentration of sulfur dioxide is necessary to protect against microorganisms but also from oxidation. It is sought that the wine kept in the cellar conditions contains 20-25 mg/l of free sulphur dioxide (Ma et al., 2022). Wine stabilisation measures include clarification, filtration and cold stabilisation of wines, while wine care measures include replenishing courts and transshipment of wine (Bakker & Clarke, 2011).

Clarifying is a physical operation to remove the particles and poised matter from wine. Young wines are usually not clear enough, so colloidal particles must be removed with the help of certain chemical substances. Turbidity is caused by colloidal particles and proteins (Stanković et al., 2004). In this paper, silica gel was used for wine clearing, which represents the amorphous form of silicon dioxide SiO_2 and is unique in its porous structure. The properties of silica gel depend on the method of preparation, but usually have a pore size of 2200 to 2600 nm and an active surface area of 750 - 800 m^2/g . Chemically is inert and non-toxic (Stanković et al., 2004; Wang et al., 2020; Zhang et al., 2021). Therefore, the new goal of this paper is to examine the influence of different concentrations and sizes of silica gel particles on the stability of red wines.

Materials and methods

Wine preparation

Grapes of the Kaberne, Vranac and Merlo varieties were purchased and according to the standard technological procedure prepared in such a way that 4 parts of Vranac, 2 parts of Kaberne and 1 part of the Merlo variety were mixed. Maceration lasted 8 days at a temperature of 21 °C. After that, grape juice was separated, and alcohol fermentation continued in vertical stainless-steel tanks. Then wine yeast is added to achieve alcoholic fermentation (*Uvaferm bayanus*, *Saccharomyces cerevisiae*) at a temperature of 19-20 °C in 4-week stretch. At the beginning of the last week, wine samples were taken and models with silica gels were prepared. Models with silica gel are prepared in such a way that the planned concentration of silica gel is added to the bottle of wine with a volume of 500 cm^3 . After adding silica gel, the models are kept for seven days in a thermostatic chamber at a temperature of 18 °C in closed colored bottles. For the first three days, each bottle is stirred by hand twice a day for 30 seconds.

Twenty-nine models have been prepared, including the reference model M0. Measurements were made on each of these models. Each individual measurement has been repeated three times to determine the reliability of the results. Four types of amorphous silica gel were used to stabilize the wine: I- SiO_2 (silica gel 60A, ACM 0-10 μm); II- SiO_2 (silica gel 60A, SCR 0-40 μm); III- SiO_2 (silica gel 60A, TSP 0-40 μm); IV- SiO_2 (silica gel 90A, SCR 0-40 μm).

Table 1. Tested wine models with added silica gel

M0	Red wine not treated with silica gel
M1.1.	0.5 g I-SiO ₂ /1l wine
M1.2.	1.0 g I-SiO ₂ /1l wine
M1.3.	1.5 g I-SiO ₂ /1l wine
M1.4.	2.0 g I-SiO ₂ /1l wine
M2.1.	0.5 g II-SiO ₂ /1l wine
M2.2.	1.0 g II-SiO ₂ /1l wine
M2.3.	1.5 g II-SiO ₂ /1l wine
M2.4.	2.0 g II-SiO ₂ /1l wine
M3.1	0,5 g III-SiO ₂ /1l wine
M3.2	1.0 g III-SiO ₂ /1l wine
M3.3	1.5 g III-SiO ₂ /1l wine
M3.4	2.0 g III-SiO ₂ /1l wine
M4.1	Mixed 0.5 g = 50%:50% = (I-SiO ₂ : II-SiO ₂)/1l wine
M4.2	Mixed 1.0 g = 50%:50% = (I-SiO ₂ : II-SiO ₂)/1l wine
M4.3	Mixed 1.5 g = 50%:50% = (I-SiO ₂ : II-SiO ₂)/1l wine
M4.4	Mixed 2.0 g = 50%:50% = (I-SiO ₂ : II-SiO ₂)/1l wine
M5.1	Mixed 0.5 g = 50%:50% = (I-SiO ₂ : III-SiO ₂)/1l wine
M5.2	Mixed 1.0 g = 50%:50% = (I-SiO ₂ : III-SiO ₂)/1l wine
M5.3	Mixed 1.5 g = 50%:50% = (I-SiO ₂ : III-SiO ₂)/1l wine
M5.4	Mixed 2.0 g = 50%:50% = (I-SiO ₂ : III-SiO ₂)/1l wine
M6.1	Mixed 0.5 g = (33.33%:33.33%:33.33%) = (I-SiO ₂ : II-SiO ₂ : III-SiO ₂)/1l wine
M6.2	Mixed 1.0 g = (33.33%:33.33%:33.33%) = (I-SiO ₂ : II-SiO ₂ : III-SiO ₂)/1l wine
M6.3	Mixed 1.5 g = (33.33%:33.33%:33.33%) = (I-SiO ₂ : II-SiO ₂ : III-SiO ₂)/1l wine
M6.4	Mixed 2.0 g = (33.33%:33.33%:33.33%) = (I-SiO ₂ : II-SiO ₂ : III-SiO ₂)/1l wine
M7.1	0.5 g : IV-SiO ₂ /1l wine
M7.2	1.0 g : IV-SiO ₂ /1l wine
M7.3	1.5 g : IV-SiO ₂ /1l wine
M7.4	2.0 g : IV-SiO ₂ /1l wine

Before carrying out the planned experimental measurements, in plastic tubes with a volume of 50 cm³, red wine from the prepared models was poured and all samples were centrifuged (Tehtnica Centric 400R) on 2000 G for 5 minutes. The content of total acids is determined by volumetric standard potentiometric titration and is expressed as tartaric acid in g/l. The color of the wine is determined spectrophotometrically (Konica Minolta, Spectrofotometer CM-5). The color was measured at wavelengths from 380 to 780 nm, every 5 nm, with D65 illuminatant and angle of the observer 10°, in a 1cm cuvette opposite distilled water as a blind test. A freezing tartare test implies exposure of filtered wine at a temperature of -4 °C for a time interval of three days. After that, an inspection was carried out on the presence of crystal tartare precipitate. If the precipitate dissolves during heating to room temperature, the wine is considered stable. However, the presence of crystalline precipitate indicates the instability of the wine. After visual inspection, the presence of the tartarate precipitate is measured for the conductivity of the wine. The wine is cooled to a temperature of 5 °C and measures the change in conductivity by adding potassium bitartrate crystals (1 g/l). A change in conductivity over 5% indicates unstable wine.

All experiments were carried out in a model of a minimum of three repetitions. Variance analysis (ANOVA) was performed over all variables in the general linear model. The statistically significant difference in the mean values of the obtained experimental data is calculated using the T – Tukey HSD test with statistical significance of (p≤0.05). On the results of the different letter code a, b, c, d... indicate the existence of a difference of that significance, and the same letter marks to the non-existence. Statistical processing was carried out using online tools (One way ANOVA with post-hoc Tukey HSD Test <https://astatsa.com/>).

Results and discussions

Total acid content

Table 2 shows four groups of models. Each group represents the same amount of added silica gel. In models marked with M1.1-M7.1, 0.5 g/l of different types and mixtures of silica gels was added to the wine. The values in the table show an impact on the content of total acids in red wine. A group marked with M1.2-M7.2 displays models that have added silica gel of 1 g/l. Analogously, groups marked with M1.3-M7.3 and M1.4-M7.4 added the maximum amounts of silica gel 1.5 g/l and 2.0 g/l respectively.

In the first group of models (M1.1 - M7.1), the M1.1 model has significant ($p \leq 0.05$) the greatest influence on the reduction of the content of total acids in wine ($0.6575^a \pm 0.0173$) compared to the model M0 (0.7325 ± 0.0043). Model M6.1 has the least impact on lowering the value of total acid content ($0.6950^a \pm 0.0043$) compared to the M0 model (0.7325 ± 0.0043).

In models treated with 2.0 g silica gel (M1.4 - M7.4) model M7.4 has the greatest influence, the value of the total acids is significantly ($p \leq 0.05$) reduced to $0.5650^c \pm 0.0043$ compared to the M0 model. Analogously with the increase in the amount of added silica gel, there was a decrease in the content of total acids in red wine.

Table 2. Comparison of obtained values for determining the content of total acids

Model	Total acid content (g/l) $\bar{X} \pm Sd$
M1.1	$0.6575^a \pm 0.0173$
M2.1	$0.6800^b \pm 0.0043$
M3.1	$0.6875^c \pm 0.0043$
M4.1	$0.6725^c \pm 0.0043$
M5.1	$0.6750^d \pm 0.0075$
M6.1	$0.6950^d \pm 0.0043$
M7.1	$0.6700^d \pm 0.0189$
M1.2	$0.6250^a \pm 0.0087$
M2.2	$0.6550^a \pm 0.0043$
M3.2	$0.6575^b \pm 0.0087$
M4.2	$0.6425^c \pm 0.0043$
M5.2	$0.6600^c \pm 0.0198$
M6.2	$0.6675^d \pm 0.0075$
M7.2	$0.6300^d \pm 0.0075$
M1.3	$0.5950^a \pm 0.0156$
M2.3	$0.6200^b \pm 0.0043$
M3.3	$0.6275^c \pm 0.0156$
M4.3	$0.6125^c \pm 0.0043$
M5.3	$0.6200^d \pm 0.0115$
M6.3	$0.6275^d \pm 0.0043$
M7.3	$0.6075^d \pm 0.0075$
M1.4	$0.5750^a \pm 0.0115$
M2.4	$0.6000^b \pm 0.0075$
M3.4	$0.5875^c \pm 0.0156$
M4.4	$0.5800^c \pm 0.0087$
M5.4	$0.5850^c \pm 0.0130$
M6.4	$0.6100^c \pm 0.0156$
M7.4	$0.5650^d \pm 0.0043$
M0	0.7325 ± 0.0043

Determination of the color by CIELab spectrophotometric

Table 3 shows the comparison of models with the same concentrations of silicagels. The values shown in the table indicate their influence on the change in the coloring value of CIELab spectrophotometric

(L*, a*, b*). Groups of red wine were treated with different images of amorphous silica gel in quantities from 0.5 to 2.0 g/l. By observing the L* value, it can be noted that in samples marked with (M2.1-M2.4) were significant increase of L* value ($p \leq 0.05$), (M2.1 $32.2133^a \pm 0.0208$; M2.2 $31.7900^a \pm 0.0436$; M2.3 $31.5533^a \pm 0.0306$ and M2.4 $31.0633^a \pm 0.0115$) compared to model M0 (21.3867 ± 0.0058). In all other cases, there was a significant decrease in the value of the L* compared to the reference model M0. By observing the a* component of red wines, the greatest reduction ($p \leq 0.05$) of the a* value of the wine was recorded on sample M1.4 ($49.6933^a \pm 0.0252$) compared to the M0, and the smallest on the sample M5.1 ($51.6500^a \pm 0.0265$).

Table 3. Comparison of the obtained wine colour values by CIELab spectrophotometric

Model	Determination of the wine color by CIELab spectrophotometric $\bar{X} \pm Sd$		
	L*	a*	b*
M1.1	$19.3867^a \pm 0.0153$	$50.7300^a \pm 0.0200$	$32.2133^a \pm 0.0208$
M2.1	$32.2133^a \pm 0.0208$	$51.1667^a \pm 0.0058$	$32.6233^a \pm 0.0451$
M3.1	$20.0700^a \pm 0.0100$	$51.4933^a \pm 0.0208$	$32.9667^a \pm 0.0503$
M4.1	$19.6200^a \pm 0.0100$	$50.9067^a \pm 0.0058$	$32.4933^a \pm 0.1159$
M5.1	$20.2833^a \pm 0.0115$	$51.6500^a \pm 0.0265$	$33.1633^a \pm 0.0702$
M6.1	$19.6167^a \pm 0.0058$	$51.0533^a \pm 0.0153$	$32.5433^a \pm 0.0351$
M7.1	$19.9167^a \pm 0.0153$	$51.3667^a \pm 0.0503$	$32.8733^a \pm 0.0513$
M1.2	$19.0700^a \pm 0.0100$	$50.3733^a \pm 0.0115$	$31.7900^a \pm 0.0436$
M2.2	$31.7900^a \pm 0.0436$	$50.8900^a \pm 0.0173$	$32.4700^a \pm 0.0800$
M3.2	$19.5300^a \pm 0.0000$	$50.9467^a \pm 0.0153$	$32.4333^a \pm 0.0462$
M4.2	$19.4833^a \pm 0.0058$	$50.8667^b \pm 0.0252$	$32.2900^b \pm 0.0520$
M5.2	$19.7467^a \pm 0.0058$	$51.0800^b \pm 0.0265$	$32.6167^b \pm 0.0404$
M6.2	$19.3333^a \pm 0.0058$	$50.7067^b \pm 0.0321$	$32.2967^c \pm 0.0321$
M7.2	$19.7767^b \pm 0.0153$	$51.1800^c \pm 0.0458$	$32.8267^c \pm 0.0058$
M1.3	$18.8733^a \pm 0.0058$	$50.1367^a \pm 0.0153$	$31.5533^a \pm 0.0306$
M2.3	$31.5533^a \pm 0.0306$	$50.3167^a \pm 0.0153$	$31.8133^a \pm 0.0058$
M3.3	$19.3133^a \pm 0.0231$	$50.6967^a \pm 0.0416$	$32.0933^a \pm 0.0862$
M4.3	$19.3100^a \pm 0.0000$	$50.6633^b \pm 0.0473$	$32.2167^b \pm 0.0945$
M5.3	$19.1933^a \pm 0.0153$	$50.5267^b \pm 0.0503$	$31.9933^b \pm 0.0115$
M6.3	$19.2100^a \pm 0.0000$	$50.5333^b \pm 0.0058$	$32.1800^c \pm 0.0819$
M7.3	$19.7367^b \pm 0.0153$	$51.1133^c \pm 0.0351$	$32.6300^d \pm 0.0361$
M1.4	$18.5067^a \pm 0.0153$	$49.6933^a \pm 0.0252$	$31.0633^a \pm 0.0115$
M2.4	$31.0633^a \pm 0.0115$	$50.3033^b \pm 0.0208$	$31.7833^b \pm 0.0651$
M3.4	$19.1933^a \pm 0.0058$	$50.4367^b \pm 0.0208$	$32.0367^b \pm 0.0929$
M4.4	$19.2867^a \pm 0.0115$	$50.5967^c \pm 0.0404$	$32.1167^c \pm 0.0252$
M5.4	$19.0267^a \pm 0.0208$	$50.2967^c \pm 0.0404$	$31.8633^c \pm 0.0681$
M6.4	$19.0067^a \pm 0.0115$	$50.2900^c \pm 0.0173$	$31.8200^c \pm 0.0436$
M7.4	$19.4800^b \pm 0.0173$	$50.8100^d \pm 0.0436$	$32.4367^d \pm 0.0208$
M0	21.3867 ± 0.0058	52.9733 ± 0.0153	34.2833 ± 0.0503

As in previous cases, the addition of silica gel resulted in a decrease in the b* value, compared to the reference model. The greatest ($p \leq 0.05$) impact on the reduction of b* value was recorded on the sample M1.4 (31.0633 ± 0.0115) compared to model M0 (34.2833 ± 0.0503). While in the M5.1

(33.1633^a±0.0702), the least impact was recorded on the reduction of the intensity of b* value in the sample.

Tartarate stability test (freezing, conductivity test)

The least impact on reducing the content of tartarate has the model M6.1 (1612.5000^c±3.5355) with a significant difference (p≤0.05) compared to model M0 (Table 4). Red wine treated in model M4.4 (1326.0000^b±1.4142) showed significant (p≤0.05) the largest decrease in the content of tartarate salts, compared to the untreated model M0.

Table 4. Comparison of the obtained values in the tartarate stability test

Model	Tartarate stability test $\bar{X} \pm Sd$
M1.1	1452.5000 ^a ±4.9497
M2.1	1533.0000 ^a ±2.8284
M3.1	1572.0000 ^a ±4.2426
M4.1	1496.0000 ^b ±2.8284
M5.1	1516.5000 ^c ±3.5355
M6.1	1612.5000 ^c ±3.5355
M7.1	1482.0000 ^c ±2.8284
M1.2	1408.0000 ^a ±1.4142
M2.2	1486.5000 ^a ±4.9497
M3.2	1553.5000 ^a ±2.1213
M4.2	1430.0000 ^b ±4.2426
M5.2	1457.5000 ^c ±3.5355
M6.2	1546.5000 ^c ±3.5355
M7.2	1466.0000 ^c ±4.2426
M1.3	1377.5000 ^a ±3.5355
M2.3	1469.5000 ^a ±2.1213
M3.3	1419.0000 ^a ±4.2426
M4.3	1425.0000 ^b ±4.2426
M5.3	1413.0000 ^c ±2.8284
M6.3	1485.0000 ^c ±4.2426
M7.3	1439.0000 ^c ±1.4142
M1.4	1366.5000 ^a ±2.1213
M2.4	1389.5000 ^a ±3.5355
M3.4	1397.5000 ^a ±3.5355
M4.4	1326.0000 ^b ±1.4142
M5.4	1349.5000 ^c ±3.5355
M6.4	1462.5000 ^c ±4.9497
M7.4	1375.0000 ^c ±4.2426
M0	1620.0000±1.4124

The content of tartarate salts decreases in wine with an increase in the concentration of amorphous silica gel in the tested models, compared to the model M0 (1620.0000±1.4124). By extracting tartarate salts in the form of precipitate, there is an increase in the stability of the tested samples. Models with added silica gel generally have a significant reduction in the content of tartarate salts compared to the M0 model, which indicates adsorption, coagulation and separation of tartarate salts in the form of precipitate, thereby contributing to the stability of the tested red wine models.

Conclusion

Red wine is prepared according to the standard technological procedure in such a way that 4 parts of Vranac, 2 parts of Kaberna and 1 part of the Merlo variety are mixed. Twenty-nine models of silica gel wine have been prepared, including the reference sample M0.

By increasing the content of silica gel in any type and relationship, there was a decrease in the content of total acids. The largest decrease was recorded in the M7.4 ($0.5650^c \pm 0.0043$). In contrast to this model, model M.6.1 had the least impact on reducing acid content ($0.6950^d \pm 0.0043$). From the presented it can be concluded that the M7.4 model has the greatest influence in the reduction of the content of total acids.

By determining the color components in the red wine, there was a decrease in the intensity of L*, a* and b* components except for samples of M2.1 ($32.2133^a \pm 0.0208$); M2.2 ($31.7900^a \pm 0.0436$); M2.3 ($31.5533^a \pm 0.0306$) and M2.4 ($31.0633^a \pm 0.0115$) that led to an increase in L* value compared to the M0 (21.3867 ± 0.0058). This indicates an increase in the white-colored component in the wine. Generally studied in the studied models of aka, there was no significant decrease in the intensity of the red and yellow color component in the wine compared to the M0 model.

The increase in the concentration of added silica gel generally has a positive effect on certain properties of red wine, all samples to which silica gel has been added have shown an increase in stability. The model 6.1 ($1612.5000^c \pm 3.5355$) showed the least impact on increasing the stability, while the M4.4 model ($1326.0000^b \pm 1.4142$) showed the greatest impact on increasing the stability of red wine compared to the model M0 (1620.0000 ± 1.4124).

References

- Aleixandre-Tudo, J. L. & du Toit, W. (2018). Cold maceration application in red wine production and its effects on phenolic compounds: A review. *LWT*, 95, 200–208.
- Bakker, J. & Clarke, R. J. (2011). *Wine: flavour chemistry*: John Wiley & Sons.
- Bisson, L. F. (2004). The biotechnology of wine yeast. *Food Biotechnology*, 18(1), 63–96. <https://doi.org/10.1081/FBT-120030385>
- Jackson, R. S. (2020). *Wine science: principles and applications*: Academic press.
- Ma, T., Wang, J., Wang, H., Zhao, Q., Zhang, F., Ge, Q., Sun, X. (2022). Wine aging and artificial simulated wine aging: technologies, applications, challenges, and perspectives. *Food Research International*, 110953. <https://doi.org/10.1016/j.foodres.2022.110953>
- Malfeito-Ferreira, M. (2021). Fine wine flavour perception and appreciation: Blending neuronal processes, tasting methods and expertise. *Trends in Food Science & Technology*, 115, 332–346. <https://doi.org/10.1016/j.tifs.2021.06.053>
- Mills, D., Phister, T., Neeley, E. & Johannsen, E. (2008). *Molecular Techniques in the Microbial Ecology of Fermented Foods*: New York. <https://content.e-bookshelf.de/media/reading/L-2252-0150ecb8fd.pdf>
- Reynolds, A. G. (2021). *Managing Wine Quality: Volume 1: Viticulture and Wine Quality*: Woodhead Publishing.
- Ribéreau-Gayon, P., Glories, Y., Maujean, A. & Dubourdieu, D. (2021). *Handbook of Enology, volume 2: The chemistry of wine stabilization and treatments*: John Wiley & Sons. <https://vinumvine.files.wordpress.com/2011/08/p-ribereau-gayon-y-glories-a-maujean-d-dubourdieu-handbook-of-enology-volume-2-the-chemistry-of-wine-stabilization-and-treatments.pdf>
- Salaha, M.-I., Kallithraka, S., Marmaras, I., Koussissi, E. & Tzourou, I. (2008). A natural alternative to sulphur dioxide for red wine production: Influence on colour, antioxidant activity and anthocyanin content. *Journal of food composition and analysis*, 21(8), 660–666. <http://dx.doi.org/10.1016/j.jfca.2008.03.010>
- Snopek, L., Mlcek, J., Sochorova, L., Baron, M., Hlavacova, I., Jurikova, T. & Sochor, J. (2018). Contribution of red wine consumption to human health protection. *Molecules*, 23(7), 1684. <https://doi.org/10.3390/molecules23071684>

- Stanković, S., Jović, S. & Živković, J. (2004). Bentonite and gelatine impact on the young red wine coloured matter. *Food Technology and Biotechnology*, 42(3), 183–188. <https://hrcak.srce.hr/file/163334>
- Sumby, K. M., Bartle, L., Grbin, P. R. & Jiranek, V. (2019). Measures to improve wine malolactic fermentation. *Applied microbiology and biotechnology*, 103(5), 2033–2051. <https://doi.org/10.1007/s00253-018-09608-8>
- Teng, B., Petrie, P. R., Smith, P. A. & Bindon, K. (2020). Comparison of water addition and early-harvest strategies to decrease alcohol concentration in *Vitis vinifera* cv. Shiraz wine: impact on wine phenolics, tannin composition and colour properties. *Australian Journal of Grape and Wine Research*, 26(2), 158–171. <https://doi.org/10.1111/ajgw.12430>
- Wang, S., Mantilla, S. M. O., Smith, P. A., Stokes, J. R. & Smyth, H. E. (2020). Astringency sub-qualities drying and pucker are driven by tannin and pH—Insights from sensory and tribology of a model wine system. *Food Hydrocolloids*, 109, 106109. <https://doi.org/10.1016/j.foodhyd.2020.106109>
- Zhang, B., Wang, X.-Q., Yang, B., Li, N.-N., Niu, J.-M., Shi, X. & Han, S.-Y. (2021). Copigmentation evidence of phenolic compound: The effect of caffeic and rosmarinic acids addition on the chromatic quality and phenolic composition of Cabernet Sauvignon red wine from the Hexi Corridor region (China). *Journal of food composition and analysis*, 102, 104037. <https://www.x-mol.com/paperRedirect/1403521360917413888>

Professional Paper

THE SEASONAL VARIATIONS OF BIOCHEMICAL COMPOSITION OF COW'S MILK ON THE SOUTHERN SERBIA TERRITORY

Jovan Ćirić^{1,2}, Slavica Ilić², Aleksandar Veličković^{1,2}, Ivan Stojković³, Dragana Stanisavljević¹, Nebojša Milosavljević¹

¹Toplica Academy of Vocational Studies – Department of Agricultural and Food Studies, Prokuplje, Serbia

²Faculty of Technology, University of Niš, Leskovac, Serbia

³Innovation Center of the Faculty of Technology and Metallurgy in Belgrade, Belgrade, Serbia

Abstract

The yield and chemical composition of cow's milk, also, the quality of milk and dairy products vary seasonally throughout the year, depending on the diet, or season. The influence of the season, relatively winter and summer, on certain important biochemical components and physical properties of milk in Southern Serbia was studied in this paper. The obtained data were processed by standard variational-statistical methods. Based on the obtained results of the research, it can be concluded that all the obtained results are following the literature as well as the valid legal norms. It was noted that there is a significant difference in quality between winter and summer milk, while variations between quality at purchase points are inappreciable. Generally, the acidity of milk is higher in the summer, while the dry matter content, as well as the added water content, is higher in the winter.

Keywords: cow's milk, quality, seasonal variations.

Introduction

Milk is one of the oldest foods known to mankind and is a mixture of fats, proteins, carbohydrates, vitamins, minerals, and other ingredients dispersed in water (Ozrenk & Inci, 2008). The composition of raw milk has a very significant impact on the quality and yield of milk products (Nešić, 2010; Scaglioni et al., 2014; Becker-Algeri et al., 2020) and the quality of milk directly depends on its physicochemical and microbiological characteristics. In general, the composition of milk varies depending on the season, lactation period, cow health, milking, genetic factors, and other daily variations (Chen et al., 2014; Heck et al., 2009). The influence of seasonal variation on the composition of milk has been studied by many authors and it has been confirmed that the concentrations of most ingredients and physiochemical properties vary significantly throughout the year (Nešić, 2010; Heck et al., 2009; Becker-Algeri et al., 2020).

Materials and Methods

The research included samples of collected milk from the purchase area of the „Milk House“ dairy in Niš at ten purchase points. These purchase points are Paraćin, Niš, Bela Palanka, Soko Banja, Gadžin Han, Aleksinac, Svrljig, Kruševac, Babušnica, and Prokuplje. The analysis of samples was performed in the internal laboratory of the dairy. Sampling was performed for 45 days in the period of January-March and June-August 2021. The content of milk fat, proteins, and dry matter were determined spectrophotometrically in the infrared area on the Milkoscan S 50. The amount of dry matter without fat (DMWF) was calculated and expressed as a percentage. The titration acidity of milk was determined by the Soxhlet-Henkel method (Fabro et al., 2006). The amount of added water was

determined by the Cryoscope 4D3. Pearson's correlation coefficient was calculated for all data related to winter and summer period samples, using Excel (Microsoft Office 365).

Results and discussion

By analyzing the milk samples from the ten purchasing areas of the "Milkhouse" dairy in Niš, during the winter period (January –March) and during the summer period (June –August), the values of acidity, specific gravity, milk fat, dry matter, dry matter without fat and proteins were obtained. The average values of these parameters as well as their dependencies are shown in Table 1. Based on the obtained results, first of all, it can be concluded that all the obtained data are in agreement with the data from the literature (Nešić, 2010). Also, there is a significant difference in the quality of winter and summer milk. The main difference is in the higher acidity of summer milk, which is a direct consequence of the higher microbiological activity of lactic acid bacteria, but also in the higher concentration of dry matter, dry matter without fat, milk fat, and proteins in the milk of the winter period. Variations in milk composition between purchase stations were significantly lower compared to seasonal variations. Similar observations were made by other researchers who published research results from other countries with different climatic conditions (Becker-Algeri et al., 2020; Ozrenk & Inci, 2008; Heck et al., 2009). The average acidity for all purchased stations of summer milk of 6,91 °SH was higher by 4.5% for winter milk samples. On the other hand, the average values of milk fat content (3.91%), dry matter (12.20%), and protein content (3.21%) were 2%, 1%, and 6% higher compared to summer milk samples. By the analysis of the values of Pearson's coefficient, it can be noticed that there is a positive and significant correlation between the parameters of winter and summer milk. Strong positive correlations were noticed between the variables of winter and summer milk of the data for milk fat and dry matter without fat, where the value of R were 0.8941 and 0.7951 and coefficients of determination (R^2) were 0.7994 and 0.6918. A moderate positive correlation with an R-value of 0.5872 and 0.6918 with coefficients of determination of 0.3448 and 0.4786 was noticed between the winter and summer data variables of the acidity and protein content results.

Table 1. Values of milk quality parameters in the period January-March and June-July

PURCHASE POINT	ACIDITY (°SH)		MILK FAT (%)		DRY MATTER (%)		DRY MATTER WITHOUT FAT (%)		PROTEINS (%)	
	Period 1	Period 2	Period 1	Period 2	Period 1	Period 2	Period 1	Period 2	Period 1	Period 2
PARAĆIN	7.00 ±0.27	6.82 ±0.21	3.83 ±0.13	3.80 ±0.12	12.04 ±0.21	11.98 ±0.18	8.21 ±0.09	8.18 ±0.15	3.12 ±0.07	3.10 ±0.08
NIŠ	6.92 ±0.26	8.08 ±0.24	3.97 ±0.16	3.85 ±0.07	12.41 ±0.17	12.30 ±0.18	8.44 ±0.22	8.18 ±0.19	3.25 ±0.11	2.36 ±0.17
BELA PALANKA	6.58 ±0.21	6.68 ±0.27	3.99 ±0.17	3.84 ±0.09	12.47 ±0.18	12.21 ±0.11	8.48 ±0.14	8.37 ±0.24	3.30 ±0.12	3.13 ±0.15
SOKO BANJA	6.68 ±0.23	6.81 ±0.23	3.94 ±0.14	3.89 ±0.11	12.25 ±0.31	12.21 ±0.17	8.31 ±0.11	8.32 ±0.05	3.22 ±0.04	3.13 ±0.14
GADŽIN HAN	6.53 ±0.24	6.82 ±0.20	3.96 ±0.11	3.84 ±0.09	12.30 ±0.24	12.08 ±0.14	8.34 ±0.16	8.24 ±0.14	3.25 ±0.11	3.12 ±0.21
ALEKSINAC	6.66 ±0.29	6.78 ±0.31	3.85 ±0.10	3.77 ±0.07	12.07 ±0.19	12.00 ±0.11	8.22 ±0.23	8.23 ±0.31	3.15 ±0.16	3.08 ±0.12
SVRLJIG	6.20 ±0.25	6.76 ±0.19	3.85 ±0.22	3.84 ±0.11	12.01 ±0.21	12.13 ±0.17	8.16 ±0.19	8.29 ±0.12	3.12 ±0.03	3.10 ±0.16
KRUŠEVAC	6.40 ±0.31	6.80 ±0.21	4.00 ±0.09	3.84 ±0.05	12.28 ±0.14	12.10 ±0.15	8.28 ±0.04	8.26 ±0.09	3.19 ±0.09	3.11 ±0.06
BABUŠNICA	6.60 ±0.16	6.81 ±0.22	3.88 ±0.14	3.84 ±0.06	12.07 ±0.19	12.08 ±0.13	8.19 ±0.12	8.24 ±0.11	3.26 ±0.05	3.10 ±0.09
PROKUPLJE	6.81 ±0.28	6.79 ±0.19	3.90 ±0.15	3.81 ±0.16	12.15 ±0.26	11.93 ±0.05	8.25 ±0.11	8.12 ±0.21	3.23 ±0.12	3.05 ±0.14
AVG	6.64 ±0.24	6.91 ±0.41	3.91 ±0.06	3.83 ±0.03	12.20 ±0.16	12.10 ±0.11	8.29 ±0.10	8.24 ±0.07	3.21 ±0.06	3.02 ±0.23

Period 1 – January -March

Period 2 – June - August

Conclusion

The season has a significant influence on the quality of milk, which was confirmed by this research with samples of the Souther Serbia territory. Due to the higher content of dry matter, proteins, and fat, milk during the winter period can be considered more suitable for industrial processing.

References

- Becker-Algeri, T.A., Souza, C., Bortoli, K., Castagnaro, D., Scaglioni, P.T., Drunkler, D. A., Dors, G., Valderrama, P. & Badiale-Furlong, E. (2020). Seasonal variation of milk quality: Physiochemical, microbiological, and toxicological. *Journal of Food Safety*, e12796. <https://doi.org/10.1111/jfs.12796>
- Chen, B., Lewis, M. J. & Grandison, A. S. (2014). Effect of seasonal variation on the composition and properties of raw milk destined for processing in the UK. *Food Chemistry*, 158, 216–223. <https://doi.org/10.1016/j.foodchem.2014.02.118>
- Fabro, M. A., Milanese, H. V., Robert, L. M., Speranza, J. L., Murphy, M., Rodriguez, G. & Castaneda, R. (2006). Determination of acidity in whole raw milk: Comparison of results obtained by two different analytical methods. *Journal of Dairy Science*, 83 (3) 859–861. [https://doi.org/10.3168/jds.s0022-0302\(06\)72149-x](https://doi.org/10.3168/jds.s0022-0302(06)72149-x)

- Heck, J. M. L., Van Valenberg, H. J. F., Dijkstra, J. & Van Hooijdonk, A. C. M. (2009). Seasonal variation in the Dutch bovine raw milk composition. *Journal of Dairy Science*, 92, 4745–4755. <https://doi.org/10.3168/jds.2009-2146>
- Nešić, V. (2013). Tehnologija mleka. Univerzitet u Nišu, ISBN:978-86-82367-85-7
- Ozrenk, E. & Inci, O. S. (2008). The effect of seasonal variation on the composition of cow milk in Van Province. *Pakistan Journal of Nutrition*, 7(1), 161–164. <https://doi.org/10.3923/pjn.2008.161.164>
- Scaglioni, P. T., Becker-Algeri, T. A., Drunkler, D. & Badiale-Furlong, E. (2014). Aflatoxin B1 and M1 in milk. *Analytica Chimica Acta*, 829, 68–74. <https://doi.org/10.1016/j.aca.2014.04.036>

Professional Paper

THE EFFECTS OF ADDITION OF FLAXSEED TO THE CHARACTERISTICS OF BREAD

Gordana Jovanović¹, Ana Vasić¹, Ljubica Mijić¹, Ana Matić¹, Bojan Damjanović¹

¹Academy of Professional Studies, Department of Medical and Business-Technological Studies, Hajduk Veljkova 10, 15000, Šabac, Serbia

Abstract

The aim of this study was to determine the effect of addition of flaxseed to bread, the physical and sensory characteristics of the obtained bread and the possibility of application of this kind of bread as functional food. For preparing the bread, flaxseeds were added to the dough in concentration of 20 and 40% calculated based on mass wheat flour. The quality of bread was assessed by determining the physico-chemical and sensory parameters 24 hours after baking, such as the height and volume of bread, mass of bread, as well as the fineness and elasticity of the bread pores. As a consequence, flaxseed can be successfully incorporated into bread formulations. The general acceptability was good with the addition of 20% of flaxseed.

Keywords: bread, flaxseed.

Introduction

Bread, as a major source of economical dietary energy and nutrients worldwide, contains high amount of carbohydrates and protein, but it has low amounts of other nutritional components such as diet fiber, monounsaturated fatty acid, and phenolic components. That is the reason why many food ingredients (food additives or functional food additives) have been included in bread formulation (Fan et al., 2007). Flaxseed as an addition can be used in bread and bakery products not only to provide nutty flavor but also to increase the nutritional and health benefit of the final product. Pohjanheimo et al. (2006) evaluated the effect of the partial supplementation of bread with flaxseed on their texture, chemical, and sensory properties. They concluded that flaxseed has a positive effect on the texture parameters during storage and nutritional composition, for example, the content of fiber and unsaturated fats. Based on the before mentioned, functional food and functional food additives have a role to provide the body with the necessary energy and nutrients, as well as to influence the preservation of health and the improvement of certain organism conditions, balancing and improving the standard of living (Milner, 2000; Roberfroid, 2002).

Flax seed is considered one of the most powerful foods in the world. Heart disease, cancer, stroke and diabetes are diseases whose risk is drastically reduced by consuming this oilseed. Fiber, omega-3 fatty acids, vitamin E, vitamin D, magnesium, selenium and zinc are important components of flax seed, but the most important for its effectiveness are lignins as its main ingredients. Lignins represent phytoestrogens that have antioxidant properties and show good effects in the treatment of hormone-dependent tumors (Matsumoto et al., 2002).

Flax seed contains both soluble and insoluble fibers, which are beneficial for digestion, intestinal health, maintenance of ideal body weight and cholesterol regulation (Cui, 2001).

Omega-3 fatty acids are also very important components of flax seed because they prevent diseases of the heart and blood vessels. These acids and lignins reduce the inflammation that accompanies

Parkinson's disease, arthritis and asthma by blocking the secretion of certain anti-inflammatory agents (Randall, 2013).

Regular consumption of flax seed is suitable for people who engage in sports activities, because its consumption reduces muscle inflammation. Thanks to the positive effect of fibers on the digestive tract, flax seed regulates the intestinal flora, which it also restores, eliminating toxins from the body and improving digestion. It acts on the stomach by lining its mucous membrane, and reduces problems with increased acidity. In addition, flax seeds are beneficial for hair and skin health, and can also relieve breast pain during menstruation. Doctors often recommend linseed as a cure for fibroids - in the form of additional therapy and prevention. These oils have a positive effect on the nervous and immune system (alleviating allergies and lupus symptoms), play an important role in calcium metabolism and have a mild diuretic effect (Shim et al., 2014).

Flax seed can be purchased in many supermarkets and health food stores. They are, usually, available in whole grain form, which is ground before use to exert its health effects. Whole flax seeds can be ground in a coffee grinder and then stored in an airtight container for several months. However, for the best effects, it is recommended to use freshly ground seeds.

Materials and Methods

The following raw materials were used in the experimental work:

- Flour for sourdough and homemade pasta T-500, manufactured by "Danubius doo" from Novi Sad,
- Kitchen salt, commercial product, manufacturer "Solana", Tuzla,
- Fresh baker's yeast, producer "Budafok", Hungary,
- Tap water for drinking.
- Furthermore, plant material used in the experiments was grounded flaxseeds.

Bread making process

The bread was prepared according to the procedure prescribed by the standard AACC method (AACC International, 2000). The raw material composition of the bread dough was as follows: flour, salt 2% (by weight of flour), yeast 2,5% (by weight of flour). Additional raw material was added according to the experimental plan (Table 1), whereby part of the flour (20 and 40%) was replaced with grounded flax seeds.

Table 1. Experimental plan

Sample	Flour (g)	Salt (g)	Yeast (g)	Flax seeds (g)	Water (g)
1	150	3	3.75	0	83.25
2	120	3	3.75	30	79.58
3	90	3	3.75	60	77.85

According to the plan of the experiment, the dough was mixed in a kneader made by Silver Crest, Germany, for 5 minutes. It was then shaped into a ball and left on the work surface, at room temperature, to ferment in the mass for 60 minutes. The dough was then hand-shaped oblong and placed in greased bread moulds (15 cm long, 5 cm wide and 7 cm high). The final fermentation was performed at a temperature of 30 °C, for 60 minutes. Bread samples were baked in a laboratory oven for 15 minutes at 250 °C. After baking, the breads were cooled for 1 h at room temperature and then stored for 24 h under controlled humidity and temperature conditions. Changes in bread quality as a function of selected independent parameters were monitored based on the results of determining the physico-chemical and sensory characteristics of the finished product.

Mass of bread: The mass of bread was measured 1 h after baking and cooling, and then after 24 h.

Volume of bread: The volume of bread was estimated 24 h after baking, and was determined by the method of squeezing millet grains (Kaluški & Filipović, 1998).

Specific volume of bread: The specific volume of bread V_{sp} (cm³/g) was determined as the ratio of the volume and weight of bread.

Moisture content: Moisture content was determined by the gravimetric method according to Ph. Jug. IV (1984). The obtained results are expressed as a percentage of moisture content (% m/m).

Ash content: The ash content was determined by the gravimetric method according to Ph. Jug. IV (1984). The obtained results are expressed as a percentage of ash (% m/m).

Determining bread quality

The quality of the bread was graded organoleptically 24 hours after baking, whereby the fineness of the crumb pore structure and elasticity were evaluated by palpation technique. Sensory parameters of bread samples (color, smell and taste) were evaluated by descriptive sensory analysis. The participants were 30 students 20-22 years of age, non-smokers, male: female ratio of 50%. The panelists were required to rinse their mouth with water between each sample. The participants evaluated the taste and colour of bread as 5- like very much, 4- like slightly, 3- neither like nor dislike, 2- dislike slightly, 1- dislike very much (Pandurang et al., 2014.) The sensory evaluation was done under white fluorescence light at room temperature of 25±2 °C. Descriptive grades of the mentioned bread crumb quality indicators (elasticity of the medium and the fineness of the pore structure) are shown in total values and graded in table for grading the bread crumb value (Kaluderski & Filipović, 1998) and marked as Value for Bread Crumb – VBC (minimum 0.0 and maximum 7.0).

Results and discussion

As planned in the experimental work, samples of bread of appropriate composition were baked. From each composition, two samples were prepared, and average values are shown in the results, in Table 2.

Table 2. Bread samples making conditions

Conditions	Sample 1	Sample 2	Sample 3
Flour temperature (°C)	22	22	22
Mixing water temperature (°C)	30	30	30
Mixing duration (min)	5	5	5
Duration and rest (min)	60	60	60
Duration of final fermentation (min)	60	60	60
Baking time (min)	15	15	15
Dough mass (g)	238.04	233.16	225.7

Table 3. Sensory properties of bread samples

Sensory properties	Sample 1	Sample 2	Sample 3
Bread weight (g)	228.31	221.68	212.08
Bread volume (cm ³)	440	340	330
Specific volume (g/cm ³)	6.31	6.04	6.27
Bread height (mm)	72	61	58
Moisture content (%)	41.92	41.72	39.2
Ash content (%)	6.31	6.04	6.27
Dough yield	158.69	194.30	250.83
Bread yield	152.47	184.73	235.64
Taste	5	4	3
Colour	5	4	3
Elasticity of the medium	Very good - (3.8)	Good - (3)	Satisfies - (2)
The fineness of the pore structure	Almost fine / a little rough (1.2)	Little rough (0.8)	Rough (0.5)
Value for Bread Crumb – VBC	5.0	3.8	2.5

Table 2 and 3 shows the results of the tested breads obtained from flour (sample 1), flour with 20% grounded flax seeds (sample 2) and bread from flour with 40% grounded flax seeds (sample 3). Considering that sample 1 was made solely out of wheat flour it is the bread that others samples were compared to. It can be concluded that the quality of bread is reduced by the addition of flax seeds. The volume of bread, as well as the height are decreasing, also values for the elasticity of the medium and the fineness of the pore structure were obtained. But a significant difference in bread quality was observed when 20% flaxseed was added compared to bread with 40% added, and that is, perhaps, the most valuable result of this research. A clear indicator is the Value for Bread Crumb – VBC, obtained by the sum of their values.

Sample 1 was bread obtained from dough with 100% flour, without any addition. Obtained bread had a very good height and volume, as well. Bread volume is one of the key parameters that determine the quality of bread. It is especially important from the point of view of consumers themselves. Other physic-chemical properties had also high values. Also, the values of elasticity of the medium and the fineness of the pore structure was very high, and accordingly the Value for Bread Crumb – VBC, as well.

When added to the base dough flaxseeds in percentages of 20% by mass of flour, obtained bread sample reduced quality. The height and volume of the bread had lower values, compared to sample 1., as well as other physical and chemical properties. Also, the values for the elasticity of the medium and the fineness of the pore structure, respectively, were lower, and therefore the Value for Bread Crumb. The VBC was average (3.8). Furthermore, the sensory characteristics of obtained bread samples were rated a little bit lower. The color was reddish, the center was well developed, elastic and light brown in color. The product had a rounded, specific and pleasant aroma. The smell and taste of bread were harmonious, they gave a mild reaction to the palate. The results of sensory testing of the samples showed that this type of the obtained product is acceptable for participants.

When it comes to bread samples to which a larger amount of flax seeds was added (40%) (sample 3), based on the obtained results, it was found that the quality of bread was not satisfactory. Both the height and volume of the bread have decreased significantly. The Value for Bread Crumb was very low (2.5). The sensory characteristics of the bread were evaluated with a quite small grade. The color of the bread was dark, the middle was compressed and moist, dark brown in color. Also, the product has an unpleasant aroma.



Figure 1. Sample of bread with 100% flour, with the addition of 20% flaxseeds and with the addition of 40% flaxseeds



Figure 2. Cross section of bread samples with 100% flour, with the addition of 20% flaxseeds with the addition of 40% flaxseeds

By sensory analysis bread samples were graded from 1 to 5, where 5.0 represents the best grade. According to the participants all three bread samples were acceptable, but that the bread samples with the addition of larger amount of flax seeds have lower sensory analysis scores compared to the control sample, i.e. classic white bread.

Due to the presence of lignins, fiber, omega-3 fatty acids, magnesium, selenium, zinc, as well as vitamins, flaxseeds are biologically valuable compounds, so working with them for the purpose of obtaining functional bread could be considered very justified. Every quantity of high-quality structures made from the flaxseeds which is found in breads made in this way, makes them foods with a significantly enriched composition. This clearly shows that these types of products, under the conditions tested, could be functional foods, and can form an essential part of our nutrition.

Conclusion

The present study on effect of flaxseed flour addition in different concentrations on physico-chemical and sensory properties of bread has established some new findings. Bread made from pure flour (sample 1) was the one to which all other samples were compared to. Physico-chemical characteristics (bread weight, height, volume and specific volume) of bread with 20% flaxseeds were increased. The color was reddish, the center was well developed, elastic and light brown in color. The product has a rounded, specific and pleasant aroma.

When it comes to sensory properties, the specific smell and bitter taste limited the amount of flaxseeds added to the bread dough. The smell and taste of bread was pleasant and acceptable.

Furthermore, the volume as well as other physical and chemical properties of bread with the addition of 40% of flaxseeds were increased. Also, the sensory properties were of lower value, because the smell and taste were bitter and moist according to the participants. The color of bread sample was dark, the middle was compressed and moist, dark brown in color.

According to all above mentioned, bread with the addition of 20% flaxseed was acceptable based on physico-chemical and sensory characteristics, and that it's use in the daily diet could be considered as well as the possibility of it being a functional food.

References

- Fan, L., Zhang, S., Yu, L. & Ma, L. (2007). Evaluation of antioxidant property and quality of breads containing *Auricularia Auricula* polysaccharide flour. *Food Chemistry*, 101(3), 1158–1163. <http://dx.doi.org/10.1016/j.foodchem.2006.03.017>
- Pohjanheimo, T. A., Hakala, M. A., Tahvonon, R. L., Salminen, S. J. & Kallio, H. P. (2006). Flaxseed in breadmaking: Effects on sensory quality, aging, and composition of bakery products. *Journal of Food Science*, 71, S343–348. <https://doi.org/10.1111/j.1750-3841.2006.00005.x>
- Milner, J. (2000). Functional foods: the US perspective. *American Journal of Clinical Nutrition*, 71, 1654–1659. <https://doi.org/10.1093/ajcn/71.6.1654S>
- Roberfroid, M. (2002). Global view on functional foods: European perspectives. *British Journal of Nutrition*, 88 (Suppl. 2) 133–138. <https://doi.org/10.1079/bjn2002677>
- Mark-Herbert, C. (2004). Innovation of a new product category-Functional foods. *Technovation*, 24 713–719. [https://doi.org/10.1016/S0166-4972\(02\)00131-1](https://doi.org/10.1016/S0166-4972(02)00131-1)
- Matsumoto, T., Shishido, A., Morita, H., Itokawa, H. & Takeya, K. (2002). Conformational analysis of cyclolinopeptides A and B. *Tetrahedron*, 58, 5135–5140. <https://doi.org/10.1016/S0040-4020%2802%2900476-3>
- Cui, S. W. (2001). *Polysaccharide gums from agricultural products: Processing, structures and functionality*. Technomic Publishing Co., Inc., Lancaster PA
- Randall, K. M., Reaney, M. J. T. & Drew, M. D. (2013). Effect of dietary coriander oil and vegetable oil sources on fillet fatty acid composition of rainbow trout. *Canadian Journal of Animal Science*, 93, 1–8. <https://doi.org/10.4141/CJAS2013-001>
- Shim, Y. Y., Gui, B., Arnison, P. G., Martin, Y. W. & Reaney, J. T. (2014). Flaxseed (*Linum usitatissimum* L.) bioactive compounds and peptide nomenclature: A review. *Trends in Food science & Technology*, 38, 5–20. <https://doi.org/10.1016/j.tifs.2014.03.011>
- AACC International, Guidelines for Measurement of Volume by Rapeseed Displacement Approved Methods of Analysis. (2000). 11th Ed. Method 10-05.01. AACC International, St. Paul MN, U.S.A.
- Kaluđerski, G. & Filipović, N. (1998). *Metode ispitivanja kvaliteta žita, brašna i gotovih proizvoda*, Tehnološki fakultet Novi Sad, Univerzitet u Novom Sad, pp 71–118.
- Ph. Jug. IV. (1984). 4th ed., *Savezni zavod za zaštitu zdravlja*, Belgrade.
- Pandurang, M., Sachin, K. S. & Shalini, S. A (2014). Effect of flaxseed flour addition on physicochemical and sensory properties of functional bread. *LWT-Food Science and Technology* 58, pp. 614–619. <https://doi.org/10.1016/j.lwt.2014.04.003>

Original scientific article

HABITS OF FLUID INTAKE WITH STUDENTS

Dragana Ilić Udovičić¹, Ana Matić¹, Danijela Damnjanović², Aleksandra Vasić¹

¹Academy of Professional Studies Sabac, Department of Medical and Business-Technological Studies, Šabac, Serbia

²Lekofarma Pharmacy Šabac, Serbia

Abstract

Water is essential for life. It is the largest single constituent of the human body, acts as a solvent, regulates body temperature, aids in food digestion and helps regulate the acid-base balance. The aim of this study was to determine the students' habits when it comes to fluid intake and assess their knowledge about the correlation of water intake and health. The research was carried out at the Academy of Professional Studies Sabac, Department of Medical and Business-Technological Studies, for a total of 95 students of the first year of studies (male 38.9%, female 61%) of average age 20.54 ± 1.95 years. The data was collected anonymously via questionnaire on food and fluid intake. The results show that female students consume on an average 1.31 ± 0.25 L water, and that the average daily intake of male students is somewhat more 1.99 ± 0.26 L. The biggest percentage of all students consumes tap water (66%), and the students that buy bottled water are mostly female 71.87%. Students have shown a good knowledge of the definition of dehydration and a higher level of knowledge was noticed with students who are physically active. In non-health related study programs knowledge was lacking for less common dehydration symptoms (headache, dizziness, lack of focus, and muscle weakness). A lack of knowledge was noticed with students regarding the needs for fluid intake and it is more notable in non-health related study programs. It is necessary to influence a change of dietary habits with students and raise awareness about the importance of water through education and promotional activities.

Keywords: water, fluid intake, dehydration, students.

Introduction

Water is one of the fundamental requirements for survival and life of human on Earth (Okanović et al., 2014; WHO, 2004). Water is the largest single constituent of the human body and is essential for cellular homeostasis. Total water intake includes drinking water, water in beverages, and water that is part of food. Low intake of total water has been associated with some chronic diseases (Leurs et al., 2010; Roncal-Jimenez et al., 2015; Šmuljić et al., 2016). Healthy individuals have considerable ability to excrete excess water and thereby maintain water balance, a Tolerable Upper Intake Level (UL) was not set for water. However, acute water toxicity has been reported due to rapid consumption of large quantities of fluids that greatly exceeded the kidney's maximal excretion rate of approximately 0.7 to 1.0 L/hour (Institute of Medicine, 2005).

Body water volume, as a percentage of fat-free mass, is highest in infants and declines in older children (Institute of Medicine, 2005) In healthy adults with a normal body mass index (BMI), water constitutes 60% of body weight (Shaheen et al., 2018).

Body water balance depends on the net difference between water gain and water loss. Water loss consists mainly of excretion of water in urine, breath, faeces and sweat.

Water loss during breathing depends on environmental factors and physical activity (on an average about 250 to 350 mL/day for sedentary persons). Urine output varies inversely with body hydration status. Kidneys are responsible for regulating the volume and composition of extracellular fluid (The minimum urine output is approximately 500 mL/day). Water loss through the skin occurs via insensible diffusion and secreted sweat. For the average adult, loss of water by insensible diffusion is approximately 450 mL/day. In hot weather, sweat evaporation provides the primary avenue of heat loss to defend the body's core temperature. Metabolic water is formed by oxidation of hydrogen-containing substrates during metabolism or energy-yielding nutrients. Oxidation of carbohydrate, protein, and fat produces metabolic water of approximately 15, 10.5, and 11.1 g/100 kcal of metabolizable energy, respectively (Institute of Medicine, 2005).

Recommendations for water intake vary. They depend on age, gender, pregnancy and lactation with women (EFSA, 2010). Adequate fluid intake is very important when the climate temperature is high and during times of intense physical activity, such as during sports or during physical activity. According to the European Food Safety Authority adult women a total daily intake of 2 L of water is necessary, and with men 2.5 L by consuming water, drinks and food (Kapsokfalou, 2013). According to the Institute of Medicine (IOM), water intake of ≥ 3.7 L daily was considered adequate for men, while ≥ 2.7 L daily hours water intake for women was considered as adequate (Institute of Medicine, 2005).

Dehydration is defined as decrease in total body water content due to fluid loss, diminished fluid intake, or both (Popkin et al., 2010). The common symptoms of mild to moderate dehydration are dry mouth/tongue, thirst, headache, lethargy, fatigue, dry skin, muscle weakness, light-headedness, dizziness and a lack of focus (Shaheen et al., 2018).

The aim of this paper is to gain an insight into the habits of students when it comes to fluid intake and knowledge level on dehydration.

Materials and Methods

Students of the first year of studies at the Department of Medical and Business-Technological Studies in Šabac participated in the research, a total of 95 students. Respondents were informed about the aim of the research and it was carried out anonymously during the summer semester of 2020/2021. A questionnaire was used for gathering data. The respondents group was consisted of students from the study program Health care (HC) and Pharmacy (P) (health related study programs), and students from non-health related study programs Gastronomy (G), Environmental Protection (EP), Information Technologies (IT), Economics (E), Engineering Management (EM) and Food Technologies (FT). All obtained results were processed using descriptive statistics in Microsoft Office Excel.

Results and discussion

A total of 95 students participated in the survey. The mean age of students was 20.54 ± 1.95 years. A third of the students ($n=29$, 30.53%) was from the study programs Pharmacy and Health care. Most students were from Šabac and Mačva district ($n=68$, 71.58%) and did not have any illness ($n=90$, 94.74%).

Processing obtained data an insight into the dietary habits of the surveyed population was gained. The data on the average fluid intake was gained by a self-assessment of the daily respondents' intake. The water intake results by study programs are presented in Figure 1.

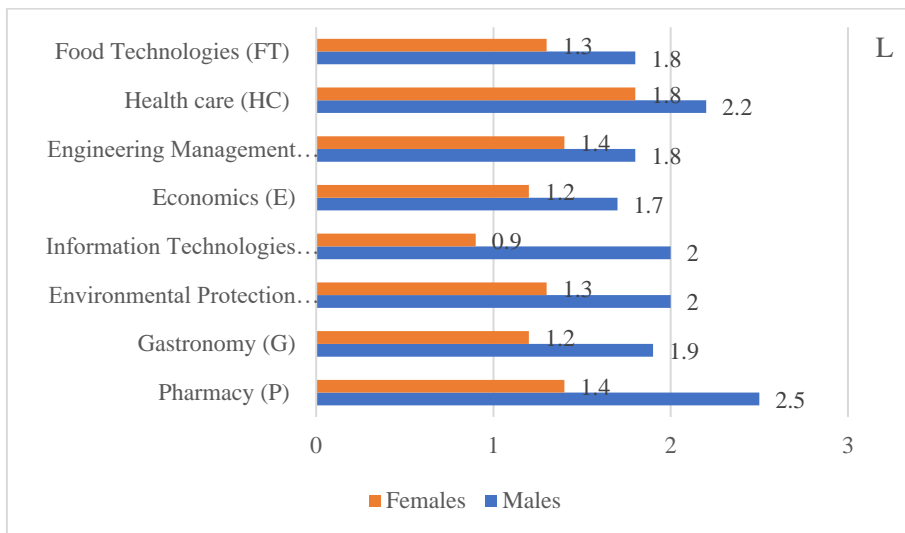


Figure 1. Average water intake in L by study programs

Females have an average intake of 1.31 ± 0.25 L water, and the interval which was reported was from 0.5 to 3.2 L. Males have a somewhat bigger average amount of 1.99 ± 0.26 L of water daily (0.5-3.5 L). Similar data was given by Banožić et al. (2015). An analysis was conducted to see whether there is a difference in the amount of water that students of health-related study programs consume compared to others (Figure 2) and the results show that the students from health-related study programs reported a bigger fluid intake. Still the total intake is somewhat lower than the recommended one for fluid intake which can be found in literature (EFSA, 2010; Institute of medicine, 2005).

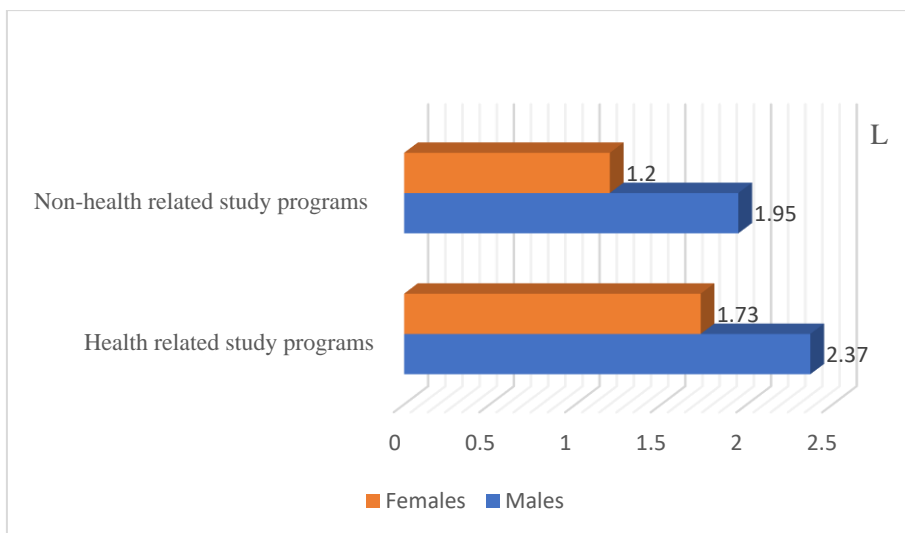


Figure 2. Average water intake in L at health and non-health related study programs

Students responded which water they choose during intake and the highest percentage of students consumes water from the tap (66%) whereas students that buy bottled water, a higher percent are female 71.87%. Similar data was given by Šmuljić et al. (2016).

Most respondents from health-related study programs showed a good knowledge of the definition of dehydration 62%, whereas such students from other study programs are 31.81%.

Numerous data from literature point out that dehydration at just 2% decreases the performance in tasks which require attention, psycho-motorics and immediate memory, as well as the assessment of the subjective state (Adan, 2012; Benton et al., 2016; Magee et al., 2017; Pross, 2017;). In order to

assess the knowledge of students and the familiarity with this fact, in the questionnaire they responded to the question Does the amount of fluids in the organism have an impact on headaches, thought process and paying attention in class. The results are shown in Figure 3. Most students from health-related study programs replied affirmatively 65.52%, whereas the percentage of other students that replied with yes is very low 15.15%. Among this population there is not enough knowledge about the importance of hydration.

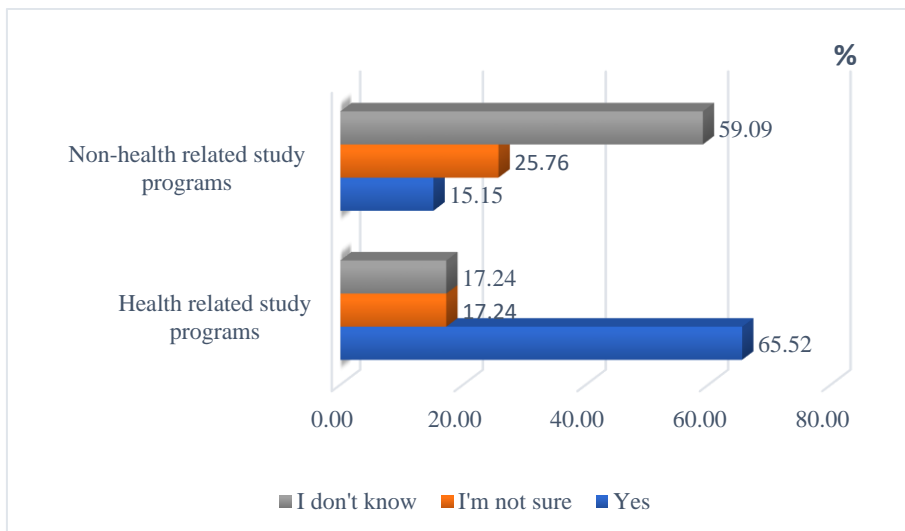


Figure 3. Respondents' answers to the question: Does the amount of fluids in the organism have an impact on headaches, thought process and paying attention in class?

Practising sports, recreationally or professionally requires knowledge and habits related to it such as intake of water and sport and energy drinks, according to the achievement of desired goals thus adequate hydration and faster regeneration of the organism after exertion (Okanović et al., 2014). Out of the total number of students surveyed 46% declared that they do sports, recreationally, every day or professionally. This group answered the question Is it important to drink fluids before, during and after a physical activity (Figure 4). Results show that a high percentage of health-related study programs (78.26%) as well as students from non-health related study programs (71.43%) that are physically active have an awareness about the importance of regular fluid intake and preventing dehydration.

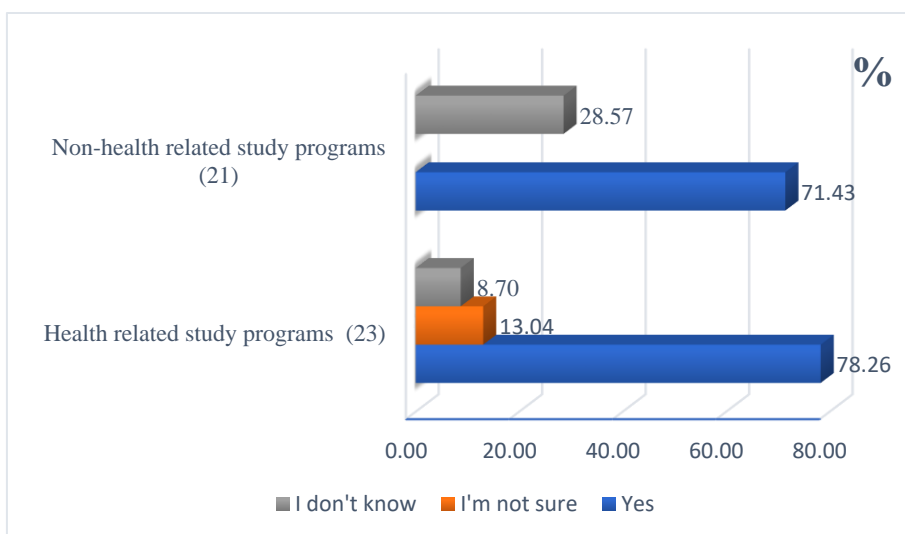


Figure 4. Is it important to drink fluids before, during and after a physical activity

In the survey the students responded to the question Which are the most frequent dehydration symptoms (Figure 5).

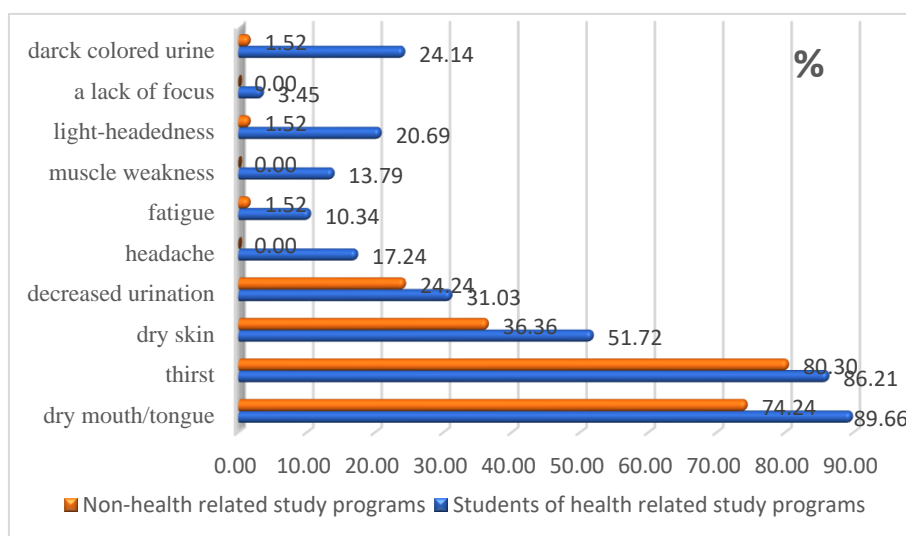


Figure 5. The most frequent dehydration symptoms

All students (in health and non-health related study programs) were well informed about the most common dehydration symptoms (dry mouth, thirst, dry tongue and dry skin) (Figure 5). However, limited knowledge about less common symptoms (headache, dizziness, a lack of focus and weak muscles) was seen with most students especially from non-health related study programs.

Conclusion

In this research about students' habits deviations can be seen from what is recommended. A lack of knowledge regarding the need for fluid intake was noted which is more pronounced with students which are not in health-related study programs. It is necessary to influence habit improvement in nutrition through training courses and promotional activities through which students should raise their awareness and acquire knowledge about appropriate hydration.

References

- Adan, A. (2012). Cognitive performance and dehydration. *Journal of the American College of Nutrition*, 31(2), 71–78. <https://doi.org/10.1080/07315724.2012.10720011>
- Banožić, M., Ljubić, A., Pehar, M., Ištuk, J. & Čačić Kenjerić, D. (2015). Dietary habits of students of the university of Mostar. *Food in health and disease: scientific- professional journal of nutrition and dietetics*, 4 (2) 105–112.
- Benton, D., Jenkins, K. T., Watkins, H. T. & Young, H. A. (2016). Minor degree of hypohydration adversely influences cognition: a mediator analysis. *The American Journal of Clinical Nutrition*, 104(3), 603–612. <https://doi.org/10.3945/ajcn.116.132605>
- European Food Safety Authority (EFSA). (2010). Scientific Opinion on Dietary Reference Values for water. *EFSA Journal*, 8(3), 1459. <https://doi.org/10.2903/j.efsa.2010.1459>
- Institute of Medicine (U.S.) Panel on Dietary Reference Intakes for Electrolytes and Water, (2005). Dietary reference intakes for water, potassium, sodium, chloride, and sulfate. Washington, DC: The National Academies Press. <https://doi.org/10.17226/10925>.

- Kapsokefalou, M. (2013). Hydration and diet, European Hydration Institute EHI, <https://www.europeanhydrationinstitute.org/hydration-diet-2/>
- Leurs, L., Schouten, L., Goldbohm, R. & Van der Brandt, P. (2010). Total fluid and specific beverage intake and mortality due to IHD and stroke in the Netherlands Cohort Study. *British Journal of Nutrition*, 104(8), 1212–1221. <https://doi.org/10.1017/S0007114510001923>
- Magee, P. J., Gallagher, A. M. & McCormack, J. M. (2017). High Prevalence of Dehydration and Inadequate Nutritional Knowledge Among University and Club Level Athletes. *International journal of sport nutrition and exercise metabolism*, 27(2), 158–168. <https://doi.org/10.1123/ijsnem.2016-0053>
- Okanović, Đ., Ilić Udovičić, D., Džinić, N. & Jokanović, M. (2014). Importance of water in sportsman nutrition. *Quality of Life*, 5(1–2), 69–72. <http://dx.doi.org/10.7251/QOL1401068O>
- Popkin, B. M., D'Anci, K. E. & Rosenberg, I. H. (2010). Water, hydration, and health. *Nutrition reviews*, 68(8), 439–458. <https://doi.org/10.1111/j.1753-4887.2010.00304.x>
- Pross, N. (2017). Effects of Dehydration on Brain Functioning: A Life-Span Perspective. *Annals of nutrition & metabolism*, 70 Suppl 1, 30–36. <https://doi.org/10.1159/000463060>
- Roncal-Jimenez, C., Lanaspaa, M. A., Jensen, T., Sanchez-Lozada, L. G. & Johnson, R. J. (2015). Mechanisms by Which Dehydration May Lead to Chronic Kidney Disease. *Annals of Nutrition and Metabolism*, 66, 10–13. <https://doi.org/10.1159/000381239>
- Shaheen, N. A., Alqahtani, A. A., Assiri, H., Alkhodair, R. & Hussein, M. A. (2018). Public knowledge of dehydration and fluid intake practices: variation by participants' characteristics. *BMC public health*, 18(1), 1346. <https://doi.org/10.1186/s12889-018-6252-5>
- Šmuljić, Z., Gajdoš Kljusurić, J., Katić, M., Čačić, J., Brlečić Bujanić, M. & Štalić, Z. (2016). Knowledge about hydration and health and fluid intake habits according to level of education. *Croatian Journal of Food technology, Biotechnology and Nutrition*, 11 (3–4), 112–121.
- WHO (World Health Organization). (2008). Guidelines for Drinking-water Quality, 3rd edition, <https://www.who.int/publications/i/item/9789241547611>

QUALITY CONTROL AND FOOD SAFETY

Original scientific article

THE CONTENT OF TOTAL IRON IN *Urtica dioica* L. FROM DIFFERENT LOCALITIES IN SERBIA

Jelena Đuričić Milanković¹, Kosana Popović¹, Mirjana Antonijević Nikolić¹, Bojana Milutinović¹, Danijela Damnjanović², Dragana Ilić Udovičić¹

¹Academy of Applied Studies Šabac, Department of Medical and Business-Technological Studies, Šabac, Serbia

²Pharmacy institution Lekofarma Šabac, Serbia

Abstract

Urtica dioica L., commonly known as “stinging nettle”, is a wild, unique herbaceous flowering plant that has been of use as a food as well as a medicinal herb for a variety of diseases centuries ago. This paper presents determination of Fe content in samples *Urtica dioica* L. collected from five localities in Serbia. The sample preparation procedure involved dry digestion in triplicate and dissolution of the ash in 6M HCl and then in 0.1 M HNO₃. The determinations of Fe content in the leaves have been performed by using spectrophotometry. Samples of nettle leaves showed the concentration of Fe in the range from 171.81 ± 9.75 mg/kg to 382.69 ± 20.25 mg/kg dry weight. The obtained values were compared with data available from literature. Finally, the content of Fe in samples were used to calculate the daily intake of Fe (*EDI*), and the target hazard quotients (*THQ*) values and contribution to daily intake of Fe for adult by consuming herbal tea of the tested stinging nettle.

Keywords: *Urtica dioica* L., iron, spectrophotometry, daily intake.

Introduction

Stinging nettle (*Urtica dioica* L., *Urticaceae*) as a weed plant widespread in the world, that has been used for over 2,000 years as a natural remedy for its therapeutic properties. Because of the high content of nutriment and bioactive compounds like minerals, vitamins and poly phenols, nettle possesses a great nutritional value and a large number of pharmacological effects (Ait Haj Said et al., 2015). In addition to elements such as zinc, magnesium, calcium, phosphorus and potassium, nettle is especially rich in iron.

Iron is an essential element for growth and development of animals, plants and humans. Iron is a component of haemoglobin present in red blood cells in the human body, and conveys oxygen throughout the body (Narain et al., 2015). It facilitates the oxidation of carbohydrates, proteins and fats to control body weight, which is a very important factor in diabetes management. Deficiency of iron in the human body is very common. Low iron content causes gastrointestinal infection, nosebleeds and myocardial infection. The most important functional indicators of iron deficiency are reduced physical work capacity, delayed psychomotor development in infants, impaired cognitive function, and adverse effects for both the mother and the fetus (FDA, 2001). These adverse consequences of iron deficiency are associated with a degree of iron deficiency sufficient to cause measurable anemia (FDA, 2001). In developing country, anaemia was reported to be a serious problem in pregnant women and preschool children (WHO, 2003). Anemia also contributes to 20% of all maternal deaths (Shonte et al., 2020). A nettle leaf in both fresh and dried forms was found to be a good source of iron. Bukva et al. (2019) examined the iron content in 35 food samples from four groups: fruits, vegetables, herbs and spices, and they concluded that the food samples can be arranged

by iron concentration in the following descending order: herbs and tea > spices > vegetables > fruits. Among the eight types of plants and teas examined, nettle was singled out as the plant with the highest measured iron content.

The Recommended Dietary Allowance (RDA) of iron for all age groups of men and postmenopausal women is 8 mg/day; the RDA for premenopausal women is 18 mg/day (FDA, 2001). The median dietary intake of iron is approximately 16 to 18 mg/day for men and 12 mg/day for women and the Tolerable Upper Intake Level (UL) for adults is 45 mg/day of iron, a level based on gastrointestinal distress as an adverse effect (FDA, 2001).

Nettle leaves can be used to make herbal tea, which is rich in minerals, vitamins, and other phytoconstituents (Paulauskiene et al., 2021). The results presented in one research report showed that *U. Dioica* retains significant amounts of minerals, vitamins, and other functional values after heat treatment (Rutto et al., 2013). The use of herbal teas is widespread in Serbia as a complementary way to treat and prevent illnesses. A World Health Organization (WHO) survey indicated that about 70–80% of the world population relies on non-conventional medicine, mainly from herbal sources, in their primary healthcare (WHO, 2002.; Kalny et al., 2007).

Alterations in chemical composition and quantity of components of stinging nettle is related to environmental growth factors such as temperature, moisture, light, soil type and nutrients (Rafajlovska et al. 2013). Also, harvesting time, development stage, form and type of organs, as well as the conditions of storage and drying are important (Grevsen et al., 2008; Biesiada et al., 2009; Krystofova et al., 2010; Kowol et al., 2011; Biesiada et al., 2010; Rafajlovska et al., 2013; Shonte et al., 2020; Paulauskiene et al., 2021).

Determination of iron content in the leaves of stinging nettle collected from different localities of Serbia and calculation of contribution to daily intake of Fe for adult by consuming herbal tea of the tested stinging nettle was set as an objective of this research.

Materials and Methods

Sampling and sample preparation

In this paper iron content in *Urtica dioica L* were analyzed. Samples of nettle leaves were collected in Serbia from five different localities (Figure 1): Fruška gora (mountain), Ljubovija, Požarevac (village Smoljinac), Šabac (village Sinošević and suburb Letnjikovac). The samples of *Urtica dioica L* were collected during September 2021. randomly in sufficient quantities (2 kg) to provide representative samples. Samples were air-dried for two weeks, then powdered and sieved through a 0.5 mm sieve (laboratory vibrating screen). The powdered samples were stored at ambient temperature and used for the analysis.

Determination of the loss of drying/water were made according to the procedures given in the general chapters of the European Pharmacopoeia (The European Pharmacopoeia, 2019; The European Pharmacopoeia, 1996).



Figure 1. Location of the sampling points for leaves collection

Spectrophotometric method

The preparation of samples was carried out by dry digestion. The herbal samples were prepared with mass of about 3 g (exact mass measured to 4 decimal places), calcined gradually by raising the temperature by 50 °C/h, from room to 450 °C, at which the sample was kept for 8 h. After cooling, ashes were dissolved in 5 ml hydrochloric acid ($c=6\text{ M}$), and the solution was evaporated in water bath to dryness. The residual precipitate was dissolved in ~10.0 ml nitric acid ($c=0.1\text{ mol/dm}^3$), filtered in volumetric flask (50 ml), washed with deionized water and diluted to mark (AOAC International, 2000). Digestion of each samples were done in triplicate.

The total iron was determined basing on the reaction with potassium-thiocyanate using the Thermo Scientific Evolution 60S UV-Visible Spectrophotometer (Mandal et al., 2017). Solutions of each samples were red to red pale color. The blank sample was prepared in the same way. Absorbance was measured at 480 nm for working and analyzed solutions. Observed calibration curve demonstrated adequate linearity, $R^2 = 0.99976$.

Calculation of health risk assessment

The contents of iron in leaves were used to evaluate the estimated daily intake (*EDI*), target hazard quotients (*THQ*) and contribution to daily intake of Fe for adult by consuming herbal tea of the tested stinging nettle.

Estimated daily intake

The estimated daily intake (*EDI*) (mg/kg body weight/day) is a fundamental parameter for metal transfer from plant to human. It can be calculated using the following equation (Zhang et al., 2018):

$$EDI = \frac{C \cdot F_{IR} \cdot TR}{W_{AB} \cdot 1000} \quad (1)$$

where C is the Fe content (mg/kg) in herbal tea, F_{IR} is the herbal tea ingestion rate (g/person/day), TR is the transference rate of the heavy metal from herbal tea to herbal tea infusion, and W_{AB} is the average body weight.

Target hazard quotient (THQ)

The targeted hazard quotient (THQ) was used to estimate the potential noncarcinogenic effects of Fe. The equation (2) was employed to calculate the THQ :

$$THQ = \frac{EDI}{RfD} \quad (2)$$

where the THQ is the target hazard quotient and is dimensionless, the EDI is the estimated daily intake (mg/kg body weight/day), and the RfD is the oral reference dose for the metal (mg/kg body weight/day) (Zhang et al., 2018, EPA US, 2007) which does not induce a lifetime harmful effect. The oral reference dose (RfD) for Fe= 0.7 mg/kg body weight/day (Chen et al., 2021; EPA US, 2000).

Results and discussion

The results of the determination of total iron in samples are given in Table 1. They are the average concentration Fe of three replicate analyses. In general, the range of concentration in which total iron was found in all samples varied from 171.81 ± 9.75 mg/kg of dry weight collected in Sinošević (sample 5), to 382.69 ± 20.25 mg/kg in nettle harvested in Ljubovija (sample 4). The samples were arranged by iron concentration in the following descending order: Ljubovija (sample 4) > Letnjikovac (Šabac, sample 2) > Fruška gora (sample 3) > Smoljinac (Požarevac, sample 1) > Sinošević (Šabac, sample 5).

In the recent decades researchers have shown that nettles are rich in iron, but reported different amounts, ranging from 7.932 mg/kg (Jan et al., 2016) to 2765 mg/kg (Radman et al., 2015) in the plant leaves. In nettle, the concentration of mineral elements varies strongly because of the different absorption of mineral elements from the soil and the time of sample collection (Shonte et al., 2020; Radman et al., 2015), especially iron (Paulauskiene et al., 2021). The quality of the analyzed stinging nettle leaves was evaluated by comparing with the literature data (Table 2) of the content of Fe in other countries. Large variations in Fe content have been noticed. The obtained results of contents Fe in samples from Serbia are in the literature range.

Table 1. Determination of loss on drying/water content (m/m%), iron content (mg/kg dry weight), estimated daily intake (EDI) (mg/kg bw/day) of iron for adults, the mean average EDI (mg/kg body weight/day), the recommended daily intake (RDI) expressed for body weight (mg/kg body weight/day), target hazard quotient (THQ) of iron and calculated contribution to daily intakes of iron (%) by consuming analyzed herbal teas of nettle from Serbia for adults (men and women)

Sample	Location (month of sampling)	Loss of drying/water content [m/m %]	Iron content [mg/ kg dry weight]	EDI for adults [mg/kg body weight/day]	THQ for adults	Contribution to daily intakes of iron by consuming herbal tea of the stinging nettle [%]	
						for men	for women
1.	Smoljinac, village near Požarevac, meadow (September)	8.14 ± 0.25	178.91 ± 14.20	$3.04 \cdot 10^{-3}$	$4.34 \cdot 10^{-3}$	2.67	1.18
2.	Letnjikovac, suburb of	8.05 ± 0.05	283.19 ± 7.84	$4.78 \cdot 10^{-3}$	$6.83 \cdot 10^{-3}$	4.19	1.86

	Šabac, courtyard (September)						
3.	Fruška gora, mountain, forest (September)	7.96 ± 0.07	209.84 ± 12.49	3.54 · 10 ⁻³	5.06 · 10 ⁻³	3.11	1.38
4.	Ljubovija, courtyard (September)	9.11 ± 0.04	382.69 ± 20.25	6.46 · 10 ⁻³	9.23 · 10 ⁻³	5.67	2.51
5.	Sinošević, village near Šabac meadow (September)	8.3 ± 0.18	171.81 ± 9.75	2.90 · 10 ⁻³	4.14 · 10 ⁻³	2.54	1.13
Recommended daily intakes (<i>RDI</i>)* (mg/day/ person) for men (women) (Harmanescu et al., 2011, FDA, 2001)			8 (18)				
The mean average of <i>EDI</i> (mg/kg body weight/day)			4.14 · 10 ⁻³				
Recommended daily intakes expressed by body weight (mg/kg body weight/day) which calculated for men (women) weighing 70 kg			1.14 · 10 ⁻¹ (2.57 · 10 ⁻¹)				

*The recommended daily intakes (*RDI*) is the average daily dietary intake level that is sufficient to meet the nutrient requirement of nearly all (97 to 98 percent) healthy individuals in a particular life stage and gender group (FDA, 2001).

Paulauskiene et al. found the highest concentrations of iron in the leaves picked in April, at the beginning of vegetation, 526.20 ± 0.12 mg/kg, while the iron content in September was 223.60 ± 0.12 mg/kg (Paulauskiene et al., 2021). The comparison of our results regarding iron content in the leaves of *Urtica dioica L* collected during autumn, with above mentioned results showed good agreement.

Table 2. Contents of Fe (mg/kg) in leaves of *Urtica dioica L*. from the literature

Literature	Content Fe (mg/kg)
Koniecznyński et al., 2007	30.76-235.37
Jan et al., 2016	7.932
Kara, 2009	999
Djurović et al., 2017	150.97
Shonte et al., 2020	167
Radman et al., 2015	2765
Bukva et al. 2019	962
This work	171.81 -382.69

Based on obtained iron content results, the iron risk to the health of that is introduced by consuming nettle tea has been assessed. According to the equation (1), the estimated daily intakes (*EDI*) values of Fe were calculated and showed in Table 1. The values of the recommended daily intakes expressed by body weight (mg/kg body weight/day) i.e. the recommended daily intakes recalculated for adults weighing 70 kg, also were given in Table 1. The *EDI* values of the Fe in samples were in the range 2.90 · 10⁻³-6.46 · 10⁻³ (mg/kg bw/day) (Table 1).

The *EDI* for Fe in all samples is less than the recommended daily intakes expressed by body weight (Table 1). This indicates that the daily intake of this metal surveyed as a five cups of the herbal tea infusion are much lower than human body needed. Consuming herbal tea can supplement Fe needed by human body, but its content is much lower than human body needs (Daničić, 2012). The estimated

values *EDI* and their comparison with the recommended daily intakes expressed by body weight are shown in Figure 2.

Research shows that a typical serving of fresh or dried nettle leaves provides approximately 5 to 30% of the recommended daily values of some mineral elements (Shonte et al., 2020). In this paper we obtained values contribution to daily intakes of Fe (%) by consuming herbal tea nettle in the interval is 2.54 -5.67 % for men and 1.13-2.51 % for women.

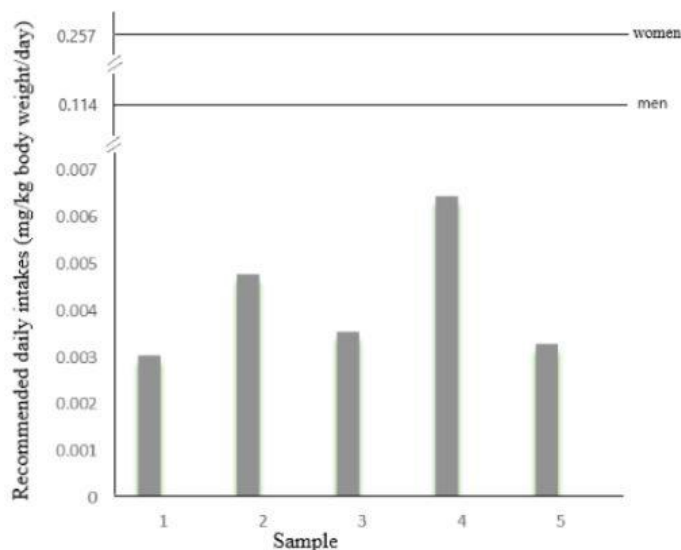


Figure 2. Estimated daily Fe intake compared with recommended daily intakes for men ($1.14 \cdot 10^{-1}$ mg/kg body weight/day) and women ($2.57 \cdot 10^{-1}$ mg/kg body weight/day)

The *EDI* values in the samples (range $2.90 \cdot 10^{-3}$ - $6.46 \cdot 10^{-3}$ mg/kg body weight/day) were all below the oral reference dose ($RfD=0,7$ mg/kg body weight/day) (Chen et al., 2021, EPA US, 2000), indicating that the drinking of the analyzed samples of stinging nettle did not appear to pose a health risk to consumers.

More authors use successfully the *THQ* methodology to estimate the potential health risks associated with long term exposure to heavy metals from food, vegetables and teas. *THQ* parameter used in health risk assessment of heavy metals provides a better picture than using a simple parameter as content of metals from soils, vegetables and tea. The target hazard quotient (*THQ*) of samples varied from $4.14 \cdot 10^{-3}$ - $9.23 \cdot 10^{-3}$ for Fe, Table 1, and were less than one, which is regarded as secure for human use.

Conclusion

This paper determined levels of Fe in five samples *Urtica dioica L.* The samples were collected from five localities in Serbia. The Fe content was determined by spectrophotometry. Samples of nettle leaves showed the concentration of iron in the range from 171.81 ± 9.75 mg/kg for sample from Sinošević (village near Šabac) to 382.69 ± 20.25 mg/kg for sample from Ljubovija. Obtained results regarding iron content in the leaves of *Urtica dioica L.* collected during autumn, compared with those of other authors showed good agreement. The analysed leaves of *Urtica dioica L.* contain Fe and could contribute to the daily dietary requirements. The noncancer health risk assessment indicated that the analyzed leaves do not pose a danger to the health of consumers.

References

- Ait Haj Said, A., Sbai el Otmani, I., Derfoufi, S. & Benmoussa, A. (2015). Highlights on nutritional and therapeutic value of stinging nettle (*Urtica Dioica*). *International Journal of Pharmacy and Pharmaceutical Sciences*, 7(10), 8–14.
https://www.researchgate.net/publication/283675999_Highlights_on_nutritional_and_therapeutic_value_of_stinging_nettle_Urtica_Dioica
- Biesiada, A., Woloszczak, E., Sokol-Letowska, A., Kucharska, A. Z. & Nawirska-Olszanska, A. (2009). The effect of nitrogen form and dose on yield, chemical composition and antioxidant activity of stinging nettle (*Urtica dioica L.*). *Herba Polonica*, 55(3), 84–93.
- Biesiada, A., Kucharska, A., Sokol-Letowska, A. & Kuš, A. (2010). Effect of the age of plantation and harvest term on chemical composition and antioxidant activity of stinging nettle (*Urtica dioica L.*). *Ecological Chemistry and Engineering A*, 17(9), 1061–1068.
<file:///D:/Documents/Downloads/Biesiada.pdf>
- Bukva, M., Kapo, D., Huseinbašić, N., Gojak-Salimović, S. & Huremović J. (2019). Iron Content in Fruits, Vegetables, Herbs and Spices Samples Marketed in Sarajevo Bosnia and Herzegovina. *Kemija u industriji*, 68 (7–8), 281–287. <https://doi.org/10.15255/KUI.2019.001>
- Chen, Y. G., He, X. L., Huang, J. H., Luo, R., Ge, H. Z., Wołowicz, A., Wawrzekiewicz, M., Gładysz-Płaska, A., Li, B., Yu, Q. X., Kołodyńska, D., Lv, G. Y. & Chen, S. H. (2021). Impacts of heavy metals and medicinal crops on ecological systems, environmental pollution, cultivation, and production processes in China. *Ecotoxicology and Environmental Safety*, 219, Article 112336. <https://doi.org/10.1016/j.ecoenv.2021.112336>
- Daničić, V. (2012). *Vitaminologija, sve o vitaminima i mineralima* [in Serbian], Tarifa, Beograd.
- Djurović, S., Pavlić, B., Šorgić, S., Popov, S., Savić, S., Pertoničević, M., Radojković, M., Cvetanović, A. & Zeković, Z. (2017). Chemical composition of stinging nettle leaves obtained by different analytical approaches. *Journal of Functional Foods*, 32, 18–26.
<http://dx.doi.org/10.1016/j.jff.2017.02.019>
- FDA (Food and Drug Administration). (2001). Dietary Reference Intakes for Vitamin A, Vitamin K, Arsenic, Boron, Chromium, Copper, Iodine, Iron, Manganese, Molybdenum, Nickel, Silicon, Vanadium, and Zinc. Report of the Panel on Micronutrients. National Academy Press, Washington, DC, Food and Drug Administration. Dietary supplements. Center for Food Safety and Applied Nutrition.
- Grevsen, K., Fretté, X. C. & Christensen, L. P. (2008). Concentration and composition of flavonol glycosides and phenolic acids in aerial parts of stinging nettle (*Urtica dioica L.*) are affected by nitrogen fertilization and by harvest time. *European Journal of Horticultural Science*, 73(1), 20–27.
- Harmanescu, M., Alda, L. M., Bordean, D. M., Gogosa, I. & Gergen, I. (2011). Heavy metals health risk assessment for population via consumption of vegetables grown in old mining area; a case study: Banat County, Romania. *Chemistry Central Journal*, 5, 64–74.
<https://doi.org/10.1186/1752-153x-5-64>
- Jan, K. N., Zarafshan, K. & Singh, S. (2017). Stinging nettle (*Urtica dioica L.*): a reservoir of nutrition and bioactive components with great functional potential. *Food Measure*, <https://doi.org/10.1007/s11694-016-9410-4>
- Kalny, P., Fijałek, Z., Daszczyk, A. & Ostapczyk, P. (2007). Determination of selected microelements in polish herbs and their infusions. *Science of the Total Environment*, 381, 99–104.
<https://doi.org/10.1016/j.scitotenv.2007.03.026>
- Kara, D. (2009). Evaluation of trace metal concentrations in some herbs and herbal teas by principal component analysis. *Food Chemistry*, 114, 347–354.
<https://doi.org/10.1016/j.foodchem.2008.09.054>

- Koniecznyński, P., Wesołowski, M. & Rafalski, P. (2007). Total and extractable iron in selected herbs collected from natural areas in Northern Poland. *Herba Polonica*, 53 (4), 27–33. <http://www.herbapolonica.pl/magazines-files/8437128-4.pdf>
- Kowol, J., Kwapuliński, J., Brodiak-Dopierala, B., Paukszto, A., Bogunia, M., Rochel, R. & Ahner B. (2011). Influence of a transboundary emission on bioavailability of metals of stinging nettle from soil. *Polish Journal of Environmental Studies*, 20(1), 115–124. <http://www.pjoes.com/pdf-88537-22396?filename=Influence%20of%20a.pdf>
- Krystofova, O., Adam, V., Babula, P., Zehnalek, J., Beklova, M., Havel, L. & Kizek, R. (2010). Effects of various doses of selenite on stinging nettle (*Urtica dioica* L.). *International Journal of Environmental Research Public Health*, 7, 3804–3815. <https://doi.org/10.3390%2Fijerph7103804>
- Mandal, Š., Keškić, N. & Marevac, N. (2017). The determination of iron levels in Menthae tea (*Mentha piperita* L.). *Bulletin of the Chemists and Technologists of Bosnia and Herzegovina*, 48, 21–26. <http://hemija.pmf.unsa.ba/glasnik/files/Issue%2048%20new/5-21-26-Mandal.pdf>
- Narain, R. & Ilango, V. (2015). Analysis of iron content of selected vegetarian food items in Dubai, UAE. *International Journal of Science, Environment and Technology*, 4(3), 543–552. <https://www.ijset.net/journal/674.pdf>
- Official Methods of Analysis of AOAC International. (2000). 17th Ed. Official Method 999.11. Gaithersburg, MD, USA: AOAC International.
- Paulauskiene, A., Tarasevičiene, Ž. & Laukagalis, V. (2021). Influence of Harvesting Time on the Chemical Composition of Wild Stinging Nettle (*Urtica dioica* L.). *Plants*, 10, 686. <https://doi.org/10.3390/plants10040686>
- Radman, S., Žutić, I., Fabek, S., Žlabur, J. Š., Benko, B., Toth, N. & Coga, L. (2015). Influence of nitrogen fertilization on chemical composition of cultivated nettle. *Emirates Journal of Food and Agriculture*, 27, 889–896. <https://doi.org/10.9755/ejfa.2015-04-089>
- Rafajlovska, V., Kavrakovski, Z., Klopcevska, J. & Srbinoska, M. (2013). Determination of protein and mineral contents in stinging nettle. *Quality of Life*, 4(1–2), 26–30. <https://doi.org/10.7251/QOL1301026R>
- Rutto, L. K., Xu, Y., Ramirez, E. & Brandt, M. (2013). Mineral Properties and Dietary Value of Raw and Processed Stinging Nettle (*Urtica dioica* L.). *International Journal of Food Science*, 1–9. <https://doi.org/10.1155/2013/857120>
- Shonte, T. T., Duodu, K. G. & de Kock, H. L. (2020). Effect of drying methods on chemical composition and antioxidant activity of underutilized stinging nettle leaves. *Heliyon*, 6, 1–10. <https://doi.org/10.1016/j.heliyon.2020.e03938>
- The European Pharmacopoeia, 10th edition, Strasbourg: Council of Europe (2019).
- The European Pharmacopoeia, 3rd edition, Strasbourg: Council of Europe (1996).
- United States Environmental Protection Agency (EPA US). (2007). Concepts, Methods and Data Sources for Cumulative Health Risk Assessment of Multiple Chemicals, Exposures and Effects: A Resource Document; EPA/600/R-06/013F, Office of Research and Development, National Center for Environmental Assessment, Cincinnati, OH, USA.
- United States Environmental Protection Agency (EPA US). (2000). Handbook for Non-Cancer Health Effects Evaluation. US Environmental Protection Agency, Washington (DC).
- World Health Organization (WHO). (2002). Traditional medicine strategy 2002–2005, Geneva.
- World Health Organization (WHO). (2003). Nutrition Unit. Fruit and vegetable promotion initiative: a meeting report, 25-27/08/03. World Health Organization.
- Zhang, J., Yang, R., Chen, R., Peng, Y., Wen, X. & Gao, L. (2018). Accumulation of Heavy Metals in Tea Leaves and Potential Health Risk Assessment: A Case Study from Puan County, Guizhou Province, China. *International Journal of Environmental Research and Public Health*, 15(1), 133–155. <https://doi.org/10.3390%2Fijerph15010133>

Professional Paper

THE PRESENCE OF PHOSPHATE IN MEAT PRODUCTS FROM THE MARKET OF REPUBLIC OF SRPSKA

Biljana Pećanac¹, Dragan Brenjo²

¹ PI Veterinary Institute of the Republic of Srpska „Dr Vaso Butozan“ Banja Luka, Branka Radičevića 18, 78000 Banja Luka, Republic of Srpska, BiH

² Agencija za bezbednost hrane, Kneza Višeslava bb, 88000 Mostar, Bosna i Hercegovina

Abstract

Phosphates and polyphosphates are the most commonly used functional additives in the food industry. The use of phosphates in the meat industry is under serious scrutiny due to the growing interest in healthier food and the association of synthetic phosphates by consumers with health risks. According to the Ordinance on food additives the maximum allowed amount of phosphoric acid and phosphate (E 338 - E 452), which can be added to meat products individually or in combination (expressed as P₂O₅), is 5 g/kg. The aim of the research is to determine the content of added phosphates expressed as phosphorus pentoxide (P₂O₅) in meat products from the market of the Republic of Srpska and compliance with regulatory requirements. To determine the amount of added phosphates, a mathematical conversion of phosphorus expressed as phosphorus pentoxide content (P₂O₅) was applied according to the Codex Alimentarius mathematical formula (Codex Stan 89-1981). In the period from May 2020 to August 2022, a total of 247 meat products were analyzed. Added phosphates were not quantified in 26% of products. The highest average value of the content of added phosphates was found in meat sausages in pieces (3.09±1.097 g/kg), and the lowest in pâtés (0.911±0.485 g/kg). Based on the obtained results, the determined amounts of added phosphates are below the allowed amounts that may be added to meat products. Given the determined amount, it is important that the use of phosphates in the meat industry is under constant supervision in order to protect the health of consumers.

Keywords: additives, meat product, added phosphates, health.

Introduction

Phosphorus is an essential nutrient and an integral part of the human body. It is used in the form of phosphate and plays an important role in the metabolism of carbohydrates, fats and proteins. We consume a large part of phosphorus through food, and there is a difference between natural and added phosphorus, which do not have the same speed and efficiency of absorption in the human body. Bioavailability of phosphorus depends on food sources. Phosphorus in meat is usually found as intracellular organic compounds that can be easily hydrolyzed to release inorganic phosphate (Uribarri, 2007).

Phosphates are one of the most commonly used food additives in poultry and meat products due to their multifunctional properties. Food safety is an imperative of modern society and this is the reason why most food additives, apart from other measures that are applied, and if used correctly, can significantly help in achieving the level of food safety (Prica et al., 2015). The use of the appropriate amount and mixture of phosphates can lead to the improvement of some properties of finished products, such as moisture retention, water retention, color protection, retardation of oxidation,

extension of shelf life, stabilization and improvement of the structure of the final product (Long et al., 2011,).

Despite its technological advantages, it has been estimated that 50% of the daily intake of phosphorus (P) in the Western world comes from "hidden phosphorus" as a food additive (Calvo et al., 2019).

The use of phosphates in meat is under serious scrutiny due to increasing interest (healthier food) and consumers' association of synthetic phosphates with health risks. These 'free industry' (inorganically bound) phosphates are efficiently absorbed in the gastrointestinal tract (Glorieux, 2017). Established is the association between high intake of phosphate additives and cardiovascular pain and mortality (Ritz et al., 2012).

The rulebook on food additives in the Republic of Srpska and Bosnia and Herzegovina is harmonized with the requirements of European regulations, i.e. the same maximum permitted amounts of phosphoric acid and phosphate (E 338 - E 452) that can be added to meat products individually or in combination (expressed as P_2O_5) prescribed is 5 g/kg. In 2019, the Committee for Food Additives and Flavorings (FAF) issued a scientific opinion evaluating the safety of phosphates (E 338-341, E 343, E 450-452) as food additives. The panel considered that phosphates are of low acute oral toxicity and there are no concerns regarding genotoxicity and carcinogenicity. No effects were reported in developmental toxicity studies (EFSA, 2019).

As the amount of natural and added phosphates cannot be calculated by the laboratory method itself, there are several mathematical formulas (possibilities) for determining natural or added phosphates. The Food Safety Agency of Bosnia and Herzegovina adopted Guidelines/guide on phosphorus and phosphates, calculation of total phosphates and recalculation of permitted amounts in meat products in order to achieve a unique methodology, display and interpretation of results in all laboratories in Bosnia and Herzegovina that participated in official food controls (Đerić & Brenjo, 2018).

Foods that contain a high amount of protein can contain a large amount of natural phosphorus. To use these formulas, it is necessary to know the amount of protein and the total amount of phosphate expressed as P_2O_5 in the sample. The added amount of phosphate can be calculated by subtracting the amount of natural phosphates from the total phosphates.

The determination of natural and added phosphates is carried out with one of the following three mathematical formulas:

1. Calculation formula according to the Codex Alimentarius Commission (Codex Stan 89-1981; 96-1981)
2. Determination of added phosphates by the Martin Dušek method (2004) (<http://fsa.gov.ba/bs>)
3. Determination of added phosphates VTT Biotechnology Method VTT – 4202 – 91 (1991)

To determine the amount of added phosphates in this study, the mathematical conversion of phosphorus expressed as the content of phosphorus pentoxide (P_2O_5) according to the Codex Alimentarius mathematical formula (Codex Stan 89-1981) was applied.

The aim of this research is to determine the content of added phosphates expressed as phosphorus pentoxide (P_2O_5) in meat products on the market of Republika Srpska and compliance with legal requirements.

Materials and Methods

In the period from May 2020 to August 2022, a total of 247 meat products belonging to different categories and groups were analyzed. The samples, according to the systematization prescribed by the Ordinance on minced meat, semi-finished products and meat products Ordinance (15), belong to five categories: sausages (permanent dry sausages (n = 47), thermally processed sausages (n=114)), dried meat products (permanent products (n=11) and semi-permanent products (n=22)), canned goods (canned minced meat, breakfast cuts (n=32) and pates (n = 8)) and bacon (permanent (n = 7) and semi-permanent (n = 6)). After receiving the samples in the laboratory, they were homogenised with

appropriate equipment, kept in a seal-tight container at 4°C and analysed within 24 h of homogenization. The total phosphorus content in the samples was determined by the standard method BAS ISO 13730:200.

To determine the amount of added phosphates in this study, the mathematical conversion of phosphorus expressed as the content of phosphorus pentoxide (P₂O₅) according to the Codex Alimentarius mathematical formula (Codex Stan 89-1981) was applied, which included the content of total phosphates and proteins, by the standard ISO method determined by standard methods BAS ISO 13730 and BAS ISO 937.

Calculation formula according to the Codex Alimentarius Commission (Codex Stan 89-1981; 96-1981):

$$\text{Natural phosphate (mg/kg P}_2\text{O}_5) = 250 \times \text{Amount of protein (\%)} \quad (1)$$

$$\begin{aligned} &\text{Total phosphate (mg/kg P}_2\text{O}_5) - \text{natural phosphate (mg/kg P}_2\text{O}_5) \\ &= \text{added phosphates (mg/kg P}_2\text{O}_5) \end{aligned} \quad (2)$$

Results and discussion

In the period May 2020 to August 2022, a total of 247 meat products belonging to different categories and groups were analyzed. The samples, according to the systematization prescribed by the regulation (7) belong to four categories: sausages (dry fermented sausages (n=47), thermally processed sausages (n=114), dried meat products (permanent products (n=11), semi-permanent products (n=22)), canned goods (canned minced meat, breakfast cuts (n=32), pates (n=8)) and bacon, permanent (n=7) and semi-permanent (n=6)). The results of proteins (%), total phosphates (g/kg) and added phosphates (g/kg) are presented by product groups according to current regulations, as well as by types of meat products for individual product groups, which is shown in Table 1 and Table 2 and Figure 1 and Figure 2.

Table 1. Results of testing protein (%), total phosphates (g/kg) and added phosphates (g/kg) in meat products presented by groups

Group of Meat Products	Proteins (%)	Min (%)	Max (%)	Total phosphates (g/kg)	Min (g/kg)	Max (g/kg)	Added phosphates (g/kg)	Min (g/kg)	Max (g/kg)
Finely chopped sausages n -33	10.99±1.052	9.14	13.72	4.73±0.379	4.08	5.47	1.99±0.238	1.50	2.39
Coarsely chopped sausages n -62	13.97±1.564	9.74	18.14	5.43±1.071	3.52	8.43	1.91±1.059	0.26	4.16
Dry fermented sausages n -47	24.60±2.92	18.26	35.8	5.70±0.825	3.94	8.39	<0.10	<0.10	<0.10
Heat-treated meat sausages in pieces n -19	13.29±1.022	10.62	14.40	6.41±1.263	4.26	8.29	3.09±1.097	1.61	4.69
Semi- dried meat products n -22	17.16±2.178	13.8	22.49	6.49±0.826	4.74	7.91	2.27±0.465	1.29	3.57

Permanent dried meat products n -11	34.78±2.753	31.11	39.25	8.29±0.811	7.47	9.88	<0.10	<0.10	<0.10
Canned meat - meat breakfast n -32	12.42±1.232	10.62	14.04	5.60±0.938	4.23	7.66	2.49±0.959	1.16	3.20
Pate n -8	10.59±1.173	8.52	11.7	3.59±0.640	2.74	4.41	0.91±0.485	0.28	1.52
Dry bacon n - 7	19.97±3.905	16.76	26.61	4.37±1.182	3.29	6.70	<0.10	<0.10	<0.10
Semi-dry bacon n -6	15.45±1,217	13.62	17.30	6.30±1.484	4.67	8.51	2.43±1.447	0.64	4.52

n- number of tested meat products

Table 2. Results of testing protein (%), total phosphates (g/kg) and added phosphates (g/kg) in meat products presented by types of products belongs to the group of dry fermented sausages

Group of Meat Products	Proteins (%)	Min (%)	Max (%)	Total phosphates (g/kg)	Min (g/kg)	Max (g/kg)	Added phosphates (g/kg)	Min (g/kg)	Max (g/kg)
Dry fermented sausages n -47	24.60±2.92	18.26	35.8	5.70±0.825	3.94	8.39	<0.10	<0.10	<0.10
Kulen sausage n -9	24.72±4.274	22.04	35.80	6.03±0.980	5.00	8.39	<0.10	<0.10	<0.10
Winter salamin - 3	28.12±0.568	27.29	28.62	6.57±0.535	5.96	6.96	<0.10	<0.10	<0.10
Srem sausage n -8	24.84±1.026	23.00	26.40	5.78±0.641	4.81	6.40	<0.10	<0.10	<0.10
Tea sausage n -18	23.68±2.166	19.99	28.23	5.31±0.513	4.47	6.26	<0.10	<0.10	<0.10
Sujuk sausage n -2	28.96±1.181	28.12	29.79	7.22±0.134	7.12	7.31	<0.10	<0.10	<0.10
Related sausages n -7	23.65±2.994	18.26	27.50	5.43±0.817	3.94	6.35	<0.10	<0.10	<0.10

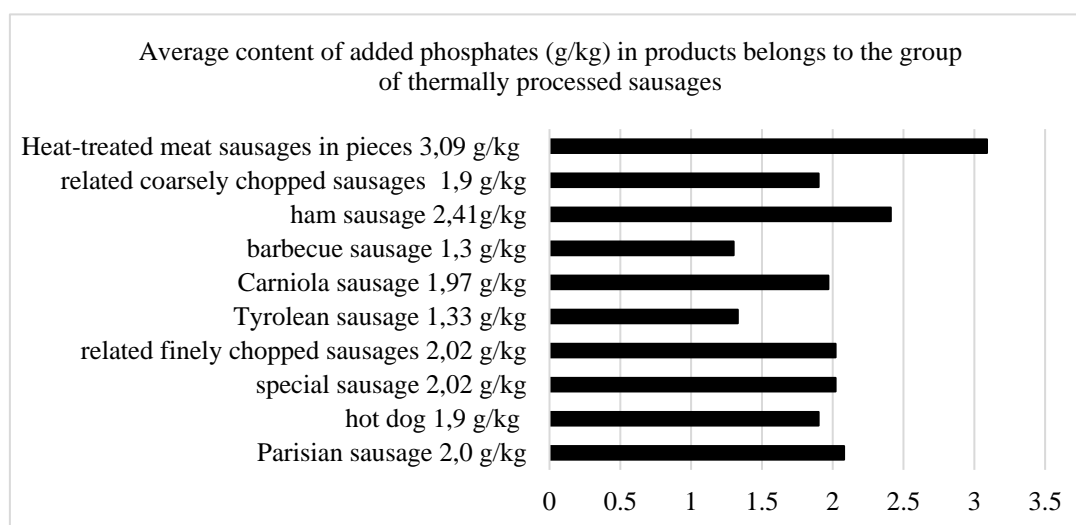


Figure 1. Results of average content of added phosphates (g/kg) in products belongs to the group of thermally processed sausages

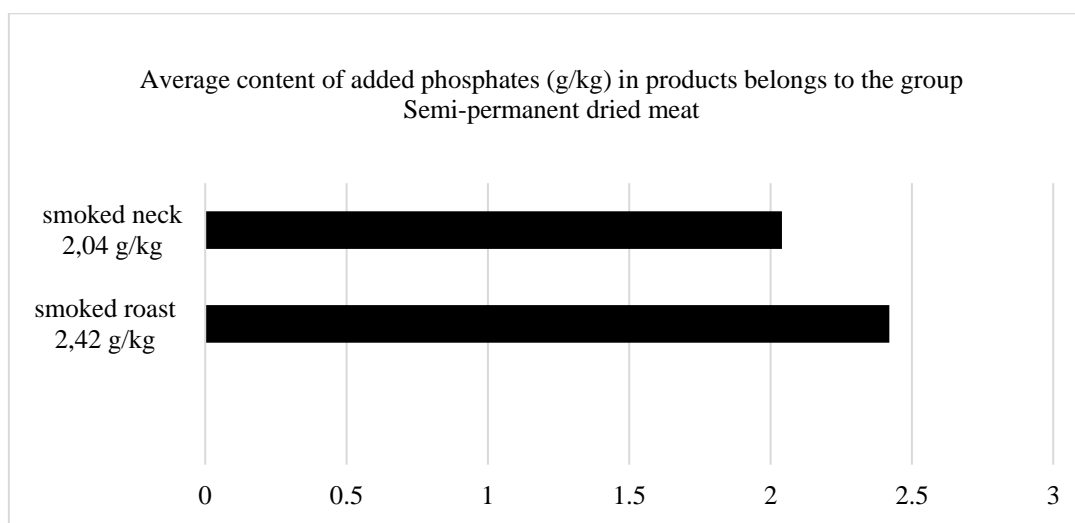


Figure 2. Results of average content of added phosphates (g/kg) in products belongs to the group of Semi-permanent dried meat

Added phosphates were not quantified in 26% of the products (< 0.10 g/kg), which belong to dry fermented sausages, dry bacon and permanent cured meat products. The results obtained in the mentioned products were also to be expected considering the technological justification of the use of phosphate in the technological production process.

The highest average value of the content of added phosphates was found in meat sausages in pieces (3.09 ± 1.097 g/kg), and the lowest average value in pâtés (0.911 ± 0.485 g/kg).

The highest amount of added phosphates was recorded in the meat sausage in pieces (4.69 g/kg), and the lowest in the Tyrolean sausage (0.26 g/kg).

In permanent products that have not been thermally processed, a more significant content of proteins was determined, and thus the share of total phosphates originating from proteins.

Thus, in 47 samples of fermented dry sausages, an average of $24.60 \pm 2.92\%$ protein was found, and the values reached up to 35.80% protein, while the total phosphates were an average of 5.70 ± 0.825 g/kg. Also, in 11 cured meat products, the average proportion of proteins is $34.78 \pm 2.753\%$, and total phosphates is 8.29 ± 0.811 g/kg, while in six samples of cured bacon, the average proportion of proteins is $19.97 \pm 3.905\%$, and total phosphates 4.37 ± 1.182 g/kg. Lower average values of protein content were found in Paris sausage ($10.58 \pm 0.62\%$) and pate ($10.59 \pm 1.173\%$), in which the lowest share of total phosphates was recorded. Depending on the content of total phosphates and proteins, we obtained the corresponding content of added phosphates.

In finely chopped sausages average amount of added phosphates with standard deviation is 1.99 ± 0.238 g/kg, and the highest recorded amount is 2.39 g/kg. In coarsely chopped sausages, the average amount of added phosphates is 1.91 ± 1.059 mg/kg, and the highest recorded amount is 4.16 mg/kg. In dry meat semi-permanent products we find 2.27 ± 0.465 g/kg of added phosphates, and a maximum of 3.57 mg/kg. A total of 6.41 ± 1.263 g/kg of total phosphates was determined in sausages made of meat in pieces, and the highest amount determined was 8.29 g/kg. A total of 2.43 ± 1.447 g/kg of total phosphates was determined in semi-permanent bacon, and the highest amount determined was 2.27 g/kg.

Pleadin et al. (2009) in the conducted research on the amount of phosphate found polyphosphate levels that exceeded the highest permitted amount of 5 g/kg in the group of semi-permanent sausages in 13 samples, of which one sample of Tyrolean sausage (5.56 g/kg), four samples of ham and eight samples of other semi-permanent sausages. In our research we found 4.66 ± 1.120 g/kg of total phosphates in Tyrolean sausage, but the added phosphates amounts were 1.33 ± 1.07 g/kg. Even when

taking into account the highest amount of total phosphates found in Tyrolean sausage of 6.82 g/kg, the amount of additional phosphate of 3.32 g/kg is less than the maximum allowed amount. Also, in our research, 6.49 ± 0.826 g/kg of total phosphates, 17.16 ± 2.178 % of protein were found in ham sausage, and based on the results obtained according to the mathematical formula, 2.27 ± 0.465 g/kg of added phosphates were determined, which is less than the allowed amount. In the related products of semi-permanent sausages, higher amounts of total phosphates (5.62 ± 1.043 g/kg) were found compared to the value determined by Pleadin et al (2009). Higher amounts of total phosphates were also found in dry fermented sausages than Pleadin et al (2009), but no added phosphates were found. In the meat industry, phosphates are used in quantities of 0.05 to 0.5%. It is important to emphasize that in permanent dried meat products with a high protein content, in the production of which polyphosphates are not even used, the analysis of total phosphorus also determined its high natural levels (Marušić, 2012).

In the research of Milešević et al. (2022), highest average and highest phosphorus content were observed in smoked meat products (6.12 ± 1.33 g/kg, 10.64 g/kg, respectively), while the lowest average values were obtained for liver sausage and pate (2.71 ± 1.05 g/kg). Although the results of Milešević et al. (2022) expressed over total phosphates, which in meat products can be up to 8 g/kg, our results are in agreement with the minimum and maximum determined total phosphates. The lowest values of 2.74 g/kg (10.59 ± 1.173 g/kg) were found in pâté, and the maximum amount of total phosphates was 9.88 g/kg (8.29 ± 0.811 g/kg) found in permanent dried meat products (smoked meat products). The most common categories of products that use phosphates are cooked sausages, hams, and other whole-muscle products. This may be attributed to the fact that moisture retention is an important parameter of their quality. Phosphates increase the water-holding capacity and, consequently, reduce drip loss and cooking loss (Polak et al., 2017).

Also, our results of total phosphates in cans (5.60 ± 0.938 mg/kg) agree with the results of Milešević et al. (2022) whose average value of total phosphates is 5.79 ± 1.01 g/kg.

Dimitrovska et al (2019) found that over 60% of beef/pork products and about 45% of poultry products exceed the legal limit of 5000 mg/kg of added phosphates expressed as P_2O_5 .

It is necessary before using any type of meat in meat preparation products, to know the amount of phosphorus in meat or meat mass, so that added synthetic phosphates and polyphosphates will not exceed the permissible limit (Prica et al., 2015).

In regulations on the conditions of use of additives and other requirements for additives and their mixtures in the Republic of Serbia and in Montenegro, the permitted use of total phosphorus expressed as P_2O_5 content is defined differently (double) in the regulations on the quality of meat products whose the specified value in the finished product must be less than 8.0 g/kg for Serbia, that is, it must not be greater than 7.0 g/kg for Montenegro.

Conclusion

Based on the obtained results, the determined amounts of added phosphates are below the amounts allowed by the Ordinance on food additives that can be added to meat products individually or in combination (expressed as P_2O_5), which is 5 g/kg for meat products. Added phosphates were not quantified in 26% of the products (< 0.10 g/kg), which belong to dry fermented sausages, dry bacon and permanent cured meat products which was to be expected considering the technological justification of the use of phosphate in the technological production process.

The highest average value of the content of added phosphates was found in meat sausages in pieces (3.09 ± 1.097 g/kg), and the lowest average value in pâtés (0.911 ± 0.485 g/kg). The highest amount of added phosphates was recorded in the meat sausage in pieces (4.69 g/kg), and the lowest in the Tyrolean sausage (0.26 g/kg). In finely chopped sausages average amount of added phosphates is 1.99 ± 0.238 g/kg, and the highest recorded amount is 2.39 g/kg. In coarsely chopped sausages, the

average amount of added phosphates is 1.91 ± 1.059 mg/kg, and the highest recorded amount is 4.16 mg/kg. In dry meat semi-permanent products we find 2.27 ± 0.465 g/kg of added phosphates, and a maximum of 3.57 mg/kg. A total of 6.41 ± 1.263 g/kg of total phosphates was determined in sausages made of meat in pieces, and the highest amount determined was 8.29 g/kg. A total of 2.43 ± 1.447 g/kg of total phosphates was determined in semi-permanent bacon, and the highest amount determined was 2.27 g/kg.

Since significant amounts of added phosphate have been found in certain groups of meat products, it is very important that the use of phosphate in the meat industry be under constant supervision in order to protect the health of consumers.

References

- BAS ISO 13730:200 - Meat and meat products - Determination of total phosphorus content – spectrophotometric method.
- BAS ISO 937:2007 - Meat and meat products - Determination of nitrogen content.
- Březinová, B. (2015). *Polyphosphates in fat production Bachelor's degree* (Unpublished Bachelor's degree thesis). Mendel University in Brno, Faculty of Agronomy, Institute of Technology.
- Calvo, M. S., Sherman, R. A. & Uribarri, J. (2019). Dietary Phosphate and the Forgotten Kidney Patient: A Critical Need for FDA Regulatory Action. *Am. J. Kidney Dis.*, 73, 542–551. <https://doi.org/10.1053/j.ajkd.2018.11.004>
- Dimitrovska, M., Ristovska, G., Chuleva, B. & Dimitrovski, D. (2019). Phosphates as food additives in meat and meat products in North Macedonia. *60th International Meat Industry Conference MEATCON, IOP Conference Series Earth and Environmental Science*, 333(1), 012054. <https://doi.org/10.1088/1755-1315/333/1/012054>
- Đerić, Z. & Brenjo, D. (2018). Phosphates in meat products - legal basis and practice (Fosfati u proizvodima od mesa – zakonski osnov i praksa). *Scientific Journal "Meat Technology"*, 56(2), 120–130.
- EFSA Journal. (2019). 17(6), 5674. <https://doi.org/10.2903/j.efsa.2019.5674>
- Glorieux, S., Goemaere, O., Steen, L. & Fraeye, I. (2017). Phosphate Reduction in Emulsified Meat Products: Impact of Phosphate Type and Dosage on Quality Characteristics. *Food Technol Biotechnol*, 55(3), 390–397. <https://doi.org/10.17113/ftb.55.03.17.5089>
- Guidelines/guide on phosphorus and phosphate, calculation of total phosphate and calculation of allowed quantities in meat products (www.fsa.gov.ba). 2015
- Long, N., Gál, R. & Buňka, F. (2011). Use of phosphates in meat products. *African Journal of Biotechnology*, 10, 19874–19882. <https://doi.org/10.5897/AJBX11.023>
- Marušić, J., Katalenić, M., Kozačinski, L., Pleadin, J., Cvrtila, Ž., Stražanac, D. & Gross-Bošković, A. (2012). Polyphosphates in meat and meat products. *Croatian Food Agency. Scientific opinion*
- Milešević, J., Vranić, D., Gurinović, M., Korićanac, V., Borović, B., Zeković, M., Šarac, I., Milićević, D. R. & Glibetić, M. (2022). The Intake of Phosphorus and Nitrites through Meat Products: A Health Risk Assessment of Children Aged 1 to 9 Years Old in Serbia. *Nutrients*, 14(2), 242. <https://doi.org/10.3390/nu14020242>
- Polak, T., Lušnic Polak, M., Tomović, V. M., Žlender, B. & Demšar, L. (2017). Characterization of the Kranjska klobasa, a traditional slovenian cooked, cured, and smoked sausage from coarse ground pork. *Journal of food processing and preservation*, 41(6), e13269. <https://doi.org/10.1111/jfpp.13269>
- Prica, N., Zivkov-Balos, M., Jaksica, S., Mihaljev, Z., Kartalovic, B., Ljubojevic, D. & Savic, S. (2015). Phosphates as food additives in meat and meat products in North Macedonia. *Procedia Food Science*, 5, 243–246.

- Pleadin, J., Perši, N., Vulić, A. & Đugum, J. (2009). Kakvoća trajnih, polutrajnih i obarenih kobasica na hrvatskom tržištu. *Hrvatski časopis za prehrambenu tehnologiju, biotehnologiju i nutricionizam* 4 (3-4), 104–108.
- Ritz, E., Hahn, K., Ketteler, M., Kuhlmann, M. K. & Mann, J. (2012). Phosphate additives in food – a health risk. *Dtsch Arztebl Int.*, 109, 49–55. <https://doi.org/10.3238%2Farztebl.2012.0049>
- Rulebook on food additives (Official Gazette of the Republic of Srpska no 96/20)
- Rulebook on minced meat, semi-finished products and meat products (Official Gazette of the Republic of Srpska no 46/15)
- Uribarri, J. (2007). Phosphorus homeostasis in normal health and in chronic kidney disease patients with special emphasis on dietary phosphorus intake. *Seminars in dialysis*, 20, 295-301. <https://doi.org/10.1111/j.1525-139x.2007.00309.x>

TEXTILE ENGINEERING

Original scientific article

OPTIMIZATION OF THE CLASSICAL DYEING PROCESS OF PES KNITWEAR

Marija Kodrić¹, Suzana Đorđević², Nevena Tomić³, Dragan Đorđević³

¹Innovation Center University of Niš, Niš, Serbia

²Technological and Artistic Professional School Leskovac, Leskovac, Srbija

³University of Niš, Faculty of Technology in Leskovac, Leskovac, Serbia

Abstract

The optimization of the classical polyester knitting dyeing procedure by varying the parameters of importance for dyeing was described by this paper. Dispersants, pH regulators, equalizers, wetting agents, etc. facilitate and accelerate the diffusion of dye into the fiber. Laboratory tests conducted in this work are aimed at determining the influence of these parameters for polyester dyeing, the amount of dispersant, equalizer, pH of dyeing solution, temperature and dyeing time has been optimized. To quantify the dye of the knitwear, after dyeing, the Kubelka-Munk equation and parameters of the CIELab system were used, through which differences in the degree of dyeing can be characterized. The test results show that all the examined parameters have a corresponding influence on the degree of dye depletion and the degree of dyeing of the knitwear. The concentration of the dispersant, the pH of the solution and the temperature of the dye stand out.

Keywords: disperse dye, polyester, dyeing, optimization.

Introduction

The growing demand for high-quality textile materials has triggered the development of high value-added synthetic fibers that complement the benefits of synthetic and natural fibers (Wada, 1992; Sudha et al., 2009).

Polyester (PES) fiber has a compact structure formed by multiple stretching and heat treatment, extremely hydrophobic character, high electronegative potential and a small number of functional groups capable of reacting with ions and dye molecules. All these characteristics limit the choice of dyes and complicate the dyeing process of this fiber (Demirel et al., 2011).

Polyester belongs to a group of synthetic fibers that have active sites where dye molecules can be adsorbed. PES contains a large number of ester groups, as well as a number of carboxyl groups located at the ends of the chain, so the dyeing of this fiber will establish hydrogen bonds with the dye molecules. PES has a pronounced hydrophobic character and compact structure, so having in mind this behavior of fibers in the dyeing solution, it is necessary to modify the usual dyeing procedure, ie increase the rate of diffusion of dye into the fibers. In general, the dyeing rate could be increased by using suitable dyes, changing the fiber structure, changing the dyeing conditions, etc. (Burkinshaw, 1995).

The dyeing process or the reaction between the dye and the polyester takes place in accordance with the sorption process. As is known, PES belongs to the group of synthetic fibers that have active sites where dye molecules can be adsorbed.

Optimization is done with the basic recipe provided by the manufacturer with the usual additions to standard recipes. The purpose is to successfully dye highly hydrophobic and crystalline fibers under

normal conditions of pressure and temperature. In recent years, many attempts have been made to improve various aspects of dyeing, new technologies have been developed to reduce fiber damage, reduce energy consumption and increase productivity (Shao et al., 2001).

Dye dispersants play an important role in paint quality and the dyeing process. Dispersion stability also depends on the nature of the various components and their interactions. To ensure good quality of the finished product, the dispersed particles in the solvent should be optimized with an adequate spray aid, including the selection of its type and quantity. Disperse dyeing of polyesters requires the use of dispersants as additives to increase dispersion stability, solubility, leveling properties and dye fastness (Dong et al., 2010).

This paper is an attempt to optimize the classic process of dyeing PES knitwear, all with the aim of achieving adequate dyeing on textiles, saving energy and time, and ultimately money.

Materials and Methods

Raw and undyed 100% polyester (polyethylene terephthalate) knitwear was used with the following basic characteristics: interlacing, yarn fineness 9.4 tex, yarn density horizontally 15 1/cm, vertically 16 1/cm, surface mass 140 g/m².

PES knitwear from the dye manufacturer's recipe is dyed with disperse dye C.I. Disperse Red 60 (Figure 1), molecular formula C₂₀H₁₃NO₄ and molar mass $M = 331.32$ g/mol, with the addition of 1 g/dm³ dispersant (Sarbid DLO conc), 1 g/dm³ equalizer (Alviron S), 0.5 g/dm³ formic acid, 1% dye, in the ratio of bath 1: 100, in the time of 60 min, at 100 °C, then rinsing with distilled water hot, cold and drying. The paper optimizes the recipe of the manufacturer in laboratory conditions, the following parameters were varied: the amount of dispersant, equalizer, pH of the dye solution, temperature and time of dyeing.

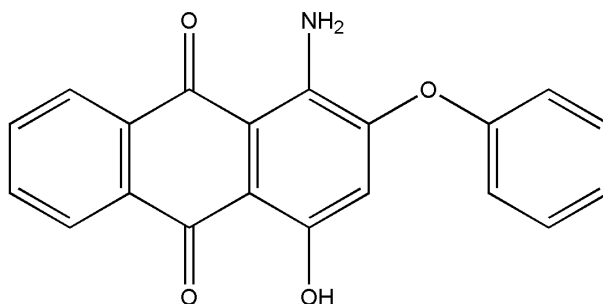


Figure 1. Structure of disperse dye C.I. Disperse Red 60

When it comes to the dye of textiles, ie. visual experience of the surface, the results of reflection spectroscopy can give certain interpretations and explanations based on the dependence of reflection and/or K/S parameter on the wave length in the visible light range for dyed textiles. As a rule, the textile pattern that has the highest reflection values shows the lowest values for the K/S parameter, which indicates its lighter shade compared to the pattern that has lower reflection values and higher K/S values, for one and the same dye.

The Kubelka and Munka formula gives the relationship between the reflection coefficient of the material and the dye content and contains a constant that depends on the dye itself and the wave length.

$$\frac{K}{S} = \frac{(1-R)^2}{2R} = A \cdot c \quad (1)$$

where: K - absorption constant for a certain wave length, S - scattering coefficient for a certain wave length, R_e - measured remission value for a certain wave length, A - proportional constant (dye concentration, wave length, etc.) and C (%) - dye concentration (Miljković et al., 2012).

The dye of the knitwear was measured using a reflection spectrophotometer (HunterLab ColorQuest XE diffuse / 80), which is connected to a personal computer or appropriate software. The device determines the reflection, Gurevich-Kubelka-Munk function and the parameters of the CIELab system, which can be used to characterize differences in the degree of dye.

Results and Discussion

The optimization was done in laboratory conditions with the basic recipe provided by the manufacturer with the usual additions according to standard recipes.

The stability of the suspension when dyeing polyester fibers can be appropriately modified by applying appropriate dispersants, but dyeing used Sarabid DLO conc. The effect of different concentrations (0.5, 1.5, 2 g/dm³) of dispersant on the dye strength of polyester in the classical dyeing process was compared with the amount of dispersant of 1 g/dm³ (from the paint manufacturer's recipe). The influence of the amount of dispersant (Sarabid DLO conc) on the ability to dye polyester with disperse dyes is shown in the diagram in Figure 2.

According to the diagram, the maximum dye strength was achieved when dyeing with the amount of dispersant 2 g/dm³, at a wave length of 510 nm and *K/S* value 6.34, which means that under these conditions most dye is bound to fiber, so this amount of dispersant is recommended when dyeing PES fibers with disperse dyes. This is more than the amount of dispersant provided by the standard recipe, 1 g/dm³ and the classic dyeing process. When dyeing with a dispersant of 0.5 g/dm³, we obtained the lowest degree of staining at a wave length of 510 nm and a *K/S* value of 4.59. It was found that the amount of dispersant has an effect on the dye strength of polyester knitwear.

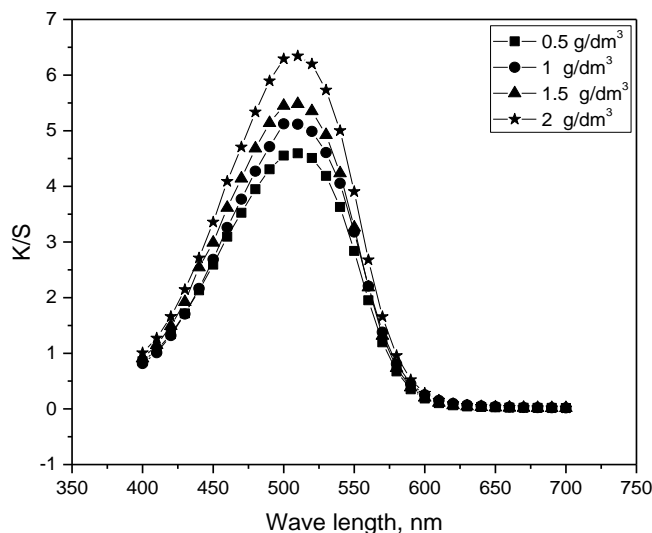


Figure 2. Influence of different dispersant concentration on polyester dyeing strength

Then, the influence of different concentrations (0.5, 2 and 3 g/dm³) of the equalizer on the dye intensity of polyester dyed by the classical dyeing process was compared with the amount of equalizer of 1 g/dm³ (from the paint manufacturer's recipe). The influence of the amount of equalizer (Alviron S) on the ability to dye polyester with disperse dyes is shown in the diagram in Figure 3. It can be seen that the dye intensity increases with increasing amount of equalizer. The maximum dye strength was achieved when dyeing with the amount of equalizer 3 g/dm³, at a wave length of 510 nm and *K/S* value of 5.48, which means that under these conditions most dye is bound to fiber, so this amount of equalizer is recommended for dyeing PES fibers disperse paints. This is more than the amount of equalizer provided by the standard recipe, 1 g/dm³ in the classic dyeing process. When staining with an equalizer of 0.5 g/dm³, we obtained the lowest degree of staining at a wave length of 510 nm and

a K/S value of 4.39. It was determined that the amount of equalizer has an effect on the dye strength of polyester knitwear.

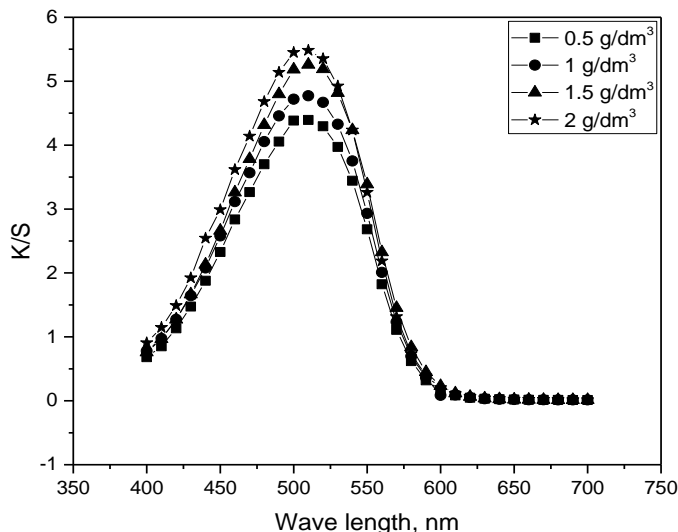


Figure 3. Influence of the amount of equalizer on polyester dyeing strength

One of the important factors of PES disperse dyeing is the dyeing time. The influence of time or length of contact between adsorbate and adsorbent on adsorption - depletion of dye for dyeing PES knitwear with the manufacturer's recipe was investigated. The influence of the time of staining with disperse dyes on the strength of staining was examined in the range of 20 to 80 min. The equilibrium time recommended by the manufacturer is 60 min.

The influence of dyeing time on the ability to dye polyester with disperse dyes is shown in the diagram in Figure 4. It can be seen that the intensity of dyeing increases with increasing dyeing time. The maximum dyeing strength was achieved when dyeing at a time of 80 min, at a wave length of 510 nm and a K/S value of 5.14, which means that under these conditions most dye is bound to fiber, so this time is recommended for dyeing PES fibers with disperse dyes. This is a longer time than the standard recipe, 60 minutes for the classic dyeing process. At a staining time of 20 min, we obtained the lowest degree of staining at a wave length of 510 nm and a K/S value of 4.13. It has been determined that the dyeing time has an effect on the dyeing strength of polyester knitwear.

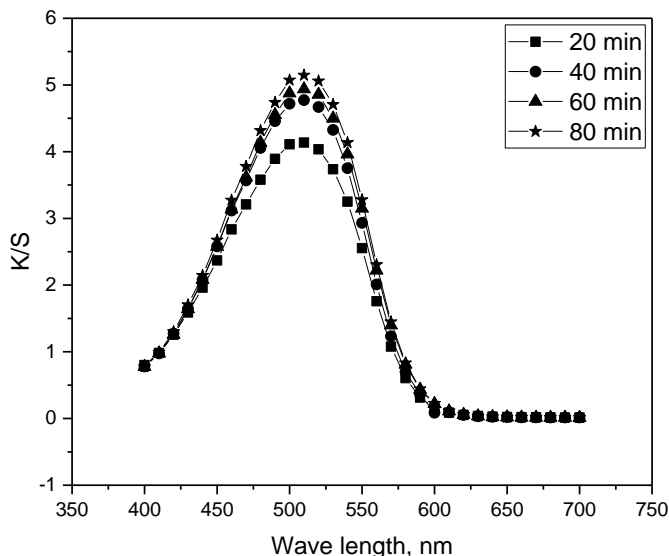


Figure 4. Influence of dyeing time on polyester dyeing strength

The speed of staining significantly depends on the temperature and in all cases the speed increases with increasing temperature. Examining the influence of temperature on the dyeing speed of different dye-fiber systems, it was found that an increase in solution temperature reflects an increase in dyeing rate or diffusion rate, but also that an increase in equilibrium depletion decreases with increasing temperature. Dyeing is an exothermic process, so it is understandable that the equilibrium adsorption of dye must decrease with increasing temperature (Novaković, 1996).

We compared the effect of temperature when dyeing polyester at 70, 80 and 90 °C with the classical dyeing procedure at a temperature of 100 °C (from the recipe of the paint manufacturer).

As can be seen from the diagram, the maximum dyeing strength was achieved when dyeing at 100 °C, at a wavelength of 510 nm, *K/S* value 6.67, so this temperature is recommended when dyeing PES fibers with disperse dyes, and this is the recommended temperature. manufacturer. At other lower temperatures, a lower staining intensity was obtained, and at a staining temperature of 70 °C, the lowest degree of staining was obtained at a wavelength of 510 nm, *K/S* value 4.77. The diagram clearly shows that the temperature has an effect on the dye strength of the polyester knitwear.

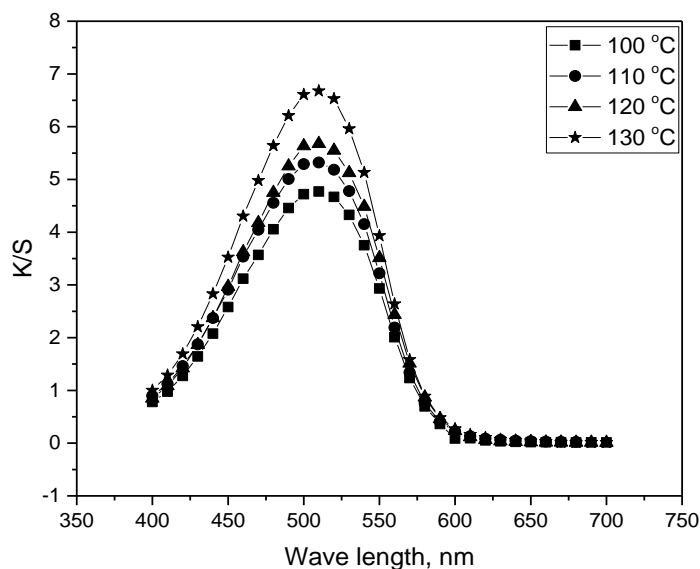


Figure 5. Influence of temperature on polyester dyeing strength

Dyeing of textile material can be seen as a chemical process in which pH plays a significant role, as well as other variables. The influence of pH (4, 4.5 and 5.5) in polyester dyeing was compared with the classical dyeing procedure (pH 5) (from the dye manufacturer 's recipe). As can be seen from the diagram, the maximum dyeing strength was achieved when dyeing at pH 4.5, at a wave length of 510 nm, *K/S* value 6.14, so this pH value is recommended when dyeing PES fibers with disperse dyes. In classical staining, we obtained the degree of staining at a wave length of 510 nm, *K/S* values of 5.11, while pH 4 and pH 5.5 values showed a lower degree of staining. The diagram clearly shows that the pH value has an effect on the dye strength of the polyester knitwear.

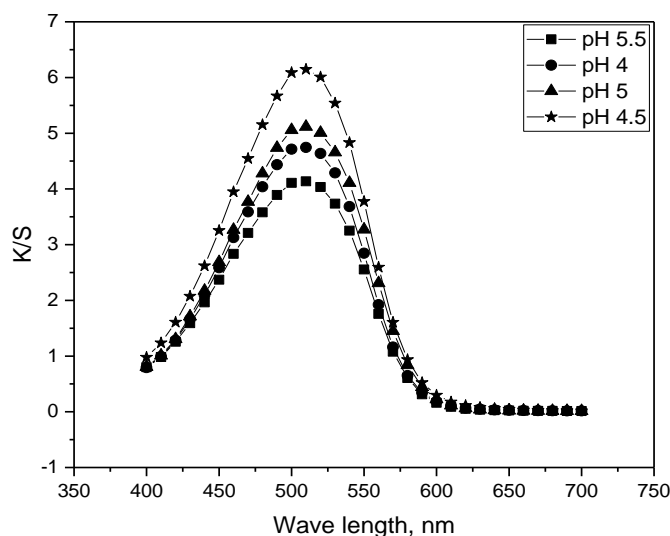


Figure 6. Influence of pH value on polyester dyeing strength

Conclusion

The results show that the optimization of the classical dyeing procedure of PES knitwear made in laboratory conditions gave better dyeing results in relation to the manufacturer's recipe. The results also show that the used C.I. Disperse Red 60 dye can be successfully applied for dyeing PES knitwear in new conditions.

The test results showed that the equalizer, dispersant, temperature and pH values have an impact on the dyeing process of PES knitwear and with increasing their concentrations better dyes were obtained. The greatest influence on the dye intensity was achieved when dyeing with the amount of dispersant 2 g/dm^3 , at a wave length of 510 nm and K/S value of 6.34, also a great influence was the change of pH value of 4.5 at a wave length of 510 nm and K/S with a value of 6.14 nm, which means that under these conditions most dyes are bound to the fiber, so this amount of dispersant and pH value of 4.5 is recommended when dyeing PES fibers with disperse dyes.

Acknowledgment: "Republic of Serbia - Ministry of Education, Science and Technological Development, Program for financing scientific research work at the Innovation Center of the University of Nis."

References

- Wada, O. (1992). Control of fiber form and yarn and fabric structure. *The Journal of The Textile Institute*, 83(3), 322–347. <https://doi.org/10.1080/00405009208631207>
- Sudha, T. B., Thanikaivelan, P., Aaron, K. P., Krishnaraj, K. & Chandrasekaran, B. (2009). Comfort, chemical, mechanical, and structural properties of natural and synthetic leathers used for apparel. *Journal of Applied Polymer Science*, 114(3), 1761–1767. <https://doi.org/10.1002/app.30589>
- Demirel, B., Yaras, A. & Elcicek, H. (2011). Crystallization Behavior of PET Materials. *BAU. Fen. Bil. Enst. Dergisi Cilt*, 13(1), 26–35. https://www.researchgate.net/profile/Ali-Yaras-2/publication/290429725_Crystallization_Behavior_of_PET_Materials/links/56977b7308ae1c427904dc10/Crystallization-Behavior-of-PET-Materials.pdf

- Burkinshaw, S. M. (1995). Chemical Principles of Synthetic Fibre Dyeing. *Blackie Chapman & Hall*, London.
- Shao, J., Liua, J. & Carr, C. (2001). Investigation into the synergistic effect between uv/ozone exposure and peroxide pad-batch bleaching on the printability of wool. *Coloration Technology*, 117(5), 270–275. <http://dx.doi.org/10.1111/j.1478-4408.2001.tb00074.x>
- Dong, X., Zheng, Z. & He, J. (2010). pH-Sensitive Dye-Polyether Derivatives as Dispersants for Its Parent Dye. Part 2: Dispersion Stability and Dyeing Performance. *Journal of Dispersion Science and Technology*, 31(9), 1188–1194. <https://doi.org/10.1080/01932690903224037>
- Miljković, M., Purenović, M., Stamenković, M. & Petrović, M. (2012). Određivanje koncentracija dve reaktivne boje u bojenom pamučnom materijalu. *Hem. Ind*, 66(2), 243–251. <https://doi.org/10.2298/HEMIND110721091M>
- Novaković, M. (1996). Teorija i tehnologija oplemenjivanja tekstila bojenjem i štampanjem. BMG, Beograd.

Original scientific article

INFLUENCE OF KNIT PATTERN ON DIMENSIONAL STABILITY OF KNITTED FABRICS

Sandra Stojanović¹, Dušan Trajković², Jelka Geršak³, Miodrag Đorđević¹

¹Department of Technology and Art, Academy of Professional Studies South Serbia, Serbia

²Department of Textile Sciences, Faculty of Technology, University of Niš, Leskovac, Serbia

³Research and Innovation Centre for Design and Clothing Engineering, Faculty of Mechanical Engineering, University of Maribor, Maribor, Slovenia

Abstract

During sport activities active wear is exposed to moisture and strain which can influence the dimensional changes of garments. For that reason, an experimental work was introduced to examine influence of knit pattern on dimensional stability and moisture content of knitted fabrics intended for active wear. Modified FAST 4 method was used for determination of Relaxation Shrinkage and Hygral Expansion of nine knitted fabrics knitted in three knit pattern groups (interlock, pique and rib knit). It has been established that knit pattern has an impact on dimension stability parameters of knitted fabrics. For knitted fabrics knitted in interlock pattern, negative values of Relaxation Shrinkage were recorded both in the wale and course direction. The density of knitted fabrics had the greatest influence on Hygral Expansion values. For pique knitted fabrics, it was found that the yarn parameters had the significant influence on the dimensional stability parameters. For samples in pique knit pattern, positive Hygral Expansion values were recorded in the course direction, while in the wale direction there was no change with the exception of the sample K5-P where 0.4% was recorded. In the case of knitted fabrics in rib knit pattern, negative Relaxation Shrinkage values were recorded with the exception of the sample K9-R, while Hygral Expansion values were positive and inversely proportional to the density. Moisture content of knitted fabrics in interlock pattern range from 1.12% to 1.31%, in pique from 1.07% to 4.02% and rip knit from 0.91% to 3.37%.

Keywords: Knit pattern, dimensional stability, Relaxation Shrinkage, Hygral Expansion, moisture content.

Introduction

Because of their good characteristic such as high elasticity, better stretch and recovery, low mass per unit area, smooth surface and comfort, porosity and air permeability knitted fabrics acquired higher popularity and wider use compared to the woven fabrics (Yesmin et al., 2014).

Knitted fabrics intended for clothing production must possess high quality. Dimensional stability is a significant impact on the construction of clothing and the quality of finished garments (Geršak, 2014). In addition, dimensional stability is one of most important factor to maintain the aesthetic appearance of knitwear during its using (Munden, 1960). Various factors such as fiber properties, yarn parameters, machine parameters and knit pattern influence the dimensional and geometrical characteristics of knitted fabrics (Emirhanova & Kavusturan, 2008; Mikučionienė & Laureckienė, 2009). Shrinkage of knitted fabric is a serious problem which occur from dimensional changes in the knitted fabrics specifically loop structure (Abu Nassif, 2019). It is known that sportswear is constantly subjected to wetting that occurs due to sweating of athletes during physical activity. It was reported

that an athlete in certain conditions can create even 2.5 liters of sweat (Shirreffs et al., 2005). In addition, shrinkage represents 20% of the total complain of clothing buyers (Munden, 1960). This problem become even more significant in recent years due to the increased popularity of different type of sportswear. When designing garments, major matter is prediction of the dimensional stability of knitted fabrics. During the exploitation of knitwear and their washing, these products are often subjected to notable dimensional changes which reduce their quality (Pešić et al., 2018). One more demand in relation to textile material intended for sportswear manufacturing is excellent moisture management properties (Senthilkumar et al., 2013).

For these reasons, it is necessary to get acquainted with the effect of dimensional changes in knitted fabrics intended for the production of sportswear. Effect of three knit pattern on dimensional stability and moisture content (MC) was investigated.

Materials and Methods

In this study, dimensional stability of knitted fabrics intendent for sportswear production were experimentally presented. For the purpose of investigation knit pattern on dimensional stability, nine different knitted fabrics in three different pattern groups (interlock, pique and rip knit) and four different row material were knitted. Structural parameters of knitted fabrics are presented in Table 1.

Table 1. Structural parameters of knitted fabrics

Sample	Knit pattern	Raw material	Yarn linear mass [tex]	Total density [cm ⁻²]	Thickness [mm]	Surface mass [g m ⁻²]
K1-I	Interlock	PES	7.4	344.0	0.312	131.62
K2-I	Interlock	PES	7.4	171.1	0.382	127.49
K3-I	Interlock	PES	7.4 3.6	194.7	0.280	135.19
K4-P	Double pique	50% PES / 50% Co	7.4 17.4	254.4	0.666	157.60
K5-P	Double pique	50% Outlast / 50% PES /	9.4 3.6	287.5	0.539	144.71
K6-P	Pique	PES	8.8	192.2	0.394	156.51
K7-R	Rib knit (honycomb)	PES	7.4	211.3	0.500	124.90
K8-R	Rib knit	PES	11.1	279.0	0.330	132.10
K9-R	Rib knit	65% PES micro / 35% Outlast	11.7 7.2	165.0	0.499	151.00

In Figure 1 visual appearance of analyzed knitted fabrics is presented.

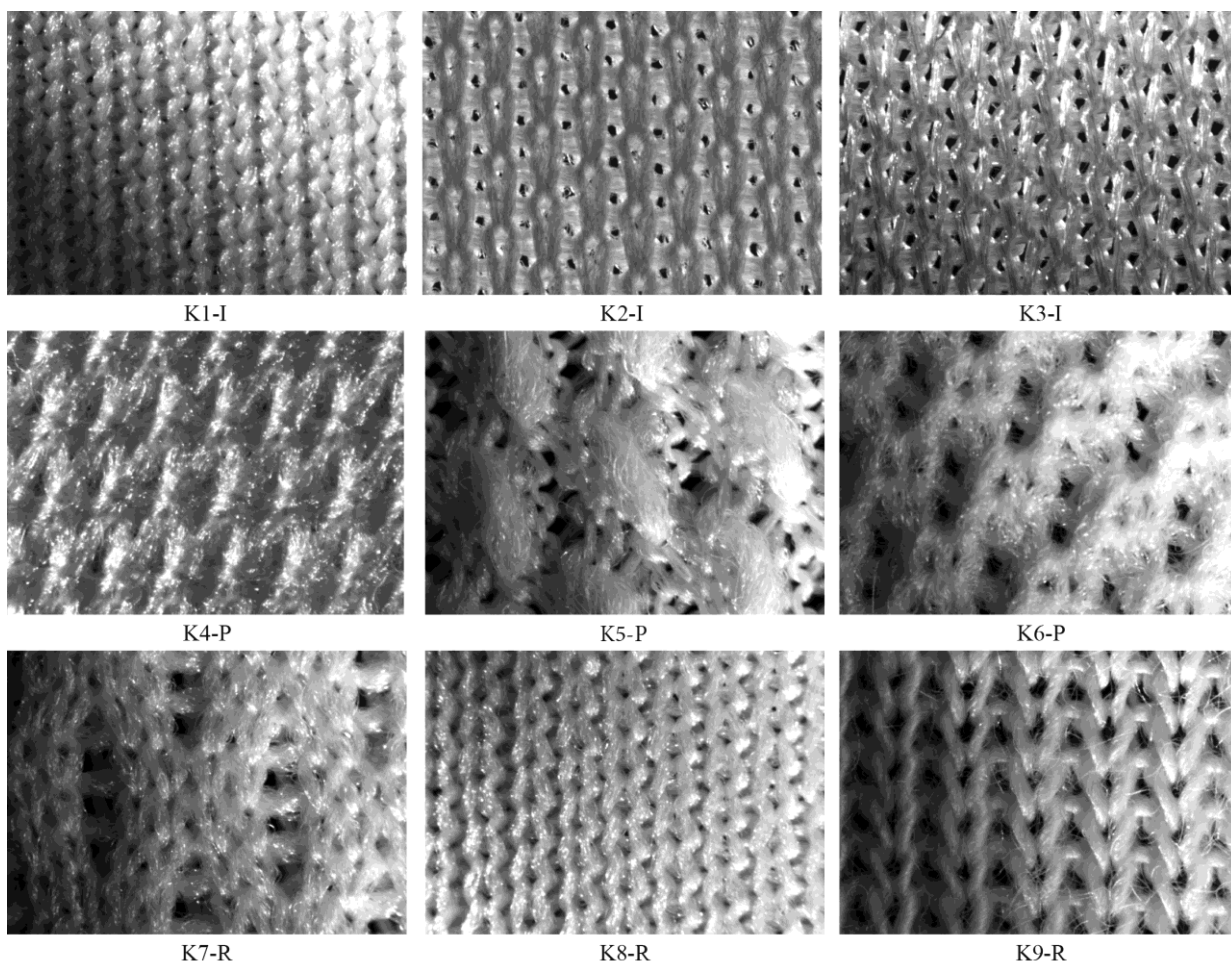


Figure 1. Visual appearance of knitted fabrics

FAST 4 method was used for determination of the dimensional stability of knitted fabrics. The results of this test method give valuable information to garment manufactures as how dimensions of textile material will change when exposed to moisture and heat. The method enables Dimensional stability to be split in to two important parameters: Relaxation Shrinkage (RS) and Hygral Expansion (HE) (Geršak, 2014).

Relaxation Shrinkage is irreversible change in textile material dimensions (shrinkage or expansion) that occurs when fabrics is exposed to heat and moisture or steam. RS is caused by the release of cohesively set strains which are imposed on fabrics during the late stage of finishing. By the FAST-4 method, RS is defined as percentage change expressed in the dimensions of textile material after wet and heat treatment.

Hygral Expansion is reversible change in the dimensions of the textile material which occurs when the moisture content of the textile material is altered. Using FAST-4 method, HE is defined as the percentage change in the dimensions of textile material after wet treatment.

For measuring the moisture content in the analysed knitted fabrics Mettler Toledo moisture Analyzer HC103 was used. The mean values of moisture content of five measurements for each sample are presented in this paper.

The knitted fabrics were conditioned in standard atmospheres specified according to the ISO 139:2005 Standard.

Results and discussion

Results of Hygral Expansion (HE) are presented in Figure 2.

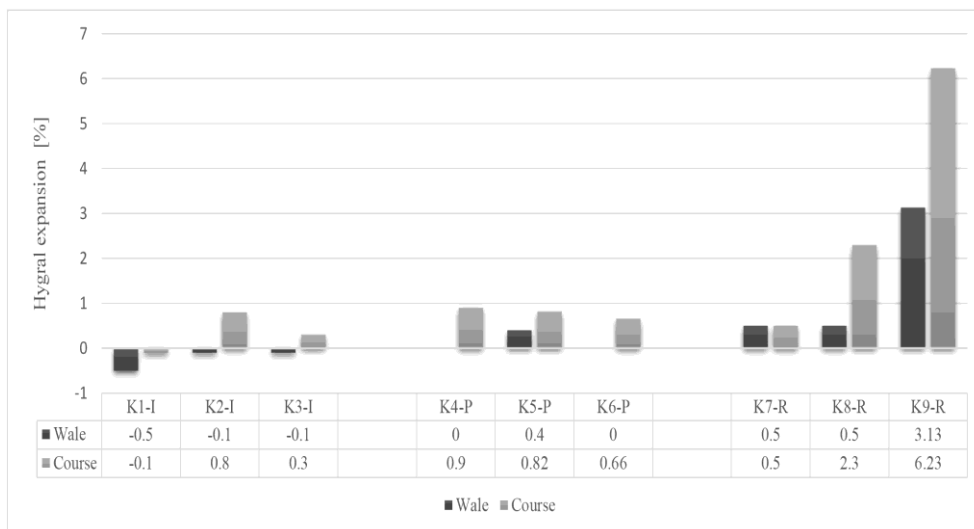


Figure 2. Results of Hygral Expansion of knitted fabrics

Relatively small HE values were recorded for knitted fabrics in interlock pattern. By analyzing the obtained results presented in Figure 2 for the samples K1-I and K2-I knitted using same yarn and in same knit pattern, it can be concluded that the density of knitted fabrics has a significant influence on the HE values. In sample K1-I, which has the highest total density, shrinkage occurred in both directions of knitted fabric. While in samples K2-I and K3-I, shrinkage in wale and stretching in the course direction were recorded after wet treatment. Higher HE values were recorded for sample K2-I in the course direction. The knitted fabric K3-I was made using two yarns, which contributed to the greater stability of this knitted fabric after wet treatment.

For knitted fabrics in double pique pattern K4-P and K5-P no changes in dimensions in wale direction occurred, while in course direction a slight expansion was recorded after wet treatment, which can be seen from obtained HE values. For knitted fabric K6-P expansion in course direction has been recorded. These results indicate that wet treatment on knitted fabrics in pique pattern has a greater influence on the change of dimensions in the wale direction, while it has insignificant influence in the course direction. In addition, the raw material composition of the samples had a smaller impact on the HE results, namely sample K4-P (50% cotton / 50% polyester) for which slightly higher values were recorded compared to other polyester (PES) samples in the pique knit pattern. All three knitted fabrics in the pique pattern have approximately equal thickness and surface mass, which indicates that the main factors contributing to the different results of HE is the total density and raw material composition.

For all knitted fabrics in rib-knit pattern positive HE values were recorded, which indicates that expansion occurred after wet treatment. For knitted fabrics K8-R there is equal expansion in both directions (0.5%), while for sample K9-R significantly higher HE values were recorded in course in comparison to wale direction.

By analyzing results of hygral expansion for all knitted fabrics samples it is evident that the highest values were recorded for samples in rib knit pattern (K8-R and K9-R) in comparison to samples in interlock and pique pattern. This means that rib knit pattern has a more unstable structure in contact with moisture and after wet processing in comparison to interlock and pique pattern.

Results of Relaxation Shrinkage (RS) are presented in Figure 3.

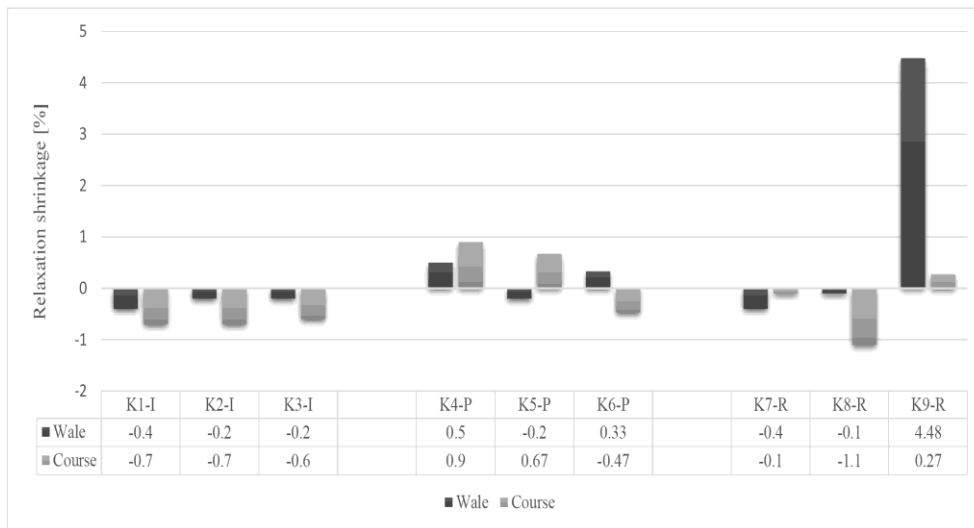


Figure 3. Results of Relaxation Shrinkage of knitted fabrics

For the knitted fabrics in interlock pattern, negative RS values were recorded both in wale and course directions. RH values in course direction range from -0.2% to -0.7% and from -0.2% to -0.6% in wale direction. When comparing K1-I and K2-I samples knitted using the same yarn, it is noticed that higher shrinkage was recorded for the K1-I knitted fabric. This knitted fabric has a higher total density, thickness and surface mass. For sample K3-I (which was made by using two yarns) slightly lower RS values were recorded in comparison to other two knitted fabrics from this group of samples, which indicates that the influence of the yarn parameters on the change of RS is not significant. Based on RH results, it can be concluded that knitted fabrics produced in interlock knit pattern have a stable structure, which can contribute to predicting the behavior of garments made from these knitted fabrics.

Knitted fabrics in double pique pattern K4-P and K5-P showed increase in RH values in wale direction, while in course direction comes to a slight expansion for K4-P sample and shrinkage for K5-P sample. This results can be explained by raw material; sample K4-P was knitted using two yarns one of them was cotton yarn (17.35 tex) while sample K5-P was knitted using two polyester (PES) yarns (9.38 tex). When cotton (Co) fibres absorb moisture, they swell which lead to change of fibres cross section, extension of fibre and increase of weight of knitted fabric. Swelling of fibres leads to dimensional changes i.e. increase of fibre diameter leads to changes in yarn and knitted fabric.

In the case of the knitted fabric K6-P, a different behavior was observed in relation to other knitted fabrics from the pique sample group. This knitted fabric shrank in the wale direction (-2.64%) while, in the course direction stretched (0.67%) after wet and heat treatment. This sample has the lowest total density and highest thickness and surface mass which contributed to this results.

All three knitted fabrics were in rib knit pattern were knitted of PES yarn of different yarn linear mass. For samples K8-R and K9-R, negative RS values were recorded, *i.e.* there was a shrinkage in both directions after wet and heat treatment. For this two knitted fabrics different percentage of shrinkage was recorded because of different structure of this knitted fabrics (rib knit and honeycomb rib knit). These two knitted fabrics have more stable structure in comparison to sample K9-R. Knitted fabrics K9-R is very elastic and unstable which, can be seen from RS and HE results.

In Figure 4 results of moisture content of analyzed knitted fabrics are presented.

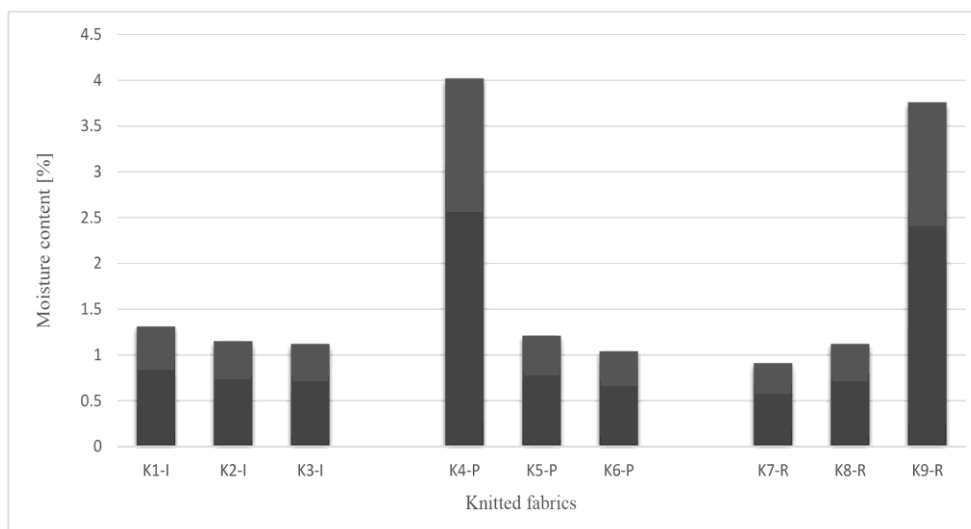


Figure 4. Results of moisture content of knitted fabrics

Moisture content values for knitted fabrics from the interlock sample group range from 1.12% to 1.31%. When comparing samples K1-I and K2-I which were knitted using same yarn, it is evident that higher moisture content value was recorded for K1-I. This sample has greater weight and total density. The lowest MC value was recorded for K3-I sample (which was knitted using two yarns) in comparison to other samples knitted in interlock pattern. This sample has the smallest thickness, which contributed to low MC results.

For knitted fabrics in a pique pattern, MC values range from 1.07% to 4.02%. In the case of these samples, the raw material composition has the greatest influence on the MC values, so the highest value was recorded for the K4-P sample (4.02%), which row material composition is 50% Co and 50% PES. It is well known that Co fibers are hydrophilic, and when absorb water swell and dry more slowly. When comparing samples K5-P and K6-P, it can be concluded that the total density is the decisive factor in determining the MC values. Regarding the knitted fabric sample with a more open construction (lower total density) K5-P, the recorded MC value is higher by 0.17% compared to the sample K6-P.

In the group samples knitted in rib knit pattern, the properties of two samples made of conventional fibers (K7-R and K8-R) and one sample made of microfibers (K9-R) were tested. For samples in rib knit pattern made using conventional fibers, higher MC values were recorded for sample K8-R, this sample have a higher total density. High results of MC were recorded for sample made using 65% PES microfiber and 35% Outlast fibers. Microfiber fabrics are characterized by ability to transfer and bind moisture, *i.e.* absorb sweat, which is achieved thanks to the capillary mechanism and the function of absorption and migration of moisture. The quality of that mechanism does not depend on the hydrophilicity of the fiber surface, but rather on the size of the fiber surface available for absorption, that is, on the fineness of the fibers. Textile surface products made of microfibers allow greater wearing comfort due to the improved capillary transfer of sweat and through the fineness of the fibers (relatively speaking) higher absorption potential on the surface of the fibers.

Conclusion

Based on the obtained results, it can be concluded that knit pattern plays a significant role in determining the dimensional stability of knitted fabrics. Low HE values were recorded in the case of knitted fabrics in the interlock knit pattern. Which means that the reversible deformation in these

knitted fabrics was insignificant after wet treatment. However, when analysing the RH results which represent irreversible deformation, shrinkage of knitted fabrics in both directions was detected. The shrinkage was more pronounced in the wale direction.

For knitted fabrics in the pique pattern, HE values equal to zero were recorded (except for sample K5-P, where the value of 0.4% was recorded), while in the course direction stretching (0.66% to 0.9%) were recorded after wet treatment. However, after wet and heat treatment, different behaviour was noted in these samples, which is evident from the RH results. The main reason for this behaviour was complex pique pattern structure.

For knitted fabrics in rib knit pattern, stretching was recorded in both directions, which can be seen from the HE results. The deformation is proportionally reversed with the reduction of the surface mass. While the RS values for these knitted fabrics are negative in both directions with the exception of sample K9-R. With these knitted fabrics, the biggest difference between HE and RS results is recorded.

It can be concluded that the knit pattern does not have a great influence on the obtained moisture content results. The raw material composition of the knitted fabric as well as the structure of the fibres from which it is made had the greatest influence on MC results. The highest MC value was obtained for the K4-P sample (50% PES /50%Co) in pique knit pattern as much as 4.02%. In addition, a high value of MC was recorded for sample K9-R in rib knit pattern, which was produced from microfibres which have an exceptional ability to absorb moisture.

References

- Abu Nassif, N. (2019). Dimensional Stability, Aesthetic and Functional Properties of Cotton:Polyester Blended Knitted Fabrics with Different Structures. *International Design Journal*, 9(4) 23–29. <https://dx.doi.org/10.21608/idj.2019.82542>
- Emirhanova, N. & Kavusturan, Y. (2008). Effects of Knit Structure on the Dimensional and Physical Properties of Winter Outerwear Knitted Fabrics. *Fibres and Textiles in Eastern Europe*, 16(2), 69–74. http://www.fibtex.lodz.pl/67_17_69.pdf
- Geršak, J. (2014). *Objektivno vrednovanje plošnih tekstilija i odjeće*. Sveučilište u Zagrebu Tekstilno-tehnološki fakultet.
- Mikučionienė, D. & Laureckienė, G. (2009). The Influence of Drying Conditions on Dimensional Stability of Cotton Weft Knitted Fabrics. *Materials Science*, 15(1), 64–65. https://www.researchgate.net/publication/266071786_The_Influence_of_Drying_Conditions_on_Dimensional_Stability_of_Cotton_Weft_Knitted_Fabrics
- Munden, D. (1960). Dimensional stability of plain-knit fabrics. *Journal of the Textile Institute Proceedings*, 51(4), 200–229. <https://doi.org/10.1080/19447016008664427>
- Pešić, M., Petrović, V., Stepanović, J. & Bešić, C. (2018). The analysis of dimensional stability of 1x1 RIB Co and Co/LY knitwear. *Industria Textila*, 69(4), 293–297. <https://doi.org/10.35530/IT.069.04.1434>
- Senthilkumar, M., Sampath, M. & Ramachandran, T. (2013). Moisture Management in an Active Sportswear: Techniques and Evaluation—A Review Article. *Journal of The Institution of Engineers*, 93, 61–68. <https://doi.org/10.1007/s40034-013-0013-x>
- Shirreffs, S., Aragon-Vargas, L., Chamorro, M., Maughan, R., Serratos, L. & Zachwieja, J. (2005). The sweating response of elite professional soccer players to training in the heat. *International journal of sports medicine*, 26(2), 90–95. <https://doi.org/10.1055/s-2004-821112>
- Yesmin, S., Hasan, B., Miah, S., Momotaz, F., Idris, M. & Hasan, R. (2014). Effect of Stitch Length and Fabric Constructions on Dimensional and Mechanical Properties of Knitted Fabrics. *World Applied Sciences*, 32(9), 1991–1995. <https://doi.org/10.5829/idosi.wasj.2014.32.09.1264>

GRAPHIC ENGINEERING AND DESIGN

Original scientific article

A METHOD OF RANKING RESPONDENTS ACCORDING TO SENSE OF COLOR DIFFERENCES

Zoran Gazibarić¹, Predrag Živković², Vladimir Cviljušac³, Miloš Ljubojević⁴

¹Banja Luka College, Banja Luka, Bosnia and Herzegovina

²University of Belgrade, Faculty of Technology and Metallurgy, Beograd, Serbia

³University of Zagreb, Faculty of Graphics Arts, Zagreb, Croatia

⁴University of Banja Luka, Faculty of Electrical Engineering, Banja Luka, Bosnia and Herzegovina

Abstract

The Farnsworth-Munsell 100 Hue Test has been used for the past 60 years in various industries as a method for evaluating an individual's ability to discern color. The respondent gets a precise result in which part of the colored space has a weaker sense of color distinction. It can also be ranked according to the overall result. For a production manager or production technician, a satisfactory result from this test is ≤ 40 points, and for a strict color assessment, a designer or a person with a very strict color evaluation criterion must have a result of ≤ 16 points. The purpose of this paper is to propose a new method of ranking respondents according to sense of color differences. Respondent's ranking results for color difference are declared in ΔE and can be compared with instrumental measurements. Respondent's rank results within the method represented in this work can be expressed by ΔE^*_{ab} , ΔE^*_{CMC} , ΔE^*_{94} or ΔE^*_{00} and can be compared directly with results obtained by instrumental measurement.

Keywords: color, method, color distinction, color difference.

Introduction

In addition to instrumental color control, the evaluation of color differences should be performed by human observer in many industry branches where color accuracy is a critical quality parameter. To rank respondents in terms of their tolerance for color differences, an original method is developed earlier (Gazibarić et al., 2021), and used to determine the sensitivity threshold (ST), barely noticeable differences (BND), and unacceptable color differences (UCD) that particular respondent perceives. The method for characterization sense for color differences of the respondent, described in the preliminary paper is based on the originally developed software Color Changer (Gazibarić et al., 2021). By establishing a quantitative indicator for each member of the test group, it is possible to rank the respondents in terms of tolerance for perceiving a color difference. The assumption is that a candidate with the narrowest tolerance for the perception of color differences is also the best candidate for evaluating color deviation in a given circulation.

The Farnsworth-Munsell 100 Hue Test (www.xrite.com, n.d.) has been used over the past 60 years in various industries to assess an individual's sense of color differences. The respondent receives a precise result in which part of the colored space she or he has a weaker sense of color distinction. It can also be ranked according to the overall result. For a production manager or production technician, a satisfactory result from this test is ≤ 40 points and for a strict color assessment that must be performed by a designer or a person with very strict criteria for assessing colors, the result of the F-

W test must be ≤ 16 points. The test can be repeated and by recording the results, the change in respondent's ability for color perception can be monitored.

The method described in this work, using the method for characterizing human sense by color differences (Gazibarić et al., 2021), has a direct link to the color difference expressed through the equation ΔE_{00} (Luo et al., 2001) from instrumental color analysis. It is emphasized that any equation can be applied to the method described in this work, so data can be compared to data read from the instrument. The test can be repeated and by recording the results, the change in respondent's ability for color differences can be monitored.

Materials and Methods

For this experiment, the CIELAB values of 24 test fields taken from the X-Rite ColorChecker Classic card based on the Color-Rendition Chart (McCamy et al., 1976) were selected. The Color-Rendition Chart has been developed to facilitate quantitative or visual assessments of color reproduced in photography, television, and print. A series of 24 colored fields includes spectral simulations of the bright and dark color of human skin, leaves, blue sky, and blue flower (chicory). Likewise, the primary colors of additive and subtractive synthesis as well as a scale of six neutral ones are included. Colored fields are the stimuli shown on the calibrated monitor (Sharma, 2002). There are a lot of research activities for evaluating color differences, that confirm the reliability of the usage of computer systems, monitors, developed software and a controlled environment. One is conducted by authors Salvadori and Goñi (Goñi & Salvadori, 2017). In their work, Szafir et al. presented color comparison fields via an Internet connection and respondents answered the test by viewing the colors on their monitors (Szafir, 2018; Szafir et al., 2014). Liang et al. conducted two separate but similar experiments at the University of Leeds (UK) and Zhejiang University (China). Both experiments to assess color differences were carried out using the Eizo screen using the ratio method (Liang et al., 2017).

For this experiment, it was not crucial to achieve absolutely accurate values on the screen as on the X-Rite ColorChecker tab, but to have the fields approximately in those parts of the color space as the fields from that card and to cover all parts of it. In addition, it is crucial for this experiment to accurately determine the difference in color, and not the absolute value of the color in the CIELAB coordinates. The table with CIELAB values of 24 test fields (Table 1) is taken from the www.babelcolor.com (www.babelcolor.com, n.d.).

Table 1. Reference color table

No.	Color name	xyY (CIE D50)			L*a*b* (CIE D50)		
		x	y	Y	L*	a*	b*
1	dark skin	0.4325	0.3788	10.34	38.44	13.61	14.53
2	light skin	0.4191	0.3748	35.25	65.95	17.91	17.87
3	blue sky	0.2761	0.3004	18.47	50.06	-4.52	-22.25
4	foliage	0.3700	0.4501	13.35	43.28	-13.21	21.94
5	blue flower	0.3020	0.2877	23.24	55.31	8.82	-24.60
6	bluish green	0.2856	0.3910	41.74	70.69	-33.03	-0.11
7	orange	0.5291	0.4075	31.17	62.65	35.35	57.86
8	purplish blue	0.2339	0.2155	11.40	40.24	9.74	-44.35
9	moderate red	0.5008	0.3293	19.79	51.60	47.80	16.90
10	purple	0.3326	0.2556	6.44	30.50	21.07	-20.02
11	yellow green	0.3989	0.4998	44.35	72.46	-23.30	57.00

No.	Color name	xyY (CIE D50)			L*a*b* (CIE D50)		
		x	y	Y	L*	a*	b*
12	orange yellow	0.4962	0.4428	43.58	71.95	19.46	68.12
13	blue	0.2040	0.1696	5.79	28.87	14.81	-50.15
14	green	0.3270	0.5033	23.07	55.15	-37.80	31.64
15	red	0.5709	0.3298	12.68	42.28	54.12	28.67
16	yellow	0.4694	0.4732	60.81	82.27	4.02	79.99
17	magenta	0.4177	0.2704	20.07	51.91	49.80	-13.82
18	cyan	0.2151	0.3037	19.03	50.72	-28.11	-27.95
19	white 9.5 (.05 D)	0.3488	0.3628	91.29	96.53	-0.47	2.42
20	neutral 8 (.23 D)	0.3451	0.3596	58.85	81.21	-0.64	0.27
21	neutral 6.5 (.44 D)	0.3446	0.3590	35.95	66.48	-0.53	0.00
22	neutral 5 (.70 D)	0.3438	0.3589	19.12	50.83	-0.64	-0.14
23	neutral 3.5 (1.05 D)	0.3423	0.3576	8.93	35.85	-0.54	-0.49
24	black 2 (1.5 D)	0.3439	0.3565	3.20	20.81	0.03	-0.39

Before performing this experiment, each potential respondent was checked for color blindness, using the Ishihara color test (Ishihara, 1918). Only respondents with normal color vision should be included in this investigation.

In this method, the two-coloured fields with known colorimetric values are presented to respondents on a screen (Figure 1).

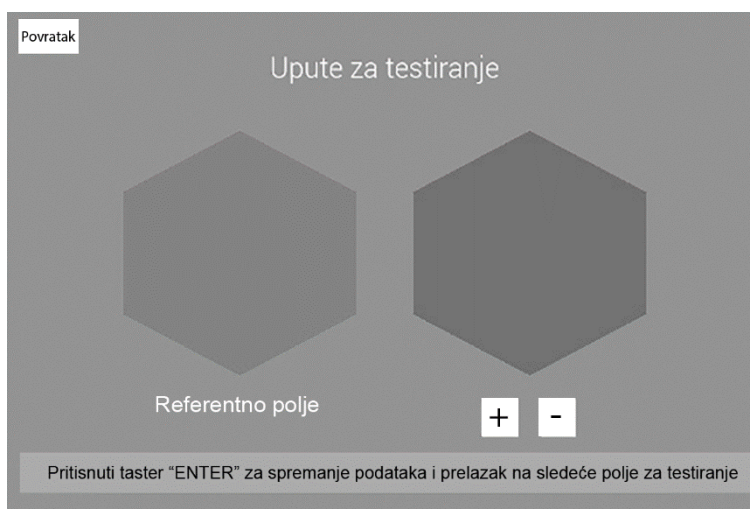


Figure 1. Colored fields on a monitor shown to respondent (translation of original signs: "Upute za testiranje" – Testing instructions; „Referentno polje“ - Referent field; „Pritisnuti taster „ENTER“ za spremanje podataka i prelazak na sljedeće polje za testiranje“ - Press the ENTER key to save the data and move to the next test field; „Povratak“- Return)

The respondent interactively answers different questions, and a program collects data on how it responds to colour differences. There are two fields on the main screen: the referent field on the left and the changeable field on the right side. The colour of the left field does not change, while the colour of the right field does. The two types of classical psychophysical testing methods were performed: method of adjustment and method of limits (Sharma, 2002)

In the test of the first type, the respondent manually changes the colour of the right field. The initial colours of the fields are different, and the respondent is supposed to adjust the colour of the changeable field on the right side to be equal to the colour of the referent field, on the left side. The

number of colours and colorimetric values for each colour can be predefined. This first type of test repeats, until all predefined initial colours are checked.

In the second test, the colour of the changeable field changes automatically. The colours of the fields are the same at the start and the respondent is supposed to signalize when he or she first notices the difference between the two fields and then again to signalize when the difference in color becomes too big and unacceptable for her or him. This test also repeats, until all predefined initial colours are checked.

These tests would give the following information about respondent:

- the respondent's sensitivity threshold (ST) for colour difference.
- the barely noticeable difference (BND).
- the unacceptable colour difference (UCD).

The hardware components of the device used for the experiment are:

- Regular PC, for everyday use.
- UHD hardware calibration monitor Eizo ColorEdge CG248-4K (diagonal: 60.45 cm; native resolution: 3840 x 2160 resolution; panel type: IPS; Dual Display Port; HDMI 185 ppi; built-in calibration sensor).
- Calibration of the monitor is performed by a built-in spectrophotometer operating with ColorNavigator 6 color management software. The monitor is calibrated at D50 standard and hooded against ambient light.

The software for the experiment was originally created "Color Changer", developed for a new method for evaluating a human observer's perception of color differences in a digital environment (Gazibarić et al., 2021).

It has the following functions:

- It allows the researcher to generate an initial set of reference-colored fields which will be shown to the subject during the experiment.
- It allows the researcher to adjust the conditions of the experiment (the size, spacing and background color of the reference and variable fields, the step of changing colors, the extent to which colors change, the speed at which colors change, the number of changes per second, to show fields randomly ...).
- It allows the researcher to define a data set for the respondent, which can include personal data of respondent, which can be important for future research. The first three functions are accomplished by creating a configuration file.
- It automatically registers the $L^*a^*b^*$ values when the respondent reacts to the variable color field.
- It automatically calculates the color difference ΔE according to the selected equation (in this work the ΔE^*_{00} was selected).
- At the end of the test, the software automatically generates a table with $L^*a^*b^*$ and ΔE^*_{00} of all fields, recorded when the respondent adjusts the color of the changeable field to be equal as the reference field or confirms the BND or UCD between reference and changeable fields.

The differences in color were evaluated by 20 respondents in 24 color test fields. Descriptive statistical analysis was carried out on all results. Statistical analysis was performed in a statistical environment R 4.0.2 (R Core Team, 2020) and in JASP statistical software (JASP Team, 2020).

Results and discussion

The result of the psychophysical visual experiment conducted in this study is the table with perceived CIELAB values of the reference and adjustable and variable hexagonal colored fields (Figure 1) shown to the subject.

Descriptive statistical analysis also allowed correction of errors that occurred during testing. Values resulting from fatigue or some other influence on the subjects who participated in the experiment or illogical results were excluded. For instance, all data on the ST, BND and UCD in which the BND was greater than UCD or where ST was greater than BND, were excluded. There was a total of 144 eliminated data (we consider the individual value of the ST, BND, or UCD), that is 5.14% of the total of 2880 data collected in this experiment (3 coordinates x 2 directions x 20 respondents x 24 color = 2880).

In this investigation, the BND was chosen to be respondents ranking criteria, and ST and UCD were used as a control result that confirmed the validity of the obtained results for BND.

Distribution of the mean value of a BND for all 24 colors per respond

Figure 2 shows the distribution of the results of determining the BND per subject. The rectangular part of the diagram shows the dispersion of the results.

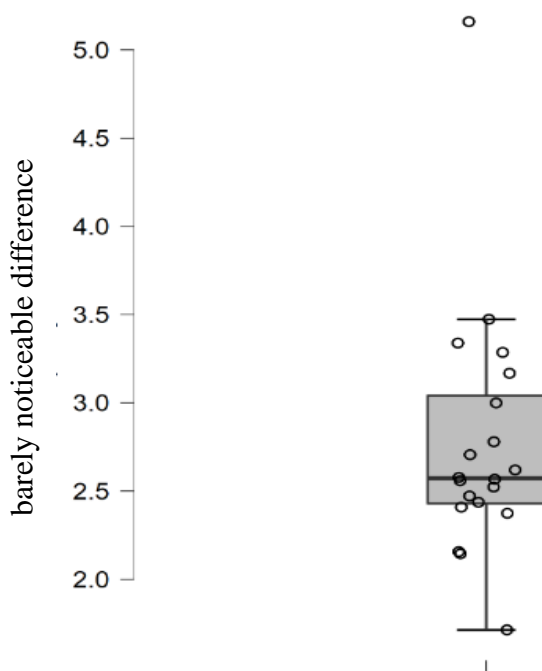


Figure 2. Distribution of the value of a BND per respondent for all 24 colors

The median value is 2.57 (ΔE^*_{00}), and the data shows dispersion (larger interquartile range). A BND of less than 2.43 (ΔE^*_{00}) has 5 respondents, or in percentages, 25% of respondents, and also 5 respondents or in percentages, 25% of respondents have higher values, with a barely noticeable difference of 3.04 (ΔE^*_{00}), with one respondent having a markedly high value, with a BND from the other respondents.

Based on the presented dispersion of the results on the diagram of the distribution of the value of a BND, it can be found that about 3/4 of the subjects reacted to a BND of less than 3.04 (ΔE^*_{00}).

Dispersion of the results for BND for all respondents by individual colors and color tolerance

Table 2 shows the mean values of BND for individual colors for all 20 subjects and standard deviations by color. The colors were ranked by the mean value of the BND in ascending order.

Table 2. Dispersion of tolerance test results in the BND of all respondents by individual colors and color tolerance

	Color	Mean	Std. Deviation	Median	Min.	Max.	Q1	Q3	Confidence interval percentage -95%	Confidence interval percentage +95%
BND	yellow green	2.18	1.21	2.09	0.39	5.19	1.38	2.83	1.65	2.71
	purple	2.35	1.36	2.17	0.39	5.71	1.50	2.94	1.76	2.95
	yellow	2.38	1.27	2.37	0.35	5.09	1.46	3.22	1.82	2.94
	green	2.39	1.28	2.33	0.35	5.58	1.51	3.02	1.83	2.95
	magenta	2.49	1.37	2.42	0.31	5.34	1.57	3.22	1.88	3.09
	bluish green	2.49	1.33	2.47	0.47	5.31	1.57	3.16	1.91	3.08
	moderate red	2.50	1.26	2.46	0.42	5.30	1.76	3.20	1.95	3.05
	purplish blue	2.51	1.27	2.35	0.60	5.21	1.65	3.21	1.96	3.07
	orange	2.59	1.51	2.64	0.34	5.86	1.52	3.40	1.93	3.25
	foliage	2.60	1.47	2.26	0.47	6.32	1.74	3.29	1.96	3.24
	orange yellow	2.61	1.29	2.48	0.56	6.08	1.88	3.08	2.05	3.18
	red	2.67	1.35	2.48	0.74	6.02	1.77	3.45	2.08	3.26
	light skin	2.71	1.35	2.64	0.63	6.28	1.81	3.24	2.12	3.30
	blue sky	2.74	1.50	2.47	0.46	6.01	1.73	3.63	2.08	3.40
	blue	2.75	1.49	2.62	0.46	6.26	1.80	3.48	2.10	3.40
	neutral 6.5 (.44 D)	2.78	1.28	2.74	0.68	6.08	2.04	3.31	2.22	3.34
	blue flower	2.80	1.73	2.56	0.17	7.13	1.87	3.44	2.04	3.56
	cyan	2.87	1.51	2.90	0.35	5.61	1.84	4.02	2.20	3.53
	dark skin	3.08	1.48	2.93	0.50	6.56	2.26	3.85	2.44	3.73
	neutral 3.5 (1.05 D)	3.18	1.59	2.89	0.70	6.99	2.25	4.07	2.49	3.88
neutral 5 (.70 D)	3.23	1.59	3.02	0.71	7.18	2.15	3.88	2.53	3.93	
white 9.5 (.05 D)	3.38	1.78	3.11	0.91	8.23	2.22	4.20	2.60	4.16	
neutral 8 (.23 D)	3.46	1.49	3.30	0.93	7.10	2.51	4.16	2.80	4.11	
black 2 (1.5 D)	3.63	1.44	3.47	1.35	6.51	2.75	4.30	3.00	4.26	

According to the dispersion of mean value of BND and standard deviation among the subjects, it can be concluded that the BND of every color is completely individual for each respondent.

The lowest mean value (ΔE^*_{00}) of BND (2.18), and the standard deviation (1.21) was obtained for yellow-green color, which leads to the conclusion that for most subjects it was easiest to determine BND for this color.

Ranking of the respondents by the BND value

The subjects were evaluated and ranked according to the mean BND value for all the colors covered by the test and by the BND value for some individual colors (yellow, blue, red, and green).

Table 3. shows the ranking of subjects according to the mean BND value shown in the test, for all the colors covered by the test for each respondent:

- mean of BND
- the percentile ranking, which shows how much of the total number of respondents sees BND value and
- Z score, which shows how BND among the respondents is higher or lower than the mean but expressed through standard deviation.

Table 3. The assessment of the subjects by mean BND values for all the colors covered by the test

Respondent	In total		
	*Height	Percentile rank	z-score
1	3.168	0.761	0.555
2	3.339	0.857	0.796
3	2.436	0.285	-0.474
4	2.567	0.476	-0.290
5	2.409	0.238	-0.513
6	2.374	0.190	-0.562
7	2.145	0.095	-0.885
8	5.160	0.952	3.360
9	2.577	0.523	-0.276
10	3.000	0.714	0.319
11	2.472	0.333	-0.424
12	3.473	0.904	0.986
13	2.559	0.428	-0.302
14	2.620	0.571	-0.216
15	2.523	0.380	-0.352
16	2.779	0.666	0.009
17	2.156	0.142	-0.868
18	2.706	0.619	-0.094
19	1.713	0.047	-1.492
20	3.286	0.809	0.722

*Height – expectation (mean) of a barely noticeable difference for all colors covered by the test.

The ranking was carried out by calculating the percentile rank of the mean BND value between each subject for all colors. The value of the percentile threshold (0.952) indicates subject No. 8 as the worst-ranked by height of a BND. Z record for respondent number 8 is (3.360).

The value of the percentile rank (0.047) indicates subject No. 19 as the top-ranked by height by a barely noticeable difference. Z record for respondent number 19 is (-1.492). It is obvious that respondent No. 7 is the second among the top ranked, and candidate 12 is penultimate, among the lowest ranked. The Z-record difference between the best and worst subjects expressed in standard deviations is (4.852).

Table 4 presents the results of the ranking of respondents according to BND for individual colors (yellow, blue, red, and green).

Table 4. Ranking the subjects by the value of a BND for yellow, red, green, and blue

Respondent	Yellow			Red			Green			Blue		
	*Height	Percentile rank	z-score	*Height	Percentile rank	z-score	*Height	Percentile rank	z-score	*Height	Percentile rank	z-score
1	2.435	0.666	0.035	1.658	0.047	-	2.858	0.761	0.758	4.400	0.904	1.990
2	2.264	0.476	-	3.246	0.857	0.720	3.046	0.857	1.062	3.461	0.857	0.873
3	3.042	0.857	0.742	1.707	0.142	-	3.158	0.904	1.243	2.838	0.571	0.131
4	1.859	0.238	-	2.275	0.428	-	2.388	0.476	-	1.733	0.142	-
5	1.727	0.190	-	2.236	0.285	-	1.696	0.190	-	0.922	0.047	-
6	1.884	0.285	-	2.290	0.476	-	2.627	0.666	0.384	2.595	0.380	-
7	2.280	0.523	-	2.123	0.238	-	1.664	0.142	-	1.722	0.095	-
8	4.888	0.952	2.891	5.230	0.952	3.124	3.789	0.952	2.265	4.488	0.952	2.094
9	2.220	0.380	-	2.240	0.333	-	1.897	0.285	-	3.053	0.714	0.388
10	2.838	0.809	0.505	2.960	0.666	0.373	2.542	0.571	0.245	3.097	0.761	0.439
11	1.726	0.142	-	2.832	0.619	0.218	2.587	0.619	0.318	2.616	0.428	-
12	2.361	0.571	-	2.556	0.523	-	3.027	0.809	1.031	2.803	0.523	0.090
13	2.236	0.428	-	3.543	0.904	1.080	2.019	0.333	-	2.268	0.285	-
14	2.619	0.714	0.249	3.239	0.809	0.711	1.837	0.238	-	2.430	0.333	-
15	1.725	0.095	-	2.695	0.571	0.052	1.323	0.047	-	3.048	0.666	0.382
16	2.374	0.619	-	3.181	0.761	0.640	2.663	0.714	0.442	2.699	0.476	-
17	1.925	0.333	-	2.063	0.190	-	2.228	0.380	-	2.223	0.238	-
18	4.003	0.904	1.861	2.270	0.380	-	2.380	0.428	-	2.925	0.619	0.235
19	0.910	0.047	-	1.668	0.095	-	1.623	0.095	-	2.013	0.190	-
20	2.777	0.761	0.433	3.032	0.714	0.460	2.452	0.523	0.099	3.213	0.809	0.578

From the presented Table 4, it is shown that respondent No. 19 for all four colors is the best or among the top-ranked candidates. On the other hand, the candidate No. 8 is again at the bottom of the list for all four selected colors. When printing spot colors, evaluating an acceptable color difference is difficult. There is no proposition in ISO standards (www.iso.org/standard/, n.d.) for acceptance limit value for spot colors. With the method conducted in this and previous work (Gazibarić et al., 2021), the criteria can be established.

Conclusion

From the Box and Whisker Plot diagram (Figure 2), it can be concluded that there is a diversity in the perception of color differences among respondents. The assumption is confirmed that individual indicators of the perception of the difference in color should be determined for each observer that is included in evaluating color in any industrial production, either the manager, designer or production technicians staff. The results of the psychophysical visual experiment conducted in this study show three main types of results that determine the ability of respondents to distinguish color differences: ST, BND, and UCD. Two types of results (ST and UCD) can be used as a control result, and BND, as a main result, can be used as a ranking criterion for an observer's sense of color differences.

The method presented in this paper is practical and available with relatively little investment and can be implemented in any company for which color matching is of great importance.

The method enables a reliable ranking of the examinee in terms of sensitivity to color differences and a quantitative assessment of his ability.

References

- Gazibarić, Z., Cviljušac, V., Živković, P. & Mrvac, N. (2021). A Method for Evaluating Human Observer's Perception of Color Differences. *Technical Gazette*, 28(6), 2094–2101. <https://doi.org/10.17559/TV-20201027193639>
- Goñi, S. & Salvadori, V. (2017). Color measurement: comparison of colorimeter vs. computer vision system. *Food Measure*, 11, 538–547. <https://doi.org/10.1007/s11694-016-9421-1>
- Ishihara, S. (1918). Tests for Color Blindness. *American Journal of Ophthalmology*, 1(5), 376. [https://doi.org/10.1016/s0002-9394\(18\)90663-x](https://doi.org/10.1016/s0002-9394(18)90663-x)
- JASP Team. JASP (Version 0.14.1)[Computer software]. Retrieved from <https://jasp-stats.org/> (2020).
- Liang, J., Georgoula, M., Zou, N., Cui, G. & Luo, M. R. (2017). Colour difference evaluation using display colours. *Lighting Research & Technology*, 0, 1–13. <https://doi.org/10.1177/1477153517739054>
- Luo, M. R., Cui, G. & Rigg, B. (2001). The development of the CIE 2000 color-difference formula: CIEDE2000. *Color Research & Application*, 26(5), 340–350. <https://doi.org/10.1002/col.1049>
- McCamy, C., Marcus, H. & Davidson, J. (1976). A Color-Rendition Chart. *Journal of Applied Photographic Engineering*, 2(3), 95–99. Retrieved from <https://home.cis.rit.edu/~cnspci/references/mccamy1976.pdf>
- R Core Team. R: A language and environment for statistical computing. Vienna: R Foundation for Statistical Computing. Retrieved from <http://www.R-project.org/> (2020).
- Sharma, G. (2002). *Digital Color Imaging Handbook*. USA: CRC Press, Inc.
- Szafir, D. A. (2018). Modeling Color Difference for Visualization Design. *IEEE Transactions on Visualization and Computer Graphics*, 24(1), 392–401. <https://doi.org/10.1109/tvcg.2017.2744359>
- Szafir, D. A., Stone, M. & Gleicher, M. (2014). Adapting Color Difference for Design. *Color and Imaging Conference, 22nd Color and Imaging Conference Final Program and Proceedings (pp. 228–233(6))*. Society for Imaging Science and Technology. Retrieved from <https://www.semanticscholar.org/paper/Adapting-Color-Difference-for-Design-Szafir-Stone/71331a4951d414e3aa24173a44c64aa595526970>
- www.babelcolor.com. (n.d.). Retrieved from https://www.babelcolor.com/colorchecker-2.htm#CCP2_data
- www.iso.org/standard/. (n.d.). Retrieved 9 17, 2022, from <https://www.iso.org/standard/57833.html>
- www.xrite.com. (n.d.). Retrieved 9 15, 2022, from <https://www.xrite.com/categories/visual-assessment-tools/fm-100-hue-test>

Preliminary Report

**AN OVERVIEW OF VARIOUS POSSIBILITIES OF 3D PRINTING
TECHNIQUES IN THE PRODUCTION OF FLEXOGRAPHIC PRINTING
PLATES**

Sandra Dedijer¹, Nemanja Kašiković¹, Magdolna Pal¹, Živko Pavlović¹, Gojko Vladić¹, Ivana Tomić¹, Bojan Banjanin¹

¹University of Novi Sad, Faculty of Technical Sciences, Department of Graphic Engineering and Design
Novi Sad, Serbia

Abstract

This paper presents an overview of different technological possibilities for making flexographic printing plates using 3D printing techniques. Through the literature overview, the most promising 3D printing techniques for flexo platemaking process in the various fields of application were presented. It has been found that among others Inkjet technology, Stereolithography and even FDM (primarily for mould manufacturing) has potential in application to platemaking for flexographic printing in principle. The previous research has shown that the choice of materials used, in conjunction with the selected 3D printing parameters plays the significant role in the final characteristics of the 3D printed flexo plate: line, dot, and text reproduction, plate thickness stability, the ink transfer ability etc. Also, the applicability of the 3D printing techniques in the field of flexo platemaking process is dependable on the possibility to adjust existing 3D printing devices for large area printing. The benefits of using 3D printing techniques in flexo platemaking that cannot be overseen are reflecting in simplification of the production process, reduction of the production costs and potentially less environmental pollution and materials waste in comparison to traditional flexographic plate making process. The findings presented in the paper showed that at this point of technological development, the 3D printing technique can at least provide the basis for the flexographic platemaking process.

Keywords: flexography, plate making process, 3D printing.

Flexography principles and flexo printing plates

Flexography is a relief printing process whereas the image areas on the printing plate are raised above the non-image areas receiving the low viscosity printing ink which is transferred directly onto a various printing substrates (Novaković et al, 2010; Dedijer et al., 2017). Flexible printing plate and usage of various printing inks provide ability to print on coated and uncoated paper and board, non-porous substrates including metallised and paper foils and polymer films, used especially in the packaging industry (Dedijer et al., 2012; Zołek-Tryznowska et al., 2015). Nowadays, more than 75% of packaging products are printed with this technique (Zołek-Tryznowska et al., 2020; Dedijer et al., 2020). The versatility of this printing technique is mainly due to flexibility of the printing plates. At the same time, this benefit could be also considered as potential drawback if the improper plate production is performed since the flexographic printing plate is one of the most influential factors on the stability and quality of the printing process (Dedijer et al., 2017). This is becoming even more obvious if we know that in the plate production phases (plate imaging, plate exposure and plate washout) printing elements are formed as well as relief depth and final plate hardness (Dedijer et al., 2012; Dedijer et al., 2017). In flexo plate production, the CtP technology is becoming standardised procedure since it has inevitable quality advantage allowing rapid, high-resolution imaging with 1:1

dot reproduction and sharp image details due to solutions which achieve stable flat top dot structure overcoming the oxygen inhibition negative effects (Dedijer et al., 2017). CtP flexo plate making process includes following sequential production phases: back exposure of the plate, computer controlled laser imaging of the black sensitive coating (ablation mask) on the plate surface, main exposure of the plate with UV light, subsequent removal of the unexposed polymer either by chemical or thermal processing method, drying (if chemical method is used) and final post-exposure (UVA and UVC) (Dedijer et al., 2012). Each of these phases can affect the final printing element reproduction in terms of proper tone value (TV) reproduction, single dot reproduction (dot area, shape and profile), line reproduction (line width and profile), as well as reproduction of text elements (clearly transferred and readable on printing substrate) (Dedijer et al., 2012; Dedijer et al., 2017). The simplification of the plate production process by introducing novel techniques such as 3D printing process, while still maintaining the optimal printing elements reproduction and plate mechanical properties, would be a great breakthrough in the flexo domain, especially if it could additionally lower or even eliminate the unwanted influences on the environment that are associated with the customary flexo plate making processes.

3D printing technologies

3D printing, also known as additive manufacturing, invented in the early 1980s (Mitsouras & Liacouras, 2017), is an emerging technology which has experienced enormous development in the past couple of decades contributing to the various branches of production and manufacturing. It is more than justified to be considered as the technology which transforms traditional manufacturing to intelligent manufacturing; it is a process which, from digital files by joining materials layer by layer build three dimensional elements from micro to macro scale (Wang et al., 2020a). The main advantages of 3D printing can be listed as follows: the freedom in design, materials saving, customization, and the ability to manufacture complex geometry with high precision (Wang et al., 2020a). Many advances have occurred in the basic 3D printing techniques enabling researchers to print a variety of materials even those such as live cells, modulus changing polymers and spacecraft grade metals (Karakurt & Lin, 2020). Moreover, 3D printing technologies in their variability can be used for a broad spectrum of need starting from in-house 3D printing of car accessories to micro batteries printing, dentist material, houses or even components needed for reparation or service of the space shuttle station (Singh et al., 2015; Wang et al., 2020a). 3D printing is qualified as cost effective manufacturing of high-quality control since it is manufacturing practice with low labour involvement and high precision manufacturing processes (Singh et al., 2015). 3D printing techniques which can be considered as the most commonly used are Fused deposition modelling, Direct ink writing, Selective laser sintering, Inkjet printing, Stereolithography and Electron beam melting (Karakurt & Lin, 2020).

Fused deposition modelling (FDM)

Fused Deposition Modelling (FDM), developed by Stratasys in Eden Prairie, Minnesota (Ramya & Vanapalli, 2016) is the most common due to its price and simplicity (Kluska et al., 2018). Although it is relatively slow compared to other 3D processes (Chadha et al., 2022), the literature findings list it to be the second most widely used rapid prototyping technology, after Stereolithography (Ramya & Vanapalli, 2016). It is a process where melted filaments made of thermoplastic polymers (i.e. ABS - acrylonitrile butadiene styrene and PLA - polylactide) which run through a hot nozzle followed by natural cooling and solidification are used to build parts (Karakurt & Lin, 2020). The melted polymer is imposed layer by layer in heated chamber in order to eliminate material shrinkage and shape deformations (Kluska et al., 2018). A support material is provided from another printer head which

after the printing process is easily removed (Kluska et al., 2018). The drawbacks of this method are reflected in used materials, the limitations in printing resolution, surface finish, porosity and mechanical and chemical properties of the printed parts (Karakurt & Lin, 2020). In terms of resolution, the FDM process is inferior in comparison to Stereolithography, but on the other side it is easier to use and more readily available (Finnes, 2015). The printing resolution primarily depends on the nozzle size, viscosity and flow characteristics of the filament while surface finish and porosity depend on the Z-axis movement control and the adherence between layers (Karakurt & Lin, 2020). Beside ABS and PLA, materials used in FDM technology are polyamide, polycarbonate, polyethylene, polypropylene and investment casting wax (Ramya & Vanapalli, 2016) finding its application in various fields, from robotics to microfluidics (Karakurt & Lin, 2020).

Direct ink writing (DIW)

Direct ink writing (DIW) is considered to be similar to FDM due to the fact that in this process a viscoelastic fluid 'ink' flows through a nozzle under an external pressure source (Karakurt & Lin, 2020). The ink is selectively deposited by using one or the combination of these methods: stress, phase change, solvent evaporation or polymerization (Karakurt & Lin, 2020). The direct ink writing technique has good flexibility for different fields and is a beneficial technique in medicine for manufacturing flexible and self-healing devices, drug encapsulations, in biomedical industry for manufacturing shape-changing stents or in the engineering for soft robotics and touch sensors but also for the ceramics for optics and cellular structure applications (Karakurt & Lin, 2020; Chadha et al., 2022). As the main drawback of this technology is considered to be the difficulty in making voids or overhanging structures (Karakurt & Lin, 2020).

Selective laser sintering (SLS)

Carl Deckard and Joe Beaman at the University of Texas at Austin invented Selective laser sintering (SLS). SLS also referred to as laser sintering, uses a laser beam as the power source to sinter powdered material (typically nylon or poly-amide) to create 3D structure (Ramya & Vanapalli, 2016; Wang et al., 2020a; Wang et al., 2020b). This technology uses high power lasers (commonly CO₂ lasers) at specific wavelengths to selectively irradiate (heat and sinter) a target powder bed such as metals, polymers, hybrids, ceramics, composites and cement whereas sintering process occurs either through chemical or mechanical effects (Karakurt & Lin, 2020; Wang et al., 2020a; Chadha et al., 2022). It is quick and accurate process allowing fast solidification compared to for example with FDM process (Karakurt & Lin, 2020; Chadha et al., 2022). The high temperature processes limit the material selection to metals with high thermal conductivity, whereas polymers for SLS processes are limited to thermoplastics, Polyamide 12 remains by far the most widely used laser sintering polymer (Wang et al., 2020a). Its high accuracy is reflected through the fact that if particle size of powder material is less than 0.1 mm, the accuracy can reach 1% (Wang et al., 2020a). Selective Laser Sintering is applicable in industries such as automobile, aerospace, medical, artware biological medicine, especially in tissue engineering and medical implantation (Wang et al., 2020a). One of the key drawbacks of this technology is the surface finishing roughness, which is related to the powder size and the porosity of fabricated structures (Karakurt & Lin, 2020).

Inkjet printing or (multi) material jetting

Inkjet printing or (multi) material jetting is a technology related to vat photopolymerization in that it relies on the same chemical principles but it does not use printers that hold the material in a vat; instead they are quite similar to inkjet printers (Mitsouras & Liacouras, 2017). This technology is printing photopolymerizable resins by selectively placing picoliter droplets on a build plate solidified using a UV light source (Karakurt & Lin, 2020). Multimaterial printers have multiple print heads,

enabling materials to be mixed during the printing, thus allowing seamless mixing of the different materials held in each head and ultimately achieving different hardness and mechanical properties of the printed parts, ranging from rubberlike to rigid (Mitsouras & Liacouras, 2017). This technology can achieve extremely fine resolution and surface finishes primarily thanks to micro droplets technology and used materials (Ramya & Vanapalli, 2016; Karakurt & Lin, 2020). The most outstanding characteristic of the system is the ability to produce almost equivalent parts as ones produced with CNC machines, but the expensive commercial printers and proprietary resins as well as slow speed for large objects are key limitations of the technology (Ramya & Vanapalli, 2016; Karakurt & Lin, 2020).

Stereolithography (SLA)

The first additive manufacturing technology, stereolithography (SLA), patented by Charles Hull in 1984, is a process of photo-hardening a series of cross sections using a computer-controlled beam of ultraviolet (UV) light to solidify liquid resin and create models, prototypes etc. (Mitsouras & Liacouras, 2017; Wang et al., 2020b). This 3D printing process is also known as Digital Light Processing (DLP). It has three basic components: first, a high intensity light source (typically ultraviolet UV-A or UV-B); second, a vat or tray that holds an epoxy- or acrylic-based photocurable liquid resin which contains monomers and oligomers; and third, a controlling system that directs the light source to selectively illuminate the resin. In SLA the high resolution is afforded by a laser beam (Mitsouras & Liacouras, 2017).

Electron beam melting (EBM)

Electron beam melting (EBM) is technology which uses an electron beam to fuse small particles of material typically preheated to just below the material melting point (Mitsouras & Liacouras, 2017). It is a powder-bed based system, the same as selective laser sintering (SLS) whereas EBM uses an electron beam for irradiation to construct metal structures. The sintering process occurs either through chemical or mechanical effects, allowing for fast solidification. Structures such as turbine blades, engines, and implants have been printed using this technology. The high temperature processes limit the material selection as well as surface finishing roughness, which is related to the powder size and the porosity of fabricated structures (Karakurt & Lin, 2020).

3D printing technologies and the reproduction of flexo plates

The versatile experimental studies have shown that the technology of additive manufacturing, represented by 3D printing, can be applied to platemaking for flexographic printing in principle (Zheng et al., 2019). It was found to be beneficial in lowering the materials waste and production time in process of exposure, development, etc. in traditional flexographic plate making and greatly reducing environmental pollution (Changlong et al.; Huang et al., 2016).

According to (Zheng, 2021) flexographic platemaking widely focuses on 3D printing technology based on inkjet technology and UV curing 3D printing technology based on stereoscopic light modelling. Still, there are studies showing that SLA technology can potentially be utilised in such a purpose since it could be beneficial in avoiding some occurring problems in inkjet such as nozzle clogging (Zheng, 2021; Zheng et al., 2019; Tsakos, 2018).

The feasibility study of flexographic platemaking based on Stereolithography apparatus 3D printing technology was conveyed by the (Zheng et al., 2019). In their experiment, they have detected the line width error and line edge straightness of the results of SLA printing technology in comparison with the results of traditional flexographic platemaking whereas the results confirmed that in general SLA 3D printing technology can be applied to platemaking for flexographic printing, and can provide

the basis for the flexographic platemaking using the technology of additive manufacturing. In terms of line width and line edge straightness, the results of SLA 3D printing showed to be roughly equivalent to those of conventional flexographic platemaking technology (Zheng et al., 2019). The drawback that was noted is that the laser spot diameter of existing SLA 3D printing equipment on the market cannot meet the needs of high precision flexographic platemaking (Zheng et al., 2019).

Zheng in his late study (Zheng, 2021) went deeper in the analysis of the process of making flexographic plate with Stereolithography 3D printing technology, the factors affecting the process and quality of platemaking. This study has showed that in principle Stereolithography can be applied to flexographic platemaking, but it has its drawbacks (Zheng, 2021). The beneficial is that SLA technology is theoretically characterised with the optical system of high exposure resolution, accurate moulding results, and the edges of the convex graphic parts of the flexible plate which are neat ensuring the quality of the platemaking results (Zheng, 2021). The main drawback which was emphasised in this study (Zheng, 2021) was that the physical properties of existing materials are different from the requirements of flexography platemaking leaning towards the fact that the key of successful implementation of SLA technology in the flexographic platemaking process lies in the development of new materials.

The experiment conducted by (Tsakos, 2018) showed that 3D printing technology can be implemented in flexographic packaging printing whereas the flexographic printing plates were printed using the FDM and SLA 3D printing method. The conducted comparison analysis with the CtP polymer flexo plates used for the same printing purpose showed that the 3D method is far more economically justified. The experiment also showed that the material selection, in terms of hardness and later surface properties, for the 3D printing process is of the most importance if we want to achieve as close as possible printing results as with dominating printing plate making techniques. The one of the emphasised drawbacks in this probe was the printing surface of the printing plate since FDM method could not provide a unified surface, which resulted in a printing with visible grids. The author has proposed the solution to this problem through spraying with appropriate coating or polishing to a smoother surface.

The successful probe in replacing conventional flexo printing plates in microcontact printing with the 3D printed ones was reported as well (Maksud et al., 2016). Flexographic printing has found important role in printed electronic, since it is allowing mass production at higher printing speed and low cost. However, CtP printing plates was found to be of insufficient fidelity in order to achieve microscale pattern size. Hence, in the experiment conducted by the (Maksud et al., 2016) a flexible rapid prototyping FDM 3D printer, allowing production of any shape of pattern, was used for developing a PDMS micro-scale printing plate which was used in reel to reel (R2R) flexographic printing process. The finest multiple solid line array with 1mm width and 2mm gap pattern of printing plate was successfully fabricated by 3D printer master mould due to size limitation of the FDM (Fused Deposition Modelling) 3D printer nozzle itself. It was found that this type of printing plate production method is valuable for micro-flexographic in printed electronic field or biomedical application since it is easy, fast and of low cost (Maksud et al., 2016). In the study of printing plate mould development by using 3D printers for micro-flexographic printing process conducted by (Hassan et al., 2020) the emphasis was on possibility to produce a master mould with solid fine lines that could be used for micro-flexographic printing for future development and application of printing in the electronic, graphic and bio-medical field. They have come up to the conclusion that micro-flexographic is a good candidate for printing micro to nano fine lines with printing plate mould property, printing plate, substrates and process parameters being the main role for a successful implementation (Hassan et al., 2020).

Huang et al. (2016), in their study gave the accent to the possibility of using hybrid light curable material for 3D printing of flexo plates. They put the focus on the hybrid UV curable material system having good adaptability, and they have studied the influence for prepolymer and monomer on the

plate forming and ink transfer ability of 3D printed flexographic plate, and determined the best material formula for the 3D printing process (Huang et al., 2016). The results showed that the materials studied has good forming effect and good ink transfer ability (Huang et al., 2016).

In the research conducted in (Vićentić & Dedijer, 2022) the possibility of making the flexographic printing plates with DLP 3D printing technology was investigated. The emphasis was on finding the possibility of making flexographic printing plates of appropriate thicknesses, with satisfactory reproduction of printing elements in the form of lines and dots of appropriate widths and diameters. The authors have concluded that on all plates there are changes in the size of the diameter of the points as well as in the line widths, which cannot be considered negligible. Based on the measurements they made, the results obtained and their analysis, the final conclusion was that the DLP 3D printing technique could not produce flexo printing plates with a satisfactory reproduction of the printing elements in terms of precision and the absence of deformations of the printing elements, but also on the other hand there is still room for improving the results in terms of finding the more appropriate printing material of lower hardness, more appropriate model base, printer calibration, positioning the model on the printer platform and other parameters that can positively contribute to the more precise formation of the printing elements on the printing plate surface (Vićentić & Dedijer, 2022).

Conclusion

In this paper we have aimed to present an overview of different technological possibilities for making flexographic printing plates using 3D printing technologies. We have given the short introduction over flexo printing technology and flexo platemaking process emphasising the their important functional and exploitation properties. The paper also includes the short overview of the mostly known 3D printing technologies. In terms of the correlation between 3D printing and flexo plate making process, the literature overview has led to the conclusion that among others, Inkjet technology, Stereolithography and even FDM (primarily for mould manufacturing) has potential in application to platemaking for flexographic printing in principle. The previous research also pointed out the importance of the choice of materials used, in conjunction with the selected 3D printing parameters in the final characteristics of the 3D printed flexo plate. Also, the applicability of the 3D printing techniques in the field of flexo platemaking process is dependable on the possibility to adjust existing 3D printing devices for large area printing. The benefits of using 3D printing techniques in flexo platemaking that cannot be overseen are reflecting in simplification of the production process, reduction of the production costs and potentially less environmental pollution and materials waste in comparison to traditional flexographic plate making process. The findings presented in the paper indicated that at this technological point, the 3D printing technique can at least provide the basis for the flexographic platemaking process.

Acknowledgment: This research (paper) has been supported by the Ministry of Education, Science and Technological Development through project no. 451-03-68/2022-14/200156 “Innovative scientific and artistic research from the FTS (activity) domain”.

References

Chadha, U., Abrol, A., Paras Vora, N., Tiwari, A., Kirubaa Shanker, S. & Kumaran Selvaraj, S. (2022). Performance evaluation of 3D printing technologies: a review, recent advances, current challenges, and future directions. *Progress in Additive Manufacturing*. <https://doi.org/10.1007/s40964-021-00257-4>

- Changlong, G., Beiqing, H. & Xianfu, W. (2015). Application of hybrid UV curing system in flexographic production through 3D printing. *Applied Mechanics and Materials*, 731, 277–282. <https://doi.org/10.4028/www.scientific.net/AMM.731.277>
- Dedijer, S., Novaković, D., Pál, M. & Pavlović, Ž. (2012). Statistical analysis of printing elements reproduction on thermally developed CTP flexo printing plates. *Journal of Graphic Engineering and Design*, 3(2), 12–22. https://www.researchgate.net/publication/281463706_Statistical_analysis_of_printing_elements_reproduction_on_thermally_developed_CTP_flexo_printing_plates
- Dedijer, S., Pál, M., Tomić, I., Pavlović, Ž., Vasić, J., Vladić, G. & Kašiković, N. (2017). Study of line and dot elements reproduction on digital flexo printing plates using FlexCel NX imaging technology. In: 1. IJCELIT 2017 - "First International Joint Conference on Environmental and Light Industry Technologies" (pp. 28–28). Rejtő Sándor Faculty of Light Industry and Environmental Protection Engineering, Budapest.
- Dedijer, S., Pál, M., Tomić, I., Poljak, S., Pavlović, Ž., Jurič, I. & Milić Keresteš, N. (2020). Statistical analysis of the influence of print run on surface roughness of digital flexo printing plates' solid tone areas. In: Dedijer, S. (Ed.) Proceedings – International Scientific Meeting "10th International Symposium GRID 2020" (pp. 281–288). Faculty of Technical Sciences, University of Novi Sad, Novi Sad. <https://doi.org/10.24867/GRID-2020-p30>
- Finnes, T. (2015). High definition 3D printing – comparing SLA and FDM printing technologies. *The Journal of Undergraduate Research*, 13, 10–25. <https://openprairie.sdstate.edu/cgi/viewcontent.cgi?article=1001&context=jur>
- Hassan, S., Yusof, M. S., Embong, Z., Ding, S. & Marwah, O. M. F. (2020). A study of printing plate mould development by using 3D printers for micro-flexographic printing process. *Journal of Advanced Manufacturing Technology*, 14 (1), 25–36 file:///D:/Documents/Downloads/5856-Article%20Text-15735-2-10-20200724.pdf
- Huang, B., Shang, X., Li, Y., Wei, X. & Guo, C. (2017). Study of printability of hybrid light curable material used in 3D printing—Product Flexographic Plate. In: Zhao, P., Ouyang, Y., Xu, M., Yang, L., Ouyang, Y. (Eds.) Proceedings – international Scientific Meeting "2016 China Academic Conference on Printing, Packaging Engineering & Media Technology" (pp. 1139–1155). Springer, Singapore. https://doi.org/10.1007/978-981-10-3530-2_140
- Karakurt, I. & Lin, L. (2020). 3D printing technologies: techniques, materials, and post-processing. *Current Opinion in Chemical Engineering*, 28, 134–143. <https://doi.org/10.1016/j.coche.2020.04.001>
- Maksud, M. I., Nodin, M. N., Yusof, M. S. & Hassan, S. (2016). Utilizing rapid prototyping 3D printer for fabricating flexographic PDMS printing plate. *ARPJ Journal of Engineering and Applied Sciences*, 11(12), 7728–7734. http://www.arpnjournals.org/jeas/research_papers/rp_2016/jeas_0616_4506.pdf
- Mitsouras, D. & Liacouras, P. C. (2017). 3D printing technologies, In F. J. Rybicki, G. T. Grant (Ed.), *3D Printing in Medicine* (pp. 5–22.). Springer. https://doi.org/10.1007/978-3-319-61924-8_2
- Novaković, D., Dedijer, S. & Mahović – Poljacek, S. (2010). A model for improving the flexographic printing plate making process. *Technical Gazette*, 17(4), 403–410. <https://hrcak.srce.hr/file/94261>
- Kluska, E., Gruda, P. & Majca-Nowak, N. (2018). The accuracy and the printing resolution comparison of different 3D printing technologies. *Transactions On Aerospace Research*, 3 (252), 69–83. <https://sciendo.com/pdf/10.2478/tar-2018-0023>
- Ramya, A. & Vanapalli, S. I. (2016). 3D printing technologies in various applications. *International Journal of Mechanical Engineering and Technology*, 7(3), 396–409. https://iaeme.com/MasterAdmin/Journal_uploads/IJMET/VOLUME_7_ISSUE_3/IJMET_07_03_036.pdf

- Singh, O. P., Abhilash, M. & Sheikh, M. A. (2015). Modern 3D printing technologies: future trends and developments. *Recent Patents on Engineering*, 9(2), 91–103. <https://doi.org/10.2174/1872212109666150213000747>
- Tsakos, D. (2018). *Implementation of 3D printing technology in flexographic packaging printing* (Master's thesis). Aalborg University, Denmark.
- Vićentić, D. & Dedijer, S. (2022). Istraživanje mogućnosti izrade štampajućih elemenata flekso štamparske forme pomoću DLP 3D tehnologije/Research of the possibility of making printing elements of flexo printing form using DLP 3D technology. *Zbornik radova Fakulteta tehničkih nauka*, 37(9), 1528–1531. <https://doi.org/https://doi.org/10.24867/19EF06Vicentic>
- Wang, Y., Xu, Z., Wu, D. & Bai, J. (2020). Current status and prospects of polymer Powder 3D printing technologies. *Materials*, 13, 1–19. <https://doi.org/10.3390/ma13102406>
- Wang, L., Jiang, S. & Zhang, S. (2020). Mapping technological trajectories and exploring knowledge sources: A case study of 3D printing technologies. *Technological Forecasting & Social Change*, 161, 1–12. <https://doi.org/10.1016/j.techfore.2020.120251>
- Zheng, L., Kong, L. & Li, C. (2019). Feasibility study of flexographic platemaking based on SLA 3D printing technology. In: Zhao, P., Ouyang, Y., Xu, M., Yang, L., Ren, Y. (Eds.) *Proceedings – International Scientific Meeting “9th China Academic Conference on Printing and Packaging”* (pp. 528–534). Springer, Singapore. doi: https://doi.org/10.1007/978-981-13-3663-8_72
- Zheng, L. (2021). Analysis of factors affecting flexographic plate-making technology based on surface imaging stereolithography. In: Zhao, P., Ouyang, Y., Xu, M., Yang, L., Ren, Y. (Eds.) *Proceedings – International Scientific Meeting “11th China Academic Conference on Printing and Packaging”* (pp. 340–346). Springer, Singapore. https://doi.org/10.1007/978-981-16-0503-1_50
- Zołek-Tryznowska, Z., Izdebska, J. & Tryznowski, M. (2015). Branched polyglycerols as performance additives for water-based flexographic printing inks. *Progress in Organic Coatings*, 78, 334–339. <https://link.springer.com/article/10.1007/s11998-018-0055-6>
- Zołek-Tryznowska, Z., Rombel, M., Petriaszwili, G., Dedijer, S. & Kašiković, N. (2020). Influence of Some Flexographic Printing Process Conditions on the Optical Density and Tonal Value Increase of Overprinted Plastic Films. *Coatings*, 10(9), 2–12. <https://doi.org/10.3390/coatings10090816> pp 2-12

Professional Paper

CONTEMPORARY APPLICATIONS OF PULP MOULDED PACKAGING

Gojko Vladić¹, Nemanja Kašiković¹, Živko Pavlović¹, Stefan Đurđević¹, Gordana Bošnjaković¹, Teodora Gvoka¹

¹University of Novi Sad, Faculty of Technical Sciences, Department of Graphic Engineering and Design, Novi Sad, Serbia

Abstract

Moulded pulp also known as moulded fibre packaging is made of paper fibres, and or other fibres, moulded to a shape of the packaging able to hold and protect the product. Classic example of the moulded pulp packaging is egg carton, but there is a possibility of producing more refined and attractively designed packaging for higher-value goods. Good environmental characteristics and possibilities for usage of paper waste for its production adds additional value. Production moulds are made from aluminium, bronze, or plastic. Lately additive manufacturing technologies made significant changes in speed of packaging development and mould production. This paper aims to present possibilities for usage of moulded pulp packaging for ecological, high value packaging with minimal time and costs for development of new packaging shapes.

Keywords: Pulp, moulding, packaging, recycling.

Introduction

Moulded pulp, also known as moulded fibre is a wood cellulose based material, well known and in use for over one century. Martin Keyes first developed it in 1903 (Twede, 2015). The most common and best-known usage of this material is production of egg packaging. Moulded pulp packaging is three-dimensional and this is the main difference from other paper based packaging materials. Moulded pulp packaging is favourable as it can be produced from recycled fibres such as recycled newspaper or other paper based products. This source of fibres for moulded pulp packaging has predominated over the years (Wever, 2007).

Moulded pulp packaging characteristics:

- Eco-friendly packaging - compostable, recyclable and biodegradable.
- Renewable material - raw materials can be all from natural wood fibre renewable resources.
- Customized colour - the most common colour natural light brown, although it can be white, black or customizable in any colour by adding a pigment to the pulp.
- Diverse technology - can be made by different techniques to achieve different results.
- Product protection - shaped according to the product it creates cushioning and protection, saving on storage and transport.
- Design shape - great number of various custom sizes and shapes are possible.
- Additional functionality - can be made waterproof, dust free, reinforced, insect and mould proof, etc.

Expanded polystyrene (EPS) is often used to provide product cushioning, support, spacing, and other packaging functions, but at high environmental costs having in mind short life cycle of packaging products. Environmental benefits and packaging sustainability drives moulded pulp packaging rising popularity as it can also be shaped in various forms similar to the EPS packaging (Ma, 2004). As the

final moulded pulp material often suffers from nonuniformity and mechanical properties depend on the pulp mix as well as the geometry of the form final properties are difficult to predict, compared to the EPS packaging. Moulded pulp packaging is heavier than EPS and the design parameters are different from EPS.

Having in mind these characteristics moulded pulp packaging found its applications as protective packaging for electronics, home appliances, and other manufactured goods. Paper plates and trays, fruit punnets, and egg packaging are typical food packaging applications. Biodegradability and compostability are two major environmental benefits of moulded pulp packaging. With advances in the production technology moulded pulp packaging is beginning to be used in packaging of liquids.

Production methods

Paper based materials for packaging usually enter the packaging production process as sheets of pre-determined size, which causes waste during production or die cutting process to be exact. Paper sheets can be folded or pressed in to shallow trays or cups during formation of the final packaging shape. In contrast to paper sheets, moulded pulp packaging is shaped directly to its final three-dimensional shape in the moulds from a slurry of paper or and other fibres. This direct moulding process enables more creative and complex geometries to be applied to the packaging. Production process is similar to paper sheet making process, with the difference that final product is three-dimensional.

Conventional mould is formed from a fine porous mesh screen. Excess water is pulled from the slurry by a vacuum or pressed out by the press. In the vacuum process the mold is submerged in the slurry where the fibres are sucked onto the surface of the screen, forming a layer of fibres. Moulds are traditionally made out of aluminium, bronze, plastics and lately are produced by various additive manufacturing processes. Most often used additive manufacturing are fused deposit manufacturing (FDM) and stereolithography (STL) or other Vat polymerization 3D printing technique depending on the size and desired precision of the mould.

FDM 3D printing technique is most affordable and it found the wide adoption and application before other 3D printing techniques based on that. It is based on extrusion of thermoplastic material in thin wire like form and depositing it in multiple layers in order to form 3D forms. This kind of material depositing forms relatively rough, stepped surfaces, which are transferred to the final moulded form. Thermoplastics used can vary in material composition thus resulting in different final results. For production of the moulds for moulded pulp production material must be water resistant, and relatively thermo stabile to withstand conditions in pulp form production.

Vat polymerization techniques (STL and DLP) offer much more precise models with fined surface. Process is based on light projection and hardening liquid polymer by polymerisation. As material is not thermoplastic, it can be engineered to be significantly more thermo stabile than those produced by FDM technique.

Hewlett-Packar offers specialized 3D printed solutions for production of moulds providing competitive advantage by accelerating tooling fabrication and expediting delivery of the final product to customers. This technology for mould production offers possibilities to optimize cycle time for forming and dewatering, using engineered fluid pathways to address special design requirements such as uneven wall thicknesses, eliminate mould sectioning, which would be difficult or impossible by traditional tooling and conventional production technologies. Materials used in 3D printing HP process are corrosion resistant and renewable, made from vegetable castor oil (Hewlett-Packar, 2021).

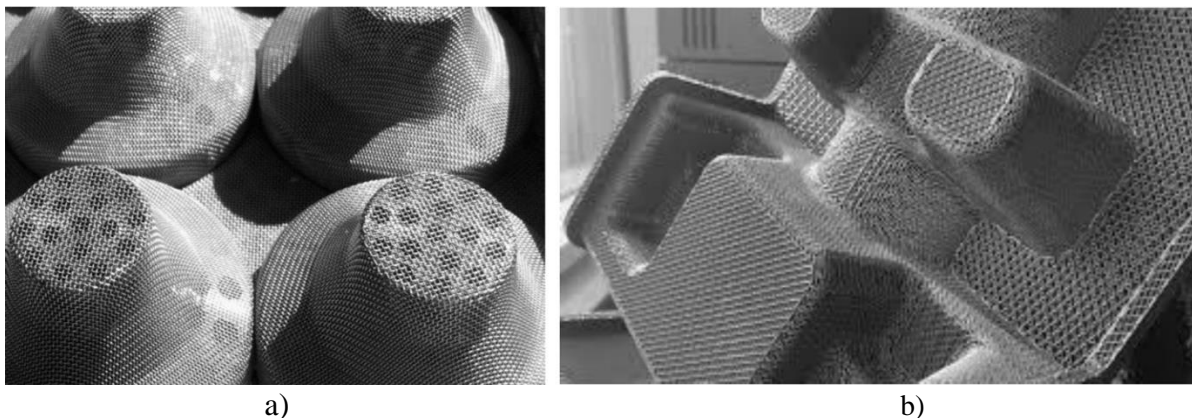


Figure 1. a) Metal mesh mould, b) 3D printed mould

There are a great number of different moulding processes but they can be classified according to the International Molded Fiber Association (IMFA) as (imfa.org, 2022):

- plain moulding,
- transfer moulding,
- precision moulding and
- special treatments.

In plain moulding, the screened mould is submerged into the hot, watery slurry of fibres, a vacuum is applied, and slurry is sucked onto the surface of the porous screened mould while most of the water passes thru the screen. Mould with deposited fibres is then lifted from slurry, than the formed shape is blown off from the mould and passed to the oven to be free-dried at 205 °C for 6–12 minutes depending on the size and thickness (imfa.org, 2022). This process results in forms with one rough side and other with less rough surface, wall thickness can vary from 4 to 12 mm, depending on the product. Packaging produced with this process, shown in Figure 2a. provides great protection capabilities for packaging of the heavy parts, furniture, bottles, etc. (imfa.org, 2022).

Transfer moulding is multistage process where two wire moulds are used. The fibres, from the cold unheated slurry, are first vacuumed onto the forming mould, then the second mould couples with the forming mould. Second mould uses a vacuum to transfer the wet form onto a drying conveyor that takes the form through the oven. The typical forming cycle can vary from a few seconds to one minute. This process produces a relatively smooth form surface on both sides, with one side slightly rougher, wall thickness varies from 1.7 to 3.5 mm. Typical applications, shown in Figure 2b are packaging for small items such as egg cartons, fruit punnets, protective packaging for electronics (imfa.org, 2022).

Precision moulding is a multi-stage process that uses a heated mould for the final drying. The form is produced by heated matched moulds, assisted by vacuum. Parts are fully dry when they leave the moulds without the need for oven drying. Forms produced are denser with smoother surfaces and more precise dimensions than those produced by plain and transfer moulding. Walls are usually form 0.8 to 1.3 mm thick. This process is used for forms with fine details, precise inserts and small items, shown in Figure 2c. There are also hybrid precision/transfer moulding processes.

Special treatments are production category for special fibre blends, additives, and items with secondary treatments like printing, embossing, die cutting, plastic coating, or lamination, shown in Figure 2d (imfa.org, 2022).

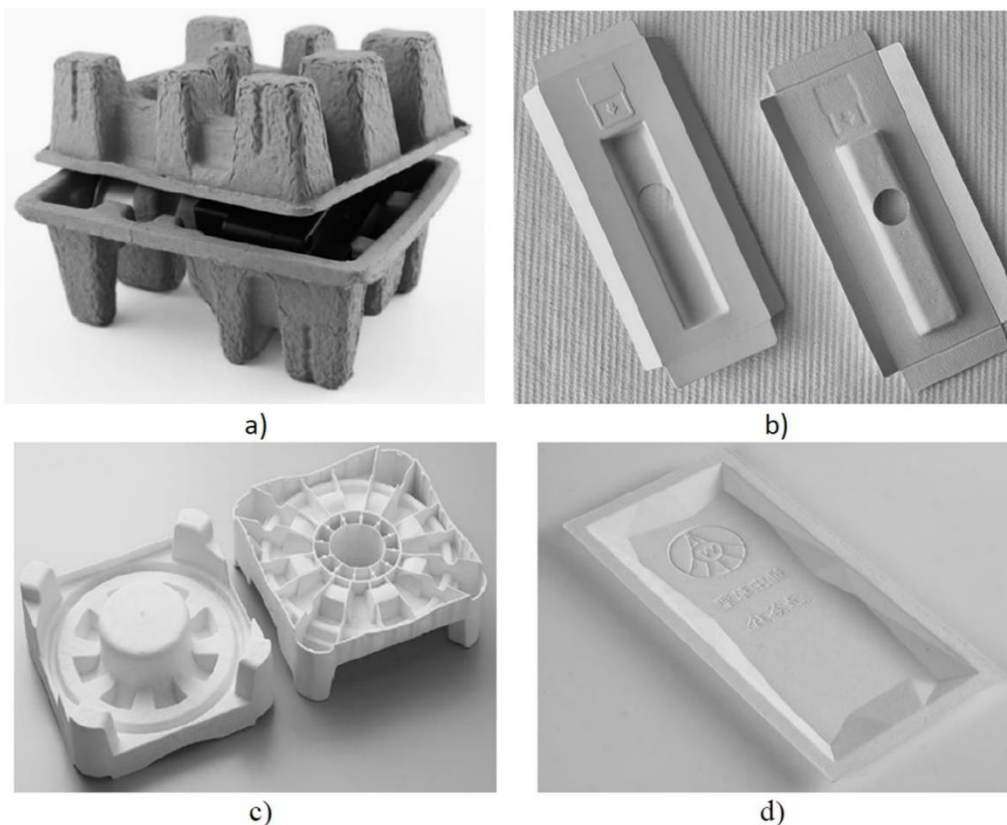


Figure 2. a) Plane moulding results, b) Transfer moulding results, c) Precision moulding results, d) Special treatment, embossing, of moulded pulp plate

Fibres used for moulded pulp packaging

Fibres can differ in processing and refinement, which result in different length, strength, colour and other characteristics. The fibre blend affects the drainage, internal bond strength, shrinkage, and biodegradability. There are two major types of fibres used in production of moulded pulp packaging. Recycled OCC fibres (Old Corrugated Container) are environmentally friendly usually used to produce stronger more robust packaging, with thicker walls for product protection, with plain moulding technology. Recycled ONP (Old newspaper) fibres are used to produce a softer thinner walled packaging, with transfer moulding technology. These materials can be combined to produce packaging for granular or liquid products. For example mixture 70 % OCC and 30 % ONP lined with plastic is used to produce liquid canisters (Mohan, 2013). Less often very smooth, sanitary forms in white colour are produced, in that case pulp from used office paper can be bleached and formed. For production of food packaging products virgin fibre or specially treated recycled papers are used to avoid contaminants. Depending on the worlds region different additional fibres can be added to the recycled paper pulp such as bagasse, bamboo, palm, or reeds giving the final product distinct characteristics (Ma, 2004). Additives also can be used to modify properties of the packaging. Waterproofing is achieved by adding colloidal rosin, while oil resistance is achieved with fluorocarbon chemicals. Some often used additives are dyes, bleach, flame-retardants, strength resins, thermosetting polymers for non-disposable items, etc. Biodegradability of the moulded pulp packaging can be improved by adding peat moss, seeds and fertilizer additives to the pulp slurry mix. Plant packaging produced in this way can be placed in the ground with the plant and support growth of the plant.

Design and application opportunities for moulded pulp packaging

From the previous sections dealing with materials and production technology it is obvious that there are only small number of limitations concerning application field, shape or size of this type of packaging. Despite wide possibilities, moulded pulp still finds its use as protective inserts or rough packaging for agriculture products. Packaging designers are slowly adopting this packaging material as commercial packaging of the high-end products. This is most often done to emphasize ecological characteristics of the product. Considering moulded pulp packing as an alternative to plastic packaging is not only a possibility but rather it should become responsibility of the designers. Food packaging has one of the shortest life cycles, as it is discarded when using the product and that product can have really short shelf life due to spoilage. In this case using long lasting materials such as plastic is irresponsible and fully biodegradable packaging should be considered. Figure 3 shows example of plastic and paper candy packaging and already present alternative used in agriculture for flower seed packaging. This simple example illustrates possibilities which are even greater if special treatments are introduced in moulded pulp packaging design.



Figure 3. Bomboniere candy plastic packagin and moulded pulp alternative used in agriculture

There are examples of using moulded pulp packaging to promote ecological responsible and environmental consciousness of the company but in reality, these attempts can be judged as green washing attempts. Figure 4 shows moulded pulp packaging by Nike, but it is a packaging for the book about Nike sneakers rather than for their product.



Figure 4. Nike book of rear and exquisite sneakers moulded pulp packaging

Conclusion

Having in mind advantages of the moulded pulp packaging regarding its ease of production, ecological characteristics, possibilities of improved mechanical properties and other considered in this paper it should be considered as a more popular packaging material. Range from rough protective packaging to refined embossed, died or printed packaging surely offers enough possibilities for designers to express their creativity and promote the product in the best way, meanwhile approaching the design process in environmentally responsible manner.

References

- Twede, D. & Selke, E. M. (2015). *Cartons, crates and corrugated board Handbook of Paper and Wood Packaging*. A DEStech Publications book.
- Ma, X., Soh, A. K. & Wang, B. (2004). A Design Database for Moulded Pulp Packaging Structure. *Packaging Technology and Science*, 17(4), 193–204. <https://doi.org/10.1002/pts.658>
- Mohan, A. M. (2013). Molded-pulp Bottle is Perfect for Protein Powder Line. *Packaging World*, 20 (2), 30–33.
- The HP Molded Fiber Advanced Tooling Solution (2022, September 14). <https://manuals.plus/m/338514c1bd15f0f7386d8e88c284b6fdeef8a31ff47da6dea9c2145c0beb1538.pdf>
- Wever, R. & Twede, D. (2007). The History of Molded Fiber Packaging; A 20th Century Pulp Story, 22nd IAPRI Symposium Proceedings (on disk). Leatherhead, UK: Pira. www.imfa.org (2022, September 14).

Original scientific article

INFLUENCE OF THE SUBSTRATE ON THE PERMANENCE OF PRINTING INK

Branka Ružičić¹, Mladen Stančić¹, Đorđe Vujčić¹, Milijana Milić¹

¹University of Banja Luka, Faculty of Technology, Banja Luka, Bosnia and Herzegovina

Abstract

One of the advantages of digital printing is the ability to transfer ink to different materials and substrates. However, most of these materials require a special type of ink that would be permanent. Colour fastness test against friction is a test to determine the long-term use quality of printed products. The purpose of this test is to determine the quantity of colour that can be transferred from the surface of a coloured substrate to a test cloth by rubbing. Also surface macro nonuniformity before and after colour fastness test was investigated. The results show significant surface change after colour fastness test on plastics, and a slightly improvement on other tested materials.

Keywords: Colour fastness, digital printing, ink permanence, friction, macro nonuniformity.

Introduction

Digital printing is essentially an inkjet process. A series of print heads pass back and forth across the substrate, spraying dyestuff onto it (Briggs-Goode, 2011). Inkjet process has a major grow in use because of possibility to print on various materials as substrates. The global digital printing market is estimated to be USD 27.54 Bn in 2022 and is projected to reach USD 37.8 Bn by 2027, growing at a CAGR of 6.54% (Research & Markets, 2022). Presently, it is desirable that one type of ink be suitable for printing on various substrates with different properties. So, in this paper colour coordinates, macro-nonuniformity of the colour patch and colour fastness depending on the substrate will be compared. Printed colours are characterized by CIE Lab coordinates and colour differences are calculated in order to determine influence of printing substrate on colour reproduction. Numerous formulas are developed for the purpose of determining colour differences, such as basic ΔE_{76} (Kašiković et al., 2013). All colour difference formulas make use of the Euclidean distance in a device independent colour space (ΔL^* , Δa^* , Δb^*) (Kim & Nobbs, 1997). Newer colour difference formulas are extended in order to address perceptual non-uniformities, while retaining the $L^*a^*b^*$ colour space. The perceptual interpretation of the color difference ΔE is not straightforward. The just noticeable difference is about 1 ΔE (Hunt, 1995) but varies for different parts of CIELAB space. A "rule of thumb" for the interpretation of the ΔE color difference for printed products is proposed: $\Delta E < 3$ hardly perceptible, $3 > \Delta E < 6$ perceptible but acceptable, $\Delta E > 6$ not acceptable (Hardeberg, 2001). Histogram Mottle Macro is a method that measures the print mottle, or the amount of non uniformity in the grayscale image. The amount of non uniformity is calculated on the basis of the histogram of the image. It measures the difference between the upper U_x and lower L_x values of the image histogram ($NU = U_x - L_x$). U_x is calculated as the mean of the intensities between median and maximum values of the histogram. L_x is calculated as the mean of the intensities between minimum and median values of the histogram. The amount of the non uniformity is expressed as the non uniformity index (NU). The greater the NU index, the surface is non-uniform, i.e. there is more amount of mottle (Image, 2008). During the transportation or handling of the material (packaging),

prints are generally exposed to a certain degree of abrasion on their surface. Therefore, the material must have a certain resistance to friction, and the printing ink must be prepared in such a way that the resistance to friction increases. Friction is affected by the composition and characteristics of the printing ink. Friction is a problem that occurs very often with matte coated papers. Due to the characteristic rough structure, their surface is significantly more abrasive compared to the surface of smoothly coated papers. If the printed surfaces are in direct contact with each other and are rubbed under pressure, the paint may peel from the substrate. It would be desirable if a "standard color" could be used with all types of materials. In order for the prints to have good friction resistance, the paint must be completely dry.

Materials and Methods

In this work, the quality of UV Ink Jet printing will be investigated depending on the material on which it is printed. The colour reproduction and difference between same ink colour on different materials, macro non-uniformity and research of ink resistance to friction were analysed. Colour reproduction was analysed by spectrophotometric measurement. The evaluation of the secondary parameters of the print quality was done using the method of digital analysis of scanned images of the samples with ImageJ software, while the experiment to determine the resistance to friction was carried out using a device designed for that research. Materials used are 10 x 10 cm plates from paper, plastic, wood, metal and canvas. Printing test form was created in Adobe Illustrator and printed with APEX UV 6090 printing machine with Epson DKS5 nozzles. The samples were scanned after printing with all automatic image corrections turned off and the scanned images were analysed in ImageJ software. Spectrophotometric coordinates were obtained using Konica Minolta cm-2600d spectrophotometer and the friction resistance was done according the JUS F.S3.021 (JUS, 1980) standard for evaluation of colour fastness.

Results and Discussion

To begin with, the colour differences between the samples are presented in Table 1.

Table 1. Colour difference between samples

Sample	Colour difference in regard to paper	Colour difference before and after friction
Paper	-	0.08
Plastic	7.34	-
Canvas	13.15	0.66
Metal	16.23	0.16
Wood	25.22	6.22

From Table 1 can be concluded that although the same ink was used with all the samples, results show completely not acceptable colour with massive change (>6) depending on the substrate underneath in regard to paper printed sample. This difference can be conducted also with visual method, as seen on Figure 1. Colour coordinates were measured again after resistance to friction test and in Table 1 are also shown the results of colour difference between samples before and after friction resistance test. Colour difference on plastic couldn't be evaluated because all the ink fell off after friction resistance test, as seen on Figure 2. Metal and paper samples didn't show colour difference after resistance to friction test, but it can be noticed slightly better result of macro nonuniformity index.



Figure 1. Visual representation of printed ink on different substrates (Paper – Plastic – Canvas – Metal – Wood)



Figure 2. Visual representation of printed ink on different substrates after resistance to friction test (Paper – Plastic – Canvas – Metal – Wood)

In Table 2 are presented results of macro nonuniformity index (NU) conducted with ImageJ software. Ideal NU value is 0.

Table 2. Macro nonuniformity index of samples

Sample	Macro nonuniformity index after printing	Macro nonuniformity index after friction
Paper	3.97	3.88
Plastic	4.68	-
Canvas	7.20	7.36
Metal	12.56	11.60
Wood	13.26	12.78

It can be concluded that paper has the most uniform patches of colour, plastic is similar to paper, then goes a substrate with patterns. NU index values are not large, so it is relatively low print mottle for all samples, and it becomes slightly lower after friction test, due to smudging of ink over the surface. As can be seen from the analysis of the results, the permanence of the ink on most of the samples remained the same, i.e., slight changes have occurred that do not visibly affect the appearance of the print. The print on the plastic was completely destroyed, the ink was mostly copied onto the cloth with which the experiment was performed. As a reason, it can be said that the surface itself is plastic, which is not resistant to this process. The difference in the measured masses of the samples before and after processing is negligible, there is none. Figure 3 show the appearance of the samples after processing.

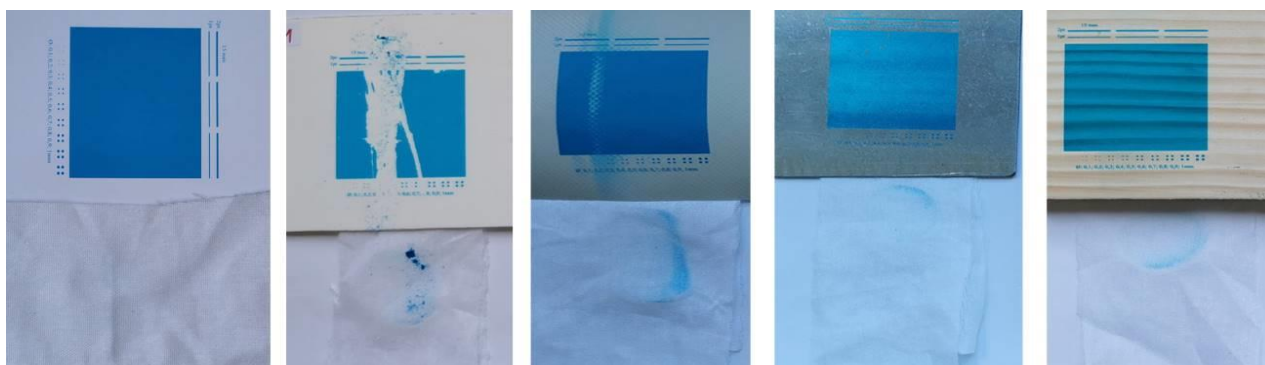


Figure 3. The appearance of the samples after resistance to friction test

Every sample, except paper has a visible trace of ink transferred to the cloth used for friction.

Conclusion

The analysis showed that the reproduction of the colour of the print on wood, metal, and even plastic and canvas have massive differences in colour compared to the reference value - paper. The colour differences can be seen with the naked eye.

By analysing the macro non-uniformity of the samples, it can be concluded that the results are the highest on materials such as wood and metal because these materials have a visibly different surface patterns, and the results of macro non-uniformity are much higher than on other materials. It is recommended to use cover white ink before printing on these substrates.

By researching the resistance of ink to friction, the results show that UV printing on plastic has low effect, because after applying the pressure, prints were completely destroyed. On other materials, after this experiment, there were no visible changes on the samples.

By re-analysing colour reproduction and macro non-uniformity after the friction resistance evaluation experiment, different results were obtained, but the differences are not large. Which does not apply to plastic samples, because as already mentioned, the ink on those samples were scratched, so the differences in these measurements are high.

For UV Ink Jet printing, there are many factors that should be paid attention to and well prepared for the best possible result. From this work, it was concluded that the substrate on which this type of printing is printed affects the very appearance of the final graphic product. Therefore, it would be desirable to prepare the printing surface well before printing.

Acknowledgments: The authors declare that the presented investigation is not in any conflict of interest. The research is financially supported by the Ministry of Scientific and Technological Development, Higher Education and Information Society of the Republic of Srpska, project No. 19.030/961-9-2/21 "Digital approach to the production of environmentally friendly packaging".

References

- Briggs-Goode, A. & Russell, A. (2011). Printed textile design, In Briggs-Goode, A., & Townsend, K., (Eds.), *Textile Design*, (pp. 105-129e). Woodhead Publishing. <https://doi.org/10.1533/9780857092564.2.105>
- Hardeberg, J. Y. (2001). Acquisition and reproduction of color images: Colorimetric and multispectral approaches, *Dissertation.com*. ISBN 1-58112-135-0
- Hunt, R. W. G. (1995). *The reproduction of colour*. Fifth Edition, Kingston-upon-Thames, Fountain Press. ISBN 0 86343 381 2
- Image, J. (2008). Slikovna analiza primeri primjene u grafičkoj tehnologiji [Online] Available at: http://materijali.grf.unizg.hr/media/PGM_slikovna%20analiza.pdf (accessed 03.09.22);
- JUS F.S3.021 (1980). Ispitivanje tekstila, gume i plastičnih masa – Određivanje postojanosti boje prema trljanju - Dio X12: Postojanost obojenja na trenje
- Kašiković, N., Vladić, G., Stančić, M., Novaković, D. & Milošević, R. (2013). Influence of substrates on colour reproduction in billboard printing. *IV International Joint Conference on Environmental and Light Industry Technologies* (pp. 392-397), Budapest: Óbuda University, 20– 22. November 2013. ISBN 978-615-5018-93-0
- Kim, D. H. & Nobbs, J. H. (1997). New weighting functions for the weighted CIELAB color difference formula. *Proc 8th Cong AIC Colour 97* (pp. 446–449) Kyoto, Japan.
- Research and Markets (2022). *Global Digital Printing Market (2022-2027) by Type, Ink Type, Application, Geography, Competitive Analysis and the Impact of Covid-19 with Ansoff Analysis*. ID: 5585730

Informative Article

REMARKS ABOUT PRINTING AUTOMATION

Thomas Hoffmann Walbeck, Živko Pavlović¹

¹University of Novi Sad, Faculty of Technical Sciences, Department of Graphic Engineering and Design, Novi Sad, Serbia,

Abstract

Automation is an important topic in the graphic arts industry. Many terms are related to automation, such as process automation, workflow automation, metadata, job tickets, WMS, MIS/ERP, AI, IoT, Print 4.0 and smart factory. These terms are also commonly used by manufacturers as buzzwords for product marketing. In this paper we will discuss these terms and also the relationships between them.

Keywords: automation, process, workflow, print production.

Introduction

Automation in production means the reduction of manual interventions, so-called human touch points. It usually implies an increase in efficiency and thus a reduction in costs. Efficiency can be increased and/or costs can be reduced without changing the degree of automation, of course. An example of this is a rise in the production speed of a machine. In everyday language, however, automation and efficiency are often mistakenly equated.

The classic driving forces for automation in print production are well known: Run length reduction, increase in the number of print jobs per day, cost pressures and the demand for faster throughput. In recent times, two significant factors have been added: Increases in material/energy costs and the shortage of skilled operators.

So perhaps it is no coincidence that so many buzzwords have become popular in recent years in connection with automation of print production: Process Automation, Workflow Automation, Metadata, WMS, MIS/ERP, Cloud Computing, Artificial Intelligence (AI), Internet of Things (IoT), Print 4.0, Smart Factory to name just the most important.

But are some of these buzz words synonyms, do they complement, or do they denote certain subfields of others? We also like to explore the question of the extent to which the terms describe classical technologies, state-of-the-art technologies or visions for the future.

In this paper, we therefore would like to clarify these terms and their interrelations.

Process Automation, Workflow Automation

Automation in print production can be roughly divided into two subcategories, both are often interdependent: process automation and workflow automation.

A process in production is a singular work step with a specific and immediate goal that is carried out independently of other work steps. According to this definition, trapping in prepress, offset printing or folding in postpress are three different processes. The make-ready of a printing press, on the other hand, is not, because this production step only makes sense in connection with the associated production run. Make-ready is only a so-called process phase; it is too specific, too directly linked to the next work step and represents a too narrow interval in the production chain. Conversely, a very

general term such as "prepress" is not a process because the tasks that occur there have very different immediate goals.

Process automation therefore always means automating a specific process. For example, the printing process on a classic offset press can be automated to a greater extent by automatic register control or by automatic color control. A trapping process in prepress can be automated by automatically generating suitable traps. Recently, the automated generation of sheet layouts has gained importance. The examples show that processes can be executed on machines or by software on computers.

Workflow automation, on the other hand, is the process of transferring documents/ information from one work step (process) to the next or to some dedicated workflow management software, often called "controller".

Automated workflow steps can be triggered by metadata. Metadata in the print area are descriptions of print products, instructions for production control, and operational data collected from the print shop floor. Metadata is to be understood in contrast to print data describing graphical content (e.g., deploying PDF). Typically, metadata is described by the Job Definition Format (JDF) and its associated Job Messaging Format (JMF) (CIP4, 2020a), by Exchange JDF (XJDF) (CIP4, 2020b), or by PrintTalk (CIP4, 2020c). This type of data is often also called "job tickets". In addition to these data standards, private XML/JSON data is also used for metadata. A relatively new possibility is the storage of job ticket data in PDF files (ISO, 2019).

Workflow and process automation are often strongly interwoven. For this reason, these two subcategories are often not properly distinguished. For example, an automatic presetting of a machine (process automation) mainly becomes powerful through the provision of certain metadata from outside (workflow automation). Therefore, the terms process automation, workflow automation and production automation are often used synonymously.

Process automation is not a new concept; a Linotype typesetting press, for example, represents a significant level of automation compared to traditional manual typesetting. Process automation has probably always been sought in human civilization. However, computer-based workflow automation in the graphic arts industry probably did not begin until the introduction of the Print Production Format (PPF) in 1995 (CIP4, 1998). Since then, this format has been used primarily to send data from the RIP to the offset presses for setting ink zone presetting values automatically. JDF has significantly advanced workflow automation since 2000.

WMS and MIS

A controller manages processes that run on devices or applications. Two special controller types play a prominent role: Workflow Management Systems (WMS), or workflow systems for short, and Management Information Systems (MIS). Both are particularly important for automation in the graphic arts industry.

A WMS usually manages several print productions processes. It consists of a core and usually several engines. The WMS core contains the workflow logic and the interfaces to the outside (for example to other controllers and also to the GUI for the operators). Each engine receives appropriate instructions (job tickets) from the core, executes one (or more) process(es), and often returns resulting data along with operational data back to the core. For example, a WMS in prepress manages the preflight, color management, trapping, imposition, RIPing, and plate setting processes. All communication to and from the engines, therefore (almost) always runs via the WMS core.

An MIS, on the other hand, primarily manages the commercial aspects of customer orders. In the early days, the most important module was cost estimation for individual print job. In recent years, however, the MIS has increasingly taken over the control of production and thus developed more and more into an Enterprise Resource Planning (ERP) system. With this development, even the original cost calculation has sometimes been abandoned altogether, as with Internet print shops (web-to-print).

These printing companies simply have to produce too many jobs per day to be able to calculate them individually in advance.

The MIS is sometimes called the "brain" of a print shop. It normally is the topmost controller in the hierarchy of all other controllers and devices. It usually creates new jobs in a database, initiates the associated job tickets and passes them on to production. The other way round it collects operational data from devices and other controllers on the shop floor and condenses it into useful information for the management. In many cases, however, the MIS today has interfaces not only to production, but also with purchasing, shipping, the customer portal, and so on.

WMS and MIS have been widely used in the graphic arts industry for about 20 years. Both are essential pillars of automation in current print shops.

Cloud Computing

The term "Cloud Computing" often refers to the delivery of IT services, software apps, and resources over the internet. Sai Vennam (Vennam, 2020) defines cloud computing to be as „on-demand access, via the internet, to computing resources—applications, servers (physical servers and virtual servers), data storage, development tools, networking capabilities, and more—hosted at a remote data center managed by a cloud services provider (or CSP) “.

This is a valid characterization for a public cloud, however, not necessarily for a private cloud. So, what is the difference between the two? In a public cloud computing services and infrastructure are managed by a third-party CSP. It is shared with multiple organizations.

In a private cloud (also called internal cloud or corporate cloud) the infrastructure is not shared with others. The management of the services and infrastructure might still be done by some third party (the private cloud provider) or by the organization itself. The latter means that the organization is responsible for the hardware and software, just as before with its own data center on premises. Furthermore, there are hybrid architectures that have both private and public cloud characteristics.

Although the IT hardware of a private cloud may be identical to that of the organization's traditional data center, the software architecture differs significantly. The traditional client-server architecture is replaced by a cloud architecture, even if it does not use the Internet, but the intranet instead.

Strictly speaking, cloud storage is not yet cloud computing. For cloud computing, dedicated software processes must run over the Internet/intranet (e.g., remote applications).

However, cloud computing has actually (almost) nothing to do with automation, but rather with scalability, flexibility and new financial models. Cloud computing, however, might be deployed as an IT architecture for advanced production automation, of course. Print 4.0, the future concept for production automation, will certainly be based heavily on cloud computing.

Cloud computing is state-of-the-art. In the graphics industry, cloud computing solutions have so far been offered mainly in the MIS/ERP area. Due to the large volume of data generated, cloud computing is currently not practical everywhere in print production. For example, the RIPing process is unlikely to be moved to the cloud in the foreseeable future (at best, the control of the local RIP) because the large volumes of data generated by this process are subsequently required on-site at the print shop. Cloud storage, on the other hand, has been used heavily for years.

Artificial Intelligence (AI)

AI could play an important role in the graphic arts industry in the future, especially in production decisions based on incomplete or uncertain information, from which no compelling instructions for action can be derived. Examples include determining an appropriate job schedule, job ganging, and sheet layout. AI will be a new possibility to enhance and automate these production processes.

A different area of AI in print shops is predictive maintenance, where many different machine data are analyzed to trigger a potential service call.

Yet another area for AI can be in content creation. For example, content for mailings, personalized catalogues or advertising brochures can be selected in a more targeted and automated way using data about the recipients.

It is currently difficult to assess whether some software is already using true AI methods such as neural networks and machine learning algorithm. Even if manufacturers claim this when marketing their products, it is difficult to verify from the outside. A job scheduler could be based on AI, but also on classical algorithms with many if-then-else queries.

Internet of Things (IoT), Print 4.0, Smart Factory

The term "Print 4.0" is derived from the term "Industry 4.0"; a name first proposed in 2011 at the Hanover Fair in Germany. It can be characterized as follows.

- Mass customization
- Highly flexible and nearly autonomous production,
- Extensive integration of manufacturers, customers, and business partners
- Linking of production with high-quality services

With Print 4.0, the focus of this concept is on the printing industry. The vision is that print buyers send their customized orders to a print provider, where they define production workflow automatically, that is, devices are booked, material/services are purchased and the products are shipped – everything without or hardly any human touch points.

With workflow and process automation, job tickets, web-to-print, and cloud computing, the printing industry is pretty well prepared for exactly this scenario. Some manufacturers already using this term in their marketing statements. But there is still a long way to go before Print Shop 4.0, also known as the smart factory, is a reality.

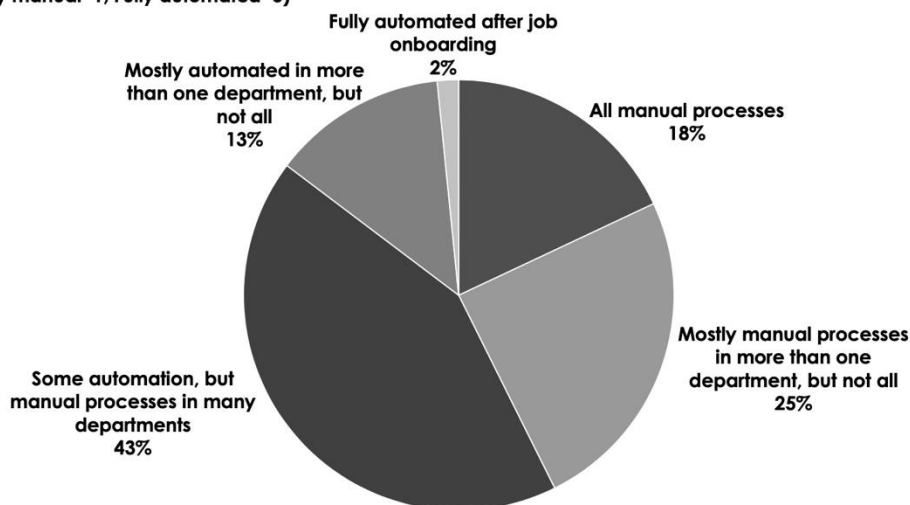
With web-to-print, there is still a limited number of products to choose from. For each type of product, a production path is defined and tested in advance, so it is largely predetermined. Thus, the products are not really individual, only the print content, and manufacturing is not negotiated between devices for each job. Apart from that, the processes are not fully automated even at the large Internet printers. The (industrial) Internet-of-Things (IoT) is the mass linking of sensors, devices and electronic components with software systems, either directly or via the cloud. This makes the IoT an important element of Industry 4.0 respectively Print 4.0; however, it should not be equated.

Discussion and Conclusion

If we refer to a technology as "classic" or "state-of-the-art" in this paper, this does not of course mean that the majority of companies are already using it. In industry, automation of production is far less advanced, as the study by KP Infotrends shows (Zwang, 2021), see Figure 1.

Q15: What best describes your current level of workflow automation?

Mean: 2.6 (Fully manual=1, Fully automated=5)



N = 122 respondents

Chart 1. Current level of workflow automation Source: NA Software Investment outlook, KP-InfoTrends 2019

In this paper, we have shown that certain terms associated with automation in print production sometimes have little to do with it (e.g., cloud computing), others are complementary (e.g., process automation and workflow automation), still others represent subsets (e.g., process/workflow automation and production automation), and finally can be used interchangeably (Print 4.0 and smart factory).

Further information about workflow automation can be found, for example, in the textbook (Hoffmann-Walbeck, 2022).

References

- CIP3 (1998). Specification of the CIP3 Print Production Format. <https://www.cip4.org/new-structure/specifications-tools/cip3-print-production-format-ppf/articles/new-structure-specifications-tools-job-definition-format-jdf-PPF-specification.html> (Accessed 9/17/2022)
- CIP4 (2020a). JDF Specification 1.7 <https://www.cip4.org/new-structure/specifications-tools/job-definition-format-jdf/articles/jdf-jmf-specification.html> (Accessed 9/17/2022)
- CIP4 (2020b). XJDF Specification 2.1. <https://cip4.atlassian.net/wiki/spaces/PUB/pages/1181122928/XJDF> (Accessed 9/17/2022)
- CIP4 (2020c). PrintTalk Specification 2.1. <https://www.cip4.org/what-is-printtalk.html> (Accessed 9/17/2022)
- Hoffmann Walbeck, T. *Workflow Automation: Basic Concepts of Workflow Automation in the Graphic Industry*, Springer. (Accessed 9/17/2022)
- ISO 2019: ISO 21812:2019 Graphic technology – Print product metadata for PDF files – Part 1 Architecture and core requirements for metadata. Available at <https://www.iso.org/standard/74407.html> (Accessed 9/17/2022)
- Vennam, S. (2020). *Cloud Computing*. <https://www.ibm.com/cloud/learn/cloud-computing> (Accessed 9/17/2022)
- Zwang, L. D. (2021): *How to participate in Industry 4.0 Part 2: State of Readiness*. <https://whattheythink.com/articles/105462-how-participate-industry-40part-1-state-readiness/> (Accessed 9/17/2022)

ENVIRONMENTAL ENGINEERING AND ECOLOGY

Original scientific article

DEPOSITION OF GOETHITE AND FERRIHYDRITE ONTO EXPANDED VERMICULITE SURFACE: CHEMICAL PROPERTIES AND POTENTIAL APPLICATION

Mladen Bugarčić¹, Aleksandar Jovanović¹, Aleksandar Marinković², Jovana Bošnjaković³, Miroslav Sokić¹, Ana Radosavljević Mihajlović¹, Milan Milivojević²

¹Institute for Technology of Nuclear and Other Mineral Raw Materials, 11000 Belgrade, Serbia

²University of Belgrade, Faculty of Technology and Metallurgy, 11000 Belgrade, Serbia

³Research and Development Institute Lola L.T.D., 11030 Belgrade, Serbia

Abstract

Current demand on adsorbent materials is in constant growth, hence scientific society is in ceaseless research subjecting cheap and optimal adsorbent. Abundant raw materials which may be utilized as adsorbent of cation species are mica minerals, and vermiculite as one of them is widely examined. Since wastewater may contain anion or/ and non-ionic pollutants it is needed to functionalize adsorbent so it may attract those species as well. Goethite and ferrihydrite are potential candidates for such modification since they: have large specific surface area (SSA), possess hydroxide group and they are not toxic to the environment. Goethite/ expanded vermiculite (Goe/EV) and ferrihydrite/ expanded vermiculite (Fer/EV) are successfully prepared and those composites have showed better adsorption related chemical properties than expanded vermiculite (EV) itself. Utilizing BET methodology, it is determined that Fer/EV possess five-time larger SSA than EV, while Goe/EV is two times larger. Measuring cation exchange capacity (CEC) it is determined that modified samples have only ~10% smaller values of CEC. Summary, both composites have shown higher affinity toward cationic dye, malachite green and also showed their adsorbent potential toward anionic dye, tartrazine. Thanks to facile preparation of such materials and its cost, it may be concluded that they are prospective choice as adsorbents, in first order of heavy metals and dyes.

Keywords: expanded vermiculite, adsorbent functionalization, goethite, ferrihydrite, wastewater treatment.

Introduction

Mica minerals are among the most abundant group of minerals that readily exist in Earth's crust (Ralph, 2017), and also they possess quite interesting properties. Vermiculite, as well as other smectites is expandable mica mineral. Vermiculite expanded form, expanded vermiculite (EV) can be facile produced via thermal process during intensive heating of vermiculite particles from ambient conditions up to 300 °C (Suvorov & Skurikhin, 2003). Thus obtained, EV is already used as heat insulator (Suvorov & Skurikhin, 2003), radiation shield (Kaur et al., 2014) as germination medium (Wisdom et al., 2017) as a matrix for phase change materials (Gencel et al., 2021; Yang et al., 2020). Beside all mentioned usability, this material may be used as adsorbent as well (Brião et al., 2021; Bugarčić et al., 2021). Thanks to its simplicity, applicability and low cost, adsorption is one of the most promising methods that can be used in wastewater management. Adsorption properties of EV towards cation species come from its moderate cation exchange capacity (CEC) from 25 to 250 cmol_{eq}/kg (Weiss et al., 1955). However, negative surface of T-O-T layers repels anions, therefore

EV couldn't be utilized as an adsorbent of anions. Such defect of material could be exceeded enriching the surface T-O-T sheets of EV with minerals with hydroxide functionality. Thanks to possibility to form hydrogen bonds hydroxide group could bind both cations and anions, that way those composites would be even superior adsorbent than EV itself. Goethite (Goe) and ferrihydrite (Fer) quite fit the requirements of the mineral with hydroxide functional group, they also possess huge surface area and they are quite stable and harmless to the environment (Baragaño et al., 2020; Malakar et al., 2022). In this study, deposition of Goe and Fer on EV surface was done by coprecipitation in thin layer of nonsolvent. Thus, prepared composite was characterized in the manner of its adsorption (towards malachite green (MG) and tartrazine (TAR)) and physicochemical properties (Cation Exchange Capacity (CEC) and BET specific surface area).

Materials and Methods

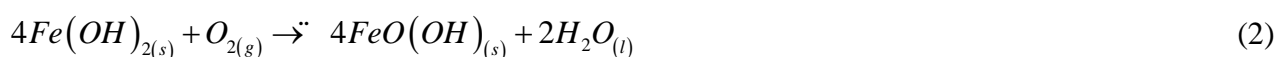
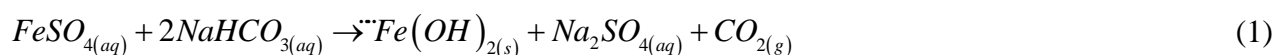
Samples of EV used for preparation of composites are provided from Vatra ltd, Beograd. All the chemicals mentioned in subsection below were of analytical grade, while dialysis bags used are obtained from Spectra/Por® Biotech made from Regenerated Cellulose (RC), MWCO 3500.

Deposition of the Goe has been performed in three identical consecutive steps. Total mass of the reagents used for goethite synthesis was calculated in the way that total mass of produced goethite in those 3 steps is 10 mas% of the EV mass. Prior to deposition EV sample is etched in two steps:

- I step using solution of peroxydisulfuric acid ($\omega=1.5$ mas%) $m:m=50$ g kg^{-1} for 15 minutes of gentle stirring (up to 50 rpm) the dispersion in a glass
- II step using solution of hydrofluoric acid ($\omega=3.0$ mas%) $m:V=50$ g dm^{-3} for 30 minutes of gentle stirring (up to 50 rpm) the dispersion in a polyethylene glass

After etching, the sample was thoroughly rinsed with deionized water (DW) until negative reaction on fluoride ions, and dried on 80°C for 2.5 hours.

Concept for preparation of goethite can be found in work of Schwertman and Cornell (Schwertman & Cornell, 2000) procedure that may be found in cited book is modified in a few details. In order to obtain Goe/EV sample 5.0000 g of EV is placed into three-necked balloon ($V=100$ cm^3) together with 10.0 cm^3 of xylene, 2.00 cm^3 of nitrogen aerated water and 0.3300 g of $\text{FeSO}_4 \cdot 7\text{H}_2\text{O}$ and vacuumed (using water jet pump) for 15 minutes and sonicated (ultrasound (US) bath, Bandelin Sonorex RK 100) another 15 minutes. After this 0.2000 g of NaHCO_3 ($n(\text{FeSO}_4 \cdot 7\text{H}_2\text{O}):n(\text{NaHCO}_3)=1:2$) is dissolved into 2.00 cm^3 of nitrogen aerated water and this solution is droplet added in balloon in nitrogen atmosphere. When evolution of CO_2 is finished, gas inlet is switched on synthetic air. This reaction is left for 24 h, after it obtained composite is filtered and rinsed with ethanol and DW until negative reaction on sulfate ions. Wet sample Goe/EV is dried on 40°C for 6 hours. This deposition of goethite is repeated three times and thus obtained composite is stored in plastic containers. Reactions that occur during synthesis of goethite can be presented with chemisms (1,2).



Procedure for preparation of 6-line ferrihydrite can be found in the book Iron Oxides in the Laboratory by Schwertman and Cornell (Schwertman & Cornell, 2000) however found procedure is changed in a few details so preparation of composite Fer/EV is done in procedure described below:

At first, it is measured 5.0000 g of EV and placed into a tube together with 1.00 cm^3 of DW in order to wet the base material. Wetting of the sample is done the same as in previous case, in assistance of

US bath (US bath, Bandelin Sonorex RK 100) and applying the vacuum (water jet pump). In another glass it as added 10.0 cm³ of xylene and 4.00 cm³ of water and put into a furnace and preheated on 75 °C when the reaction mixture reached this temperature it is added 2.0000 g of unhydrolyzed Fe(NO₃)₃·9H₂O together with already wet EV sample and rapid stirred for 1 minute. Glass together with reagents is moved in oven again for 10 minutes and after the polymerization of iron (III) hydroxides is done, the glass is cooled rapidly plunging it into ice water, and after cooling the sample is centrifuged (3000 rpm for 3 minutes), the liquid phase is decanted and solid raw sample is placed into dialysis bag where the sample is dialyzed for 5 days (water is changed 3 times a day). When the dialysis is done, solid sample is rinsed with DW and ethanol and dried on 60 °C for 6 hours.

In order to determine cation exchange capacity (CEC) mass concentrations of sodium, potassium, magnesium, calcium and iron were done for all samples, methodology used for CEC determination was done according to work of Daković et al (Daković et al., 2005).

Determination of samples specific surface area (SSA) was done by Brunauer–Emmett–Teller (BET) methodology on Micrometrics ASAP 2020 in linear part of nitrogen BET adsorption isotherm on the temperature of nitrogen boiling ($p = p_{atm}$). Before nitrogen adsorption all the samples were degassed on vacuum for a 10 h at 150 °C. Adsorption was done using nitrogen 99.9 vol.% purity.

Adsorption of malachite green and tartrazine ($c_i=10 \text{ mg dm}^{-3}$) were done on 298 K in a batch system ($m:V=8:60 \text{ g dm}^{-3}$) Concentration of the dyes during adsorption was measured using UV/Vis spectrophotometer Shimadzu 1800 measuring absorption of the light in the wavelength range from 200 to 800 nm on the pre-filtered aliquot sample. Concentration is calculated via Beer-Lambert law equation (3).

$$c = \frac{A}{\varepsilon \cdot l} \quad (3)$$

In the expression (3) A is the absorbance on the wavelength of strongest peak, while $\varepsilon \cdot l$ value was obtained via calibration (determined as a slope of linear part of the function A vs c for standardized solutions of used dyes).

Results and discussion

Determined values of CEC together with contribution of each cation in summary CEC value are given within Table 1. As it can be seen from Table 1 the largest contribution of CEC value in raw sample is provided by presence of magnesium ions in interlayer. On the other hand, composite Goe/EV was obtained via co-precipitation method using sodium salt as a reagent, for that reason sodium ions gave larger contribution to CEC than others present. In the case of Fer/EV composite there were no other reagents used than iron (III) salt and water, so the CEC value is similar as for the start material (EV) with slightly higher contribution of iron (III) ions when compared with EV sample (see Table 1).

Table 1. Cation exchange capacity of EV and its composite and their SSA measured utilizing BET methodology

	Cation Exchange Capacity/cmole _c kg ⁻¹						S _{BET} / m ² g ⁻¹
	Ca ²⁺	Mg ²⁺	Na ⁺	K ⁺	Fe ³⁺	Σ	
EV	6.1	32.1	0.8	0.9	0.1	40.0	3.28
Goe/EV	3.2	4.8	27.8	0.5	0.2	36.5	6.61
Fer/EV	3.0	30.6	0.7	0.8	1.1	36.2	15.1

Results of SSA determined via BET methodology are placed in Table 1, and as it can be seen both modifications (Goe/EV and Fer/EV) possess higher SSA than bas material EV. And this is expected since Goe and Fer prepared utilizing routes described by Schwertman and Cornell have SSA of 80 and 200 m² g⁻¹ respectively (Schwertman & Cornell, 2000). However, since the yield of the oxides are

not the same (6-line ferrihydrite is much less yielded than goethite) SSA of Fer/EV is only about 150 % higher than Goe/EV.

Measuring absorbance of standardized solutions of MG and TAR were utilized to determine values of $\varepsilon \cdot l$ slope and their respectively values are xx and zz $\text{dm}^3 \text{g}^{-1}$.

With determined values of $\varepsilon \cdot l$ absorbance results (A) from adsorption experiments are simple recalculated into c using equation (3) and adsorption capacity is calculated using expression (4).

$$q_t = \frac{c_i - c_t}{m_{ads}} * V \quad (4)$$

Where q_t (mg g^{-1}) is adsorption capacity after amount of time, c_t and c_i (mg dm^{-3}) are measured and initial concentration of the dyes in a solutions, m_{ads} (g) is of used adsorbent and V (dm^3) is volume of the solution in the batch. The results of adsorption experiments are presented at Figures 1 and 2 as function of achieved adsorption capacity versus contact time of adsorbent with adsorbate solution.

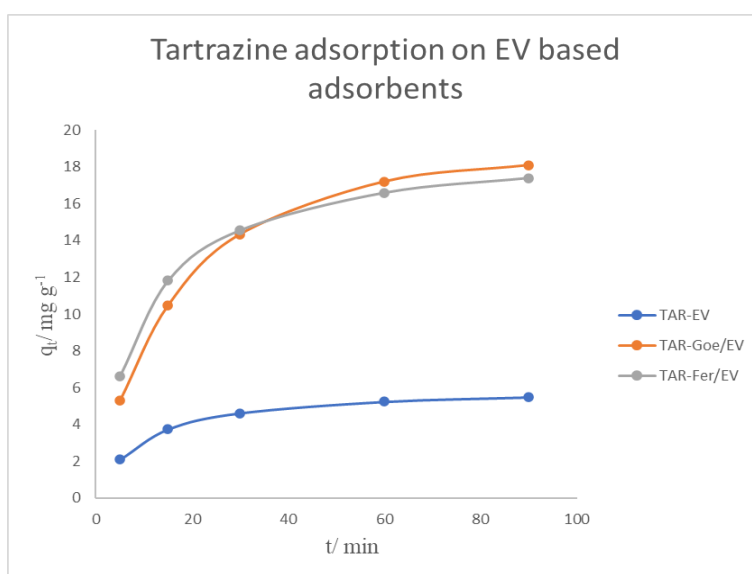


Figure 1. Tartrazine adsorption trend on EV and its modifications

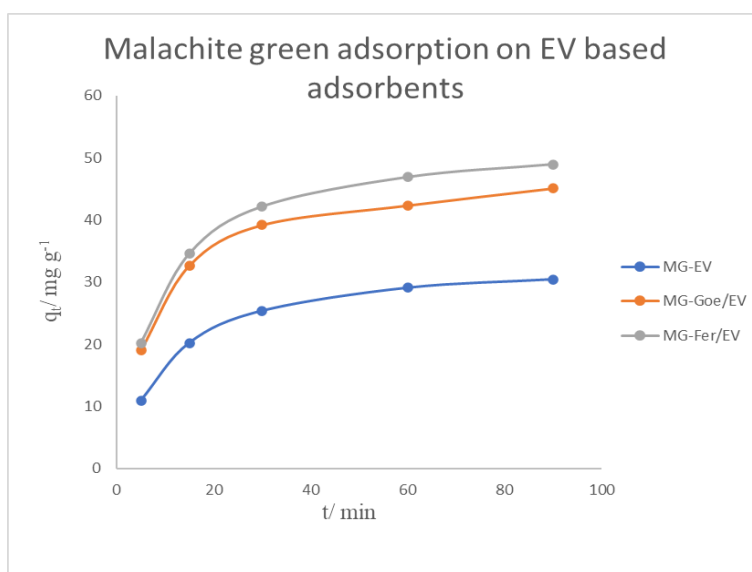


Figure 2. Malachite green adsorption trend on EV and its modifications

As it can be seen from Figure 1, prepared composites possess much higher adsorption capacities towards tartrazine than EV itself. This is expected as a result since EV itself possesses negative surface (T-O-T layer) and thanks to this property EV can't attract negatively charged molecules such as tartrazine and adsorption capacity towards anion species is limited. In the presence of Goe and Fer negatively charged molecules of tartrazine anion could be attracted on support surface and adsorption capacity is better. From the same figure it can be seen that adsorption trend of this dye on Goe/EV is slower however at certain point Goe/EV overcomes Fer/EV composite. Most likely this is due to limiting mass transfer through inner pores of Fer which possess significantly larger SSA than Goe, however inner pores during the adsorption become more and more unavailable and adsorption reaches equilibrium state.

Adsorption capacity of cationic dye, MG on both composites surpassed the base material (EV) adsorption capacity towards same dye as it can be seen from Figure 2. Composite Fer/EV possesses better adsorption properties towards MG than Goe/EV composite, thanks to bigger SSA, as it can be seen from Table 1. Molecular structures of TAR and MG can also help in understanding such results, at Figures 3 are given structures of TAR and MG.

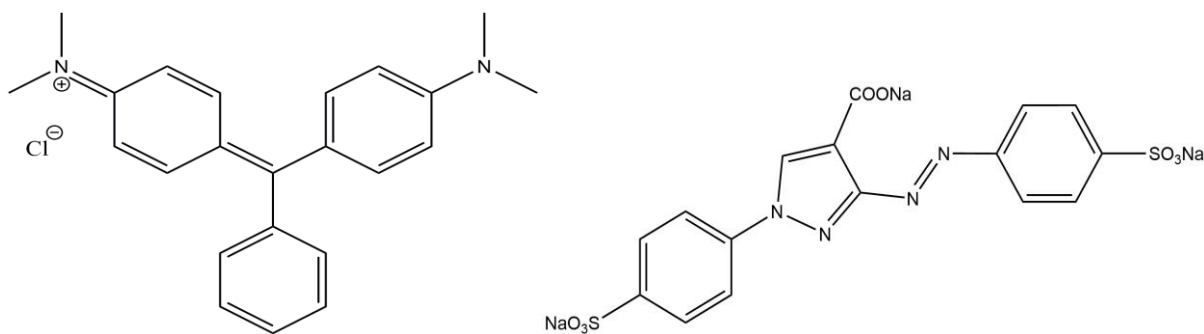


Figure 3. Molecular structures of MG (left) and TAR (right)

As it can be seen from structures MG compound is a salt where positive charge is carried by nitrogen atom and this charge is dispersed through all the benzene rings thanks to complete aromatic behavior of this cation. This cation easily bonds on T-O-T structure of EV matrix all followed by ion exchange with cations in interlayer and adsorption on particles of oxides present on the surface of EV in the case of composites. Structure of TAR shows another salt where negative charge is carried by two sulfonate anion and carboxylate anion so total charge of the anion is -3. This anion is repulsed by the EV surface of T-O-T layer, however presence of Goe and Fer supports the bonding of anion thanks to ion-dipole interaction in the smaller intensity and hydrogen bond in higher intensity.

Conclusion

Deposition of both Goe and Fer on the surface of EV alters the adsorption properties of EV towards the dyes. Presence of these two iron oxides enable the adsorption of anionic dyes and in the same time improve the adsorption capacity of cationic dyes. Thanks to higher CEC and improved SSA obtained composites are prospective choice for adsorption of cationic species in the first place and anionic species in decent amount for such materials in a second place.

References

Baragaño, D., Alonso, J., Gallego, J. R., Lobo, M. C & Gil-Díaz, M. (2020). Zero valent iron and goethite nanoparticles as new promising remediation techniques for As-polluted soils.

- Chemosphere*, 238. <https://doi.org/10.1016/j.chemosphere.2019.124624>
- Brião, G. de V., da Silva, M. G. & Vieira, M. G. A. (2021). Expanded vermiculite as an alternative adsorbent for the dysprosium recovery. *Journal of the Taiwan Institute of Chemical Engineers*, 127, 228–235. <https://doi.org/10.1016/j.jtice.2021.08.022>
- Bugarčić, M., Lopičić, Z., Šoštarić, T., Marinković, A., Rusmirovic, J. D., Milošević, D. & Milivojević, M. (2021). Vermiculite enriched by Fe(III) oxides as a novel adsorbent for toxic metals removal. *Journal of Environmental Chemical Engineering*, 9(5). <https://doi.org/10.1016/j.jece.2021.106020>
- Daković, A., Tomašević-Čanović, M., Dondur, V., Rottinghaus, G. E., Medaković, V. & Zarić, S. (2005). Adsorption of mycotoxins by organozeolites. *Colloids and Surfaces B: Biointerfaces*, 46(1), 20–25. <https://doi.org/10.1016/j.colsurfb.2005.08.013>
- Gencel, O., Sarı, A., Ustaoglu, A., Hekimoglu, G., Erdogmus, E., Yaras, A., Sutcu, M. & Cay, V. V. (2021). Eco-friendly building materials containing micronized expanded vermiculite and phase change material for solar based thermo-regulation applications. *Construction and Building Materials*, 308(September), 125062. <https://doi.org/10.1016/j.conbuildmat.2021.125062>
- Kaur, S., Singh, S. & Singh, L. (2014). Physio-chemical properties of gamma-irradiated vermiculite and their significance for radiation protection and thermoluminescence. *American Mineralogist*, 99(10), 2018–2024. <https://doi.org/10.2138/am-2014-4873>
- Malakar, A., Snow, D. D., Kaiser, M., Shields, J., Maharjan, B., Walia, H., Rudnick, D. & Ray, C. (2022). Ferrihydrite enrichment in the rhizosphere of unsaturated soil improves nutrient retention while limiting arsenic and uranium plant uptake. *Science of the Total Environment*, 806, 150967. <https://doi.org/10.1016/j.scitotenv.2021.150967>
- Ralph, J. (2017). *The Most Common Minerals on the Earth*. https://www.mindat.org/a/common_minerals
- Schwertman, U. & Cornell, R. M. (2000). *Iron Oxides in the Laboratory* (Second edi). Wiley VCH Verlag GmbH.
- Suvorov, S. A. & Skurikhin, V. V. (2003). Vermiculite - A promising material for high-temperature heat insulators. *Refractories and Industrial Ceramics*, 44(3), 186–193. <https://doi.org/10.1023/A:1026312619843>
- Weiss, A., Koch, G. & Hofmann, U. (1955). Zur Kenntnis von Saponite. *Berichte Der Deutsche Keramische Gesellschaft*, 22, 12–17. <https://scholar.googleusercontent.com/scholar.bib?q=info:Q5yqbVpi-sEJ:scholar.google.com/&output=citation&scisig=AAGBfm0AAAAAXKMVzWA5qMcHu7ZrPzq3LPxN4DHvfcGT&scisf=4&ct=citation&cd=-1&hl=en>
- Wisdom, B., Nyembezi, M. & Agathar, K. (2017). Effect of different vermiculite and pine bark media substrates mixtures on physical properties and spiral rooting of radish (*Raphanus sativus* L.) in float tray system. *Rhizosphere*, 3(January), 67–74. <https://doi.org/10.1016/j.rhisph.2017.01.002>
- Yang, Z., Li, J., Luan, X. & Song, S. (2020). Effects of acid leaching and organic intercalation on the thermophysical properties of paraffin/expanded vermiculite composite phase change materials. *Applied Clay Science*, 196(June), 105754. <https://doi.org/10.1016/j.clay.2020.105754>

Original scientific article

REMOVAL OF XENOBIOTICS FROM WASTEWATERS USING PHOTOLYSIS UNDER SUN-LIGHT IRRADIATION: EXPERIMENTAL APPROACH AND PROCESS DESIGN

Aleksandar Jovanović¹, Mladen Bugarčić¹, Nataša Knežević², Jovana Bošnjaković³, Jelena Lukić⁴, Antonije Onjia², Aleksandar Marinković²

¹Institute for Technology of Nuclear and Other Mineral Raw Materials, 11000 Belgrade, Serbia

²University of Belgrade, Faculty of Technology and Metallurgy, 11000 Belgrade, Serbia

³Research and Development Institute Lola L.T.D., 11030 Belgrade, Serbia

⁴Innovation Center of Faculty of Technology and Metallurgy, 11000 Belgrade, Serbia

Abstract

Conventional wastewater treatment processes are increasingly difficult to fulfill strict standards of achieving the required quality. Therefore, it is necessary to apply processes that in an efficient and economically justified way reach the necessary limits in order to discharge wastewater into the recipient. The process of photolysis represents the degradation of the starting pollutant practically to water and carbon dioxide. The whole process takes place under the action of a UV lamp that imitated solar irradiation. The process is environmentally justified since, unlike some other advanced oxidation processes - AOPs, there is no use of additional, hazardous, chemicals which possibly results in the precipitates formation that are leading to further treatment. In this paper, photolytic degradation of pesticide thiophanate methyl was performed in doubled wall quartz reactor equipped with a thermoregulation system. Reaction was forced under Osram ULTRA VITALUX UV lamp (300W). Kinetics of photodecomposition process was followed by pseudo-first order. In certain time periods, specimens were sampled, filtered and monitored by UV spectrophotometer Shimadzu 1800 with an aim to determine the concentration of xenobiotic. Complete degradation of present xenobiotics was obtained after 240 min. With an aim to enhance the degradation process, hydrogen peroxide was added as a boosting agent which cause a shortening in demanded time (150 min) for complete degradation. Verification of the success of decomposition was confirmed by the obtained values of chemical oxygen demand (COD), which reveal that the established system has a basis for real application in industrial or municipal wastewater.

Keywords: wastewater treatment, pesticide degradation, photolysis, AOPs, COD.

Introduction

Due to the excessive or improper use of pesticides, the rising demand for food production worldwide has not only produced a major decline in food quality and severe environmental effects (Abhilash & Singh, 2009). Various pesticides used in agricultural techniques to assure crop quality and food safety might cause the release of these compounds into non-target environmental matrices, such as freshwater bodies (Bustos et al, 2019). This is a serious issue because pesticides are typically recognized to have harmful qualities that can make exposure to these chemicals potentially lethal. In terms of human health, pesticide exposure has been linked to an increase in the occurrence of some forms of cancer and birth abnormalities, among other disorders (Kaur & Kaur, 2018). Furthermore, it is generally understood that these substances might pose a health danger to other living species (Damalas & Eleftherohorinos, 2011). A fungicide called thiophanate methyl was frequently applied

to crops to prevent fungal infections (Correia et al., 2016). It is not particularly persistent in soil or water systems, has a low aqueous solubility, and is not particularly volatile. Although it is not poisonous to mammals, it can irritate, cause skin sensitivity, and even be mutagenic (Jia et al., 2020). Most aquatic species and earthworms are poisonous to it, while birds and bees are less susceptible. Due to high water pollution with different organic compounds, many researchers are trying their best to develop techniques for the removal and degradation of them. Wastewaters from industrial factories and agricultural fields present a tremendous problem for modern society, in the area of health care and sustainability (Ungureanu et al., 2020). Therefore, oxidative process like photolysis is increasingly used in smaller wastewater treatment plants (Liu et al., 2011; Anisuzzaman et al., 2022). This process provides the degradation of many classes of organic compounds and biological pollutants. Photolysis is a process of degradation of various pollutants under the action of UV irradiation, where the parent molecule is converted into smaller ones.

The goal of this study was to thoroughly investigate the degradation of thiophanate methyl (TPM) under simulated sunlight in order to develop an appropriate technique for its removal from water. Measurement of chemical oxygen demand (COD) will help in further explanations of process efficiency. The effects of hydrogen peroxide addition and the distance of the UV lamp on degradation were examined. The reaction kinetics was further investigated using UV-VIS.

Materials and Methods

All used chemicals are analytically pure and without the need for further purification. Pesticide thiophanate methyl was obtained from Sigma Aldrich (European Commission, 2022). Hydrogen peroxide was also acquired from Sigma Aldrich. Photolytic experiments were performed in a doubled-wall quartz glass reactor (Figure 1). For irradiation of pesticide solutions, Osram Ultra Vitalux UV lamp nominal wattage of 300 W (UVA : UVB = 13.6 : 3) was used. During irradiation, the reactor is consistently cooled down by coolant water in the reactor jacket to avoid uncontrolled heating of the treated solutions. Photolytic tests in this study were carried out with starting TPM concentrations of 5 and 10 mg dm⁻³. For initial experiments, in the reactor 150 dm⁻³ of the abovementioned fungicide solutions were added. In certain periods, 3.0 dm⁻³ of the solution was taken and recorded via UV spectrophotometry. All measurements were taken in triplicate. In photolytic experiments, the concentration of TPM was measured using UV-VIS Spectrophotometer 1800, Shimadzu, Japan. COD was measured by EPA 410.4: 1993 standard.

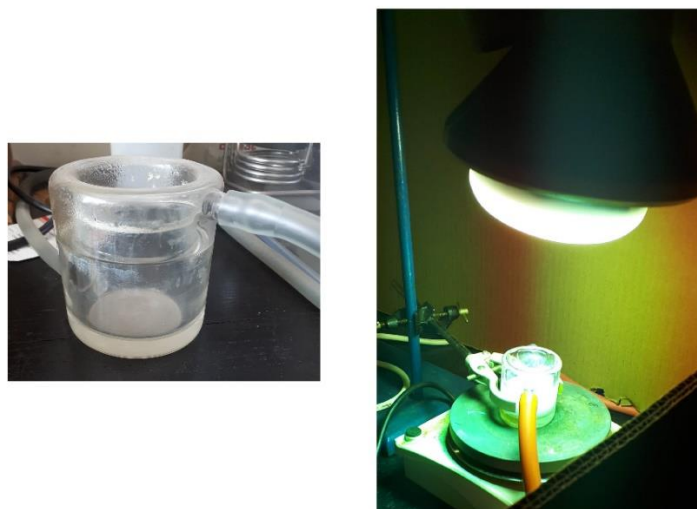


Figure 1. The reactor used for photolytic experiments

Results and discussion

At low concentrations of the organic pollutant, a pseudo-first order equation can be used to estimate the kinetics of photolytic reactions (Yusuff et al., 2020). In the Figure 2 are shown obtained curves with different symbols for all tests. They are representing the degradation of the present pollutant by sun-imitated irradiation and by sun-imitated irradiation with an addition 5% solution of H₂O₂.

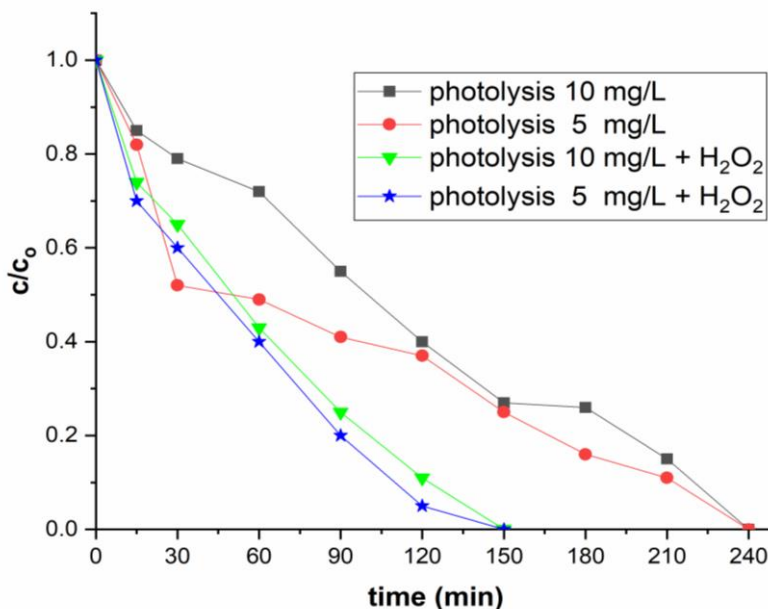


Figure 2. Degradation of TPM under different conditions

Photolytic tests reveal the relatively average degradation of TPM, which indicates the stability of this pesticide (which is in agreement with literature from Introduction). Results show that for both TPM concentrations, 5 and 10 mg dm⁻³, the needed time for complete decomposition was 240 min.

This is the reason for advancing photolytic reaction with the addition of H₂O₂ in order to fasten degradation of presented organic. The formation of peroxide radicals reduces the duration of the process due to accelerated oxidation of the pollution, which drives the degradation reaction and justify the necessity for an advanced process. Therefore, acquired results prove usage of this combination - 150 min as the required time for total decomposition of TPM (Figure 2).

By varying the distance of the lamp from reactor (from 100 to 400 mm), it was concluded that a distance of 200 mm has the best impact on degradation reactions. When the distance was the higher then 200 nm, photolytic degradation was lower by approximately 15% for 300 mm and approximately 25% for 400 mm. This can be explained by dissipation of emitted light. Contrastingly, when the gap between the reactor and UV lamp was smaller, solution of TPM started to evaporate because of inability of the system to cool the working solution.

Measurement of COD values are shown in Figure 3.

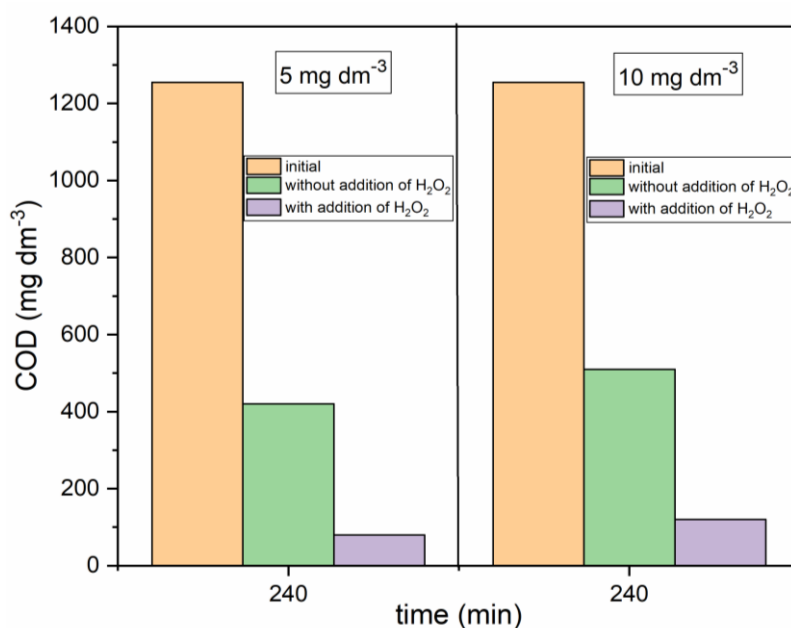


Figure 3. Monitoring of COD values prior and after the degradation of TPM

Determined initial value of COD for TPM solution was 1255 mg dm⁻³. Following the 240 min of photolytic reactions, obtained values were 510 and 420 for 10 and 5 mg dm⁻³, respectively. After the addition of 5% solution of H₂O₂, values of COD were decreased, 120 and 80 for 10 and 5 mg dm⁻³, respectively. This shows that the used system showed significant improvements.

Conclusion

Typical wastewater treatment systems are becoming increasingly difficult to meet stringent quality standards. As a result, in order to discharge wastewater into the recipient, processes that are efficient and economically justified must be used. Therefore, entire procedure is carried out under the influence of a UV light that simulates sun irradiation. The kinetics of the photodecomposition process was followed by pseudo-first order. Complete degradation of the present TPM was obtained after 240 min. With an aim to enhance the degradation process, hydrogen peroxide was added as a boosting agent which cause a shortening in demanded time (150 min) for complete degradation. Also, it was concluded that the optimal reactor-to-lamp distance was 200 mm. The estimated chemical oxygen demand (COD) values were used to evaluate the decomposition's success: 80 mg dm⁻³ for the concentration of TPM of 5 mg dm⁻³, which reveal that the established system has a basis for real application in industrial or municipal wastewater.

References

- Abhilash, P. C. & Singh, N. (2009). Pesticide use and application: an Indian scenario. *Journal of Hazardous Materials*, 165(1–3), 1–12. <https://doi.org/10.1016/j.jhazmat.2008.10.061>
- Anisuzzaman, S. M., Joseph, C. G., Pang, C. K., Affandi, N. A., Maruja, S. N. & Vijayan, V. (2022). Current Trends in the Utilization of Photolysis and Photocatalysis Treatment Processes for the Remediation of Dye Wastewater: A Short Review. *ChemEngineering*, 6(4). <https://doi.org/10.3390/chemengineering6040058>
- Bustos, N., Cruz-Alcalde, A., Iriel, A., Fernández Cirelli, A. & Sans, C. (2019). Sunlight and UVC-254 irradiation induced photodegradation of organophosphorus pesticide dichlorvos in aqueous matrices. *Science of the Total Environment*, 649, 592–600.

- <https://doi.org/10.1016/j.scitotenv.2018.08.254>
- Correia, M., Rodrigues, M., Paíga, P. & Delerue-Matos, C. (2016). Fungicides. In B. Caballero, P. M. Finglas, & F. B. T.-E. of F. and H. Toldrá (Eds.) (pp. 169–176). Oxford: Academic Press. <https://doi.org/https://doi.org/10.1016/B978-0-12-384947-2.00342-1>
- Damalas, C. A. & Eleftherohorinos, I. G. (2011). Pesticide exposure, safety issues, and risk assessment indicators. *International Journal of Environmental Research and Public Health*, 8(5), 1402–1419. <https://doi.org/10.3390/ijerph8051402>
- European Commission. (2022). *SDS Thiophanate-methyl*.
- Jia, K., Cheng, B., Huang, L., Xiao, J., Bai, Z., Liao, X. & Lu, H. (2020). Thiophanate-methyl induces severe hepatotoxicity in zebrafish. *Chemosphere*, 248(28), 125941. <https://doi.org/10.1016/j.chemosphere.2020.125941>
- Kaur, K. & Kaur, R. (2018). Occupational Pesticide Exposure, Impaired DNA Repair, and Diseases. *Indian Journal of Occupational and Environmental Medicine*, 22(2), 74–81. https://doi.org/10.4103/ijoem.IJOEM_45_18
- Liu, Y. S., Ying, G. G., Shareef, A. & Kookana, R. S. (2011). Photolysis of benzotriazole and formation of its polymerised photoproducts in aqueous solutions under UV irradiation. *Environmental Chemistry*, 8(2), 174–181. <https://doi.org/10.1071/EN10141>
- Ungureanu, N., Vlăduț, V. & Voicu, G. (2020). Water Scarcity and Wastewater Reuse in Crop Irrigation. *Sustainability*, 12(21), 9055. <https://doi.org/10.3390/su12219055>
- Yusuff, A. S., Taofeek Popoola, L. & Aderibigbe, E. I. (2020). Solar photocatalytic degradation of organic pollutants in textile industry wastewater by ZnO/pumice composite photocatalyst. *Journal of Environmental Chemical Engineering*, 8(4), 103907. <https://doi.org/https://doi.org/10.1016/j.jece.2020.103907>

Original scientific article

SOLAR STABILITY OF COMMERCIAL PESTICIDES THAT CONTRIBUTE TO THE QUALITY OF GRAPES AND FRUITS

Maria M. Savanović^{1,2}, Aleksandra Jovanoski Kostić¹, Andrijana Vukojević^{1,2}, Stevan Armaković^{1,2}, Jelena Kalajdžić³, Biserka Milić³, Mladen Kalajdžić³, Svetlana Pelemiš⁴, Sanja J. Armaković^{1,2}

¹University of Novi Sad, Faculty of Sciences, Trg Dositeja Obradovića 3, Novi Sad 21000, Serbia

²Association for the International Development of Academic and Scientific Collaboration (AIDASCO), 21000 Novi Sad, Serbia

³University of Novi Sad, Faculty of Agriculture, Trg Dositeja Obradovića 8, 21000 Novi Sad, Serbia

⁴University of East Sarajevo, Faculty of Technology Zvornik, Karakaj bb, 75400 Zvornik, Republic of Srpska, Bosnia and Herzegovina

Abstract

Pesticides are chemicals that are widely used in agriculture. They have several benefits, such as controlling harmful organisms and weeds that destroy crops and threaten people's lives. They also help farmers increase crop yields to provide enough food resources for a growing population, decrease food costs, and prevent sickness caused by moldy food. But there is a thin line between positive and negative effects of pesticide use. Therefore, after the treatment of plants with pesticides, it is necessary to monitor their stability in the environment. If the plants do not absorb pesticide, it reaches the surface and groundwater. This research aimed to assess the positive effects and solar stability of commercial pesticides Ormoroc and Globaryll used to treat grapevine and fruits. Ormoroc and Globaryll increased fruit weight, diameter and fruit firmness of sour (cv. Erdi botermo) and sweet (cv. Regina) cherries. The stability of Ormoroc and Globaryll was monitored at room temperature in the dark. Under these conditions, they were highly stable. The more significant investigation for the environment is the solar stability of these pesticides. Our results indicate the decomposition of the mentioned compounds under UV radiation. As UV light is a part of solar radiation, these results suggest that applying investigated formulations and their degradation using solar radiation is one of the foundations of sustainable agriculture.

Keywords: Ormoroc, Globaryll, Direct photolysis, UV radiation.

Introduction

With increasing food demand, agriculture modernization, and pesticide marketing, pesticide use has increased. The widespread use of pesticides is inevitable in agriculture. The average amount of pesticides used per hectare increased from 0.32 kg/ha in 1990 to 0.39 kg/ha in 2019 (Faostat, 2021). However, pesticide use for agriculture rose from 338 tons of active ingredients in the 1960s to 82,560 tons in 2019. The increase in pesticide use results from increased demand for food attributed to population increases from 16.7 million in 1991 to 43.0 million in 2021 (Ssemugabo et al., 2022). The question is whether these chemicals have toxic and hazardous environmental effects which arise from their continuous use in agriculture. This topic has attracted humankind's attention and has become a global ecological inquiry. Various studies have revealed that the exposure of humans to high concentrations of residual pesticides in food and water leads to serious chronic effects, including effects on reproduction, carcinogenesis, and neurotoxicity. However, when these chemicals are properly used according to regulations, they positively impact fruit quality, thereby ensuring higher

fruit yields in a world where the lack of food is an increasing problem (Da Silva et al., 2013; Hileman, 1994).

A commercial pesticide Ormoroc (active component 1-naphtylacetic acid) is a plant growth regulator with a similar structure to the auxin indole-3-acetic acid, a natural plant growth hormone important for seed and root development. It has been widely used in agriculture for over 60 years as a component in many commercial plant rooting and horticultural formulations (Kocaman & Güven, 2016). It is used for root cuttings, to prevent fruit drop shortly before harvest, and as a fruit thinning agent for fruits such as apple, pear, peach, and grape (Link, 2000). Its action mainly involves inducing the abscission of flower buds. Due to its application on various crops, trace amounts of 1-naphtylacetic acid are found in fruits and vegetables. It may also be expected to be present in surface and ground waters due to its incomplete plant adsorption. In literature, 1-naphtylacetic acid is considered harmful to aquatic organisms with a LC_{50} of 4 mg/dm^3 for fish and a half-lifetime of 38 days in water (Da Silva et al., 2013).

A commercial formulation of the pesticide Globaryll (active component 6-benzyladenine, also called 6-benzylaminopurine) is a synthetic cytokinin that stimulates cell division in plants. Among other actions, it spurs plant growth, sets blossoms, and improves fruit quality (Zhang et al., 2010). Since it is widely used, it was found in the environment in low concentrations. Therefore, 6-benzyladenine toxicity was assessed through various studies. In mammals, 6-benzyladenine is shown to be harmful if swallowed. This substance is of low acute toxicity after dermal and inhalation exposure, it is neither a skin or eye irritant nor a skin sensitizer. The risk to birds and mammals from consumption of contaminated drinking water with 6-benzyladenine was assessed as low. The risk to bees, earthworms, non-target soil micro-organisms, non-target plants, and the function of wastewater treatment plants was assessed as low (European Food Safety, 2010; Wu et al., 2014).

This study observed the positive effects of Ormoroc and Globaryll on increased fruit weight, diameter, and fruit firmness of sour (cv. Erdi botermo) and sweet (cv. Regina) cherries. To our knowledge, stability studies of commercial formulations Ormoroc and Globaryll in aqueous solutions have not been conducted. Therefore, a kinetic study on its hydrolysis and photolysis was undertaken. Ormoroc and Globaryll stability were monitored at $25 \text{ }^\circ\text{C}$ in the dark. The solar stability of these pesticides was assessed under the influence of UV irradiation.

Materials and Methods

The experiment was conducted during the season 2022 on the sour (cv. Erdi botermo) and sweet (cv. Regina) cherry trees. The trees of both cultivars were planted in 2019, with planting distance $5 \times 3 \text{ m}$ (sour cherry), and $4 \times 1.5 \text{ m}$ (sweet cherry). Standard agrotechnical procedures including pruning, irrigation, fertirrigation, removing grass cover between rows, the control of weeds, pests and diseases were performed during the growing season.

The trial was set up in a completely randomized block design with three replications and three trees per replication (9 trees per treatment). The trees were sprayed with backpack sprayer (STIHL SR-420) with run-off (800 l per hectare). The chemical used were Ormoroc (containing 7.5% active ingredient (a.i) 1-naphtylacetic acid) and Globaryll (containing 9.5% a.i. 6-benzyladenine). The following bioregulator treatments were applied after full bloom: 20 mg/dm^3 1-naphtylacetic acid, 100 mg/dm^3 6-benzyladenine and untreated control.

At harvest, 30 fruits were randomly chosen for the analyses of the fruit size (weight, diameter, height and width) and fruit firmness. Fruit firmness was measured with Fruit Texture Analyser, FTA-25 (Güss System, RSA) penetrometer fitted with 5 mm diameter prob and measured values were expressed in kg/cm^2 .

For observing bioregulators stability in water, commercial formulations of Ormoroc (Rocca frutta, Italy) and Globaryll (Globachem, Belgium) were used as obtained. The stock solutions of 0.05

mmol/dm³ of Ormoroc and Globaryll were made using ultrapure water (UPW). The solutions were protected from light and stored in a dark place at 25 °C.

Hydrolysis of Ormoroc and Globaryll solution was carried out in the dark in a volumetric flask (Duran®). Experiments were performed at 25 ± 1 °C. Hydrolysis of Ormoroc and Globaryll dissolved in UPW was monitored for one month. Ormoroc and Globaryll hydrolysis monitoring samples were taken in the chosen time intervals.

Direct photolysis was carried out in a cell made of Pyrex glass (total volume of *ca.* 40 cm³, liquid layer thickness 35 mm), with a plain window where the light beam was focused. Experiments were performed using 20 cm³ of 0.05 mmol/dm³ Ormoroc or Globaryll solutions. The cell was equipped with a magnetic stirring bar and water circulating jacket. Before irradiation, the photochemical cell was placed on a magnetic stirrer and thermostated at 25 ± 1 °C with mixing in a stream of O₂. The O₂ flow was 3.0 cm³/min in all degradation experiments. A high-pressure mercury lamp (125 W, Philips, HPL-N, emission bands at 290, 293, 296, 304, 314, 335, and 366 nm, with maximum emission at 366 nm) was used as the UV irradiation source.

Kinetics of Ormoroc and Globaryll removal from the water was measured spectrophotometrically. The absorption maximums of Ormoroc and Globaryll were 222 nm and 269 nm, respectively. Absorption spectra were recorded on a double-beam T80+ UV/Vis Spectrometer (UK) at a fixed slit width (2 nm), using quartz cell (1 cm optical length) and computer-loaded UV Win 5 data software. Absorption spectra were recorded between 200 nm to 400 nm.

The data was processed by factorial ANOVA using Software Statistica version 14.0 (StatSoft Inc., Tulsa, USA). Duncan post hoc test was used to test the significance of differences (P≤0.05) among the mean values.

Results and discussion

Globaryll increased fruit weight and fruit diameter of Erdi botermo, while Ormoroc had no effect (Table 1). Booth, Ormoroc and Globaryll increased Regina fruit weight compared to control (15.9 and 11.4%, respectively). These treatments also increased Regina fruit firmness, while the fruit diameter was increased only by Globaryll treatment. Our results are in agreement with Zeman et al. (2013) who observed increasement of the Regina fruit weight up to 11.9% in 1-naphtylacetic acid treatment.

Table 1. Fruit size and fruit firmness of sour (cv. Erdi botermo) and sweet (cv. Regina) cherry fruits treated with bioregulators

Treatment	Sour cherry				Sweet cherry					
	Fruit weight	Fruit height	Fruit diameter	Fruit width	Fruit firmness	Fruit weight	Fruit height	Fruit diameter	Fruit width	Fruit firmness
Contol	5.6 ^b	19.1 ^a	21.5 ^b	19.3 ^a	5.1 ^a	8.8 ^b	25.1 ^a	25.4 ^b	22.2 ^a	15.3 ^b
Ormoroc	5.8 ^b	19.4 ^a	21.7 ^b	19.6 ^a	5.5 ^a	9.8 ^a	26.2 ^a	26.3 ^{ab}	23.1 ^a	17.0 ^a
Globaryll	6.4 ^a	19.9 ^a	22.4 ^a	19.9 ^a	5.3 ^a	10.2 ^a	26.2 ^a	27.1 ^a	23.3 ^a	18.4 ^a
Statistical significance	*	ns	*	ns	ns	*	ns	*	ns	*

The means in columns with the different lowercase letter do significantly differ according to the Duncan post hoc test (P≤0.05).

The results indicate the benefits of applying bioregulators to the examined plant species. However, since pesticides reach the surface and underground water after treating plants, this study analyzed hydrolysis and direct photolysis in water to test the stability of commercial formulations of the investigated compounds.

Hydrolysis is an important degradation pathway for substances in the environment, besides photolysis or redox reactions (de Melo Plese et al., 2005). Studies by many authors suggest that abiotic

transformations, such as hydrolysis and photolysis, could be significant for the environmental outlay of substances occurring in nature (Alexandrino et al., 2017; Armaković et al., 2018). As a starting point, we have monitored the Ormoroc and Globaryll hydrolysis in UPW at 25 ± 1 °C (Figure 1). After 28 days, 22.3% of Ormoroc hydrolyzed under these conditions (Figure 1a). Therefore, since Ormoroc and its active component 1-naphtylacetic acid did not show toxic and hazardous effects on the environment, hydrolysis proved to be an effective way for the degradation of Ormoroc residues in the environment. On the other hand, as can be seen (Figure 1b), Globaryll did not hydrolyze after 28 days. It was reported that the active component of Globaryll, 6-benzyladenine showed stable hydrolysis (pH 5, 7, and 9). Photolysis may contribute to the degradation of 6-benzyladenine in water (European Food Safety, 2010). With that in mind, as well as the absorption spectra of Ormoroc and Globaryll, our further studies were directed to direct UV photolysis.

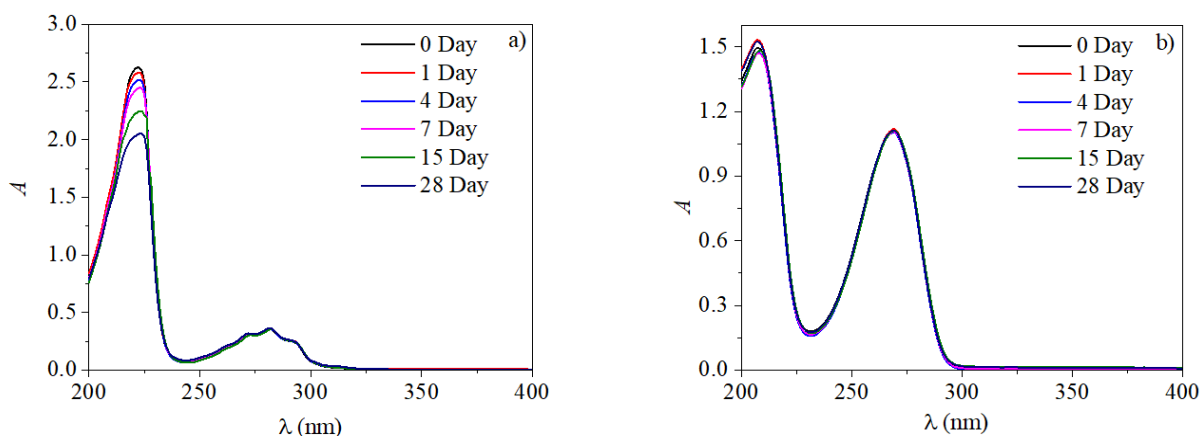
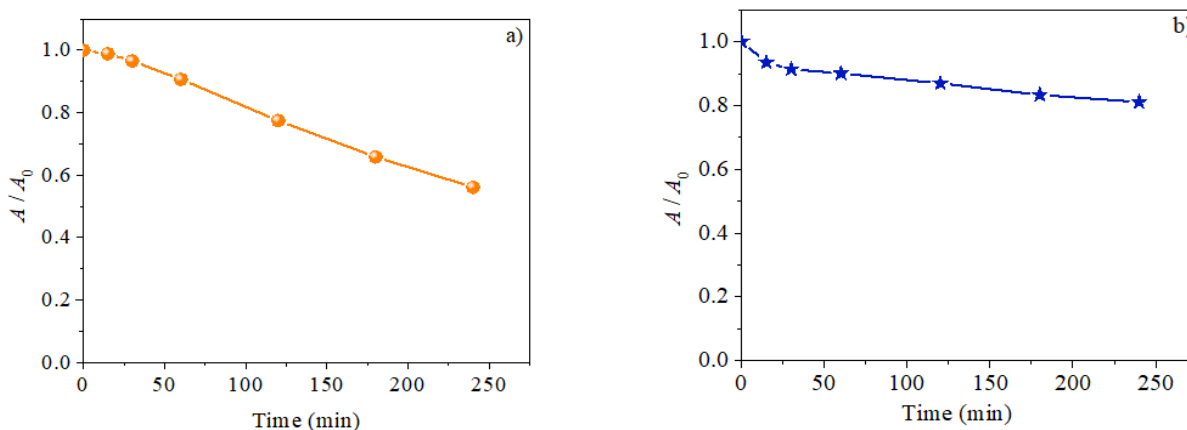


Figure 1. Absorption spectra after hydrolysis of Ormoroc (0.05 mmol/dm^3) (a) and Globaryll (0.05 mmol/dm^3) (b) in observed intervals of time

The efficiency of direct photolysis depends on the target compounds' ability to absorb the emitted light and on the relevant quantum yields. The efficiency of direct photolysis of Ormoroc was performed at natural pH (8.0) under the influence of UV irradiation (Figure 2a). It was found that 43.9% of Ormoroc was degraded by direct photolysis after 240 min of irradiation. In the case of Globaryll (Figure 2b), degradation efficiency was 18.9% under UV irradiation at natural pH (8.0). Since UV light is a part of solar radiation, these results suggest that investigated formulations could be degraded in the environment using solar radiation. Figures 2c and 2d show absorption spectra of Ormoroc and Globaryll direct photolysis.



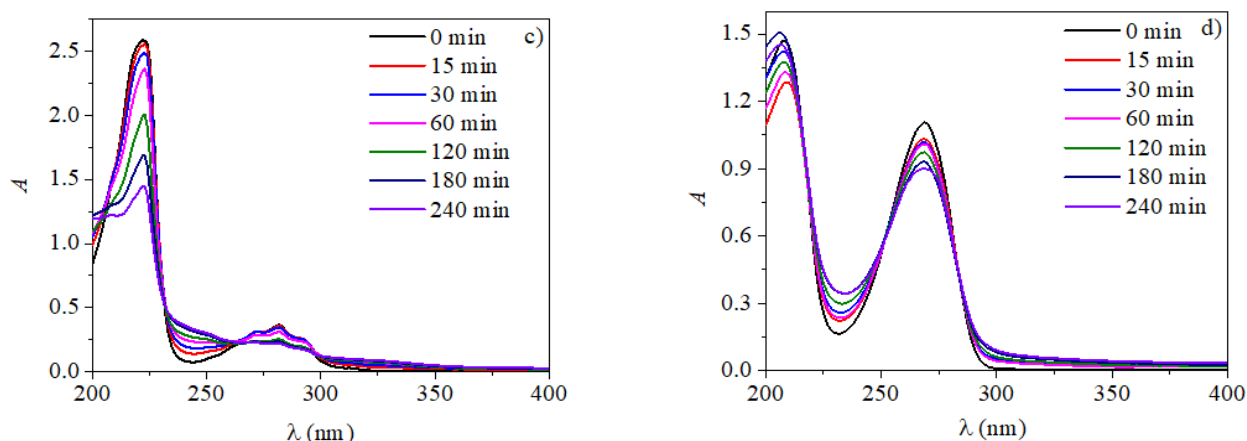


Figure 2. Kinetics of direct photolysis of Ormoroc (0.05 mmol/dm^3) (a) and Globaryll (0.05 mmol/dm^3) (b), and absorption spectra obtained during direct photolysis of Ormoroc (c) and Globaryll (d) in observed intervals of time

Conclusion

With the increasing food demand, pesticide use has increased globally. These chemicals are used widely in agriculture because of their benefits, such as controlling harmful organisms and weeds that destroy crops and threaten people's lives. They help farmers to provide better growth of crops which increases agricultural productivity. However, a line is thin between the positive and negative effects of pesticide use. Therefore, it is necessary to monitor their stability in the environment. Hydrolysis and photolysis are suggested as effective and economical ways of removing these substances from the environment.

This paper assesses the positive effects and solar stability of commercial pesticides Ormoroc and Globaryll used to treat grapevine and fruits. They have increased fruit weight, diameter and fruit firmness of sour (cv. Erdi botermo) and sweet (cv. Regina) cherries. Hydrolysis was an important degradation pathway for Ormoroc. After 28 days of Ormoroc hydrolysis at $25 \pm 1^\circ\text{C}$, 22.3% of Ormoroc was hydrolyzed. An effective way for degradation of both, Ormoroc and Globaryll was direct UV photolysis. After 240 min of direct hydrolysis, 43.9% and 18.9% of Ormoroc and Globaryll were degraded, respectively. Since sunlight contains UV light, these results suggested that investigated formulations could be degraded in the environment by using solar radiation.

References

- Alexandrino, D. A. M., Mucha, A. P., Almeida, C. M. R., Gao, W., Jia, Z. & Carvalho, M. F. (2017). Biodegradation of the veterinary antibiotics enrofloxacin and ceftiofur and associated microbial community dynamics. *Science of The Total Environment*, 581, 359–368. <https://doi.org/10.1016/j.scitotenv.2016.12.141>
- Armaković, S. J., Armaković, S., Četojević-Simin, D. D., Šibul, F. & Abramović, B. F. (2018). Photocatalytic degradation of 4-amino-6-chlorobenzene-1, 3-disulfonamide stable hydrolysis product of hydrochlorothiazide: Detection of intermediates and their toxicity. *Environmental Pollution*, 233, 916–924. <https://doi.org/10.1016/j.envpol.2017.08.090>
- Da Silva, E. S., Wong-Wah-Chung, P., Burrows, H. D. & Sarakha, M. (2013). Photochemical degradation of the plant growth regulator 2-(1-Naphthyl) acetamide in aqueous solution upon UV irradiation. *Photochemistry and Photobiology*, 89(3), 560–570. <https://doi.org/10.1111/php.12050>
- De Melo Plese, L. P., Paraiba, L. C., Foloni, L. L. & Trevizan, L. R. P. (2005). Kinetics of carbosulfan hydrolysis to carbofuran and the subsequent degradation of this last compound in irrigated

- rice fields. *Chemosphere*, 60(2), 149–156.
<https://doi.org/10.1016/j.chemosphere.2005.02.049>
- European Food Safety. (2010). Conclusion on the peer review of the pesticide risk assessment of the active substance 6-benzyladenine. *EFSA Journal*, 8(10), 1–49.
<https://doi.org/10.2903/j.efsa.2010.1716>
- Faostat, F. A. O. (2021). Pesticide indicators—Agri-Environmental indicator on the use of pesticides per area of cropland. *Food and Agricultural Organisation: Rome, Italy*.
- Hileman, B. (1994). Environmental estrogens linked to reproductive abnormalities, cancer. *Chemical and Engineering News*, 72(5), 19–23. <http://dx.doi.org/10.1021/cen-v072n005.p019>
- Kocaman, A. Y. & Güven, B. (2016). In vitro genotoxicity assessment of the synthetic plant growth regulator, 1-naphthaleneacetamide. *Cytotechnology*, 68(4), 947–956.
<https://doi.org/10.1007%2Fs10616-015-9847-z>
- Link, H. (2000). Significance of flower and fruit thinning on fruit quality. *Plant Growth Regulation*, 31(1), 17–26. <http://dx.doi.org/10.1023/A:1006334110068>
- Ssemugabo, C., Guwatudde, D., Ssempebwa, J. C. & Bradman, A. (2022). Pesticide residue trends in fruits and vegetables from farm to fork in Kampala Metropolitan area, Uganda—A mixed methods study. *International Journal of Environmental Research and Public Health*, 19(3).
<https://doi.org/10.3390/ijerph19031350>
- Wu, X., He, J., Chen, J., Yang, S. & Zha, D. (2014). Alleviation of exogenous 6-benzyladenine on two genotypes of eggplant (*Solanum melongena* Mill.) growth under salt stress. *Protoplasma*, 251(1), 169–176. <https://doi.org/10.1007/s00709-013-0535-6>
- Zeman, S., Jemrić, T., Čmelik, Z., Fruk, G., Bujan, M. & Tompić, T. (2013). The effect of climatic conditions on sweet cherry fruit treated with plant growth regulators. *Journal of Food, Agriculture & Environment*, 11(2), 524–528. <https://www.bib.irb.hr/604460>
- Zhang, H., Horgan, K. J., Reynolds, P. H. S. & Jameson, P. E. (2010). 6-Benzyladenine metabolism during reinvigoration of mature *Pinus radiata* buds in vitro. *Tree Physiology*, 30(4), 514–526.
<https://doi.org/10.1093/treephys/tpp130>

Original scientific article

COMPARATIVE ASSESSMENT OF ZINC IONS SORPTION AND RETENTION BY PROSPECTIVE UNCONVENTIONAL SOIL ADDITIVES

Ivana Smičiklas¹, Marija Egerić¹, Mihajlo Jović¹

¹„VINČA” Institute of Nuclear Sciences - National Institute of the Republic of Serbia, University of Belgrade, Belgrade, Serbia

Abstract

Mining, combustion of coal and waste, and steel processing are the main industrial activities that trigger the emission of large amounts of Zn, which reach the soil and pose a risk to its services, functions, and groundwater quality. A frequently associated process is soil acidification, reducing soil's ability to retain incoming toxic metals. The soil treatments with reactive, low-cost, and locally available materials might be a straightforward approach to decreasing the mobility of toxic metals and alleviating the environmental risks. This study aimed to compare Zn ions sorption and retention by several unconventional soil additives (seashell waste, bone char, and red mud) against the performance of acidic soil. Batch experiments of Zn ions sorption were initially performed using solutions with different Zn concentrations, followed by the determination of sorbed Zn stability in an acidic medium. The waste materials exhibited higher pH values and superior Zn sorption capacities with respect to the soil. The desorption experiment exposed different mechanisms of Zn ions fixation by studied materials. While the substantial amounts of Zn sorbed by seashells, red mud, as well as soil were released in the scope of the ion exchange and carbonate fraction, sensitive to pH decrease, the bone char preserved Zn in more stable fractions. The investigated waste materials can potentially prevent Zn leaching through the soil profile, with the bone char demonstrating the most significant capability for long-term retention performance.

Keywords: soil additives, zinc, sorption, retention, soil remediation.

Introduction

The overall mean zinc (Zn) concentration in soil is 50–55 mg/kg and typically does not exceed 300 mg/kg (Noulas et al., 2018). Zinc ions are essential in numerous plant metabolic processes, thus, their deficiency causes reduced growth, tolerance to stress, and chlorophyll synthesis (Sharma et al., 2013). It is also essential for animals' and humans' health, affecting gastrointestinal, central nervous, immune, skeletal, and reproductive systems (Roohani et al., 2013). While the scarcity of available soil Zn represents an important soil quality issue and a cause of malnutrition problems in some parts of the world, Zn concentrations in the soil are rising in many other areas worldwide due to anthropogenic additions.

Characteristic industrial activities that generate and emit the most of Zn are mining, steel processing, and coal and waste combustion (Wuana & Okieimen, 2011). Like other heavy metals, Zn becomes a contaminant in the soil if its total concentrations are elevated compared to natural background levels and its distribution in the soil shifts towards chemical forms with greater mobility and bioavailability. The pollution in croplands results in soil–plant–food transfer of Zn and exposure of numerous living organisms through this chain.

Soil contamination and surface runoff infiltration to the groundwater aquifers result in groundwater contamination with Zn and other toxic metals. Given that groundwater is the most significant source of drinking water in the European Union and the resource for agriculture and industry (EC, 2008), the safety of its quality in part refers to the prevention of metals leaching from the contaminated soil. Numerous techniques for on-site or off-site treatment of the soil contaminated with Zn are developed. Methods based on the physical separation of Zn from soil matrix include chemical leaching using a variety of agents such as carboxyalkylthiosuccinic acid (CETSA), copolymer of maleic and acrylic acid (MA/AA), ethylenediamine tetra acetic acid (EDTA) (Xia et al., 2019), citric acid (Gu et al., 2018; Hu et al., 2021), tartaric acid (Alman-Abad et al., 2020), but also inorganic acids (HCl, H₂SO₄, and H₃PO₄) (Ko et al., 2006). Phytoremediation (Yan et al., 2020), electro-kinetic remediation (Rezaee et al., 2017) and microbial-induced remediation of Zn pollution (Zhan & Qian, 2016) are also proposed. Furthermore, stabilization/solidification of soil Zn can be achieved using appropriate agents. Recently, cost-effective materials, like limestone calcined clay cement, a low-carbon/cost cementitious material (Reddy et al., 2020), or cement–soda residue (Zha et al., 2021), were found applicable for Zn solidification. The perspective approach is *in situ* stabilization of Zn in soil not by targeting encapsulation but by using amendments (Kumpiene et al., 2008). The role of amendments is to change the chemical forms of Zn in the soil, making it less mobile and less available to plants. Zinc can be chemically stabilized by mixing the soil with liming materials (Martin & Ruby, 2004), phosphate salts (Wuana & Okieimen, 2011), bentonite (Chaves et al., 2017), zeolite, sepiolite, and palygorskite (Ye et al., 2022).

The useful amendment for reducing Zn environmental availability should be effective, inexpensive, available, easy to apply, and non-toxic to the plants. The aim of this study was to evaluate the prospects of several low-cost materials as additives for Zn stabilization in the soil. The sorption and retention of Zn ions by waste-derived materials (seashell waste, bone char, and red mud) were tested in the range of Zn concentrations, and their performance was compared with the Zn sorption/retention ability of a model acidic soil.

Materials and Methods

Waste-derived materials with different compositions were selected, i.e., calcium carbonate-based seashell powders, calcium phosphate-based animal bones, and Fe-oxide-rich bauxite residue. A composite sample of seashells from the shores of the Aegean Sea in Greece (SW), as well as the samples of *Mytilus galloprovincialis* (MG) shells collected from the mussel farms in the Boka Kotorska bay (Montenegro). The material denoted BC was obtained by the treatment of animal (bovine) bones at 400 °C in an air atmosphere (Dimović et al., 2009). Both the seashells and BC were ground to pass the 0.2 mm sieve. The bauxite residue (red mud, RM) was collected from the Zvornik Alumina Refinery, Republic of Srpska, BiH, and used as a fine powder after rinsing with water and drying at room temperature (Egerić et al., 2019). For comparison, the acidic soil sampled near the mining and metallurgical complex in Bor, Serbia, was used (Egerić et al., 2019).

The sorption of Zn ions was first examined in a series of batch experiments by mixing the investigated solid samples and Zn solutions at a solid-to-solution ratio 1g/10 mL. The solutions with Zn ions concentrations in the range 10⁻⁴ – 5×10⁻³ mol/L were prepared from Zn(NO₃)₂ salt in the inert background electrolyte (10⁻² mol/L NaNO₃). The initial pH of all solutions was set to pH 5.0±0.2. The suspensions were agitated at room temperature using an end-over-end shaker (10 rpm) for 48 h. Subsequently, the solid and liquid phases were separated by centrifugation (10 min, 9000 rpm) and filtration. The residual Zn concentrations in the supernatants were measured by Inductively Coupled Plasma Optical Emission Spectroscopy (ICP-OES, Perkin Elmer Avio 200), and the quantities of Zn sorbed were calculated from the difference between initial and final concentrations. Final pH values

in liquid phases were measured as well, and the concentrations of Ca ions released into the solution following the Zn ions sorption.

For the Zn desorption experiments, residues from sorption experiments were resuspended in 0.11 mol/L acetic acid at the solid-to-solution ratio of 1g/40mL and agitated at room temperature (21 ± 2 °C) for 16 h. These conditions correspond to the first step of the sequential extraction scheme recommended by the European Community Bureau of Reference (BCR) (Ure et al., 1993), which separates the most mobile metal fraction. After centrifugation (10 min, 9000 rpm) and filtration, the extracted Zn concentrations were measured using ICP-OES.

Results and discussion

Two biological materials were used in the experiments. By their composition, mussel shells are a very rich source of biogenic calcium carbonate (>95%) regardless of the shellfish (Egerić et al., 2018), while (BC) obtained from animal bones is a calcium-phosphate product with the structure of non-stoichiometric hydroxyapatite (Dimović et al., 2009). The RM was composed of oxide compounds and desilication products that result from the Bayer process, with the largest share of hematite (Egerić et al., 2019). The soil was characterized as clay loam, non-carbonate, with an acidic reaction with water (pH 4.93) (Egerić et al., 2019).

As shown in Figure 1a., investigated additives have sorbed Zn ions with very high efficiency viewing the entire range of initial Zn concentrations, specifically SW 98.2-99.7%, MG 96.6-98.7%, B 98.7-99.7%, and RM 99.5-99.9%. Quite the contrary, the soil exhibited a sharp decline in Zn removal efficiency from 93.3% to 62.3%, with a rise in Zn addition.

The experiment outlined the finite capacity of the acidic soil for Zn, which inevitably leads to the leaching of Zn into deeper soil layers or watercourses at higher loads. Amendments, on the other hand, provide sorption sites with a higher affinity for Zn ions with respect to the soil and the pH conditions favorable for limiting the water-soluble fraction of the metal (Figure 1b).

At a given solid-to-solution ratio (1:10), the highest pH values in solution are detected after reaction with RM (10.1-9.1), followed by SW (9.2-7.6), MG (8.6-7.5), BC (7.8-7.4), and finally the soil (5.4-4.8). Processing Bauxite ore via the Bayer process requires the use of a strong base (NaOH), so the residue is strongly alkaline (typically with $\text{pH} > 12$). By washing the red mud with water, the free base was removed but the product still exhibits alkaline properties due to the presence of desilication products (DSP) with high pH and buffering capacity (Gräfe et al., 2011). Seashells and BC as well provide H^+ neutralization through reaction with bio-carbonate and bio-apatite phases. Since pH is one of the most significant soil quality indicators (Bünemann et al., 2018), adding investigated material could benefit the acidic soil through an increase in pH. However, the materials' mechanisms and capacities for pH regulation differ significantly.

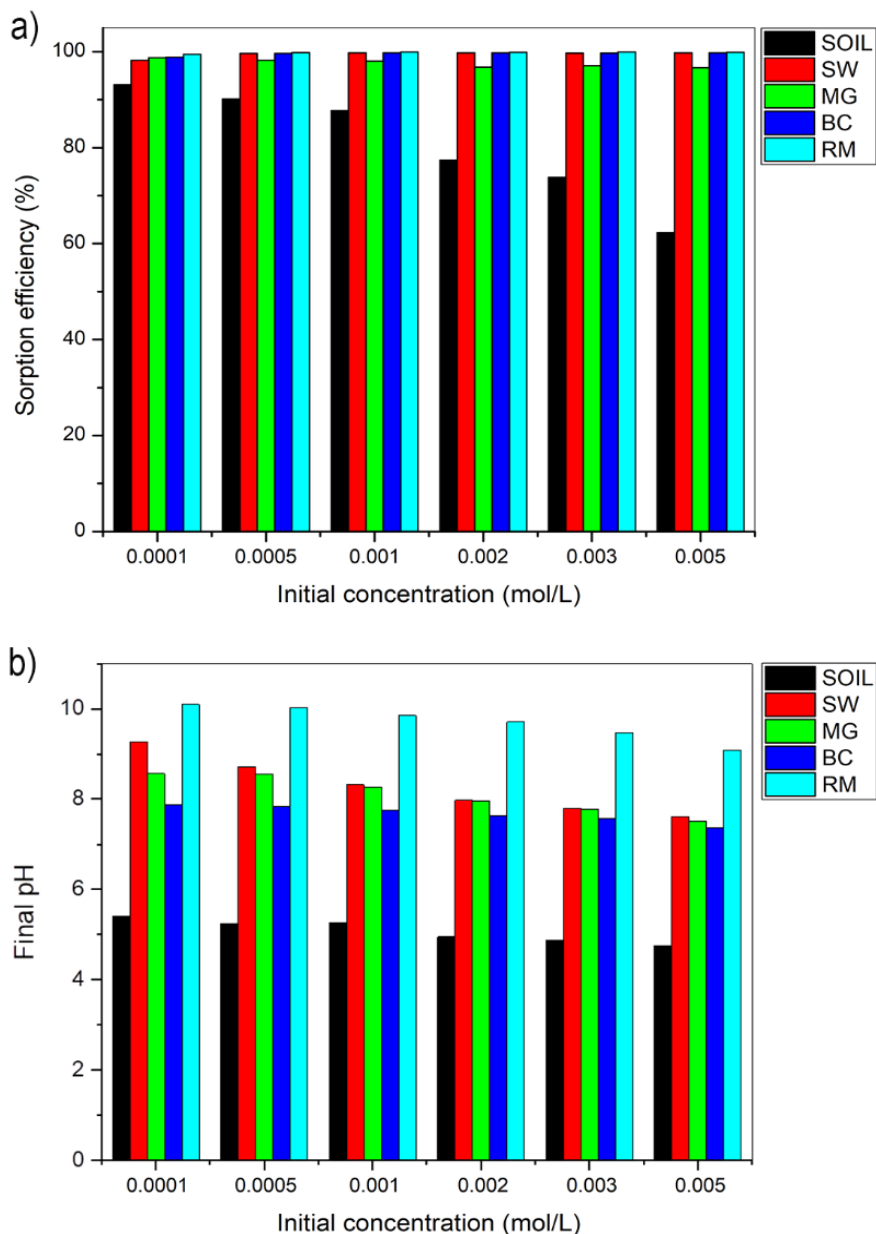


Figure 1. The influence of initial Zn concentration in the solution on the a) Zn sorption efficiency (%) by the investigated unconventional additives and the model soil, and b) final pH values of the solution. Initial pH =5.0, solid-to-solution ratio 1:10, contact time 48 h

After the Zn sorption by all tested materials, the final pH values decreased with the increasing concentration of sorbate (Figure 1b). Over the examined range of Zn concentrations, the final pH values declined by about 1 pH unit using RM and seashell powders, by 0.7 pH units using soil, and by 0.5 pH units using BC. These pH changes may indicate the specific sorption of Zn ions by active protonated surface groups and the release of H⁺ ions into the solution.

Relationships between the amounts of Zn ions sorbed and Ca ions released by the additives and the soil are shown in Figure 2. It is noticeable that the application of seashell powders leads to the greatest increase in aqueous Ca concentration (molar ratio Ca:Zn>1:1) due to a partial dissolution of the samples and Zn binding by displacement of Ca in carbonates or precipitation of Zn-carbonate phase. The ratio of sorbed and released ions was linear for the BC and the soil, indicating the ion exchange process and/or dissolution/precipitation mechanism in the case of BC. For the same amount of sorbed

Zn, the RM released the smallest amounts of Ca (Figure 2). RM provides numerous active centers for Zn ion sorption as a composite material with a high hematite content. The addition of different forms of iron, such as hydrous oxides, steel shot, steel sludge, furnace slag, and zero-valent iron, has previously been shown to reduce the leachability and bioaccessibility of soil zinc (Martin & Ruby, 2004). Metal oxides can strongly bind metals through specific sorption and co-precipitation (Derakhshan Nejad et al., 2018).

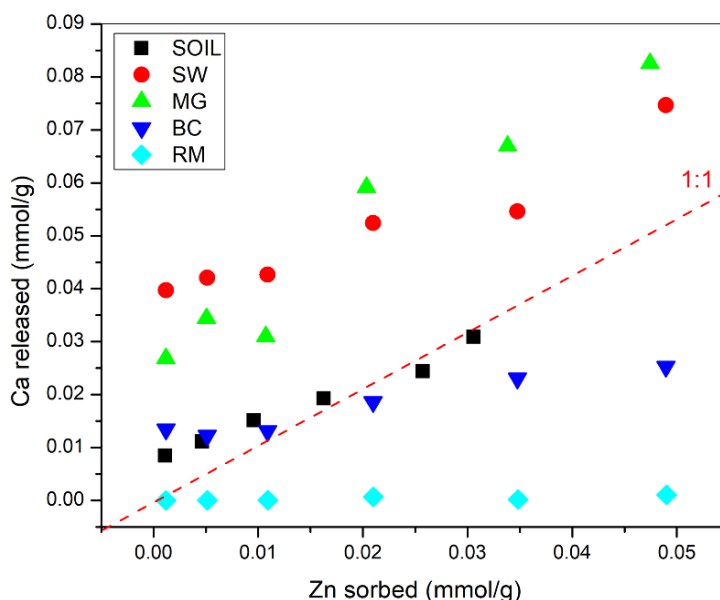


Figure 2. Relationship between the sorbed amounts of Zn and amounts of Ca ions released into the solution by investigated samples

The BCR method proved to be applicable for the assessment of Zn mobility in the soil, showing correlations with the soil constituents and the plant contents (Fernández-Ondoño et al., 2017). The fraction of Zn in the most mobile phase of the BCR extraction protocol was determined to assess the long-term stability of Zn sorbed by different samples. The results of exposure of the residues obtained following Zn sorption to the acetic acid solution are summarized in Figure 3. It can be concluded that Zn extraction in the scope of the ion exchange and carbonate fraction generally increases with the increase in the Zn load, but absolute amounts differ markedly between studied materials.

For soil, maximally, 58% of the sorbed Zn was found in the most mobile fraction. Seashell powders SW and MG accumulated the highest share of Zn in the acid-soluble fraction (up to 86%), whereas the percentage in RM reached 64%, at the highest Zn load. Previously, the positive correlation between Zn concentration extracted within BCR1 soil fraction was established with the content of CaCO_3 in the soil, as well as with the percentages of Fe_{ox} in some soils (Fernández-Ondoño et al., 2017). In practice, this indicates the potential re-mobilization of Zn ions if the pH of the medium drops sufficiently, which would require periodic repetition of the treatment. On the other hand, with less than 1 % extracted with acetic acid, additive BC proves to accumulate Zn in more stable fractions. Results implied that Zn was immobilized as metal-phosphate precipitates resistant to soil acidification, in accordance with the previous research conducted using various phosphate-based amendments (Kumpiene et al., 2008).

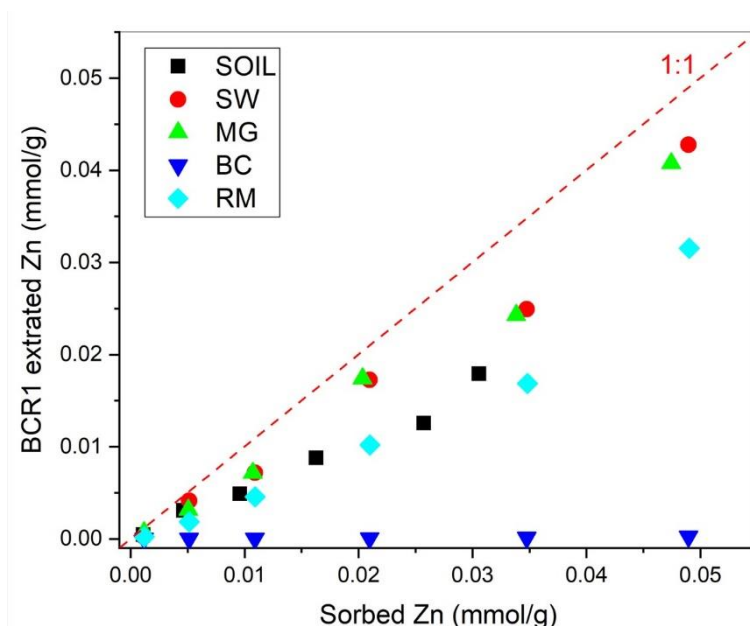


Figure 3. Relationship between the sorbed amounts of Zn and amounts of Zn extracted in the scope of the acid-soluble (BCR1) fraction

Generally, alkaline materials, Fe-oxides, phosphorus materials, and clays were found to be the most efficient amendments for Zn immobilization in the soil (Kumpiene et al., 2008). Identifying and applying waste materials and by-products of various industries, which according to their composition, correspond to one of these classes and do not pose a risk to the living world, is a step toward sustainable soil management. After screening out the efficiency of the potential additives, experiments should be conducted with the specific soil to determine the best soil/additive ratio for the field-fixing treatment.

Conclusion

The materials studied in this work are available, cheap, easy to handle and apply, and show higher capacity at binding Zn compared to model acidic soil. Consequently, they may be an effective alternative to frequently used soil remediation agents, like limestone, lime, or natural minerals. Application in the soil also has positive effects on reducing the accumulated amounts of these waste materials. Considering their alkaline nature, treatments with selected materials would affect the increase in the soil pH, thus improving soil capacity for natural attenuation of mobility and leaching of toxic metals. Comprehensive research is needed to optimize the addition rates of such unconventional additives, considering not only toxic metals' mobility but other essential properties of the soil and its future use.

References

- Alman-Abad, Z. S., Pirkharrati, H., Asadzadeh, F. & Maleki-Kakelar, M. (2020). Application of response surface methodology for optimization of zinc elimination from a polluted soil using tartaric acid. *Adsorption Science & Technology*, 38(3–4), 79–93. <https://doi.org/10.1177/0263617420916592>
- Bünemann, E. K., Bongiorno, G., Bai, Z., Creamer, R. E., De Deyn, G., de Goede, R., Fleskens, L., Geissen, V., Kuyper, T. W., Mäder, P., Pulleman, M., Sukkel, W., van Groenigen, J. W. & Brussaard, L. (2018). Soil quality – A critical review. *Soil Biology and Biochemistry*, 120,

- 105–125. <https://doi.org/10.1016/j.soilbio.2018.01.030>
- Chaves, L., Tito, G. & De Brito Chaves, I. (2017). Bentonite application in the remediation of zinc contamination soil. *Chemical Engineering Transactions*, 58, 745–750. <https://doi.org/10.3303/CET1758125>
- Derakhshan Nejad, Z., Jung, M. C. & Kim, K.-H. (2018). Remediation of soils contaminated with heavy metals with an emphasis on immobilization technology. *Environmental Geochemistry and Health*, 40(3), 927–953. <https://doi.org/10.1007/s10653-017-9964-z>
- Dimović, S., Smičiklas, I., Plečaš, I., Antonović, D. & Mitrić, M. (2009). Comparative study of differently treated animal bones for Co²⁺ removal. *Journal of Hazardous Materials*, 164(1), 279–287. <https://doi.org/10.1016/j.jhazmat.2008.08.013>
- EC (2008). European Commission, Groundwater Protection in Europe, Luxembourg: Office for Official Publications of the European Communities, 35 pp. ISBN 978-92-79-09817-8. <https://ec.europa.eu/environment/water/water-framework/groundwater/pdf/brochure/en.pdf>
- Egerić, M., Smičiklas, I., Dojčinović, B., Sikirić, B., Jović, M., Šljivić-Ivanović, M. & Čakmak, D. (2019). Interactions of acidic soil near copper mining and smelting complex and waste-derived alkaline additives. *Geoderma*, 352, 241–250. <https://doi.org/10.1016/j.geoderma.2019.06.015>
- Egerić, M., Smičiklas, I., Mraković, A., Jović, M., Šljivić-Ivanović, M., Antanasijević, D. & Ristić, M. (2018). Experimental and theoretical consideration of the factors influencing cationic pollutants retention by seashell waste. *Journal of Chemical Technology & Biotechnology*, 93(5), 1477–1487. <https://doi.org/10.1002/jctb.5516>
- Fernández-Ondoño, E., Bacchetta, G., Lallena, A. M., Navarro, F. B., Ortiz, I. & Jiménez, M. N. (2017). Use of BCR sequential extraction procedures for soils and plant metal transfer predictions in contaminated mine tailings in Sardinia. *Journal of Geochemical Exploration*, 172, 133–141. <https://doi.org/10.1016/j.gexplo.2016.09.013>
- Gräfe, M., Power, G. & Klauber, C. (2011). Bauxite residue issues: III. Alkalinity and associated chemistry. *Hydrometallurgy*, 108(1–2), 60–79. <https://doi.org/10.1016/j.hydromet.2011.02.004>
- Gu, F., Zhang, Y., Tang, Q., Lu, C. & Zhou, T. (2018). Remediation of Zn(II)- and Cu(II)-contaminated soil using citric acid and citric acid-containing wastewater. *International Journal of Civil Engineering*, 16(11), 1607–1619. <https://doi.org/10.1007/s40999-018-0300-5>
- Hu, W., Niu, Y., Zhu, H., Dong, K., Wang, D. & Liu, F. (2021). Remediation of zinc-contaminated soils by using the two-step washing with citric acid and water-soluble chitosan. *Chemosphere*, 282, 131092. <https://doi.org/10.1016/j.chemosphere.2021.131092>
- Ko, I., Lee, C.-H., Lee, K.-P., Lee, S.-W. & Kim, K.-W. (2006). Remediation of soil contaminated with arsenic, zinc, and nickel by pilot-scale soil washing. *Environmental Progress*, 25(1), 39–48. <https://doi.org/10.1002/ep.10101>
- Kumpiene, J., Lagerkvist, A. & Maurice, C. (2008). Stabilization of As, Cr, Cu, Pb and Zn in soil using amendments – A review. *Waste Management*, 28(1), 215–225. <https://doi.org/10.1016/j.wasman.2006.12.012>
- Martin, T. A. & Ruby, M. V. (2004). Review of in situ remediation technologies for lead, zinc, and cadmium in soil. *Remediation Journal*, 14(3), 35–53. <https://doi.org/10.1002/rem.20011>
- Noulas, C., Tziouvalekas, M. & Karyotis, T. (2018). Zinc in soils, water and food crops. *Journal of Trace Elements in Medicine and Biology*, 49, 252–260. <https://doi.org/10.1016/j.jtemb.2018.02.009>
- Reddy, V. A., Solanki, C. H., Kumar, S., Reddy, K. R. & Du, Y.-J. (2020). Stabilization/solidification of zinc- and lead-contaminated soil using limestone calcined clay cement (LC3): An environmentally friendly alternative. *Sustainability*, 12(9), 3725.

- <https://doi.org/10.3390/su12093725>
- Rezaee, M., Kargar Ghomeshe, P. & Mohammad Hosseini, A. (2017). Electrokinetic remediation of zinc and copper contaminated soil: A simulation-based study. *Civil Engineering Journal*, 3(9), 690–700. <https://doi.org/10.21859/cej-03096>
- Roohani, N., Hurrell, R., Kelishadi, R. & Schulin, R. (2013). Zinc and its importance for human health: An integrative review. *Journal of Research in Medical Sciences : The Official Journal of Isfahan University of Medical Sciences*, 18(2), 144–157. <http://www.ncbi.nlm.nih.gov/pubmed/23914218>
- Sharma, A., Patni, B., Shankhdhar, D. & Shankhdhar, S. C. (2013). Zinc – An indispensable micronutrient. *Physiology and Molecular Biology of Plants*, 19(1), 11–20. <https://doi.org/10.1007/s12298-012-0139-1>
- Ure, A. M., Quevauviller, P., Muntau, H. & Griepink, B. (1993). Speciation of heavy metals in soils and sediments. An account of the improvement and harmonization of extraction techniques undertaken under the auspices of the BCR of the Commission of the European Communities. *International Journal of Environmental Analytical Chemistry*, 51(1–4), 135–151. <https://doi.org/10.1080/03067319308027619>
- Wuana, R. A. & Okieimen, F. E. (2011). Heavy metals in contaminated soils: A review of sources, chemistry, risks and best available strategies for remediation. *ISRN Ecology*, 1–20. <https://doi.org/10.5402/2011/402647>
- Xia, Z., Zhang, S., Cao, Y., Zhong, Q., Wang, G., Li, T. & Xu, X. (2019). Remediation of cadmium, lead and zinc in contaminated soil with CETSA and MA/AA. *Journal of Hazardous Materials*, 366, 177–183. <https://doi.org/10.1016/j.jhazmat.2018.11.109>
- Yan, A., Wang, Y., Tan, S. N., Mohd Yusof, M. L., Ghosh, S. & Chen, Z. (2020). Phytoremediation: A promising approach for revegetation of heavy metal-polluted land. *Frontiers in Plant Science*, 11(359), 1–15. <https://doi.org/10.3389/fpls.2020.00359>
- Ye, S., Wang, L. & Liu, T. (2022). Study of solidification and stabilization of heavy metals by passivators in heavy metal-contaminated soil. *Open Chemistry*, 20(1), 1–9. <https://doi.org/10.1515/chem-2021-0101>
- Zha, F., Liu, C., Kang, B., Yang, X., Zhou, Y. & Yang, C. (2021). Acid rain leaching behavior of Zn-contaminated soils solidified/stabilized using cement–soda residue. *Chemosphere*, 281, 130916. <https://doi.org/10.1016/j.chemosphere.2021.130916>
- Zhan, Q. & Qian, C. (2016). Microbial-induced remediation of Zn²⁺ pollution based on the capture and utilization of carbon dioxide. *Electronic Journal of Biotechnology*, 19, 29–32. <https://doi.org/10.1016/j.ejbt.2015.11.003>

Original scientific article

A GREEN ADSORBENT BASED ON WHEAT STARCH FOR REMOVAL OF SELECTIVE ORGANIC POLLUTANTS FROM AQUEOUS SOLUTIONS

Nataša Karić¹, Marija Vukčević², Marina Maletić¹, Mirjana Ristić², Aleksandra Perić-Grujić², Katarina Trivunac²

¹Innovation Center of Faculty of Technology and Metallurgy, 11120 Belgrade, Serbia

²University of Belgrade, Faculty of Technology and Metallurgy, 11120 Belgrade, Serbia

Abstract

The objective of this study was to evaluate the adsorption efficiency of a cationic functionalized wheat starch, obtained with betaine hydrochloride and glycidyl trimethylammonium chloride by an environmentally friendly process without the use of organic solvents. Surface functional groups of samples were characterized by Fourier transform infrared spectroscopy, the morphology of the materials was examined using scanning electron microscopy, the nitrogen content was determined by elemental analysis, while UV-VIS spectroscopy and liquid chromatography-tandem mass spectrometry were used for adsorption investigation. The efficiency of obtained cationic starches to adsorb the anionic and cationic dyes, as well as selected pharmaceuticals and pesticides was investigated. Adsorption experiments were performed in a batch system to determine the effect of contact time, initial concentration, and pH of the solution on the removal efficiency of crystal violet dye, which was chosen as the model for the detailed study of adsorption. Pseudo-first and pseudo-second order models were used to examine the adsorption kinetic, while Langmuir and Freundlich isotherm models were applied to equilibrium adsorption data. The results showed that environmentally and economically acceptable adsorbents prepared in this study could be effective in removing the examined organic pollutants.

Keywords: eco-friendly process, modification, starch, adsorption, organic pollutants.

Introduction

The production and consumption of chemical products by consumers are associated with growing environmental pollution and negative impacts on the health of the population. This growing environmental pollution that has attracted significant global scientific attention, in addition to the activities of the chemical and pharmaceutical industries, can be attributed to other anthropogenic activities such as urbanization, mining, agriculture, and domestic activities that also largely contribute to the higher pollution index (Wen et al., 2017). Global water pollution with organic pollutants is one of the biggest challenges of the 21st century. Most of these organics are only partially removed in conventional wastewater treatment plants, and many of these pollutants are released into the environment and can be found in their various parts. Due to the ecotoxicological effects, bioaccumulation, and carcinogenic effects of organic pollutants or their degradation products on the environment and humans, the wastewater must be properly treated before being discharged into the environment (Ge et al., 2016). The adsorption technique has proven to be one of the most attractive methods for wastewater treatment due to its simplicity, speed, efficiency, and availability of cheap adsorbents based on polysaccharides, such as starch, cellulose, chitin, chitosan, and lignin (Lawchoochaisakul et al., 2020).

The aim of this work was to evaluate the possibility of using cationic starches obtained by an environmentally friendly process as adsorbents to remove selected organic pollutants from aqueous solutions. Two starch derivatives were used, starch modified with betaine hydrochloride (CSt-B) and glycidyl trimethylammonium chloride (CSt-G). The adsorption efficiency of anionic (methyl orange, MO, and alizarin red S, ARS) and cationic (crystal violet, CV, and methylene blue, MB) dyes, as well as selected pesticides (imidacloprid, acetamiprid, dimethoate, carbamazepine, atrazine, propazine, malathion, tebufenozide) and pharmaceuticals (metabolites of metamizole 4AAA and 4FAA, lorazepam, diazepam, and clopidogrel) was also investigated. Based on the obtained results for the efficiency of absorption, as well as due to the smaller number of works dealing with its removal from wastewater, crystal violet dye was chosen as a model for a detailed study of adsorption. In order to determine the optimal reaction conditions, the kinetics of adsorption, adsorption isotherms, as well as the influence of the initial pH values were examined.

Materials and Methods

Wheat starch was purchased from Žito Promet, Serbia (moisture content $\leq 15.0\%$, ash content 0.46–0.55%, carbon content - 39.96%, and hydrogen content - 21.3%).

The modification of wheat starch was performed by a dry process of mixing starch with a cationic reagent in the presence of plasticizer and reaction catalysts according to the procedure described earlier (Karić et al. 2021).

Surface structure and morphology were studied by scanning electron microscopy (FE-SEM, TESCAN Mira3 XMU), while Fourier-transform infrared spectroscopy was used for the structural characterization of the materials (Nicolet iS10 spectrometer, Thermo Scientific).

The efficiency of dye adsorption was investigated at a constant adsorbent mass (0.1 g), initial concentration (50.0 mg dm⁻³) and solution volume (50.0 mL) for 180 min. The concentration of the dye in the solution was analyzed using a UV-VIS spectrophotometer. The adsorption efficiency of pesticides and pharmaceuticals was tested at a constant adsorbent mass (0.05 g), initial concentration (500.0 mg dm⁻³) and solution volume (50.0 mL) for 180 min. The concentration of tested pesticides and pharmaceuticals in the solution was analyzed by liquid chromatography-tandem mass spectrometry (LC-MS/MS). The influence of different initial concentrations (25.0 to 500.0 mg dm⁻³) and initial pH of the CV dye solution (25.0 mg dm⁻³, pH adjusted to 2-9) on the adsorption efficiency was determined at a constant mass of adsorbent (0.05 g) and the volume of the solution (25.0 mL) during 180 min. The kinetics of CV adsorption of the dye was investigated in the interval from 5 to 180 min at constant adsorbent mass (0.2 g), solution volume (100.0 mL) and initial concentration (50.0 mg dm⁻³).

The adsorption capacity, q (mg g⁻¹) and the removal efficiency, R (%) of selected pollutants from aqueous solutions can be calculated according to the equations (1) and (2) (Lin et al., 2017), respectively:

$$q = \left(\frac{C_0 - C_t}{m} \right) \cdot V \quad (1)$$

$$\% R = \left(\frac{C_0 - C_t}{C_0} \right) \cdot 100 \quad (2)$$

where C_0 and C_t (mg dm⁻³) are the concentration of an organic pollutant at the initial time and after time t (min), V is the volume of solution (cm³), and m is the amount of the adsorbent (g).

The nonlinear form of Langmuir model (Langmuir, 1918) and Freundlich model (Freundlich, 1906) are expressed by the equations (3) and (4), respectively:

$$q_e = \frac{q_{max} \cdot K \cdot C_e}{1 + K \cdot C_e} \quad (3)$$

$$q_e = K_f \cdot C_e^{1/n} \quad (4)$$

where q_e is the equilibrium adsorption capacity of the adsorbent (mg g^{-1}), q_{max} is the maximum adsorptive capacity of the adsorbent (mg g^{-1}), and C_e is the equilibrium concentration after adsorption (mg dm^{-3}), K is the Langmuir isotherm constant which describes the affinity between pollutants and adsorbents, K_F is Freundlich adsorption equilibrium constant which positively related to the adsorption capacity ($\text{dm}^3 \text{g}^{-1}$) and $1/n$ is the constant of adsorption intensity and describes surface heterogeneity.

The pseudo-first order model (Lagergren, 1898) and the pseudo-second order model (Ho & Mckay 1999) were expressed by the equations (5) and (6), respectively:

$$q_t = q_e \cdot (1 - e^{-k_1 \cdot t}) \quad (5)$$

$$q_t = q_e - \left(\frac{1}{q_e} - k_2 \cdot t \right)^{-1} \quad (6)$$

where q_t is the amount of pollutant adsorbed at the time t (mg g^{-1}), q_e is the adsorption quantity at equilibrium (mg g^{-1}), k_1 is the pseudo-first-order kinetic rate constant (min^{-1}), and k_2 is the pseudo-second-order kinetic rate constant ($\text{mg g}^{-1} \text{min}^{-1}$).

Results and discussion

The FTIR spectra of unmodified starch and cationic starch are shown in Fig. 1.

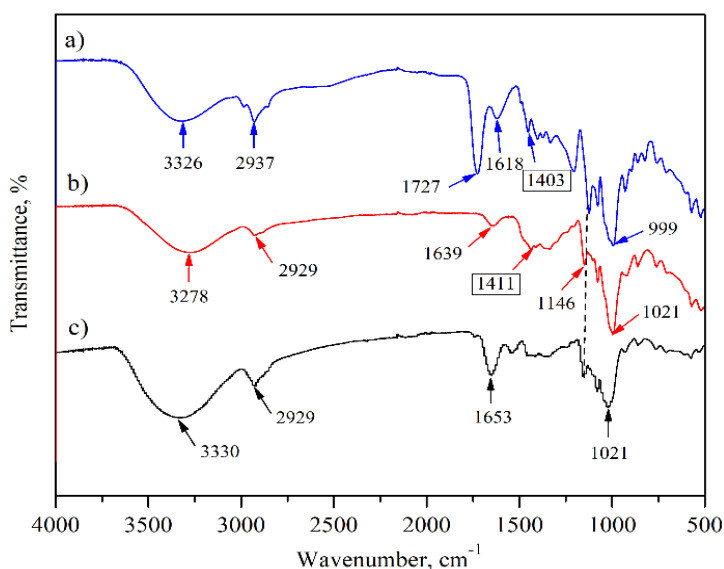


Figure 1. FTIR spectra of a) CSt-B, b) CSt-G, and c) unmodified starch

All the spectra showed a typical peak of starch backbone: wide hydroxyl bands at 3330, 3326, and 3278 cm^{-1} , the peaks at about 2929 and 2937 cm^{-1} which belong to C–H stretching vibrations, the peaks at 1653, 1618, and 1639 cm^{-1} for H–O–H bending vibration, the signal at 1146 cm^{-1} of the C–O stretching vibrations of the glucose unit, the peaks at 1021 and 999 cm^{-1} attributed to the C–O–C stretching vibrations of the anhydroglucose unit (AGU) (Lawchoochaisakul et al., 2021). The

absorption peak at 1727 cm^{-1} at the FTIR spectra of CSt-B (Fig. 1a) was assigned to the stretching vibration of C=O of the ester carbonyl group, indicating the formation of ester bonds between starch and BHC. In addition to the characteristic peaks for starch structure (Fig. 1a) the presence of additional bands at 1403 and 1411 cm^{-1} on cationic starches spectra (Fig. 1a and 1b) are attributed to the stretching vibration of C–N bonds from quaternary ammonium cationic group (Nasir et al., 2020). The SEM micrographs of the unmodified starch and starch materials after cationization are shown in Fig. 2.

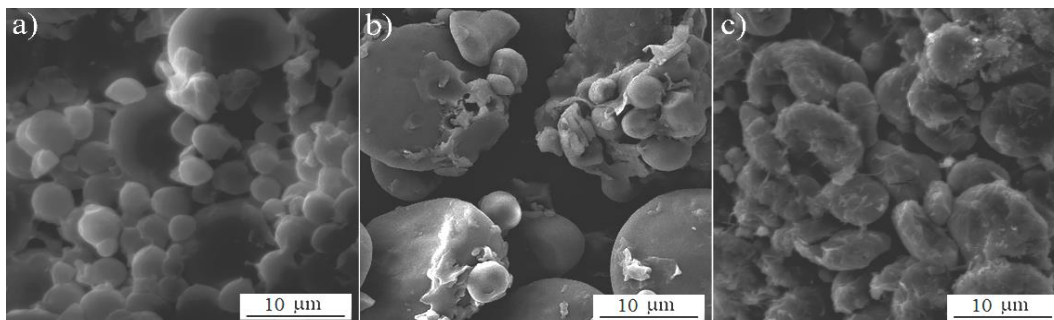


Figure 2. SEM micrographs of a) unmodified starch, b) CSt-B, and c) CSt-G

Fig. 2a shows that the surface of unmodified starch granules is smooth and the granules are spherical or oval. Micrographs of cationic starches (Fig. 2b and 2c) show that the surface of the granules became uneven, with protrusions and holes. Granules partially (Fig. 2b) or completely (Fig. 2c) lose their clear shape, due to partial or complete gelatinization and agglomeration of granules after cationization (Liu et al., 2017). The results of the efficiency of removing MO, CV, ARS, and MB dyes from individual solutions are shown in Fig. 3a, while the results of the efficiency of removing selected pharmaceuticals and pesticides from the multicomponent solution are shown in Fig. 3b.

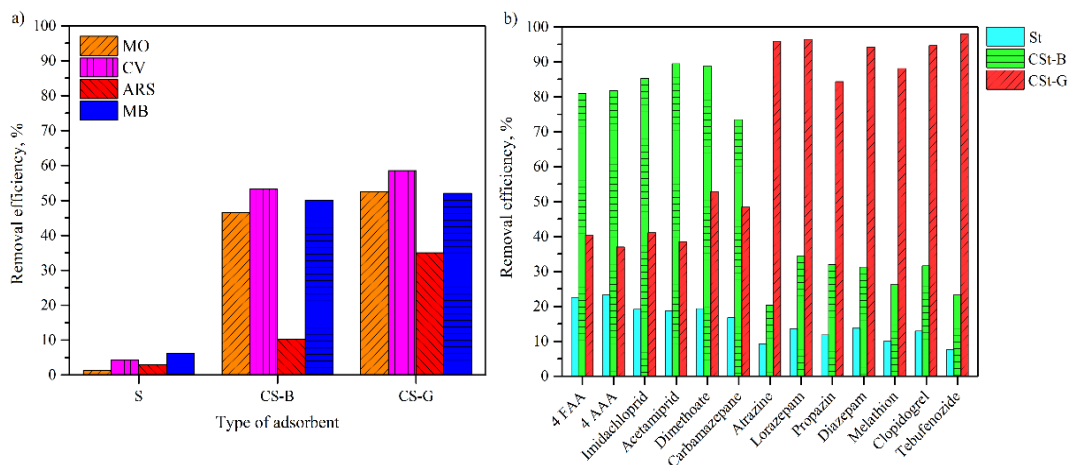


Figure 3. Adsorption efficiency of examined materials toward a) anionic and cationic dyes and b) pharmaceuticals and pesticides

Fig. 3a shows the comparative results of the efficiency of CSt-G and CSt-B in removing different dyes. The tested materials proved to be the most effective adsorbents for the removal of cationic dye, CV. Both materials showed similar efficiency in removing MB dye, while the removal efficiency of MO, CV, and ARS was slightly better for the CSt-G material. The lowest efficiency was obtained for the removal of ARS dye, especially in the case of adsorption with CSt-B. Fig. 3b shows that CSt-B material was more effective in removing most of the tested pharmaceuticals, while CSt-G material was more effective in removing lorazepam, diazepam, and clopidogrel. Also, CSt-G material proved to be more effective in removing all tested pesticides compared to CSt-B material. Considering that polarity of selected pesticides and pharmaceuticals decreases along the X-axis (from the most polar

4-AAA to the less polar tebufenozide), it was noticed that CSt-B showed higher efficiency for the removal of polar compounds, while CSt-G was more efficient in the removal of nonpolar compounds. The influence of the initial pH value of the solution, as well as adsorption time, on the removal efficiency of CV, is given in Fig. 4a. Removal efficiency increases with pH, and the highest removal efficiency for both materials was achieved at pH 9. The adsorption capacity of both types of adsorbents increases significantly in the first 60 minutes of adsorption (Fig. 4b), almost reaching the equilibrium, after which increases slightly up to 180 min. The fast adsorption in the first 15 min can be explained in terms of the high concentration gradient and the availability of a large number of active sites for the adsorption. The pseudo-second order model has a greater ability to describe the kinetic behavior of the adsorption process, indicating that adsorption occurs through the chemisorption reaction (Baloo et. al., 2021).

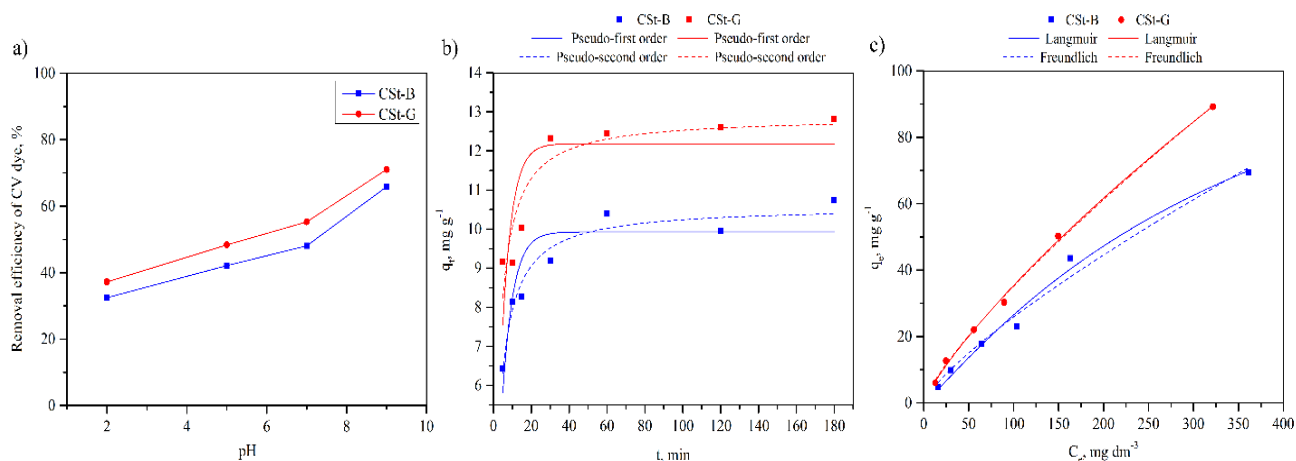


Figure 4. Effect of pH solution (a), time (b), and initial concentration (c) on the removal efficiency of CV dyes

Fig. 4c shows that equilibrium adsorption capacity increases with an initial concentration on CV solution, although the characteristic plateau was not reached in the examined concentration range. Also, both Langmuir and Freundlich adsorption isotherms equally well describe the adsorption of CV on both types of materials.

Conclusion

Modified starch derivates, prepared with betaine hydrochloride (CSt-B) and glycidyltrimethylammonium chloride (CSt-G), were used as adsorbents for the removal of different organic pollutants from water. An increase in the removal efficiency of selected organic pollutants indicated that applied modification has a positive effect on starch adsorption properties. For the adsorption of pesticides and pharmaceuticals, CSt-B showed higher affinity to adsorb more polar, and CSt-G less polar compounds. On the other hand, similar behavior in the adsorption of dyes was observed for both CSt-G and CSt-B samples, with sample CSt-G being slightly more efficient. Adsorption of crystal violet onto both modified starch was highly dependent on solution pH, reaching its maximum at pH 9. For both cationic starches, adsorption equilibrium was attained very rapidly, after 60 minutes. The kinetic data were well described by the pseudo-second order model, while the data obtained from the isotherm study fit well with both Langmuir and Freundlich models. The results of this study indicate that the cationization of wheat starch by the process without the use of expensive and toxic chemicals can be successfully used for the preparation of effective and eco-friendly adsorbents to remove organic pollutants from aqueous solutions.

Acknowledgment: This work was financially supported by the Ministry of Education, Science and Technological Development of the Republic of Serbia (Contract No. 451-03-9/2022-14/200135 and 451-03-9/2022-14/200287).

References

- Baloo, L., Isa, M. H., Sapari, N. B., Jagaba, A. H., Wei, L. J., Yavari, S., Razali, R. & Vasu, R. (2021). Adsorptive removal of methylene blue and acid orange 10 dyes from aqueous solutions using oil palm wastes-derived activated carbons. *Alexandria Engineering Journal*, 60(6), 5611–5629. <https://doi.org/10.1016/j.biortech.2016.09.060><https://doi.org/10.1016/j.aej.2021.04.044>
- Freundlich, H. (1906). Adsorption in solutions. *Journal of Physical Chemistry*, 57, 384–410.
- Ge, H., Wang, C., Liu, S. & Huang, Z. (2016). Synthesis of citric acid functionalized magnetic graphene oxide coated corn straw for methylene blue adsorption. *Bioresource Technology*, 221, 419–429. <https://doi.org/10.1016/j.biortech.2016.09.060>
- Ho, Y. S. & Mckay, G. (1999). Pseudo-second order model for sorption processes. *Process Biochemistry*, 34(5), 451–465. [https://doi.org/10.1016/S0032-9592\(98\)00112-5](https://doi.org/10.1016/S0032-9592(98)00112-5)
- Karić, N., Vukčević, M., Ristić, M., Perić-Grujić, A. Marinković, A. & Trivunac, K. (2021). A green approach to starch modification by solvent-free method with betaine hydrochloride. *International Journal of Biological Macromolecules*, 193, 1962–1971. <https://doi.org/10.1016/j.ijbiomac.2021.11.027>
- Lagergren, S. (1898). Zur theorie der sogenannten adsorption gelöster stoff. *Kungliga Svenska Vetenskapsakademiens Handlingar*, 24(4), 1–39.
- Langmuir, I. (1918). The adsorption of gases on plane surfaces of glass, mica and platinum. *Journal of the American Chemical Society*, 40(9), 1361–1403. <https://doi.org/10.1021/ja02242a004>
- Lawchoochaisakul, S., Monvisade, P. & Siriphannon, P. (2021). Cationic starch intercalated montmorillonite nanocomposites as natural based adsorbent for dye removal. *Carbohydrate Polymers*, 252, 1–26. <https://doi.org/10.1016/j.carbpol.2020.117230>
- Lin, Q., Wang, K., Gao, M., Yunshan, B., Lei, C. & Ma, H. (2017). Effectively removal of cationic and anionic dyes by pH-sensitive amphoteric adsorbent derived from agricultural waste-wheat straw. *Journal of the Taiwan Institute of Chemical Engineers*, 76, 65–72. <https://doi.org/10.1016/j.jtice.2017.04.010>
- Liu, C., Hong, J. & Zhen, X. (2017). Effect of heat-moisture treatment on morphological, structural and functional characteristics of ball-milled wheat starches. *Starch/Staerke*, 69, 1–9. <https://doi.org/10.1002/star.201500141>
- Nasir, N. M., Abdulmalek, E. & Zainuddin, N. (2020). Preparation and optimization of water-soluble cationic sago starch with a high degree of substitution using response surface methodology. *Polymers*, 12(11), 1–13. <https://doi.org/10.3390/polym12112614>
- Su, Y., Du, H., Huo, Y., Xu, Y., Wang, J., Wang, L., Zhao, S. & Xiong, S. (2016). Characterization of cationic starch flocculants synthesized by dry process with ball milling activating method. *International Journal of Biological Macromolecules*, 87, 34–40. <https://doi.org/10.1016/j.ijbiomac.2015.11.093>
- Wen, Y., Schoups, G. & van de Giesen, N. (2017). Organic pollution of rivers: Combined threats of urbanization, livestock farming and global climate change. *Scientific Reports*, 7, 1–9. <https://doi.org/10.1038/srep43289>

Original scientific article

EFFECT OF ALKALI MODIFICATION ON ADSORPTION EFFICIENCY OF FLY ASH

Nataša Karić¹, Sara Živojinović², Marija Vukčević², Marina Maletić¹, Aleksandra Perić-Grujić², Katarina Trivunac²

¹Innovation Center of Faculty of Technology and Metallurgy, Karnegijeva 4, 11120 Belgrade, Serbia

²University of Belgrade, Faculty of Technology and Metallurgy, Karnegijeva 4, 11120 Belgrade, Serbia

Abstract

As coal combustion in thermal power plants generates huge amounts of waste such as bottom ash and fly ash, there is a need to find new applications for these materials. One of the ways of its reuse is chemical or thermal modification of the ash in order to obtain new materials, which can be further used as adsorbents of various pollutants from water. The subject of this research was the alkali modification and alkali activation of fly ash in purpose to increase the adsorption capacity towards heavy metal ions. The success of modification process and characterization of the obtained materials was monitored by Fourier transform infrared spectroscopy, X-ray fluorescence spectroscopy and scanning electron microscopy. The concentration of zinc and cadmium ions after adsorption was determined by atomic absorption spectroscopy. The kinetics of the adsorption process on the most efficient adsorbent were examined and the experimental data were compared with pseudo-first and pseudo-second order models. The achieved results show a positive effect of alkaline modification of fly ash on adsorption efficiency of both metals, while alkaline activation gives an exceptionally effective adsorbent in the case of zinc.

Keywords: fly ash, environment, modification, heavy metal, waste reuse.

Introduction

Burning coal in thermal power plants produces huge amounts of ash. Fly ash (FA) is deposited in several large-scale landfills and has a negative impact on the environment and human health. Fly ash is considered a pollutant because it contains acidic, toxic and sometimes radioactive substances. Fly ash particles have a direct harmful effect on human health and the environment (Vilakazi et al., 2022). Due to size of fly ash particles, the wind easily blows them to greater distances from the thermal power plant and they can remain in the air for a long time, which increases the possibility of their inhalation. Fly ash landfills also cause degradation of agricultural land, which requires some control and monitoring. As a way to reduce the amount of waste, the possibility of using ash in construction as an additive to cement and concrete, and in road construction, has been observed (Krithika & Kumar, 2020). Application for soil stabilization and photocatalyst production were also investigated (Indiramma & Sudharani, 2018; Jala & Goyal, 2006). Likewise, great interest is focused on the development of efficient adsorbents for the removal of dyes and heavy metals from water (Hussain et al., 2022; Banerjee et al., 2003; Sahoo et al., 2013). The advantage of using fly ash is its availability and low cost. Through different modification processes, it is possible to improve the adsorption and selective characteristics of the obtained adsorbents (Zhuang et al., 2016; Kato et al., 2019; Pengthamkeerati et al., 2008). Modification can be mechanical, thermal and chemical. Mineral acids (nitric and hydrochloric), sodium and calcium hydroxide, alkaline silicate solution can be used as modification agents (Sočo et al., 2016; Wang et al., 2005; Gollakota et al., 2019).

Materials and Methods

Fly ash containing SiO₂ (58.40%), Al₂O₃ (21.80%), Fe₂O₃ (4.21%), CaO (2.83%) from power plant in Serbia was used. The material was sieved, then washed with deionized water and dried at temperature of 105 °C in oven (sample FA₀). Two different modification procedure of fly ash, based on literature with slight difference, were performed. In first, washed and dried fly ash was mixed with 2M NaOH in a cuvette (1:3) and put on a shaker (120 rpm) to mix for 7 days. After that, obtained material was washed with about 1.5 l of distilled water and dried in the oven for 24 hours at a temperature of 60 °C (sample labelled FA₁). During second modification, FA was mixed well with diatomaceous earth in a plastic mold and sodium silicate was added (2:1:2). For better mixing, a few drops of 16M NaOH were added. The sample was placed in the oven for 2 h at 105 °C to dry, and then left in a closed mold at room temperature to age for 15 (sample marked as FA₂), and 30 days (sample marked as FA₃).

The morphological characteristics of the surface of unmodified and modified materials were examined by scanning electron microscopy - SEM (SEM JEOL JSM-6610LV). The content of functional groups on the surface of the material was determined by Fourier transform infrared spectroscopy - FTIR (Nicolet iS10, Thermo Scientific). The efficiency of unmodified and modified fly ash to adsorb Cd and Zn ions from aqueous solution was tested in batch system at room temperature. Concentration of metal ions after adsorption were determined by atomic absorption spectroscopy. The adsorption efficiency (%E) of the prepared adsorbents in the removal of metal ions was calculated using the following equation (1):

$$\% E = \frac{(C_0 - C_e)}{C_0} \times 100 \quad (1)$$

where C_e is the equilibrium and C_0 is the initial concentration of metal ions in solution (mg dm⁻³).

The two kinetic models, the pseudo-first order model (equation (2)) and the pseudo-second order model (equation (3)) were used to calculate the adsorption rate:

$$q_t = q_e \cdot (1 - e^{-k_1 \cdot t}) \quad (2)$$

$$q_t = q_e - \left(\frac{1}{q_e} - k_2 \cdot t \right)^{-1} \quad (3)$$

where q_t is the amount of metal ions adsorbed at the time t (mg g⁻¹), q_e is the amount of metal ions adsorbed at equilibrium (mg g⁻¹), k_1 is the pseudo-first-order kinetic rate constant (min⁻¹), and k_2 is the pseudo-second-order kinetic rate constant (mg g⁻¹ min⁻¹).

Results and discussion

The SEM micrographs of the unmodified and modified fly ash are shown in Fig. 1. Both treatments, alkali modification and alkali activation, changed the surface of starting material. With the addition of NaOH (Fig. 1b), the surface of the material becomes rougher and more porous in comparison to unmodified fly ash (Fig. 1a). Surface of alkali activated fly ash (Fig. 1c and 1d) contains cracks and a heterogeneous matrix containing unreacted fly ash particles.

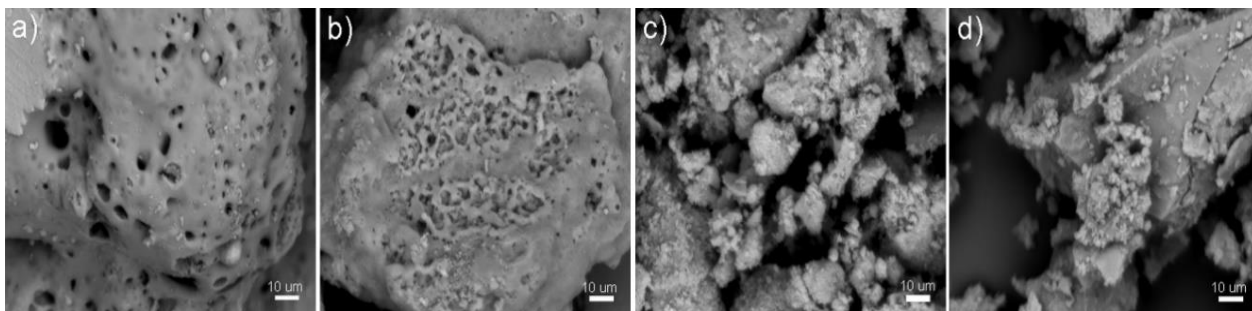


Figure 1. SEM micrographs of a) unmodified fly ash, b) FA₁, c) FA₂, and d) FA₃ samples

FTIR spectra of unmodified and modified materials before and after adsorption are shown in Fig. 2a. Sharp peaks at around 1000 and 780 cm⁻¹, can be ascribed to the stretching of asymmetric Si - O -Si and symmetric Si - O -Si bond, respectively. The small shifts to lower values in the range around 1000 cm⁻¹ and absence of peak at 797 cm⁻¹ in FA₂ and FA₃ spectra confirms formation of alkali activated materials. The band at 1450-1500 cm⁻¹ originated from atmospheric carbonation of materials surface. After adsorption, changes in the intensity of bands around 1000 cm⁻¹ are visible, indicating the interaction of these groups with metal ions.

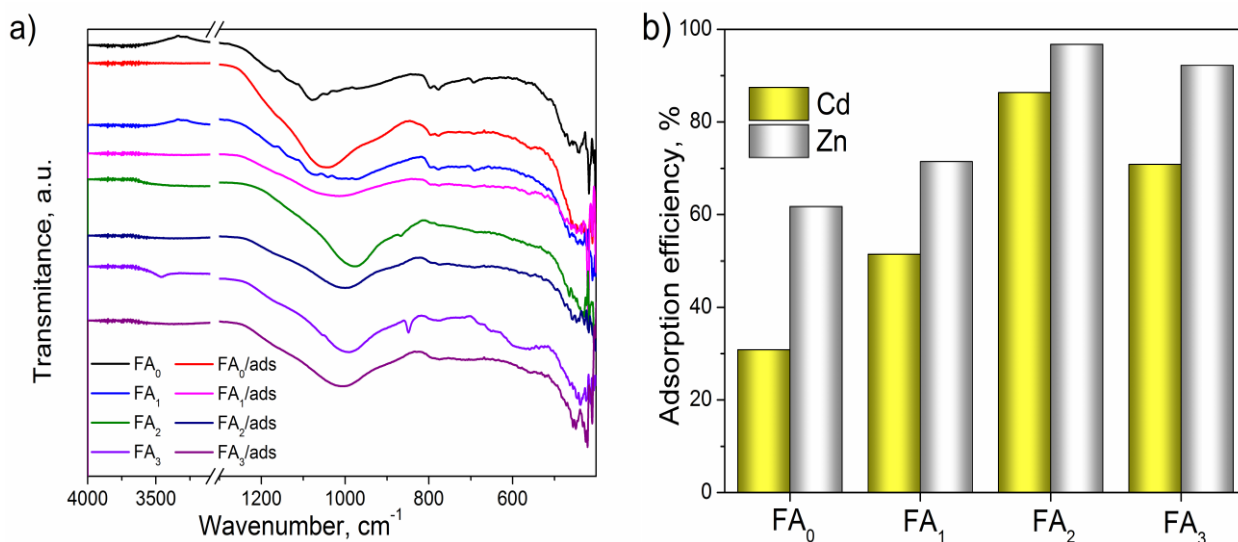


Figure 2. FTIR spectra (a) and adsorption efficiency (b) of unmodified and modified materials

The adsorption efficiency of the prepared adsorbents towards Zn and Cd ions is shown in Fig. 2b. An improvement in the efficiency of modified materials compared to the unmodified fly ash is evident. This increase is more pronounced in the case of zinc ions adsorption. Alkali-activated samples (FA₂ and FA₃) have proven to be the most effective in Zn and Cd adsorption. This is the consequence of introducing the polymeric Si-O-Al-O- bonds into the structure of materials during alkali activation, which increase the number of active sites for metal ion binding. These conclusions are consistent with the FTIR results.

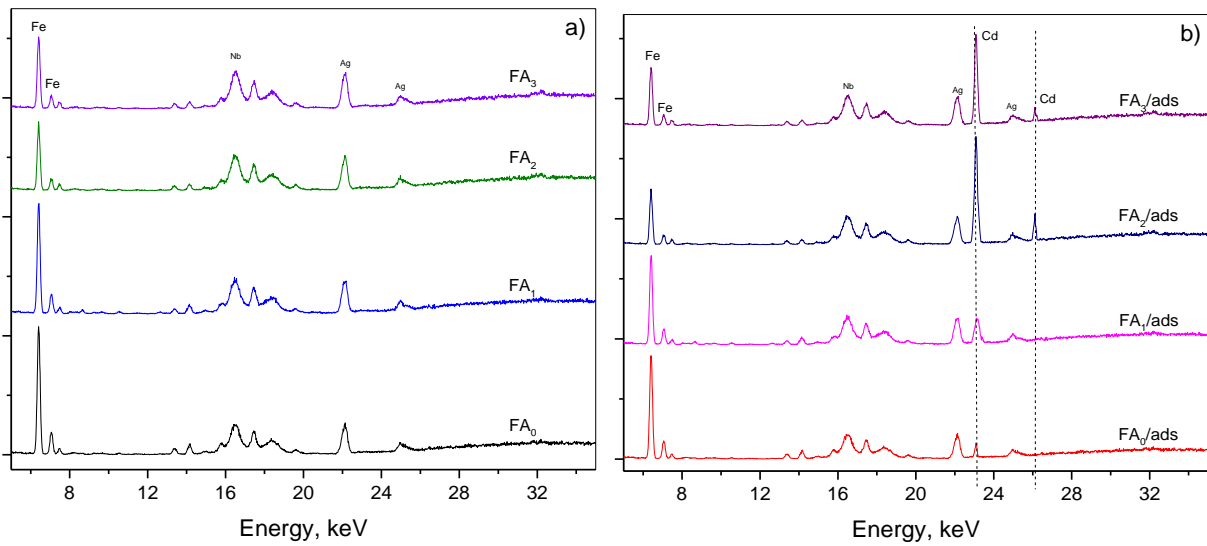


Figure 3. XRF spectra of adsorbents a) before and b) after adsorption of cadmium

Adsorption of cadmium, in the range of 5-50 keV can be confirmed by XRF spectrum. The peaks corresponding to the $K\alpha_1$ and $K\beta_1$ lines of cadmium, at values 23.17 and 26.09, respectively, confirm that cadmium ions are adsorbed on the surface of examined materials (Fig. 3b), since there is no confirmation of their presence on the samples surface before the adsorption (Fig. 3a). Also, the most intense peaks of cadmium are observed for adsorbent FA₂, which confirms the previously obtained results.

To evaluate the adsorption kinetic data and investigate the adsorption mechanism, the pseudo-first order and pseudo-second order equations were used. Graphical comparison of experimental data and applied models is shown in Fig. 4. Calculated kinetic constants and correlation coefficients for Zn and Cd adsorption are shown in Table 1.

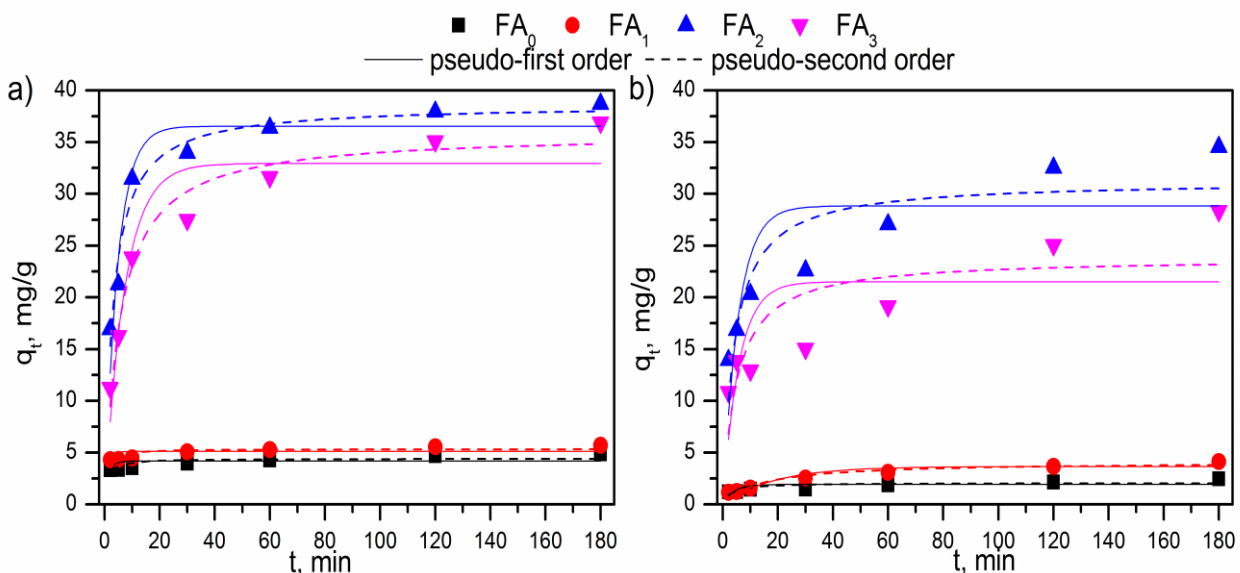


Figure 4. Kinetic adsorption models of metals a) Zn and b) Cd on unmodified fly ash (FA₀) and modified samples FA₁, FA₂, and FA₃

Based on the results of kinetic models, it can be seen that the process of metal adsorption on all investigated materials was relatively fast and that equilibrium was reached at about 30 min for both metals. The alkali activated materials showed higher adsorption capacity especially towards Zn ions

(Fig. 4a). The calculated value of the correlation coefficient (R^2) is used as a criterion for explaining the kinetics of the adsorption process. According to Table 1, it can be concluded that in the examined process there is a better agreement with the pseudo second-order model, and that chemisorption takes place.

Table 1. Kinetic parameters for Cd and Zn adsorption onto examined samples

	Sample	Pseudo-first order			Pseudo-second order			$q_{e,exp}$
		$q_{e,cal}$	k_1	R^2	$q_{e,cal}$	k_2	R^2	
Cd	FA ₀	1.917	0.27029	0.25466	2.062	0.18004	0.53397	2.465
	FA ₁	3.643	0.05356	0.81858	4.093	0.01744	0.9047	4.117
	FA ₂	28.82	0.17861	0.57461	31.25	0.00757	0.77737	34.53
	FA ₃	21.50	0.17193	0.30742	23.80	0.00845	0.55253	28.33
Zn	FA ₀	4.170	0.69652	0.12527	4.408	0.23180	0.5331	4.861
	FA ₁	5.108	0.84559	0.13628	5.338	0.26688	0.57163	5.716
	FA ₂	36.53	0.21267	0.89327	38.63	0.00847	0.95737	38.70
	FA ₃	32.93	0.13842	0.8745	35.90	0.00497	0.95992	36.89

Conclusion

In this study, influence of alkali modification and alkali activation of fly ash on its ability to remove the polluting substances from aqueous solutions was analyzed. During the modification process, changes occurred both on the surface and in the structure of the material, which was confirmed by the applied instrumental methods. The adsorption efficiency increases after both type of modification of fly ash. By alkali activation of fly ash, more effective adsorbent towards heavy metal ions was obtained. Alkali-activated materials are more effective due to polymeric Si-O-Al-O- bonds introduced into the structure of materials thus increasing the number of active sites for metal ion binding.

The positive impact that applied alkali modification and alkali activation had on the adsorption characteristics of fly ash requires continued investigation of the possibility of using adsorbents obtained in this way for the removal of other inorganic and organic pollutants.

Acknowledgment: This work was supported by the Science Fund of the Republic of Serbia within project „Serbian Industrial Waste towards Sustainable Environment: Resource of Strategic Elements and Removal Agent for Pollutants - SIW4SE“ (Contracts No. 7743343).

References

- Vilakazi, A. Q., Ndlovu, S., Chipise, L. & Shemi, A. (2022). The Recycling of Coal Fly Ash: A Review on Sustainable Developments and Economic Considerations. *Sustainability*, 14(4), 1958. <https://doi.org/10.3390/su14041958>
- Gollakota, A. R. K., Volli, V. & Shu, CM. (2019). Progressive utilisation prospects of coal fly ash: A review. *Science of the Total Environment*, 672, 951–989. <https://doi.org/10.1016/j.scitotenv.2019.03.337>
- Sočo, E. & Kalembkiewicz, J. (2016). Comparison of adsorption of Cd(II) and Pb(II) ions on pure and chemically modified fly ashes. *Chemical and Process Engineering*, 37(2), 215–234. <https://doi.org/10.1515/cpe-2016-0018>
- Indiramma, P. & Sudharani, CH. (2018). Scanning Electron Microscope Analysis of Fly Ash, Quarry Dust Stabilized Soil. In: Frikha, W., Varaksin, S., Viana da Fonseca, A. (eds) Soil Testing, Soil Stability and Ground Improvement. GeoMEast 2017. Sustainable Civil Infrastructures. Springer, Cham. https://doi.org/10.1007/978-3-319-61902-6_22

- Krithika, J. & Ramesh Kumar, G. B. (2020). Influence of fly ash on concrete – A systematic review. *Materials Today: Proceedings*, 33(1), 906–911. <https://doi.org/10.1016/j.matpr.2020.06.425>
- Kato, K., Xin, Y., Hitomi, T. & Shirai, T. Surface modification of fly ash by mechano-chemical treatment. *Ceramics International*, 45 (1), 849–853. <http://dx.doi.org/10.1016/j.ceramint.2018.09.254>
- Pengthamkeerati, P., Satapanajaru, T. & Chularuengoaksorn, P. Chemical modification of coal fly ash for the removal of phosphate from aqueous solution, *Fuel*, 87(12), 2469–2476. <https://doi.org/10.1016/j.fuel.2008.03.013>
- Sahoo, P. K., Tripathy, S., Panigrahi, M. K. & Equeenuddin, Sk. Md. (2013). Evaluation of the use of an alkali modified fly ash as a potential adsorbent for the removal of metals from acid mine drainage. *Applied Water Science*, 3(3), 567–576. <https://doi.org/10.1007/s13201-013-0113-2>
- Jala, S. & Goyal, D. (2006). Fly ash as a soil ameliorant for improving crop production—a review. *Bioresource Technology*, 97(9), 1136–1147. <https://doi.org/10.1016/j.biortech.2004.09.004>
- Banerjee, S. S., Jayaram, R. V. & Joshi, M. V. (2003). Removal of Nickel(II) and Zinc(II) from Wastewater Using Fly Ash and Impregnated Fly Ash. *Separation Science and Technology*, 38(5), 1015–1032. <https://doi.org/10.1081/SS-120018121>
- Wang, S., Boyjoo, Y. & Choueib, A. (2005). A comparative study of dye removal using fly ash treated by different methods. *Chemosphere*, 60(10), 1401–1407. <https://doi.org/10.1016/j.chemosphere.2005.01.091>
- Zhuang, X. Y., Chen, L., Komarneni, S., Zhou, C. H., Tong, D. S., Yang, H. M., Yu, W. H. & Wang, H. (2016). Fly ash-based geopolymers: clean production, properties and applications. *Journal of Cleaner Production*, 125, 253–267. <https://doi.org/10.1016/j.jclepro.2016.03.019>
- Hussain, Z., Chang, N., Sun, J., Xiang, S., Ayaz, T., Zhang, H. & Wang, H. (2022). Modification of coal fly ash and its use as low-cost adsorbent for the removal of directive, acid and reactive dyes, *Journal of Hazardous Materials*, 422, 126778. <https://doi.org/10.1016/j.jhazmat.2021.126778>

Informative Article

USE OF AGRICULTURAL WASTE AS RAW MATERIALS FOR OBTAINING GLASS AND GLASS-CERAMICS: A REVIEW

Vladimir S. Topalović¹, Jelena D. Nikolić¹, Veljko V. Savić¹, Srdjan D. Matijašević¹, Marija S. Djošić¹, Snežana N. Zildžović¹, Snežana R. Grujić²

¹Institute for the Technology of Nuclear and other Mineral Raw Materials-Belgrade, Serbia

²University of Belgrade, Faculty of Technology and Metallurgy-Belgrade, Serbia

Abstract

Global trends are moving towards a circular economy to replace the deeply grounded linear economics and waste management. Circular economy implies and the protection of human rights through sustainable development, global security natural resources, combating climate change, energy security, insurance sufficient amounts of food, reducing inequalities, preservation of health and a cleaner environment and the rights of future generations to resources, etc. The policy of procurement of raw materials in the circular economy is focused on the use of secondary raw materials. A big challenge for modern production is to use different types of waste to obtain new products without the use of raw materials. This kind of production requires new knowledge, adaptation of existing technologies or new technologies, new jobs, etc. Large amounts of vegetative residues are produced annually by agriculture. Agricultural waste is very often incinerated or disposed of on land and is still not used. Most of the agricultural waste ashes consist of silicon dioxide along with other oxides which may vary according to region and atmosphere of the local conditions. This paper gives an overview of the possibilities of using agricultural waste for obtaining glass and glass ceramics. Previous research has shown that various types of glass and glass-ceramics can be successfully obtained from agricultural waste, which can be used in construction, medicine, various composites, etc.

Keywords: glass, agricultural waste, recycling.

Introduction

Minerals in organic waste have been used for a long time in the concrete industry, production of carbides, nitrides and others. This type of waste is not widely used primarily because it is less known which minerals are present in plants. What is more, plants have a significant content of water and organic components that must be removed before use.

Glass and glass ceramics are most often (traditionally) produced from high purity proportions of pure chemicals. They can also be prepared from cheaper raw materials such as wastes because the glass-ceramic process has been established as a suitable way to valorise mining and industrial wastes (Giro-Paloma et al., 2019). Most of the elements from the periodic table necessary for obtaining different types of glass are found in various plants, except for B, Li, Ge and Sn (for example, B is important element for display glasses). The amount of certain minerals that are undesirable in glass, Fe₂O₃, for example, is not significant in plants. On the other hand, S and Cl are present in some plant, that are desirable as fining agents for glass production (Cornejo et al., 2014). In recent times, a few researchers have reported that the food waste could be used as the resource material to obtaining the glasses and

glass-ceramics for numerous applications. In this paper, a brief overview of previous research is given.

Materials and Methods

In order to obtain glass from food waste, it is necessary to first dry the waste and then heat it at a certain temperature to remove unwanted components (such as H₂O, CO_x and NO_x). Typically, a second heat treatment produces the mineral desired for glass batching. Certain food wastes, such as eggshells, which are primarily CaCO₃, do not need this heat treatment and may be used directly as a raw material.

Results and discussion

The mineral content of organic waste varies widely depending on the type of plant, thereby providing the ability to batch a variety of glass and glass-ceramic compositions. This diversity allows significant flexibility in production these engineered materials. In Table 1 present the chemical compositions of three common glasses and the ash of various food wastes.

Table 1. Oxide content in three common glasses and present in ash of various food waste (Cornejo et al., 2014)

	SiO ₂	CaO	K ₂ O	Na ₂ O	MgO	Al ₂ O ₃	P ₂ O ₅	Fe ₂ O ₃	SO ₃	B ₂ O ₃
GLASS										
Containers	65-75	10	0	14	3	<1	0	0	<1	0
Display	50-60	0-4	0-5	0-5	0-3	10-17	0	0	0	8-15
Bioactive	0-55	22-27	0-9	6-24	0-8	0-28	1-3	-	0	0-51
FOOD WASTE										
Rice husk	97.8	0.6	1.3	-	0.24	trace	-	trace	-	-
Corn husk	35.7	5.8	20.2	5.1	9.9	0.4	22.5	0.3	-	-
Egg shell	0.1	98.6	0.1	0.1	0.8	-	-	-	-	-

Naghizadeh et al. (2015) have fabricated a 3 D scaffold using polycaprolactone and silicate based bioactive glass-ceramic. Bioactive glass (50SiO₂-25Na₂O-25CaO (mol %)) was obtained by the sol-gel process, and rice slag was used as a source of Si. In vitro test showed the formation of HA after both 7 and 14 days, on the surface of the scaffold. The toxicity rate of the glass powder demonstrated that it was not directly toxic to the hMSCs and cell proliferation in culture after 3 days. For a series of bioactive glasses, Kaur et al. (2021) used rice husk and eggshells to obtain bioactive glasses (basic composition SiO₂-P₂O₅-MgO-CaO) that can be employed in bone implants and drug delivery applications. Using the sol-gel process, Essien et al. (2016) obtained bioactive glass of ternary system of CaO-MgO-SiO₂, as raw materials they also used rice slag and eggshells. Their results show that there was absence of agglomeration of glass particles. Consequently, a good surface area is achieved, which is important for the reaction of glass in the body fluid. In the study of Chen et al. (2017), they used rice husk, to develop a novel mesoporous bioactive glass and found that the glass a well-ordered hexagonal mesoscopic structure, high surface area, high pore volume and the capacity to support the formation of hydroxyapatite layer that can be attached to the bone.

The study of Sharma & Singh (2019) demonstrated that wheat straw ash and mineral oxides based glass-ceramic can be promising sealant materials for solid oxide fuel cells application. Wheat straw ash exhibits good thermal stability with insulating nature even at 700 °C. The same authors (2020) prepared four samples with varying (wt%) of rice husk (RHA) and eggshells (ESP), composition (100-x)RHA*(x)ESP, where x=30, 40, 50 and 60 (only 70RHA*30ESP did not have glassy nature). The as-quenched samples are transparent with a blue tint. They assumed that the blue color may arise due to the presence of some transition trace elements like Ti as observed in EDS and XPS analysis.

Two different crystalline forms of SiO₂, cristoballite and tridymite, were formed. The calculated density of the present glasses is lower, while the hardness is slightly higher than the similar type of glass-ceramics synthesized from commercially available oxides. The hardness of the samples is 590-630 HV. Optical band gap is in wide semiconductor range, 3.2-3.5 eV. Low/moderate dielectric constant with low dielectric loss is observed in the present glasses and glass-ceramics, which can be exploited to use them in microelectronic applications.

Optical properties of soda-lime-silica glasses doped with peanut shell powder investigated by Aktas et al. (2016). They are different amounts of the peanut shell powders (0.5, 1, 3 and 5 wt.%) mixed with the soda-lime-silica glass powder and the melt-quench technique prepared glasses. The density of the glasses decreased with increasing peanut shell powder content. The pure soda-lime-silica glass was colourless and transparent, whereas it became dark green after adding the peanut shell powder.

Andreola et al. (2013) described the fabrication of glass-ceramic tiles by using rice husk ash. The RHA glass frit was prepared from a composition (wt.%) of 46.52RHA, 13.84Al₂O₃, 13.16MgO, 22.17Na₂CO₃ and 4.33B₂O₃ by melting at 1450 °C followed by quenching in water. These glass-ceramics were found to produce nepheline (Na₂O·Al₂O₃·2SiO₂) and forsterite (2MgO·SiO₂) crystal phases. Their bending strength, Young's modulus, shear modulus, Poisson's ratio and Mohs hardness were found to vary in the ranges of 24-39 MPa, 43-61 GPa, 17-23 GPa, 0.14-0.30 and 6-9, respectively. Regarding technological features, the sintered materials showed bending strength values and Mohs hardness higher with respect to commercial glass-ceramics. Bottom ash from biomass combustion, coming from a thermoelectric power plant in Faenza (Italy), was exploited as an alternative raw material in porcelain stoneware bodies (Conte et al., 2022). No significant variations with respect to technological parameters, such as particle size distribution, springback, green and dry bulk density were identified, indicating that the introduction of ash, within certain limits, guarantees the maintenance of the required properties of the semi-finished products along the production line.

Farias et al. (2022) used coffee husk ash, highly attractive raw material with potential as a low cost K₂O source to produce glass-ceramics for solid oxide cell applications. They determined that this glass-ceramic consists of two distinct crystalline phases, diopside and nepheline, embedded into the glassy matrix. Thermal expansion coefficients were found between 9 and 10x10⁻⁶ °C⁻¹, suggesting excellent mechanical compatibility with other cell components operating at intermediate temperatures.

The research of Iwaszko et al. (2020) showed that vitrified material is characterized by very low ion leachability, comparable to the ion leachability of glass, therefore its potential use e.g. in the building materials industry does not require additional protective or adaptation activities. Their research has shown the possibility of vitrifying wastes (The Virginia mallow) generated during biomass torrefaction.

A group of researchers from Spain (Jordan et al., 2018) examined the possibilities of obtaining glass and glass-ceramics from different types of waste. They concluded that vitrification of waste (palm wood, natural peat and earthworm humus) occurs at lower melting temperatures (from 1200 to 1300 °C). The straw and palm leaf could be located in the K₂O-CaO-SiO₂ ternary system, far from the eutectic points. The high K₂O content in these wastes will facilitate the vitrification process and could give rise to controlled soluble glasses. The peat and humus biomass wastes can be located in the CaO-Al₂O₃-SiO₂ system, which is a very common ternary composition diagram for waste such as slags, fly ash, etc. The composition are close to the eutectic triple point formed by wollastonite, anorthite and gehlenite.

Conclusion

This paper presents some of the research into the possibility of using food waste to obtain different glasses and glass ceramics. Most food wastes contain valuable minerals that could serve as raw

materials for the production of glass, ceramics and glass-ceramics. Previous research has shown that glass, ceramics and glass-ceramics obtained from food waste can be successfully used as biomaterials or sealing materials at high temperatures. Additionally, they can be used in the production of ceramic tiles, as well as construction material in the building industry, etc. The goal of our research is to show the possibilities of using materials that we consider waste. Also, our goal is to show what treasures are hidden in food waste.

Acknowledgment: This work was supported by the Ministry of Education, Science and Technological Development of the Republic of Serbia (Contract No. 451-03-68/2022-14/200023 and Contract No. 451-03-68/2022-14/200135).

References

- Aktas, B., Albaskar, M., Yalcin, S. & Dogru, K. (2016). Optical properties of soda-lime-silica glasses doped with peanut shell powder. *Archives of Materials Science and Engineering*, 82(2), 57–61. <https://doi.org/10.5604/01.3001.0009.7104>
- Andreola, F., Martin, M. I., Ferrari, A. M., Lancellotti, I., Bondioli, F., Rincon, J. M., Romero, M. & Barbieri, L. (2013). Technological properties of glass-ceramic tiles obtained using rice husk ash silica precursor. *Ceramic International*, 39, 5427–5435. <https://doi.org/10.1016/j.ceramint.2012.12.050>
- Chen, S., Chou, P., Chan, W. & Lin, H. (2017). Preparation and characterization of mesoporous bioactive glass from agricultural waste rice husk for targeted anticancer drug delivery. *Ceramics International*, 43, 2239–2245. <http://dx.doi.org/10.1016/j.ceramint.2016.11.007>
- Conte, S., Buonamico, D., Magni, T., Arletti, R., Dondi, M., Guarini, G. & Zanelli, C. (2022). Recycling of bottom ash from biomass combustion in porcelain stoneware tiles: Effects on technological properties, phase evolution and microstructure. *Journal of the European Ceramic Society*, 42, 5153–5163. <https://doi.org/10.1016/j.jeurceramsoc.2022.05.014>
- Cornejo, I. A., Ramalingam, S., Fish, J. S. & Reimanis, I. E. (2014). Hidden treasures: Turning food waste into glass. *American Ceramic Society Bulletin*, 93(6), 26–30. <https://bulletin-archive.ceramics.org/2014-08/>
- Essien, E. R., Atasie, V. N. & Udobang, E. U. (2016). Microwave energy-assisted formation of bioactive CaO-MgO-SiO₂ ternary glass from bio-wastes. *Bulletin of Materials Science*, 39(4), 989–995. <https://doi.org/10.1007/s12034-016-1251-6>
- Farias, M. B., Araujo, A. J. M., Medeiros, V. S., Macedo, D. A., De Miranda, A., Paskocimas, C. A. & Nascimento, R. M. (2022). Use of coffee husk ash for preparation of glass-ceramics as potential sealants for solid oxide cells. *Ceramics International*, 48, 23145–23150. <https://doi.org/10.1016/j.ceramint.2022.04.295>
- Giro-Paloma J., Manosa, J., Maldonado-Alameda, A., Quina, M. J. & Chimenos, J. M. (2019). Rapid sintering of weathered municipal solid waste incinerator bottom ash and rice husk for lightweight aggregate manufacturing and product properties. *Journal of Cleaner Production*, 232, 713–721. <https://doi.org/10.1016/j.jclepro.2019.06.010>
- Iwazsko, J., Zajemska, M., Zawada, A., Szwaja, S. & Poskart, A. (2020). Vitrification of environmentally harmful by-products from biomass torrefaction process. *Journal of Cleaner Production*, 249, 119427. <https://doi.org/10.1016/j.jclepro.2019.119427>
- Jordan, M. M., Almendro-Candel, M. B., Navarro-Pedreño, J., Guirao, D., Acosta, A. & Rincón, J. M. (2018). First evaluation of vitrification capability of palm tree biomass wastes and sewage sludge. *Materials Letters*, 229, 71–73. <https://doi.org/10.1016/j.matlet.2018.06.099>

- Kaur, D., Reddy, M. S. & Pandey, O. P. (2021). Agro waste as a source of bioactive glass for targeted drug delivery and bone implantation. *Journal of Drug Delivery Science and Technology*, 65, 102669. <https://doi.org/10.1016/j.jddst.2021.102669>
- Naghizadeh, F., Kadir, M. R. A., Doostmohammadi, A., Roozbahani, F., Iqbal, N., Taheri, M. M., Naveen, S. V. & Kamarul, T. (2015). Rice husk derived bioactive glass-ceramic as a functional bioceramic: Synthesis, characterization and biological testing. *Journal of Non-Crystalline Solids*, 427, 54–61. <http://dx.doi.org/10.1016/j.jnoncrysol.2015.07.017>
- Sharma, G. & Singh, K. (2019). Agro-waste ash and mineral oxides derived glass-ceramics and their interconnect study with Cofer 22 APU for SOFC application. *Ceramics International*, 45, 20501–20508. <https://doi.org/10.1016/j.ceramint.2019.07.029>
- Sharma, G. & Singh, K. (2020). Dielectric and optical properties of glasses and glass-ceramics synthesized from agro-food wastes. *Materials Chemistry and Physics*, 246, 122754. <https://doi.org/10.1016/j.matchemphys.2020.122754>

Original scientific article

PHOTOCATALYTIC DECOMPOSITION OF DIFENOCONAZOLE FROM WASTEWATERS

Jovana Bošnjaković¹, Nataša Knežević², Srećko Manasijević¹, Aleksandar Jovanović³, Mladen Bugarčić³, Aleksandar Marinković²

¹Research and Development Institute Lola L.T.D., Kneza Višeslava 70A, 11030 Belgrade, Serbia

²Faculty of Technology and Metallurgy, University of Belgrade, Karnegijeva 4, 11120 Belgrade, Serbia

³Institute for Technology of Nuclear and Other Raw Materials, Bulevar Franše d'Eperea 86, 11000 Belgrade, Serbia

Abstract

Due to the rapid development of industry and growth of population, water consumption is increased. Beside this, releasing of xenobiotics, which represent significant pollutants into watercourse, like heavy metal ions, pesticides, paints, and solvents, made this problem much bigger. Therefore, they can enter into aquatic organisms directly from industrial plants or into human bodies indirectly through agricultural products. New technologies, including photocatalytic decomposition, are necessary for wastewater treatment as a highly efficient and low-cost process. Photocatalysis implies the degradation of various types of harmful organic substances to simple molecules such as CO₂, SO₂, ions, and water. The applied process has no detrimental effect on the environment and does not require additional chemicals for precipitation of the products. In this work, photodegradation of the pesticide difenoconazole (DFC) using a TiO₂-based photocatalyst was examined using doubled wall thermoregulated quartz reactor. As a replacement for UVC radiation, solar imitated Ultra Vitalux (UV) lamp (300W) was used. Determination of DFC concentration was performed using a UV method. Degradation kinetics follows pseudo-first order. After 120 minutes, the DFC was completely degraded. Chemical oxygen demand (COD) also confirmed that successfully indicating that this process can be used in treating of industrial wastewater.

Keywords: photodegradation, xenobiotics, environmental, DFC, wastewater.

Introduction

Pesticides are products of biological or chemical origin intended for the protection of plants and animals from harmful insects, diseases. The use of pesticides has a negative impact on the ecosystem in which they are applied. In order to maintain agricultural production, reducing the use of pesticides is of great importance. They are used in agriculture for more than fifty years. About five hundred different pesticides have been registered (Sakkas et al., 2011). The classification is made depending on the purpose, chemical structure, mechanism of action (Sakkas et al., 2011). They can be divided into herbicides, insecticides, fungicides, bactericides, physiotropes, hemosterilants (Marican & Durán-Lara, 2018). In the Republic of Serbia, usage of pesticides in agricultural production is still in small quantities. In recent decades, pesticides are increasingly present in underground, surface and drinking water (Moore et al., 2007; Palma et al., 2009; Šunjka, 2012). Together with other pollutants, which are present in wastewater, they can have a very severe impact on human health due to high toxicity, carcinogenicity, bioaccumulation (Eriksson et al., 2007). Less than 0.1% of the applied amount reaches the target organisms and about 99.9% is lost to the environment (Pimentel, 1995). They get into water and soil through direct use, washing off crops, and runoff from the soil surface

(Jing et al., 2011). In order to improve the protection of the environment, the management of pesticide residues represents a special challenge.

Pesticides-polluted waters is a major problem for the environment and requires systematic monitoring. The need for the development of new technologies that could be used in the treatment of wastewater contaminated with pesticides arose due to their long-term degradation by photolysis and high stability in the environment (Bavcon Kralj et al., 2007). Photodegradation and biological treatment are the widely used techniques in wastewater treatment (Oller et al., 2011). Biological treatment (BT) is the degradation of pollutants in the soil and natural waters by fungi and bacteria. However, due to the low efficiency and long duration of the purification process, BT is not widely used in industry (Hincapié et al., 2005). Also, due to the high toxicity of pesticides towards microorganisms, wastewater can not be treated by biological methods and its biodegradation is not possible (Chiron et al., 2000). The most suitable technique for removing pesticides from wastewater is photodegradation. During the photodegradation process, oxidation-degradation reactions take place during which organic radicals are generated. The intermediate radicals that were formed during the degradation process are captured by dissolved molecular oxygen and are further guided through peroxy radicals, thus increasing the efficiency of the degradation process (Tomašević et al., 2009). The advantage of this process compared to other processes is that it results in a complete transformation of harmful substances (Tomašević et al., 2009).

The aim of this work is to investigate the possibility of removing DFC from wastewater using the photocatalytic degradation process utilizing TiO₂ as a photocatalyst.

Materials and Methods

Degradation of DFC by means of heterogeneous photocatalysis was carried out with the help of TiO₂ P25 (Degussa) photocatalyst. For the purposes of the experiment, a cylindrical glass thermostated reactor with a volume of 100 cm³ was used. The double walls in which the thermostatic water circulates in the reactor made it possible to maintain the reaction temperature.

The initial concentration of DFC solution was 15 ppm, while the mass of TiO₂ was 10 mg. The suspension is mixed during the irradiation process on a magnetic stirrer (500 rpm). In this way, an even distribution of TiO₂ particles was achieved. The apparatus was placed in a digester, in which protection from daylight was provided. In certain time intervals, sampling was carried out for the purposes of analytical testing. After sampling from the reactor, filtration was performed through a nylon filter (Cronus, 13 mm, 0.22 μm).

The change in pesticide concentration was monitored on a UV/Vis spectrophotometer (Shimadzu 1800) in the range from 200 to 400 nm, in quartz cuvettes with an optical path of 1 cm. Residual concentrations were sampled at certain time intervals (0, 10, 20, 30, 60, 90 and 120 min). Degradation kinetics were determined at 235 nm.

The degree of removal of DFC and the reaction rate constant (*k*) were used as a measure of the catalytic activity of TiO₂ in photocatalytic degradation processes. With the help of the Langmuir-Hinshelwood (Li et al., 2021) kinetic model, the pseudo-first-order degradation rate constant was determined.

$$\ln c/c_0 = -k \cdot t \quad (1)$$

where *k* is the reaction constant, pseudo first order.

Results and discussion

Absorption spectra of adsorbate medium given as a series are provided in the Figure 1. As it can be seen from the Figure 1, absorption maximums lowers as the contact time increases. The changes in

the adsorption spectra during the degradation of DFC during 2h of irradiation are presented. The rate of photocatalytic degradation of DFC is influenced by its initial concentration. Research has shown that the speed of the process decreases with increasing pesticide concentration. In Figure 2, it can be seen how the initial concentration of DFC affects the photocatalytic degradation, in the presence of the optimal concentration of TiO₂. An increase in the initial concentration of the substrate leads to an increasing number of DFC molecules adsorbed on the surface of the catalyst, which leads to a decrease in the efficiency of the photocatalytic process (Nezamzadeh-Ejehieh & Moeinirad, 2011). Also, organic molecules have the ability to absorb light, as well as catalyst particles, and this leads to a decrease in the photoactivity of semiconductors (Nezamzadeh-Ejehieh & Moeinirad, 2011).

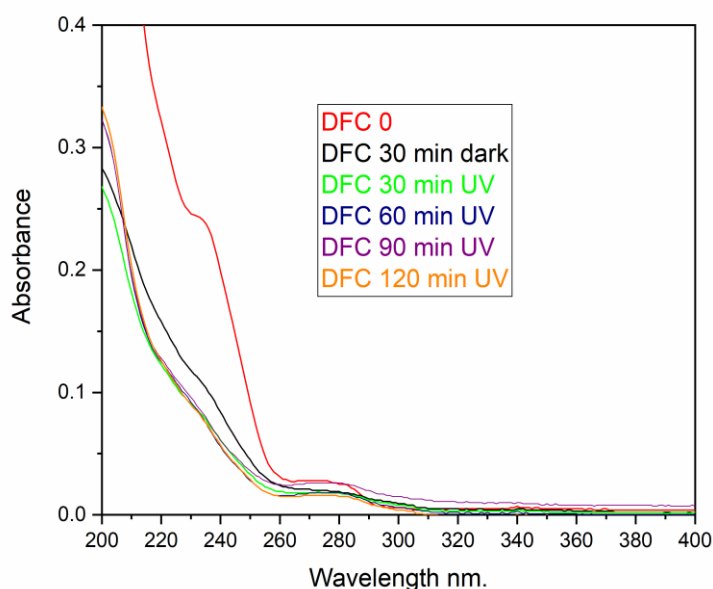


Figure 1. UV adsorption spectrum of DFC in the presence of 10 mg/L TiO₂

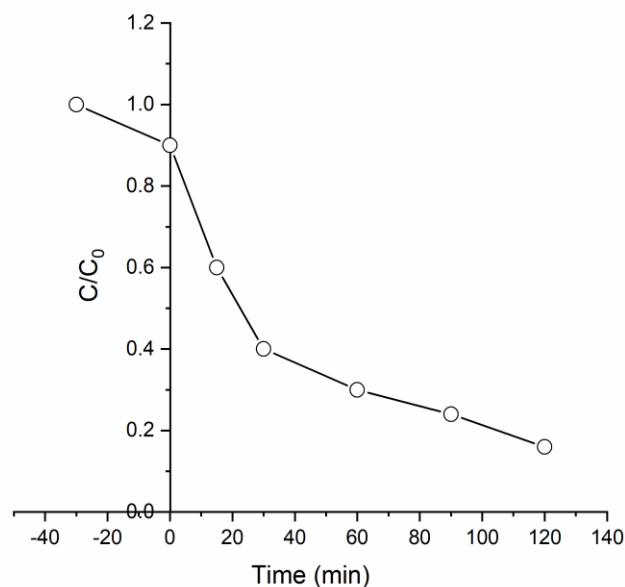


Figure 2. Effect of DFC concentration on the rate of photocatalytic degradation in wastewater

Conclusion

The subject of this work was the removal of DFC from wastewater by photocatalytic degradation. Photocatalytic degradation was studied with the help of nanogranulometric photocatalyst TiO₂ P25 (Degussa), in a thermostated quartz reactor. The change in DFC concentration was monitored on a UV/Vis spectrophotometer. The degradation kinetics is pseudo-first order. After 120 minutes, DFC was fully degraded. Based on the presented results, it can be concluded that DFC was successfully degraded from wastewater with the help of TiO₂ photocatalyst, which implies that applied system has a viable path in future investigation and optimization.

Acknowledgements: This work was supported by the Ministry of Education, Science and Technological Development of the Republic of Serbia (Contract No., 451-03-1270/2022-14/2685, 451-03-68/2022-14/200066, 451-03-68/2022-14/200023, 451-03-68/2022-14/200135).

References

- Bavcon Kralj, M., Černigoj, U., Franko, M. & Trebše, P. (2007). Comparison of photocatalysis and photolysis of malathion, isomalathion, malaoxon, and commercial malathion-Products and toxicity studies. *Water Research*, 41(19), 4504–4514. <https://doi.org/10.1016/j.watres.2007.06.016>
- Chiron, S., Fernandez-Alba, A., Rodriguez, A. & Garcia-Calvo, E. (2000). Pesticide chemical oxidation: State-of-the-art. *Water Research*, 34(2), 366–377. [https://doi.org/10.1016/S0043-1354\(99\)00173-6](https://doi.org/10.1016/S0043-1354(99)00173-6)
- Eriksson, E., Baun, A., Mikkelsen, P. S. & Ledin, A. (2007). Risk assessment of xenobiotics in stormwater discharged to Harrestrup Å, Denmark. *Desalination*, 215(1–3), 187–197. <https://doi.org/10.1016/j.desal.2006.12.008>
- Hincapié, M., Maldonado, M. I., Oller, I., Gernjak, W., Sánchez-Pérez, J. A., Ballesteros, M. M. & Malato, S. (2005). Solar photocatalytic degradation and detoxification of EU priority substances. *Catalysis Today*, 101(3-4 SPEC. ISS.), 203–210. <https://doi.org/10.1016/j.cattod.2005.03.004>
- Jing, J., Liu, M., Colvin, V. L., Li, W. & Yu, W. W. (2011). Photocatalytic degradation of nitrogen-containing organic compounds over TiO₂. *Journal of Molecular Catalysis A: Chemical*, 351, 17–28. <https://doi.org/10.1016/j.molcata.2011.10.002>
- Li, T., Abdelhaleem, A., Chu, W., Pu, S., Qi, F. & Zou, J. (2021). S-doped TiO₂ photocatalyst for visible LED mediated oxone activation: Kinetics and mechanism study for the photocatalytic degradation of pyrimethanil fungicide. *Chemical Engineering Journal*, 411(July 2020), 128450. <https://doi.org/10.1016/j.cej.2021.128450>
- Marican, A. & Durán-Lara, E. F. (2018). A review on pesticide removal through different processes. *Environmental Science and Pollution Research*, 25(3), 2051–2064. <https://doi.org/10.1007/s11356-017-0796-2>
- Moore, M. T., Lizotte, R. E., Knight, S. S., Smith, S. & Cooper, C. M. (2007). Assessment of pesticide contamination in three Mississippi Delta oxbow lakes using *Hyalella azteca*. *Chemosphere*, 67(11), 2184–2191. <https://doi.org/10.1016/j.chemosphere.2006.12.026>
- Nezamzadeh-Ejhi, A. & Moeinirad, S. (2011). Heterogeneous photocatalytic degradation of furfural using NiS-clinoptilolite zeolite. *Desalination*, 273(2–3), 248–257. <https://doi.org/10.1016/j.desal.2010.12.031>
- Oller, I., Malato, S. & Sánchez-Pérez, J. A. (2011). Combination of Advanced Oxidation Processes and biological treatments for wastewater decontamination-A review. *Science of the Total Environment*, 409(20), 4141–4166. <https://doi.org/10.1016/j.scitotenv.2010.08.061>

- Palma, P., Kuster, M., Alvarenga, P., Palma, V. L., Fernandes, R. M., Soares, A. M. V. M., López de Alda, M. J., Barceló, D. & Barbosa, I. R. (2009). Risk assessment of representative and priority pesticides, in surface water of the Alqueva reservoir (South of Portugal) using on-line solid phase extraction-liquid chromatography-tandem mass spectrometry. *Environment International*, 35(3), 545–551. <https://doi.org/10.1016/j.envint.2008.09.015>
- Pimentel, D. (1995). Amounts of pesticides reaching target pests: Environmental impacts and ethics. *Journal of Agricultural and Environmental Ethics*, 8(1), 17–29. <https://doi.org/10.1007/BF02286399>
- Sakkas, V. A., Calza, P., Vlachou, A. D., Medana, C., Minero, C. & Albanis, T. (2011). Photocatalytic transformation of flufenacet over TiO₂ aqueous suspensions: Identification of intermediates and the mechanism involved. *Applied Catalysis B: Environmental*, 110, 238–250. <https://doi.org/10.1016/j.apcatb.2011.09.006>
- Šunjka, D. B. (2012). *Ostaci atrazina i njegovih degradacionih produkata u podzemnim vodama Srbije*. Doktorska disertacija, Poljoprivredni fakultet, Univerzitet u Novom Sadu.
- Tomašević, A. V., Avramov Ivić, M. L., Petrović, S. D., Jovanović, M. B. & Mijin, D. Ž. (2009). A study of the electrochemical behaviour of methomyl on a gold electrode in a neutral electrolyte. *Journal of the Serbian Chemical Society*, 74(5), 573–579. <https://doi.org/10.2298/JSC0905573T>

Original scientific article

UTILIZATION OF CONSTRUCTION MATERIAL AND UNSATURATED RESIN FROM WASTE PET AS A STABILIZER FOR DESORBED METAL ION Pb^{2+}

Nataša Knežević¹, Jovana Bošnjaković², Aleksandar Jovanović³, Mladen Bugarčić³, Srećko Manasijević², Aleksandar Marinković¹

¹Faculty of Technology and Metallurgy, University of Belgrade, Karnegijeva 4, 11120 Belgrade, Serbia

²Research and Development Institute Lola L.T.D., Kneza Višeslava 70A, 11030 Belgrade, Serbia

³Institute for Technology of Nuclear and Other Raw Materials, Bulevar Franše d'Eperea 86, 11000 Belgrade, Serbia

Abstract

Wastewater management covers various techniques developed to provide purified water that would do minimum harm to the environment. Applying adsorption leaves a saturated adsorbent that should be regenerated or stabilized so it can't release pollutants into the environment. Lead, one of the most toxic pollutants, can be efficiently removed utilizing the adsorption process. After the consecutive adsorption and desorption processes, the lead must be processed to significantly reduce and prevent the risk to human health and environmental pollution. As one of the most efficient technologies for treating this toxic pollutant, stabilization has been tested by converting a desorbed lead to its salt lead-phthalate (LP). Obtained LP is used as a component in the production of construction materials and composites with unsaturated polyester resins (UPR). A standard leaching test (Toxicity Characteristic Leaching Procedure - TCLP) was performed to determine the toxicity of the waste material used as an additive. The concentration of leached lead from the construction material with the addition of $Ca(OH)_2$ can be as high as 54 mg/L, which significantly exceeds the permitted limits. After adding cement, lead concentration is lower - 13 mg/L. The acquired results from the sample with UPR show that the concentration of released lead is as low as 0.01 mg/L. Such results indicate complete crosslinking of the UPR and strong binding of the lead ions. Applying the S/S technique together with the utilization of UPR would be an environmentally friendly operation and easily applicable procedure for stabilizing Pb^{2+} .

Keywords: lead, construction materials, (re)valorization of waste material, TCLP, resin composites.

Introduction

The removal of pollutants from wastewater, such as heavy metals, is attracting a lot of attention from scientists because of their negative impact on the environment and human health (Schwarzenbach et al., 2010). The most frequently present heavy metals and metalloids in wastewater are mercury, cadmium, lead, chromium, zinc, copper, nickel, cobalt, arsenic, antimony, etc. Their toxicity, persistence, high prevalence, and mobility are some of the obstacles that can be overcome by stabilization/solidification (S/S) technology (Yaashikaa et al., 2021). The stabilization process is used as the final step in the treatment of hazardous waste before it is landfilled. This chemically stabilizes and physically modifies the waste, in this case, desorbed lead, into a low-permeability solid matrix. In addition to waste disposal, the quality of the obtained composites is easier to handle and transport (Wiles, 1987).

The subject of this study is the stabilization of desorbed lead metal in the form of a very stable lead-phthalate salt ($C_8H_4O_4Pb$) (Stewart et al., 1947; Liming He et al., 2019) by adding calcium hydroxide ($Ca(OH)_2$), cement, and unsaturated polyester resins synthesized from the products of catalytic depolymerization of PET more than bifunctional alcohols (diol component) and maleic anhydride (MA) (Rusmirovic, 2016; Knežević et al., 2022). The possibility of applying the desorbed pollutant as an addition to construction material and polymer matrixes was tested by the standard toxicity characteristic leaching procedure (TCLP) (USEPA, 1990).

The aim of the research is the simultaneous disposal of waste material (desorbed lead) (Moon, 2022) which acquires a useful value, first in saving natural resources for the production of building materials and as a filler when using the newly created UPR composites for the production of floors in vehicles. As a novelty, the TCLP results obtained indicate an environmentally acceptable and health-safe disposal of desorbed metals by a composite UPR stabilization process.

Materials and Methods

1. Materials

Construction material samples were made in the form of a cube with dimensions of 25x65x135 mm by mixing $Ca(OH)_2$ (Carmeuse, "Jelen Do" a.d., Serbia) and portland cement ("Lafarge", Beocin, Serbia) with the addition of sand ("Tr Gravel", Serbia), distilled water and synthesized lead-phthalate salts (as a substitute for TOCell with bound lead ions). The resin-based composites were homogenized by mixing UPR, methyl ethyl ketone peroxide (MEKP, "Sigma-Aldrich", Germany) as the initiator and cobalt octoate (Co-oct, "Sigma-Aldrich", Germany,) as the accelerator with the addition of the recycling component, salt lead-phthalate.

Leaching fluids were prepared using glacial acetic acid (CH_3COOH , "Fluka AG", Switzerland) and 1N sodium hydroxide (NaOH, "Lachema", Czech,) with the addition of deionized water.

2. Methods

By mixing $Ca(OH)_2$ /cement, lead-phthalate, sand, and water in a ratio of 2:1:8:2, building material samples were made and thermostated for 7 days at a temperature of 24 °C. UPR-based composites were prepared by the emulsion mixing method by dispersing lead-phthalate in the UPR matrix. The created molds were cross-linked using MEKP (3 wt.%) as an initiator and Co-oct (3 wt.%) as the accelerator in standard polytetrafluoroethylene molds for uniaxial tensile tests (ASTM D882 test standard dimension 60x10x4 mm with narrowed neck area – 15x4x4 mm) and flammability measurements.

The leaching experiment (Leaching experiment - Toxicity Characteristic (TCLP)) was performed in order to confirm the disposal of the desorbed lead after adsorption-desorption cycles (Moon, 2022). One of the reasons for applying the solidification/stabilization method is to reduce the amount of hazardous waste that is disposed of in landfills, as it converts potentially hazardous waste into non-hazardous waste and recycles it while meeting the maximum allowable concentration after the leaching test. It is a standard batch leaching test developed by the US EPA (Method 1311) for waste classification (USEPA, 1990).

The solution used for the toxicity test was made up of 0.300 mL CH_3COOH and 3.500 mL 1N NaOH with the addition of deionized water to a normal beaker volume of 50 mL. The pH value of the obtained solution was 4.75. 25 g of the sample was placed in the extraction vessel and 50 mL of the prepared solution was added. The suspension was mixed on a rotary extractor for 1 day (24 h). After extraction, the solutions were filtered and the resulting filtrate was used to determine the metal concentration (As, Se, Pb, Cr, Cd, Ba) using the ICP-OES technique. As pH values affect the content of heavy metals and their leaching, increased metal leaching is expected in an acidic environment (Brunauer et al., 1938).

Material characterization

Fourier transforms infrared (FTIR) spectra were recorded in absorbance mode with a Nicolet™ iS™ 10 FT-IR Spectrometer (ThermoFisher SCIENTIFIC) equipped with Smart iTR™ Attenuated Total Reflectance (ATR) Sampling accessories.

Results and discussion

1. FTIR analysis

Fourier transform infrared spectra (FTIR) was used to identify the functional groups present in the newly formed building material and their changes after the extraction of heavy metals. Figure 1 shows the FTIR spectrum of the cement/lead-phthalate composite before and after the leaching experiment.

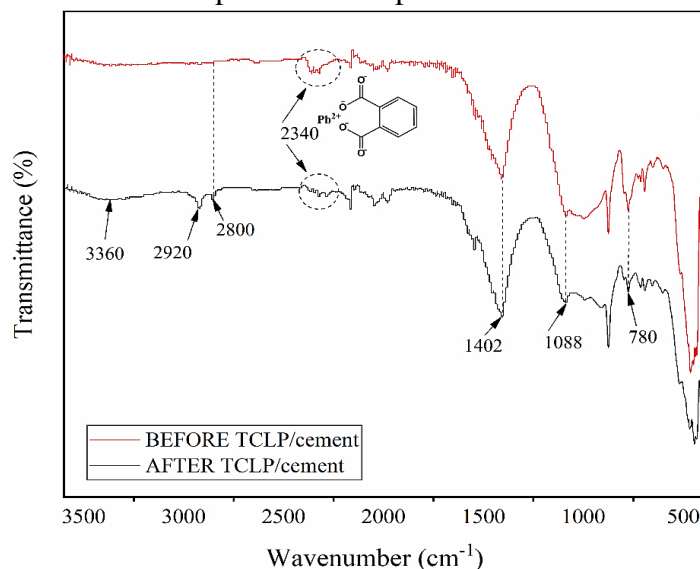


Figure 1. FTIR spectrum of cement/lead-phthalate sample

When examining the FTIR spectra of complexes –OH absorption bands of aqua ligands present at 3360 cm^{-1} correspond to the asymmetric and symmetric stretching vibration of water molecules. Small peaks at 2920 cm^{-1} and 2800 cm^{-1} originate from C-H stretching vibrations in the aromatic methoxy groups and the methyl and methylene groups of the side chain. The presence of lead in the sample before TCLP indicates a peak at 2340 cm^{-1} whose intensity decreased after the removal of heavy metals. The band at 1402 cm^{-1} can be attributed to the C–H bending of the methylene group. The intensity change was recorded at 1088 cm^{-1} , a characteristic peak for valence vibrations of C-O groups in carboxyl groups. The reduced intensity of the band at the wavelength of 780 cm^{-1} indicates the release of heavy metals after the completion of the leaching test (Dursun et al., 2009).

2. Production and testing of construction materials

The concentration of leached heavy metal ions was determined by optical emission spectrometry with inductively coupled plasma - ICP-OES (Thermo Scientific™ iCAP 7200 system).

By using glacial acetic acid as an agent in the leaching experiment, it was determined that significantly higher concentrations of lead ions are released from the analyzed samples with $\text{Ca}(\text{OH})_2$, which is considered a health-unsafe method of lead-phthalate stabilization. Low metal concentrations after treating the sample with cement can be attributed to better stability of the crystal structure and lower solubility of cement in the prepared TCLP solution. Of all the results of the TCLP test as the main criterion for the manipulation of the generated waste, the cross-linking of heavy metal with a polymer matrix (UPR), indicate that lead can be safely disposed of as an environmentally acceptable

material and the obtained composites can be further used for industrial purposes. The results of the leaching test of the samples (Figure 2) are shown in Table 1.



Figure 2. Laboratory samples for testing the release of heavy metals: a) with Ca(OH)_2 , b) with cement, c) with UPR

Table 1. Concentrations of released metals from formed composites

Element	The concentration of elements after leaching, mg L^{-1}			Limit
	Ca(OH)_2	Cement	UPR	
Pb	54	13	0.1	5.0
As	< 0.02	< 0.02	Not Detected*	5.0
Se	< 0.02	< 0.02	Not Detected	1.0
Cr	< 0.01	< 0.01	Not Detected	5.0
Cd	< 0.005	< 0.005	Not Detected	1.0
Ba	0.19	0.22	0.002	100

*Not Detected (< 0.001 mg L^{-1})

The results of the TCLP test show that the leaching of Pb^{2+} ions (54 mg L^{-1}) with the addition of Ca(OH)_2 is far greater than the maximum allowed value, which is close to 5 mg L^{-1} , according to national regulations (U. S. EPA, 1992). A drastically lower degree of leaching of desorbed metal (13 mg L^{-1}) was recorded in materials with the addition of cement as a stronger binding agent. The lowest level of leaching of lead ions occurs in the composite made with unsaturated polyester resin and lead-phthalate (0.1 mg L^{-1}). The results obtained by the leaching of UPR composites give the possibility of using a stabilized pollutant for the construction of trains, floors in warehouses, buildings, etc., with improved non-combustible properties and proof of eco-safety. In this way, a process has been developed to remove polluting substances without any additional pollution.

Conclusion

This study presents the results of the immobilization procedure of previously desorbed lead using building materials and resins made from waste PET. The results of the stabilization test showed that the most effective use of unsaturated polyester resins as a matrix for the stabilization of lead-phthalate salts, which meets the regulations on hazardous waste disposal and environmental protection. While the stabilizer Ca(OH)_2 was the least effective.

FTIR spectroscopy used to characterize the produced modules with Ca(OH)_2 and cement before and after the leaching test shows the changes occurring in the structure of the synthesized composites. The presence of lead in the sample before TCLP indicates a peak at 2340 cm^{-1} , the intensity of which decreased after the removal of heavy metals, which further confirms the effectiveness of the applied stabilization method.

The presented study is part of the contemporary trend related to polemics about energy or other methods of exploitation of waste material, i.e. hazardous waste, to achieve economic benefits, i.e.

marketable products, while satisfying the current legislation. The proposed technology must be a good achievement in the treatment of hazardous waste that produces non-hazardous stabilized materials. The developed methodology fulfills the principles of waste management, material recycling, resource conservation, and environmental protection.

Acknowledgments: This work was supported by the Ministry of Education, Science and Technological Development of the Republic of Serbia (Contract Nos., 451-03-1270/2022-14/2685, 451-03-68/2022-14/200066, 451-03-68/2022-14/200023, 451-03-68/2022-14/200135).

References

- Yaashikaa, P. R., Senthil Kumar, P., Saravanan, A. & Dai-Viet N. Vo. (2021). Advances in biosorbents for removal of environmental pollutants: A review on pretreatment, removal mechanism and future outlook. *Journal of Hazardous Materials*, 420, 126596 <https://doi.org/10.1016/j.jhazmat.2021.126596>
- Wiles, C. C. (1987). A review of solidification/stabilization technology. *Journal of Hazardous Materials*, 14, 5–27.
- Stewart, A., Pitrot, A. R., Leonard, M. & Kebrich, L. M. (1947). Complex salts are containing lead phthalate and lead salts of aliphatic acids. *United States Patent Office*, 2, 415,917.
- He, L., Zhou, J., Dai, S. & Ma, Z. (2019). Influence of Combustion Modifiers on the Cure Kinetics of Glycidyl Azide Polymer Based Propellant-Evaluated through Rheo-Kinetic Approach. *Polymers*, 11, 637. <https://doi.org/10.3390/polym11040637>
- Rusmirovic, J. (2016). *Dynamic-mechanical and thermal properties of composites based on unsaturated polyester resins and modified silicon-dioxide and cellulose nanoparticles*, (Doctoral dissertation). University of Belgrade, Faculty of Technology and Metallurgy, Belgrade.
- USEPA. (1990). Toxicity Characterization Leaching Procedure (TCLP), EPA Method 1311. USEPA, Washington, DC, USA.
- Brunauer, S., Emmett, P. H. & Teller, E. (1938). Adsorption of gases in multimolecular layers. *Journal of the American chemical society*, 60(2), 309–319. <https://doi.org/10.1021/ja01269a023>
- Dursun, A. K., Ibrahim, U. & Gokce, S. (2009). Bis(N, N-diethylnicotinamide) p-chlorobenzoate complexes of Ni(II), Zn(II) and Cd(II). *Journal of Thermal Analysis and Calorimetry*, 95(1), 247–251.
- USEPA (US Environmental Protection Agency). (1992). Toxicity Characteristic Leaching Procedure. Method 1311, Rev.0. In SW-846: test methods for evaluating solid waste, physical/chemical methods. Washington, DC: Office of Solid Waste.
- Schwarzenbach, R. P., Egli, T., Hofstetter, T. B., Von Gunten, U. & Wehrli, B. (2010). Global Water Pollution and Human Health. *Annu. Rev. Environ. Resour.*, 35, 109–136. <https://doi.org/10.1146/annurev-environ-100809-125342>
- Knežević, N., Jovanović, A., Bošnjaković, J., Milošević, M., Rančić, M., Marinković, A., Gržetić, J. & Gamoudi, H. (2022). Fire-resistant composites based on acrylic-functionalized lignin and polyester resin obtained from waste poly(ethylene terephthalate). *Scientific Technical Review*, 72(2), 32–37. <https://doi.org/10.5937/str2202032K>
- Moon, D. H. & Koutsospyros, A. (2022). A. Stabilization of Lead-Contaminated Mine Soil Using Natural Waste Materials. *Agriculture*, 12, 367. <https://doi.org/10.3390/agriculture12030367>

Original scientific article

BIOCHAR AS EFFICIENT TOOL FOR SOIL AMMENDEMENT

Zorica Lopičić¹, Anja Antanasković¹, Tatjana Šoštarić¹, Vladimir Adamović¹, Marina Orlić¹, Jelena Petrović¹, Jelena Avdalović²

¹Institute for Technology of Nuclear and Other Mineral Raw Materials, Belgrade, Serbia

²University of Belgrade-Institute of Chemistry, Technology and Metallurgy, Belgrade, Serbia

Abstract

Food production generates significant amounts of waste, especially in fruits and vegetables processing industries (FVPI), where biodegradable lignocellulosic waste (LCW) represents approx. 25-30% of processed raw materials. In most cases, this type of waste is landfilled, representing unsustainable practices with significant environmental hazards. Biochar, a highly carbonaceous organic material obtained from thermochemical conversion of LCW biomass, pose significant positive characteristics with multifunctional purpose. Biochar application might remove emerging contaminants from wastewater, and its application on soils improves soil properties such as fertility leading to improved crop productivity, soil pH regulation and soil CEC improvement, as well as microbial activities enhancement. In this paper, the characterization of biochar obtained via slow pyrolysis of peach stone (PS) is done along with its possible application as a soil amendment. This preliminary investigation revealed that the properties of the biochar produced from PS are in line with those necessary to act as a suitable agent for soil amendment.

Keywords: lignocellulosic waste, peach stone, biochar, soil amendment, circular economy.

Introduction

In the European Thematic Strategy for Soil Protection, the EC has recognized the main threats to the soil in the EU. These hazards are marked as loss of soil organic matter, soil compaction, erosion, desertification, salinization, soil acidification, loss of biodiversity, landslides and soil contamination (European Commission, 2020). Soil contamination can be a trigger for other degradation processes because it affects the ecosystem and causes toxicity to organisms, reducing biodiversity, which is associated with the loss of organic matter in the soil, imbalance of nutrients and consequent soil erosion. Regardless of the technology that pollutes the environment, improper disposal of waste or an accident, the land becomes first which is affected by contamination. Pollution spreads quickly through all mediums of the environment, into groundwater or surface water and ultimately affects the health population (SEPA, 2018). Accordingly, the only way to solve existing environmental problems, as well as related health problems, represents remediation of contaminated soil, maintaining and improving soil quality and preventing further contamination. Therefore, in order to sustain soil productivity, the crucial challenge is to maintain adequate levels of organic matter in the soil to preserve its physical, chemical and biological integrity.

Biochar is the product of biomass pyrolysis, a process whereby organic substances are broken down at temperatures ranging from 350 °C to 700 °C in a reduced oxygen thermal process. According to Lehmann and Stephen (2009), biochar applications have an effect on soil improvement, waste management, climate change mitigation and energy, and consequently might have social and economic benefits. Biochar improves soil physiology and increases productivity, assisting with crop

residue management. It also reduces soil acidity, while the essential mineral uptake increases. The significant quantities of K and phosphorus and lower amounts of Mg, Ca, Cu, Zn and Fe, which are presented in biochar, reflects its potential to be applied as fertilizer, too (Mwampamba et al., 2013). Globally, biochar has been considered a soil amendment tool, due to its suitable cation exchange capacity (CEC), which improves the soil pH, water-holding capacity and affinity for plant nutrients (Nsamba et al., 2015). In addition, biochar plays an important role in improving soil health by increasing crop yield and absorbing atmospheric carbon dioxide (Srinivasarao et al., 2013).

Demand for food has drastically increased in the last decades. This has consequently increased the amounts of organic waste, which goes to landfills every day, but also raised the application of chemical fertilizers in the soil to support increased food production. The fruits and vegetables processing industries (where biodegradable waste represents 25-30% of processed raw materials), generates significant amounts of waste which are in most cases, landfilled, representing unsustainable practice with environmental hazards. Recently the interest of many researchers have been raised in producing biochar from such bio-residues and using the obtained product as a soil amendment, due to the urgent need to find an alternative to chemical fertilizers. Fertilizers made of waste biomass available in abundant amounts, might promote global food production, enhance CO₂ capture, and reduce waste generated improving soil health and the overall environment.

Since the peaches (*Prunus persica* L.) have an important role in Serbia's fruit production with an average of five years of production approx. 45,000 t, which generates approx. 9,000 t peach stones waste (Statistical office of the Republic of Serbia, 2022), have been chosen as lignocellulosic biomass for biochar preparation. The specific aim of the present work was to investigate the characteristics of the waste peach stones biochar from the corner of its possible agriculture application in an environmentally sustainable manner.

Materials and Methods

Material: Peach stones were obtained from the Juice Factory Vino Župa Aleksandrovac, Serbia, where they have been classified as waste. They were washed, dried at room temperature, grinded by the vibrating disk mill Siebtechnik – TS250 (Siebtechnik GmbH, Germany), and sieved into a fraction between 0.1 to 0.5 mm (PS). Further, PS was pyrolysed at 500 °C under oxygen-limited conditions in a Nabertherm 1300 muffle furnace (Nabertherm, Germany) at the heating rate of 10 °C min⁻¹, for 1 h. The obtained biochar (PS-B) was stored in containers with polypropylene caps in a dark place.

Methods: Scanning Electron Microscopy (SEM) analysis was performed under a vacuum, where samples were coated with gold and observed using a JEOL JSM-6610 LV model (JEOL Ltd., Japan). Mass yield (%) of PS-B was expressed as the unit weight of biochar to the unit weight of dry PS times 100. For elemental analysis (C, H, N and S) Vario-EL III; CHNS-O Elementar Analyzer (Hanau, Germany) has been used. Analysis of moisture, volatile matter (VM) and ash were performed according to the ASTM D1762-84 (2007) standard. Fixed carbon (FC) was calculated by subtracting the ash, moisture and VM content from 100. The determination of the mineral content was performed by using atomic adsorption spectrometers (Perkyn Elmer AAS Analyst 300). The value of the suspension pH (pH_{sus}) was determined according to ASTM D6851-02 standard: 0.2 g of samples were suspended in 30 cm³ of distilled water, and left for 72 h with occasional stirring, after which suspension pH value was measured by using a pH meter SensION3 (Hach, USA). The point of zero charge (pH_{pzc}) values were determined by using a method described by Milonjić et al. (1975).

Results and discussion

The SEM micrographs of PS and PS-B (Fig. 1) revealed the changes after pyrolysis. It can be seen that the PS-B sample has a significantly higher surface area and porosity. It is evident also that PS-B

contains larger (20-30 μm) and smaller (1-3 μm) diameter pores. The porosity is increased by forming the pores located inside the larger ones, compared to the raw sample. The formation of secondary pores indicates the release of volatile matter during this treatment (Peiris et al., 2019). Previously done BET analysis, (Lopičić et al., 2021) confirmed SEM analysis results: specific surface area (SSA) increased from 0.545 m^2g^{-1} (PS) to 159.1 m^2g^{-1} (PS-B) where PS-B has a highly developed micro- and meso- pore structures in comparison to PS. Increased surface area and biochar porosity are highly beneficial to soil water retention capacity.

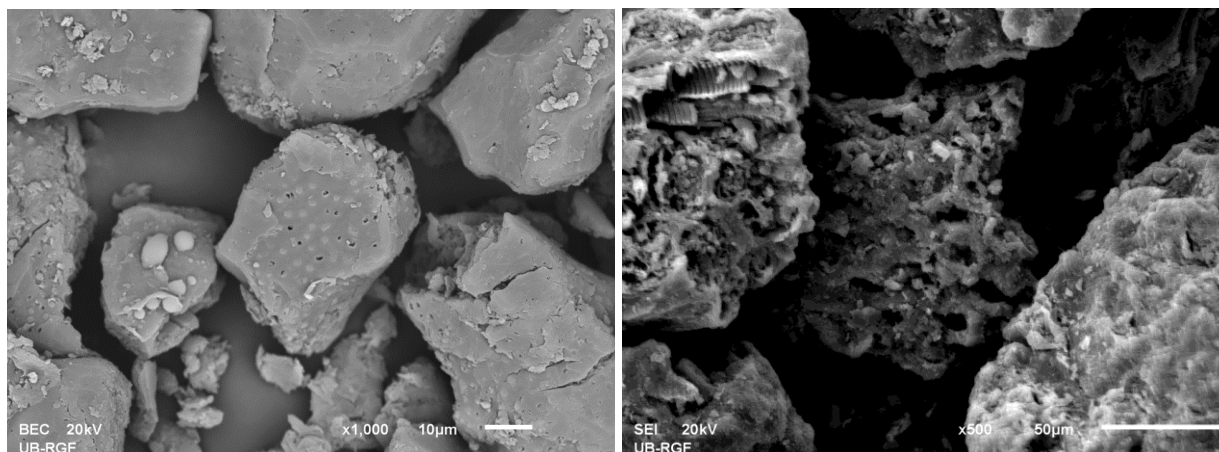


Figure 1. SEM micrographs of raw (PS) – left, and biochar sample (PS-B) - right

Such a larger surface area with a highly porous structure is suitable for absorbing soluble organic and inorganic nutrients and for providing a favourable environment for the growth of useful soil microbes. The advantages of biochar as a soil amendment are multiple. The presence of the microbes on biochar surface significantly increases microbial biomass carbon in soil compared with chemical fertilizers (Panwar et al., 2019). Another advantage of biochar as a soil amendment agent is carbon sequestration, which arises from the fact that biochar, is capable to absorb atmospheric carbon dioxide. According to Ahmad et al. (2014), the sorption of organic contaminants present in the soil depends mainly on surface area and pore size, thus biochar, in general, shows greater sorption capacity for organic than inorganic contaminants. However, ion exchange, electrostatic attraction and precipitation are dominant mechanisms for the remediation of inorganic pollutants by biochar.

Table 1 summarizes key parameters collected from the literature concerning biochar characteristics produced from different feedstock at pyrolysis temperature of 500 °C. In this table, the main physicochemical characteristics of biochar PS-B are also given. As can be seen, poultry manure and sewage sludge generate a higher biochar yield in comparison to agro residues and woody biomasses. This is related to the presence of inorganic components in feedstock, which is in accordance with relatively high ash content. However, high biochar yield can be achieved from agro waste too, if it has a high level of minerals and lignin (Sohi et al., 2010).

Table 1. Characteristics of biochars produced from different feedstock at pyrolysis temperature 500 °C

Feedstock	Yield*	VM*	FC*	Ash*	pH	C*	H*	O*	N*	Ref
Corn cobs	18.9	-	-	13.3	7.8	77.60	3.05	5.11	0.85	Mullen et al., 2010
Corn stover	17.0	-	-	32.8	7.2	57.29	2.86	5.45	1.47	
Orange peel	26.9	-	-	4.3	-	71.40	2.25	20.30	1.83	Chen & Chen, 2009
Pine needles	26.1	-	-	2.8	-	81.67	2.26	14.96	1.11	Chen et al., 2008
Rapeseed plant	35.6	17.5	69.6	12.9	-	75.03	2.62	7.79	1.41	Karaosmanoğlu et al. 2000
Poultry manure	72.0	7.3	68.6	24.0	11.0	51.56	1.87	40.32	5.50	Ahmad et al., 2014
Peach stone	28.14	25.20	71.89	0.73	5.76	69.37	2.74	27.49	0.30	This paper

*data reported in (Lopičić Z. et al., 2021)

Elemental composition and their calculated molar ratios are often used to reveal the temperature effects on the functional chemistry of biochars: an increase in pyrolysis temperature results in lower molar H/C and O/C ratios, thereby indicating dehydration and deoxygenation of the biomass (Ahmad et al., 2014). From Table 1 is evident that PS-B characteristics are in accordance with characteristics of biochar from a similar feedstock. The share of H and O decreased over C, leading to products with higher C concentration, due to the loss of biomass's volatile compounds during the process of pyrolysis. This can be seen by the high content of FC and low VM content. In addition, the value of H/C (0.04) and O/C (0.4) molar ratios indicate the stronger aromatic and stable structure of biochar, and the lower number of polar functional groups on the surface of PS-B (Lopičić et al., 2021). The values of these parameters are significant because they determine the stability of biochar in soil. According to Spokas (2014), who investigated the stability of biochar in soil, a lower O/C ratio results in more stable biochar. Accordingly, when the O/C molar ratio is > 0.6 , biochar will possess a half-life of < 100 years; if the range is 0.2–0.6, the half-life range is 100 - 1000 years, and if the molar O/C ratio is less than 0.2, the half-life will be more than 1000 years (Spokas, 2014). Therefore, biochar remains in soil longer if the molar ratio of O/C in biochar is lower. Obtained results for PS-B indicate that its half-range in the soil will be more than 500 years.

The low ash content of 0.73% for the PS-B indicates that most of the biochar is made from the combustible phase. Nevertheless, the value of pH_{SUS} of PS-B is higher (5.76) in comparison to raw PS (4.10). The reason for that can be found in feedstock composition (PS) and the number of present minerals in it, like potassium, magnesium and calcium ions. According to Lopičić (2017), the content of essential elements in the ash of PS are: calcium (4.2%), magnesium (6.99%) and potassium (25.4%), as well as phosphorus (26.88%). The analysis of major components of mineral matter in ashes of PS-B revealed that the K, Ca and Mg are major components of the ashes. The content of K was 19.9%, Mg was 9%, while the Ca content was also significant. The amount of Fe was approximately 2% for both samples, while the number of other components analysed was. This mineral composition is beneficial for promoting plant growth, suggesting that PS-B can be used in soil enrichment and approves that this material can be used as a supplement in agricultural practice. The pH_{pzc} was also determined because it describes the acid-base sorbent behaviour at which the net surface charge of the sorbent becomes electrically neutral. The biochar surface charge has been significantly changed after pyrolysis by increasing the pH value of the point zero charge pH_{pzc} from 4.8 (PS) to 6.0 (PS-B). These results show the basic character of the PS-B. These results agree with the overall literature about biochars that typically indicate basic properties.

Conclusion

In this paper, peach stones, renewable, waste material, which is reutilized from landfills, were pyrolysed to obtain biochar (PS-B). In order to determine PS-B's potential as a soil amendment, its characterization has been performed. The pyrolysed sample contains a large multi-porous surface area, with increased aromaticity compared to the native sample. Biochar PS-B has the potential to remain in soil longer since the molar ratio of O/C in biochar is low (0.4). Mineral content and value of pH_{SUS} also approve that can be used as a supplement in agricultural practice, while the value of pH_{pzc} shows a basic character of biochar PS-B indicating its potential to reduce the soil acidity. The results clearly indicate that PS-B has potential for soil improvement, which at the same time reduces the number of landfill wastes and decreases greenhouse gas emissions by carbon sequestering and reduction of methane emissions from landfills.

Acknowledgements: This work was supported by the Ministry of Education, Science and Technological Development of the Republic of Serbia (grant no 451-03-68/2022-14/200023).

References

- Ahmad, M., Rajapaksha, A. U., Lim, J. E., Zhang, M., Bolan, N., Mohan, D., Vithanage, M., Lee, S. S. & Ok, Y. S. (2014). Biochar as a sorbent for contaminant management in soil and water: A review. *Chemosphere*, 99, 19–33. <https://doi.org/10.1016/j.chemosphere.2013.10.071>
- Chen, B., Zhou, D. & Zhu, L. (2008). Transitional adsorption and partition on nonpolar and polar aromatic contaminants by biochars of pine needles with different pyrolytic temperatures. *Environmental Science & Technology*, 42(14), 5137–5143. <https://doi.org/10.1021/es8002684>
- Chen, B. & Chen, Z. (2009). Sorption of naphthalene and 1-naphthol by biochars of orange peels with different pyrolytic temperatures. *Chemosphere* 76(1), 127–133. <https://doi.org/10.1016/j.chemosphere.2009.02.004>
- European Commission. (2020). EU soil strategy for 2030. https://ec.europa.eu/environment/soil/soil_policy_en.htm, accessed in June 2022.
- Karaosmanoğlu, F., Işığigür-Ergüdenler, A. & Sever, A. (2000). Biochar from the straw–stalk of rapeseed plant. *Energy Fuels*, 14(2), 336–339. <https://doi.org/10.1021/ef9901138>
- Lehmann, J. & Joseph, S. (Eds.). (2009). Biochar for environmental management: An introduction, In J. Lehmann & S. Joseph (Eds.), *Biochar for Environmental Management: Science and Technology* (1st ed.). (pp. 1–12). Applied Routledge, London. <https://doi.org/10.4324/9781849770552>
- Lopičić, Z. (2017, September 21). *Sorption properties and thermal behaviour of Prunus persica L. waste biomass*, (Doctoral Dissertation), University of Belgrade, Faculty of Technology and Metallurgy, Belgrade. <https://uvidok.rcub.bg.ac.rs/handle/123456789/2110>
- Lopičić, Z., Avdalović, J., Milojković, J., Antanasković, A., Lješević, M., Lugonja, N. & Šoštarić T. (2021). Removal of diesel pollution by biochar - support in water remediation. *Hemijska industrija*, 75(6), 329–339. <https://doi.org/10.2298/HEMIND210514029L>
- Milonjić, S., Ruvarac, A. & Sušić, M. (1975). The heat of immersion of natural magnetite in aqueous solutions. *Thermochimica Acta*, 11, 261–266. [https://doi.org/10.1016/0040-6031\(75\)85095-7](https://doi.org/10.1016/0040-6031(75)85095-7)
- Mullen, C. A., Boateng, A. A., Goldberg, N. M., Lima, I. S., Laird, D. A. & Hicks, K. B. (2010). Bio-oil and bio-char production from corn cobs and stover by pyrolysis. *Biomass and Bioenergy*, 34(1), 67–74. <https://doi.org/10.1016/j.biombioe.2009.09.012>
- Mwampamba, T. H., Owen, M. & Pigaht, M. (2013). Opportunities, challenges and way forward for the charcoal briquette industry in Sub-Saharan Africa. *Energy for Sustainable Development*, 17(2), 158–170. <https://doi.org/10.1016/j.esd.2012.10.006>
- Nsamba, H. K., Hale, S. E., Cornelissen, G. & Bachmann, R. T. (2015). Sustainable technologies for small-scale biochar production - a review. *Journal of Sustainable Bioenergy Systems*, 5, 10–31. doi: 10.4236/jsbs.2015.51002
- Panwar, N. L., Pawar, A. & Salvi, B. L. (2019). Comprehensive review on production and utilization of biochar. *SN Applied Sciences*, 1(168). <https://doi.org/10.1007/s42452-019-0172-6>.
- Peiris, C., Nayanathara, O., Navarathna, C. M., Jayawardhana, Y., Nawalage, S., Burk, G., Karunanayake, A. G., Madduri, S. B., Vithanage, M., Kaumal, M. N., Mlsna, T. E., Hassan, E. B., Abeyesundara, S., Ferez, F. & Gunatilake, S. R. (2019). The influence of three acid modifications on the physicochemical characteristics of tea-waste biochar pyrolyzed at different temperatures: a comparative study. *RSC Advances*, 9(31), 17612–17622. <https://doi.org/10.1039/c9ra02729g>
- SEPA. (2018). Ka dekontaminaciji zemljišta u RS [Towards soil decontamination in the RS]. , <http://www.sepa.gov.rs/download/zemljiste/KaDekontaminacijiZemljista.pdf>

- Sohi, S. P., Krull, E., Lopez-Capel, E. & Bol, R. (2010). A review of biochar and its use and function in soil. In: Sparks, D. L. (Ed.), *Advances in Agronomy*. Academic Press, Burlington, (pp. 47–82). [https://doi.org/10.1016/S0065-2113\(10\)05002-9](https://doi.org/10.1016/S0065-2113(10)05002-9)
- Spokas, K. A. (2014). Review of the stability of biochar in soil: predictability of O:C molar ratios. *Carbon management*, 1(2), 289–303. <https://doi.org/10.4155/cmt.10.32>
- Srinivasarao, C., Gopinath, K. A., Venkatesh, G., Dubey, A. K., Wakudkar, H, Purakayastha, T. J., Pathak, H., Jha, P., Lakaria, B. L., Rajkhowa, D. J. Mandal, S., Jeyaraman, S., Venkateswarlu, B. & Sikka, A. K. (2013). Use of biochar for soil health enhancement and greenhouse gas mitigation in India: potential and constraints. *NICRA Bulletin*, 1, 1–51. <http://www.nicra-icar.in/nicrarevised/images/Books/Biochor%20Bulletin.pdf>
- Statistical office of the Republic of Serbia. <https://www.stat.gov.rs>, accessed 14.09.2022

Original scientific article

A STUDY OF PV SYSTEM APPLICATION ON THE SUSTAINABLE DEVELOPMENT IN SERBIA

Dragana Todorović¹, Slavica Jovanović¹, Tijana Kevkić¹, Marija Stojanović Krasić², Nenad Milojević³, Branko Drljača¹

¹University of Priština, Faculty of Sciences and Mathematics, Kosovska Mitrovica, Serbia

²University of Niš, Faculty of Technology, Leskovac, Serbia

³University of Niš, Faculty of Sciences and Mathematics, Niš, Serbia

Abstract

Climate change is one of the most significant environmental problems and is affecting the entire global population. Renewable sources of energy (RES) are vital to deal with this problem. Solar energy, especially photovoltaic (PV) technologies, is one of the most promising renewable energy sources and is, therefore, one of the fastest-growing industries in this field. Thus, this paper focuses on the performance analyses of rooftop on-grid PV system in real climatic conditions in Niš (Serbia) in 2019 and its environmental benefits. Besides, the life cycle assessment (LCA) for the PV system, based on a case study in Niš, is also given in this paper. Based on this study, energy from PV systems could potentially be a part of the solution for Serbia's future energy demands, as well as for the preservation of the environment and the establishment of sustainable development in Serbia.

Keywords: PV system, PV system Efficiency, Performance Ratio, LCA, EPBT.

Introduction

Mankind has lately been faced with climate change and now it is becoming an increasing concern. The sudden increase in population, with a manifold increase in global industrial and other human activities, has led to the increased use of fossil fuels and the uncontrolled global degradation of the environment. In order to restore the ecological balance and sustainable development of mankind, it is necessary to make greater use of renewable sources of energy (RES). The renewable energy applications contribute to GHG emissions reduction with a concomitant reduction of fossil fuel use. Among the available alternative energies, photovoltaic (PV) energy is one of the most promising renewable energies. PV energy is clean, simple in design, and requires very little maintenance. Many studies show that PV systems will have an important share in the electricity of the immediate future. This applies both to developed and developing countries (Bhubaneswari, 2011).

The developments in PV systems are mainly driven by the agenda to reduce carbon emissions of energy systems. Over the last thirty years, hundreds of life cycle assessments (LCAs) have been conducted and published for a variety of residential and utility-scale solar photovoltaic (PV) systems. Life cycle assessment (LCA) is a valuable tool for providing a comprehensive view of technology's environmental burdens and for analyzing renewable energy alternatives to conventional energy systems, especially for estimating greenhouse gas (GHG) emissions (Georgitsioti et al, 2019; Gerbinet et al, 2014; Muteri et al, 2020).

In this paper, the impact of PV system application on sustainable development in Serbia is reflected in estimating life cycle greenhouse gas (GHG) emissions of rooftop grid-connected (on-grid) PV systems based on a case study in Niš. The aim of this work was to focus on environmental hotspots, key parameters, and methodological insights through the LCA analysis of the PV system in a specific

location. Based on experimental measurements the CO₂ emission rate and the embodied energy payback time for solar PVs in Niš, in 2019 are presented in this paper.

Materials and Methods

This paper is focused on GHG emissions estimations of the PV systems during their lifecycle. To evaluate this the index g-CO₂, eq/kWh, which refers to the amount of GHG emissions released from each kilowatt-hour produced, will be used. The other index that will be accounted for in this study is the energy payback time (EPBT), which refers to the time it takes for a PV system to produce the same amount of energy that was used during production. The *GHG emission* estimates for solar PVs is based on Eq. [1]:

$$GHG = \frac{W}{G_{opt} \times \eta \times PR \times LT \times A} \quad (1)$$

where *GHG* is the mass emissions of *GHGs* weighted by their global warming potential (GWP) per unit of electricity generated (g CO₂-eq/kWh), $W = I \cdot E_{out}$ - is the GWP-weighted mass of GHGs emitted over the lifetime of the PV system (g CO₂-eq), G_{opt} is the POA irradiation (solar irradiation on the optimally-inclined plane) (kWh/m²/yr), η is the lifetime average PV system efficiency (%), *PR* is the performance ratio, *LT* is the system lifetime (yr), and *A* is the total module surface (PV array area) (m²).

Generally, the operation period of a PV system (the PV system lifetime) is assumed to be 25 years since the PV module warranties provided by the PV manufacturers are usually around 30 years and the performance of a system decreases over time due to various degradation mechanisms (Alsema, 2012; Georgitsioti et al, 2019; Gerbinet et al, 2014; Muteri et al, 2020; Sherwani et al, 2010).

PV system Efficiency

The *PV system Efficiency* (η) is defined as the ratio of energy output from the PV system to input energy from the sun and is defined as (Milosavljević et al, 2015):

$$\eta = \frac{\sum_i E_{out}}{A \times \sum_i G_{opt}} \quad (2)$$

where n – is a number of days in a year and E_{out} – is a total amount of electrical energy generated by PV system and transmitted to the power grid (Wh).

Performance Ratio

Performance Ratio of PV system is the ratio between the specific yield factor Y_f and the reference yield factor Y_r , where *reference yield* Y_r is defined as the ratio between the total POA irradiation and the reference irradiation of 1 kW/m² and *specific yield factor* Y_f (kWh/kW) is the ratio of the PV system electricity generated and the total PV system installed power (Milosavljević et al, 2015; Milosavljević, 2018; Milosavljević et al, 2022). PV system PR is given by Eq [3]:

$$PR = \frac{Y_f}{Y_r} = \frac{\frac{E_{out}(\text{kWh})}{P_{max}(\text{kW})}}{\frac{G_{opt}(\text{kWh/m}^2)}{1(\text{kW/m}^2)}} \quad (3)$$

The reference yield factor Y_r presents the solar irradiation resource for the PV system and is a function of the geographical location and PV array orientation, while the Y_f is a parameter used to normalize the energy produced with respect to the size of the PV system. Therefore, the PR presents the rate of effective energy generated with the energy that the system would produce if it continuously operated on its STC efficiency. So, the PR includes all PV system losses (optical and electric losses), gives the correlation of the PV system quality between installations in different locations and PV array orientations and does not directly depend on input parameters like the meteo inputs, module efficiency, and PV array orientation (Milosavljević et al, 2015; Milosavljević, 2018; Milosavljević et al, 2022).

Embodied energy payback time EPBT

The embodied energy payback time $EPBT$ (year) is the ratio of the embodied energy E_{em} (kWh/m²), which is the amount of energy required to produce the material in its product form, to the amount of energy obtained per year from the product E_{out} (kWh/m²/year). Embodied energy E_{em} for a PV system can be expressed as follows:

$$E_{em} = E_p + E_s + E_f + E_t + E_{BOS} \quad (4)$$

where E_p is the embodied energy required for the purification and processing of silicon (kWh); E_s is the embodied energy of silicon ingot slicing; E_f is the embodied energy for PV module fabrication (kWh); E_t is the energy to transport PV modules from factory to installation site (kWh); E_{BOS} is the embodied energy for components such as support structure, inverter, electrical wirings (kWh) (Li et al, 2013; Nawaz et al, 2006; Pantić et al, 2014). The typical values for the silicon monocrystalline PV module as given in (Li et al. 2013; Nawaz et al, 2006) are $E_p = 666$ kWh/m², $E_s = 120$ kWh/m², $E_f = 190$ kWh/m², and $E_{BOS} = 358$ kWh/m².

Based on experimental measurements in real climatic conditions in 2019, POA irradiation on the PV array area, the PV system Efficiency and Performance Ratio, and GHG emission estimates are calculated. On other hand, the calculated EPBT shows how long it takes before energy investments are compensated by energy yield.

PV system in Niš, Serbia

For the experimental examination of PV system operation, a fixed on-grid 2 kW_p PV system was installed on the roof of the Faculty of Sciences and Mathematics in Niš (Latitude: 43°19'28.99"N, Longitude: 21°54'11.99"E), Serbia (Fig.1). The PV system consists of 10 monocrystalline silicon (c-Si) solar modules (Shenzhen Sunco Solar Technology Co.), serially interconnected in a string; DC and AC distribution boxes; single phase inverter (Sunny Boy 2000HF), monitoring devices (Sunny SensorBox and Sunny WEBBox), and accompanying elements (conductors, cables, etc.). Solar modules and Sunny SensorBox were fixed on the building roof with an inclination angle of 32° to the South and are free from any shading effect, while other devices were set up inside the building. By adequate conductors and cables solar modules are connected to DC box, inverter, AC box (RO-AC) and the city power grid. At the output of AC distribution box there is alternating (AC) voltage 230V, 50Hz (Milosavljević et al, 2015; Milosavljević, 2018; Milosavljević et al, 2022).



Figure 1. Fixed on-grid 2 kW_p PV system in Niš, Serbia

For the PV systems monitoring, remote diagnostics, and data acquisition, Sunny WEBBox is used as the central communication interface. It is connected to the inverter and Sunny SensorBox by Bluetooth. This device enables continuous recording of the PV system electrical parameters into the internal memory of 12.5 MB. Sensor unit Sunny SensorBox measures global solar irradiation and ambient temperature. The Sunny SensorBox is connected with the Sunny WEBBox through an SMA Power Injector with Bluetooth. Thus, all measurement values (DC current and voltage, AC current and voltage, power at the output from the solar modules, PV system power, solar irradiation and ambient temperature) are each 5 minutes directly recorded on SD memory card or by FTP server (Milosavljević et al, 2015; Milosavljević, 2018; Milosavljević et al, 2022).

Results and discussion

The experimental values of solar irradiation on an optimally inclined (32°) and South oriented plane (POA irradiation) in Niš, as well as, amount of PV electricity produced by 2 kW_p fixed on-grid PV system with c-Si solar modules oriented to the South at an optimal angle of 32°, in 2019 in Niš, are given in this section. Besides, the PV system performance parameters, GHG emission estimates, and EPBT, described in Section 2, are also given and discussed.

Graphics of the changes in the experimental values of the electrical energy (E_{out}) generated by given PV system in Niš, depending on the POA irradiation (G_{opt}) in 2019 is given in Figure 2.

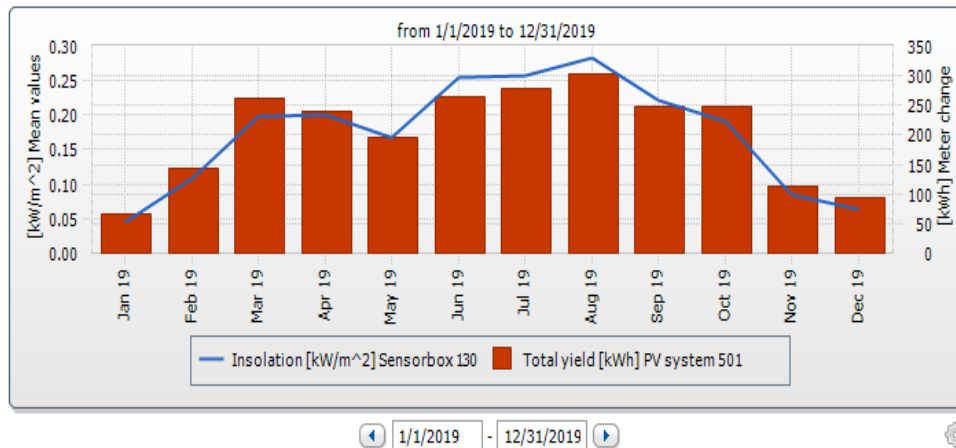


Figure 2. Graphics of the changes in the experimental values of the electrical energy (E_{out}) generated by given PV system, and the POA irradiation (G_{opt}) in 2019, in Niš

Statistical processing and analysis of measurements show that the experimental monthly average daily solar irradiation on optimally-inclined surface ranged between 1.42 (January) and 8.82 kWh/m²/day (August), while the monthly values of electricity generation from the PV system in Niš range between 66.89 kWh (January) and 303.05 kWh (August). It should be noted that experimental values of PV system electricity generation are values that the PV system, with a total surface of PV area of 16.59 m², transmits to the electricity distribution network.

Graphics of the experimental values of the monthly energy efficiency (η) of 2 kW_p PV system in 2019, in Niš is given in Figure 3.

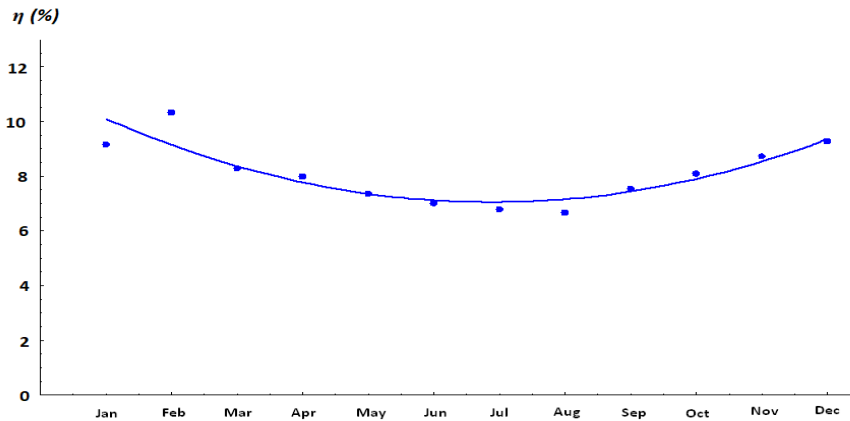


Figure 3. Graphics of the experimental values of the monthly energy efficiency (η) of 2 kW_p PV system in 2019, in Niš

Figure 3 shows that the experimental monthly energy efficiency (η) of 2 kW_p PV system in 2019, in Niš ranged from 6.68% (in August) to 10.34% (in February). The energy efficiency is the lowest in the summer months, which is explained by the increase in the ambient temperature that causes solar modules heating which leads to a decrease in the energy efficiency of the PV system. With the increase in solar modules temperature, there is an increase in the thermal vibration of cristal lattice atom of materials used to produce solar cells, which in turn impedes directed movement of free carriers of charging resulting in open circuit voltage decrease and solar cells power degradation. Besides, it should be noted that the PV system performances are usually specified under standard test conditions, but the performance of the PV system under real conditions differs from the expectations derived from the results under standard test conditions due to a variety of continuously changing conditions. The experimental monthly values of PR of the given PV system in 2019 are given in Figure 4.

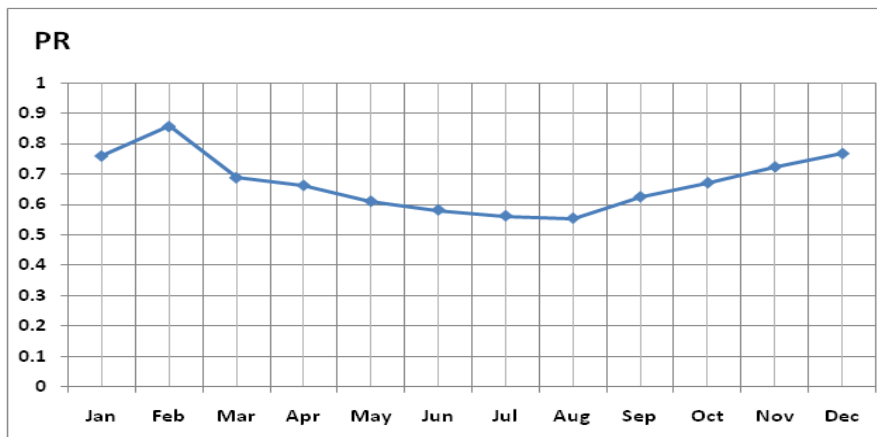


Figure 4. The experimental monthly values of PR of the given PV system in 2019

As PR is a quantitative characteristic of all losses in the PV system, due to losses that occur in summer due to the increase in PV module temperature, PR values are smaller in the summer than in the winter and, in the general case, are in the range between 0.6 and 0.8. The experimental monthly values of PR range from 0.55 (August) to 0.86 (February), as shown in Figure 3, while the annual mean experimental value of PR is 0.67.

GHG emission estimates and EPBT for solar PVs

Based on experimental measurements values, the GHG emission estimates and EPBT for rooftop on-grid 2 kW_p PV system with c-Si solar modules are 56.5 g CO₂-eq/kWh and 9.01 years, respectively. It should be noted that the energy to transport PV modules from factory to installation site (E_t) is not taken into account. If E_t were taken into a calculation, the EPBT would be less.

Conclusion

This research provides the basic environmental hotspots, key parameters, and methodological insights through the LCA analysis of the PV system in a specific location. Based on experimental obtained results in 2019, in Niš, presented in this paper, it could be concluded that:

- Total annual value of the global solar irradiation on the surface oriented southward, at the optimal angle of 32° in relation to the horizontal surface in Niš, was 1929.51 kWh/m²;
- Rooftop on-grid 2 kW_p PV system in Nis generated 2455.621 kWh of electrical energy;
- The annual energy efficiency of 2 kW_p PV system in Niš was 8.1% and the annual mean value of the PV system PR in Nis was 67%;
- The annual value of the CO₂ emission rate and EPBT for rooftop on-grid 2 kW_p PV system, with c-Si solar modules, are 56.5 g CO₂-eq/kWh and 9.01 years, respectively.

Total lifecycle emissions associated with PV energy production are lower than those of fossil fuel energy production. During their 20-30 year lifetimes, solar modules generate more electricity than was consumed during their production. The energy payback time quantifies the minimum useful life required for a solar module to generate the energy that was used to produce the module, and the average energy payback time is around 9 years. Thus, silicon PV modules have a low life cycle environmental impact compared to most conventional forms of energy such as coal and natural gas. The greatest carbon emissions caused by the use of PV modules are those associated with module production. Energy Pay Back Times (EPBT) vary between 2 and 10 years for various solar climates around the world. Overall, silicon PV panels payback the required upfront energy costs of production well before their useful lifetime and are a net energy generators for the majority of their useful life. It should also be taken into account that the obtained results would probably slightly modify depending on which measurement year was used.

Acknowledgement: Authors thank the Ministry of Education, Science and Technological Development of the Republic of Serbia for support under Contract No. **451-03-68/2022-14** and the Faculty of Sciences and Mathematics in Kosovska Mitrovica (University of Priština in Kosovska Mitrovica, Department of Physics) for support under the project **ИЈ-0201**. Additionally, corresponding author would like to thank all researchers from the Solar Energy Laboratory in Niš (Faculty of Sciences and Mathematics, Department of Physics) for long-term cooperation.

References

Alsema, E. A. (2012). Environment and health, *Energy payback time and CO₂ emissions of PV systems* (pp. 1097–1117). Practical Handbook of Photovoltaics.

- Bhubaneswari, P., Iniyar, S. & Goic, R. (2011). A review of solar photovoltaic technologies. *Renewable and Sustainable Energy Reviews*, 15(3), 1625–1636. <https://doi:10.1016/j.rser.2010.11.032>
- Georgitsiotti, T., Pearsall, N., Forbes, I. & Pillai, G. G. (2019). A combined model for PV system lifetime energy prediction and annual energy assessment. *Solar Energy*, 183(7), 738–744. <https://doi.org/10.1016/j.solener.2019.03.055>
- Gerbinet, S., Belboom, S. & Léonard, A. (2014). Life Cycle Analysis (LCA) of photovoltaic panels: A review. *Renewable and Sustainable Energy Reviews*, 38(C), 747–753. <https://doi:10.1016/j.rser.2014.07.043>
- Li, D. H. W., Chow, S. K. H. & Lee, E. W. M. (2013). An analysis of a medium size grid-connected building integrated photovoltaic (BIPV) system using measured data. *Energy and Buildings*, 60, 383–387. <https://doi.org/10.1016/j.enbuild.2013.02.007>
- Milosavljević, D. D., Pavlović, T. M. & Piršl, D. S. (2015). Performance analysis of a grid-connected solar PV plant in Niš, Republic of Serbia. *Renew. Sust. Energ. Rev.* 44(C), 423–435. <https://doi:10.1016/j.rser.2014.12.031>
- Milosavljević, D. D. (2018). Influence of meteorological parameters on the operation of a grid-connected PV solar plant. *University Thought*, 8(1), 56–61. <https://doi:10.5937/univtho8-17271>
- Milosavljević, D. D., Kevkić, T. S. & Jovanović, S. J. (2022). Review and validation of photovoltaic solar simulation tools/software based on case study. *Open Physics*, 20(1), 431–451. <https://doi.org/10.1515/phys-2022-0042>
- Muteri, V., Cellura, M., Curto, D., Franzitta, V., Longo, S., Mistretta, M. & Parisi, L. M. (2020). Review on Life Cycle Assessment of Solar Photovoltaic Panels. *Energies*, 13(1), 252, 1–38. <https://doi:10.3390/en13010252>
- Nawaz, I. & Tiwari, G. N. (2006). Embodied energy analysis of photovoltaic (PV) system based on macro- and micro-level. *Energy Policy*, 34(17), 3144–3152. <https://doi.org/10.1016/j.enpol.2005.06.018>
- Pantić, L. S., Pavlović, T. M. & Milosavljević, D. D. (2014). A practical field study of performances of solar modules at various positions in Serbia. *Thermal Science*, 19(2), 511–523. <https://doi.org/10.2298/TSCI140313081P>
- Sherwani, A. F., Usmani, J. A. & Varun. (2010). Life cycle assessment of solar PV based electricity generation systems: A review. *Renewable and Sustainable Energy Reviews*, 14(1), 540–544. <https://doi.org/10.1016/j.rser.2009.08.003>

Original scientific article

TIME AND SEASONAL VARIATIONS OF PARTICULATE MATTER (PM) AND GASEOUS POLLUTANTS CONCENTRATIONS IN AMBIENT AIR OF VALJEVO, SERBIA

Jelena Đuričić Milanković^{1,2}, Dragana Đorđević³, Slavica Ilić¹

¹Academy of Applied Studies Šabac, Department of Medical and Business-Technological Studies, Hajduk Veljkova 10, Šabac, Serbia

²ICTM Institution of National Importance, University of Belgrade, Njegoševa 12 (Studentski trg 14–16), Belgrade, Serbia

³Centre of Excellence in Environmental Chemistry and Engineering–ICTM Institution of National Importance, University of Belgrade, Njegoševa 12 (Studentski trg 14–16), Belgrade, Serbia

Abstract

According to the latest European Commission Report "Status of Environment and Climate in the Western Balkans" the mortality rate that can be linked to air pollution in the Western Balkans is more than twice as high as the EU 27 average. The same report states that the dominant impact on mortality has PM_{2.5}. Valjevo is one of the cities in Serbia in which air quality has belonged to the third category (excessively polluted air) for many years due to exceeding the limit values for PM₁₀ and PM_{2.5}. In this paper, average concentrations and time and seasonal variations of particulate matter (PM₁₀ and PM_{2.5}) as well as gaseous pollutants (SO₂, NO₂, NO, NO_x, CO) measured at the automatic air quality monitoring station Valjevo in the period from December 2020 till May 2022 were analyzed. The daily mean concentrations of PM₁₀ and PM_{2.5} were 56.5 and 40.9 μg m⁻³, with maximum daily mean values of 318.8 and 246.4 μg m⁻³, respectively. The highest mean concentration of PM₁₀ and PM_{2.5} was measured during the winter period (78.3 and 64.2 μg m⁻³), followed by autumn, spring and summer with the lowest measured mean concentration (29.6 and 13.4 μg m⁻³). During the winter period, the major part of the PM₁₀ mass was in fine mode (PM_{2.5}) (82.9%) rather than coarse mode (PM_{10-2.5}) (17.1%), which can be attributed to the intensive combustion of biomass and fossil fuels for heating in households, industry and the public sector during this period.

Keywords: air pollution, PM_{2.5}, PM₁₀, Valjevo.

Introduction

Exposure to air pollution is the main environmental risk of early death and in 2019 is estimated to have contributed to 5.9–7.5 million premature deaths globally (Health Effects Institute HEI, 2020). Heart disease and stroke are the most common reasons for premature death attributable to air pollution, followed by lung diseases and lung cancer (WHO, 2018). Air pollution affects the whole population, certain groups are more vulnerable to its effects on health, such as children, elderly people, pregnant women and those with pre-existing health problems (EEA, 2019). Although air pollution has considerable economic impacts, cutting lives short, increasing medical costs and reducing productivity through working days lost across the economy (EEA, 2019).

Europe's most serious pollutants, in terms of harm to human health, are PM, NO₂ and ground-level O₃. The European Environment Agency (EEA) reports that in 2016, fine particles (PM_{2.5}) caused around 412,000 premature deaths of European citizens, NO₂ caused 71,000 and O₃ 15,000 (EEA, 2019). The same agency warns that high concentrations of pollution have the most visible effect, but

long-term exposure to lower doses poses a greater danger to human health. According to the latest report of the European Commission "Status of Environment and Climate in the Western Balkans" (Belis et al., 2022) in 2019, the annual mortality rate (premature deaths per 100,000 inhabitants) attributable to air pollution (mainly PM_{2.5}) in the Western Balkans (WB) was considerably higher than the EU27 average and in certain cases more than doubled it. The same report states that Serbia, Bosnia and Herzegovina and Albania contributed to nearly 90% of the total PM_{2.5} emissions in the WB region. In particular, the three-year PM_{2.5} average (2016–2018) is above the exposure concentration obligation (20 µg/m³) in most of the region and the main contributors of this pollutant are coal fuelled power plants and biomass burning for domestic heating (Belis et al., 2019). Air pollution in the WB contributes between 4% and 19% of total premature mortality in 18 selected WB cities and reduces life expectancy by between 0.4 and 1.3 years (UNEP, 2019).

The main sources of outdoor air pollution in Serbia include the energy sector (thermal power plants, district heating plants and individual household heating), the transport sector (an old vehicle fleet), waste dump sites and industrial activities (oil refineries, the chemical industry, mining and metal processing and the construction industry) (WHO, 2019). Air pollution significantly contributes the overall burden of disease and premature death in Serbia, having higher estimates of premature death due to air pollution than most countries in the European Union (WHO, 2019). According to the report of the WHO Regional Office for Europe (WHO, 2019) that included an extensive analysis of air quality and its impacts on health in Serbia for 11 Serbian cities the overall health impact of air pollution for the whole of the urban areas in Serbia (not just the 11 cities studied in detail) was estimated at 6 394 attributable deaths. According to the same report in Serbia for 11 Serbian cities exposure to PM_{2.5} accounts for 3585 premature deaths per year, including 1796 in Belgrade, where air pollution has by far the highest impact in absolute terms. But when estimates per 100 000 of the population at risk the mortality rates for the 11 cities the existing concentration of PM_{2.5} appears to be associated with the highest relative health impacts of air pollution in Valjevo (18.8%) (WHO, 2019). Valjevo is one of the cities in Serbia in which air quality has belonged to the third category (excessively polluted air) for many years due to exceeding the limit values for PM₁₀ and PM_{2.5}. In this paper, average concentrations and time and seasonal variations of particulate matter (PM₁₀ and PM_{2.5}) as well as gaseous pollutants (SO₂, NO₂, NO, NO_x, CO) measured at the automatic air quality monitoring station Valjevo in the period from December 2020 till May 2022 were analyzed. The air pollution level in the Valjevo during the observed period was assessed concerning the corresponding limit/ recommended values defined by national and other legislation dealing with air quality standards.

Materials and Methods

Study area

The city of Valjevo is located in the northwestern part of central Serbia. According to the data of the 2011 population census, a total of 90,312 inhabitants live in the Valjevo area, of which 69,223 live in the city center and suburbs, and 21,089 live in rural areas (Air quality plan for the period from 2016 to 2021, 2016). Valjevo covers an area of 2,256 ha and was formed in a basin surrounded by a mountain range, on the banks of the Kolubara River. The borders of the city are geographically clearly defined by the eastern slopes of the Vlašić mountain and the upper reaches of the Ub river, in the north, the peaks of the Valjevski mountains, in the west and south, and the Kolubara basin in the central part. The climate of this area can be characterized as moderate-continental, with certain specificities that manifest as elements of subhumid and microthermal climate. This type of climate conditions cold winters and warm to subtropical summers. The minimum annual temperature ranges up to -26.4 °C, and the maximum up to +42.4 °C. The area is such that there are great temperature extremes and very cold winters, with frequent severe frosts, and the snow cover, regardless of its

thickness, lasts from mid-December to the beginning of March (Air quality plan for the period from 2016 to 2021, 2016). The sources of air pollutant emissions in the city during the winter months basically include home heating and road traffic, while industry is an additional source. Coal and wood are predominantly used for domestic heating.

Automatic air quality monitoring station

Automatic air quality monitoring stations in Valjevo is managed by the Serbian Environmental Protection Agency (SEPA). Daily mean concentrations of air pollutants and meteorological data for Valjevo station was downloaded from the website of the Serbian Environmental Protection Agency (<http://www.amskv.sepa.gov.rs/pregledpodatakazbirni.php>). Concentrations of air pollutants from this station in the period from December 2020 till May 2022 were analyzed. Valjevo automatic air quality monitoring station monitors air pollutants (PM₁₀, PM_{2.5}, SO₂, NO₂, NO, No_x and CO) and meteorological parameters (wind speed, wind direction, surface pressure, temperature and relative humidity). The air sampling takes place hourly, using Teledyne API Model 100E for SO₂, Teledyne API Model 200A for NO/NO₂/NO_x, Teledyne API Model 300A for CO, TCR TECORA Skypost HV for PM₁₀ and GRIMM EDM 180 for PM_{2.5}. Measuring station Valjevo is an urban background station located at latitude 19° 53' 56" N and longitude 44° 16' 22" N. The automatic measuring station Valjevo is located within the city zone, which is characterized as residential and commercial. The locations of the station Valjevo are shown on the map in Fig. 1.

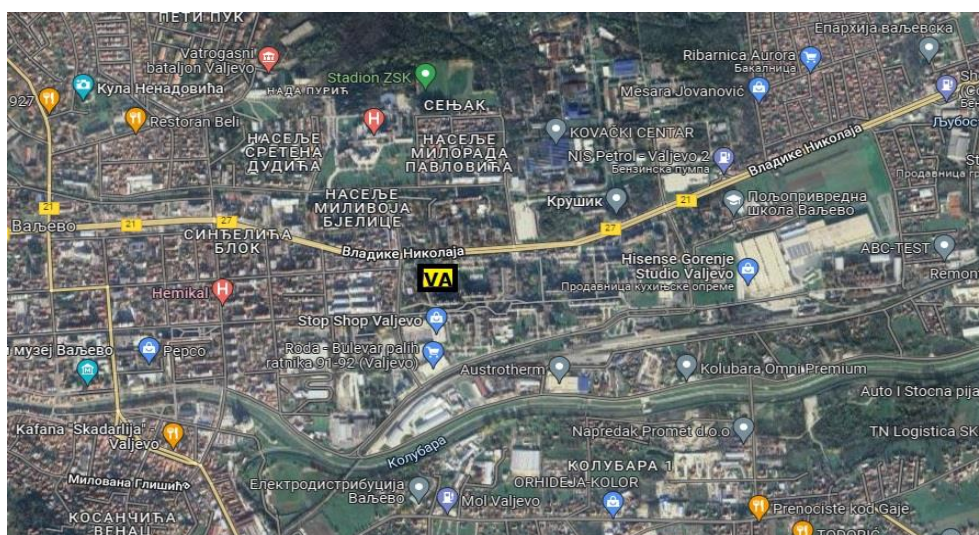


Figure 1. Map of the Valjevo with locations of the automatic air quality monitoring station VA (Source of the city map: <https://www.google.com/maps/@44.2725575,19.8936586,2245m/data=!3m1!1e3>)

Results and discussion

Mass concentrations of PM₁₀ and PM_{2.5} fractions and gaseous air pollutants for entire period and for seasons

Summary statistics of daily mean concentrations ($\mu\text{g m}^{-3}$) of different fractions of particulate matter observed at automatic air quality monitoring station Valjevo for entire period (December 2019 to May 2022) and for heating and non-heating seasons are shown in Tab. 1. The mass concentrations of PM₁₀ at the VA measuring station in the observed period were in the range from 9.9 to 318.8 $\mu\text{g m}^{-3}$ (with a mean value of 56.5 $\mu\text{g m}^{-3}$). The mass concentrations of fine mode PM_{2.5} (particles with a diameter of less than 2.5 μm) ranged from 4.9 to 246.4 $\mu\text{g m}^{-3}$ (with a mean value of 40.9 $\mu\text{g m}^{-3}$) (Tab. 1). The WHO estimate of the annual mean PM_{2.5} concentration in Serbia is 19.4 $\mu\text{g}/\text{m}^3$, with a slightly higher mean in urban than in rural areas: 21.0 $\mu\text{g}/\text{m}^3$ and 19.4 $\mu\text{g}/\text{m}^3$, respectively (WHO,

2016), and the average annual mean PM_{2.5} concentration calculated by WHO for the European Region as a whole is 14.0 µg/m³ (WHO, 2019). Therefore, the mean value of the PM_{2.5} concentration measured for the observed period for Valjevo was two times higher than the average annual value of PM_{2.5} in Serbia and 2.8 times higher than the mean annual PM_{2.5} concentration calculated by WHO for the European Region as a whole.

In this study PM_{2.5}/PM₁₀ ratios ranged from 0.04 to 0.99 with a mean value of 0.70 (Tab. 1). This is in agreement with results of Jeričević et al. (2016). During the colder part of the year PM_{2.5}/PM₁₀ was higher than 0.9 at almost all examined stations and lower during the warmer part of the year. The value of PM_{2.5}/PM₁₀ ratios of 0.04 observed during the non-heating season is due to the occurrence of an extremely high concentration of mean daily PM₁₀ concentration of 318.8 µg m⁻³ which was measured during June 15, 2021. If this value were excluded, the minimum value of PM_{2.5}/PM₁₀ ratios would be 0.22. Unusually for June, extremely high concentration of mean daily PM₁₀ concentration caused a short-term bad state of air quality in many places in Serbia, and the dominant reason for this phenomenon was the transfer of Saharan dust.

Table 1. Statistical summary of daily mean concentrations of different fractions of particulate matter and gaseous air pollutants observed at automatic air quality monitoring station Valjevo for entire period (December 2019 to May 2022) and for heating and non-heating seasons

	Total (n = 500) Mean ± SD Min. – Max. Range	Heating season ^a (n = 309) Mean ± SD Min. – Max. Range	Non - heating season (n = 191) Mean ± SD Min. – Max. Range
PM ₁₀ (µg/m ³)	56.5 ± 36.4 9.9 - 318.8 308.9	73.4 ^b ± 32.4 19.4 - 262.4 243.0	29.2 ^b ± 23.9 9.9 - 318.8 308.9
PM _{2.5} (µg/m ³)	40.9 ± 29.6 4.9 - 246.4 241.5	56.5 ^b ± 27.2 10.2 - 246.4 236.2	15.7 ^b ± 7.9 4.9 - 52.4 47.4
PM _{10-2.5} (µg/m ³)	15.6 ± 17.6 0.3 - 305.6 305.3	16.9 ± 13.8 0.3 - 114.0 113.7	13.5 ± 22.2 1.4 - 305.6 304.2
PM _{2.5} /PM ₁₀	0.70 ± 0.18 0.04 - 0.99 0.95	0.78 ± 0.15 0.37 - 0.99 0.62	0.56 ± 0.14 0.04 - 0.93 0.89
SO ₂ (µg/m ³)	19.9 ± 8.3 2.5 - 59.4 56.9	19.4 ± 8.3 2.5 - 59.4 56.9	20.8 ± 8.3 3.9 - 39.9 36.0
NO ₂ (µg/m ³)	26.4 ± 10.4 7.0 - 96.2 89.2	30.9 ^b ± 9.8 7.0 - 96.2 89.2	18.8 ^b ± 6.4 9.9 - 41.1 31.2
NO (µg/m ³)	24.2 ± 21.4 3.0 - 174.5 171.5	32.3 ^b ± 23.1 3.0 - 174.5 171.5	10.9 ^b ± 7.4 3.3 - 44.1 40.8
NO _x (µg/m ³)	63.4 ± 41.6 16.6 - 309.9 293.2	80.3 ^b ± 43.0 18.5 - 309.9 291.4	35.4 ^b ± 17.2 16.5 - 100.5 84.0
CO (mg/m ³)	1.0 ± 0.5 0.2 - 5.8 4.6	1.2 ^b ± 0.6 0.2 - 5.8 5.6	0.7 ^b ± 0.2 0.2 - 1.3 1.1

^a15 October–15 April

^bSeasonal variation (p < 0.05)

During the transition from a warm to a cold period, an increase in the mean value of the mass concentration of particulate matter was observed. During the non-heating season, the mean daily

value of PM₁₀ concentration ranged from 9.9 to 318.8 µg m⁻³ with a mean value of 29.2 µg m⁻³, while the values during the heating season (15. October – 15. April) ranged from 19.4 to 262.4 µg m⁻³ with a mean value of 73.4 µg m⁻³. The mean daily value of PM₁₀ and PM_{2.5} concentrations was statistically significantly higher during the heating season compared to the non-heating season (Tab. 1). The mean value of PM₁₀ concentration measured during the heating season is about two and a half times higher compared to the non-heating season. The mean daily PM_{2.5} concentration during the heating season was 56.5 µg m⁻³, which was more than three times higher than the mean PM_{2.5} concentration measured during the non-heating season (Tab. 1). The same trend of increasing concentrations during the transition from a warm to a cold period is also observed for gaseous pollutants NO₂, NO, NO_x and CO. The mean daily value concentrations of these gaseous pollutants was statistically significantly higher during the heating season compared to the non-heating season (Tab. 1).

Table 2. Descriptive statistics of concentrations of different fractions of particulate matter (PM₁₀, PM_{2.5} and PM_{10-2.5}) and gaseous pollutants by seasons

	Winter (n=170)	Spring (n=148)	Summer (n=91)	Autumn (n= 91)
	Mean ± SD	Mean ± SD	Mean ± SD	Mean ± SD
	Min. – Max.	Min. – Max.	Min. – Max.	Min. – Max.
	Range	Range	Range	Range
PM ₁₀ (µg/m ³)	78.3 ± 35.6 19.4 - 262.4 243.0	50.6 ± 26.2 11.8 - 180.7 168.9	29.6 ± 32.7 9.9 - 318.8 308.9	52.4 ± 32.5 14.6 - 166.4 151.8
PM _{2.5} (µg/m ³)	64.2 ± 30.2 11.6 - 246.4 234.9	32.9 ± 18.0 5.0 - 118.6 113.6	13.4 ± 4.7 4.9 - 28.5 23.5	38.0 ± 26.0 7.8 - 129.3 121.5
PM _{10-2.5} (µg/m ³)	14.2 ± 12.8 0.3 - 55.1 54.8	17.7 ± 13.8 0.3 - 114.0 113.7	16.0 ± 31.7 1.4 - 305.6 304.2	14.4 ± 8.6 1.1 - 50.9 49.9
SO ₂ (µg/m ³)	21.11 ± 8.60 2.48 - 59.36 56.88	16.57 ± 7.69 2.54 - 39.77 37.23	25.20 ± 5.31 14.38 - 39.89 25.51	17.87 ± 8.20 4.60 - 37.88 33.28
NO ₂ (µg/m ³)	32.87 ± 11.39 7.04 - 96.19 89.15	24.10 ± 6.69 10.53 - 45.34 34.81	15.82 ± 3.02 9.88 - 24.55 14.67	27.99 ± 8.79 11.17 - 45.99 34.82
NO (µg/m ³)	37.22 ± 24.67 3.01 - 174.50 171.49	14.72 ± 7.3 3.48 - 56.02 52.54	7.55 ± 2.63 3.33 - 15.86 12.53	31.54 ± 22.49 4.22 - 133.48 129.26
NO _x (µg/m ³)	89.74 ± 46.86 18.50 - 309.89 291.39	46.68 ± 16.65 16.53 - 131.07 114.54	27.36 ± 6.27 16.65 - 47.08 30.43	76.30 ± 41.66 17.74 - 245.39 227.65
CO (mg/m ³)	1.37 ± 0.68 0.24 - 5.76 5.52	0.85 ± 0.33 0.21 - 2.68 2.47	0.79 ± 0.05 0.72 - 0.93 0.21	0.91 ± 0.42 0.38 - 3.34 2.96

The highest mean concentration of PM₁₀ and PM_{2.5} was measured during the winter period (78.3 and 64.2 µg m⁻³), followed by autumn, spring and summer with the lowest measured mean concentration (29.6 and 13.4 µg m⁻³). The same trend can be observed for NO₂, NO, NO_x and CO (Tab. 2). During the winter, the mean value of the PM_{2.5} concentration was about five times higher than the mean value of the PM_{2.5} concentration measured during the summer (Tab. 2). This can be explained by increased emissions of fine particles due to the use of wood, biomass, and fossil fuels in domestic heating during the colder part of the year (Sarigiannis et al., 2014). However, air quality does not depend only on pollutant emissions. In addition to emissions, meteorology and terrain topography also have a significant impact on air quality. Valjevo has an unfavorable geographical position, it is located in a basin surrounded by a mountain range, which additionally negatively affects air quality. High

concentrations of pollutants in the air during the colder part of the year can occur due to frequent occurrences of temperature inversion, which are characteristic of valleys surrounded by mountain ranges, preventing the vertical mixing of air masses, which leads to the accumulation of pollutants in the lower layers of the atmosphere. During the winter period, the major part of the PM₁₀ mass was in fine mode (PM_{2.5}) (82.9%) rather than coarse mode (PM_{10-2.5}) (17.1%), which can be attributed to the intensive combustion of biomass and fossil fuels for heating in households, industry and the public sector during this period. The summer period was characterized by the distribution of 47.3% coarse mode, while fine mode accounts for 52.7% of the total PM₁₀ mass.

Comparison of mean daily concentrations of air pollutants with the values prescribed by EU legislation and WHO recommendations

According to European Regulation (EU Directive 2008/50/EC) the daily limit value for PM₁₀ is 50 µg m⁻³, and that value should not be exceeded more than 35 days per year (EU, 2008). National legislation (Regulation on conditions for monitoring and air quality requirements (Official Gazette of RS No. 11/2010, 75/2010 and 63/2013) prescribes a daily limit value of PM₁₀ concentration equal to the value prescribed in Directive 2008/50/EC (EU, 2008). EU legislation, as well as national legislation, does not prescribe a daily concentration limit of PM_{2.5} (Tab. 3). According to the new guidelines for global air quality of the World Health Organization (WHO, 2021), the recommendation for daily mean concentration for PM₁₀ is 45 µg m⁻³ and the daily mean concentration for PM_{2.5} is 15 µg m⁻³, defined as the 99th percentile (equivalent to 3 - 4 exceedance days per year) of the annual distribution of 24-hour average concentrations (Tab. 3).

During the observed period from December 2019 to May 2022, the measured daily mean concentrations of PM₁₀ at the Valjevo station were above 50 µg m⁻³ (EU, 2008) for 204 days (40.8% of the time). When the mean daily concentrations for PM₁₀ are compared with WHO recommendations, the number of days with exceedances of the recommended value of 45 µg m⁻³ was 232 days (46.4% of the time). Measured daily mean concentrations of PM_{2.5} were above the values recommended by the WHO Air Quality Guidelines (AQG) (15 µg m⁻³) for 413 days (82.6 % of the time). In Serbia, the state-managed system for monitoring air quality showed that the concentrations of air pollutants, particularly PM, in cities regularly exceeds the levels recommended in the WHO AQG (WHO, 2019). WHO indicates that most epimedemological studies performed on the large population have been unable to determine a threshold concentration below which ambient particulate matter has no health effect (WHO, 2006b). Long-term PM exposure has been described as more significant, regarding the influence on human health, compared to the short-term exposure (Liu et al., 2015).

Table 3. Comparison of the European limits values and the WHO recommendations 2005 AQG and 2021 AQG for the protection of human health

	Averaging time	EU Limit Values ¹	WHO Recommendations	
		Limits	2005 AQG ²	2021 AQG ³
PM ₁₀ (µg/m ³)	annual	40	20	15
	24 hour	50 (35 exceedances permitted)	50 ⁴	45 ⁴
PM _{2.5} (µg/m ³)	annual	25 (stage 1) ⁵ , 20 (stage 2) ⁶	10	5
	24 hour	-	25 ⁴	15 ⁴
NO ₂ (µg/m ³)	annual	40	40	10
	24 hour	-	-	25 ⁴
	1 hour	200 (18 exceedances permitted)	200	200
SO ₂ (µg/m ³)	24 hour	125 (3 exceedances permitted)	20 ⁴	40 ⁴
	1 hour	350 (24 exceedances permitted)	-	-

CO (mg/m ³)	24 hour	-	-	4 ⁴
	1 hour	-	35	35

¹ EU limit values for the protection of human health according to the EU Directive 2008/50/EC

² WHO air quality guidelines for particulate matter, ozone, nitrogen dioxide and sulfur dioxide - Global update. 2005.

³ WHO global air quality guidelines. Particulate matter, ozone, nitrogen dioxide, sulfur dioxide and carbon monoxide. 2021.

⁴ 99th percentile (i.e. 3-4 exceedance days per year).

⁵ Date by which limit value is to be met 1.1.2015. ⁶ Date by which limit value is to be met 1.1.2020.

EU legislation (Directive 2008/50/EC) (EU, 2008) and domestic legislation (Regulation on conditions for monitoring and air quality requirements (Official Gazette of RS No. 11/2010, 75/2010 and 63/2013)) prescribes a daily limit value for SO₂ concentration of 125 µg m⁻³, which should not be exceeded more than 3 times a calendar year. During observed period daily mean concentrations of SO₂ was under 125 µg m⁻³. WHO AQG recommend a daily mean SO₂ concentration of 40 µg m⁻³ (WHO, 2021). During the observed period the measured daily mean concentrations of SO₂ at Valjevo station were above the recommended value by the WHO AQG for four days (0,8% of the time).

For mean daily NO₂ concentrations, the comparison with EU legislation was not possible, because for the concentration of NO₂ in ambient air EU directive prescribe only mean hourly values and mean annual value, but not the mean daily value. WHO AQG recommend a daily mean NO₂ concentration of 25 µg m⁻³ (WHO, 2021). During the observed period the measured daily mean concentrations of NO₂ at the Valjevo station were above 25 µg m⁻³ for 251 days (50.2 % of the time). The measured daily mean concentrations of CO at the Valjevo station were above 4 mg m⁻³ (WHO, 2021) for only one day. From Tab. 4, it can be seen that exceeding the limit/recommended values for PM₁₀, PM_{2.5} and NO₂ predominantly occur during the heating season for PM₁₀ 62.78% of time (according to EU regulation) and 69.26% of time (according to WHO recommendations), for PM_{2.5} 92.56% of time (according to WHO recommendations) and for NO₂ 72.17% of time (according to WHO recommendations). An important source of particulate matter emissions during the heating season is residential heating with coal and wood. Coal combustion is an important source of suspended particles and gases (Tsitouridou & Anatolaki, 2007), while combustion of biomass for residential heating can be singled out as one of the largest sources of fine particles in the global troposphere (Vicente & Alves, 2018). In addition to the sources of emissions, the location

Table 4. The number of days and % the time with exceedances of the limit/recommended value for PM₁₀, PM_{2.5} and NO₂ during heating and non-heating seasons observed at automatic air quality monitoring station Valjevo in the period from December 2019 to May 2022

		Heating season (n = 309)		Non-heating season (n = 191)		
		Limit/recommended value (µg/m ³)	the number of days with exceedances of the limit/recommended value	% of the time	the number of days with exceedances of the limit/recommended value	% of the time
PM ₁₀	EU ¹	50	194	62.78	10	5.24
	WHO AQG ²	45	214	69.26	18	9.42
PM _{2.5}	WHO AQG ²	15	286	92.56	127	66.49
NO ₂	WHO AQG ²	25	223	72.17	28	14.66

¹EU limit values for the protection of human health according to the EU Directive 2008/50/EC

² WHO global air quality guidelines. Particulate matter, ozone, nitrogen dioxide, sulfur dioxide and carbon monoxide. 2021.

of the city core, which is located in the basin, contributes significantly to the high concentrations of suspended particles at the investigated measurement site during the heating season. Meteorological factors are often an additional cause of high concentrations of suspended particles during the heating season.

Conclusion

In this paper, average concentrations and time and seasonal variations of particulate matter (PM₁₀ and PM_{2.5}) as well as gaseous pollutants (SO₂, NO₂, NO, NO_x, CO) measured at the automatic air quality monitoring station Valjevo in the period from December 2020 till May 2022 were analyzed. The assessment of air quality was carried out taking into account the limit values defined by Serbian and European legislation and also WHO AQG.

The mass concentrations of PM₁₀ at the VA measuring station in the observed period were in the range from 9.9 to 318.8 $\mu\text{g m}^{-3}$ (with a mean value of 56.5 $\mu\text{g m}^{-3}$), while the mass concentrations of fine mode PM_{2.5} particles ranged from 4.9 to 246.4 $\mu\text{g m}^{-3}$ (with a mean value of 40.9 $\mu\text{g m}^{-3}$). The mean value of the PM_{2.5} concentration measured for the observed period for Valjevo was two times higher than the average annual value of PM_{2.5} in Serbia and 2.8 times higher than the mean annual PM_{2.5} concentration calculated by WHO for the European Region as a whole.

During the transition from a warm to a cold period of year, an increase in the mean value of the mass concentrations of particulate matter and for gaseous pollutants NO₂, NO, NO_x and CO was observed. The mean daily value of PM₁₀, PM_{2.5}, NO₂, NO, NO_x and CO concentrations was statistically significantly higher during the heating season compared to the non-heating season.

The highest mean concentrations of PM₁₀, PM_{2.5}, NO₂, NO, NO_x and CO was measured during the winter period followed by autumn, spring and summer. During the winter, the mean value of the PM_{2.5} concentration was about five times higher than the mean value of the PM_{2.5} concentration measured during the summer. This can be explained by increased emissions of fine particles due to the use of wood, biomass, and fossil fuels in domestic heating during the colder part of the year, but also the meteorological conditions during the winter months and unfavorable geographical location of Valjevo which additionally negatively affect the air quality.

When the mean daily concentrations for PM₁₀ are compared with WHO recommendations, the number of days with exceedances of the recommended value of 45 $\mu\text{g m}^{-3}$ was 232 days (46.4% of the time), while measured daily mean concentrations of PM_{2.5} were above the values recommended by the WHO AQG (15 $\mu\text{g m}^{-3}$) for 413 days (82.6% of the time). During the observed period the measured daily mean concentrations of NO₂ at the Valjevo station were above WHO AQG (25 $\mu\text{g m}^{-3}$) for 251 days (50.2% of the time), while daily mean concentrations of SO₂ and CO at Valjevo station were above the recommended value by the WHO AQG for four days and only one day, respectively. It was observed that exceeding the WHO AQG recommended values for PM₁₀, PM_{2.5} and NO₂ predominantly occur during the heating season for PM₁₀ 69.26% of time, for PM_{2.5} 92.56% of time and for NO₂ 72.17% of time.

The results of this analysis can form the basis of a policy to improve the quality of air in Valjevo. Effective action to reduce air pollution and its impacts requires a good understanding of its causes and how pollutants affect humans, society and the economy. Decreasing the use of solid fuels for household heating, improving planning to increase the energy efficiency of houses and buildings, increasing the use of low-emission fuels, improving communication and awareness of risks are some of the actions that could directly reduce pollution air and protect people's health and improve the quality of life.

References

- Belis, A. C., Pisoni, E., Degraeuwe, B., Peduzzi, E., Thunis, P., Monforti-Ferrario, F. & Guizzardi, D. (2019). Urban pollution in the Danube and Western Balkans regions: the impact of major PM_{2.5} sources. *Environmental International Journal*, 133, 105158. <https://doi.org/10.1016/j.envint.2019.105158>
- Belis, C., Djatkov, D., Lettieri, T., Jones, A., Wojda, P., Banja, M., Muntean, M., Paunovic, M., Niegowska, M. Z., Marinov, D., Poznanović, G., Pozzoli, L., Dobricic, S., Zdruli, P. & Vandyck, T. (2022). Status of environment and climate in the Western Balkans, EUR 31077 EN, *Publications Office of the European Union*, Luxembourg. <https://doi.org/10.2760/374068>
- EEA. (2019). *Air quality in Europe — 2019 report*. European Environment Agency. Luxembourg, Luxembourg: Publications Office of the European Union. <https://www.eea.europa.eu/publications/air-quality-in-europe-2019>
- EU. (2008). Directive 2008/50/EC of the European Parliament and of the Council of 21 May 2008 on ambient air quality and cleaner air for Europe. *Official Journal of the European Union*, OJ L 152, 11.6.2008, 1–44. <https://eur-lex.europa.eu/legal-content/EN/TXT/PDF/?uri=CELEX:32008L0050&from=en>
- Health Effects Institute HEI, (2020). State of Global Air 2020. *Health Effects Institute*, Boston, MA, pp. 1–28. <https://www.healthdata.org/policy-report/state-global-air-2020>
- Jeričević, A., Džaja Grgičin, V., Telišman Prtenjak, M., Vidič, S. & Bloemen, H. (2016). Analyses of urban and rural particulate matter mass concentrations in Croatia in the period 2006–2014. *Geofizika*, 33, 2, 157–181. <https://doi.org/10.15233/gfz.2016.33.8>
- Liu, Z., Hu, B., Wang, L., Wu, F., Gao, W. & Wang, Y. (2015). Seasonal and diurnal variation in particulate matter (PM₁₀ and PM_{2.5}) at an urban site of Beijing: analyses from a 9-year study. *Environmental Science and Pollution Research*, 22, 627–642. <https://doi.org/10.1007/s11356-014-3347-0>
- Air quality plan for the period from 2016 to 2021, (2016). Valjevo (in serbian). https://valjevo.rs/Dokumenta/GradValjevo/Zastita_Sredine/Plan%20kvaliteta%20vazduha,%202012022016.pdf
- Regulation on conditions for monitoring and air quality requirements. *Official Gazette of Republic of Serbia*, 11/2010, 75/2010 and 63/2013. (in Serbian). <https://www.paragraf.rs/propisi/uredbaslovima-monitoring-zahtevima-kvaliteta-vazduha.html>
- Sarigiannis, D. A., Karakitsios, S. P., Kermenidou, M., Nikolaki, S., Zikopoulos, D., Semelidis, S., Papagiannakis, A. & Tzimou, R. (2014). Total exposure to airborne particulate matter in cities: the effect of biomass combustion. *Science of The Total Environment*, 493, 795–805. <https://doi.org/10.1016/j.scitotenv.2014.06.055>
- Tsitouridou, R. & Anatolaki, C. (2007). On the wet and dry deposition of ionic species in the vicinity of coal-fired power plants, northwestern Greece. *Atmospheric Research*, 83, 93–105. <https://doi.org/10.1016/j.atmosres.2006.03.005>
- UNEP. (2019). Air Pollution and Human Health: the Case of the Western Balkans. *United Nations Environment Programme*. https://www.developmentaid.org/api/frontend/cms/uploadedImages/2019/06/Air-Quality-and-Human-Health-Report_Case-of-Western-Balkans_preliminary_results.pdf
- Vicente, E. D. & Alves, C. A. (2018). An overview of particulate emissions from residential biomass combustion. *Atmospheric Research*, 199, 159–185. <https://doi.org/10.1016/j.atmosres.2017.08.027>
- WHO. (2006a). WHO Air quality guidelines for particulate matter, ozone, nitrogen dioxide and sulfur dioxide: Global update 2005: Summary of risk assessment. Geneva, Switzerland: *World Health Organization*. <https://apps.who.int/iris/handle/10665/69477>

- WHO. (2006b). World Health Organization. Regional Office for Europe & Joint WHO/Convention Task Force on the Health Aspects of Air Pollution. Health risks of particulate matter from long-range transboundary air pollution. Copenhagen: *WHO Regional Office for Europe*. <https://apps.who.int/iris/handle/10665/107691>
- WHO. (2016). Ambient air pollution: a global assessment of exposure and burden of disease. Geneva: *World Health Organization*. <https://www.who.int/phe/publications/air-pollution-globalassessment/en>
- WHO. (2018). Burden of disease from the joint effects of household and ambient air pollution for 2016. *World Health Organization*. https://cdn.who.int/media/docs/default-source/air-quality-database/aqd_2018/ap_joint_effect_bod_results_may2018.pdf
- WHO. (2019). Health impact of ambient air pollution in Serbia - A call to action. Copenhagen, Denmark: *WHO Regional Office for Europe*. https://serbia.un.org/sites/default/files/2019-10/Health-impact-pollution-Serbia_0.pdf
- WHO. (2021). WHO global air quality guidelines: particulate matter (PM_{2.5} and PM₁₀), ozone, nitrogen dioxide, sulfur dioxide and carbon monoxide. *World Health Organization*. <https://apps.who.int/iris/handle/10665/345329>

Original scientific article

ORGANIC BIO-DEGRADABLE WASTE IN FRUIT PRODUCTION

Milica Đeković Šević¹, Zoranka Malešević¹, Milan Šević², Tamara Bartošek³

¹Academy of Vocational Studies Sumadija, Department in Aranđelovac, Josifa Pancica 11, Aranđelovac, Serbia

²Agricultural Advisory and Professional Service Belgrade, Stojana Novakovica 2, Mladenovac, Serbia

³Public utility company "Bukulja" Aranđelovac, Branislava Nusica 1, Aranđelovac, Serbia

Abstract

Within this work, a research was conducted on the quantities of generated organic, bio-degradable waste generated in fruit production, primarily waste generated by pruning fruit at a specific location, a pear plantation. The amount of pruned material per tree was measured, and research on growing technology, impact on the living world and the environment was conducted. The exact amounts of organic biomass, flows and the way in which agricultural fruit waste is treated and how it is managed have been determined. It was concluded that this type of waste represents a serious potential resource, which can be used in different ways (as an energy source and as a raw material for compost). However, the situation on the ground shows that this type of agricultural waste is managed in an unsustainable and irresponsible way. In this studies is present a model of sustainable management application, managing waste in a responsible way without negative impact and pressure on the environment.

Key words: organic bio-degradable waste, agricultural production, waste management.

Introduction

Waste is any material that is not desirable by human standards, which is discarded in various ways and needs to be disposed of. Agricultural residues is generated as a result of the work of agricultural production, food and wood industry, and in general, it is present in significant quantities. Agricultural residues include all the organic materials which are produced as by-products from arable farming, fruit growing, viticulture, animal husbandry, gardening and other types of agricultural production (Plečević, 2018; Dyjakon, 2019). Globally, 140 billion metric tons of biomass is generated every year from agriculture (UNEP 2009).

The task of fruit production is to provide sufficient quantities of fruit as a food source, for human consumption or further processing (Šoškić, 2016). However, in intensive fruit production, there is the formation of large amounts of waste resulting from pruning. Fruit production in the world is constantly growing. From 392 million tons in 1993, production increased to 504 million tons in 2003, and after 10 years, ie in 2013, it reached 638 million tons. The leading country in the world in terms of production volume in the world is China with almost 85 million tons, followed by India, Brazil, The United States of America and Italy. In Europe, the average annual production is 72.48 million tons (average between 1993 and 2013) according to FAOSTAT data. The largest production volumes are in Italy, Spain and France (Keserović, 2016). The most represented cultivated fruit species in the leading countries in terms of production are the species from the group of subtropical and tropical (southern) fruits, and the most common fruit species from the temperate climate zone is the apple. With a production of about 16 million tons pear ranks sixth among fruit trees in the world (after citrus fruits, bananas, apples, mangoes and olives). Pear ranks second, among continental fruit trees after

apple (Mratinić, 2000). With the increase in the area on which fruit is grown, the amount of waste generated by pruning also increases. Many countries in the world are developing programs for the sustainable management of pruning waste (Spinelli & Picchi, 2010; Spinelli et al., 2011; Najibeh et al., 2020). In fact, pruning residues could replace traditional wood assortments for bioenergy and industrial use (Ntalos & Grigoriou, 2002; Bernetti et al., 2004).

In the total agricultural production of the Republic of Serbia, fruit growing and viticulture occupies a very high place, in terms of volume, importance, economic profitability and tradition. The growth trend in the last 20 years is evident, and it has been extremely pronounced in the last 10 years. New plantings are constantly sprouting, new cultures and new varieties of existing ones are being introduced, new planting and cultivation technologies, modern mechanization.

The largest areas under orchards are located in Western Serbia (the city of Čačak), Šumadija (Topola municipality), the Danube region (the city of Smederevo and the municipality of Grocka) and parts of Southern Serbia. Although there are significant areas under fruit in Vojvodina, they are still significantly smaller than in these parts of Serbia. Also, Eastern and South-Eastern Serbia are areas with much less orchards.

According to the official data of FAOSTAT for the period from 1993 to 2013, the average annual fruit production in the Republic of Serbia is 1.453 million tons, with an upward trend in production. Plums are mostly produced, followed by apples, raspberries and cherries.

The total area under pears in Serbia is 7.343 hectares, which places us in 10th place in Europe. By far the largest areas are in the municipality of Leskovac (362 hectares), followed by Čačak (287 hectares), Šid (215 hectares), Kraljevo (202 hectares) and Grocka (196 hectares) (Republican Institute of Statistics, Belgrade, 2017). Large areas under pear orchards are also located in the municipality of Leskovac, and this is contributed by very favorable climatic conditions, but also the orientation of producers towards the processing of this fruit species into quality fruit brandy. Apart from these municipalities, the pear is significantly present in other parts of Srem, in Mačva, parts of western Serbia and Šumadija.

On the territory of the municipality of Arandjelovac, fruit growing has a long tradition. In this paper, the municipality of Arandjelovac will be the focus of research, and in the experimental part of the paper where field research and measuring the amount of generated bio-degradable waste in fruit production will be presented, this focus will be narrowed to the village of Darosava. On the territory of the village of Darosava, there is a location where measurements were made, ie a pear plantation. But many other factors related to the work were observed within this, relatively smaller space, in order to be able to investigate as closely as possible the factors related to the topic of the work. Observing the area of the municipality of Arandjelovac and the narrower village of Darosava, it is possible to see a broader picture of the situation in the entire Republic of Serbia because the situation is quite the same in other parts of the country. The method of production, cultivated varieties, size of holdings, population structure and many other factors are very similar, and all the problems related to fruit production, product placement and waste management are almost identical.

Pruning of fruit trees is performed in order to form a growing form, regulate fertility and rejuvenate fruit trees. Depending on the time of pruning, pruning can be summer (green) and winter (mature). It is a very professional job for which you need to have a certain level of knowledge and experience. The intensity of pruning itself depends on the following factors: fruit species, fruit age, fruit variety, number and fertility of fruiting buds. Younger trees are generally more lush and such trees are pruned a little less, that is, fruit trees that do not bear fruit should be pruned minimally because pruning encourages new growth (Keserović, 2016; Mratinić, 2000). The most common pear varieties grown in Serbia are: June Beauty (Bella di Giugno), Butirre Precoce Morettini, Carmen, Santa Maria, Williams, Abbate Fetel and Cure (Le Cure). Current cultivars and cultivation forms require intensive pruning (Mratinić, 2000). Winter pruning is one of the most important jobs done in an orchard. Fruits are pruned in the period when they are in the phase of biological dormancy, from the period of leaf

fall to bud movement. When pruning is later, during late winter and early spring, it adversely affects the development of fruit trees. It can be justified in excessively lush and barren fruit trees, which systematically reduces lushness. In fruit species that bloom earlier and can be damaged by late spring frosts, later pruning, after assessing possible damage, may also be justified (Keserović, 2016). Since only winter pruning has been practiced at the location (plantation) where the research was conducted, since its formation, ie planting, the paper will focus only on it (Figure 1).



Figure 1. Winter pruning at the research site

Materials and Methods

The research was conducted at the location of a pear plantation in the area of the village of Darosava. The plantation is located in the area of the village of Darosava, on the north-western side of the hill Orlovica, at an altitude of about 300 meters (Figure 2).



Figure 2. Pear plantation

It covers an area of slightly more than 4.5 ha and has 4.500 seedlings or fruit trees. So far, it consists of four different varieties of pear, namely: Williams, June Beauty, Santa Maria and Butirre Precoce Morettini. The main cultivated variety is Williams, other varieties are less represented. It has been formed so far in 2013, is privately owned and is in the full-fledged phase. At the time of the research, the plantation was six years old and that is an important fact because the fruit trees will still develop and grow, and thus the amount of waste generated by pruning will increase. In conversation with experts and technical persons responsible for the maintenance of the plantations, it was learned that this increase will amount to between 30 to 40% more pruned material compared to the current situation. The tree is expected to reach its full growth by 15 years of planting. The measurement of the amount of pruned organic matter lasted for almost two months, during the winter pruning, in November and the beginning of December 2018. The quantities that are pruned from each tree individually were measured (Figure 3).



Figure 3. Quantity of pruned material from one pear tree

In order to make the data as accurate as possible in the final sum, the measurement was performed on two different parts of the plantation, in two different sectors. One measurement was performed in the upper sector and the other in the lower sector of the plantation, and the results obtained in these two sectors differ.

Results and discussion

During pruning and as part of the research, the exact number of pruned branches was counted and the thickness of the cut branches was measured. The number of cut branches and their total weight are given in the following tables (Tables 1, 2, 3 and 4), the thickness of the pruned branches is from 0.5 cm to a maximum of 5 cm in diameter.

As for the thickness of pruned branches, i.e. their volume, it amounts to from 0.5 cm to a maximum of 5 cm in diameter, and expressed as a percentage of pruned substances seems to be:

- Over 50% of the pruned material consists of the thinnest branches, 0.5 cm thick in diameter;
- About 40% are branches of the axis 1 to 1.5 cm in diameter;
- Approximately 5% are branches that are 2 to 3 cm in diameter;
- Only one or at most two pruned branches have between 3 and 5 cm in diameter, and it is mostly the highest, frontal branch on the tree or less often a branch that grows in the wrong way.

Table 1. Quantities of pruned bio-degradable waste in the upper sector of the plantation

Tree	1	2	3	4	5	6	7	8	9	10
Quantity (kg)	3	3.5	3.5	4.5	3	3.7	3.9	3.3	4	3.5

Table 2. Number of pruned branches in the upper sector of the plantation

Tree	1	2	3	4	5	6	7	8	9	10
Number of branches	172	174	168	190	173	179	182	174	185	175

Table 3. Quantities of pruned bio-degradable waste in the lower sector of the plantation

Tree	1	2	3	4	5	6	7	8	9	10
Quantity (kg)	4	4.4	4	4.5	4.1	4.2	3.6	4.1	4.6	3.9

Table 4. Number of pruned branches per tree in the lower sector of the plantation

Tree	1	2	3	4	5	6	7	8	9	10
Number of branches	181	189	182	195	184	185	171	182	197	175

The tables show the results, that the measured quantities of pruned material and the number of pruned individual branches are very similar, approximate in number and weight. This is a direct consequence of the technology of growing and pruning fruit trees, because fruit trees are formed into a uniform, almost completely identical shape of the canopy and the entire tree (Figure 4).



Figure 4. Uniform shape of pruned pear trees

The thickness of the pruned branches provides data on the character of agricultural waste generated by fruit pruning. It is clear that the largest part of this type of bio-degradable agricultural waste consists of very thin branches and twigs, which in fruit production are undesirable material. They are always removed first in order to form fruit of the best possible quality on thicker, perennial, fruit-bearing branches. These quantitative data are important parameters within this paper, as they provide a picture of what can be done further within the framework of sustainable management of agricultural bio-degradable waste generated in fruit growing. It is necessary to have a clear picture of what and how much quantities are available in fruit growing, in order to plan sustainable management of this

type of non-hazardous waste. If all the parameters are known exactly, it is much easier to optimally use all the potentials of this resource, and instead of putting new pressure on the environment, it can be used to improve the quality of the environment and reduce the consumption of various other resources.

If we start from the analysis of the obtained results of measuring the amount of pruned material from Table 5 and Table 7, the following data are obtained:

- The average amount of pruned material in the process of pear fruit production during one year is 3.865 kg per tree;
- There are 4500 trees on the plantation;
- At the annual level, the total amount of pruned material is 17392.5 kg.

The amount of over 17 t represents a serious potential of bio-degradable material. If we take into account that the trees will continue to grow in volume and develop in the next 5 to 7 years, the amount of pruned material will also increase, according to experts who are in charge of maintaining the plantation by about 30 to 40%. This means that in the phase of its full growth, after 15 years from planting, between 20 and 25 tons of pruned biomass will be generated annually on the site. It must be acknowledged that this is a very serious potential, if it is managed sustainably and responsibly. Otherwise, if managed as before, irresponsibly and unsustainably, that amount represents a huge pressure on the environment.

If we look at the number of pruned branches and their volume and share, we come to the following conclusions given in Table 5.

Table 5. Relationship between the number and volume of pruned branches in percent

Number of pruned branches per tree	Between 170 and 190
Branches 0.5 cm thick in diameter	Over 50% of the total pruned material
Branches from 1cm - 1.5cm in diameter	About 40% of the total pruned material
Branches of 2cm - 3cm in diameter	Only about 5%
Branches between 3cm - 5cm in diameter	Only one or at most two pruned branches, mostly apical or bearing

This data is important because of the consideration of the possibility of using this bio-degradable waste in further processing. Namely, it is clear that this cut material is very small, and that determines the further technological course of processing. Also, due to the technology of fruit growing, it contains traces of agro-chemical preparations that are used in the production process. All these factors determine the possibilities of using this biomass. One of the simplest uses is as an energy source. Pruned material can be used as a household energy source or distributed for sale. The technological procedure is relatively simple and consists of the following phases (Table 6).

Table 6. Technological procedure of processing of cut organic material into energy source

Technological process of processing	
• Collection of cut material	• In the field (plantation, orchard)
• Transport	• To the processing plant (if required)
• Storage	• At the processing plant or in the field
• Drying	• At the processing plant (but also in the field)
• Processing into a product (pellet, wood chips, etc.)	• At the processing plant, but it is also possible in the field with the help of specialized machinery
• Storage of the finished product	• In a warehouse or household, depending on the purpose
• Sell or use	• Depending on the purpose

This type of use is very simple, but also very efficient. Pruned fruit waste has a very high energy value and can be used as a very good energy source. Since most fruit producers are in rural areas and live in houses, a minimal investment in the modification of the household heating system and a slightly larger investment in processing equipment is sufficient. It is very interesting that agricultural producers have lately been very interested in this type of management of agricultural, fruit, forest and similar organic waste. During the field research, it was found out that some equipment for processing such organic matter is already being procured, which was completely unused until only a few years ago. All that is still in its infancy, but it is a positive hint. Simply put, modern society puts economic conditions first, and producers of fruits and other agricultural crops see here the possibility of making additional funds and profits. The aggravating circumstance is certainly, and the fact that there are no incentives from the state, local self-government and similar organizations for the procurement of equipment. With such incentives, a large part of agricultural producers, not only fruit growers, would certainly think of waste as an energy source.

Another type of use of biodegradable waste generated in the fruit production process could be the production of compost, which could further have dual use, as an inert material needed for a sanitary landfill or as organic matter needed for reclamation and revitalization of exploited mining land.

Since the cut bio-degradable material is homogeneous, it is relatively bad for the composting process, and since it also contains certain amounts of agro-chemical preparations, its quality would not be top quality. But it is quite the right quality for a certain use. One of the possibilities that could be applied is the use of the obtained compost at the city sanitary landfill as an inert material. In this way, multiple environmental and economic benefits would be achieved:

- land degradation due to land exploitation as an inert material would be reduced;
- less bio-degradable waste would end up in the landfill and thus automatically increase its working and operational life;
- less agricultural waste would end up incinerated or disposed of in the environment;
- reduced waste disposal costs;
- direct environmental benefit.

As far as use in the reconstruction of exploited mining land is concerned, little inter-local cooperation between the two neighboring municipalities is needed, little systemic investment and education, and the result could be excellent. The exploited areas are huge, a large human and financial investment is needed in their revitalization and reclamation, and the application of compost obtained in this way could play a big role in the initial phase. Rudarski Kombinat Kolubara is located very close to the municipality of Arandjelovac, funds and investment in equipment and transport could be provided by the state, the Ministry of Mining and Energy, and the result could be mutually beneficial, both environmentally and economically, for both municipalities but also for citizens.

These are just two types of sustainable management of bio-degradable agricultural waste from fruit production, and it is certain that in addition to investing in the education of production entities and the procurement of equipment, there may be more. It is quite clear that the current way of managing this type of waste is unsustainable and irresponsible, and that a different, sustainable and responsible management is possible. Not only is it possible, but it is also necessary.

Based on the above, it can be concluded that there is an ecological and economic justification for the processing and use of organic waste generated in fruit production. There are sufficient quantities on an annual basis that it would be economically justified to invest in processing and use it as an energy source or as a raw material for compost.

Conclusions

The municipality of Arandjelovac is climatically and geographically very favorable for the development of fruit production, and has a long tradition of this production, and in the development

plans of the municipality, fruit production has a place. There is a lot of bio-degradable waste generated in fruit production, primarily with pruned fruit material, and there is a trend of increase, due to the increase of areas under fruit crops.

At the moment, this cut material is being managed completely unsustainably and irresponsibly. Most of it ends up burned or disposed of directly in the environment, left to rot and decay. A small part, mostly from large holdings, ends up deposited in the sanitary city landfill, and negatively affects the capacity and lifespan of the landfill. And instead of using this organic material as an environmentally friendly energy source, raw material for obtaining compost and the like, it additionally negatively affects the quality of the environment.

With the active involvement of all entities, fruit producers, local self-government organizations, citizens, it is possible to use this type of organic waste as a potential. It is necessary to actively work on education and raising the level of awareness, but above all, economic incentives and organization are needed, because currently, the economic effect dictates all flows. The individual farmer simply looks primarily at the economic side of the problem. There is an obligation of the state and local authorities to combine environmental, social and societal benefits, with economic viability. It is clear that the potential for exploitation exists, it is necessary to improve the current situation.

References

- Bernetti, I., Fagarazzi, C. & Fratini, R. (2004). A methodology to analyze the potential development of biomass energy sector: an application in Tuscany. *Forest Policy and Economics*, 6(3–4), 415–432. <https://doi.org/10.1016/j.forpol.2004.03.018>
- Dyjakon, A. (2019). The influence of apple orchard management on energy performance and pruned biomass harvesting for energetic applications. *Energies*, 12(4), 632–616. <https://doi.org/10.3390/en12040632>
- Plećević, Lj. (2018). Upravljanje otpadom. Arandelovac, Srbija: Visoka škola strukovnih studija Arandelovac-Arandelovac.
- Keserović, Z. (2016). Voćarstvo i vinogradarstvo, Poljoprivredni fakultet Novi Sad, Srbija: Novi Sad-Feljton.
- Mratinić, E. (2000). Kruška, Beograd, Srbija Partenon.
- Ntalos, G. & Grigoriou, A. (2002). Characterisation and utilisation of vine prunings as a wood substitute for particleboard production. *Industrial Crops and Products*, 16(1), 59–68. [https://doi.org/10.1016/S0926-6690\(02\)00008-0](https://doi.org/10.1016/S0926-6690(02)00008-0)
- UNEP. (2009). Converting waste agricultural biomass into a resource, compendium of technologies: United Nations Environment Programme. p. 441.
- Najibeh, G., Rafaele, S., Ramin, N. & Akbar, N. (2020). Utilization of woody pruning residues of apple trees. *Forest Science and Technology*, 16(4), 216–223. <https://doi.org/10.1080/21580103.2020.1845822>
- Spinelli, R. & Picchi, G. (2010). Industrial harvesting of olive tree pruning residue for energy biomass. *Bioresource Technology*, 101(2), 730–735. <https://doi.org/10.1016/j.biortech.2009.08.039>
- Spinelli, R., Magagnotti, N., Nati, C., Cantini, C., Sani, G., Picchi, G. & Biocca, M. (2011). Integrating olive grove maintenance and energy biomass recovery with a single-phase pruning and harvesting machine. *Biomass and Bioenergy*, 35, 808–813. <https://doi.org/10.1016/j.biombioe.2010.11.015>
- Statistika voćarske proizvodnje - Rezultati istraživanja o voćnjacima (2017). Republički zavod za statistiku. <https://www.stat.gov.rs/sr-latn/oblasti/poljoprivreda-sumarstvo-i-ribarstvo/visegodisnjizasadi/>
- Šoškić, M. (2016). Savremeno voćarstvo. Beograd, Srbija: Partenon.

MATERIAL SCIENCE AND METALLURGY

Professional Paper

SIMULATION OF THE IMPACT OF PREHEATING TEMPERATURE ON RAILWAY ALUMINOTHERMIC WELDING

Gvozden Jovanović¹, Vaso Manojlović², Miroslav Sokić¹, Alen Delić³, Milorad Gavrilovski⁴

¹Institute for Technology of Nuclear and Other Mineral Resources - ITNMS, Belgrade, Serbia

²University of Belgrade, Faculty of Technology and Metallurgy, Belgrade, Serbia

³TTU energetik d.o.o., Tuzla, Bosnia and Herzegovina

⁴University of Belgrade, Faculty of Technology and Metallurgy, Innovation Center, Serbia

Abstract

For more than a century, railway rails have been joined using the aluminothermic welding process. The flexibility, compactness of the weld, and ease of execution are all advantages of this process. It is not necessary to use external energy to finish the operation. It is provided by the exothermic effect of the chemical reactions of the elements of the aluminothermic combination. The design of the mold with the pouring system, which should ensure even pouring of thermal steel, without turbulence, then even heat dissipation or cooling in order to obtain an appropriate micro and macro structure of steel, free of internal and external defects, is an important factor in producing a welded joint of the required quality. As a result, the design of the mold was continually developing, necessitating the adoption of expensive experimental approaches in industrial settings. To eliminate costly and time-consuming industrial experiments, software applications are being employed to imitate traditional casting methods that can be used in the casting of thermite steel during the fabrication of welded railway connections. This study presents a simulation of casting thermite steel in the mold cavity, i.e., in the weld joint, for the 49E1 rail using the NovaFlow & Solid CV software package

Keywords: aluminothermic welding, simulation modeling, Novacast, welded joint, preheating influence.

Introduction

Using Casting simulations for classic casting technologies is an innovative approach that basically simulates the filling of a mold with metal, as well as its hardening, and gives the possibility of simulating the production of castings. The simulation approach, in any event, saves manufacturing costs and optimizes the technical casting process (Delić et al., 2022). Most commercial casting procedures, as well as the thermite steel casting method for aluminothermic rail welding (NovaCast, 2015), may be simulated. The simulation depicts the effects of various inflow routes and feeding systems. Defects in castings such as macro and micro inclusions owing to excessive turbulence, cold joints, shrinkage, and porosity may be prevented by improving the design of the input system and gas vents (Ravi, 2008; Ravi, 2010; Delić et al., 2018; Delić et al., 2019).

The simulation program's primary input data is a 3D CAD model for creating molds. The fundamental parameters of the aluminothermic process, such as thermite steel and mold properties, as well as heat transmission characteristics of the metal, sand mold, pouring temperature, and so on, are then entered into the software. Output data includes animated visualizations of mold filling, thermite steel solidification, and further cooling to room temperature. Total filling time, mold erosion, partial filling, and gas entrapment may all be predicted using mold filling simulation. The temperature and cooling

rate in the casting solidification simulation are used to forecast the location of shrinkage porosity based on Niyama and other criteria. It is also possible to model further cooling to room temperature, which is important for forecasting microstructure, mechanical characteristics, residual stresses, and curl.

This study shows how to utilize casting simulation in aluminothermic welding to bypass the way of practical trial and error, particularly how different preheating times and temperature distribution influence casting. By optimizing the design of the ingate system, feeders, and ventilation, casting problems such as oxide inclusions caused by excessive turbulence, undercooling, shrinkage, and slag inclusions may be prevented.

Materials and Methods

The steel used for simulation is commercial railway steel R260 or EN 1.0623 and the type of rails are 49E1. The chemical composition is presented in Table 1, while some other thermal characteristics are presented in Table 2.

Table 1. Chemical composition of steel that is used as an input into NovaCast database

Element mass%								
C	Si	Mn	P	S	Cu	Sn	V	Al
0.54	0.35	1.07	0.025	0.20	0.11	0.001	0.11	0.31

Table 2. Thermal casting characteristics of the steel used according to the NovaCast database

Liquidus Temperature, °C	1478.6	Solidus Temperature, °C	1401.5	Eutectic Temperature, °C	1139.9
CLF up %	70.0	CLF down %	45.0	CLF press%	35.1
Qcr kJ/kg	172.6	Qet kJ/kg7	235.7		

Simulation set up.

The simulation is carried out using the software program NovaFlow& Solid CV (Novacast business, Sweden) (NovaCast, 2015). The finite volume method was utilized instead of the finite element method. The model is divided into small hexagons (cubes) and edge cells by altering the network parameters, resulting in a mathematical approximation that fully conforms to the original model. In such instance, the size of the cells is no longer as important, hence larger cells could be used (total number of cells 495261). The four perspectives of the model are presented in Figure 1.

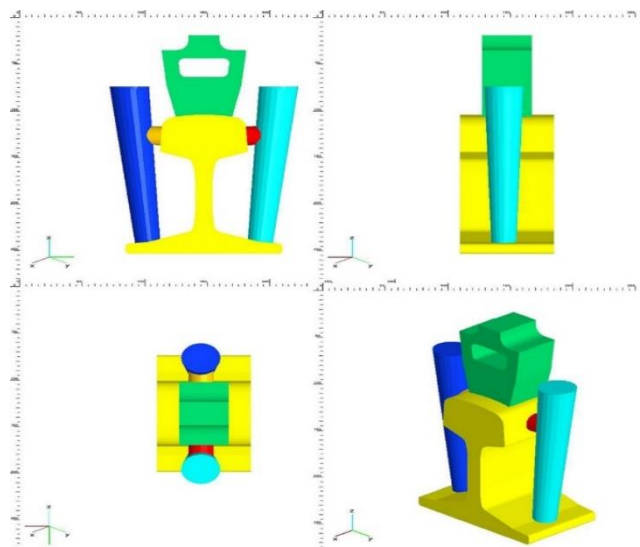


Figure 1. Casting model from the front, side, top, and angle perspective

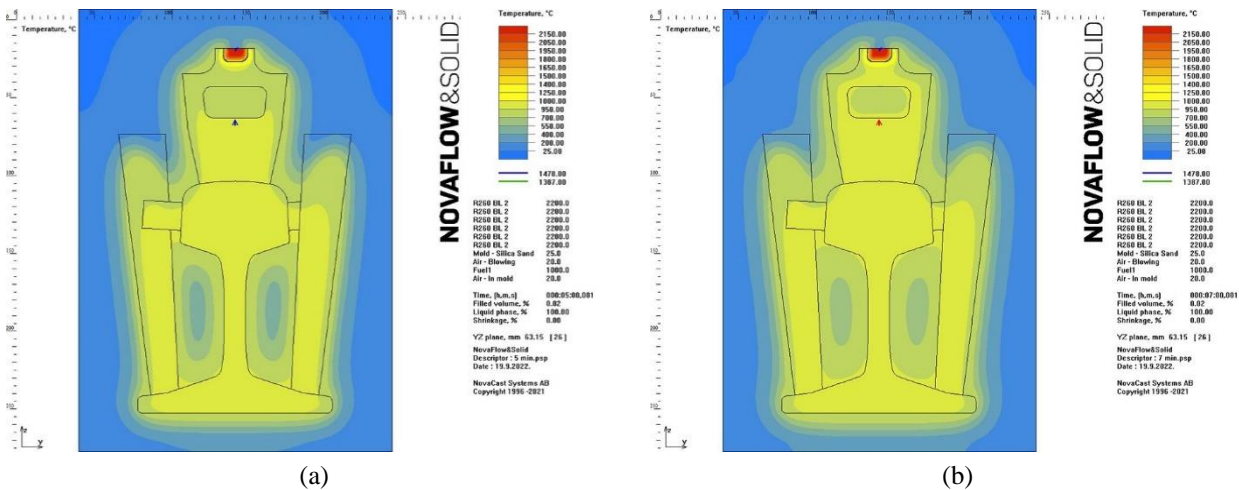
The model shown in Figure 1 consists of six elements: the rail canting (bright yellow), ingate system, and feeders (red, dark yellow, blue, and teal). The one and only gating point was placed at the center of the uppermost part of the ingate system. The molten metal flow was injected in a circle of 10 mm in diameter. Gravity casting was chosen for the filling parameters with a pressure height of 300 mm, making the flow 1.149 kg/s. The overall casting mass was calculated to be 5.370 kg and the casting temperature was set at 2200 °C. The shrinkage model was set at a high gravity influence, with a standard 83% gravity influence coefficient. In the solver setting option, conversion, gas at filling, bubble formation, and turbulence were all taken into account for quasi-equilibrium model calculation without segregation. In all simulations, the surface heat transfer model was taken into account.

Simulations were conducted with the preheating option turned on. Here the mold material (silica sand) is set to the room temperature of 25 °C while the cavity medium (air) is heated with a burner (1000 °C) from the right side of the flow divider for 4 different times (300 s, 420 s, 510 s, and 600 s). The shape of the burner area is circular, 30mm in diameter, and the flow was set at 0.1 L/s, while the initial temperature of the cavity medium was 20 °C and its flow was set at 0 L/s. These conditions were chosen in an attempt to more accurately represent realistic conditions and temperature distribution since the flow divider is not present during preheating.

In the future, in order for the model to be closer to real conditions, two sets of solid steel rails will be added on each side of the casting mold. This way, the colling and heating temperature distribution will be improved. Furthermore, because the burner is typically located about 40 cm above ground, the temperature, diameter, and gas flow would be adjusted to accurately recreate these conditions.

Results and discussion

As it can be seen from Figure 2, the starting temperature distribution at the start of casting is heavily influenced by preheating time. This difference is still present at the end of casting (Figure 3), while it is negligible at the end of solidification (Figure 6).



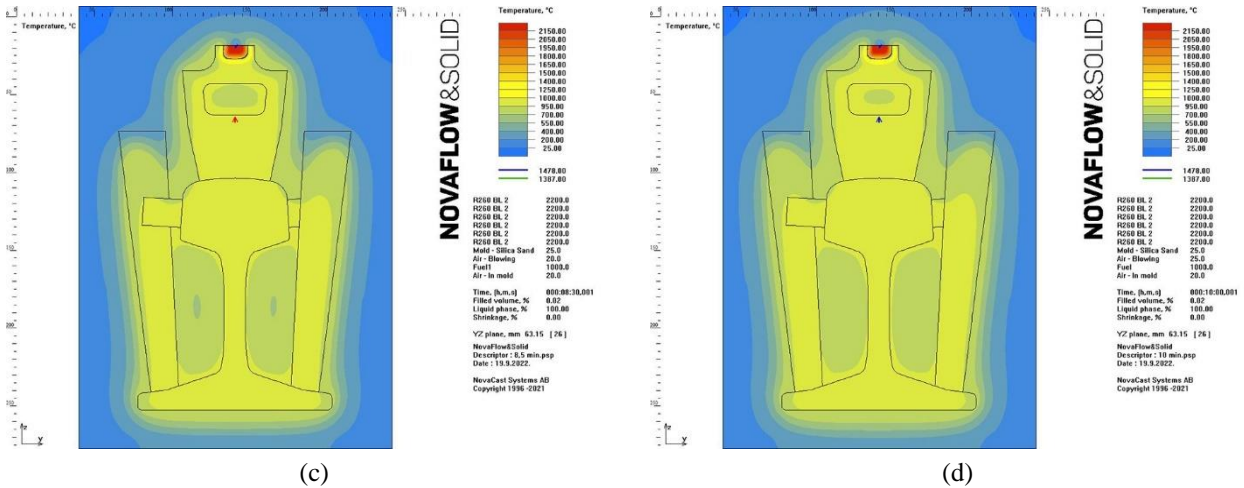


Figure 2. Temperature distribution at the start of casing for diferent preheating times: (a) 500 s ; (b) 420 s ; (c) 510 s ;(d) 600 s

The biggest differences in preheating times are evident in the sand mold heating that is between the rail canting and feeders. Clearly, at the lowest preheating time, the middle of that area is around 500 °C and it rises with the increase of preheating time to 750 °C. This same temperature distribution is maintained till the end of the casting shown in figure 3, with a maximum difference of a couple of degrees Celsius. It's also worth noting that the bottom edge of the rail has a cold spot.

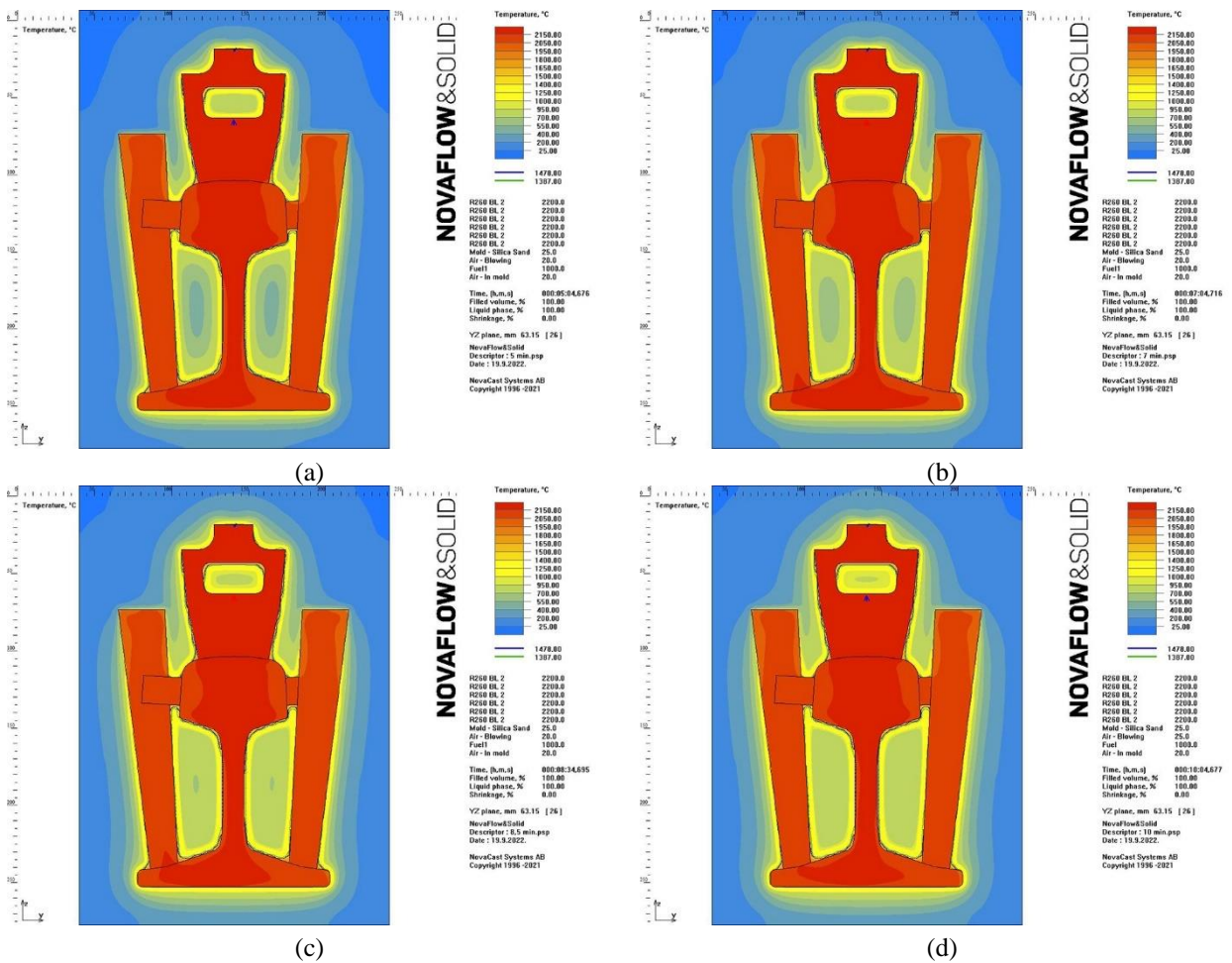


Figure 3. Temperature distribution at the end of casing for different preheating times: (a) 500 s ; (b) 420 s ; (c) 510 s ;(d) 600 s

Both Figures 2 and 3 show a cross-section of the casting model right in the middle of the x axis. However, in order to adequately show shrinkage (Figures 4) and local solidification time (Figure 5), the cross-section that divides the two feeders right in the middle is shown. The top arrows in figures 3 and 4 represent the gating point, while the bottom arrow represents the burner point, both of which are located in the center of the model. Since both figures 4 and 5 represent the end of solidification when the liquid phase reaches 0%, the same view point is kept for the temperature distribution at the end (Figure 6).

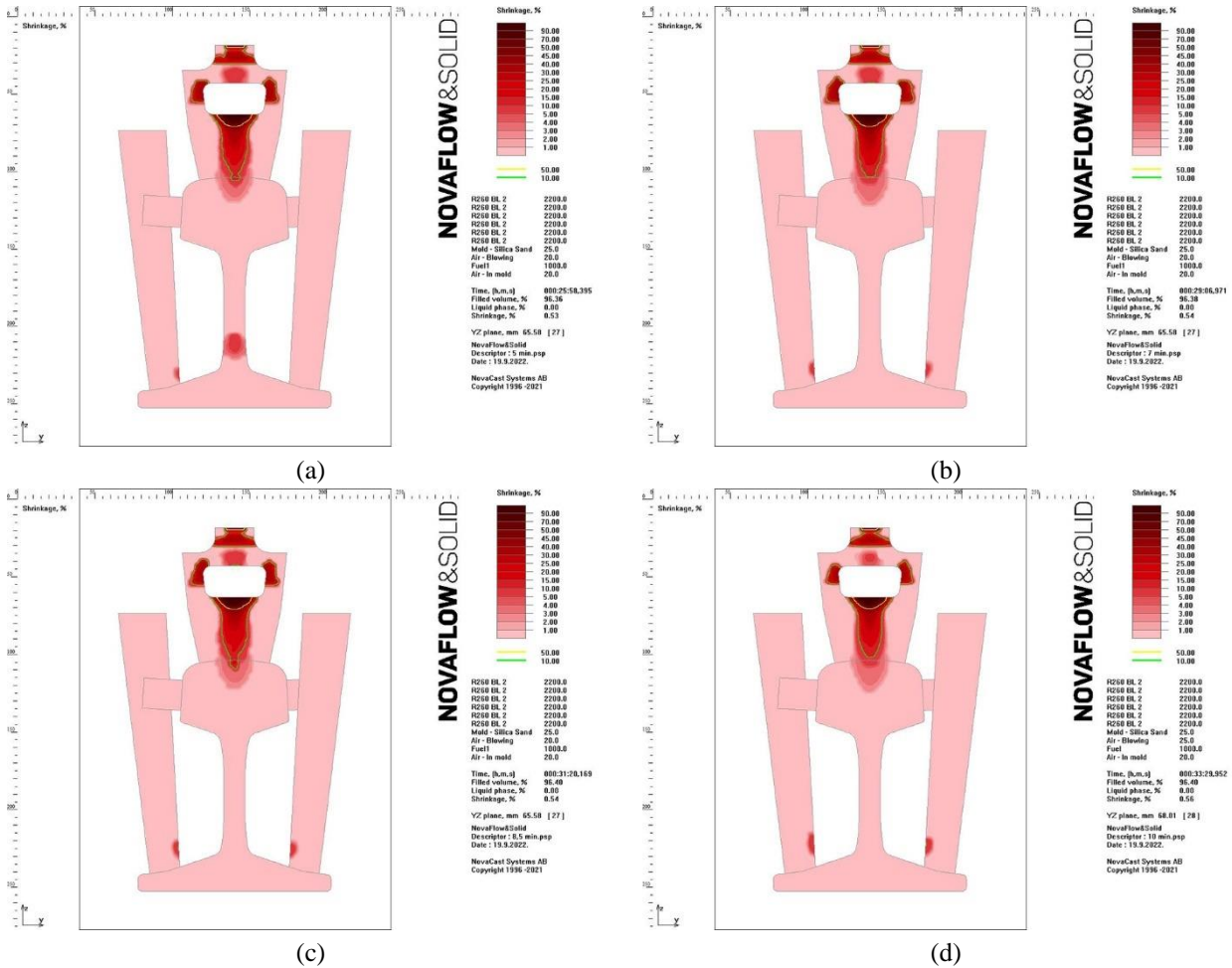


Figure 4. Shrinkage fields at the end of solidification for different preheating times: (a) 500 s ; (b) 420 s ; (c) 510 s ; (d) 600 s

Shrinkage is considered one of the most important results from this simulation in regards to solidification. Most of the shrinkage is concentrated in the feeder that is also used as an ingate system. From figure 4 (a), it is clear that the preheating time of 5 min is inadequate since it causes shrinkage at the neck of the rail. This effect is absent from other preheating times, but at the bottom of the feeders it becomes more prevalent. The preheating time of 600 s is shown to be sufficient since it moves the feeder shrinkage away from the rail casting and the shrinkage in the ingate feeder above the rail head is minimized (Figure 4 (b)).

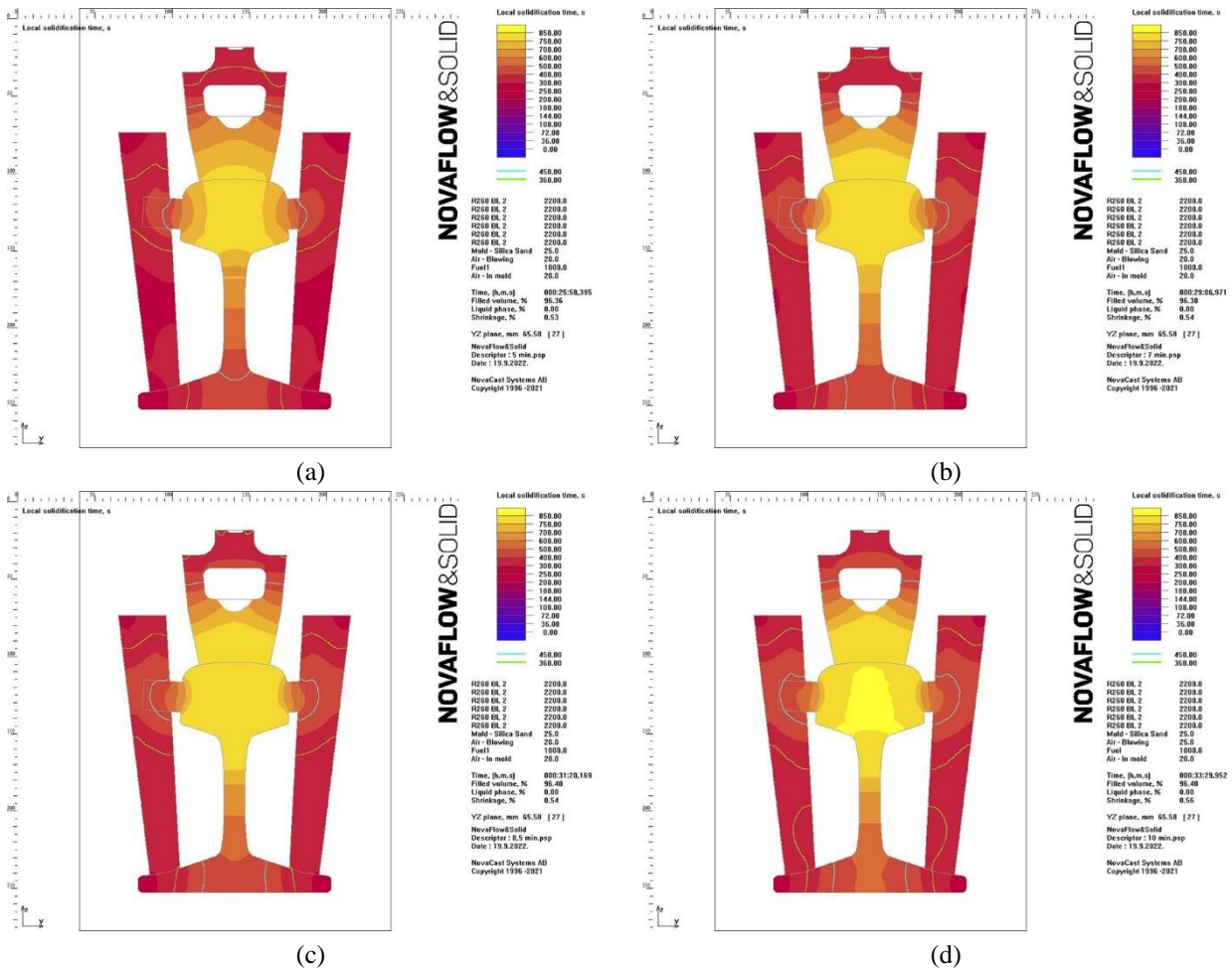
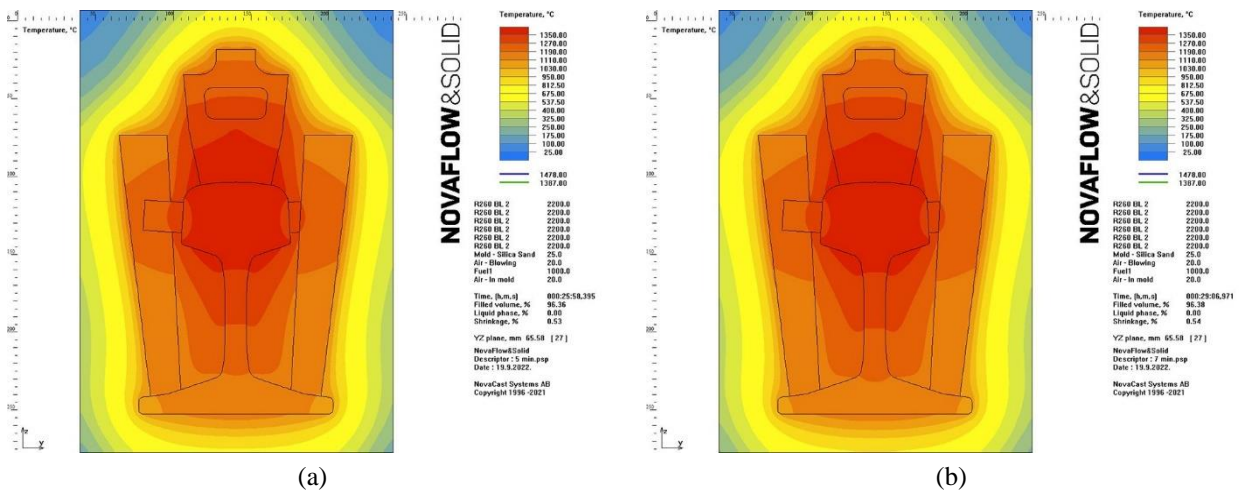


Figure 5. Local solidification times at the end of solidification for different preheating times: (a) 500 s; (b) 420 s; (c) 510 s; (d) 600 s

If we observe the temperature distribution at the end of casting before solidification starts, we can see a direct correlation between figures 3 and 5. Local solidification time increases as preheating time increases. However, at the end of solidification, there is little difference in temperature distribution between preheating times as it can be observed in Figure 6. There is clear evidence of gas entrapment below the flow divider in both Figures 5 and 6, but this doesn't affect the quality of the rail casting since the ingate feeder will be removed.



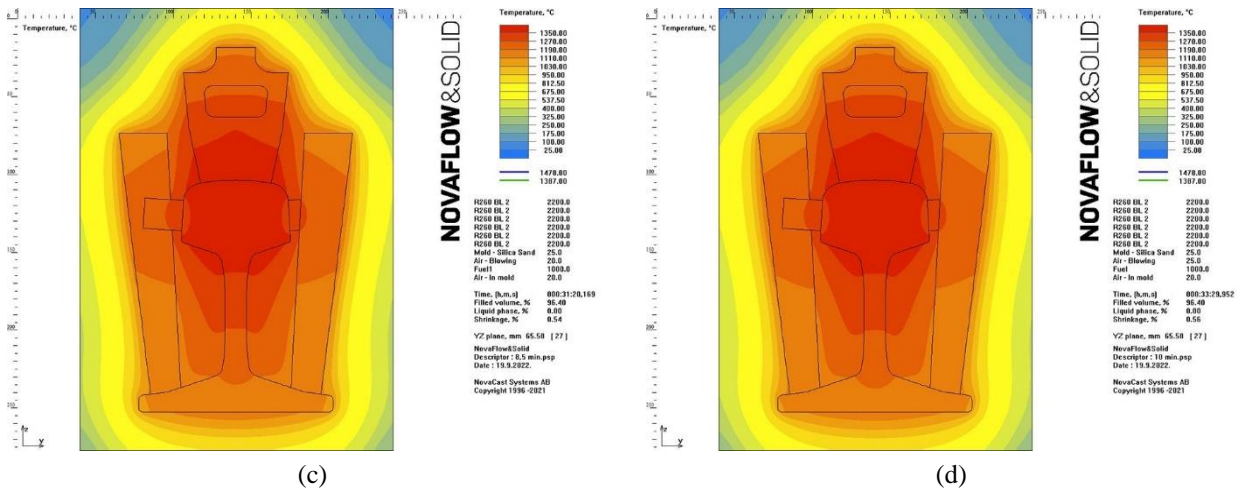


Figure 6. Temperature distribution at the end of solidification for different preheating times:
(a) 500 s; (b) 420 s; (c) 510 s ; (d) 600 s

Conclusion

It was shown in this study that the software NovaFlow and Solid CV effectively simulate the aluminothermic process of railway rail welding and may considerably contribute to the optimization of the process's techno-economic parameters. The simulation showed that there is a considerable difference in shrinkage due to preheating temperature distribution. Preheating for 600 s showed the best results, which is similar to practical experience. It may also help to improve welded connection quality by anticipating defects in the seam and at the contact point of the extra and base material. Its suitability was shown by the manufacture of test welded joints that met the quality parameters defined by simulation in the program, in the particular example of welding the type 49E1 260 rails, avoiding the significant investment of producing a large number of test welded joints.

References

- Delić, A. (2018). *Investigation of the relationship between the microstructure and properties of refractory austenitic steel HK30 modified with niobium in order to improve the properties at high temperatures* (Unpublished doctoral dissertation). University of Zenica, Faculty of Metallurgy and Technology, Zenica.
- Delić, A., Oruč, M., Rimac, M., Gigović-Gekić, A. & Sunulahpašić, R. (2019). The influence of solution annealing on microstructure and mechanical properties heat-resistant cast Steel HK30 modified by Niobium. *Metallurgical and Materials Engineering*, 25(3), 237–245. <https://doi.org/10.30544/430>
- Delić, A., Manojlović, V., Sokić, M. & Gavrilovski, M. (2022). Optimization of mold design for aluminothermic welding of railway tracks by software simulation. *Tehnika*, 77(3), 311–317. <https://doi.org/10.5937/tehnika2203311D>
- Nova Cast Systems AB (2015). Nova Flow & Solid (6.0) [Computer software]. Nova Cast Systems AB.
- Ravi, B. (2008). Casting simulation and optimization: benefits, bottlenecks and best practices. *Indian Foundry Journal*, 54(1), 47. http://efoundry.iitb.ac.in/Academy/TechnicalPapers/2008/2008IFJ_CastingSimulation.pdf
- Ravi, B. (2010). Casting simulation—best practices. *Transactions of 58th IFC, Ahmedabad*, 19–29. <http://efoundry.iitb.ac.in/Academy/TechnicalPapers/2010/58thIFC-Ravi.pdf>

OTHERS

Original scientific article

STUDY OF ISOTHERMAL, KINETIC, AND THERMODYNAMIC PARAMETERS FOR SORPTION OF VANADIUM

Tamara T. Tadić¹, Bojana M. Marković¹, Aleksandra B. Nastasović¹, Ljiljana T. Suručić², Zvezdana P. Sandić³, Antonije E. Onjia⁴

¹University of Belgrade - Institute of Chemistry, Technology and Metallurgy, Njegoševa 12, 11000 Belgrade, Serbia

²Faculty of Medicine, University of Banja Luka, Save Mrkalja 14, 78000 Banja Luka, Republic of Srpska, B&H

³University of Banja Luka, Faculty of Natural Science and Mathematics, Mladena Stojanovića 2, 78000 Banja Luka, Republic of Srpska, B&H

⁴Faculty of Technology and Metallurgy, University of Belgrade, Karnegijeva 4, 11000 Belgrade, Serbia

Abstract

This study evaluated the equilibrium, kinetics, and thermodynamics of vanadium sorption from aqueous solution onto nanocomposite functionalized with diethylene triamine in batch conditions. The effects of temperature, solution pH, and initial concentration of vanadium were examined. The maximum sorption capacity of vanadium on the tested sorbent was achieved at pH 6. The sorption capacity increased with increasing temperature and initial concentration. The equilibrium adsorption data were analyzed using Langmuir, Freundlich, Temkin, Jovanovic, Toth, Sips, Khan, and Redlich–Peterson isotherm models. The kinetics data were studied using pseudo-first-order, pseudo-second-order, the fractional power, Elovich, and Avrami models. A non-linear fitting method was used to compare the best fitting of the equilibrium and kinetic data. The sorption equilibrium data were best represented by the Langmuir, Khan, Toth, and Redlich–Peterson isotherms. The adsorption kinetics was estimated to follow the pseudo-second-order kinetic model. The mechanism of vanadium sorption was analyzed with intra-particle, Bangham, Boyd, and liquid film diffusion models. It was observed that the sorption process was controlled by the film-diffusion as well as the pore-diffusion. Thermodynamic parameters (change of standard enthalpy (ΔH°), standard entropy (ΔS°), and standard free energy (ΔG°)) suggested that the sorption of vanadium onto functionalized nanocomposite was a spontaneous and endothermic process.

Keywords: sorption, vanadium, kinetics, isotherms, thermodynamics.

Introduction

Vanadium (V) is a transition element that exists in several oxidation states in the range from +2 to +5, while tetravalent and pentavalent vanadium are the most commonly used forms (Ścibior et al., 2020). Due to its good physicochemical properties, vanadium is widely used in many industries such as petrochemical, electrochemical, and metallurgical industries (Luo et al., 2017). It plays an important role in contemporary science thanks to its application in producing ceramics, alloys, glasses, and redox batteries (Dakroury et al., 2022; Peng, 2019). An important source of vanadium is represented by minerals, such as vanadinite, patronite and carnotite (Luo et al., 2017). Also, it is used in steel production to improve strength, malleability, and resistance (Ścibior et al., 2020). The rapid growth of the industry has resulted in environmental pollution by vanadium. At the trace level, V has positive effects on plants and algae. On the other hand, huge amounts of V could be released into the environment through industry, contaminating wastewater, groundwater, and soils (Rivas et al., 2019; Ścibior et al., 2020). Vanadium compounds toxicity increase with increasing valence. Through the

food chain, vanadium could reach the human body and cause various health diseases and disorders (Barceloux & Barceloux, 1999). During the production of heat and electricity, exposure to vanadium occurs. Much attention has been focused on the removal of vanadium pollution. Various methods have been employed for removing vanadium from aqueous solutions, such as solvent extraction, sorption, chemical precipitation, and ion exchange (Li et al., 2011; Mthombeni et al., 2015). Among the mentioned methods, sorption is the most economical and effective method due to its flexibility, low cost, simple operation, and high efficiency. Various natural and synthetic materials have been used as sorbents for the removal of vanadium from aqueous solutions, such as natural soil colloids (Luo et al., 2017), di-2-ethylhexyl phosphoric acid (Li et al., 2011), amine extracts (Yang et al., 2016), polymers (Rivas et al., 2019), etc.

In this work, nanocomposite functionalized with diethylene triamine was used as a sorbent for the removal of vanadium. The effects of initial pH value, operative temperature, and initial concentration of vanadium in solution onto sorption capacity were investigated. In addition, the isotherms, kinetics, and thermodynamics of the sorption process were discussed.

Materials and Methods

In the present study, all the chemicals were analytical reagent grade. A stock solution of vanadium (100 mg/dm^3) was prepared by dissolving a NH_4VO_3 (Merck, Germany) in deionized water (Milli-Q Millipore, conductivity $18 \text{ M}\Omega/\text{cm}$). The batch sorption experiments were performed in 100 ml erlenmeyer flasks by contacting 10 g/L of sorbent with a certain concentration of vanadium solution. The effects of process parameters on sorption capacity were investigated by varying initial pH values (3 - 8), initial concentration of the metal solution ($1 - 100 \text{ mg/dm}^3$), and temperature (298 - 343 K). The residual vanadium concentration in the aqueous solution was determined by ICP-OES (Thermo Scientific iCAP 6500, USA). All experiments were repeated in duplicate. Based on obtained results, the kinetic, isotherm, and thermodynamic parameters were determined. The sorption capacity at a given time (Q_t , mg/g) and at equilibrium (Q_e , mg/g) were calculated using equations 1 and 2, respectively:

$$Q_t = \frac{(C_0 - C_t)V}{m} \quad (1)$$

$$Q_e = \frac{(C_0 - C_e)V}{m} \quad (2)$$

where C_0 (mg/dm^3) is the initial concentration of vanadium solution, C_t (mg/dm^3) and C_e (mg/dm^3) are the concentrations of vanadium solutions at time t , and at equilibrium, respectively, V (dm^3) is the volume of the aqueous phase, and m (g) is the mass of the sorbent.

Results and discussion

The pH value of vanadium solution is a very important parameter of the sorption process because it affects the surface chemistry of the sorbent and vanadium ions specification. The effect of pH values of vanadium solution on sorption capacity was investigated in an initial pH range between 3 and 8 at $T = 298 \text{ K}$ using 10 g/dm^3 sorbent dose for 60 min. It was observed from Figure 1a that as the initial pH value was increased, the capacity of vanadium sorption increased and the maximum sorption capacity was reached at pH 6. With a further increase in the initial pH value, the sorption capacity decreased. It is known that the dominant form of vanadium at pH lower than 4 is VO^{2+} , while neutral and anionic forms exist at pH above 4 (Guzmán et al., 2002). At pH around 6, amino groups on nanocomposite were protonated, thus, the interaction between anionic forms of vanadium and active

sites of sorbent was more efficient. The influence of initial metal concentration was examined at $\text{pH} = 6$, $T = 298 \text{ K}$ for 60 min. The increase of initial vanadium concentration from 1 to 100 mg/dm^3 resulted in an increase in sorption capacity from 0.07 mg/g to 4.97 mg/g (Figure 1b). This can be accounted to the increase in the number of vanadium ions to the constant amount of active sites on the sorbent. To investigate the effect of temperature, the sorption capacity was determined at 298, 310, 329, and 343 K -at pH value 6, with a sorbent dose of 10 g/dm^3 for 60 min. The results are presented in Figure 1c. As can be seen, the sorption capacity slightly increases with increasing the temperature. The observed behavior can be attributed to the increase in the rate of diffusion of vanadium ions to the active sites on the sorbent (Atsar et al., 2021).

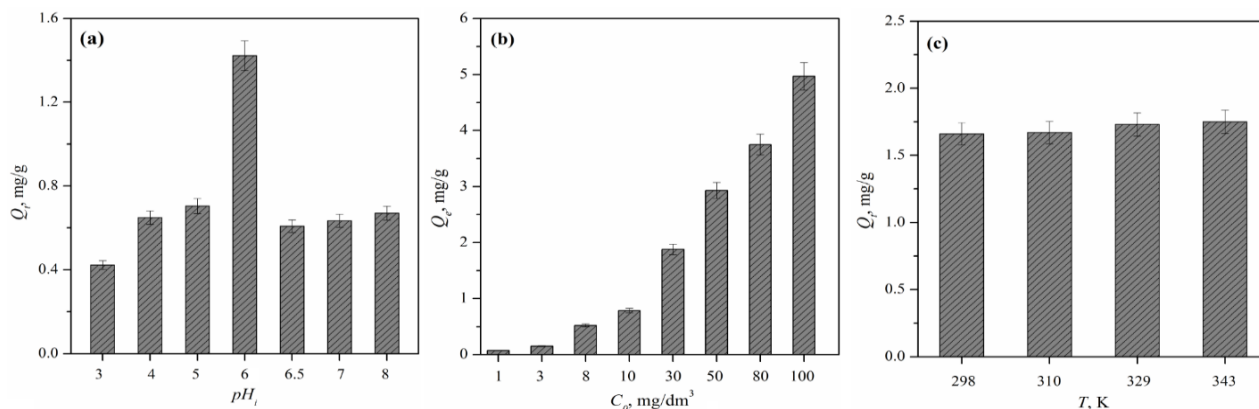


Figure 1. Effect of (a) initial pH, (b) initial concentration and (c) temperature on the sorption capacity of vanadium

To examine the binding interaction between sorbent and vanadium ions, experimental data at equilibrium were analyzed using two-parameters models, namely Langmuir, Freundlich, Temkin, and Jovanovic as well as three-parameters isotherms, namely Redlich-Peterson, Sips, Toth and Khan (Marković et al., 2014; Nastasović et al., 2022). The non-linear regression was used for fitting the curves by applying the Microsoft Excel Solver function. The isotherm models were analyzed using three statistical error functions, namely coefficient of determination (R^2), the sum of square error (SSE), and Chi-square (χ^2) (Kuetze et al., 2020). The obtained parameters for two-parameters and three-parameters isotherm models are presented in Tables 1 and 2, while isotherm fitting curves are portrayed in Figure 2.

With maximal R^2 and minimal SSE and χ^2 , the Langmuir model better described the experimental data compared to other two-parameters isotherm models, indicating monolayer sorption and the homogenous nature of sorbent. All three-parameters isotherm models showed good agreement with experimental data since their R^2 values were high (≥ 0.993). The obtained results indicate that three-parameters isotherms better describe the sorption process than two-parameters models. Also, it can be seen that the Redlich-Peterson and Khan isotherm models have the same and maximal R^2 value (0.994) and minimal values of SSE and χ^2 (0.097 and 0.035, respectively), indicating that sorption of vanadium was a hybrid process and does not follow ideal monolayer adsorption.

Table 1. Parameters of two-parameters isotherm models for the sorption of vanadium onto amino-functionalized nanocomposite

Isotherm model	Parameter	Value	R ²	SSE	χ ²
Langmuir	K_L , L/mg	0.02	0.992	0.066	0.094
	$Q_{max,L}$, mg/g	8.63			
Freundlich	K_F , L ⁿ mg ¹⁻ⁿ /g	0.27	0.988	0.093	0.042
	n	1.37			
Temkin	b_T , kJ/mol	1.45	0.943	1.053	3.451
	K_T , L/mg	0.27			
Jovanovic	K_J , L/g	0.02	0.991	0.104	0.152
	$Q_{max,J}$, mg/g	7.63			

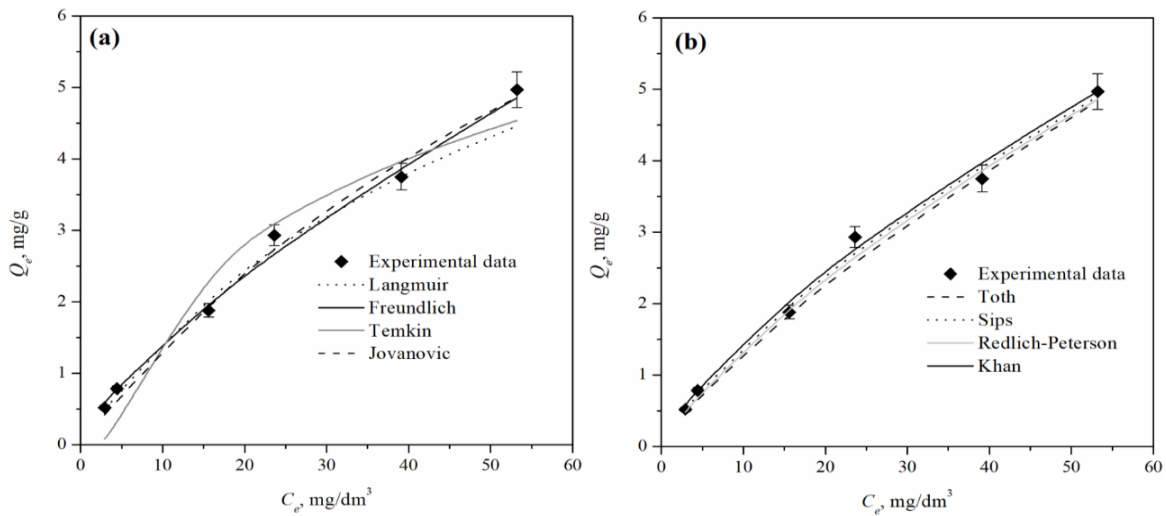


Figure 2. Predicted curve non-linear fits for the (a) two-parameter and (b) three-parameter isotherms of vanadium sorption by amino-functionalized nanocomposit

Table 2. Parameters of three-parameters isotherm models for the sorption of vanadium onto amino-functionalized nanocomposite

Isotherm model	Parameter	Value	R ²	SSE	χ ²
Redlich-Peterson	A , L/g	0.32	0.994	0.097	0.035
	B , L/mg	0.50			
	g	0.40			
Sips	$Q_{m,s}$, mg/g	28.86	0.993	0.100	0.036
	$K_S \cdot 10^3$, L/mg	2.76			
Toth	β	0.83	0.994	0.103	0.040
	$Q_{m,T}$, mg/g	70.19			
	$K_T \cdot 10^3$, L/g	3.29			
Khan	t	0.42	0.994	0.097	0.035
	$Q_{m,K}$, mg/g	0.76			
	K_K	0.28			
	n_K	0.30			

To investigate the kinetics of the vanadium sorption onto nanocomposite functionalized with diethylene triamine five models were used, namely pseudo-first-order, pseudo-second-order, Elovich, Avrami, and Fractional power kinetic models (Nastasović et al., 2022). The non-linear regression method was used to determine the kinetic parameters. The three statistical error functions (R², SSE, and χ²) were applied to test the best fitting kinetic models. The estimated kinetic parameters are presented in Table 3, while kinetics fitting curves are shown in Figure 3.

Table 3. Kinetic parameters for sorption of vanadium onto amino-functionalized nanocomposite

Kinetic model	Parameter	Value	R ²	SSE	χ ²
Pseudo-first-order	k ₁ , 1/min	0.14	0.787	0.267	0.395
	Q _e ^{cal} , mg/g	1.42			
Pseudo-second-order	k ₂ , 1/min	0.18	0.998	0.001	0.001
	Q _e ^{cal} , mg/g	1.48			
Elovich	α, mg/g min	4.91	0.992	0.004	0.003
	β, g/mg	5.35			
Avrami	k _{AV} , 1/min	0.07	0.997	0.002	0.002
	Q _e ^{cal} , mg/g	10.49			
	n	0.17			
Fractional power	k _{FP} , mg/g min	0.71	0.888	0.076	0.084
	ν, 1/min	0.16			

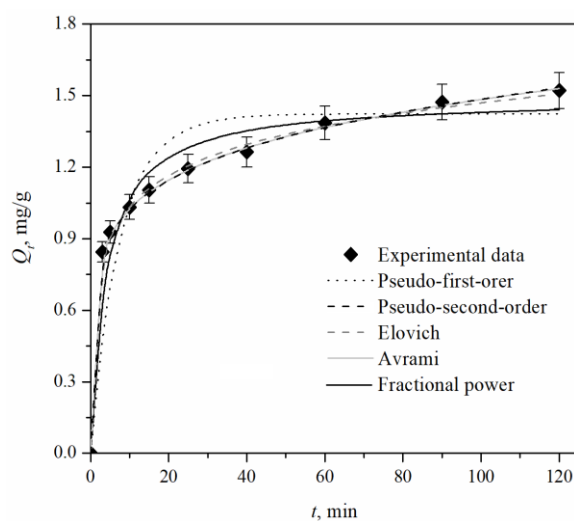


Figure 3. Non-linear kinetic models fitting for sorption of vanadium by nanocomposite functionalized with diethylene triamine

Based on statistical error functions presented in Table 3, the non-linear model of pseudo-second order is best suited to describe the sorption of vanadium. The Q_e^{calc} value (1.48 mg/g) from the pseudo-second-order was close to the Q_e^{exp} value (1.52 mg/g), meaning that chemisorption plays an important role in the vanadium sorption onto amino-functionalized nanocomposite.

The liquid film diffusion, intra-particle diffusion, Bangham, and Boyd models (Nastasović et al., 2022) were used to understand the sorption mechanism. The results are presented in Figure 4 and Table 4. As can be seen from obtained results, the high values for R² for liquid film diffusion, intra-particle diffusion, Bangham, and Boyd models, as well as multilinear intra-particle diffusion plot, suggest the simultaneous influence of film and pore diffusion onto vanadium sorption by the investigated sorbent.

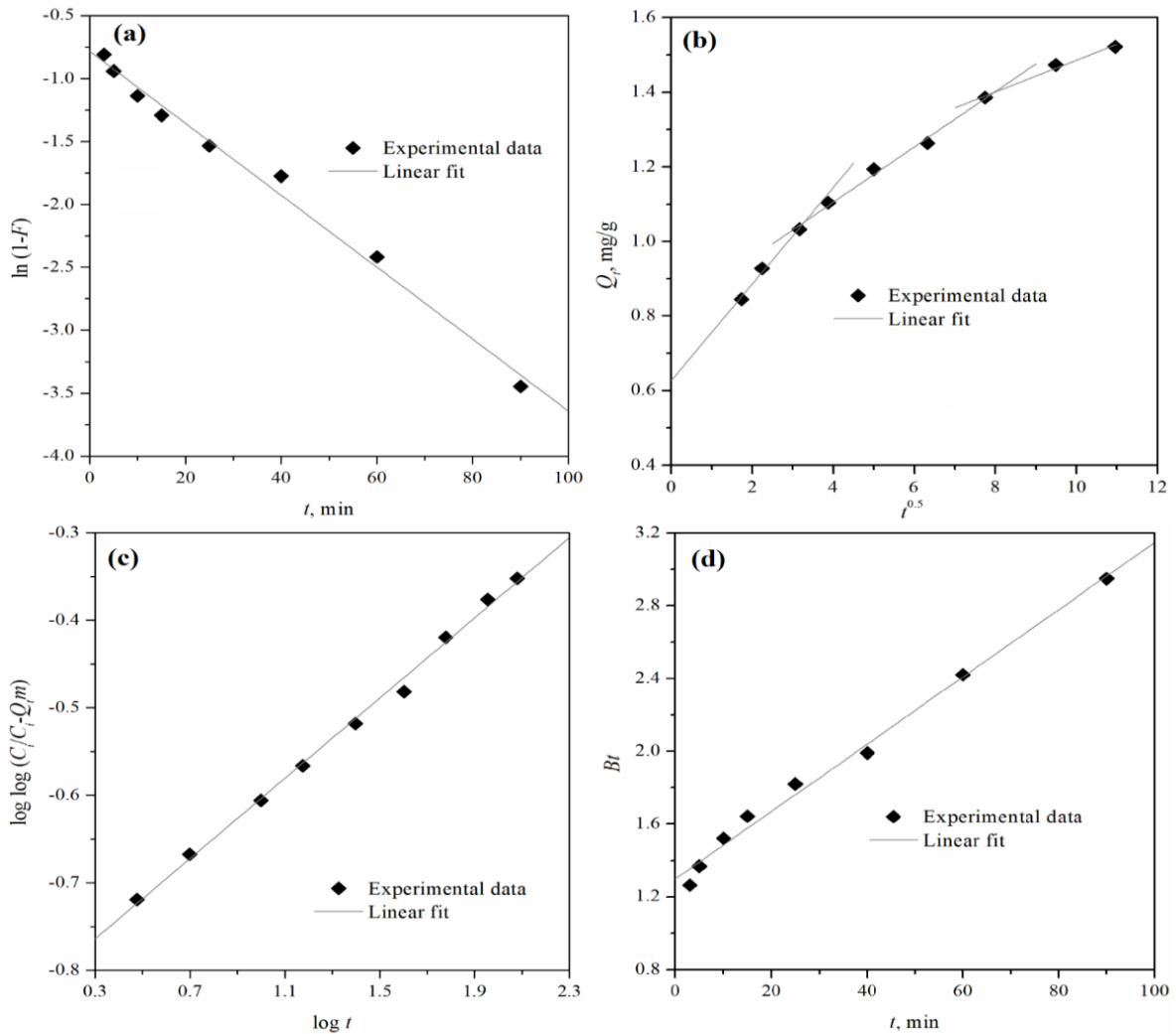


Figure 4. Linearized plots of (a) liquid film diffusion, (b) intra-particle diffusion, (c) Bangham and (d) Boyd models for the sorption of vanadium onto nanocomposite functionalized with diethylene triamine

Table 4. Parameters for sorption mechanism of vanadium onto amino-functionalized nanocomposite

Parameters	Values	Parameters	Values
Intra-particle diffusion		Liquid film diffusion	
$k_{id,1}$, mg/g min ^{0.5}	0.13	$k_{LFD} \cdot 10^2$, 1/min	2.86
$C_{id,1}$	0.63	C_{LFD}	-0.79
R_1^2	0.990	R^2	0.990
$k_{id,2}$, mg/g min ^{0.5}	0.07	Bangham model	
$C_{id,2}$	0.81	$k_B \cdot 10^3$, 1/g	0.68
R_2^2	0.992	α	0.23
$k_{id,3}$, mg/g min ^{0.5}	0.04	R^2	0.996
$C_{id,3}$	1.06	Boyd model	
R_3^2	0.987	R^2	0.991

The standard Gibb's free energy change (ΔG°), the standard enthalpy change (ΔH°) and the standard entropy change (ΔS°) were calculated from Van't Hoff equation (Marković et al., 2017). The thermodynamic parameters are given in Table 5. The positive values of ΔS° (0.31 kJ/K mol) typify a high degree of randomness and reversible process. The positive ΔH° value (69.5 kJ/mol) suggests that the sorption is endothermic and chemisorption in nature (Dada et al., 2020). The negative ΔG°

values at all studied temperatures indicate that sorption of vanadium is thermodynamically favourable and spontaneous.

Table 5. Thermodynamic parameters for vanadium sorption by amino-functionalized nanocomposite

T, K	ΔG° (kJ/mol)	ΔH° (kJ/mol)	ΔS° (kJ/Kmol)	$T\Delta S^\circ$ (kJ/mol)
298	-22.98			92.55
313	-26.71			96.28
328	-31.61	69.5	0.31	102.18
343	-36.95			106.53

Conclusion

This study has investigated the possible application of amino-functionalized nanocomposite as sorbent for the removal of vanadium from aqueous solutions. The sorption capacity was dependent on the initial pH value of vanadium solution, temperature as well as initial metal concentration. Isotherms models confirmed that sorption of vanadium was a hybrid process and did not follow ideal monolayer adsorption. The sorption followed the pseudo-second-order kinetics model, as confirmed by statistical error functions. The mechanism investigation has shown that intra-particle diffusion was not the only rate-limiting step. Thermodynamic parameters suggested that the sorption of vanadium onto functionalized nanocomposite was a spontaneous, thermodynamically favourable, and endothermic process.

Acknowledgment: This work was supported by the Ministry of Education, Science and Technological Development of the Republic of Serbia (Grants No. 451-03-68/2022-14/200026 and 451-03-68/2022-14/200135).

References

- Atsar, F. S., Kukwa, D., Wuana, R. A. & Arwenyo, B. (2021). Kinetics and thermodynamic studies: Adsorption of Pb, Cr and Ni ions from spent lubrication oil (SLO) using acid modified clay. *American Journal of Analytical Chemistry*, 12(5), 109–120. <https://doi.org/10.4236/ajac.2021.125009>
- Barceloux, D. G. & Barceloux, D. (1999). Vanadium. *Journal of Toxicology: Clinical Toxicology*, 37(2), 265–279. <https://doi.org/10.1081/CLT-100102425>
- Dada, A. O., Adekola, F. A., Odebunmi, E. O., Dada, F. E., Bello, O. M., Akinyemi, B. A., Bello, O. S. & Unukoro, O. G. (2020). Sustainable and low-cost *Ocimum gratissimum* for biosorption of indigo carmine dye: kinetics, isotherm, and thermodynamic studies. *International journal of phytoremediation*, 22(14), 1524–1537. <https://doi.org/10.1080/15226514.2020.1785389>
- Dakroury, G. A., El-Shazly, E. A. A., Eliwa, A. A., Mubark, A. E. & El-Azony, K. M. (2022). Utilization of titanium nanocomposites as prospective materials for recycling of vanadium (V) from waste solutions. *Journal of Molecular Liquid*, 366, 120170. <https://doi.org/10.1016/j.molliq.2022.120170>
- Guzmán, J., Saucedo, I., Navarro, R., Revilla, J. & Guibal, E. (2002). Vanadium interactions with chitosan: Influence of polymer protonation and metal speciation. *Langmuir*, 18(5), 1567–1573. <https://doi.org/10.1021/la010802n>
- Kuete, I.-H. T., Tchuifon, D. R. T., Ndifor-Angwafor, G. N., Kamdem, A. T. & Anagho, S. G. (2020). Kinetic, isotherm and thermodynamic studies of the adsorption of thymol blue onto powdered activated carbons from *Garcinia cola* nut shells impregnated with H₃PO₄ and KOH: Non-linear regression analysis. *Journal of Encapsulation and Adsorption Sciences*, 10, 1–27. <https://doi.org/10.4236/jeas.2020.101001>

- Li, X., Wei, C., Deng, Z., Li, M., Li, C. & Fan, G. (2011). Selective solvent extraction of vanadium over iron from a stone coal/black shale acid leach solution by D2EHPA/TBP. *Hydrometallurgy*, 105, 359–363. <https://doi.org/10.1016/j.hydromet.2010.10.006>
- Luo, X., Yu, L., Wang, C., Yin, X., Mosa, A., Lv, J. & Sun, H. (2017). Sorption of vanadium (V) onto natural soil colloids under various solution pH and ionic strength conditions. *Chemosphere*, 169, 609–617. <https://doi.org/10.1016/j.chemosphere.2016.11.105>
- Marković, B. M., Stefanović, I. S., Hercigonja, R. V., Pergal, M. V., Marković, J. P., Onjia, A. E. & Nastasović, A. B. (2017). Novel hexamethylene diamine-functionalized macroporous copolymer for chromium removal from aqueous solutions. *Polymer International*, 66(5), 679–689. <https://doi.org/10.1002/pi.5306>
- Marković, D. D., Lekić, B. M., Rajaković-Ognjanović, V. N., Onjia, A. E. & Rajaković, Lj. V. (2014). A new approach in regression analysis for modeling adsorption isotherms. *The Scientific World Journal*. 2014, 930879. <https://doi.org/10.1155/2014/930879>
- Mthombeni, N. H., Mbakop, S. & Onyango, M. S. (2015). Magnetic zeolite-polymer composite as an adsorbent for the remediation of wastewaters containing vanadium. *International Journal of Environmental Science and Development*. 6(8), 602–605. <http://dx.doi.org/10.7763/IJESD.2015.V6.665>
- Nastasović, A., Marković, B., Suručić, Lj. & Onjia, A. (2022). Methacrylate-based polymeric sorbents for recovery of metals from aqueous solutions. *Metals*, 12(5), 814. <https://doi.org/10.3390/met12050814>
- Peng, H. (2019). A literature review on leaching and recovery of vanadium. *Journal of Environmental Chemical Engineering*, 7(5), 103313. <https://doi.org/10.1016/j.jece.2019.103313>
- Rivas, B. L., Espinosa, C. & Sánchez, J. (2019). Application of the liquid-phase polymer-based retention technique to the sorption of molybdenum(VI) and vanadium(V). *Polymer Bulletin*, 76, 539–552. <https://doi.org/10.1007/s00289-018-2397-8>
- Ścibiora, A., Pietrzyk, Ł., Plewa, Z. & Skiba, A. (2020). Vanadium: Risks and possible benefits in the light of a comprehensive overview of its pharmacotoxicological mechanisms and multi-applications with a summary of further research trends. *Journal of Trace Elements in Medicine and Biology*, 61, 126508. <https://doi.org/10.1016/j.jtemb.2020.126508>
- Yang, X., Zhang, Y., Bao, S. & Shen, C. (2016). Separation and recovery of vanadium from a sulfuric-acid leaching solution of stone coal by solvent extraction using trialkylamine. *Separation and Purification Technology*, 164, 49–55. <https://doi.org/10.1016/j.seppur.2016.03.021>

Original scientific article

REMOVAL OF LINDANE FROM AQUEOUS SOLUTION BY GLYCIDYL METHACRYLATE BASED CHELATING MACROPOROUS COPOLYMER: KINETICS AND MECHANISM

Tamara T. Tadić¹, Bojana M. Marković¹, Mila V. Ilić¹, Aleksandra B. Nastasović¹, Antonije E. Onjia²

¹University of Belgrade - Institute of Chemistry, Technology and Metallurgy, Njegoševa 12, 11000 Belgrade, Serbia

²Faculty of Technology and Metallurgy, University of Belgrade, Karnegijeva 4, 11000 Belgrade, Serbia

Abstract

Lindane belongs to the persistent organic pollutants (POPs) group, which can cause carcinogenic, endocrine, and neurological problems in an organism. The widespread presence of lindane in the environment demands efficient methods of its removal. In the present work, we investigated the removal of lindane from an aqueous solution using a synthesized macroporous copolymer surface modified with different functional groups through two-step post-functionalization. The modified copolymer was characterized by Fourier transform infrared spectroscopy (FTIR-ATR), scanning electron microscopy (SEM), and mercury intrusion porosimetry. For the kinetics of lindane sorption, pseudo-first-order, pseudo-second-order, Elovich, Avrami, and fractional power models were used via linear and non-linear regression analyses. The quality of the fitting of each model to experimental data was assessed based on seven error functions: coefficient of determination (R^2), Marquardt's percent standard deviation (MPSD), Chi-square statistic test (χ^2), hybrid fractional error function (HYBRID), the sum of the errors squared (SSE), sum of the absolute errors (EABS), and average relative error (ARE). The investigation of error estimation methods showed that the pseudo-second-order model best fits the experimental kinetics data for both regression analyses. The mechanism of lindane sorption was investigated by subjecting the data to the liquid film diffusion model, intraparticle diffusion model, Bangham, and Boyd models. The results showed that intraparticle diffusion was not the sole rate-controlling step; film-diffusion also affected the sorption process.

Keywords: chelating polymer, glycidyl methacrylate, lindane, kinetics, mechanism.

Introduction

Lindane (γ -hexachlorocyclohexane, γ -HCH) is an organochlorine pesticide. It is commonly used in agriculture as an insecticide and in pharmaceutical products as an ingredient in lotions and shampoos to control scabies and lice (Zhang et al., 2020). Due to its chemical stability, high lipid solubility, and migration over long distances, lindane can persist in the environment and cause widespread and long-term contamination (Benimeli et al., 2008). According to US EPA, lindane has been classified as mutagenic, genotoxic, and teratogenic (Khan et al., 2021). During the production of hexachlorocyclohexane (HCH) four isomers (α , β , γ , δ) are formed, but only the γ -HCH isomer has insecticidal activity. During the creation of lindane, a large amount of other waste isomers (α - and β -hexachlorocyclohexane) is created, so the production of γ -HCH isomer is non-effective (Vijgen et al., 2011). In 2009, the Stockholm Convention listed lindane and its α and β isomers as persistent organic pollutants (POP). After that, lindane, along with its α and β isomers, was banned or restricted in many countries (Zhang et al., 2020). Broad lindane applications represent severe threats to the environment and human health. Due to its slow degradation, high lipid solubility, and chemical

stability, lindane residues have been leaching underground for years and contaminating surface and groundwater (Kumar & Pannu, 2018). However, in some developing countries (India), lindane is still used due to its versatility in controlling pests and low cost (Jain et al., 2022).

Lindane can affect the endocrine system and central nervous system. In addition, due to lipophilicity, lindane can accumulate in human breast milk and in organs that are rich in fat. Many studies reported that exposure to lindane could be associated with various types of cancer (prostate, lung, breast, etc.) (Jayaraj et al., 2016; Mortazavi et al., 2019).

Since lindane contaminates water through household and agriculture, its removal is important. Modification in various ways allows porous polymer materials to be applied for the sorption of different types of materials. Macroporous copolymer based on glycidyl methacrylate and ethylene glycol dimethacrylate (PGME) is considered as an excellent starting point for surface modification and post-functionalization via reaction of the epoxy ring with nucleophilic groups. PGMA is one of the most adaptable reactive polymers with excellent adsorption properties and the ability to reuse and regenerate, which makes it a promising adsorbent.

Materials and Methods

Starting material, PGME was modified in two-step post-functionalization. In the first step, the reaction with diethylene triamine (PGME-deta) was performed (Malović et al., 2007), and in the second step, with chelating agent (ethylenediaminetetraacetic dianhydride) according to the procedure described in the literature (Su et al., 2017). PGME-deta and chelating agent (1:1) were added to the flask with N,N-dimethylformamide (DMF) and the mixture was kneaded for 4 hours at 80 ± 0.2 °C. The obtained chelating copolymer was subsequently washed, dried, and characterized by Fourier transform infrared spectroscopy (FTIR-ATR), scanning electron microscopy (SEM), and mercury intrusion porosimetry.

The mechanism and kinetics of lindane sorption were determined in a non-competitive batch process at unadjusted pH (pH=6.3) and room temperature (25 ± 0.2 °C). The sorbent (0.90 g) was contacted with 90 cm³ of lindane aqueous solution with a concentration of 150 µg/dm³ and shaken on an orbital shaker for 180 min, at a speed of 450 °/min. At appropriate time intervals, 5 cm³ of the solution was sampled with a micropipette and prepared for measurement by GC-ECD. All measurements were performed in duplicate, and the results were expressed as the mean value.

Sorption capacity (Q_t , µg/g) was calculated from:

$$Q_t = \frac{(C_0 - C_t)V}{m} \quad (1)$$

where: C_0 (µg/dm³) and C_t (µg/dm³) stand for the initial and final lindane concentration at time t , respectively, V (dm³) is the solution volume, and m is the mass of the chelating copolymer.

FTIR spectra were taken in ATR mode in the range 4000–400 cm⁻¹ using a Nicolet SUMMIT FT-IR Spectrometer (Thermo Fisher Scientific, Waltham, MA, USA). SEM micrographs were obtained on JEOL JSM-6610LV instrument (JEOL Ltd., Tokyo, Japan). Pore size distributions were determined by a high-pressure mercury intrusion porosimeter Carlo Erba Porosimeter 2000 (Washington, DC, USA, software Milestone 200). The specific surface area, S_{Hg} was calculated from the cumulative pore volume distribution curve as described in the literature (Nastasović et al., 2022). Lindane detection was determined on a gas chromatograph, Agilent 7890A GC coupled with an electron capture detector (ECD). TG-5MT capillary column (30 m × 0.25 mm × 0.25 µm) was used. The injection mode was splitless, while the temperature regime was set in the following way: 50 °C for 3 min, then increased at a rate of 30 °C/min to 210 °C and held at this temperature for 20 min. Hydrogen was used as the carrier gas with a 60 mL/min flow rate.

Results and discussion

Characterization of the sorbent

The introduction of reactive groups improves adsorption capacities, selectivity, and the pH range for sorption (Galhoum, 2019). Adsorption ability of GME-based polymer can be enhanced by two-step post-functionalization, firstly by ring-opening of the epoxy ring with diethylene triamine (deta), and secondly, by the introduction of a chelating agent through reaction with amine groups of deta. The post-functionalization of the chelating polymer was confirmed using FTIR-ATR spectrometry (Figure 1).

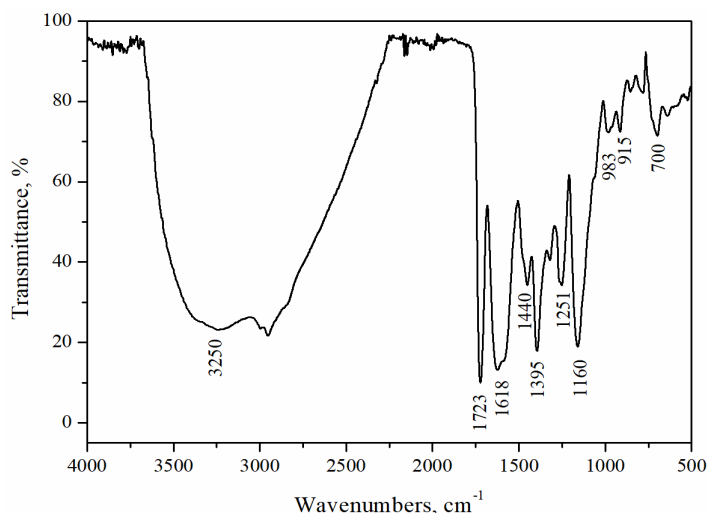


Figure 1. FTIR-ATR spectrum of the chelating copolymer

A broad band at 3800–2200 cm^{-1} in the FTIR-ATR spectrum of chelating copolymer originates from the presence of $-\text{NH}_2$ and $-\text{OH}$ groups (overlapping bands for O-H and N-H amine stretching) (Peng et al., 2008; Tadić et al., 2022). A band at $\sim 1620 \text{ cm}^{-1}$ corresponding to $-\text{NH}$ bending mode (Galhoum et al., 2019), while C-N stretching vibrations of the tertiary aliphatic amine were observed at 1160 cm^{-1} (Hwang et al., 2013). The peak at 1440 cm^{-1} was attributed to the vibration of the double covalent bond in $-\text{COOH}$ (Wang et al., 2013).

As seen from SEM micrographs in Figure 2a, the particles were smooth spheres, while the micrographs of particle surface and cross-section (Figure 2b and 2c) clearly show a three-dimensional globular porous structure. The S_{Hg} value of the chelating copolymer calculated from the cumulative pore volume distribution curve was $35 \text{ m}^2/\text{g}$.

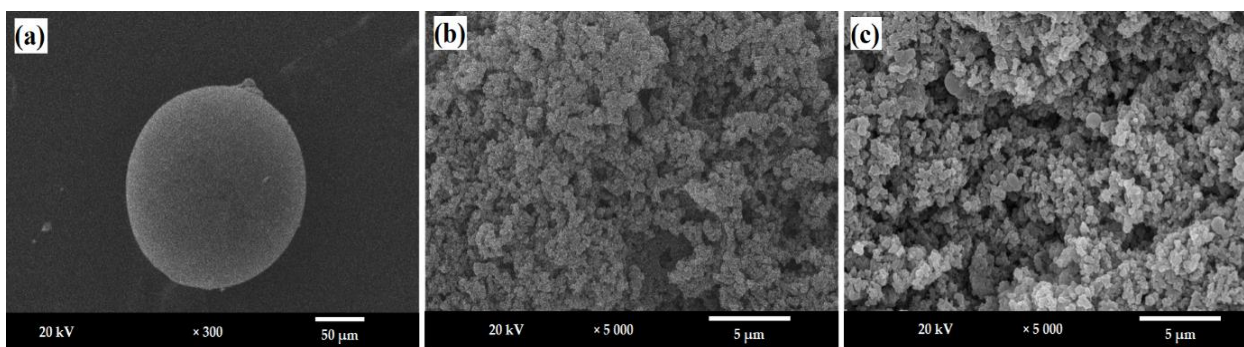


Figure 2. SEM micrographs of (a) particle beads (magnification 300×), (b) particle surface (magnification 5000×) and (c) cross-section (magnification 5000×) for chelating copolymer

Lindane sorption kinetics

The kinetic mechanism of lindane sorption on chelating copolymer was determined by linear and non-linear forms of pseudo-first-order, pseudo-second-order kinetic model, Elovich, Avrami and fractional-power model (Nastasović et al., 2022). Non-linear regression was used to fit the experimentally obtained data in the program Origin 9.0[®], OriginLab Corporation. The following error functions were used to match the applied kinetic models with the experimental data: determination coefficient (R^2), sum squared error (SSE), squared angular errors (SAE), average relative error (ARE), hybrid fractional error function (HYBRID), Marquardt's percent standard deviation (MPSD), and chi-square test (χ^2) (Marković et al., 2014; Sivarajasekar & Baskar, 2019). Figure 3 shows the comparison of the fits for different linear and non-linear kinetic models, while Tables 1 and 2 summarize calculated kinetic parameters and the relevant correlation coefficients for linear and non-linear kinetic models, respectively.

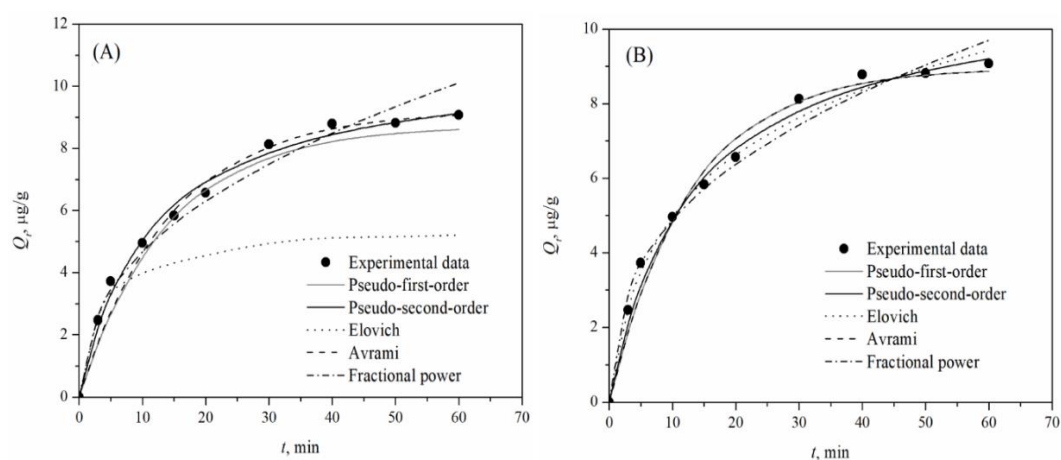


Figure 3. Kinetics model (A) linear and (B) non-linear plots for sorption of lindane onto chelating copolymer

For both linear and non-linear models, the higher R^2 values and the lowest values of other error functions suggest a better fit. According to values presented in Table 1, pseudo-second-order was the best suitable to describe the kinetic data of lindane sorption. Also, the error values indicated that the non-linear method is a better way to obtain the kinetic parameters describing the lindane sorption onto a chelating copolymer.

Table 1. Linear regression analysis for sorption kinetics of lindane onto chelating copolymer

Model	Parameter	Value	R^2	SSE	SAE	ARE	HYBRID	MPSD	χ^2
Pseudo-first-order	$k_1 \cdot 10^2$, 1/min	7.44	0.951	2.483	4.004	9.654	8.751	15.956	0.814
	Q_e^{cal} , µg/g	8.70							
Pseudo-second-order	$k_2 \cdot 10^3$, g/µg min	8.43	0.986	0.653	2.115	4.388	1.693	5.900	0.120
	Q_e^{cal} , mg/g	10.80							
Elovich	α , µg/g min	2.17	0.592	58.928	19.352	28.807	102.069	35.740	11.739
	β , g/mg	0.43							
Avrami	$k_{AV} \cdot 10^2$, 1/min	8.32	0.965	1.700	2.801	7.947	6.892	14.607	0.634
	Q_e^{cal} , µg/g	9.19							
	n	0.87							
Fractional-power	k_{FP} , µg/g min	0.43	0.956	2.160	3.757	6.790	4.285	8.691	0.286
	ν , 1/min	1.76							

Table 2. Non-linear regression analysis for sorption kinetics of lindane onto chelating copolymer

Model	Parameter	Value	R^2	SSE	SAE	ARE	HYBRID	MPSD	χ^2
Pseudo-first-order	$k_1 \cdot 10^2$, 1/min	8.04	0.969	1.501	2.800	7.178	5.336	1.521	0.443
	Q_e^{cal} , µg/g	8.94							

Pseudo-second-order	$k_2 \cdot 10^3, \text{g}/\mu\text{g min}$ $Q_e^{cal}, \text{mg/g}$	7.25 11.11	0.993	0.373	1.603	3.070	0.837	3.975	0.059
Elovich	$\alpha, \mu\text{g/g min}$ $\beta, \text{g/mg}$	1.51 0.38	0.987	0.602	2.018	3.639	1.214	4.619	0.086
Avrami	$k_{AV} \cdot 10^2, 1/\text{min}$ $Q_e^{cal}, \mu\text{g/g}$ n	8.87 8.94 0.91	0.969	1.501	2.800	7.178	5.336	12.331	0.443
Fractional-power	$k_{FP}, \mu\text{g/g min}$ $\nu, 1/\text{min}$	2.06 0.38	0.967	1.578	3.004	6.251	4.449	11.195	0.277

The mechanism of lindane sorption was investigated by linear analysis with the liquid film diffusion model, intraparticle diffusion model, as well as Bangham, and Boyd models. The results given in Table 3 and Figure 5 showed that intraparticle diffusion was not the sole rate-controlling step; film-diffusion also affected the sorption process.

Table 3. Parameters for sorption mechanism of lindane onto chelating copolymer

Model	Parameter	Value	R ²
Intra-particle diffusion	$k_{id,1}, \mu\text{g/g min}$	1.37	0.990
	$C_{id,1}, \mu\text{g/g}$	0.43	
	$k_{id,2}, \mu\text{g/g min}$	0.20	0.989
	$C_{id,2}, \mu\text{g/g}$	7.49	
Bangham	$k_B \cdot 10^4, \mu\text{g/g min}$	9.90	0.982
	α	0.55	
Liquid film diffusion	$k_{LFD} \cdot 10^2, 1/\text{min}$	7.44	0.972
	C_{LFD}	-0.05	

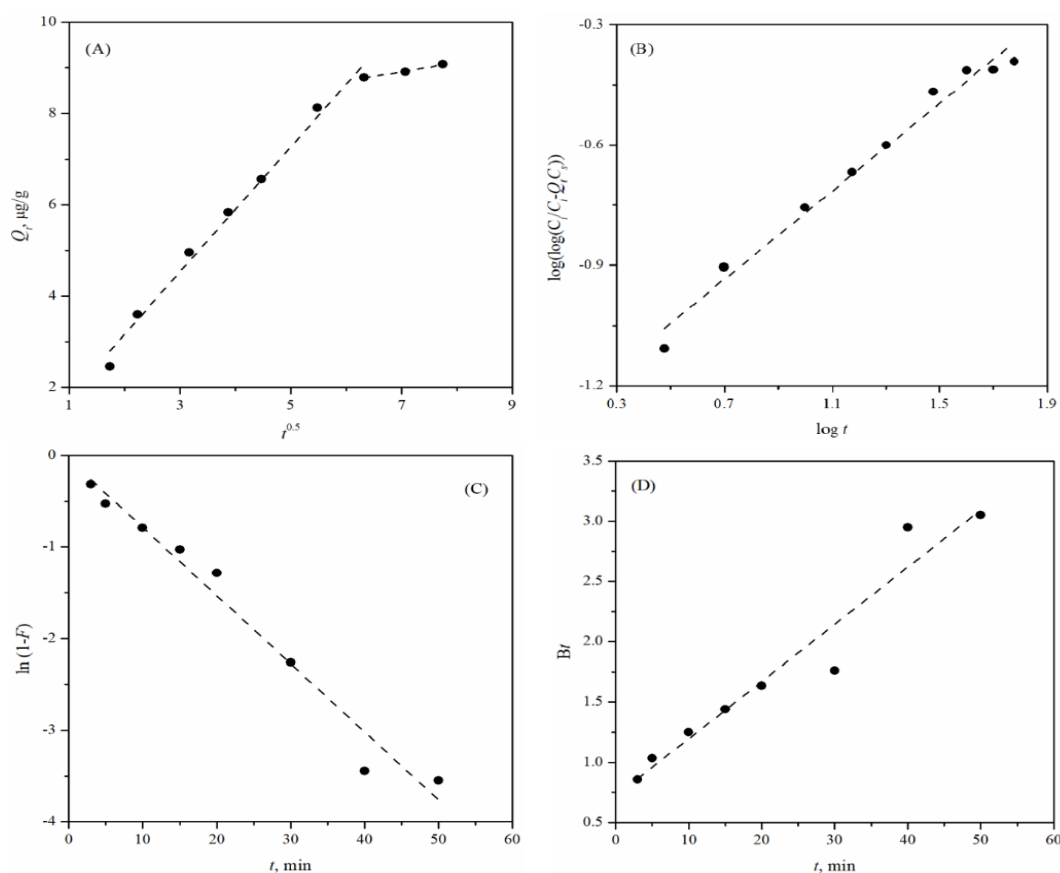


Figure 4. Linear plots for the (A) intra-particle diffusion, (B) Bangham, (C) liquid film diffusion and (D) Boyd models for the sorption of lindane onto chelating copolymer

Conclusion

In this study, PGME was chemically modified in two-step post-functionalization with diethylene triamine and chelating agent and tested as lindane sorbent. The characterization results confirmed post-functionalization and spherical porous structure of copolymer with a specific surface area of 35 m²/g. The linear and non-linear forms of pseudo-first-order, pseudo-second-order, Elovich, Avrami, and fractional power models were used to analyze the kinetics of lindane sorption. The fitting of each model to experimental data, assessed based on seven error functions, showed that the pseudo-second-order model best fit for the experimental kinetics data for both regression analyses. Also, the error values indicated that the non-linear method is a better way to obtain the kinetic parameters of lindane sorption onto chelating copolymer. The mechanism of lindane sorption was investigated with the liquid film diffusion model, intraparticle diffusion model, Bangham, and Boyd models. It was shown that intraparticle diffusion and film-diffusion affected the lindane sorption process.

Acknowledgment: This work was supported by the Ministry of Education, Science and Technological Development of the Republic of Serbia (Grants No. 451-03-68/2022-14/200026 and 451-03-68/2022-14/200135).

References

- Benimeli, C. S., Fuentes, M. S., Abate, C. M. & Amoroso, M. J. (2008). Bioremediation of lindane-contaminated soil by *Streptomyces* sp. M7 and its effects on *Zea mays* growth. *International Biodeterioration & Biodegradation*, 61(3), 233–239. <https://doi.org/10.1016/j.ibiod.2007.09.001>
- Galhoum, A. A. (2019). Facile synthesis of functionalized polyglycidyl methacrylate-magnetic nanocomposites for enhanced uranium sorption. *RSC Advances*, 9(66), 38783–38796. <https://doi.org/10.1039/C9RA06874K>
- Galhoum, A. A., Elshehy, E. A., Tolani, D. A., El-Nahas, A. M., Taketsugu, T., Nishikiori, K., Akashi, T., Morshedy, A. S. & Guibal, E. (2019). Synthesis of polyaminophosphonic acid-functionalized poly(glycidyl methacrylate) for the efficient sorption of La(III) and Y(III). *Chemical Engineering Journal*, 375, 121932. <https://doi.org/10.1016/j.cej.2019.121932>
- Hwang, C. W., Kwak, N. S. & Hwang, T. S. (2013). Preparation of poly(GMA-co-PEGDA) microbeads modified with iminodiacetic acid and their indium adsorption properties. *Chemical Engineering Journal*, 226, 79–86. <https://doi.org/10.1016/j.cej.2013.04.041>
- Jain, P., Kapoor, A., Rubeshkumar, P., Raju, M., Joseph, B., Bhat, P., Ganeshkumar, P., Kesavachandran, C. N., Patel, D. K., Manickam, N. & Kaur, P. (2022). Sudden deaths due to accidental leakage of lindane from a storage tank in a village, Sitapur, Uttar Pradesh, India, 2020: A field epidemiological investigation. *Environmental Epidemiology*, 6(3), e213. <https://doi.org/10.1097/EE9.0000000000000213>
- Jayaraj, R., Megha, P. & Sreedev, P. (2016). Review Article. Organochlorine pesticides, their toxic effects on living organisms and their fate in the environment. *Interdisciplinary Toxicology*, 9(3–4), 90–100. <https://doi.org/10.1515/intox-2016-0012>
- Khan, S., Sohail, M., Han, C., Khan, J. A., Khan, H. M. & Dionysiou, D. D. (2021). Degradation of highly chlorinated pesticide, lindane, in water using UV/persulfate: Kinetics and mechanism, toxicity evaluation, and synergism by H₂O₂. *Journal of Hazardous Materials*, 402, 123558. <https://doi.org/10.1016/j.jhazmat.2020.123558>
- Kumar, D. & Pannu, R. (2018). Perspectives of lindane (γ -hexachlorocyclohexane) biodegradation from the environment: A review. *Bioresources and Bioprocessing*, 5(1), 29. <https://doi.org/10.1186/s40643-018-0213-9>

- Malović, Lj., Nastasović, A., Sandić, Z., Marković, J., Đorđević, D. & Vuković, Z. (2007). Surface modification of macroporous glycidyl methacrylate based copolymers for selective sorption of heavy metals. *Journal of Materials Science*, 42(10), 3326–3337. <https://doi.org/10.1007/s10853-006-0958-y>
- Marković, D. D., Lekić, B. M., Rajaković-Ognjanović, V. N., Onjia, A. E. & Rajaković, Lj. V. (2014). A new approach in regression analysis for modeling adsorption isotherms. *The Scientific World Journal*. 2014, 930879. <https://doi.org/10.1155/2014/930879>
- Mortazavi, N., Asadikaram, G., Ebadzadeh, M., Kamalati, A., Pakmanesh, H., Dadgar, R., Moazed, V., Paydar, P., Fallah, H. & Abolhassani, M. (2019). Organochlorine and organophosphorus pesticides and bladder cancer: A case-control study. *Journal of Cellular Biochemistry*, 120(9), 14847–14859. <https://doi.org/10.1002/jcb.28746>
- Nastasović, A., Marković, B., Suručić, Lj. & Onjia, A. (2022). Methacrylate-based polymeric sorbents for recovery of metals from aqueous solutions. *Metals*, 12(5), 814. <https://doi.org/10.3390/met12050814>
- Peng, J., Zou, F., Liu, L., Tang, L., Yu, L., Chen, W., Liu, H., Tang, J. & Wu, L. (2008). Preparation and characterization of PEG-PEI/Fe₃O₄ nano-magnetic fluid by co-precipitation method. *Transactions of Nonferrous Metals Society of China*, 18(2), 393–398. [https://doi.org/10.1016/S1003-6326\(08\)60069-2](https://doi.org/10.1016/S1003-6326(08)60069-2)
- Sivarajasekar, N. & Baskar, R. (2014). Adsorption of Basic Magenta II onto H₂SO₄ activated immature Gossypium hirsutum seeds: Kinetics, isotherms, mass transfer, thermodynamics and process design. *Arabian Journal of Chemistry*, 12(7), 1322–1337. <https://doi.org/10.1016/j.arabjc.2014.10.040>
- Su, S., Liu, Q., Liu, J., Zhang, H., Li, R., Jing, X. & Wang, J. (2017). Enhancing adsorption of U(VI) onto EDTA modified *L. cylindrica* using epichlorohydrin and ethylenediamine as a bridge. *Scientific Reports*, 7(1), 44156. <https://doi.org/10.1038/srep44156>
- Tadić, T., Marković, B., Radulović, J., Lukić, J., Suručić, Lj., Nastasović, A. & Onjia, A. (2022). A core-shell amino-functionalized magnetic molecularly imprinted polymer based on glycidyl methacrylate for dispersive solid-phase microextraction of aniline. *Sustainability*, 14(15), 9222. <https://doi.org/10.3390/su14159222>
- Vijgen, J., Abhilash, P. C., Li, Y. F., Lal, R., Forter, M., Torres, J., Singh, N., Yunus, M., Tian, C., Schäffer, A. & Weber, R. (2011). Hexachlorocyclohexane (HCH) as new Stockholm Convention POPs—A global perspective on the management of Lindane and its waste isomers. *Environmental Science and Pollution Research*, 18(2), 152–162. <https://doi.org/10.1007/s11356-010-0417-9>
- Wang, X., Zhou, Z. & Jing, G. (2013). Synthesis of Fe₃O₄ poly(styrene–glycidyl methacrylate) magnetic porous microspheres and application in the immobilization of *Klebsiella* sp. FD-3 to reduce Fe(III)EDTA in a NO_x scrubbing solution. *Bioresource Technology*, 130, 750–756. <https://doi.org/10.1016/j.biortech.2012.12.010>
- Zhang, W., Lin, Z., Pang, S., Bhatt, P. & Chen, S. (2020). Insights into the biodegradation of lindane (γ -Hexachlorocyclohexane) using a microbial system. *Frontiers in Microbiology*, 11, 522. <https://doi.org/10.3389/fmicb.2020.00522>

Original scientific article

THE USE OF SOFT FOOD AS A VEHICLE FOR DRUG DELIVERY TO PEDIATRIC POPULATION – EFFECTS ON DISSOLUTION OF PROPRANOLOL

Maja Mirjanić¹, Aneta Stojmenovski¹, Biljana Gatarić², Nataša Bubić Pajić², Anđelka Račić²

¹University of Banja Luka – Faculty of Medicine, Department of Pharmacy, Banja Luka, Bosnia and Herzegovina

²University of Banja Luka – Faculty of Medicine, Department of Pharmaceutical Technology and Cosmetology, Banja Luka, Bosnia and Herzegovina

Abstract

The development of pediatric formulations showed to be an exceptionally complex process and therefore the use of soft food as a vehicle may be the only option for delivering the drug to the pediatric population. The aim of this study was to evaluate the effect of co-administration with peach puree and vanilla pudding on the dissolution performance of oral powder of propranolol under pediatric simulating conditions. Propranolol is a beta-blocker used to treat hypertension and infantile hemangioma in pediatric patients. Significant effect on dissolution of propranolol from the oral powder co-administrated with food was shown in comparison to the administration with water. Drug dissolution was the highest when the oral powder was mixed with pudding (95.73%) and the lowest when the powder was mixed with peach puree (67.15%), while administration with water resulted in 80,64% of drug released. These differences may be a result of different pH and composition of the vehicles, which impact drug solubility and consequently drug dissolution performance. The alterations in drug solubility and dissolution performance could also affect its bioavailability, which could ultimately compromise the safety and therapeutic effect of the drug. Thus, peach puree and pudding may not be acceptable vehicle for administration of propranolol in pediatric patients, which emphasizes the importance of considering the effect of the co-administration with food on drug performance during pediatric formulation development.

Keywords: soft food, vehicle, propranolol, dissolution, bioavailability.

Introduction

It is well known that children are not small adults due to the identified complex physiological differences (Johnson & Ke, 2021). Thus, it is important to ensure that children have access to medications that are approved and manufactured exclusively for them. New pediatric formulation could improve medication adherence and safety, reduce dosing errors and ease drug administration (Juárez-Hernández & Carleton, 2022). In order to encourage the development of pediatric drug formulation the European Medicines Agency (EMA) and United States Food and Drug Administration (FDA) made significant regulatory changes (EMA, 2012; FDA, 2018a). However, the development of pediatric formulations showed to be an exceptionally complex process and only 221 new pediatric drugs and indications became available in Europe since 2007 (EMA, 2017; Khan et al., 2022). Furthermore, currently available pediatric drug formulations cover only a small proportion of the full therapeutic requirement for effective treatment of pediatric patients (Khan et al., 2022). If the appropriate drug formulation for the pediatric patient is not available, small volumes of liquids (5 or 15 ml) such as breast milk or infant formula and/or soft foods may be the only option

for delivering the specific drug to the patient (FDA, 2018). Since in small children both gastric capacity and the amount of fasted gastric fluid are considerably smaller from those of adolescents, even a small volume of vehicle may alter the gastric environment and intraluminal conditions in the small intestine, which might cause changes in the *in vivo* performance of the drug formulation (Freerks et al., 2022). According to the draft guidance “*Use of Liquids and/or Soft Foods as Vehicles for Drug Administration: General Considerations for Selection and In Vitro Methods for Product Quality Assessments*” published in 2018 by the FDA (FDA, 2018), it must be shown that liquids and/or soft foods, which are intended to be used as vehicles for specific drug formulation, do not alter the performance of the drug formulation and could be considered well tolerated and suitable for administration in the targeted patient populations. One of the most important parameters, which must be considered when choosing a vehicle for the administration of oral dosage forms to pediatric patients is the pH value. It is well known that the pH value of fluids and soft foods can influence drug solubility and dissolution rate, but also its stability and *in vivo* performance of drug formulation. However, Freerks et al. (2022) stated that although the pH value of the vehicle is important, it is not the only parameter that should be considered during the compatibility evaluation of liquids and soft foods as potential vehicles for drug administration to pediatric patients. Namely, authors examined the composition and physicochemical properties of one of each of the vehicles listed in the FDA draft guidance document “*Use of Liquids and/or Soft Foods as Vehicles for Drug Administration*” and observed that despite similar pH, vehicles can have very different composition and other physicochemical properties that could impact drug product quality.

The aim of this study was to evaluate the effect of co-administration with peach puree and vanilla pudding on the dissolution performance of oral powder of propranolol under pediatric simulating conditions. Propranolol is a non-cardioselective beta blocker used as the hydrochloride to treat hypertension, arrhythmias, phaeochromocytoma, hyperthyroidism, haemangiomas and tetralogy of Fallot, as well as prophylaxis of migraine in children (Brayfield, 2014). Propranolol hydrochloride (Figure 1) is a weak base (pKa 9.23) with pH-dependent solubility: solubility at pH 1.2 is 225 mg/mL, while at pH 6.8 it is 130 mg/mL (Jovanović et al., 2021). According to the biopharmaceutics classification system (BCS) propranolol hydrochloride has been reported to be a class I (high permeability and high solubility) compound (Jovanović et al., 2021). It should be noted that this BCS refers to adult administration since age-specific pediatric BCS is not yet established (Guimarães et al., 2022). Currently, a commercial preparation of propranolol for children is authorized in United States (Hemangeol[®] 4.28 mg/mL oral solution, Pierre Fabre Pharmaceuticals, Inc., Parsippany, NJ) and Europe (Hemangiol[®] 3.75 mg/mL oral solution, Pierre Fabre Medicament Production, Gien, France) and can be prescribed by the physician. If the commercial formulation is not available or if the price of authorized drug product is unacceptable for health care system, a required dose can be administered by manipulating commercially available propranolol tablets or using a compounded preparation (Smithson et al., 2017).

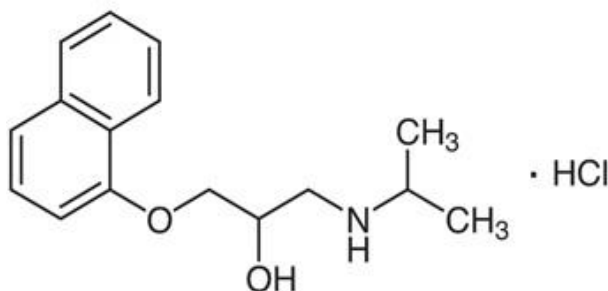


Figure 1. Chemical structure of propranolol hydrochloride
(IUPAC name: 1-naphthalen-1-yloxy-3-(propan-2-ylamino)propan-2-ol;hydrochloride)

Materials and Methods

Materials

Propranolol hydrochloride was purchased from TCI EUROPE N.V. (Belgium). Lactose monohydrate, sodium hydroxide, concentrated hydrochloric acid and potassium dihydrogen phosphate were obtained from Lach-Ner (Czech Republic). All chemicals were of analytical grade. The food products investigated in the study are shown in Table 1.

Table 1. The investigated food products

Soft food	Brand name	Manufacturer
Vanilla pudding	Pudding Zott Zottis Dessert Vanilla 0,8%	Zott SE&Co. KG, Dr. Steichele-Str.4, 86690 Mertingen, Germany
Peach puree	Lino [®] breskva	For Podravka dd: Hamé s.r.o., Na Drahách 814, 686 04 Kunovice, Czech Republic

Media preparation

0.1 M hydrochloric acid pH 1.2 and phosphate buffer pH 6.8 were prepared according to the USP 41 (2018) procedure.

Composition of the investigated food products

The specific information about the composition of investigated soft food products was acquired from the product labels and analysed.

pH value measurement

The pH value of investigated food products was measured with a digital pH-meter (Cyberscan pH 11, Eutech, Malaysia) at 25 °C. The pH-meter was first calibrated with the standard buffer solutions of pH 4.0, 7.0, and 10.0. pH measurements were conducted immediately after opening the soft food container.

Oral powder preparation

The oral powders containing 10 mg of propranolol hydrochloride and lactose monohydrate as excipient were prepared manually by mixing the pharmaceutical ingredients with porcelain mortar and pestle.

Sample preparation

The oral powders were added to 10 ml of purified water or 10 mL (approximately 10 g) of peach puree and vanilla pudding, at room temperature. The samples were then manually mixed with a glass stirring rod, for 30 s.

Dissolution study

Dissolution studies were conducted with a mini-paddle apparatus (Erweka DT 720 apparatus configured with 400 mL mini glass vessels and rotating mini paddles; Erweka, Germany). Experiments were performed at constant temperature of 37 ± 0.5 °C in a two-stage method: in pH 1.2 (volume 100 mL), for 1 h, followed by pH 6.8 (volume 200 mL), for 3 h (Martir et al., 2020). The agitation speed of the mini-paddle was set to 100 rpm. Two-milliliter samples were withdrawn at 5, 15, 30, 45, 60, 75, 90, 120, 180 and 240 min. After each sampling the collected volume was substituted with the corresponding media. The samples were firstly vortexed (VELP Scientifica, Italy) for 1 min and then centrifuged (8000 rpm, 15 min, 4 °C) (Eppendorf 5424R centrifuge, Eppendorf AG, Hamburg, Germany). The supernatant was filtered through 0.22 µm membrane filters (Chromafil X-tra PTFE-20/25, Macherey-Nagel, Germany). The filtrates were analyzed by UV

spectrophotometry (UV-1800 spectrophotometer, Shimadzu, Japan) at previously measured absorbance maximum (λ_{\max}) of propranolol in corresponding media.

Data analysis

Comparison of the obtained dissolution profiles was performed using a model-independent approach, which includes the determination of a similarity factor (f_2), according to the equation (1) as follows:

$$f_2 = 50 \times \log \left\{ \left[1 + \frac{1}{n} \sum_{t=1}^n (R_t - T_t)^2 \right]^{-0.5} \times 100 \right\} \quad (1)$$

where n is the number of time points, R_t is the dissolution value of the reference product at time t , and T_t is the dissolution value of the test product at time t . Dissolution profiles are considered similar if f_2 values are greater than 50 (i.e. 50-100) (FDA, 2017).

Results and discussion

The dissolution profiles of propranolol hydrochloride from oral powder after administration with water and selected soft food are presented in Figure 2.

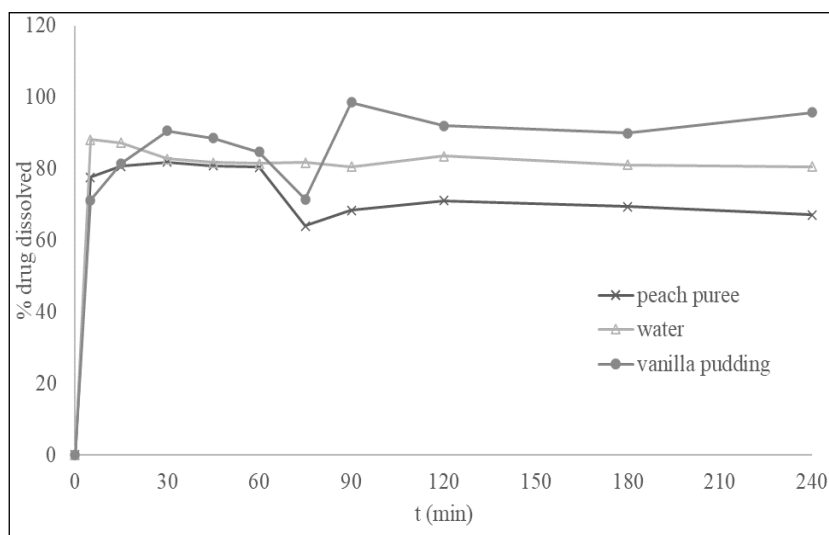


Figure 2. Percentage of propranolol hydrochloride dissolved from oral powder after administration with water and selected soft food products

The results of model-independent analysis indicate that the co-administration of propranolol hydrochloride oral powder with selected soft food products has significant effect on drug dissolution in comparison to the administration with water. Namely, the similarity factor f_2 between dissolution curves of propranolol hydrochloride obtained when the oral powder was administered with water and peach puree or with water and vanilla pudding was 49.96 and 48.53, respectively. These differences may be a result of different pH and composition of the vehicles, which impact drug solubility and consequently drug dissolution performance. As already mentioned, propranolol hydrochloride is a weak base (pKa 9.23) with pH-dependent solubility i.e., its solubility decreases with the increase of pH due to a decrease in the drug ionisation percentage. This practically means that drug solubilisation and dissolution are higher when the oral powder is mixed with a more acidic vehicle. The pH values of peach puree and vanilla pudding were 3.75 and 6.62, respectively. Therefore, it would be expected that drug dissolution is higher when the powder was mixed with peach puree in comparison to the administration with vanilla pudding as less acidic vehicle, which is not the case. Drug dissolution was

the highest when the oral powder was mixed with pudding (95.73%) and the lowest when the powder was mixed with peach puree (67.15%), while administration with water resulted in 80.64% of drug released (Figure 2). These unexpected results could be explained with the difference in the composition of the vehicles (Table 2).

Table 2. The composition of investigated food products

Soft food	Composition
Vanilla pudding	Whey, pasteurized milk, sugar, modified starch, starch, skimmed milk powder, carrageenan, carob bean gum, color, vanilla flavoring
Peach puree	Peach 75%, apple 10%, fructose, water, rice flour, citric acid, vitamin C (L-ascorbic acid)

The lower drug dissolution observed when the oral powder was mixed with peach puree, in comparison with when mixed with vanilla pudding, is probably due to the presence of starch in its composition (rice flour contains approximately 78% starch), which forms a net gel around the formulation and negatively impacts drug dissolution (Martir et al., 2020). Although vanilla pudding also contains starch (Table 2), its effect on drug dissolution is not so expressed like in the case of peach puree, because peach puree also contains fruit pieces (Table 2), which further strengthen a net gel formed around the formulation (Martir et al., 2020). These results confirm that although the pH value of the vehicle is important, it could be misleading if considered separately from other parameters during the compatibility evaluation of liquids and soft foods as potential vehicles for drug administration to pediatric patients (Freerks et al., 2022; Martir et al., 2020). In the case of propranolol hydrochloride, peach puree and vanilla pudding may not be acceptable vehicle for administration of propranolol in pediatric patients since the alterations in drug solubility and dissolution performance could also affect its bioavailability, which could ultimately compromise the safety and therapeutic effect of the drug.

Conclusion

In some cases, the use of soft food as a vehicle may be the only option for delivering the drug to the pediatric population. This study aimed to assess the impact of practices of drug co-administration with soft food on the dissolution behavior of propranolol hydrochloride. Results show that drug dissolution was significantly affected by the different vehicles. The alterations in drug solubility and dissolution performance could also affect its bioavailability, which could ultimately compromise the safety and therapeutic effect of the drug. Thus, peach puree and pudding may not be acceptable vehicle for administration of propranolol in pediatric patients, which emphasizes the importance of considering the effect of the co-administration with food on drug performance during pediatric formulation development.

References

- Brayfield, A. (2014). *Martindale: the complete drug reference*. Pharmaceutical Press.
- EMA. 2017. (2022, August 2). 10-year Report to the European Commission. https://health.ec.europa.eu/system/files/202006/paediatrics_10_years_ema_technical_report_0.pdf
- EMA. 2012. (2022, August 2). Guideline on pharmaceutical development of medicines for paediatric use. https://www.ema.europa.eu/en/documents/scientific-guideline/guideline-pharmaceutical-development-medicines-paediatric-use_en.pdf

- FDA. 2018a. (2022, August 13). E11(R1) Addendum: Clinical investigation of medicinal products in the pediatric population. <https://www.fda.gov/media/101398/download>
- FDA. 2018. (2022, August 13). Use of Liquids and/or Soft Foods as Vehicles for Drug Administration: General Considerations for Selection and In Vitro Methods for Product Quality Assessments. 2018. <https://www.fda.gov/media/114872/download>
- FDA. 2017. (2022, August 20). Guidance for industry - Waiver of in vivo bioavailability and bioequivalence studies for immediate release solid oral dosage forms based on a biopharmaceutics classification system. <https://www.gmp-compliance.org/files/guidemgr/UCM070246.pdf>
- Freerks, L., Sucher, W., Tarnow, M.-J., Eckert, C. & Klein, S. (2022). Vehicles for Drug Administration to Children: Results and Learnings from an In-Depth Screening of FDA-Recommended Liquids and Soft Foods for Product Quality Assessment. *Pharmaceutical Research*, 39(3), 497–509. <https://doi.org/10.1007/s11095-022-03208-y>
- Guimarães, M., Maharaj, A., Edgington, A., Vertzoni, M. & Fotaki, N. (2022). Understanding the Impact of Age-Related Changes in Pediatric GI Solubility by Multivariate Data Analysis. *Pharmaceutics*, 14(2), 356. <https://doi.org/10.3390/pharmaceutics14020356>
- Johnson, T. N. & Ke, A. B. (2021). Physiologically based pharmacokinetic modeling and allometric scaling in pediatric drug development: where do we draw the line? *The Journal of Clinical Pharmacology*, 61, S83–S93. <https://doi.org/10.1002/jcph.1834>
- Jovanović, M., Tomić, N., Cvijić, S., Stojanović, D., Ibrić, S. & Uskoković, P. (2021). Mucoadhesive gelatin buccal films with propranolol hydrochloride: Evaluation of mechanical, mucoadhesive, and biopharmaceutical properties. *Pharmaceutics*, 13(2), 273. <https://doi.org/10.3390/pharmaceutics13020273>
- Juárez-Hernández, J. E. & Carleton, B. C. (2022). Pediatric Oral formulations: Why don't our kids have the medicines they need? *British Journal of Clinical Pharmacology*. 88(10), 4337–4348. <https://doi.org/10.1111/bcp.15456>
- Khan, D., Kirby, D., Bryson, S., Shah, M. & Mohammed, A. R. (2022). Paediatric specific dosage forms: Patient and formulation considerations. *International Journal of Pharmaceutics*, 121501. <https://doi.org/10.1016/j.ijpharm.2022.121501>
- Martir, J., Flanagan, T., Mann, J. & Fotaki, N. (2020). Impact of food and drink administration vehicles on paediatric formulation performance part 2: dissolution of montelukast sodium and mesalazine formulations. *AAPS PharmSciTech*, 21(7), 1–15. <https://doi.org/10.1208/S12249-020-01815-9>
- Smithson, S. L., Rademaker, M., Adams, S., Bade, S., Bekhor, P., Davidson, S. & Phillips, R. (2017). Consensus statement for the treatment of infantile haemangiomas with propranolol. *Australasian Journal of Dermatology*, 58(2), 155–159. <https://doi.org/10.1111/ajd.12600>

SPONSORS



OPTIMA
G R U P A



MODRIČA
OIL REFINERY

HOFSTETTER



LABORATORIJSKA OPREMA, PRIBOR, HEMIKALIJE
PROIZVODNJA, ZASTUPANJE, TRGOVINA, SERVIS

Miše Stupara 5
78000 Banja Luka
Republika Srpska

tel./faks: +387.51.300.651
mob.: +387.65.525.146
sinex@blic.net
www.sinex-lab.rs



Već 14 godina opremamo vaše laboratorije. Zajedno istražujemo, pronalazimo nova rešenja, radujemo se uspesima i novim idejama. U našoj ponudi već se nalazi preko 20.000 artikla.



↻ Sistem za tretman infektivnog medicinskog otpada
✓ CMB Christof Group, Austrija



↻ Laboratorijski nameštaj
✓ TLOS, Zagreb

↻ Hemikalije (p.a. hemikalije ▪ HPLC rastvarače ▪ Standarde za AAS i ICP ▪ standardne rastvore, pufere, indikatore ▪ farmaceutske hemikalije ▪ hemikalije čistoće ultrapure i for trace analysis)

- ✓ PROLABO/BDH - WWR International, Austrija
- ✓ CARLO ERBA Reagenti, Italija
- ✓ LACH:NER, Češka Republika
- ✓ MOLAR, Mađarska



↻ Testovi i reagensi
✓ INVITROGEN, USA
✓ INNOGENETICS, Belgija
✓ DFI, Korea



↻ Mikrobiološke podloge, antibiogram diskovi i medicinska plastika
✓ BIOLAB, Mađarska
✓ INTERSCIENCE, Francuska
✓ VWR International, Austrija



↻ Laboratorijski aparati i instrumenti
✓ RAYPA, Španija
✓ VELD, Italija
✓ INTERSCIENCE, Francuska
✓ HANNA, Nemačka
✓ FALC, Italija
✓ KERN, Nemačka
✓ OPTECH, Nemačka



↻ Staklo i porcelan
✓ HEINZ HERENZ, Nemačka
✓ BCT Simax, Češka

↻ Metalni laboratorijski pribor
✓ BOCHEM, Nemačka
✓ HEINZ HERENZ, Nemačka
✓ HANHART, Nemačka

↻ Referentni materijali
✓ LGC PROMOCHEM, Nemačka

↻ Filter papir i sistemi za filtraciju
✓ ALBET, Španija



SVE NA JEDNOM MESTU ZA VAŠU LABORATORIJU!



Trgo Fortuna Plus
grafički materijali



East Code

www.eastcode.net



ЈП "ДЕП-ОТ" д.о.о.

РЕГИОНАЛНА ДЕПОНИЈА БАЊА ЛУКА

Булевар Војводе Живојина мишића 23, Бања Лука, тел: +387 51 258 320; fax: +387 51 258 321

ЖР: 5550070020927813, Нова Банка, Бања Лука; 5620998132697192, НЛБ Банка, Бања Лука

ПИБ: 401664160004



prehteh
— D.O.O. —

ЛЭС

ПРОЈЕКТ



ОПШТИНА ЧЕЛИНАЦ

Челинац - мјесто за добар живот!



**HIDROGRADNJA
NISKOGRADNJA
VISOKOGRADNJA**

PROIZVOĐNJA I PRODAJA:
SEPARISANIH AGREGATA,
DROBLJENIH AGREGATA,
KVARCNOG PIJESKA,
Tel: 056/310-400



**KESO
GRADNJA**

mb impeX



EKO-EURO TIM
Krupa na Vrbasu

CSK
print



PETROGRAFIJA
ŠTAMPARIJA



EUROINSPEKT

"EURO-INSPEKT" d.o.o.
ISPITNA LABORATORIJA



EURO LAB

LABORATORIJSKA OPREMA - ZASTUPSTVA, VELETRGOVINA, SERVIS



**University of Banja Luka
Faculty of Technology**

Vojvode Stepe Stepanovića br. 73
78 000 Banja Luka
Tel./Faks: +387 51 434 357
e-mail: savjetovanje@tf.unibl.org
web: www.tf.unibl.org